International Atomic Energy Agency

INDC(CCP)-43/L

INDC   INTERNATIONAL NUCLEAR DATA COMMITTEE

USSR State Committee on the Utilization of Atomic Energy
Nuclear Data Information Centre

NUCLEAR CONSTANTS

Issue No. 7

Translated by
the International Atomic Energy Agency

Vienna, July 1974

72-5354
Translated from Russian

USSR STATE COMMITTEE ON THE UTILIZATION OF ATOMIC ENERGY

NUCLEAR DATA INFORMATION CENTRE

NUCLEAR CONSTANTS

Issue No. 7

EDITORIAL BOARD

C O N T E N T S

Chapter I.   NUCLEAR PHYSICS CONSTANTS

Chapter II. REACTOR CONSTANTS AND
PARAMETERS

Chapter III. RADIATION SHIELDING CHARACTERISTICS
AND PARAMETERS.
RADIATION AND NUCLEAR SAFETY

DELAYED NEUTRONS AND THE PHYSICS OF FISSION

B. P. Maksyutenko

New method for determining relative yields of delayed neutrons
====

In reactor kinetics calculations it is necessary to know the absolute and relative yields of delayed neutrons resulting from the fission of various substances by neutrons of different energies. The yield of delayed neutrons from the ith precursor Y_i can be found if one known the yield of a given mass in fission, $P(A_i)$, the probability $P(Z_i, Z_{pi})$ of a given charge Z_i occurring in the given mass A_i in the case of the most probable charge Z_{pi}, and the probability of radiation of delayed neutrons by this precursor P_{ni}:

$$Y_i = P(A_i) \ P_{ni} \ \Sigma \ P(Z_i, Z_{pi}) \tag{1}$$

where Σ denotes that a cumulative yield is being considered. Since P_{ni} is independent of energy, $P(A_i)$ can be determined experimentally, and we would only have to find $P(Z_i, Z_{pi})$ in order to calculate Y_i for any energy of fission-producing neutrons. However, the intensity of existing fast neutron sources is not high enough to make this feasible. At the present time the charge distribution has been established only for the case of ^{235}U fission by thermal neutrons and 15 MeV neutrons. Thus we are left with the purely experimental method of determining the delayed neutron yields. This involves analysing the whole of the delayed neutron decay curve and determining the ratio of the yields from different precursors (for example, Y_i/Y_1, where Y_1 is the yield of a group with half-life ~55 sec), and then finding the total absolute yield (from all precursors together, in another experiment). These data may be also used to calculate the absolute yield of delayed neutrons from any precursor.

With the aid of radiochemical and mass spectrometric methods it has so far been possible to identify 37 fragment-precursors, i.e. to establish their Z_i and A_i values and, in addition, their P_{ni} values and their half-lives. Unfortunately expansion of the decay curve by the best available method – the least squares method – serves to segregate only six contributors at most. Hence we get only a very rough solution, because each of the six separate groups represents the relative yield of delayed neutrons from several precursors. It would be desirable to segregate a larger number of these in the expansion. M.Z. Tarasko has found a way of doing this $\diagup 1,2\diagup$ and has demonstrated its possibilities by obtaining a numerical solution for a system of equations with a thirtieth-order Gilbert matrix. Now the question is to what extent a given specific statistical selection (i.e. a given experimental result) is adequate for extracting a larger number of exponents. This will be illustrated below by comparing the results obtained by expansion of the delayed neutron decay curve resulting from thermal fission of ^{235}U with radiochemical data. But now let us consider the possibilities offered by this expansion.

In Table 1 the delayed neutron precursors are arranged in descending order of half-life. Some of them have widely differing half-lives whilst others agree within the limits of experimental error. The latter have been grouped together. In the expansion of the decay curve, as we can see from Table 1, the net yields of three bromine isotopes (with masses 87, 88, 89) can be determined. Thence we can find the probability of a given charge occurring in fission:

$$P(Z_i, Z_{pi}) = \frac{Y_i}{P_{ni}\ P(A_i)} \qquad (2)$$

where the right-hand side is determined entirely from experimental data. Since from Eq. (2) we know that

$$P(Z, Z_p) = \frac{1}{\sigma\sqrt{2}_\pi}\ \exp\left(-\frac{(Z - Z_p)^2}{2\sigma_Z^2} \right) , \quad (\Delta Z_p = Z - Z_p), \quad (3)$$

and since from Eq. (3) it is apparent that

$$Z_p = kA + \ell , \qquad (4)$$

we can now proceed to the $P(Z, A)$ dependence $\boxed{4}$. The scheme for this transformation of co-ordinates, i.e. the transition from A = const., assumed by Wahl $\boxed{2}$, to Z = const., is illustrated in Fig. 1.

Such a transformation results in a quadratic parabola on the semi-logarithmic scale:

$$\ell n\ P(Z, A) = aA^2 + bA + q \tag{5}$$

where the coefficients a, b and q are a combination of the coefficients k, ℓ and σ. Assuming A = 87, 88, etc. and solving the system of equations in expression (5), we obtain the values of k, ℓ and σ as well as Z_p and ΔZ_p for the bromine isotopes.

In addition, we can find the distribution of the probabilities of radiation along the A axis for these fragments (since Z = const.):

$$P(A_i)_{Z = const.} = Y_i/P_{ni}$$

Thus, as shown schematically in Fig. 2, we find two distributions,

$$P(A_i)_Z = const. \quad \text{and} \quad P(Z_i)_A = const.$$

in two mutually perpendicular planes. If the primary mass distribution is used in this construction, we obtain the fragment energy surface without allowance for the gamma radiation energy.

Now let us turn again to the determination of Z_p for fragments and to delayed neutron yields from the other precursors. The values of $P(Z, A_i)$ can be found for two isotopes of iodine (with masses 137 and 138) using expression (2) in the same way as for the bromine isotopes. Let us assume that the distribution width is the same in both cases (i.e. for bromine and iodine isotopes); it can easily be shown that the relationship between the values of $P(Z, A)$ for the three isotopes of bromine and iodine (the latter are denoted by strokes) should then be the following:

$$\frac{P_1 P_3}{P_2^2} = \frac{P'_1 P'_3}{P'^2_2} \tag{6}$$

where the indices 1, 2, 3 denote the values of $P(Z\ A)$ for bromine–87, 88 and 89 and iodine–137, 138 and 139. All the quantities in expression (6) are known except P'_2 – the value of $P(Z, A)$ for iodine–139. By determining this

and then using the corresponding values of P_{II} and $P(A)$ for iodine-139, we
find the delayed neutron yield from this precursor. In this way we isolate
the contribution of the iodine-139 precursor from the delayed neutron yield
of the group of precursors with a mean half-life of ~2 sec.

Furthermore, as can be seen from Table 1, apart from the isotopes there
are also isobars, for example bromine-87, selenium-87 and arsenic-87; bromine-88
and selenium-88, etc. Since

$$\frac{Y_i}{Y_1} = \frac{P_{ni}}{P_{n_1}} \cdot \frac{P(Z-1, Z_p)}{P(Z, Z_p)} \tag{7}$$

(the subscript 1 refers, for example, to bromine-87 and the subscript i to
selenium-87) and

$$\ell n \frac{P(Z-1, Z_p)}{P(Z, Z_p)} = \frac{1}{\sigma 2} (Z-Z_p-0.5), \tag{8}$$

it is possible, using the value of Z_p determined for a fragment with mass 87,
to calculate from equation (8) the ratio of the probabilities of occurrence
of a given charge and then to determine from equation (7) the ratio of the
delayed neutron yield from selenium-87 to that from bromine-87. A similar
calculation can be done for [87]As.

After isolating the delayed neutron contribution of the precursors
[139]I and [88]Se in the group with a half-life of ~2 sec, we know that the
remainder must be the contribution from the precursor [85]As plus a slight
addition from [92]Kr. In the same way it is possible to separate the contribution
of [87]Se from [93]Rb and split up the group with a half-life of 5.9 sec.

We can sum up the procedure as follows. First we use the new method of
expanding the decay curves, to classify the precursors according to the only
criterion available - the precursor half-life. The second stage involves
constructing the charge distribution for the bromine isotopes and then using
it to calculate the delayed neutron yields from the pure precursors contained in
the groups, which are a mixture of the yields from precursors with half-lives
coinciding within the limits of experimental error.

From the above analysis it is clear that we can not only determine the delayed neutron yields from a larger number of precursors than is possible with the normal least squares method but that we can also find the charge distribution parameters for any energy of fission-inducing neutrons. Apart from the above formulae the following relationship derived from Eq. (3) may be used to determine ΔZ_p in the case of individual precursors:

$$2\sigma^2 \ln \frac{P(Z_i, Z_{pi})}{P(Z_1, Z_{p_1})} = \Delta Z_{p_i}^2 - \Delta Z_{p_1}^2 \tag{9}$$

Here the subscript 1 relates to bromine-87 and the subscript i to any other precursor.

Thus, if expansion to a larger number of exponentials is performed, we can:

1. Find the relative yields of delayed neutrons from pure precursors instead of a mixture of them, and furthermore from that part of the precursors which makes the predominant contribution to the total delayed neutron yield in both thermal and fast fission;

2. Find the charge distribution parameters and the most probable charge for delayed neutron precursor fragments resulting from fast fission of various substances; and

3. Determine the energy surfaces of fission fragments (bromine isotopes) and investigate how these change with a variation in energy of the neutrons causing fission.

Cumulative yields of fission products for Z = const. We propose to show that there is another method of determining delayed neutron yields which is based not on the charge and mass distribution but on knowing the cumulative yields of precursor fragments (fission products).

Let us assume that the distribution of cumulative fission product yields when Z = const. is:

$$P(A, A_p) = \frac{1}{\sigma_Z \sqrt{2\pi}} \, e^{-\frac{(A-A_p)^2}{2\sigma_Z^2}}$$

where $P(A, A_p)$ is the probability of a fragment of mass A occurring with the most probable value of A_p (for given Z) and σ_Z is the distribution width. Table 2 shows calculated values of σ_Z and A_p for isotopes of bromine, krypton, rubidium, iodine and caesium based on data in Ref. $\underline{/6\underline{7}}$. Fig. 3 shows the fission product mass distributions for Z = const. The mean width $\bar{\sigma}_Z$ = 1.482 $\overset{+}{-}$ 0.085. The values closest to this are observed in the case of rubidium, iodine and caesium isotopes, their mean value being $\bar{\sigma}_Z$ = 1.509 $\overset{+}{-}$ 0.064. The width of the krypton isotope distribution differs considerably from the mean.

The relationship between Z and A_p is illustrated in Fig. 4. The straight lines running through the points for the bromine and rubidium isotopes and through the second pair of points - for iodine and caesium isotopes - are parallel, the slope being:

$$K = \frac{Z_2 - Z_1}{A_{p_2} - A_{p_1}} = \frac{2}{3.89} = 0.515$$

The point for krypton isotopes falls outside this relationship. If the same rule is assumed in this case, the krypton isotopes should be assigned the value A_p = 90. The broken curve in Fig. 3 shows the distribution of krypton isotope fission products on the assumption that its width is 1.509 and the peak is at A_p = 90.

Table 3 shows values of $A-A_p$ for isotopes of bromine, krypton, rubidium, iodine and caesium as well as experimentally determined and calculated fission product yield probabilities normalized to the yield of rubidium isotopes for σ_Z = 1.509. In Fig. 5 the small circles indicate experimentally determined values of $P(A, A_p)$.

As can be seen from Table 2, the Gaussian distribution parameters were calculated for three mass numbers in each group of isotopes. The yields of rubidium isotopes, for example, are known for six mass numbers and differ by three orders of magnitude. However, as can be seen from Table 3 and Fig. 5, there is good agreement with the calculated values.

The results obtained can now be used to determine the delayed neutron yields. Since

$$P(A, A_p) = Y_i / P_{ni},$$

the delayed neutron yields of three bromine isotopes (with masses 87, 88, 89) can be used to find the distribution parameters for $P(A, A_p)$ and then the delayed neutron yields from ^{90}Br and ^{91}Br. Since the distribution width is identical and the delayed neutron yields of ^{137}I and ^{138}I are known, the yield of ^{139}I and its delayed neutron yield can be found. In short, the whole of the procedure described in the previous section can be carried out using the law established for the mass distribution with Z = const. instead of the charge distribution. The accuracy of determination of the delayed neutron yields will be better, moreover, since there is no need in these calculations to make use of mass yield measurements.

Practical applications. As we have mentioned, the mathematical possibilities of the new method have been demonstrated by obtaining a numerical solution of a system of equations with a 30th order Gilbert matrix $/1/$. Now we must investigate to what extent our experimental results (from the point of view of statistics and resolution) enable us to solve the problem in hand, which is to isolate a larger number of precursors than can be segregated by the least squares method.

The total count we normally obtain under the decay curve when investigating the yields (depending on the energy of the fission-producing neutrons and on the element) is from half a million to several million pulses (in the series of measurements from 5 to 20). This statistical accuracy would seem adequate for determining a larger number of parameters than the six obtained by the least squares method. There are other factors affecting the accuracy of the results but dealing with them all would occupy a whole book. We shall concentrate on one principal factor. In this case the problem should be formulated as follows: what must be the total count under the composite decay curve and what must be the channel widths in the measurements for it to be possible to determine the initial intensities of two or more exponents with given half-lives when the curve is expanded into its components. This condition may be written comparatively easily for a composite curve consisting of two exponents, although the equation obtained is quite difficult to solve but, when there are more than two, even the formulation is unknown. In that case the only feasible method which we found for checking the correctness of the expansion of the decay curve was a series of mathematical experiments, in which the complete decay curve is expanded for different half-life combinations (the basis for their selection can be proved sound). A delayed neutron decay curve resulting from thermal fission of ^{235}U

was used for this purpose and the results of the expansion are compared
with radiochemical and mass spectrometric data in the section below entitled
"Analysis of results".

Another equally difficult problem is calculating the errors in the ratio
of the group yields, but we shall not dwell on this here for the reasons
mentioned above. We have selected the simplest method, whereby both the
results themselves and the errors are determined as the mean of the results
of expanding seven decay curves, each of which is the sum of seven to nine
exponents obtained in individual measurements.

A further mathematical problem is that of analysing precursor build-up
and decay. Heretofore the decay curve has been represented as a sum of exponents:

$$N = \sum_i a_i \exp(-\lambda_i t) \tag{10}$$

where N is the counting rate and a_i and λ_i are the initial intensity and
decay constant of the ith group of delayed neutrons. This is valid as long
as we are considering beta decay of precursor fragments formed instantaneously
during fission (direct yield). In the case of ^{87}Br and ^{88}Br the yield of their
precursors from beta decay of ^{87}Se and ^{88}Se is appreciable and allowance should
be made for the cumulative yield of bromine isotopes via the chain

$$^{87}Se \xrightarrow{\ \beta\ } \ ^{87}Br \xrightarrow{\ \beta\ } \ ^{87}Kr$$
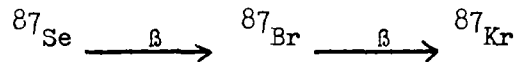
This gives Eq. (10) the form

$$N = \sum_i a_i e^{-\lambda_i t} + a_{se}(e^{-\lambda_{Br} t} - e^{-\lambda_{Se} t}) \tag{11}$$

i.e. contributors with negative yield appear. Fig. 6 shows the decay of bromine
after disconnection of the source of fission-producing neutrons as well as the
build-up and decay of bromine resulting from decay of selenium. Although the
latter contribution is small, the beginning of the decay curve is distorted.
A detailed analysis of this problem indicated that when the decay curve is
expanded from the sixth second after removal of the source there are no significant
distortions in the results.

Precursor half-lives. Many factors have pointed to an incorrect
determination of the half-lives of several isotopes. Analysis of various
ways of expanding the decay curves has corroborated this suspicion, and we
were obliged to resort to a systematic recalculation of half-lives.

Ref. $\sqrt{5\_7}$ indicated a linear dependence of the logarithm of the
half-life T on the mass number A of a precursor fragment for bromine
and iodine isotopes, i.e.

$$\ln T = rA + b \tag{12}$$

(see Fig. 7). The physical reason for this relation is the linear dependence
of the beta decay energy Q_β on A, so that Eq. (12) may also be written

$$\ln T = r'Q_\beta + b' \tag{13}$$

Fig. 8 shows the family of curves for even and odd isotopes of bromine,
krypton, rubidium, iodine and caesium. Their behaviour is regular with
the exception of the rubidium isotopes. The nuclei of the rubidium isotopes
have no anomalous features distinguishing them from the neighbouring element-
isotopes of bromine and krypton and such an anomaly in the half-life dependence
on A is not justified. Using the most reliable half-life values for ^{89}Rb, ^{90}Rb
and ^{91}Rb we found from Eq. (12) the half-lives of the rubidium isotopes with
mass numbers 92, 93 and 94 and corrected the value of the half-life for ^{139}I.
This was the first correction which we had to make to the precursor table (see
Table 11).

Probability of delayed neutron radiation. Of course distortions in the
determination of half-lives were also bound to cause distortions in the
experimentally determined values of P_{II} for the isotopes in question. Analysing
the different ways of expanding the decay curves confirms this conclusion,
which was in fact the reason for carrying out the investigations.

Amiel $\sqrt{6\_7}$ showed that the proportion of beta decays resulting in
delayed neutron radiation P_{II} is related to the energy ΔE by the expression

$$P_n = K(\Delta E)^m \tag{14}$$

where

$$\Delta E = Q_\beta - B_n$$

Here Q_β is the beta decay energy of a precursor fragment and B_n is the neutron
binding energy in the emitter nucleus. The best value of m found by Amiel on
the basis of all available experimentally determined values for P_{II} is 1.51.

Fig. 9 shows the dependence of P_n on ΔE in double logarithmic scale. As with the half-lives, the rubidium isotopes display anomalous behaviour. The dependence of ΔE on A for Z = const. was investigated and found to be linear, i.e.

$$\Delta E = sA + p \qquad (15)$$

Table 4 shows the results of calculating the coefficient S for even and odd isotopes of the above elements (in cases where this is possible) and for all isotopes irrespective of parity. From Figs 10 and 11 and Table 4 it can be seen that the light fragments - bromine, krypton and rubidium isotopes - have practivally the same value of the coefficient S, whilst in the case of the heavy fragments the values differ for even and odd A. This table also presents values of A_0 - the mass corresponding to $\Delta E = 0$, i.e. $P_{II} = 0$. Thus for all the above elements we have established the lower limit for the mass of a fragment at which the isotope of a given element can no longer be a delayed neutron precursor ($P_{II} = 0$ for all $A < A_0$). The ultimate aim of the investigation was to correct the values of P_{II} for rubidium isotopes and to calculate it for those isotopes for which experimental data were lacking. We assumed that the most reliable values of P_{II} were those determined for bromine isotopes, so we used them to find m for the light fragments and to calculate P_{II} for rubidium and krypton isotopes. Table 5 shows the calculated values of m for both light and heavy fragments. An anomalous value is observed for odd iodine isotopes. The value of P_{II} for ^{137}I is one of the most reliable. On the other hand, the m obtained from experimentally determined P_{II} for odd caesium isotopes is the same as that obtained from two calculated values of P_{II} for odd xenon isotopes (m = 1.676 and 1.688). Using m = 1.69, we get $P_{II} = 17.2\%$ for ^{139}I. Expansion of the decay curve shows that this is approximately twice the true value. The reason for this anomaly is hard to explain at present.

After correcting the values of the half-lives and P_{II}, the precursor table looks somewhat different: there is now a group with a half-life of 14 sec (^{92}Rb) whilst the group with a half-life of 2.67 sec (^{94}Rb) disappears. There is also a change in the delayed neutron yields from various precursors. These were found by multiplying the calculated values of $P(A, A_p)$ by the corrected values for P_{II}. This is the second correction we made to the precursor table.

Methods of measurement and results. Now let us turn to the method of measurement used. We shall not describe it in detail, since it is quite well known, but shall dwell only on a few important details. A sample of powdered, 90% enriched ^{235}U enclosed in a cylindrical aluminium container 35 mm in diameter and weighing 0.7 g was irradiated for 5 min and then transferred to the counter unit located 2.5 m from the target. At that instant the neutron source was disconnected. The neutrons were obtained from the T(p,n)^{3}He reaction in a Van de Graaff generator and were slowed down by a polyethylene block. The decay curves were recorded by a 512-channel analyser with a channel width of one second.

The decay curves were expanded from the 6th second after conclusion of irradiation of the sample. The channel width was set at one second from the 6th to the 60th channel and at 5 seconds thereafter to the end of the decay curve.

The procedure for expanding the decay curves is described in Ref. $\boxed{7}$. Initially expansion is done by the least squares method and Table 6 shows the results of such expansion to four exponentials. To obtain a more precise comparison, the same half-lives were used as in Ref. $\boxed{8}$ for the case of thermal fission of ^{235}U. In Ref. $\boxed{8}$ the expansion was performed to six exponentials, but in fact 12 parameters were determined (relative yields and half-lives). Since the problem was non-linear in this case, it is not surprising that the accuracy of the results in Ref. $\boxed{8}$ is inferior, despite the very good statistical accuracy. Our problem is linear (only the relative yields are determined) and the number of parameters is only one-third of that in Ref. $\boxed{8}$.

After preliminary expansion by the least squares method, giving the background and total count in the period from termination of irradiation to commencement of recording and from termination of recording to infinity, the area under the curve is normalized and the curve is expanded by the new method $\boxed{1, 7}$. Table 7 shows the results of expanding the measured decay curves. Also given are the ratios of the yields of the delayed neutron groups obtained by calculation, incorporating the corrections mentioned above. Table 8 presents the results of expanding by the least squares method $\boxed{8}$ into nine groups (this can be done artificially). Table 9 shows the relative delayed neutron yields obtained by radiochemical and mass spectrometric methods $\boxed{6}$. Table 10 shows relative delayed neutron yields

calculated from the relative fission product yields, the charge distribution and the P_{II} systematics (we shall call these "systematics data").

Comparison of the results shows that expansion of the decay curves by the new method gives considerably better agreement with the radiochemical investigations than the least squares method (9 exponentials).

It should be noted that the new method has further possibilities and that the results can be even better. For this we need more accurate determination of the half-lives by radiochemical and mass spectrometric methods and more accurate definition of P_{II}.

This concludes the first stage in the calculation of the relative delayed neutron yields which involves using the only criterion we have available at present – the half-life – to segregate contributors with half-lives from 55 to 1.7 sec (the shortest-lived group with T = 1.7 sec of course includes the residue of all shorter-lived groups and is thus essentially a "barrier" group).

The second stage involves using physical laws to separate precursors having half-lives that coincide within the limits of experimental error, since the mathematical possibilities are now exhausted. The relation

$$P(A, A_p) = Y/P_n$$

enables the mass distribution parameters to be calculated for bromine isotopes (masses 87, 88, 89). These parameters allow us to determine the delayed neutron yields from other bromine isotopes. Further, knowing that the distribution width is the same for isotopes of different elements, and knowing also the delayed neutron yields and values of P_{II} for two isotopes of iodine (137 and 138) and rubidium (92 and 93), we can find the delayed neutron yields for any iodine or rubidium isotope. These elements make by far the largest contribution to the total delayed neutron yield. Moreover, although the measurement and treatment of the decay curve are commenced when the contribution of the short-lived groups is practically zero, it is still possible to determine their yield.

Thus, although we started off with the more modest and limited aim of trying to identify the contributions of the pure precursors of bromine isotopes, the possibilities of the mathematical method and the physical laws are such as to enable us to segregate the bulk of the precursors.

An investigation of the delayed neutron yields from fast fission of various nuclei is also a basis for studying fission fragment mass and charge distribution behaviour.

Analysis of results. We have deliberately left this section to the end so as not to obscure the main arguments.

Resolution. By this term we mean here the accuracy of determination of the relative yields of contributors to the composite decay curve. This is governed by the channel grouping selected (the choice of channel widths in the analyser), the statistical accuracy of the measurements and the method of calculation. The following table demonstrates that under sufficiently rigorous conditions - a difference in half-life of 6-7% - the yields differ by factors of 1.5-2 (the yields of the 15.5 and 14.4 sec and the 6.3 and 5.9 sec groups). This means that the yields are still not equalized: in the limiting case where the half-lives are the same the yields must have an equal probability. This shows that the choice of width grouping is correct, the statistics are completely satisfactory and the method is sufficiently accurate. The weak contributors, as experience shows, cannot be isolated even with a large difference in half-lives (for example ^{134}Sb, the yield of which is 7% of the yield of bromine-87).

T (sec)	Y_i/Y_1
55.65	1
24.4	4.10
15.5	1.59
14.4	1.08
6.3	0.58
5.9	0.84
4.45	4.8
2.1	6.57
1.7	1.24

Comparison of calculations by the new method and the method of least squares.
Even the artificial version of the calculation by the least squares method
(Table 8) gives correct yield ratios (i.e. in agreement with radiochemical and
mass spectrometric data - Tables 9 and 10, groups 1 and 2) only for ^{137}I and
^{87}Br; the yield of ^{88}Br is distorted by an additional contribution (~30%) from
^{92}Rb; the yield of ^{138}I is 2.5 times too low (300% error of determination) and
the following groups represent the yield from a mixture of four or five precursors.

. The new method of calculation makes it possible to identify the yields of
a larger number of contributors in the same half-life range, i.e. it has better
resolution and, moreover, it gives much better agreement with the radiochemical
data, as can be seen by comparing Tables 7, 9 and 10. This is the great advantage
of the new method. However, its possibilities have yet to be exhausted. More
accurate results (even better agreement with radiochemical data) will be
obtainable if certain half-life values are determined more accurately.

Calculation of delayed neutron yields from short-lived isotopes and
identification of contributors from mixed groups. Below we calculate the
delayed neutron yields from ^{90}Br (T = 1.6 sec), ^{139}I (T = 3.2 sec) and
^{140}I (T = 0.8 sec). Since the decay curve is analysed only from the sixth
second after the source of fission-inducing neutrons has been switched off, the
contribution of groups with short half-lives is only a few per cent and includes
components from other contributors with similar half-lives. Therefore the
accuracy with which the yield of a group with T 1.6-1.7 sec can be determined
by direct expansion of the decay curve is low whilst the contribution of the
group with T ~0.8 sec cannot be determined at all. On the other hand, the
contribution of ^{139}I cannot be separated from the contribution of ^{93}Rb and ^{137}Te
(see Table 7) because their half-lives are identical. Using the cumulative
yields from isotopes of bromine with masses 87, 88 and 89 and of iodine with
masses 137 and 138, (obtained by expansion of the decay curve) together with
the values for P_{II}, we were able to determine the delayed neutron yields of
the above isotopes from expressions 5a and 6.

It would be possible to show the errors associated with calculating the
yields of isotopes which are not obtained directly by expansion of the decay
curves, or which are isolated from mixed groups. However, a better illustration
can be obtained by comparing the calculation results with existing experimental
data from radiochemical investigations. The results are given in the table below.

The good agreement between the calculated and radiochemical (experimental) data is a fine illustration of the possibilities of the new method. It might be considerably better still in the case of the iodine isotopes if there were not some uncertainty in the value of P_{II}.

A	Y_i/Y_1		P_{II} %	$P(A,A_p)$	
	exp.	calc.		exp.	calc.
Bromine isotopes					
87	1	–	2.5	0.400	
88	1.78^+	–	4	0.445	
89	2.82^+	–	7	0.400	
90	$2.80 + 3.76^{++}$	3.45	12		0.288
Iodine isotopes					
137	3.91^+	–	4.8	0.815	
138	$1.2^+ + 1.78^{++}$	–	2.5	0.490	
139	1.17^{++}	0.94	6		0.156
140	$0.56 + 0.51^{++}$	0.32	12		0.026

+ From expansion of our decay curve.

++ Data from radiochemical investigations.

Charge distribution. We shall not return to this problem because it has been considered in previous papers $\llbracket 1,9 \rrbracket$. In particular, it is shown in Ref. $\llbracket 9 \rrbracket$ how the method of successive approximations can be used to isolate the direct yield from the cumulative yield for bromine isotopes. The accuracy with which the charge can be determined is 0.1-0.2 charge units – essentially just as good as the direct method.

Explanations for Tables 7-10

1. a_i is the absolute delayed neutron yield from the ith precursor in 10^4 fissions;

2. "Total" is the number of delayed neutrons from a given precursor recorded from the end of irradiation to infinity:

$$N_{ni} = \int_0^\infty a_i e^{-\lambda_i t} dt = a_i \tau_i \qquad (16)$$

This quantity characterizes the relative statistical accuracy of the yield determination for each precursor. $\Sigma\, N_{ni}$ is the total delayed neutron yield from all groups from the end of irradiation to infinity. Since the calculation is performed in ralative units, the tables include values for $a_i T_i$. It is a familiar fact that even with a different set of expansion parameters – half-lives – one can obtain practically the same accuracy of fitting to the experimental data. This is clear from the figures presented.

REFERENCES

/1/   TARASKO, M.Z., FEI (Institute of Physics and Power Engineering, Obninsk) Preprint No. 156 (1969).

/2/   WAHL, A.C. et al., Phys. Rev. 126 (1962) 1112.

/3/   PAPPAS, A. et al., Int. Conf. peaceful Uses atom. Energy (Proc. conf. Geneva, 1955) 7, UN, New York (1956) 19.

/4/   MAKSYUTENKO, B.P., TARASKO, M.Z., FEI Preprint No. 145 (1968).

/5/   STEHNEY, A.F., PERLOW, G.J., Int. Conf. peaceful Uses atom. Energy (Proc. Conf. Geneva. 1958) 15, UN, Geneva (1958) 384.

/6/   AMIEL, S., Physics and Chemistry of Fission (Proc. Conf. Vienna, 1969) 1 IAEA Vienna (1969) 569.

/7/   MAKSYUTENKO, B.P., TARASKO, M.Z., Physics and Chemistry of Fission (Proc. Conf. Vienna, 1969) 1 IAEA Vienna (1969) 939.

/8/   KEEPIN, G.R., Fizičeskie osnovy kinetiki jadernyh reaktorov (The physical bases of fast reactor kinetics) (Russian translation of English original) Atomizdat, Moscow (1967).

Table 1

Delayed neutron precursors and values of P_{II} and Z_p

No.	$T_{I/2}$ sec	Precursor	P_{II} %	Z_p
1	2	3	4	5
I.	55,65 ± 0,20	Br^{87}	2,5 ± 0,4	34,52 .
2.	24,4 ± 0,4	I^{137}	4,8 ± I,3	53,26 ± 0,I2
	24,9 ± 0,2	Cs^{141}	0,073±0,0II	54,97 ± 0,04
3.	15,85 ± 0,I0	Br^{88}	4,0 ± I,4	34,9I .
4.	II,3 ± 0,3	Sb^{134}	0,03± 0,02	5I,77 ± 0,II
5.	6,3	I^{138}	2,5 + 0,6	53,45 ± 0,I0
6.	5,89 ± 0,04	Rb^{93}	I,65± 0,30	37,39 ± 0,I0
	5,8 ± 0,5	Se^{87}	0,4 ± 0,I	34,52
7.	4,48 ± 0,02	Rb^{92}	0,0I2±0,004	36,8I ± 0,04
	4,45 ± 0,30	Br^{89}	7 ± 2	35,42 ± 0,I2
8.	3,5 ± 0,5	Te^{137}	. ? .	53,26 ± 0,I2
9.	2,67 ± 0,04	Rb^{94}	II,I± I,I	37,84 ± 0,I5
I0.	2,2 ± 0,3	Se^{88}	6,4± 2,5	34,9I
	2,028 ± 0,0I2	As^{85}	22,0± 5.	33,68 .
	2,0 ± 0,5	I^{139}	6,0± I,7	53,82 ± 0,I2
	I,86 ± 0,0I	Kr^{92}	0,04± 0,0007	36,8I ± 0,04
II.	I,73 ± 0,0I	Xe^{141}	0,054±0,009	54,97 ± 0,04
	I,696 ± 0,02I	Sb^{135}	8±2	52,40 ± 0,I5
	I,69 ± 0,I3	Cs^{143}	I,I3±0,25	55,92 ± 0,I0
	I,68 ± 0,02	Cs^{142}	0,27±0,07	55,36 ± 0,04
I2.	I,6 ± 0,6	Br^{90}	II,5±0,4	35,84 ± 0,I0
I3.	I,4 ± 0,4	As^{87}	. ? .	34,52 .
	I,29 ± 0,0I	Kr^{93}	2,6±0,5	37,39 ± 0,I0
	I,24 ± 0,02	Xe^{142}	0,45±0,08	55,36 ± 0,04
I4.	I,05 ± 0,I4	Cs^{144}	I,I0±0,25	56,40 ± 0,25
	> I	Xe^{143}	?	55,92 ± 0,09
	> I	Xe^{144}	?	56,40 ± 0,25
	> I	Xe^{145}	?	56,88 .
I5.	~ 0,8	I^{140}	I2±8	54,34 ± 0,03
I6.	> 0,I5	Kr^{95}	?	38,40 ± 0,I9
I7.	. ~ 0,4.	Br^{91}	. ? .	36,32 ± 0,09
	0,36 ±0,02	Rb^{95}	7,I0±0,93	38,40 ± 0,I9
	~ 0,3	I^{141}	?	54,97 ± 0,04

Table 1 (continued)

1	2	3	4	5
18.	$0,23 \pm 0,02$	$R\beta^{96}$	$12,7 \pm 1,5$	$38,20 \pm 0,24$
	$\sim 0,2$	Kr^{94}	?	$37,84 \pm 0,15$
19.	$0,135 \pm 0,010$	$R\beta^{97}$	> 20	$39,14$

+ The grouping of precursors with half-lives below 1.7 sec is arbitrary, as can be seen from the table.

Table 2

Distribution width and values of A_p for cumulative yields of fission products

Bromine isotopes		Krypton isotopes		Rubidium isotopes		Iodine isotopes		Caesium isotopes	
A	$P(A,A_p)$	A	$P(A,A_p)$	A	$P(A,A_p)$	A	$P(A,A_p)$	A	$P(A,A_p)$
87	2,28	92	1,68	92	5,18	137	4,11	141	4,60
88	2,78	93	0,53	93	4,0	138	2,68	142	3,1
89	2,42	94	0,08	94	1,9	139	1,10	143	1,43
σ	1,721		1,165		1,434		1,469		1,623
A_p	88,09		91,64		91,98		136,57		140,46

Table 3

Distribution of mass yields of fission products for Z = const.

Element	A	$A - A_p$	$P(A,A_p)$ exper.	$P(A,A_p)$ norm. exper.	$P(A,A_p)$ calc.
Br	87	- 1,09	2,28	4,24	4,0
	88	- 0,09	2,78	5,17	5,17
	89	0,91	2,42	4,50	4,30
	90	1,91	1,40	2,60	2,33
	91	2,91	0,40	0,744	0,82
Rb	92	0,02	5,18	5,18	5,18
	93	1,02	4,0	4,0	4,12
	94	2,02	1,9	1,9	2,11
	95	3,02	0,66	0,66	0,70
	96	4,02	0,17	0,17	0,149
	97	5,02	0,02	0,02	0,0205
I	137	0,43	4,11	4,98	4,97
	138	1,43	2,68	3,24	3,30
	139	2,43	1,10	1,33	1,41
	140	3,43	0,24	0,291	0,389
Cs	141	0,54	4,60	4,86	4,86
	142	1,54	3,1	3,27	3,07
	143	2,54	1,43	1,51	1,25
	144	3,54	0,41	0,43	0,33
Kr	90	0	-	-	5,17
	91	1	-	-	4,14
	92	2	1,68	2,14	2,14
	93	3	0,53	0,678	0,728
	94	4	0,08	0,102	0,153

Table 4

Values of coefficients S and A_o in the relation $\Delta E = S\,A + p$

Element	Value of S			Value of A_o		
	Even A	Odd A	All A	Even A	Odd A	All A
As	2,100	-	2,100	83,56	-	83,25
Se	-	-	0,610	-	-	85,57
Br	0,993	0,848	0,930	86,05	85,60	85,84
Kr	0,990	0,890	0,932	91,75	90,32	91,47
Rb	0,923	0,908	0,921	91,52	91,39	91,48
Y	-	0,970	0,970	-	96,87	-
Sn	-	-	2,510	-	-	132,97
Sb	1,50	-	1,50	133,09	-	132,92
Te	-	-	0,400	-	-	134,88
I	0,320	0,640	0,676	120,38	134,75	134,96
Xe	0,205	0,318	0,295	140,00	140,41	140,51
Cs	0.425	0,480	0,465	139,55	140,08	139,93

Table 5

Values of P_{II} and m for delayed neutron precursors

Element	A	Assumed value of P_{II}	m	Experimental value of P_{II}	Calculated value	
					Our own values	Ref. [6]
1	2	3	4	5	6	7
Br	87	2,5 ± 0,5		2,5 ± 0,5		
	88	4,0 ± 1		4,0 ± 1		
	89	7 ± 2	1,29	7 ± 2		
	90	12 ± 3		12 ± 3		
	91	-		-	13,9	13,8 ± 1,6
	92	-		-	18,6	20,2 ± 2,3
Kr	92	-		0,040±0,007	0,32	0,5
	93	-	1,29	3,3±0,5	4,28	3,5 ± 2,7
	94	-		-	5,44	4,7 ± 0,5
	95	-		-	8,77	8,3 ± 1,0
Rb	92	-		0,012 ±0,004	0,70	0,5

Table 5 (continued)

1	2	3	4	5	6	7
Rb	93	-		1,8 ± 0,5	3,21	2,5 ± 1,9
	94	-	1,29	7,5 ± 1,9	5,60	4,8 ± 0,5
	95	-		7,1 ± 0,9	8,8	8,3± 1,0
	96	-		12,7 ± 1,5	12,1	12,1± 1,4
	97	-		20	15,8	16,6± 1,9
Y	97	-		-	0,14	0,5
	98	-	1,29	0,8 ± 0,4	1,20	0,8
	99	-		-	4,9	4,2 ± 0,5
I	138	2,5 ± 0,6		2,5 ± 0,6	-	3,8 ± 2,9
	140	12± 8	2,56	12 ± 8	-	9,8 ± 1,1
Cs	142	0,27± 0,1	2,35	0,27± 0,1	-	
	144	1,10± 0,3	1,10	1,10± 0,3	-	
I	137	4,8 ± 1,3		4,8 ± 1,3	-	2,2 ± 1,7
	139	6 ± 2	0,292 ?	6 ± 2	-	6,7 ± 0,8
Cs	141	0,073±0,011	1,68	0,073± 0,011	-	0,5
	143	1,13± 0,25		1,13± 0,25	-	3,0 ± 2,3
	145	-		-	6,9	4,7 ± 0,5
Xe	143	1,5 ± 1,1	1,69	-		1,5 ± 1,1
	145	2,2 ± 1,7		-		2,2 ± 1,7
I	137+		1,69		2,94	2,2 ± 1,7
	139				17,2	6,7 ± 0,8

+ We assumed that: P_{II} (^{137}I) = 4.8; m = 1.69.

Table 6

Relative delayed neutron yields in thermal fission of ^{235}U
obtained through expansion of the decay curve
by the least squares method

$T_{1/2}$ sec	Own data	Data from Ref. [8]+
55,72	I	I
22,72	6,159 ± 0,054++	6,65 ± 0,65
6,22	5,757 ± 0,054	5,95 ± 0,89
2,30	11,23 ± 0,19	12,0 ± 1,3

+ Expansion into six groups by least squares method.

++ The error in the half-life is not taken into account; if it were, the error in the yield ratio for any group would be from 4 to 5%.

Table 7

Relative delayed neutron yields obtained through expansion of the ^{235}U decay curves by the new method

No. group	T^{+} sec	T sec	Precursor	$Y_i/Y_i{}^{++}$		$Y_i/Y_i{}^{x}$
I.	55,65	55,65	Br^{87}	I		I
2.	24,4	24,9	Cs^{141}	0,06	3,73	3,91±0,I4
		24,4	I^{137}	3,67		
3.	I6,3	I6,3	Br^{88}		2,06	I,78±0,I0
4.	I4,0	I4,0	Rb^{92}	0,67	0,72	I,II±0,09
		II,3	Se^{134}	0,05		
5.	6,3	6,3	I^{138}	I,27	I,35	I,22±0,I0
		5,9	Se^{87}	0,08		
6.	4,45	4,45	Br^{89}	-	3,02	2,82±0,I8
7.	3,3	3,5	Te^{137}	0,II		
		3,3	Rb^{93}	2,45	3,87	4,32±0,28
		3,2	I^{139}	I,3I§*		
8.	2,I	2,5	Cs^{142}	0,I5		
		2,2	Se^{88}	0,87		
		2,I5	As^{85}	I,64	2,98	3,27±0,33
		2	Y^{98}	0,3I		
		I,86	Kr^{92}	0,0I		
9.	I,7	I,73	Xe^{141}	0,0I		-
		I,696	Sb^{135}	0,60	0,86	2,I4±0,40
		I,69	Cs^{143}	0,25		
		I,6	Br^{90}		2,82	

Total = 237.2

+   The half-life on which the expansion of the decay curve was based.

++ Calculated value.

x   From expansion of the decay curve.

§   When P_{II} = 5%.

Table 8

Results of expanding to nine exponentials by the least squares method[+]

Group No.[*]	T sec	Y_i/Y_i
I	54,5	I
2	24,4	3,63 ± 0,90
3	I6,3	2,9 ± I,2
4	6,3	0,5 ± I,6
5	4,4	6,2 ± 2,0
6	.2,0	2,2 ± 2,7
7	(I,6 + 2,4)	6,7 ± 2,2 Total = 238.62

+   Data from Ref. $\sqrt{8\_7}$.

*   We show only seven of the nine groups since the other two have shorter half-lives and cannot be compared with our results.

Table 9

Relative delayed neutron yields in thermal fission of ^{235}U (radiochemical data)

Group No.	T sec	Precursor	a_i	a_i/a_i	Total
1	2	3	4	5	6
I	54,5	Br^{87}	5,9 ± 0,4	I	55,65
2	24,4	I^{137}	2I,7 ± 3,6		
	24,9	Cs^{141}	0,345± 0,05	3,82 ± 0,69	93,14
3	I6,3	Br^{88}	I2,I ± 3,3	2,I5 ± 0,60	34,08
4	II,3	Sb^{134}	0,280± 0,004	0,048± 0,00I	0,54
5	6,3	I^{138}	I0,3 ± I,6		
	5,86	Rb^{93}	. 6,60.	-	-
	5,9	Se^{87}	0,56 ± 0,I4	3,05 ± 0,5I	I8,48
6	4,5	Br^{89}	I8,8 ± 5,7	-	-
	4,48	Rb^{92}	0,06 ± 0,02	3,3 ± I,0	I4,68
7	2,67	Rb^{94}	I7,2 ± 2,4	2,98 ± 0,46	7,96
8	2,028	As^{85}	9,7 ± 0,6		

Table 9 (continued)

1	2	3	4	5	6
	2,0	I^{139}	12,7 ± 3,6		
	2,2	Se^{88}	5,1 ± 2,0		
	1,86	Kr^{92}	0,07	4,83 ± 0,74	9,76
9	1,696	Sb^{135}	3,5 ± 0,3		
	1,69	Cs^{143}	1,6		
	1,68	Cs^{142}	0,84	1,0 ± 0,1	1,70
	1,73	Xe^{141}	0,06		
10	1,6	Br^{90}	16,2 ± 5,2	2,8 ± 0,9	4,48
11	1,4	As^{87}	?	?	
	1,29	Kr^{93}	1,38		
	1,24	Xe^{142}	0,14	0,26 ± ?	0,34+?

$$\Sigma = 240,81$$

Table 10

Relative delayed neutron yields in thermal
fission of ^{235}U (systematics data)

No. group	T sec	Precursor	a_i	a_i/a_i	Total
1	54,5	Br^{87}	5,7	1	55,65
2	24,4	I^{137}	19,7		
	24,9	Cs^{141}	0,33	3,59	87,60
3	16,3	Br^{88}	12,1 ± 3,3	2,23	35,33
4	11,3	Sb^{134}	0,18	0,032	0,36
5	6,3	I^{138}	6,73		
	5,89	Rb^{93}	7,2		
	5,9	Se^{87}	0,44	2,59	15,65
6	4,5	Br^{89}	16,94		
	4,48	Rb^{92}	0,06	3,05	13,55
7	2,67	Rb^{94}	14,2	2,54	6,79
8	2,028	As^{85}	8,0		
	2,0	I^{139}	6,60		
	2,2	Se^{88}	4,16		
	1,86	Kr^{92}	0,07	3,43	6,94

Table 10 (continued)

1	2	3	4	5	6
9	I,696	Sb^{135}	3,88		
	I,69	Cs^{143}	I,64		
	I,68	Cs^{142}	0,84		
	I,73	Xe^{141}	0,06	I,14	I,94
IO	I,6	Br^{90}			
II	I,4	As^{87}	?	?	?
	I,29	Kr^{93}	I,75	-	
	I,24	Xe^{142}	0,14	0,31	0,40
					$\Sigma = 230,6I$

Table 11

Half—lives calculated from systematics and obtained
by identification

Element	$T_{calc.}$, sec	$T_{ident.}$, sec
Rb^{92}	I4,0 ± I,2	4,48
Rb^{93}	3,3 ± 0,5	5,9
Rb^{94}	0,8	2,67
I^{139}	3,2	2,5
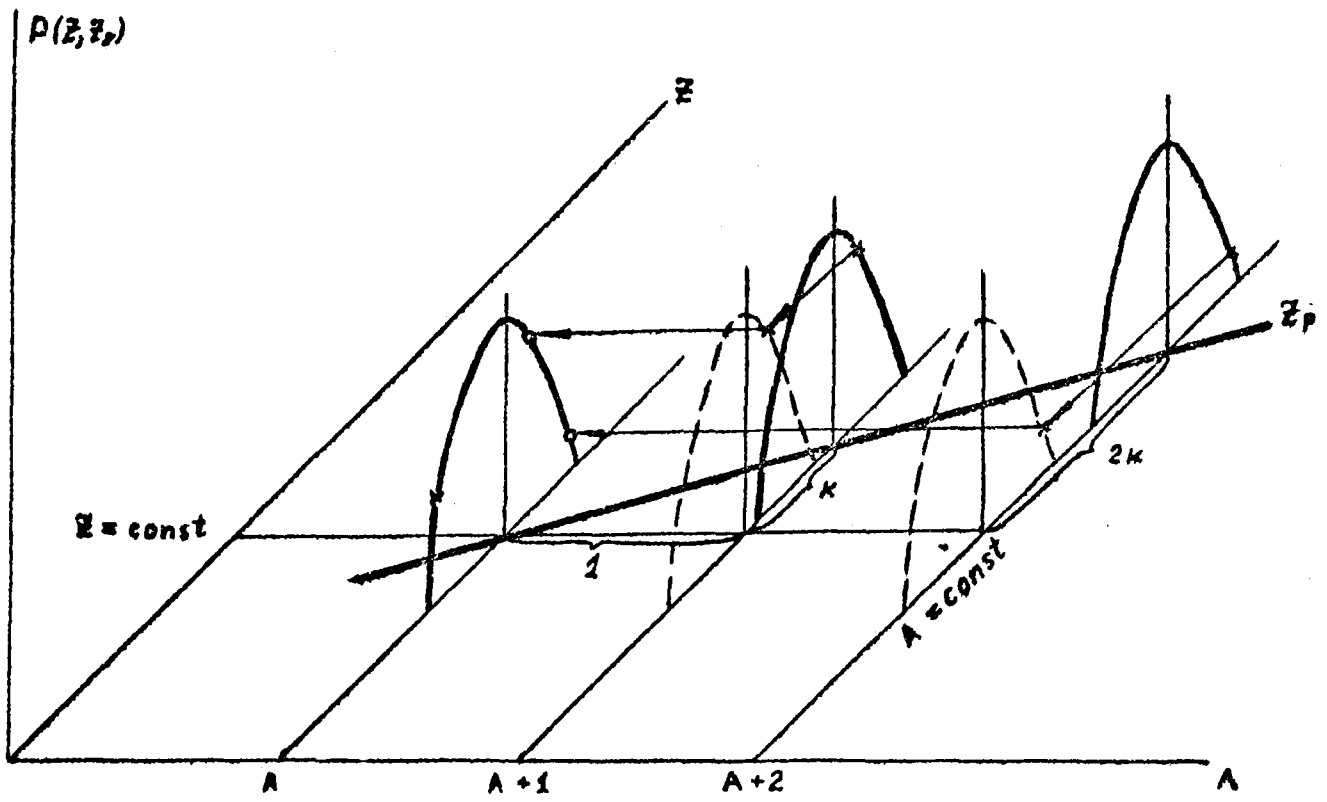
Fig. 1   Scheme for constructing the charge distribution curve for Z = const.
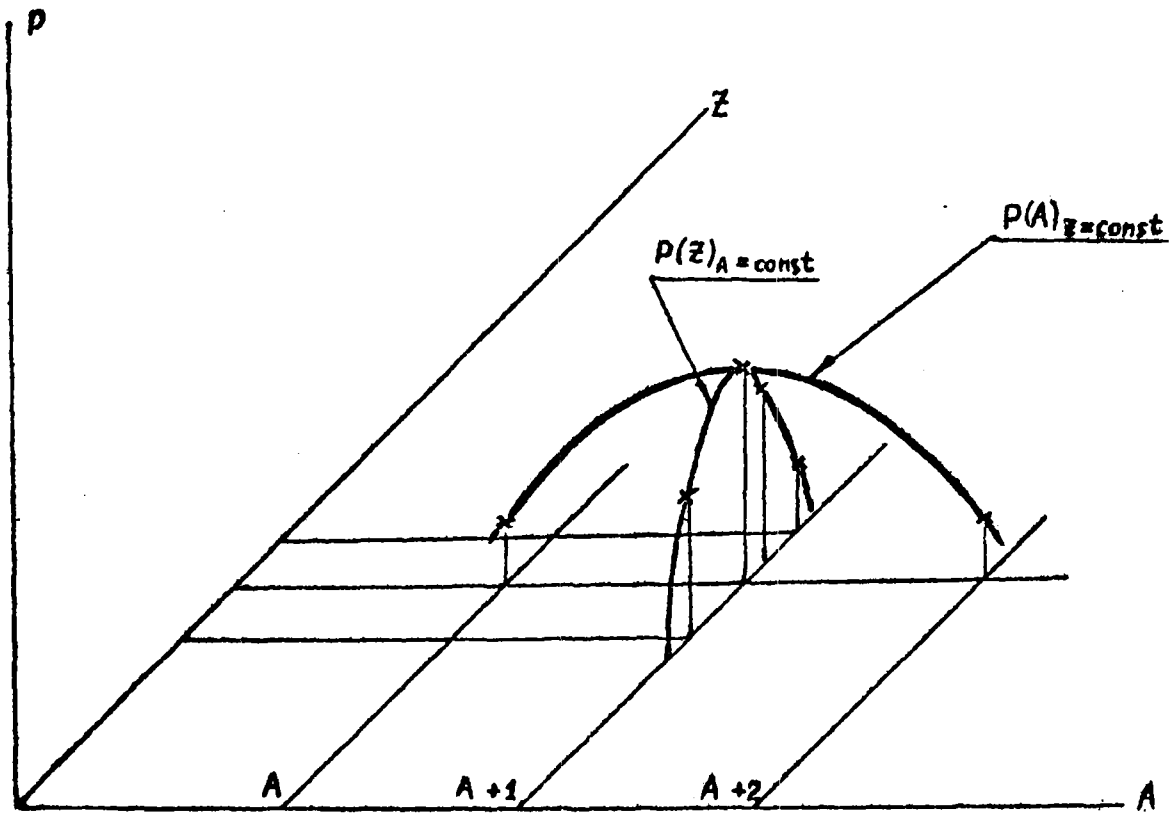
Fig. 2   Radiation probability distribution.
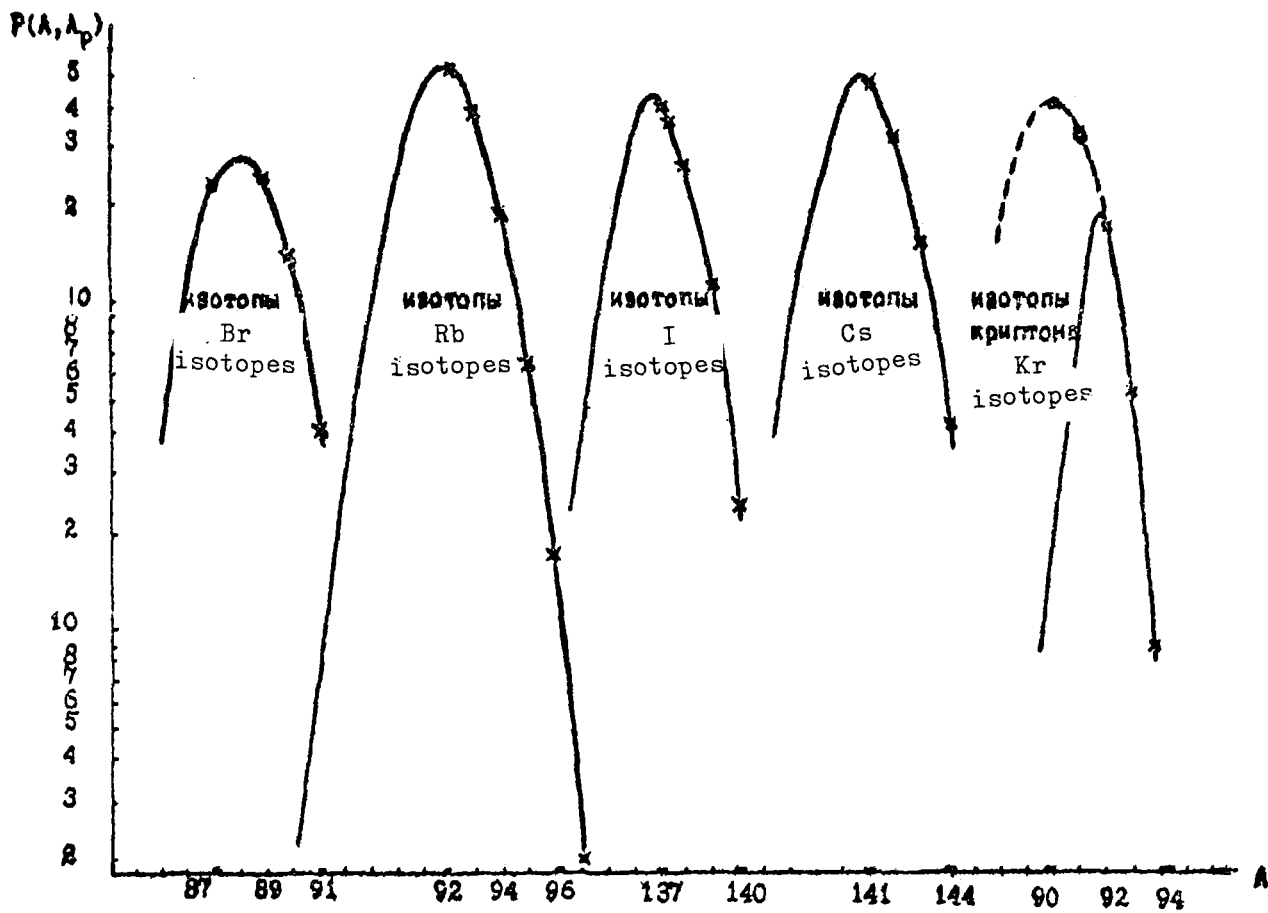
Fig. 3   Fission product mass distribution for Z = const.
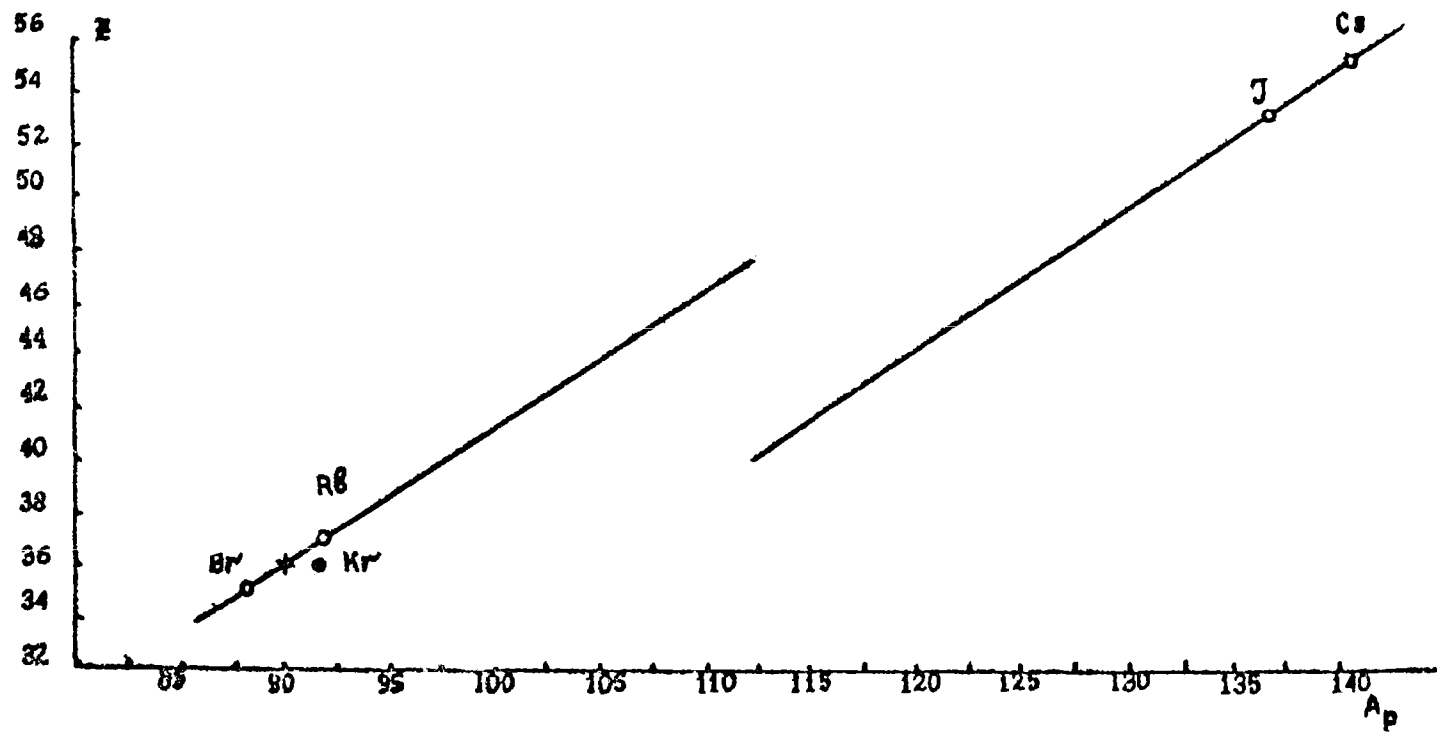
Fig. 4   Z versus A_p.
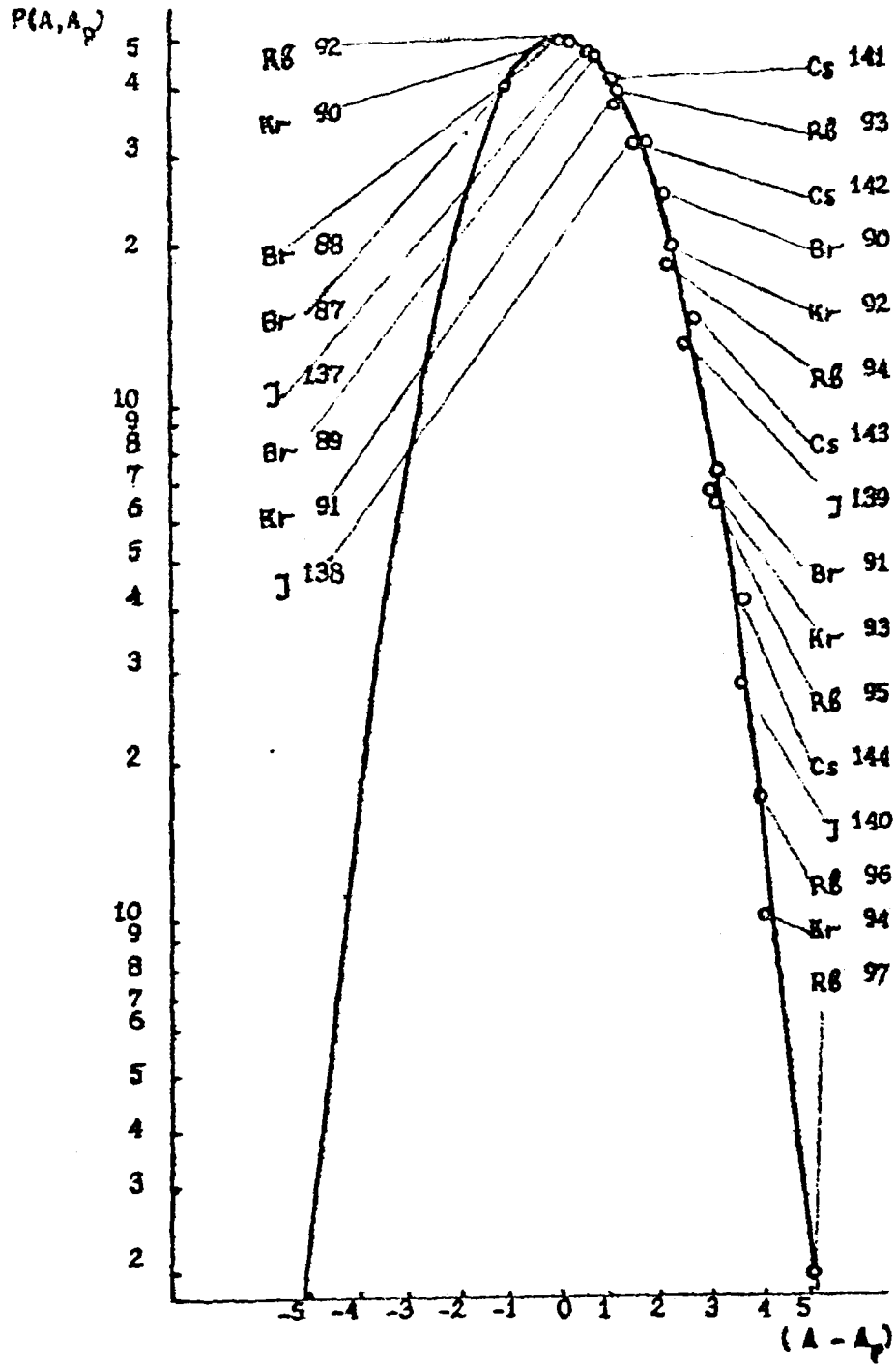
Fig. 5   Fission product mass distribution.
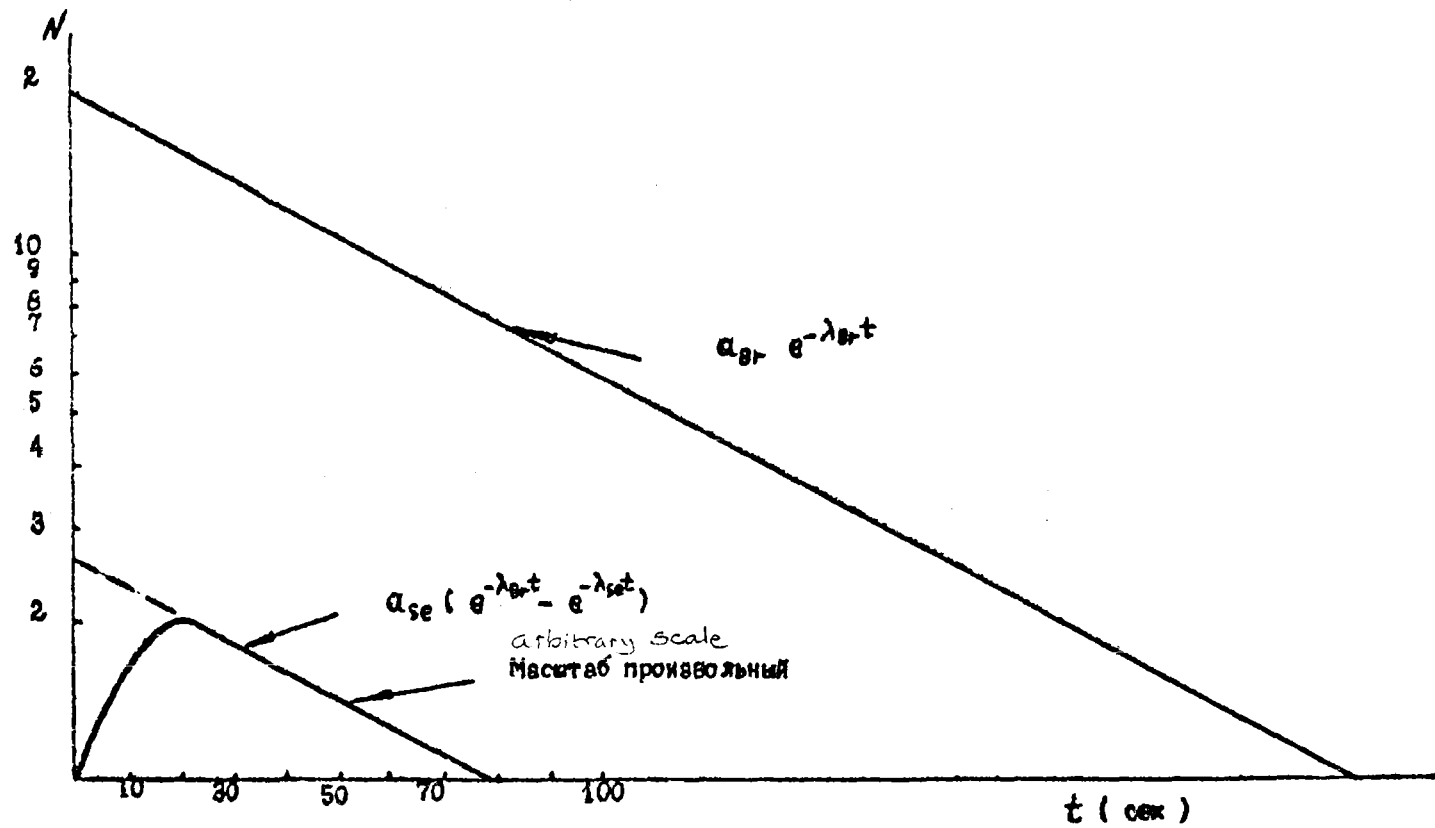
Fig. 6   Build-up and decay in the Se $\xrightarrow{\beta}$ Br chain.

Arbitrary scale
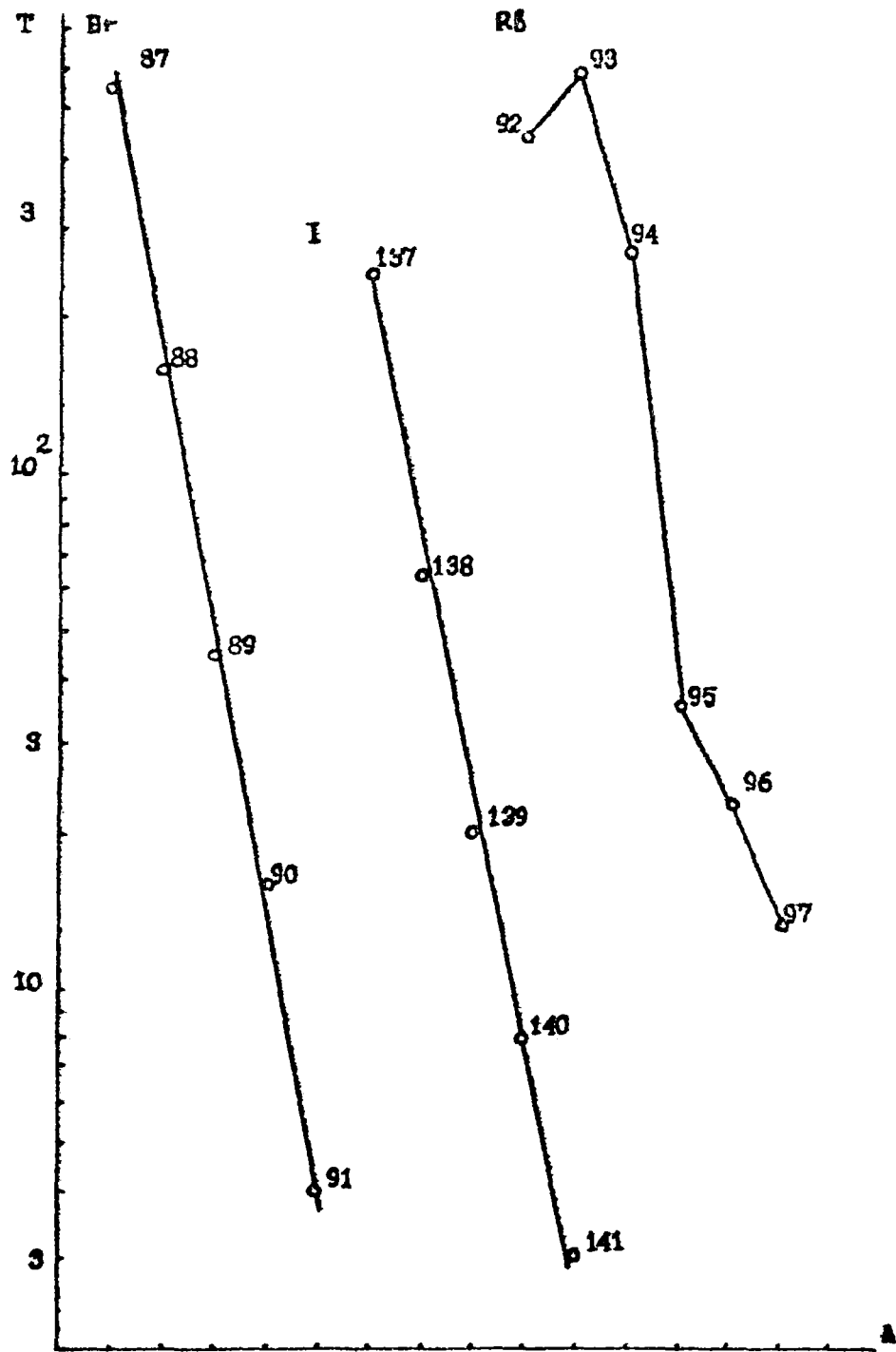
Fig. 7   Dependence of T on A.
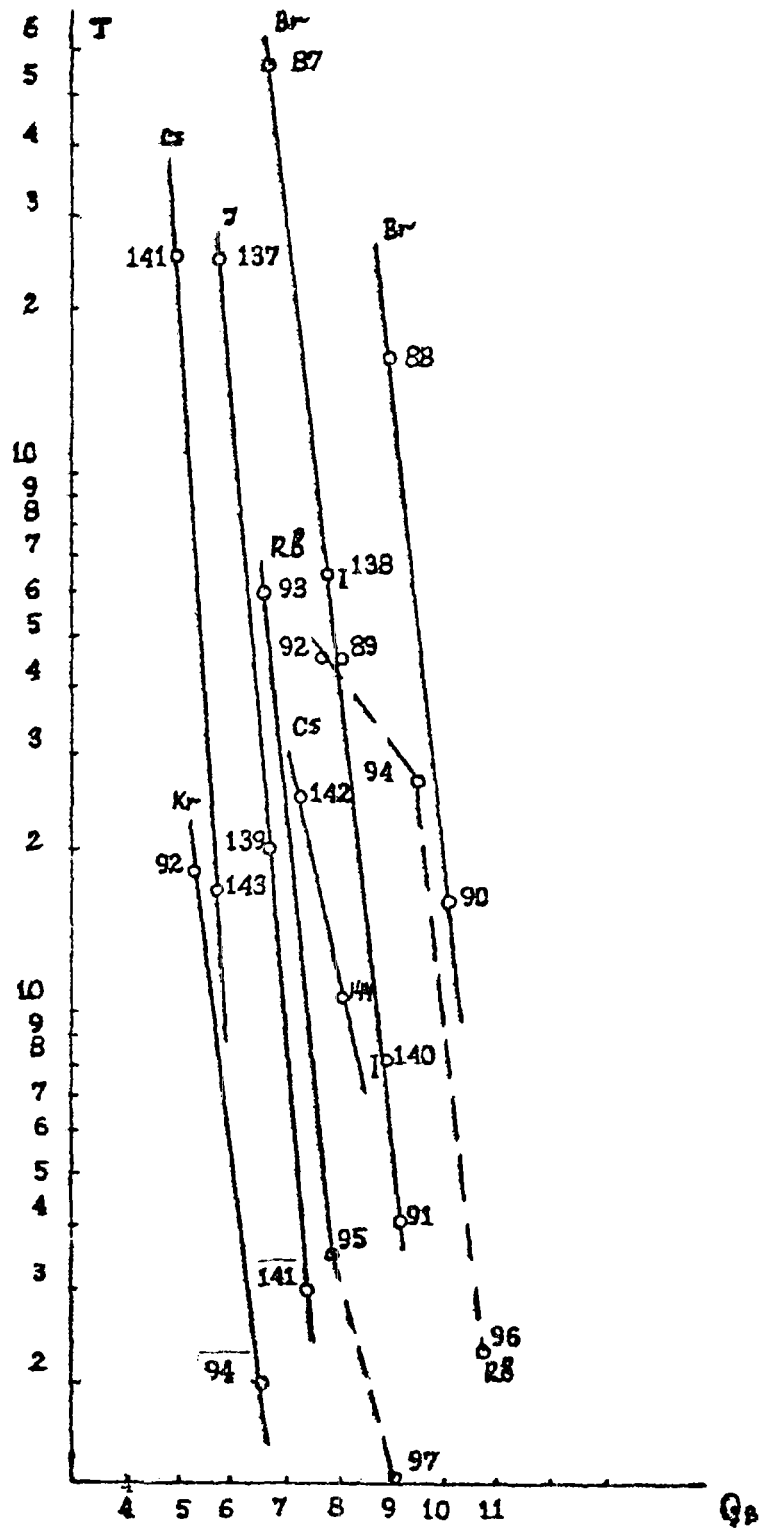
Fig. 8   Dependence of T on Q_β.
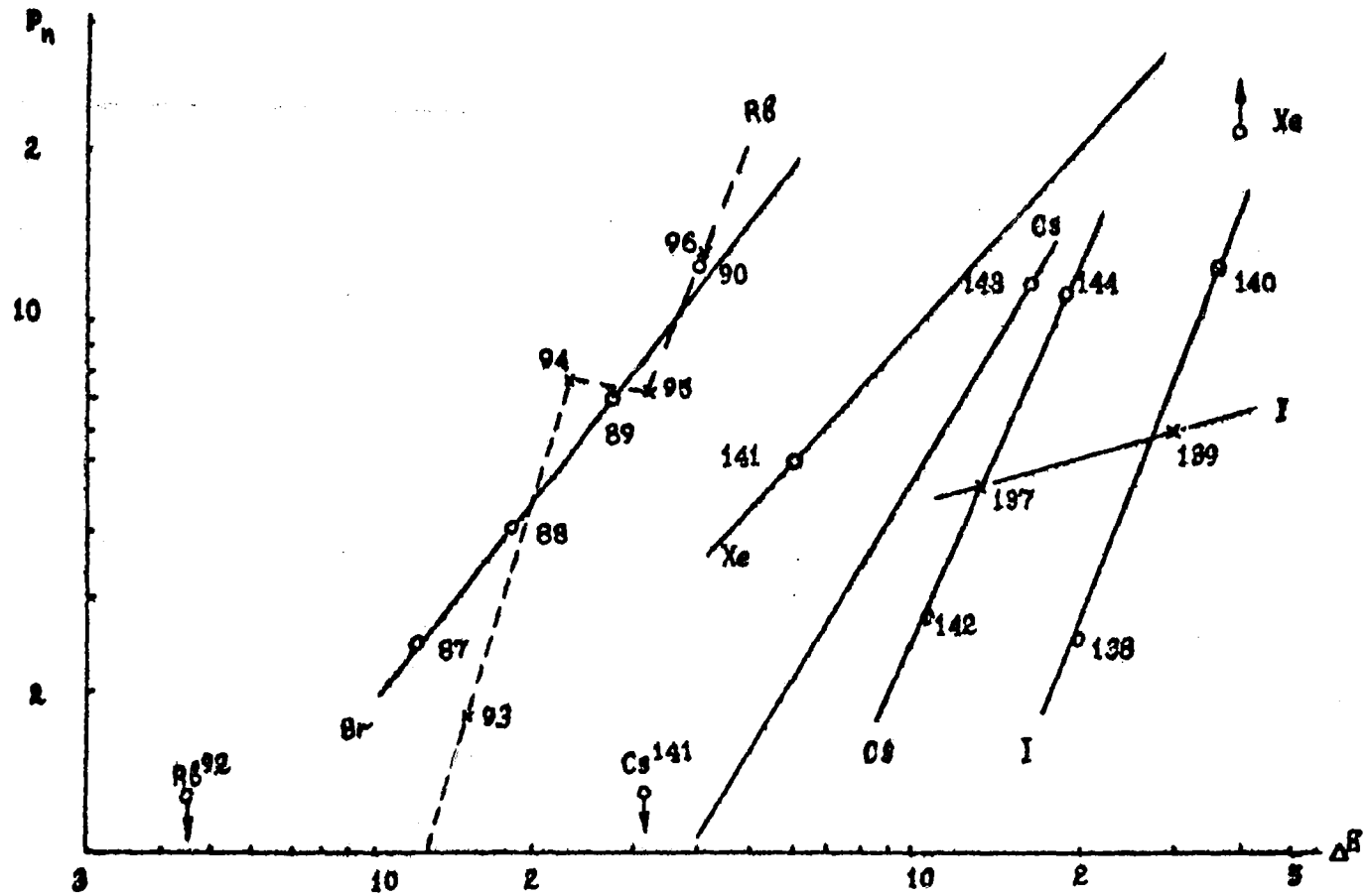
Fig. 9   Dependence of P_n on ΔE.
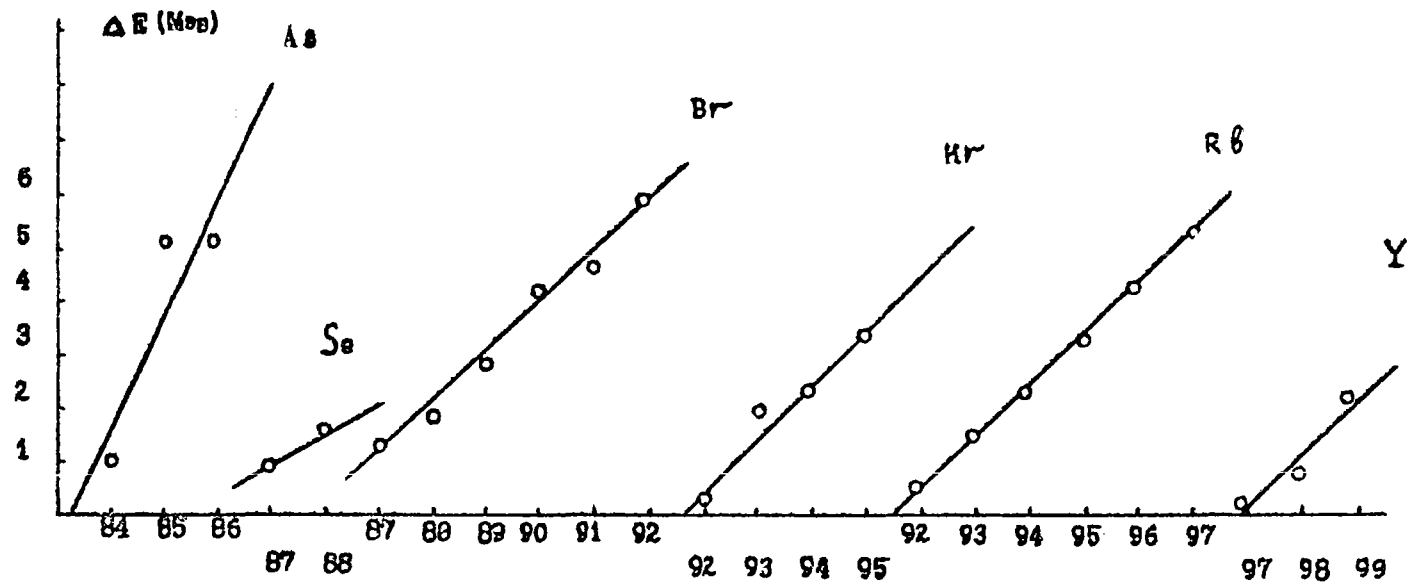
Fig. 10   Dependence of ΔE on A.

MeV
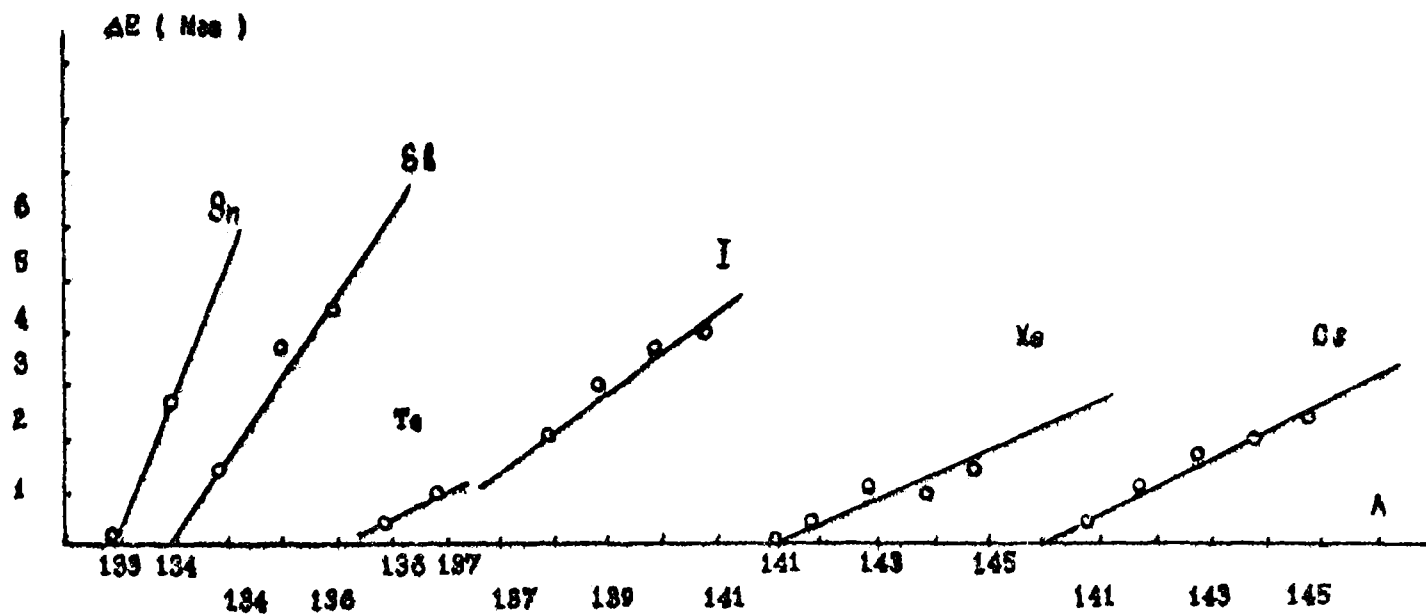
Fig. 11 Dependence of $\triangle E$ on A.

MEASUREMENT OF ^{235}U AND ^{239}Pu FISSION CROSS-SECTIONS WITH A NEUTRON SLOWING-DOWN TIME SPECTROMETER

A.A. Bergman, A.E. Samsonov, Yu.Ya. Stavissky,
V.A. Tolstikov, V.B. Chelnokov

Introduction

The fission cross-sections of ^{235}U and ^{239}Pu were measured on a neutron spectrometer using the neutron slowing-down time in lead [1, 2]. The energy range of the spectrometer enables the relative energy dependence of the cross-sections to be determined from ~ 50 keV down to thermal. The cross-section curves were normalized to the thermal fission cross-section obtained from additional measurements in a graphite prism moved up against the main lead moderator prism */.

Method of measuring cross-sections

In the main measuring channel of the lead moderator (Fig. 1) we studied the count in a fission chamber containing a layer of the material of interest as a function of slowing-down time, $I_f(t)$. The neutron density $I_B(t)$ was measured with a detector having an efficiency proportional to ~ $1/v$ (BF_3-counter). Then, as shown in Ref. [2], we have

$$\frac{I_f(t)}{I_B(t)} = K_f < \sigma_f(E).\sqrt{E} > = K_f . \sigma_f(\bar{E}) .\sqrt{\bar{E}} .(1 + \delta) \qquad (1)$$

where $v(t)$ is the mean neutron velocity at an instant of slowing down, $\sigma_f(E)$ is the fission cross-section for nuclei of the substance under study, $< \sigma_f(E) \sqrt{E}>$ represents averaging over the neutron spectrum $N(E,t)$ in the moderator at time t, δ is a small correction allowing for the substitution $< \sigma_f(E)\sqrt{E}>\to\sigma_f(\bar{E}).\sqrt{\bar{E}}$ and related to the width of the neutron energy spectrum $N(E,t)$ and the energy dependence of the cross-section under investigation, $\sigma_f(E)$, and K_f is the normalizing factor.

The mean neutron energy and the slowing-down time t (μsec) are connected by the relation [2]

$$\bar{E} = 183 / (t + 0.3)^2 \quad [keV] \qquad (2)$$

---

*/ This method of normalizing cross-sections in a graphite prism was proposed by A.A. Bergman.

If the correction δ can be neglected, the expression for determining the neutron energy dependence of the cross-section takes the form

$$\sigma_f(\bar{E}) = \frac{I_f(t)}{I_B(t)} \cdot \frac{1}{K_f \sqrt{\bar{E}}}$$ (3)

The energy dependence of the cross-sections can be normalized $\boxed{2}$ to resolved resonances having known parameters $\boxed{3}$ or to the thermal cross-section. However, with weak spectrometer resolution it is not always possible to isolate resonances with reliably determined parameters in the cross-section being measured. Furthermore, if the cross-sections have low resonances with energies of the order of a few tens of eV, the statistical measuring accuracy in the thermal region will be unsatisfactory in consequence of the large drop in neutron density in the moderator $\boxed{2}$:

$$I_B(t) = \text{const.} \; t^{-0.35} \cdot e^{-t/T}$$ (4)

where T is the mean neutron lifetime ($\sim$ 890 μsec) in the lead prism, and in consequence of the long times relative to the neutron burst ($\sim$ 2000 μsec) to which the thermal region corresponds in this case ($\sim$ 1/v law). A sufficiently intense thermal neutron spectrum can be obtained in a graphite prism placed close to the main lead moderator prism (Fig. 1). When the times relative to the neutron burst exceed 1500 μsec, virtually total thermalization occurs in a graphite prism with a characteristic dimension of $\sim$ 1 m. This permits the thermal fission cross-sections of ^{235}U and ^{239}Pu to be reliably normalized.

Method of normalizing to the thermal cross-section in a graphite prism

A graphite prism with dimensions of 120 x 60 x 60 cm was used for normalization to the thermal cross-section. A boron detector was employed to investigate the dependence of neutron density $I_B^{th}(t)$ in the graphite prism on the time relative to the neutron burst. The results of measurements of $I_B^{th}(t)$ in Fig. 2 show that the curve of $\ln I_B^{th}(t)$ has a linear trend which sets in at $t > 1000$ μsec after formation of an equilibrium spectrum. In this time range the integral neutron density in the graphite prism is ten times higher than in the measuring channel of the lead prism.

The graphite prism was also used to investigate the time dependence of the fission chamber count, $I_f^{th}(t)$. By analogy with Eq. (1) we have

$$\frac{I_f^{th}(t)}{I_B^{th}(t)} = K_f <\sigma_f(E) \cdot \sqrt{E} >^{th} \qquad (5)$$

from which we obtain an expression for calculating the normalizing factor from measurements in the graphite prism:

$$K_f = \frac{I_f^{th}(t)}{I_B^{th}(t)} \cdot \frac{1}{\bar{\sigma}_f^{th}\sqrt{E}^{th}} \qquad (6)$$

where $\bar{\sigma}_f^{th}$ is the thermal cross-section averaged over the Maxwellian spectrum in the graphite prism with mean energy $\bar{E}^{th}$.

Results of measurements and their treatment

The energy dependence $\sigma_f(E)$ for ^{235}U was investigated with a fission chamber containing 15 mg PuO_2, and the dependence $\sigma_f(E)$ for ^{239}Pu with a fission chamber containing 1.6 mg and 12.4 mg PuO_2. The chambers were filled with a mixture of argon (200 mmHg) and CO_2 (10 mmHg).

The amplifier circuit of the ionization chamber includes an amplifier with a "Siren" type discriminator. The time dependence of the detector counts was studied with the 256-channel analyser of the Measuring and Recording Centre at the Lebedev Physics Institute of the USSR Academy of Sciences [4].

The results of the measurements contain a correction for the deviation of the boron cross-section $\sigma_{10_B}(n,\alpha)$ from the $\sim 1/v$ law. The correction was calculated with allowance for an expression describing the energy dependence $\sigma_{10_B}(E)$ derived from Ref. [5],

$$\sigma_{10_B} \text{ (barn)} = \frac{610.3}{\sqrt{E \text{ (eV)}}} - 0.286 \qquad (7)$$

and is $\sim 10\%$ when $E = 40$ keV and $\sim 2\%$ when $E = 2$ keV.

The correction for weak spectrometer resolution, δ, is calculated on the basis of theoretical estimates of the resolution [2]. To determine δ we expand $<\sigma_f(E) \cdot \sqrt{E}>$ in terms of $E - \bar{E}$, restricting ourselves to the first two terms:

$$<\sigma_f \cdot \sqrt{E}> = (\sigma_f\sqrt{E})\Big|_{\bar{E}} + \frac{\bar{E}^2}{2} \cdot \frac{d^2(\sigma_f \cdot \sqrt{E})}{dE^2}\Big|_{\bar{E}} \cdot \frac{\Delta\bar{E}^2}{\bar{E}^2} \qquad (8)$$

Obviously, the correction δ is a relative quantity in the second term of the expansion:

$$\delta = \frac{\overline{E}^2}{2\sigma_f} \left(\frac{d^2\sigma_f}{dE^2} + \frac{1}{E} \cdot \frac{d\sigma_f}{dE} - \frac{1}{4} \cdot \frac{\sigma_f}{E^2} \right) \Bigg|_{\overline{E}} \cdot \frac{\Delta\overline{E}^2}{\overline{E}^2} \tag{9}$$

If the cross-section obeys the $\sigma_f \sim 1/v$ law, then $\delta = 0$; if $\sigma_f = \text{const.}$, then

$$\delta = -\frac{1}{8} \cdot \frac{\Delta\overline{E}^2}{\overline{E}^2} \tag{9a}$$

The correction to the cross-sections estimated in accordance with Eq. (9) is not more than 2% at $E \simeq 50$ keV, when the resolution of the spectrometer is at its worst ($\sim 100\%$).

Discussion of results

The results of the measurements of the energy dependence of the fission cross-sections of ^{235}U and ^{239}Pu nuclei are shown in Fig. 3. The fission cross-section ratio $\sigma_f\,^{239}\text{Pu}/\sigma_f\,^{235}\text{U}$ is shown in Fig. 4.

The cross-sections were normalized to the thermal spectrum in the graphite prism. The thermal cross-section values used for calculating the normalizing factor are given in Table 1. The normalizing factors calculated for the fission cross-section of ^{239}Pu on the basis of the resonance at $E_o = 0.296$ eV and the resolved group of resonances at $E_o = 7.85-32.3$ eV with well-known parameters $/3\_7$ agree within the error limits with the value calculated from the thermal cross-section (Table 2).

The standard deviation of the measurements is due mainly to the normalizing error, the statistical error ($\sim 2\%$) and the error in extrapolating the time/energy relation (2) into the range of small ($E < 1$ eV) and large ($E > 10$ keV) energies $/2\_7$. The error in normalizing to the thermal cross-section ($\sim 3\%$) is largely attributable to statistics and counting instability in the graphite prism.

It should be noted that the effect of diffusion cooling, estimated from formulae given in Ref. $/6\_7$, reduces the temperature of the spectrum in the graphite prism by 12%. But, as follows from the graphs in Ref. $/7\_7$, the value of $\sigma_f^{th}\sqrt{E^{th}}$ used for normalizing the fission cross-sections does not vary more than 0.2% as a result of this.

The results of our measurements of $\sigma_f(E)$ for ^{235}U in the energy range above 5 keV are on average 9-12% lower than the data recommended by Hart $/8\_7$ and the disagreement with the results of Knoll $/9\_7$ at 30 keV is about 10%.

In the 0.07–10.0 keV energy range our results are in good agreement within the limits of measuring error with averaged selected data $/$10–14$/$ which we assigned to the mean value of the averaged range of energies.

The results of our measurements of $\sigma_f(E)$ for ^{239}Pu in the energy range E < 6 keV agree with the averaged data reported from Harwell $/$5$/$ and the recommended data of Hart $/$8$/$ and Fursov et al. $/$15$/$.

For energies E > 6 keV there is a systematic deviation averaging 12–15% from the data given in Refs $/$5, 8, 15$/$. The disagreement with the averaged selected data $/$14, 16, 17$/$ is probably also partially due to the inadequate resolution of our method of measurement compared with those used by the authors of the selected data.

The values obtained for the cross-section ratio $^{239}\sigma_f / ^{235}\sigma_f$ are in good agreement with averaged values of Gilboy and Knoll $/$18$/$. Agreement with the recommended values of Hart $/$8$/$ is very good. The recommended data of Davey $/$19$/$ appear somewhat high compared with our experimental data.

Table 1

Thermal cross-section values used for normalizing the
graphite prism measurements

	^{235}U	^{239}Pu
E = 0.0253 eV	580.2 ± 1.8 barn [20]	741.6 ± 3.1 barn [20]
f	0.977 [7]	1.052 [7]
$\bar{\sigma}_f^{th}$	566.8 barn	740.6 barn

Table 2

Normalizing factors calculated for measurements
on ^{239}Pu using a fission chamber

Method of calculation	K_f
From the thermal cross-section in the graphite prism	0.487 ± 0.015
From the group of resonances at E_o = 7.85-32.3 eV	0.500 ± 0.057
From the resonance at E_o = 0.296 eV	0.514 ± 0.051

Table 3

Numerical values of ^{235}U fission cross-section

E, eV	σ_f, barn	E, eV	σ_f, barn
43500	1,84 ± 0,14	105	22,11 ± 0,88
28100	2,07 ± 0,13		
19700	2,33 ± 0,13		
13900	2,55 ± 0,13		
11200	2,80 ± 0,14		
8840	3,01 ± 0,14		
7180	3,28 ± 0,15		
5940	3,55 ± 0,15		
4700	4,00 ± 0,16		
3600	4,61 ± 0,18		
2570	5,35 ± 0,21		
1970	6,24 ± 0,24		
1660	6,88 ± 0,27		
1400	7,56 ± 0,28		
1170	8,13 ± 0,33		
950	8,66 ± 0,35		
800	9,88 ± 0,39		
700	10,58 ± 0,43		
580	11,75 ± 0,47		
460	12,26 ± 0,49		
370	13,97 ± 0,56		
310	15,50 ± 0,62		
265	18,22 ± 0,73		
220	20,05 ± 0,80		
185	19,57 ± 0,78		
165	20,05 ± 0,80		
145	20,53 ± 0,82		
125	21,32 ± 0,85		

Table 4

Numerical values of ^{239}Pu fission cross-section

E, eV	σ_f, barn	E, eV	σ_f, barn
43500	1,41 ± 0,11	105	26,0 ± 1,0
28100	1,44 ± 0,10		
19700	1,54 ± 0,09		
13900	1,65 ± 0,09		
11200	1,72 ± 0,08		
8840	1,85 ± 0,08		
7180	1,97 ± 0,08		
5940	2,14 ± 0,09		
4700	2,33 ± 0,09		
3600	2,53 ± 0,10		
2570	2,80 ± 0,11		
1970	3,31 ± 0,13		
1660	3,94 ± 0,16		
1400	4,54 ± 0,18		
1170	5,42 ± 0,22		
950	5,75 ± 0,23		
800	5,86 ± 0,24		
700	6,20 ± 0,25		
580	7,88 ± 0,32		
460	9,43 ± 0,38		
370	9,61 ± 0,39		
310	11,87 ± 0,48		
265	15,02 ± 0,60		
220	16,55 ± 0,66		
185	16,62 ± 0,66		
165	16,57 ± 0,66		
145	17,42 ± 0,70		
125	19,68 ± 0,79		

Table 5

Numerical values of fission cross-section ratio
$$\sigma_f(E)^{239}Pu/\sigma_f(E)^{235}U$$

E, eV	$\sigma_f^{239}/\sigma_f^{235}$	E, eV	$\sigma_f^{239}/\sigma_f^{235}$	E, eV	$\sigma_f^{239}/\sigma_f^{235}$
43500	0,763 ± 0,086	3100	0,537±0,031	460	0,767±0,043
28100	0,691 ± 0,63	2220	0,519±0,30	370	0,687±0,040
19700	0,657 ± 0,054	1790	0,530±0,030	310	0,761±0,043
13900	0,643 ± 0,046	1500	0,604±0,034	265	0,823±0,047
11200	0,611 ± 0,040	1250	0,636±0,036	220	0,823±0,047
8840	0,615 ± 0,040	1070	0,666±0,038	185	0,846±0,048
7180	0,599 ± 0,037	880	0,640±0,036	165	0,820±0,047
5940	0,603 ± 0,035	760	0,570±0,033	145	0,847±0,048
4700	0,580 ± 0,033	640	0,625±0,036	125	0,916±0,052
3600	0,548 ± 0,031	520	0,775±0,043	105	1,175±0,067

REFERENCES

[1] BERGMAN et al., Int. Conf. Peaceful Uses Atom. Energy (Proc. Conf. Geneva, 1955) Izdat. Akad. Nauk SSSR, 4 (1957) 166.

[2] SHAPIRO, F.L., Trudy FIAN (Lebedev Physics Institute of the USSR Academy of Sciences), 24 (1964) 3.

[3] STEHN, I.R., GOLDBERG, U.D. et al., Neutron cross-sections, BNL-325, Suppl. 2, Second edition, 1965.

[4] SHTRANIKH, I.V., et al., Trudy FIAN 42 (1968) 69.

[5] Proceedings of IAEA experts' meeting, Winfrith, 1969.

[6] WEINBERG, A., WIGNER, E., Fizičeskaja teorija jademyh reaktorov (Physical Theory of Nuclear Reactors) Izdat. inostrannoj literatury (1961).

[7] HUGHES, J., Nejtronnye effektivnye sečenija (Neutron cross-sections) Izdat. inostrannoj literatury (1959).

/¯8¯/ HART, W., Evaluated fission cross-section in the energy range
1 keV to 15 MeV. UK-USSR seminar, paper UK-10, June 1968.

/¯9¯/ KNOLL, G.F., POENITZ, W.P., I. Nucl. Energy, AB 21 (1967) 643.

/¯10¯/ VAN SHI-DI et al., in Physics and Chemistry of Fission
(Proc. Symp. Salzburg, 1965) Vol. 1, IAEA, Vienna (1965) 287.

/¯11¯/ MOSTOVAYA, T.A., BESPALOV, O.G., Bjul. inf Centr. jad. Dannyh,
issue No. III 10 (1966).

/¯12¯/ MICHAUDON, A., BERGERE, R., COIN, A., JOLY, R., J. de Physique
21 (1960) 429.

/¯13¯/ YEATER, M.Z., MILLS, W.P., GAERTTNER, E.R., Phys. Rev. 104
(1956) 479.

/¯14¯/ JAMES, J.D., SCHOMBERG, M.G., Average fission cross-sections and
resonance integral contributions between 10 eV and 20 keV
deduced from SCISRS data tapes AERE-M 2157, Harwell, 1969.

/¯15¯/ FURSOV, B.I., SHPAK, D.L., SMIRENKIN, G.N., Private communication
1965.

/¯16¯/ BOLLINGER, L., COTÉ, R., THOMAS, G., Int. Conf. peaceful uses
atom. Energy (Proc. Conf. Geneva, 1958) 15, UN, Geneva (1958) 127.

/¯17¯/ FRIEDMAN, J.M., PLATT, M., SCISRS-Sigma Centre Information
Storage and Retrieval System BNL-883 (T-357).

/¯18¯/ GILBOY, W.B., KNOLL, G.F., The fission cross-sections of some
plutonium isotopes in the neutron energy range 5-150 keV,
KFK-450, October 1966.

/¯19¯/ DAVEY, W.G., Nucl. Sci. Engng. 26 (1966) 149.

/¯20¯/ HANNA, G.C., WESTCOTT, C.H. et al., Atom. Energy Rev. 7 No. 4 (1969).
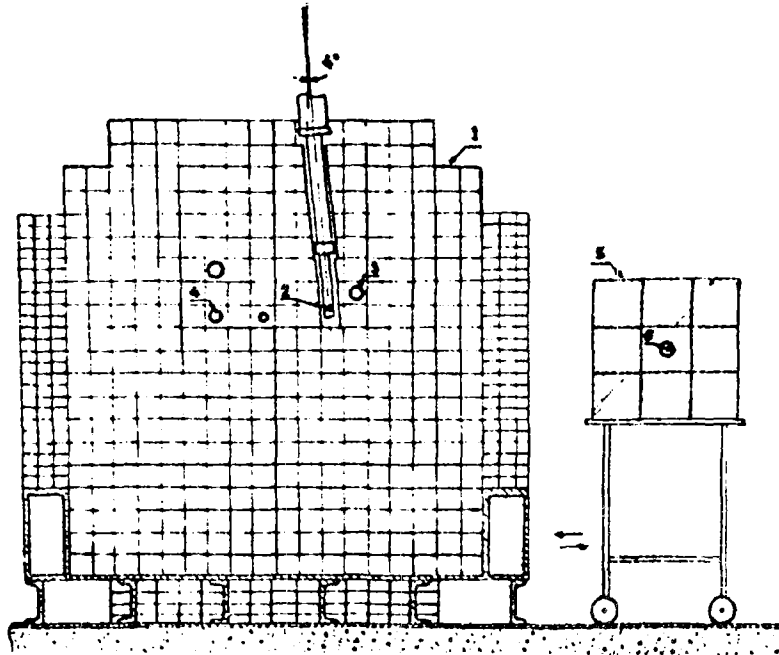
<u>Fig. 1</u>   Scheme of main lead moderator prism and of the graphite
prism for normalizing cross-section curves to the thermal
value.

Key:

1 = prism of lead moderator

2 = position of zirconium-tritium target

3 = channel in which fast neutron burst is recorded

4 = main measuring channel

5 = graphite prism

6 = measuring channel of graphite prism
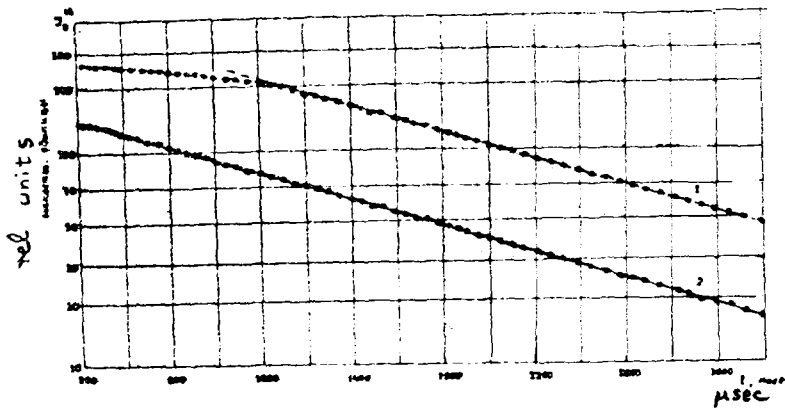
Fig. 2   Dependence of neutron density in the graphite prism on time
relative to the neutron burst, $I_B^{th}(t)$.

Key:

1 = graphite prism located at the side of the lead moderator
      closest to the target
2 = graphite prism at the side furthest from the target
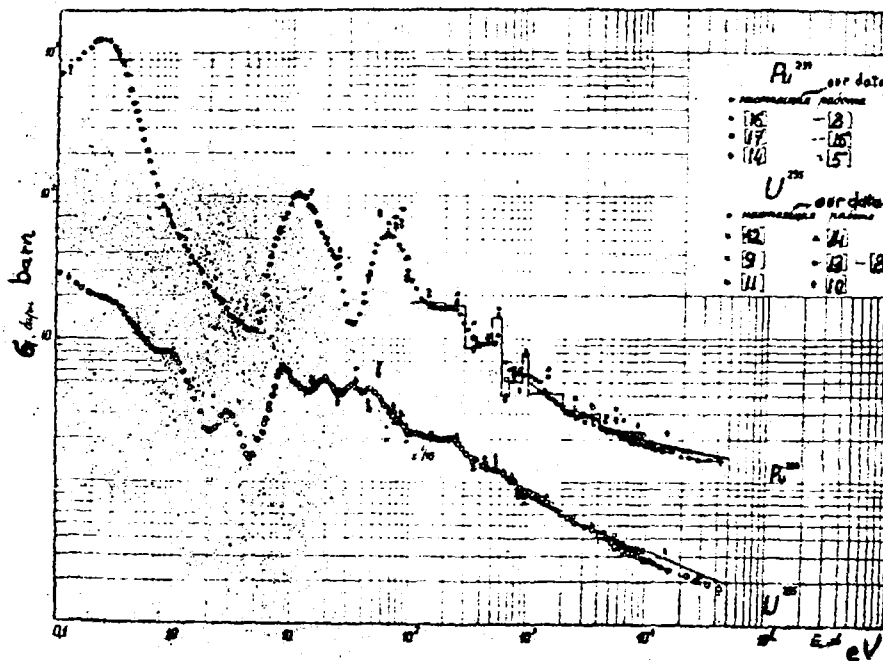
Fig. 3   Energy dependence of fission cross-sections of ^{235}U and
^{239}Pu nuclei.
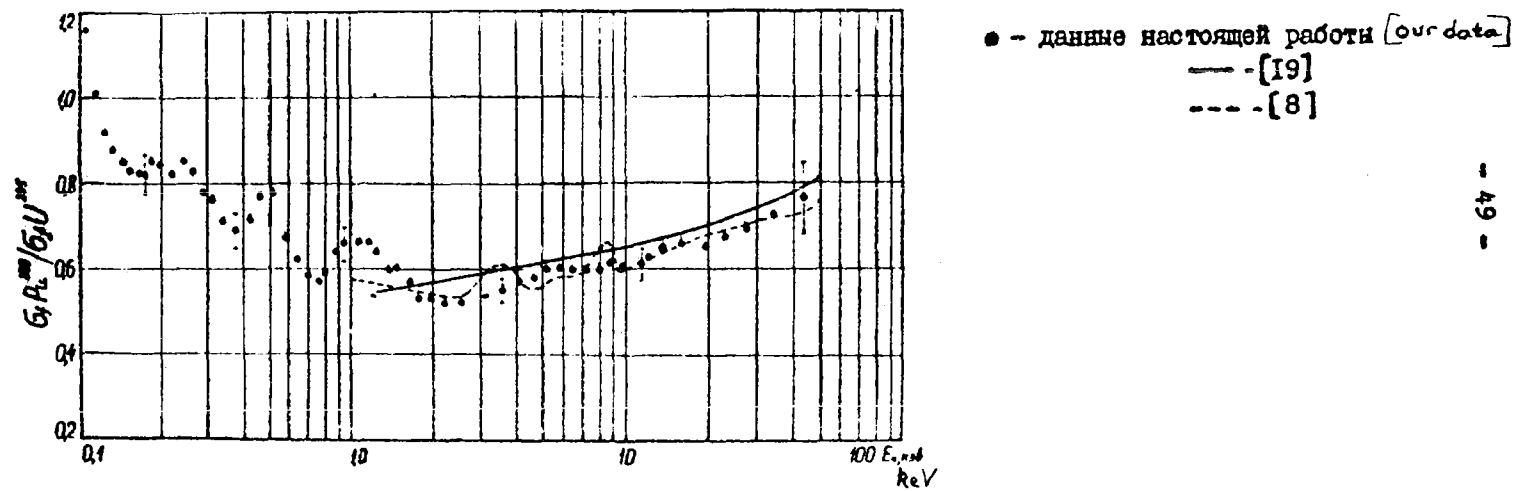
Fig. 4   Energy dependence of the fission cross-section ratio,
$\sigma_f^{239}/\sigma_f^{235}$.

MEASUREMENT OF THE PARAMETER α(E) FOR ^{239}Pu WITH A
NEUTRON SLOWING-DOWN TIME SPECTROMETER

A.A. Bergman, Yu.Ya. Stavissky, V.B. Chelnokov, A.E. Samsonov,
V.A. Tolstikov, A.N. Medvedev

Introduction

Systematic measurements of the parameter $\alpha(E) = \sigma_c(E)/\sigma_f(E)$ — the
ratio of the neutron radiative capture cross-section to the fission cross-
section — for plutonium-239, which largely determines the conversion ratio
of fast reactors, are being performed in many laboratories. Estimates of
$\alpha(E)$ from experimental values of the total cross-sections and the fission
cross-sections indicate that the accuracy with which $\alpha(E)$ can be obtained
is no better than 30% $\boxed{1\_}$. Therefore, direct measurements are very
important.

The difficulty with direct measurements of $\alpha(E)$ lies in separating the
radiative capture and fission events, since both are accompanied by the
emission of prompt gamma rays. Where time-of-flight measurements are
concerned, the experimental values contain a considerable uncertainty due
to scattering on nuclei of the specimen and to the difficulty of measuring
the background. The method with which we are concerned here, using a
neutron slowing-down time spectrometer with a lead prism $\boxed{2, 3\_}$, permits
measurements of $\alpha(E)$ in the energy range below ~ 50 keV. The essence of
the method is that sample and detector are placed in an isotropic neutron
field which is not affected by neutron scattering on nuclei of the sample
or the detector material. The low gamma background of the spectrometer
makes it possible to record gamma rays with a gas proportional counter,
in which the recording efficiency is proportional to the radiation energy
$\boxed{4, 5\_}$. The efficiency of recording a capture or fission event is
accordingly proportional to the total energy of the gamma cascade and is
independent of possible variations in the gamma-ray spectrum.

The relative energy dependence of $\alpha(E)$ was normalized with a well-
thermalized neutron spectrum produced in a graphite prism placed close
to the main lead moderator prism. The necessary thermal spectrum
constants are already known with a high degree of accuracy $\boxed{6, 7\_}$.

1. Measuring procedure, detectors and counting equipment

A sample of ^{239}Pu and a gamma detector were placed in the measuring channel of a lead moderator (Fig. 1) and the dependence of the detector count on the slowing-down time, $I_\gamma(t)$, was measured:

$$I_\gamma(t) = \text{const.} \left[\varepsilon_c \cdot \sigma_c(E) + \varepsilon_f \cdot \sigma_f(E) \right] \cdot \varphi(t)$$

$$= K_\gamma \left[\sigma_c(E) + \beta \cdot \sigma_f(E) \right] \cdot \varphi(t) \tag{1}$$

where $\beta = \varepsilon_f/\varepsilon_c$ is the ratio of the efficiencies of recording a fission event and a capture event from instantaneous gamma rays, $\varphi(t)$ is the neutron flux, and $K_\gamma(\bar{n}_x, M_x, \varepsilon_c^x)$ is the normalizing factor, which depends on the effective thickness of the sample $\bar{n}_x$, the count of the monitor M_x and the efficiency of recording a capture event for nuclei of the sample under investigation.

Measurements with the gamma detector were alternated with counts in a fission chamber, $I_f(t)$, containing layers of ^{239}Pu:

$$I_f(t) = K_f \cdot \sigma_f(E) \cdot \varphi(t) \tag{2}$$

where $K_f(\bar{n}_K, M_K, \varepsilon_K)$ is the normalizing factor, which depends on the effective thickness of the layer in the chamber, $\bar{n}_K$, the count of the monitor, M_K, and the efficiency of the chamber, ε_K.

Dividing expression (1) by (2), we obtain the basic expression for determining $\alpha(E)$:

$$\alpha(E) = \frac{K_f}{K_\gamma} \cdot \frac{I_\gamma(t)}{I_f(t)} - \beta \tag{3}$$

The mean neutron energy E (keV) and the slowing-down time t (μsec) are linked by the empirical relationship $\overline{\int 3 \int}$

$$E = 183/(t + 0.3)^2 \tag{4}$$

For recording prompt gamma rays from fission and radiative capture, a gas proportional counter is used $\overline{\int 4, 5 \int}$ in which the efficiency of recording gamma rays is approximately proportional to their energy. In this case the efficiency of recording capture and fission events is affected very little by variations in the gamma-ray spectrum and is determined solely by the total gamma-ray energy per interaction:

$$\varepsilon_c = \text{const} \cdot B_n$$

$$\varepsilon_f = \text{const} \cdot E_f \tag{5}$$

where B_n is the neutron binding energy in the nucleus and E_f is the total gamma-ray cascade energy per fission event.

From expression (5) it follows that the normalizing constants K_f/K_γ and β, which are characteristics of the detectors, are constant over the investigated range of energies.

The amplifier circuit of the detectors incorporates a UIS-2 broad band anti-saturation amplifier. The time dependence of the detector count was analysed by the Measuring and Recording Centre of the Lebedev Physics Institute $\boxed{8}$. Since the time resolution of the spectrometer is ~ 15%, the analyser has groups of channels with pulse widths ranging from 0.25 μsec at the beginning to 64 μsec at the end of the cycle.

The low resolution of the spectrometer rules out reliable determination of the normalizing constants from resonances with well-known values of $\alpha(E_0)$, so the usual practice is to normalize on the basis of the thermal values. As the graphite prism (Fig. 1) is moved up to the lead "cube" and fed with the neutron pulse from the lead, alternate measurements are made inside it of ΔI_f^{th} with the fission chamber and of ΔI_γ^{th} of the sample in question with the gamma counter as well as of $\Delta I_{\gamma st}^{th\gamma}$ of a non-fissionable standard sample:

$$\Delta I_f^{th} = K_f \cdot \sigma_f^{th} \cdot \Delta\varphi^{th} \tag{6}$$

$$\Delta I_\gamma^{th} = K_\gamma \cdot (\sigma_c^{th} + \beta \, \sigma_f^{th}) \cdot \Delta\varphi^{th} \tag{7}$$

$$\Delta I_{\gamma st}^{th} = K_\gamma^{st} \cdot \sigma_{cst}^{th} \cdot \Delta\varphi^{th} \tag{8}$$

where σ_f^{th}, σ_c^{th} and σ_{cst}^{th} are the thermal fission and radiative capture cross-sections averaged over the neutron spectrum in the graphite prism and $\Delta\varphi^{th}$ is the thermal neutron flux.

Relations (7) and (8) are dependent because the condition in expression (5) is fulfilled for the proportional gamma counter, so that for samples with uniform geometry we have

$$\frac{K_\gamma}{K_\gamma^{st}} = \frac{\bar{n}_x \cdot M_x \cdot \varepsilon_c^x}{\bar{n}_{st} \cdot M_{st} \cdot \varepsilon_c^{st}} = \frac{\bar{n}_x \cdot M_x \cdot B_n^x}{\bar{n}_{st} \cdot M_{st} \cdot B_n^{st}} \tag{9}$$

After simple transformations we obtain from relations (6), (7) and (8) the normalizing constants:

$$\beta = \frac{\sigma_{c\,st}^{th}}{C_1 \cdot \sigma_f^{th}} \cdot \frac{\Delta I_\gamma^{th}}{\Delta I_{\gamma st}^{th}} - \alpha^{th} \tag{10}$$

$$\frac{K_f}{K_\gamma} = (\alpha^{th} + \beta) \cdot \frac{\Delta I_f^{th}}{\Delta I_\gamma^{th}} \tag{11}$$

where $\alpha^{th} = \sigma_c^{th}/\sigma_f^{th}$ is the ratio of the thermal radiative capture and fission cross-sections averaged over the thermal spectrum.

2. Measurements in the lead cube

The measurements in the lead moderator of the spectrometer were performed with a neutron burst frequency of 312.5 and 625 Hz and a burst duration of ~ 0.5 μsec.

Measurements of the effect due to the sample were alternated with measurements of the gamma background (background sample in gamma counter) and measurements of the natural radioactive background from the specimen as well as measurements with the fission chamber. During the measurements the mean square spread of the counts in the channels was monitored, an especially important procedure in the case of small slowing-down times.

In measurements with the gamma detector the signal to background ratio is ~ 25% in the energy range 0.1–2.0 keV and ~ 15% in the energy range 2.0–8.0 keV. Above E ≃ 8.0 keV the signal to background ratio deteriorates owing to the increase in background close to the neutron burst; this means that it is essential for the position of the burst to remain stable relative to the beginning of the cycle.

(a) Allowing for activation

The activation of the specimen, A, was determined from the ratio of the count rate during measurement with a sample in the gamma counter $I_\gamma(t)$ to the count rate during measurement with the fission chamber $I_f(t)$ at the end of a cycle lasting 3200 μsec, when it can be assumed with sufficient certainty that the cross-section under investigation follows the ~ 1/v law:

$$\frac{I_\gamma(t) - A}{I_f(t)} = \frac{\Delta I_\gamma^{th}}{\Delta I_f^{th}} \tag{12}$$

The correction for activation of the specimen decreases sharply with decrease in t and does not exceed 1% in the 0.1–50 keV energy range.

(b) <u>Allowing for recycle neutrons</u>

The correction for the contribution of recycle neutrons in a 3200 μsec cycle is negligible. The contribution of recycle neutrons in a 1600 μsec cycle is determined from the time dependence $I_\gamma(t)$ in measurements with a 3200 μsec cycle, in the time range from 1600 to 3200 μsec.

The correction for the contribution of recycle neutrons in a series of measurements with a 1600 μsec cycle is ~ 0.5% in the 0.1-50 keV energy range.

(c) <u>Correction for counting losses</u>

The correction for counting losses is determined by the finite resolving time ($\tau \simeq 4$ μsec) of the counting system. This correction is important with small t because of the higher background close to the neutron burst. It was introduced in the results of the measurements with the sample and in the background measurements, in accordance with the expressions

$$n(t) = \frac{m(t)}{1 - \eta} \tag{13}$$

$$\eta = \frac{1}{f \cdot \Delta_K} \cdot \int_{t-\tau}^{t} m(t) dt \tag{14}$$

where $m(t)$ is the number of pulses counted in the channel situated in the range from t to $t + \Delta_K$ per unit time, $n(t)$ is the number of pulses entering that channel per unit time, and f is the neutron burst repetition frequency.

The correction for counting losses is ~ 4% at $E \simeq 50$ keV and drops sharply to ~ 0.5% at $E \simeq 5$ keV.

(d) <u>Correction for spectrometer resolution</u>

The correction to $\alpha(E)$ for poor spectrometer resolution ($\Delta E/E \simeq 35\%$ at $E \simeq 1$ keV and $\Delta E/E \simeq 70\%$ at $E \simeq 40$ keV) was calculated from the theoretical evaluations of the neutron spectrum in Ref. $\lceil 3 \rfloor$.

The correction for resolution in the 0.1-50 keV energy range does not exceed ~ 5%.

3. Measurements in the graphite prism

The measurements in the graphite prism which is moved towards the main prism of the lead moderator were performed with a neutron burst frequency of 312.5 Hz and a width of ~ 2.0 μsec.

(a) <u>Thermalization of the neutron spectrum</u>

A well-thermalized spectrum is necessary for normalizing the constants obtained from the graphite prism measurements to thermal values.

Measurements with a boron detector (BF_3-counter) in the graphite prism (Fig. 2) show that the thermal neutron density decreases with a constant relaxation of $\alpha_0 = 710$ sec^{-1}. Using this value and data from Refs $\lfloor 9, 10 \rfloor$ estimates were made of the thermalization time in the graphite prism and these indicated that a thermal spectrum with near-Maxwellian distribution is established at times of $t > 1000$ µsec.

To check the establishment of thermal equilibrium, measurements were made of the ratio of the count from the ^{239}Pu fission chamber to that of the boron detector, and of the ratio of the count from the gamma detector with the cadmium sample to that of the boron detector (Fig. 3), as functions of time relative to the neutron burst. As can be seen from Fig. 3, an equilibrium thermal spectrum can be guaranteed at $t > 1500$ µsec.

(b) <u>Allowing for activation</u>

For the measurements in the graphite prism with the gamma counter, allowance must be made for activation of the sample, which is quite significant in the case of ^{239}Pu. This is done on the assumption that the length of the cycle (3200 µsec) is small compared with the lifetimes of the radioactivities produced. We take the difference between the counts of the gamma detector over two equal time intervals of ~ 800 µsec at the end of a cycle, ΔI_γ^{th}. A similar procedure is followed for the fission chamber count, in that the quantities ΔI_γ^{th} and ΔI_f^{th} in the ratio $(\Delta I_\gamma^{th}/\Delta I_f^{th})$ are reduced to a single thermal flux.

(c) <u>Allowing for neutron flux depression</u>

The flux depression in the prism during the cycle due to neutron absorption in the specimen was estimated from the experimental ratio of the count from the boron detector with the cadmium sample inserted in the channel of the prism to the count without the cadmium sample (Fig. 4). The results of the measurements show that the effect of depression in the time range up to 3200 µsec is not more than 5%. Allowing for the difference in absorption in the samples under investigation and the cadmium sample, we find that this effect is less than 0.5% for the samples under investigation.

Absorption during passage of neutrons through the sample was allowed for on the assumption that each neutron traversing the sample covers an identical path equal to the mean distance through the sample $\bar{\ell}(\bar{n} = N\bar{\ell}$, at/$cm^2)$. As shown in Ref. $\boxed{11\_7}$, when $\bar{n}\sigma \sim 5$, the difference in the paths traversed may be neglected without giving rise to errors greater than 3-5%. In our samples $\bar{n}\sigma \sim 0.2$, so that this difference can be neglected.

The relative reduction in the count due to attenuation of the neutron flux is

$$\mu = \frac{\int \varrho(v) \cdot v(1 - \ell^{-\bar{n}\sigma}) \, dv}{\bar{n}\sigma^{th} \cdot \int \varrho(v) \cdot v_o \, dv} = 1 - \frac{\bar{n}\sigma^{th}}{V} + \frac{(\bar{n}\sigma^{th})^2}{3} \tag{15}$$

where $\varrho(v)$ and v are neutron density and velocity respectively, $\sigma(v) = \sigma^{th}v_o/v$ is the neutron absorption cross-section and σ^{th} is the absorption cross-section at an energy equal to kT ($v_o = 2200$ m/sec).

The numerator in expression (15) describes the neutron absorption in the sample with allowance for attenuation of the neutron flux, whilst the denominator represents absorption without attenuation of the flux. Integration was performed after expanding the exponential term. Succeeding terms of the expansion give divergent integrals but the validity of expression (15) was verified by numerical integration for different thicknesses of the samples investigated.

A correction for absorption was introduced in the results of the measurements with samples and also in the background measurement (background container of the gamma counter). The correction for absorption in the samples used in the measurements in the graphite prism did not exceed 13%.

4. Results and discussion

Measurements with the proportional gamma counter were performed for PuO_2 samples of different effective thicknesses ($\bar{n} = 4.4 \times 10^{21}$; 4.2×10^{20} and 1.7×10^{20} at/cm^2) with a ^{240}Pu content of $\sim 1.8\%$. For normalizing purposes measurements were also carried out in the graphite prism with samples of ^{107}Ag and ^{109}Ag ($\bar{n} = 4.3 \times 10^{21}$ at/cm^2) and ^{197}Au ($\bar{n} = 1.8 \times 10^{21}$ at/cm^2). The fission effect was measured with ionization fission chambers filled with a mixture of A (200 mmHg) and CO_2 (10 mmHg). Because of the high intensity of the spectrometer only a comparatively

small quantity of fissile material need be used in the chamber and it is
fairly easy to separate the fission fragment count from the alpha particle
background.   For our measurements we used fission chambers containing
1.6 and 12 mg $^{239}PuO_2$.

The thermal cross-sections used for determining the normalizing
constants are given in Table 1.   The absolute error due to normalization
is shown in Table 2 as a function of $\alpha(E)$.   From the measurements in the
graphite chamber we obtained the value $\beta = 0.802 + 0.056$.

The results of our measurements of the energy dependence of $\alpha(E)$ for
^{239}Pu are shown in Fig. 5 and compared with the data of other authors.
The numerical values of $\alpha(E)$ are shown in Table 3.   Our own data in the
0.2-7 keV energy range are in agreement with averaged data obtained by the
time-of-flight method in linear accelerators $\boxed{16\text{-}18\_}$ and in the neutron
spectrometer of the cyclotron at the Institute of Experimental and
Theoretical Physics $\boxed{15\_}$.

In conclusion, the authors wish to thank I.M. Frank and I.Ya. Barit
for the opportunity to conduct measurements on the neutron slowing-down-
time spectrometer;   F.L. Shapiro for his interest in the work and useful
discussions;   V.N. Konov, G.V. Muradyan and Yu.V. Ryabov for their
discussions of the method and the results;   I.V. Shtranikh and colleagues
of the Radioelectronics Department of the Lebedev Physics Institute for
organizing and carrying out the work at the Measuring and Recording Centre
of the Institute;   and N.N. Gonin, Yu.A. Dmitrienko, V.M. Polyakov,
B.I. Ryzhikov and I.V. Syutkinaya for their assistance in the measurements
and in the processing of the results.

REFERENCES

$\boxed{1\_}$ BARRE, I.Y., L'HERITEAU, I.P., RIBON, P., Report CEA-N-989,
EANDC (EUR) - 111, 1968.

$\boxed{2\_}$ BERGMAN, A.A., ISAKOV, A.I., et al., Int. Conf. Peaceful Uses
Atom. Energy (Proc. Conf. Geneva, 1955) 4, Izdat. Akad. Nauk SSSR
(1957) 166.

$\boxed{3\_}$ SHAPIRO, F.L., Trudy FIAN SSSR (Proc. Lebedev Physics Institute
of the USSR) 24 (1964) 3.

$\boxed{4\_}$ POPOV, Yu.P., Trudy FIAN SSSR (Proc. Lebedev Physics Institute
of the USSR) 24 (1964) 111.

_/5_/ BERGMAN, A.A., SAMSONOV, A.E. et al., in Nuclear Data for
Reactors (Proc. Conf. Helsinki, 1970) 2 IAEA, Vienna (1970) 51.

_/6_/ GOLDBERG, M.D., MUGHABGHAB, S.F. et al., Neutron Gross-
sections, suppl. 2 to BNL-325, second edition, 1966.

_/7_/ HANNA, G.C., WESTCOTT, C.H. et al., Atom. Energy Rev., 7, 4
(1969).

_/8_/ SHTRANIKH, I.V., KLABUKOV, A.M., SAMSONOV, A.E., Trudy FIAN SSSR
(Proc. Lebedev Physics Institute of the USSR) 42 (1968) 69.

_/9_/ BECKURTS, K., WIRTZ, K., Nejtronnaja Fizika (Neutron Physics)
Atomizdat (1968).

_/10_/ ANTONOV, A.V., Trudy FIAN SSSR (Proc. Lebedev Physics Institute
of the USSR) 14 (1962) 147.

_/11_/ KHOKHLOV, Yu.K., Preprint No. 110 FIAN SSSR (Lebedev Physics
Institute of the USSR) Moscow (1967).

_/12_/ HOPKINS, I.C., DIVEN, B.C., Nucl. Sci. Engng. 12 (1962) 169.

_/13_/ DE SAUSSURE, G. et al., in Nuclear Data for Reactors (Proc.
Conf. Paris, 1966) 2 IAEA Vienna (1967) 233.

_/14_/ RYABOV, Yu.V., KUROV, M.A., et al., in Nuclear ata for eactors
(Proc. Conf. Helsinki, 1970) 1 IAEA (1970) 345.

_/15_/ BELYAEV, F.N., IGNATEV, K.G., SUKHORUCHKIN, S.I., et al., in
Nuclear Data for Reactors (Proc. Conf. Helsinki, 1970) 1 IAEA,
Vienna (1970) 339.

_/16_/ GWIN, R., WESTON, L.W. et al., Nucl. Sci. Engng. 40 (1970) 306.

_/17_/ CZIRR, J., LINDSEY, J., in Nuclear Data for Reactors (Proc.
Conf. Helsinki, 1970) 1 IAEA, Vienna (1970) 331.

_/18_/ SCHOMBERG, M., SOWERBY, M., et al., in Nuclear Data for Reactors
(Proc. Conf. Helsinki, 1970) 1 IAEA, Vienna (1970) 315.

Table 1

Thermal cross-sections used for normalization

Values at E = 0.0253 eV	f	Values for Maxwellian spectrum
^{239}Pu $\quad \sigma_f = 741.6 \pm 3.1$ barn $[7]$	1.055	$\sigma^{th} = 780.2$
$\alpha = 0.3659 \pm 0.0039 \ [7]$	1.088	$\alpha^{th} = 0.3982$
^{197}Au $\quad \sigma_c = 98.6 \pm 0.3$ barn $[6]$	1.005	$\sigma_c^{th} = 99.1$
^{107,109}Ag $\quad \sigma_c = 63.6 \pm 0.6$ barn $[6]$	1.004	$\sigma_c^{th} = 63.8$

Note: $\sigma_x^{th} = f \cdot \sigma_x (E = 0.0253$ eV) where f is the Westcott factor $[9]$.

Table 2

Absolute error in $\alpha(E)$ due to normalization

$\alpha(E)$	$\pm \Delta\alpha$
0,40	0,06
0,60	0,07
0,80	0,08
1,00	0,10
1,20	0,11

Note: The normalization error derives largely from the measuring statistics in the graphite prism (1-2%), the error in the absolute weight of the samples (~ 4%) and the uncertainty in the dependence of the gamma counter efficiency on the gamma-ray energy (~ 4%).

Table 3

Numerical values of $\alpha(E)$ for ^{239}Pu

E, keV	$\alpha(E)$
6,0	0,96 ± 0,12
5,0	I,00 ± 0,12
4,0	I,05 ± 0,15*)
3,2	I,08 ± 0,12
2,6	1,15 ± 0,12
2,17	1,36 ± 0,12
I,77	I,40 ± 0,12
I,47	I,I9 ± 0,15*)
I,23	I,18 ± 0,II
I,05	I,15 ± 0,10
0,92	I,16 ± 0,10
0,80	I,13 ± 0,10
0,70	I,20 ± 0,II
0,60	I,20 ± 0,II
0,53	I,15 ± 0,10
0,47	0,95 ± 0,13*)
0,40	I,01 ± 0,09
0,35	I,16 ± 0,10
0,30	I,10 ± 0,10
0,27	0,94 ± 0,10
0,23	0,90 ± 0,10
0,20	0,81 ± 0,09

Note: The table shows the statistical error in the measurements of $\alpha(E)$ except in cases marked with an asterisk, where the total error is given.
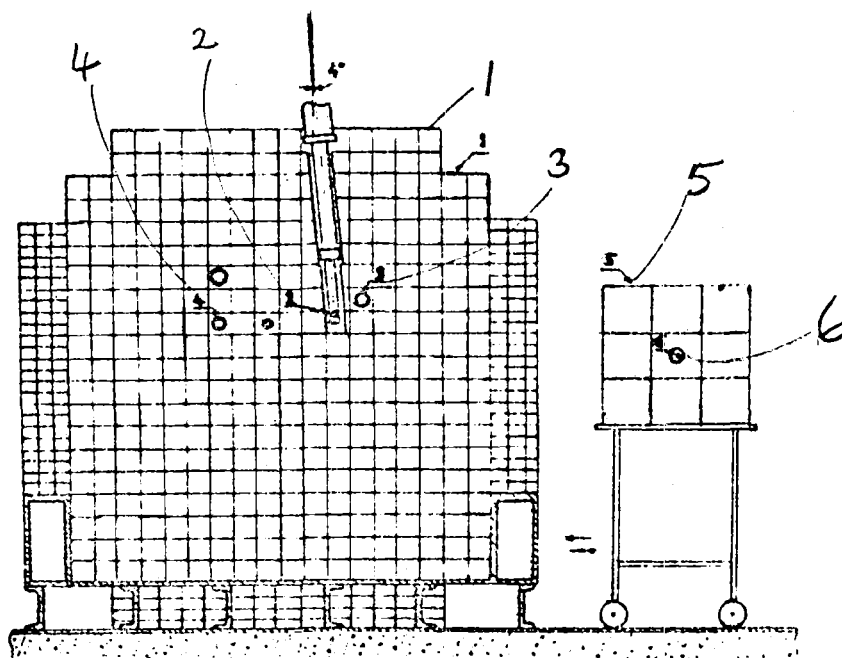
Fig. 1   Measuring set-up

1 = Lead "cube"

2 = Position of zirconium-sodium target

3 = Channel in which the fast neutron burst is recorded

4 = Main measuring channel

5 = Graphite prism, 60 x 60 x 120 cm^3

6 = Channel of graphite prism
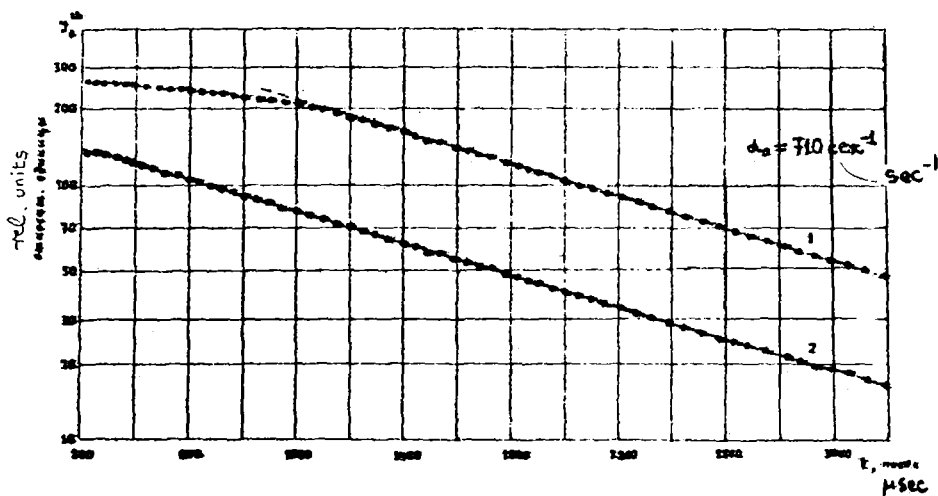
Fig. 2   Dependence of neutron density in the graphite prism on time
relative to the neutron burst $I_B^{th}(t)$:

1 = Graphite prism placed at the side of the lead "cube" closest
to the target;

2 = Graphite prism placed at opposite side.
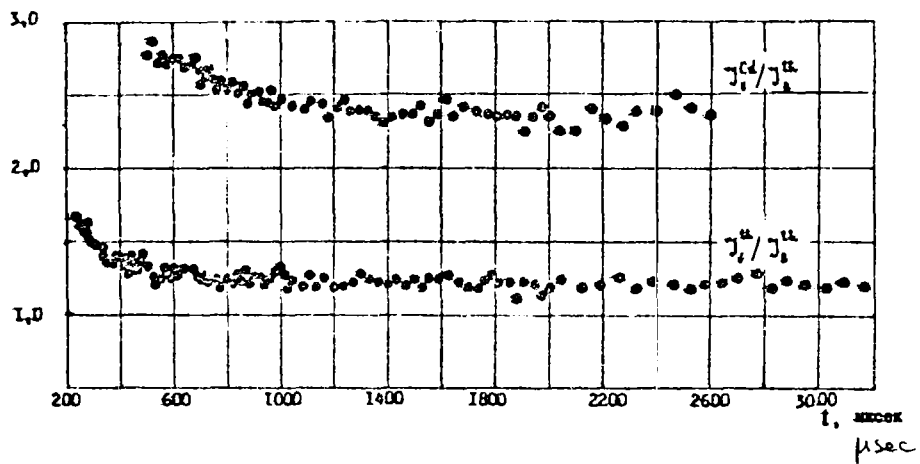
Fig. 3   Ratios of the count rate of the ^{239}Pu fission chamber $I_f^{th}(t)$ and the count rate of the gamma detector with cadmium sample $I_\gamma^{Cd}(t)$ to the count rate of the boron detector $I_B^{th}(t)$ in the graphite prism.
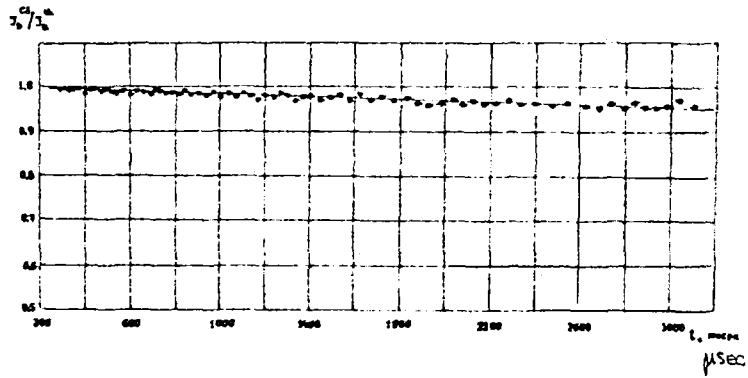
<u>Fig. 4</u>   Ratio of the count rate of the boron detector with cadmium
sample in the channel of the graphite prism $I_B^{Cd}(t)$ to the
count rate without cadmium $I_B^{th}(t)$ as a function of time
relative to neutron burst.
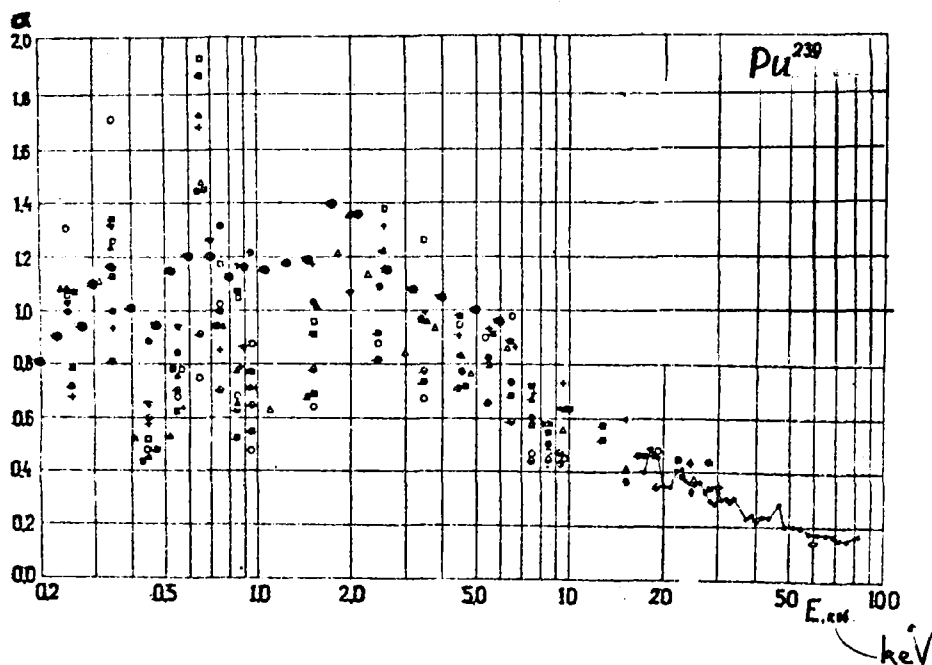
Fig. 5   Energy dependence of α(E) for [239]Pu.

•   Own data

▲   Sukhoruchkin, 1970
    Ryabov, 1970

⊙   Scintillation tank

◉   Fission chamber 220 nsec/m

○   Fission chamber 15 nsec/m

◇   Hopkins, Diven, 1962

◆   Spivak, 1956

⁄   De Saussure et al.1966

◆   Andreev, 1958
    Gwin et al, 1970
■   metal foils
▫   fission chamber
▪   Sowerby et al. 1970
△   Czirr, Lindsey, 1970
+   Farrell et al., 1970
▼   Muradyan, 1971

◇   Kazansky, 1971

ENERGY AND MASS DISTRIBUTIONS OF FISSION FRAGMENTS PRODUCED IN SPONTANEOUS ^{244}Cm FISSION

I.D. Alkhazov, O.I. Kostochkin, S.S. Kovalenko
L.Z. Malkin, K.A. Petrzhak, V.I. Shpakov

The authors present the results of bilateral measurements of the kinetic energies of fragments from spontaneous fission of ^{244}Cm which were carried out using surface-barrier silicon detectors.

A preparation of isotopically pure ^{244}Cm (< 0.001 wt% ^{242}Cm) approximately 3 mm in diameter, coated onto an aluminium base, was placed between two semiconductor detectors. The thickness of the preparation together with its carrier was less than 10 $\mu g/cm^2$. The thickness of the base was 80 $\mu g/cm^2$. The distance between the detectors was set at 1 cm. The diameter of the sensitive area of the detectors was 7 mm. The working surfaces of the detectors were diaphragmed to avoid losses in the pulse amplitude measurements when fragments strike the edges of the sensitive area of the detectors. The geometrical efficiency of recording fission fragments was 7%. The detectors used in the measurements were selected from commercially available models on the basis of energy resolution, reverse current and the permissible bias voltage. The resolution of the detectors used, measured with ^{239}Pu alpha particles was about 1–2%, the reverse current was no more than tenths of a microampere and the bias voltage was not less than 25 V.

The energy calibration of the apparatus was carried out with the aid of unilateral fragment spectra from thermal fission of ^{235}U, using the method proposed by Schmitt $\boxed{1}$.

The time resolution of the apparatus (4×10^{-7} sec) permitted an alpha particle loading of the detector of the order of 3–4 $\times 10^4$ sec^{-1}. On that basis approximately three spontaneous fissions per minute were recorded. The probability of alpha particle pulses covering fragment pulses was about 3%.

To avoid drift of the detector characteristics due to radiation damage caused by the high alpha activity of the ^{244}Cm preparation, not more than 10^4 spontaneous fission events were recorded by one pair of detectors. In all, about 65 000 spontaneous fissions of ^{244}Cm were recorded.

The peak to valley ratio was 14:1 in the ^{235}U calibration spectra and 4:1 in the ^{244}Cm energy spectra. The peak to valley ratio in the ^{244}Cm mass distribution was 15:1. The comparable value obtained by Bennett and Stein $\lfloor 2 \rfloor$ for ^{252}Cf was 12:1.

The accuracy with which the energies and accordingly the masses of the fission fragments can be measured depends on the stability of operation of the apparatus during measurement, the accuracy of the energy calibration, the superposition of alpha particle pulses on fragment pulses and the statistical measuring errors. During measurement the continuous stability of both the amplification circuits and of the pulse height measurement was checked every 30 minutes with the aid of a precision pulse height generator and a reference ^{239}Pu alpha particle source and, in addition, the positions of the peaks in the unilateral fragment spectra were checked every three hours. Peak displacement did not exceed 1%.

The calibration errors are compounded from errors in Schmitt's calibration formulae $\lfloor 1 \rfloor$ and errors in the determination of the positions of the peaks in the unilateral spectra of ^{235}U and ^{244}Cm fragments. The errors in the coefficients do not in any case exceed the errors given by Schmitt $\lfloor 3 \rfloor$ for the kinetic energies of fragments from thermal fission of ^{235}U, i.e. 0.6%. The errors in fixing the peaks are determined by the statistics accumulated in each series of measurements with one pair of detectors. As already indicated, the number of ^{244}Cm fission events was of the order of 10^4, the same as the number of fissions in the calibration spectrum. An idea of the accuracy of the energy calibration may be gained from the following consideration. Schmitt $\lfloor 1 \rfloor$ proposes determining the calibration constants from the formulae

$$a = \frac{A_1}{P_L - P_H} \qquad a' = \frac{A_2}{P_L - P_H} \qquad b = A_3 - aP_L \qquad b' = A_4 - a'P_L$$

where P_H and P_L represent the position of the peaks of heavy and light groups of fragments in the unilateral energy spectrum, and A_1, A_2, A_3 and A_4 are constants relating to the particular fissionable nucleus. The constants for ^{244}Cm were determined from the position of the ^{235}U and ^{244}Cm peaks in each series of measurements. The constants for the different series did not differ from each other by more than 0.2%. Their mean values are as follows:

$$A_1 = 23.952$$
$$A_2 = 0.0355$$
$$A_3 = 91.437$$
$$A_4 = 0.1398$$

The correction to the mean values of the kinetic energies to allow for overlapping of the pulses from alpha particles and fragments is the product of the overlapping probability and the height of the pulse from the alpha particle, i.e. not more than 200 keV. The appropriate correction was made to the data given below. An over-all estimate of the above measuring errors showed that the standard deviations in the determination of the mean kinetic energies and the masses are no more than ~ 1%.

The results of the measurements were reduced to a form corresponding to fragments before the emission of prompt fission neutrons by a method similar to that proposed by Schmitt $\sqrt{3}\sqrt{}$. To determine the number of neutrons emitted after fission, the total number of neutrons in each fission event was measured with a liquid scintillation counter and the distribution of neutrons between fragments as a function of mass was calculated from Terrell's "universal" curve $\sqrt{4}\sqrt{}$.

The data obtained are shown in Tables 1-3. Table 4 shows the mean total kinetic energy $<E_K>$, the mean energies $<E_L>$ and $<E_H>$ and the mean masses $<M_L>$ and $<M_H>$ of the light and heavy peaks, the standard deviations of the mass distribution σ_M and the total kinetic energy distribution σ_{E_K}. The table also includes similar data from the literature. It will be seen that our own data differ from those of other authors. These discrepancies can be explained as follows. In Ref. $\sqrt{8}\sqrt{}$, where the measurements were performed with semiconductor detectors, no correction was made for the mass-dependent pulse-height defect of pulses from fission fragments, so that the fragment energies are too low. Moreover, in Ref. $\sqrt{8}\sqrt{}$ and also Ref. $\sqrt{7}\sqrt{}$, the energy calibration was based on old and too low values of the kinetic fragment energies for thermal fission of ^{235}U obtained by Fraser and Milton $\sqrt{9}\sqrt{}$. If Schmitt's data $\sqrt{3}\sqrt{}$ had been used in Ref. $\sqrt{7}\sqrt{}$, the results would have agreed well with ours. In Ref. $\sqrt{6}\sqrt{}$, the total kinetic energy is clearly too high owing to the poor time resolution of the equipment.

REFERENCES

[1] SCHMITT, H.W., GIBSON, W.M., NEILER, J.H., WALTER, F.J., THOMAS, T.D., in Physics and Chemistry of Fission (Proc. Conf. Salzburg, 1965) 1 IAEA Vienna (1965) 531.

[2] BENNETT, M.J., STEIN, W.E., Phys. Rev. 156 (1967) 1277.

[3] SCHMITT, H.W., NEILER, J.H., WALTER, F.J., Phys.Rev. 141 (1966) 1146.

[4] TERRELL, J., Phys. Rev. 127 (1962) 880.

[5] SMITH, A., FIELDS, P., FRIEDMAN, A., Int. Conf. peaceful Uses atom. Energy (Proc. Conf. Geneva 1958) UN 15 392.

[6] MALKIN, L.Z., et al. Atomn. Energ. 15 (1963) 249.

[7] BOLSHOV, V.I., et al. Atomn. Energ. 17 (1964) 28.

[8] VEI-VEN, E., CHELNOKOV, L.P., Preprint No. 2317 of the Joint Institute for Nuclear Research, Dubna, 1965.

[9] MILTON, J., FRASER, J., Can. J. Phys. 40 (1962) 1626.

Table 1

Distribution of the number of ^{244}Cm spontaneous fissions in relation to the total kinetic energy and mass of the light fragment before neutron escape

Mass

MeV	86	88	90	92	94	96	98	100	102	104	106	108	110	112	114	116	118	120	122
220										1	2	4	7	9	7	3	2	1	
218										1	4	9	14	18	14	8	3	2	1
216										5	8	21	30	29	23	11	4	2	
214								1	1	9	16	36	50	47	35	16	4	2	
212							1	2	4	21	36	64	77	76	55	24	7	3	1
210							2	4	10	58	83	108	114	113	76	35	10	4	1
208						2	4	8	23	72	151	160	166	156	103	47	14	4	2
206						3	5	19	52	125	194	235	218	197	129	60	19	6	2
204						4	9	41	104	191	267	310	287	254	152	69	24	10	5
202				1	3	6	20	77	155	261	351	385	559	272	172	84	51	12	7
200				2	4	9	37	122	224	341	450	454	401	303	190	94	55	16	11
198			1	2	6	17	64	176	306	419	511	507	438	330	206	105	39	17	11
196			2	4	11	31	101	230	360	476	556	544	457	340	214	107	39	18	12
194		1	2	7	16	56	145	283	418	533	570	539	459	335	207	102	38	20	12
192		1	2	10	31	84	179	332	463	558	576	522	436	306	189	90	34	22	17
190		3	3	17	50	99	214	361	488	575	572	495	396	270	164	82	34	20	18
188		5	10	29	67	121	236	386	490	545	532	459	354	235	141	74	33	23	20
186		10	21	44	83	140	247	331	466	505	491	415	297	198	122	68	52	24	19
184	5	16	30	57	98	162	261	356	431	455	434	358	248	171	108	62	30	24	20
182	7	20	38	69	112	181	275	327	564	387	362	296	210	144	94	57	29	22	18
180	10	23	44	75	120	187	257	2L	311	327	294	238	168	116	78	49	26	21	19
178	14	29	50	81	130	182	231	250	274	268	232	184	150	92	61	41	24	22	22
176	19	34	54	88	127	165	203	222	228	217	180	142	104	64	49	34	22	22	22
174	24	39	60	87	119	150	173	188	177	164	138	111	83	61	42	30	20	20	19
172	27	42	59	78	108	133	145	156	138	123	105	87	67	48	38	28	18	20	20
170	28	42	54	74	99	117	124	122	102	93	80	58	55	45	34	25	17	19	19
168	28	42	55	69	88	96	102	95	75	69	52	52	43	36	30	23	15	15	14
166	29	43	52	61	69	76	82	72	59	53	48	40	34	30	27	21	13	12	10
164	27	47	47	49	51	59	62	55	52	40	37	31	27	25	23	19	11	10	11
162	26	34	39	37	39	47	48	42	36	31	30	26	25	22	21	18	13	12	13
160	24	31	36	35	35	38	36	32	28	26	24	23	22	20	19	16	11	12	12
158	22	26	28	30	27	27	26	25	22	20	19	21	21	20	18	15	10	10	9
156	20	23	23	22	21	20	20	20	17	15	16	19	18	17	16	13	9	10	10
154	16	18	19	20	18	16	17	18	13	12	11	15	13	11	12	11	8	9	11

Table 2

Mean total kinetic energy $<E_K>$ of ^{244}Cm spontaneous fission fragments
and its standard deviation in relation to light fragment mass

$M_л$/аеи/	86	88	90	92	94	96	98	100	102	104	106
$<E_K>$/МэВ/	166,9	168,9	170,8	173,5	176,0	178,3	181,3	184,4	186,8	188,8	190,4
σ_{E_K}/МэВ/	8,4	9,0	9,1	9,3	9,4	9,8	9,9	10,2	10,0	10,2	10,4

$M_л$/аеи/	108	110	112	114	116	118	120	122
$<E_K>$/МэВ/	191,2	192,3	193,2	192,6	190,2	187,2	182,2	179,3
σ_{E_K}/МэВ/	10,8	10,6	11,8	12,8	13,8	14,5	14,3	13,6

Table 3

Mean light fragment mass $<M_L>$ and its standard deviation σ_M as a function of E_K

E_K MeV	154	156	158	160	162	164	166	168	170	172	174	176	178	180	182	184	186
$<M_A>$ amu	99,9	99,4	99,3	99,3	99,5	99,3	99,4	100,0	100,7	101,0	101,4	102,0	102,5	103,0	103,5	104,0	104,5
σ_M amu	11,5	11,1	10,7	10,4	10,1	9,6	9,1	8,8	8,6	8,3	7,9	7,5	7,1	6,7	6,5	6,2	6,0

E_K MeV	188	190	192	194	196	198	200	202	204	206	208	210	212	214	216	218	220
$<M_A>$ amu	105,0	105,5	105,9	106,3	106,8	107,2	107,6	108,0	108,3	108,7	109,2	109,5	109,8	110,3	110,8	111,3	111,5
σ_M amu	5,7	5,4	5,3	5,1	5,0	4,9	4,7	4,6	4,4	4,3	4,2	4,0	3,9	3,7	3,6	3,7	3,6

Table 4

Energy and mass distribution characteristics of fragments from spontaneous fission of ^{244}Cm

	Smith et al.[5]	Malkin et al.[6]	Bolshov et al.[7]	Vei–Ven Chelnokov[8]	Our own data
Mean total kinetic energy (MeV) $<E_K>$	185.5		$182.3^{\pm}2.3$	$180.2^{\pm}3$	$188.6^{\pm}1.6$
Standard deviation of total kinetic energy distribution (MeV) σ_{E_K}			11.9		11.5
Standard deviation of mass distribution (amu) σ_M				Half width 19	5.9
		Most probable values			Mean values
Energy of light fragment peak (MeV) E_L	105.5	$117^{\pm}4$		$103.4^{\pm}1.5$	$107.5^{\pm}1.2$
Energy of heavy fragment peak (MeV) E_H	80	$86^{\pm}3$		$76.8^{\pm}1.5$	$81.1^{\pm}1.0$
Mass of light fragment peak (amu) M_L				$104^{\pm}0.5$	$104.6^{\pm}1.0$
Mass of heavy fragment peak (amu) M_H				$140^{\pm}0.6$	$139^{\pm}1.4$

ABSOLUTE FISSION FRAGMENT YIELDS FROM ^{241}Pu FISSION
INDUCED BY SLOW NEUTRONS

N.V. Skovorodkin, A.V. Sorokina, S.S. Bugorkov,
K.A. Petrzhak, A.S. Krivokhatsky

For the development of reactor engineering we need to know the fission
characteristics of ^{241}Pu, including its fission product yields. At the
commencement of this investigation data were available on the stable isotope
yields of the heavy fragment peak $/$1, 2$/$ and the yields of various radioactive
isotopes (^{135}I, ^{137}Cs, ^{140}Ba) $/$3$/$ and, when our investigation was finished,
two further publications appeared $/$4, 5$/$ which for all practical purposes
do not duplicate our data. Using the radiochemical method we determined
directly the absolute cumulative yields of ^{89}Sr, ^{90}Sr, ^{95}Zn, ^{99}Mo, ^{111}Ag,
^{112}Pd, ^{115}Cd, ^{115m}Cd, ^{132}Te, ^{140}Ba, ^{141}Ce and ^{144}Ce, and we also determined
the relative (to ^{144}Ce) cumulative yields of 16 radioactive isotopes of rare
earth elements and ^{91}Y resulting from slow fission of ^{241}Pu. The targets
were irradiated in a water-moderated and cooled reactor with a neutron
spectrum having a cadmium ratio for gold of ~ 3.

The plutonium for the targets was cleaned by ion exchange. The
targets were dissolved in the presence of isotopic carriers and special
conditions were created to promote exchange of antimony, molybdenum and
zirconium with the carriers. The separation and cleaning of all the
isotopes was done by ion exchange chromatography with a minimum of deposition.
The chemical yield of Mo and Ce was determined by colorimetry, the yield
of Sr by the complexometric method and the yield of the other isotopes by
gravimetric analysis. The rare earth elements and yttrium were also
separated by ion exchange chromatography using alpha-hydroxy isobutyrate
of ammonium $/$6$/$. The carrier employed was lanthanum so that we were
able to separate all the elements virtually without carrier.

The absolute number of disintegrations was measured in a $4\pi\beta$ flow-
type propane counter. The active substance was coated on gold-plated
organic films with a surface density of ~ 10 mg/cm^2. The maximum surface
density of the active substance was 50 mg/cm^2. The absolute activity of
the rare earth isotopes was measured in the $4\pi\beta$ counter through an Al
filter with a thickness of 6 mg/cm^2. The correction for beta particle
absorption was determined experimentally for each isotope. The decay

curves were analysed by computer by the least squares method. The standard deviation of the total number of atoms of all the various isotopes was 1.5–2% except for ^{141}Ce and ^{144}Ce where it was 2.7 and 3.3% respectively.

The number of fissions in the plutonium target for radiochemical analysis was determined from the number of tracks produced in a mica detector by the fission of a known amount of plutonium coated on the mica detector, which was irradiated in the reactor together with the target in a special assembly. To allow for the contribution of ^{239}Pu fissions, we used ^{239}Pu and ^{241}Pu fission cross-sections determined for the reactor spectrum in Ref. $\sqrt{7\_7}$. The fission fragment recording efficiency of the mica was determined with a calibrated ^{252}Cf source as 96.7 $\pm$ 0.7%. The contribution from ^{239}Pu fissions was not more than 5–8%. The standard deviation of the values obtained for the number of fissions in the plutonium target was 2–2.5%. The yields obtained are given in Tables 1 and 2. In the calculations allowance was made for the cumulative yield of precursors $\sqrt{6\_7}$.

Table 1

Absolute cumulative yields

Isotope	Half-life used	Absolute cumulative yield in %
Sr^{89}	50, 36 days (d)	1,21 ± 0,03
Sr^{90}	28,1 years (yr)	1,46 ± 0,04
Zr^{95}	65,2 d	4,08 ± 0,12
Mo^{99}	66,96 h	6,15 ± 0,16
Ag^{111}	7,5 d	0,586± 0,015
Pd^{112}	21,6 h	0,223± 0,058
Cd^{115}	53,5 h	0,0341± 0,0010
Cd^{115m}	43 d	0,0056± 0,0002
Te^{132}	77,7 h	4,49 ± 0,12
Ba^{140}	12,80 d	5,64 ± 0,11
Ce^{141}	32,51 d	4,81 ± 0,14
Ce^{144}	284,3 d	4,08 ± 0,14

Table 2

Relative and absolute cumulative yields

Isotope	Half-life used	Yield relative to ^{144}Ce */	Absolute cumulative yield in %
La ^{141}	3,85 h	1,10 ± 0,02	4,50 ± 0,17
Ce ^{141}	32,51 d	1,17 ± 0,02	4,78 ± 0,18
Ce ^{143}	33,40 h	0,952 ± 0,020	3,88 ± 0,16
Pr ^{143}	13,59 d	1,06 ± 0,01	4,31 ± 0,15
Pr ^{145}	5,98 h	0,739 ± 0,022	3,01 ± 0,14
Nd ^{147}	11,06 d	0,574 ± 0,008	2,34 ± 0,09
Pm ^{147}	2,64 yr	0,577 ± 0,023	2,35 ± 0,13
Nd ^{149}	1,8 h	0,361 ± 0,010	1,47 ± 0,06
Pm ^{149}	53,09 h	0,373 ± 0,014	1,52 ± 0,06
Pm ^{151}	28,40 h	0,207 ± 0,010	0,846 ± 0,050
Sm ^{153}	47,1 h	0,128 ± 0,003	0,522 ± 0,022
Sm ^{156}	9,4 h	0,0401 ± 0,0010	0,163 ± 0,007
Eu ^{156}	15,21 d	0,0417 ± 0,0007	0,170 ± 0,006
Eu ^{157}	15,15 h	0,0319 ± 0,0008	0,130 ± 0,006
Gd ^{159}	18,0 h	0,0113 ± 0,0002	0,0462 ± 0,0018
Tb ^{161}	7,20 d	0,00200 ± 0,00004	0,00815 ± 0,00032
Y ^{91}	58,8 d	0,409 ± 0,007	1,67 ± 0,06

*/ The slight differences in the relative yields compared with Ref. [6] are explained by the fact that our table includes the results of one further experiment. The yields for ^{156}Sm, ^{156}Eu and ^{153}Sm have been calculated on the basis of a more accurate half-life for ^{156}Sm, 9.4 ± 0.1 h [8].

REFERENCES

[1] FARRAR, H., CLARKE, W.B., THODE, H.G., TOMLINSON, R.H.,
Can. J. Phys., 42 (1964) 2063.

[2] RIDER, B.F., RUIZ, C.P., PETERSON, J.P., SMITH, F.R.,
USAEC Document GEAP-5505 (1967).

[3] OKAZAKI, A., WALKER, W.H., Can. J. Phys., 43 (1965) 1036.

[4] LISMAN, F.L., MAECK, W.J., REIN, J.E., FOSTER, R.E.,
ABERNETHEY, R.M., DELMORE, J.E., EMEL, W.A., KUSSY, M.E.,
McATEE, R.E., WORKMAN, G.D., Idaho Nuclear Corporation
Report IN1277 (TID-4500) (1969).

[5] CROALL, I.F., WILLIS, H.H., AERE-R 6154 (1969).

[6] SKOVORODKIN, N.V. et al., Radiokhimiya, 1970 (in press).

[7] BIGHAM, C.B., CRRP-1183 (AECL-1910) (1964).

[8] Nucl. Data Sheets, 1964, v. 5, No. 6.

CALCULATED CROSS-SECTIONS FOR ELASTIC AND INELASTIC SCATTERING OF 0.3-1.5 MeV NEUTRONS BY ATOMIC NUCLEI

I.K. Averyanov, A.E. Savelev, B.M. Dzyuba

Introduction

In a previous paper we considered an optical model of elastic and inelastic scattering of 2-6 MeV neutrons.[*]

The object of the calculations described here is to investigate the optical potential parameters for lower incident neutron energies $(E_n = 0.3-1.5$ MeV). The optical potential parameters were determined from experimental data on differential elastic scattering cross-sections for neutrons with energies of 0.3, 0.5, 0.8 and 1.5 MeV; the scattering nuclei had A = 23-238. The Hauser-Feshbach method was used for estimating the differential cross-sections for elastic scattering of neutrons by a compound nucleus.

Results of calculations

As before, we used the standard optical potential:

$$V(r) = V_1 \left\{ 1 + \exp\left(\frac{r - R}{a}\right) \right\}^{-1} + i\, V_2 \exp\left\{ -\left(\frac{r - R}{b}\right)^2 \right\}$$

$$+ V_3 \left(\frac{\hbar}{\mu c}\right)^2 \frac{1}{r} \frac{d}{dr} \left\{ 1 + \exp\left(\frac{r - R}{a}\right) \right\}^{-1} (\vec{\sigma}\, \vec{l}), \quad R = r_o A^{1/3}$$

The geometric parameters of the optical potential, r_o, a, b and the parameter of the spin-orbital interaction V_3 were fixed as constants for all nuclei and for all incident neutron energies. The parameters V_1 and V_2 were varied to obtain a satisfactory description of the experimental data on the differential cross-sections for elastic scattering of neutrons.

The results of the calculations are compared with the corresponding experimental data in Figs 1-9 of Appendix I. In the figures points indicate the experimental data, the broken lines indicate the theoretical differential cross-sections for potential elastic scattering and the solid lines are the sum of the theoretical differential cross-sections for potential elastic scattering and the differential cross-sections for elastic scattering by a

---

[*] AVERYANOV, I.K., SAVELEV, A.E., DZYUBA, B.M., Bjul. inf. Centr. jad. Dannym, issue No. 6 (1969) 236.

compound nucleus. The constant potential parameters and the parameters V_1 and V_2 obtained by the trial and error method for all the nuclei under investigation are shown in Table 1.

It is clear that for nuclei starting with Zn and increasing in weight, the parameter V_2 is constant for all nuclei and varies only with neutron energy (at E_n = 1.5 MeV V_2 is constant for all nuclei). The parameter V_1 varies at all energies, decreasing as the atomic weight of the target nucleus increases. This variation is due to the dependence of V_1 on the neutron excess in the nucleus. For certain nuclei lighter than Zn, a considerable spread of V_1 and V_2 values is observed at neutron energies below 1 MeV. This is connected with specific features of these nuclei which are apparent in the resonance structure of the cross-sections.

In Figures 1-3 of Appendix II the theoretical differential cross-sections for inelastic scattering of neutrons (curves) are compared with the corresponding experimental data (points). The theoretical curves were obtained by the Hauser-Feshbach method for calculating the elastic and inelastic scattering cross-sections for scattering of neutrons by a compound nucleus. The optical potential parameters used in deriving the theoretical curves in Appendix II are presented in Table 2.

All the experimental data on the differential cross-sections for elastic and inelastic scattering of neutrons and also the target nuclei characteristics were taken from Refs $\sqrt{}$1-26$\sqrt{}$.

A comparison of the parameters V_1 and V_2 in Tables 1 and 2 shows that as a rule they are in good agreement.

The satisfactory agreement of the theoretical differential cross-sections with the experimental data allows the hope that with the aid of the parameters in Table 1 it may be possible to predict with a certain degree of accuracy the differential cross-sections for elastic and inelastic scattering of neutrons by nuclei for which experimental data are still lacking. This is possible for nuclei which are characterized by a smooth dependence of the cross-sections on neutron energy (Zn and heavier nuclei). In the case of lighter nuclei it is possible to predict the cross-sections averaged over the resonances.

Table 1

$$a = 0.65 \ f; \quad b = 0.98 \ f; \quad r_o = 1.25 \ f; \quad V_3 = 6 \ MeV$$

	$E_n = 0.3$ MeV		$E_n = 0.5$ MeV		$E_n = 0.8$ MeV		$E_n = 1.5$ MeV	
	MeV		MeV		MeV		MeV	
	V_1	V_2	V_1	V_2	V_1	V_2	V_1	V_2
Na	65,0	2,0					67,0	4,6
Mg	54,5	2,0						
Al	56,0	2,0					59,0	4,6
Si	55,0	2,0	57,0	2,5	56,0	3,5	59,0	4,6
P							56,0	4,6
K	55,0	38,0					52,6	4,6
Ca							54,0	4,6
Ti			45,0	5,0				
Cr	45,0	5,0	45,0	5,0	47,0	5,0		
Fe	44,0	5,0	45,0	5,0	50,0	15,0		
Co					56,0	3,5	49,0	4,6
Ni	56,0	2,0						
Cu							49,0	4,6
Zn	53,3	2,0	54,8	2,5	56,8	3,5	48,0	4,6
Y							48,0	4,6
Zr	54,8	2,0			54,2	3,5	48,0	4,6
Nb							48,0	4,6
Cd	49,0	2,0	50,3	2,5	49,4	3,5		
Sn	47,4	2,0	48,5	2,5	47,5	3,5		
Te	47,0	2,0						
Ba			45,3	2,5	44,3	3,5		
Au							46,0	4,6
Hg	47,5	2,0	45,0	2,5	46,0	3,5		
Pb	45,5	2,0	45,0	2,5	45,0	3,5	45,0	4,6
Bi	46,5	2,0	45,0	2,5	45,0	3,5		
Th							41,0	4,6
U	41,8	2,0	41,0	2,5	40,0	3,5		

Table 2

a = 0.65 f; b = 0.98 f; r_o = 1.25 f; V_3 = 6 MeV

Nucleus	MeV		
	E_n	V_1	V_2
Na^{23}	0,98	66,0	4,0
	1,50	67,0	4,6
V^{51}	1,61	49,8	4,7
Mo^{95}	0,78	59,0	3,5
Ag^{107}	1,10	50,0	4,1
Ta^{181}	0,71	42,5	3,2
W^{184}	0,50	42,9	2,5
Th^{232}	0,56	41,7	2,7
U^{238}	0,55	40,8	2,7

Key to Figures (Appendix I and II)

Мэв   = MeV

мб/стер = mb/sr

θи.м.   = Centre of mass angle (cma)

$\xi_{ур}$ = Level

Appendix 1
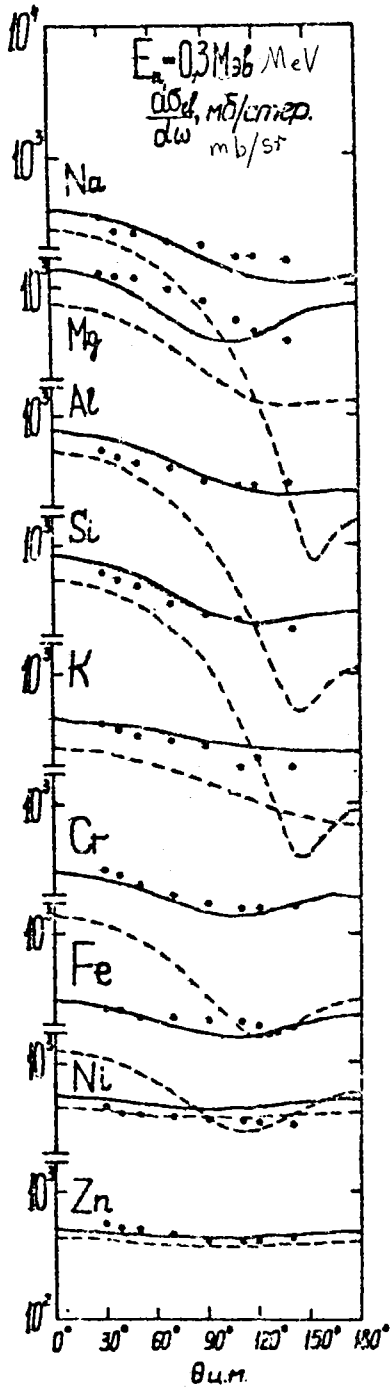
Fig. 1
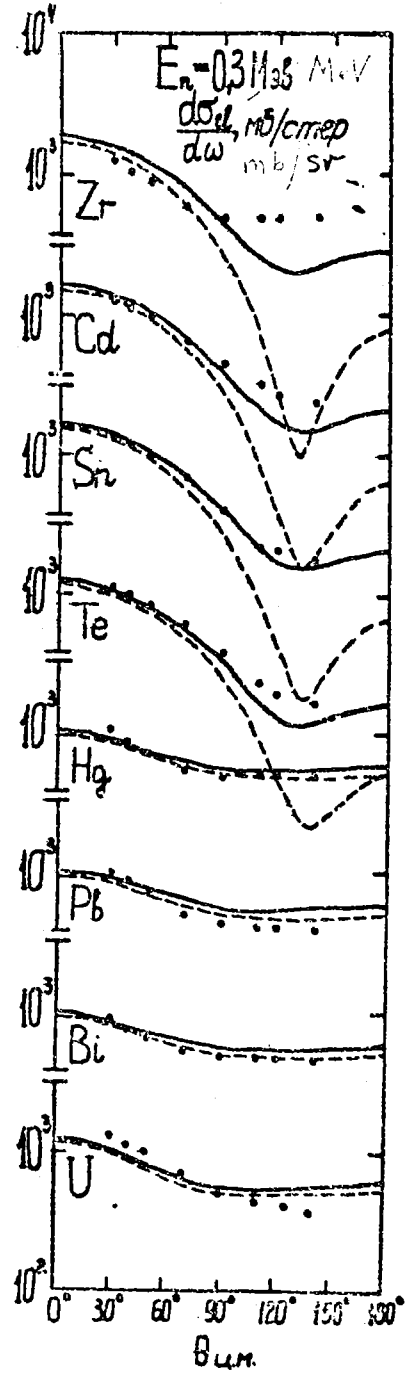
Fig. 2
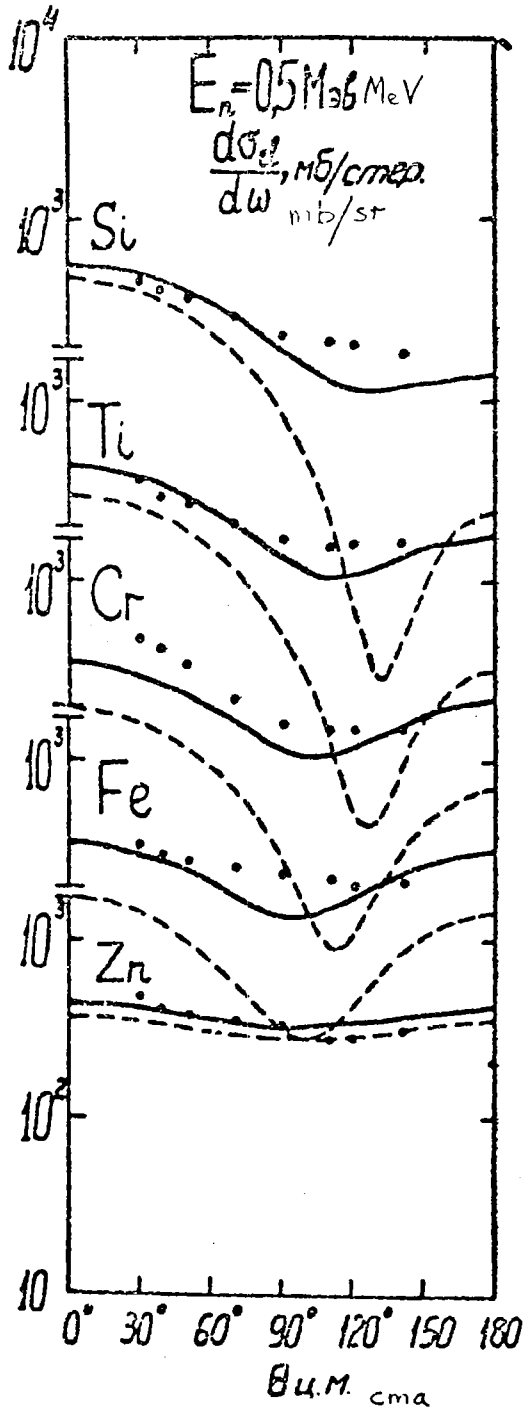
Fig. 3
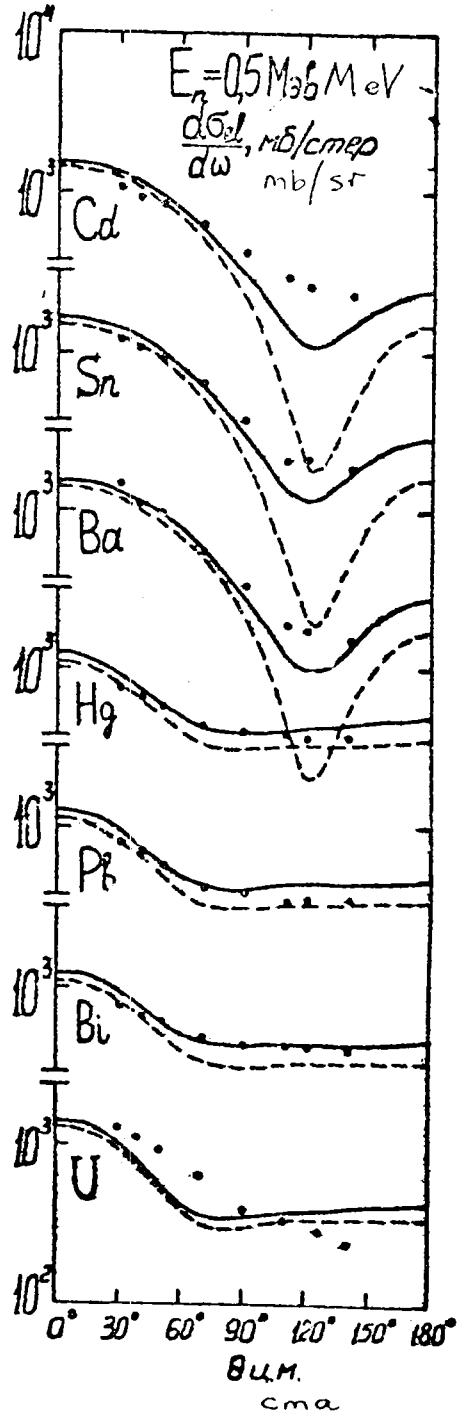
Fig. 4
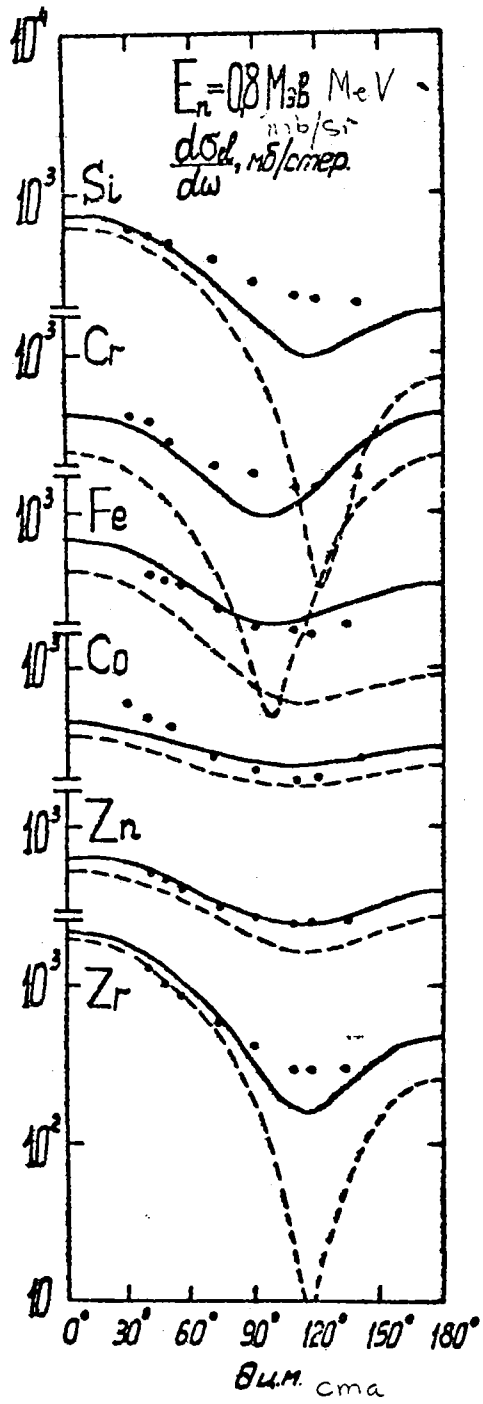
Fig. 5
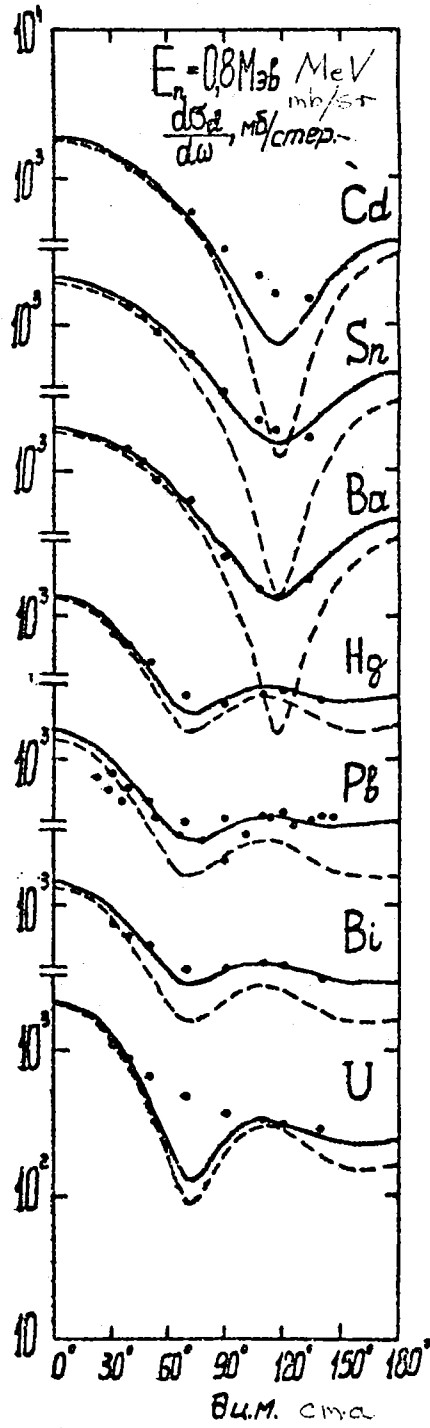
Fig. 6
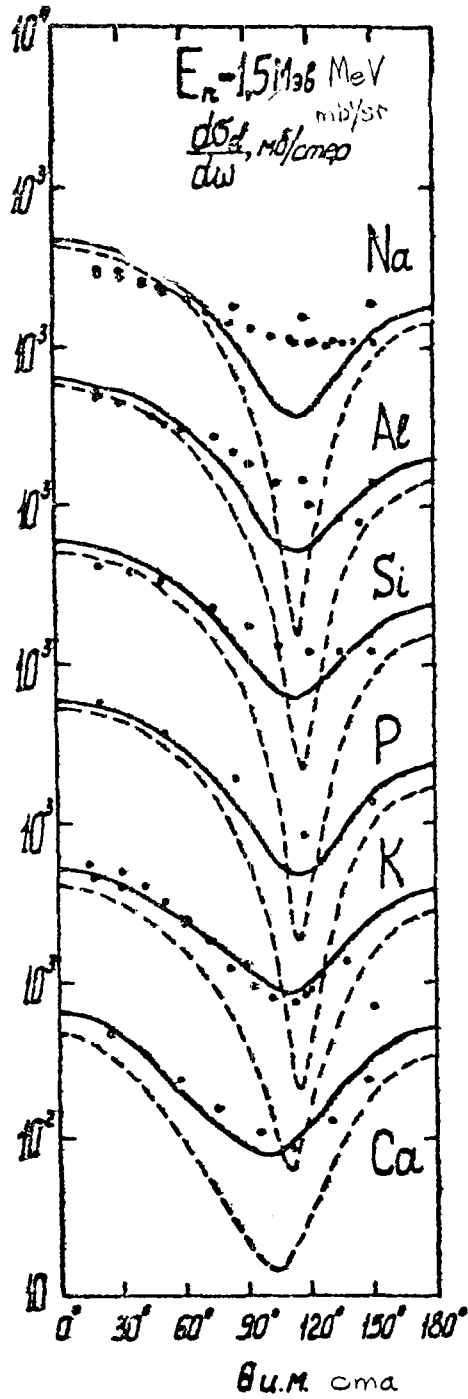
Fig. 7
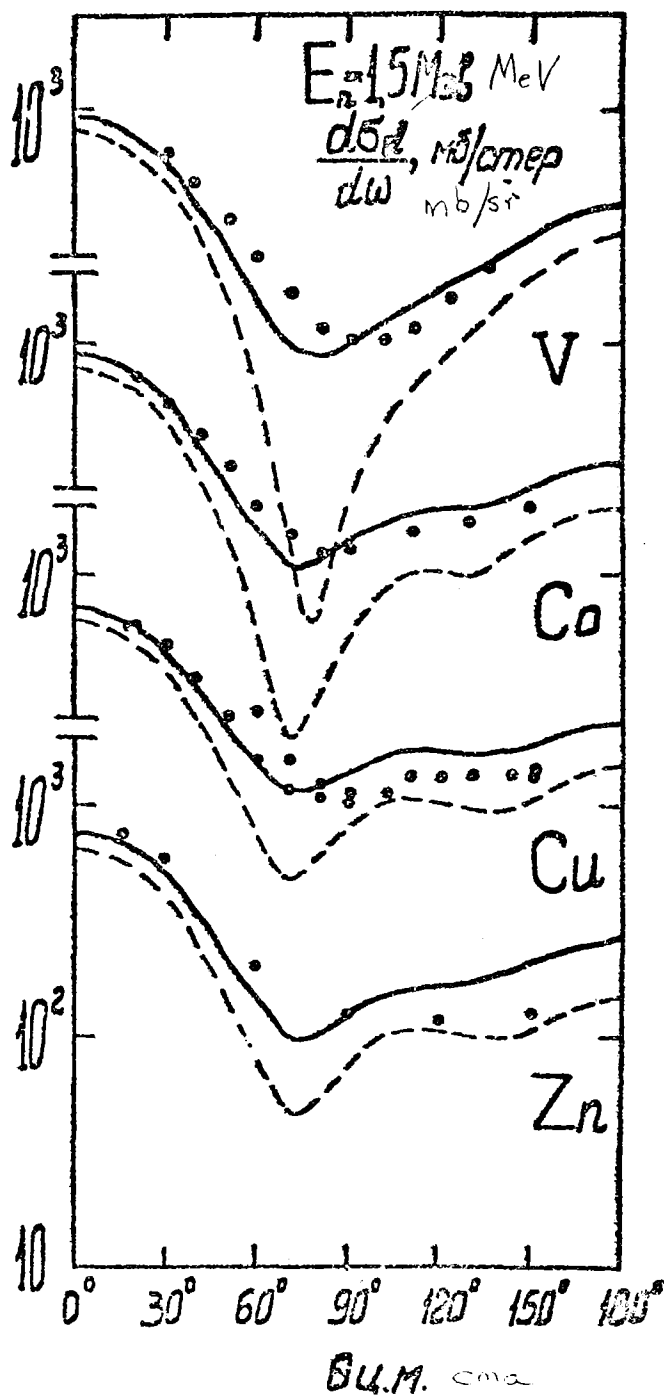
Fig. 8
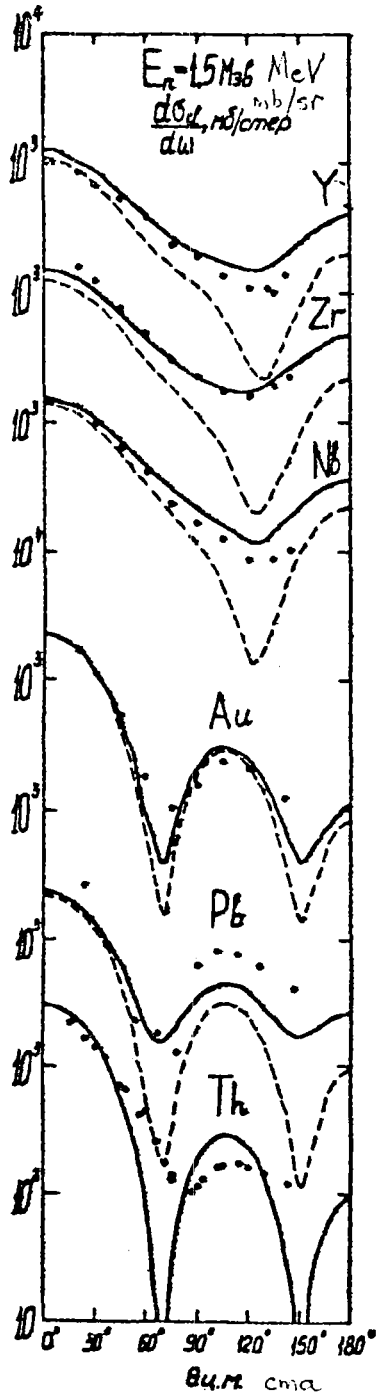
Fig. 9

Appendix II
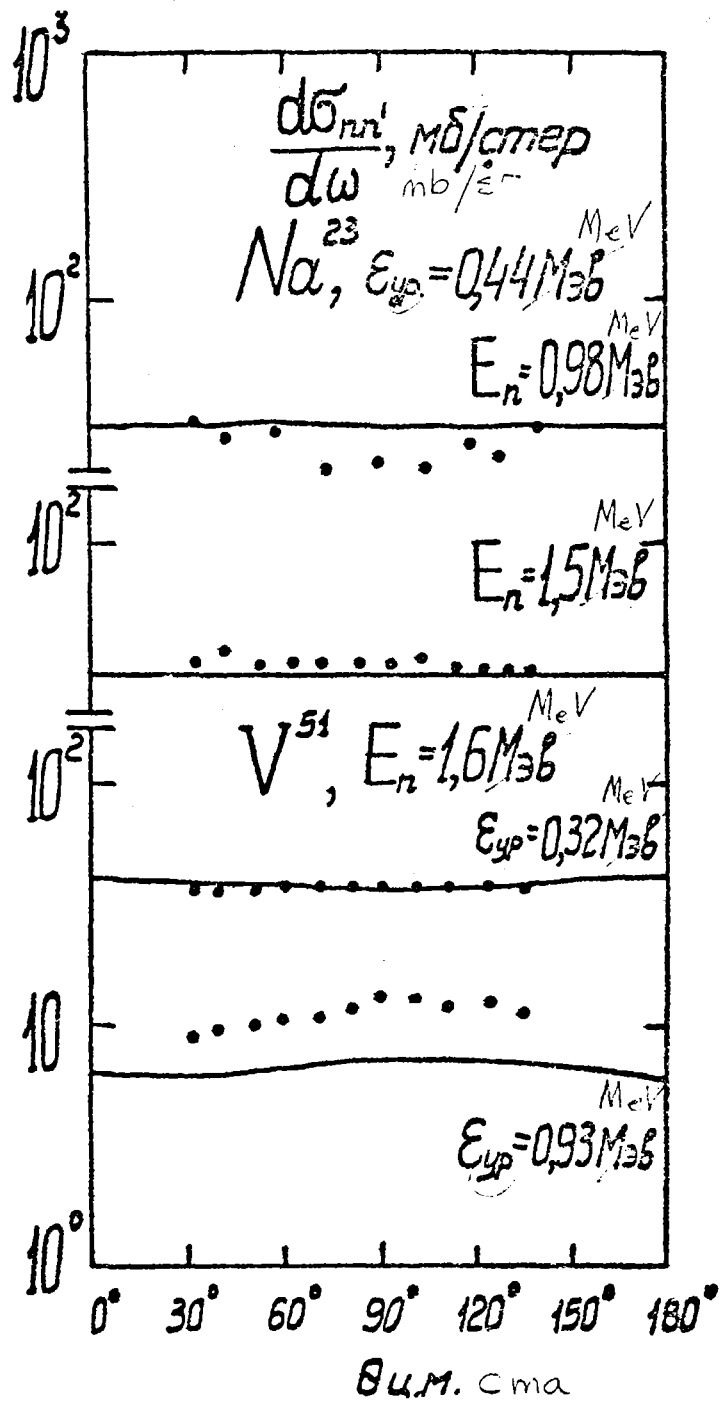
Fig. 1
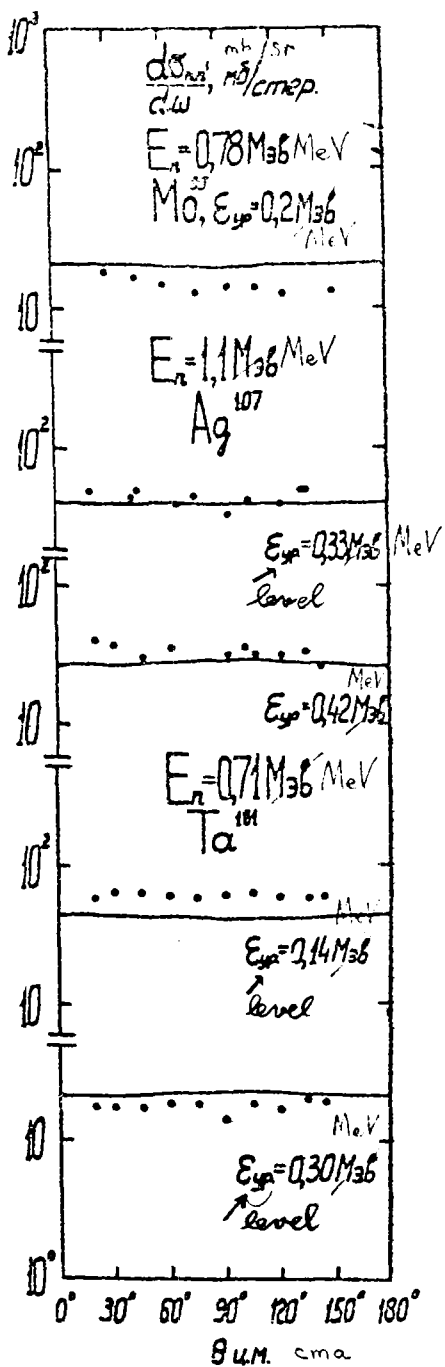
Fig. 2
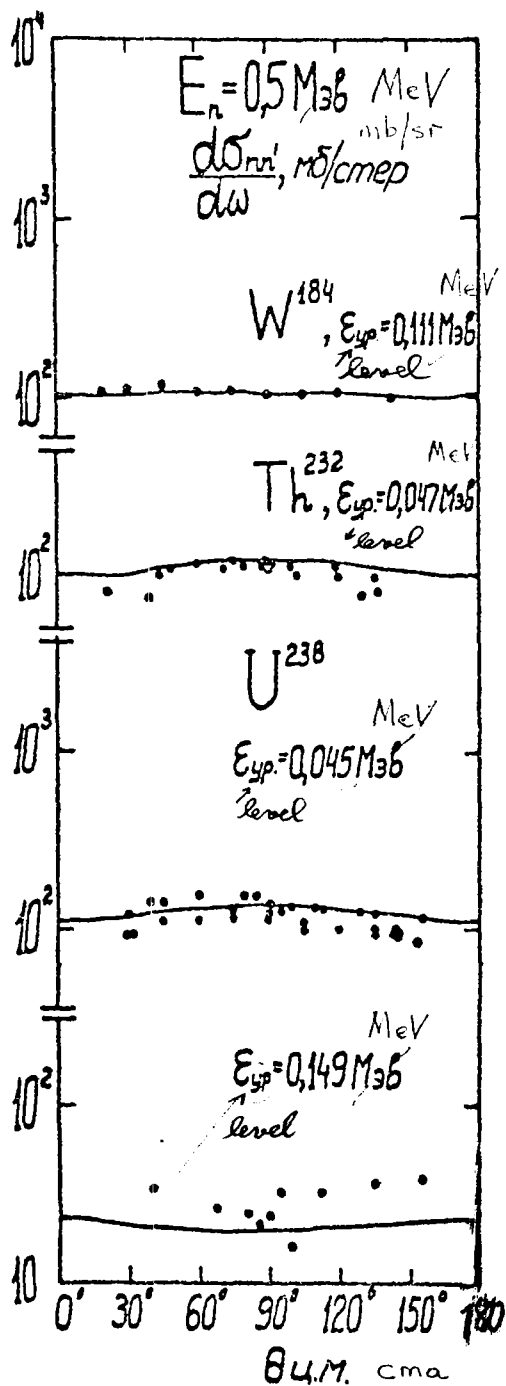
Fig. 3

REFERENCES

[1] DARDEN, S.E., PERKINS, R.B., WATSON, R.B., Phys. Rev., 100 (1955) 1315.

[2] CRANBERG, L., LEVIN, J.S., Phys. Rev., 109 (1958) 2063.

[3] SMITH, A.B., Phys. Rev., 126, (1962) 718.

[4] TOWLE, J.H., GILBOY, W.B., Nucl. Phys., 32 (1962) 610.

[5] CASWELL, R.S., J. Res. Nat. Bur. Standards, A66 (1962) 389.

[6] REITMANN, D., ENGELBRECHT, C.A., SMITH, A.B., Nucl. Phys. 48 (1963) 593.

[7] SMITH, A.B., Z. Phys., 175 (1963) 242.

[8] KORZH, I.O., SKLYAR, M.T., Ukr. fiz. Ž 8 (1963) 1389.

[9] BNL-400, Second Edition, 1963.

[10] KORZH, I.O. et al., Ukr. fiz. Ž 9 (1964) 577.

[11] KORZH, I.O. et al., Ukr. fiz. Ž 9 (1964) 929.

[12] PASECHNIK, M.V. et al., Atomn. Energ. 16 (1964) 207.

[13] Bjul. inf. Centr. jad. Dannym, Issue No. 1 (1964).

[14] ELWYN, A.J., MONAHAN, J.E., LANE, R.O., LANGSDORF, A., Nucl. Phys., 59 (1964) 113.

[15] TOWLE, J.H., GILBOY, W.B., Nucl. Phys., 72 (1965) 515.

[16] CHIEN, J.P., SMITH, A.B., Nucl. Sci. Engng., 26 (1966) 500.

[17] FOWLER, J.L., Phys. Rev., 147 (1966) 870.

[18] BARNARD, E., FERGUSON, A.T.G., McMURRAY, W.R., VAN HEERDEN, I.J., Nucl. Phys., 80 (1966) 46.

[19] KORZH, I.O. et al., Ukr. fiz. Ž 11 (1964) 563.

[20] Bjul. inf. Centr. jad. Dannym, Issue No. 3 (1966).

[21] SMITH, A.B., HAYES, R., Nucl. Phys., A93 (1967) 609.

[22] Bjul. inf. Centr. jad. Dannym, Issue No. 4 (1967).

[23] TOWLE, J.H., Nucl. Phys., A117 (1968) 657.

/ 24 /   FASOLI, U., TONIOLO, D., ZAGO, G., BENZI, V., Nucl. Phys.,
          A125 (1969) 227.

/ 25 /   HOLMQVIST, B., Ark. Fys., 38 (1969) 403.

/ 26 /   DZHELEPOV, B.S., PEKER, L.K. Shemy raspada radioaktivnyh jader
          (Decay schemes of radioactive nuclei), A-100, izdat. "Nauka"
          Moscow (1966).

          DZHELEPOV, B.S. et al., Shemy raspada radioaktivnyh jader
          (Decay schemes of radioactive nuclei), A-100, izdat. Acad.
          Nauk SSSR, Moscow, 1963.

OPTIMUM PARAMETERS OF THE NEUTRON OPTICAL POTENTIAL OF THE ^{238}U NUCLEUS

G.V. Anikin, A.G. Dovbenko, L.Ya. Kazakova, V.E. Kolesov,
V.I. Popov, G.N. Smirenkin, A.S. Tishin

Introduction

In the 20 years which have passed since the first papers on the optical model appeared $\sqrt{}$1, 2$\sqrt{}$, it has become common practice to calculate the cross-sections for the interaction of fast neutrons with different nuclei by a method based on solution of the Shroedinger equation with complex potential. Essentially the optical model is the only sufficiently universal means of calculation capable of reproducing the main features of the experimental data on fast neutron scattering which characterize the entrance channel of a reaction.

With the statistical theory first developed by Hauser and Feshbach $\sqrt{}$3$\sqrt{}$ it is also possible to calculate the cross-sections of the inelastic processes accompanying the formation of a compound nucleus. Thus with suitable development the optical model could become the basis for a theoretical description and evaluation of experimental data on the neutron cross-sections of a wide range of elements which are very important for reactor construction.

A detailed description of the various nuclear reactions requires knowledge of the "sticking" probabilities $T_{\ell,j}$ for different values of the orbital and total moments, imparted by a neutron to a compound nucleus. In the optical calculation the probabilities $T_{\ell,j}$ are obtained quite naturally. However, in Ref. $\sqrt{}$4$\sqrt{}$ it is shown that their values depend very much on the shape and values of the parameters of the optical potential employed. Unfortunately, there is as yet no agreement as to what the analytical form or the potential parameters in the optical model should be. It is true that definite progress has been made in the interpretation of the optical potential. Some authors have tried to obtain it from the familiar characteristics of the nucleon-nucleon interaction (see for example Ref. $\sqrt{}$5$\sqrt{}$). But in most cases we find a purely practical approach to the problem, based on a desire to find a good, and as far as possible economic, means of approximating experimental results of a particular kind; in this respect our study is no exception. Our main problem was to find an optical potential for ^{238}U which would provide a more or less reliable basis for calculating neutron cross-sections, in particular for channel analysis of the fission process and also for interpreting

experimental data on small-angle neutron scattering $[6]$. ^{238}U was chosen as one of the heavy nuclei which have been subjected to the most thorough experimental investigation. Besides, the use of an optical model and its physical substantiation are in practice closely related problems.

An important physical criterion of the optical potential is its universality in the sense that for a given nucleus the same potential parameters must at least give the best fit of the theoretical values to the experimental ones for different types of interaction cross-sections. In the ideal case the potential selected for the best description of the entrance channel characteristics, for example the total cross-sections, should automatically provide good agreement between other theoretical cross-sections and the experimental values.

In our work, potentials derived from the condition that they must give the best description of the total cross-sections and the angular distributions of elastically scattered neutrons, are further evaluated in terms of their description of inelastic scattering.

Recently developed non-local interaction theories $[7]$ indicate that the parameters of the local potential should have a specific energy dependence. The dependence observed in practice applied only to the real part of the potential. For the bulk of the imaginary part it is usual to obtain an increase with rising neutron energy instead of the predicted decrease $[8]$.

The ^{238}U nucleus is non-spherical. For such nuclei there exist cross-section calculations based on the use of a generalized optical model $[9]$. Experience shows that calculations involving a non-spherical potential are very time-consuming even when modern computers are used $[10]$.

Bearing in mind above all the convenience of practical evaluations and calculations, we have concentrated our attention here on finding the average parameters of a potential in simple form, in the range of energies relevant to fast reactor physics. In selecting the parameters we considered experimental data on the scattering of 0.075-15.2 MeV neutrons.

The energy-independent parameters for the ^{238}U nucleus published earlier by Auerbach and Moore $[11]$ relate to a narrower energy range (0.57-1.25 MeV). It is undesirable to use these parameters beyond the limits of the stated range $[4]$, since they give a low value of the cross-section for the formation of a compound nucleus.

Procedure for fitting the parameters

The shape of the optical potential was selected as

$$-U_o = V_o \cdot f(r) + i(W_1 \cdot f(r) + W_2 \cdot g(r)) + V_{so} \cdot h(r)\vec{\ell}\vec{\sigma} \ .$$

The form factor of the real part of the potential is written in the usual form proposed by Woods and Saxon:

$$f(r) = \left[1 + \exp\left(\frac{r - R_1}{a}\right) \right]^{-1} \ .$$

It is also used for the "volume" component of the absorption term, which includes moreover a second component allowing for the contribution of "surface" absorption. The radial dependence of the latter is in the form of a derivative of the real part:

$$g(r) = 4 \exp\left(\frac{r - R_2}{b}\right) / \left[1 + \exp\left(\frac{r - R_2}{b}\right) \right]^2 \ .$$

However, this expression includes additional parameters — the radius R_2, which determines the localization of the absorption peak, and the parameter b defining the width of this peak. The Thomas form is used in the spin-orbital term for $h(r)$:

$$h(r) = \left(\frac{\hbar}{m_\pi c}\right)^2 \frac{1}{r} \left| \frac{df(r)}{dr} \right| \ .$$

In these formulae $R_1 = r_1 \sqrt[3]{A}$, $R_2 = r_2 \sqrt[3]{A}$, A is the atomic weight of the nucleus, m_π is the mass of a π-meson, c is the velocity of light and $\hbar$ is Planck's constant.

Calculation of the cross-sections and the fitting of the parameters was done with a programme similar to that published in the paper by Popov et al. $\boxed{12}$. The potential parameters were selected solely on the basis of experimental data characterizing the reaction entrance channel, i.e. the total cross-section and the angular distributions of elastically scattered neutrons.

The calculated angular distributions included a correction for elastic scattering by a compound nucleus. This correction, which is quite considerable at low energies, was calculated semi-empirically as the difference between the calculated cross-section for the formation of a compound nucleus and the experimental cross-section for inelastic interactions divided by 4π, with the assumption of isotropic scattering.

The automatic procedure for fitting the parameters may be summed up as follows:

1. The initial potential was used to calculate the total and differential cross-sections for 14 neutron energies in the chosen energy range. Then we estimated the sum of the squares of the relative deviations of the theoretical curves from the experimentally determined cross-sections, i.e.

$$H^2 = H_1^2 + H_2^2 = \frac{1}{14} \left[\frac{1}{N} \sum_{n=1}^{14} \sum_{i=1}^{N} \left(\frac{\sigma^{exp.}(\vartheta_i, E_n) - \sigma^{theor.}(\vartheta_i, E_n)}{\sigma^{exp.}(\vartheta_i, E_n)} \right)^2 \right.$$
$$\left. + B \cdot \sum_{n=1}^{14} \left(\frac{\sigma_t^{exp.}(E_n) - \sigma_t^{theor.}(E_n)}{\sigma_t^{exp.}(E_n)} \right)^2 \right]$$

(1)

    The factor B allows for the best statistical accuracy of the experimental total cross-sections compared with the angular distributions;

2. A test method was used to determine the direction of variation of one of the parameters in which H decreases. In the selected direction the parameter was varied successively 2-3 times by a standard step, the value of which was selected separately for each parameter. If the relative minimum in H was not attained, the step was doubled but the change of a given parameter with increased step was continued only in the following parameter variation cycle whereupon the same procedure was repeated for another parameter;

3. If the step exceeded the standard value in reaching the relative minimum for any of the parameters, it was halved until the position of the minimum could be found with the accuracy of the standard step. For the parameters V_o, V_{so}, W_1 and W_2 the standard step was 0.1 MeV and for the parameters a, r_1 and r_2 it was 0.01 f. Attainment of the absolute minimum was noted by the absence of a reduction in H with variation of any of the parameters in either of the two directions.

It should be noted that at the end of the H^2 minimizing process it is more economical to use the other procedure included in the programme, whereby the transition to the following parameter is made only after the relative minimum is attained. This reduces the number of tests.

The programme provides for limiting the variation of a parameter if the rate of decrease in the sum H^2 does not exceed a given level. It is clearly advantageous to use this procedure in two cases – at the commencement of the operation, when it is desirable to segregate the group of parameters which have the strongest effect on the minimization process (we shall call these "strong" parameters), and in the case where one of the parameters has a tendency to drift into the physically unreal region without any significant improvement in the approximation of the experimental data. This situation often occurs with "weak" parameters, for example the spin–orbit parameter.

The use in our programme of the quantity H^2 instead of the more usual χ^2, where the errors in the experimental values come under the summation sign in the denominator, derives, on the one hand, from the absence of errors in a certain number of the angular distributions employed and, on the other hand, from a desire to assign slightly more weight to the differential cross–sections at large scattering angles. The latter contain much more information about the detailed structure of the optical potential than the first diffraction peak, although it makes a major contribution to the integral elastic scattering cross–section.

Results

The form of the optical potential used here enables three of·its variants to be investigated, i.e. potentials with purely surface absorption ($W_1 = 0$), purely volume absorption ($W_2 = 0$) and combined absorption ($W_1 \neq 0, W_2 \neq 0$). The investigation was performed as follows. For the surface and volume variants we found those sets of parameters which gave the best approximation of the total cross–sections alone ($B = 10^6$) and the angular distributions alone ($B = 0$) as well as sets which took both these groups of experimental data into account ($B = 9$). The groups of parameters obtained are given in Table 1, the top line of which shows the values of B (see formula (1)) that determine the nature of the experimental data to which the corresponding group of parameters relates. The factor $B = 9$ means that the accuracy with which we know the total cross–sections is at least three times better than the accuracy of the angular distributions.

It should be noted that the attempt to describe the total cross–sections alone did not yield a set of parameters with combined absorption. The automatic search gave either surface or volume absorption.

The last two lines of the table show figures for H_1 and H_2, i.e. the standard deviations of the theoretical curves from the experimental values (for the total cross-sections this is the averaged curve).

Figs 1-3 show cross-sections calculated with the parameters from Table 1 and compare them with experimental data taken largely from Refs $\boxed{13\,\boxed}$ and $\boxed{14\,\boxed}$. Fig. 4 reproduces inelastic neutron scattering cross-sections with excitation of different levels of the ^{238}U nucleus, also in comparison with experimental data. As in Fig. 3, the results are given for a group of parameters selected with the coefficient B = 9 for the three types of absorption. The cross-sections $\sigma(n,n')$ were calculated using the programme of Kolesov and Dovbenko $\boxed{15\,\boxed}$, compiled with allowance for the Hauser-Feshbach statistical theory but with no allowance for level width fluctuations.

Discussion of results

1. The main conclusion to be drawn is that for a ^{238}U nucleus it is possible to find groups of parameters which, on average, satisfactorily reproduce the experimental data on neutron scattering over the whole range of energies relevant to reactor physics.

2. If the object is to describe all the experimental data on scattering, the best results are supplied by the potential with combined absorption. Generally speaking, the difference in the results obtained with the three types of parameters is quite small and each individual type of cross-section can be reproduced by any of them.

3. From Table 1 it can be seen that the groups with B = 0 and with B = 10^6 differ appreciably, especially in regard to the parameter a. A possible reason for this is the non-spherical nature of the ^{238}U nucleus, which was not allowed for in our calculation. It may be that for reproducing the angular distributions it is essential to have a sharper nuclear boundary, whereas the total cross-section of prolate and chaotically grouped nuclei as a whole can be effectively described by a potential with a more blurred edge.

4. Around 15-18 MeV in the case of the spin-orbit coupling, as can be seen from Table 1, there is an individual isolated minimum in the value of H^2, if the search is performed with B = 0 or B = 9, i.e. allowing for the angular distributions. The reason for this is as follows: in the range around 15-18 MeV the parameter V_{so} fluctuates when we try to follow the energy dependence of the parameters of any of the three potentials without defining any one of them. However, with such values of the spin-orbit parameter it is impossible to get a good description of the total cross-sections with an energy-independent optical potential.

Of course, in the search for a compromise it is the "weak" parameters which are farthest from their true values. Besides, the real value of the parameter V_{so} can be established only with the aid of neutron polarization data.

5. Note that in the 0.6–2 MeV energy range the theoretical curves badly reproduce the experimental angular distributions. In Ref. $\boxed{11}$ there is an analogous situation with energies of 1.17 and 1.25 MeV, although the parameters in that case were selected for a narrower energy range. If we assume variation of the parameters with energy, an ideal description of the experimental angular distributions is possible for virtually all the neutron energies under consideration here. However, some of the parameters reveal an energy dependence which is difficult to explain physically. Thus, for example, the parameter a in the potential with volume absorption at energies 0.6–1.25 MeV decreases to 0.2–0.3 f. With surface absorption in the same energy range the parameters W_2 and V_{so} increase 3 or 4 times. Without excluding the possibility of errors in the experimental data, we may take it that the irregularity in the variation of the parameters probably arises from the simplified form of the interaction potential.

Table 1

Neutron optical potential groups

Absorption	Surface				Volume				Combined	
No. of group	I	II	III	IV	I	II	III	IV	II	III
B	10^6	9	9	0	10^6	9·	9	0	9	9
V_0, MeV	41,5	43,2	41,9	43,3	44,3	43	39,1	42,2	40,9	38,9
τ_1, f	1,31	1,28	1,3	1,29	1,25	1,26	1,35	1,31	1,31	1,35
a, f	0,36	0,29	0,25	0,27	0,6	0,56	0,36	0,3	0,46	0,31
W_1 MeV	–	–	–	–	3,6	4,5	4,2	5	2,1	1,5
W_2 MeV	4	4,7	5,6	10	–	–	–	–	5	5
τ_2 f	1,17	1,17	1,05	1,1	–	–	–	–	1,06	1,26
b, f	0,95	1,0	0,95	0,72	–	–	–	–	0,72	0,64
V_{so} MeV	4,9	3,3	17,8	18,5	0	3,1	14,9	17	0	16,4
H^2	0,137	0,077	0,054	0,037	0,1	0,057	0,058	0,04	0,061	0,054
$H_a^2 \times 10^{-3}$	0,17	1,2	3,6	7	0,79	1,2	2,2	9,7	0,64	1,4
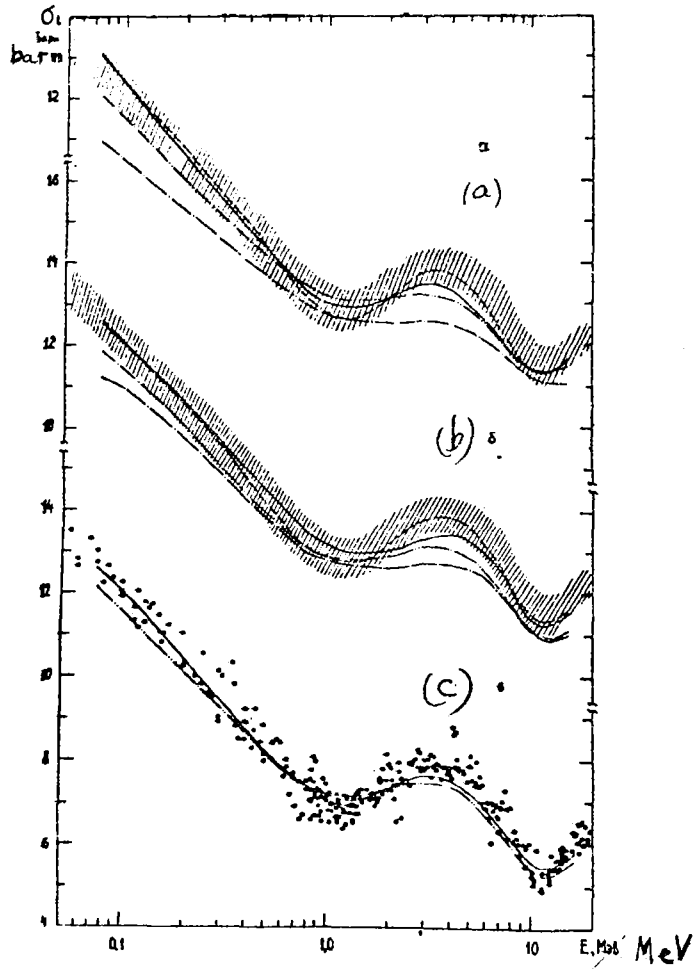
Fig. 1   Total interaction cross-sections for ^{238}U calculated
with volume (a), surface (b) and combined (c) absorption.
The theoretical curves correspond to the parameter group
numbers given in Table 1:

— — — I, ——— II, —— · · —— III, —— · —— IV.
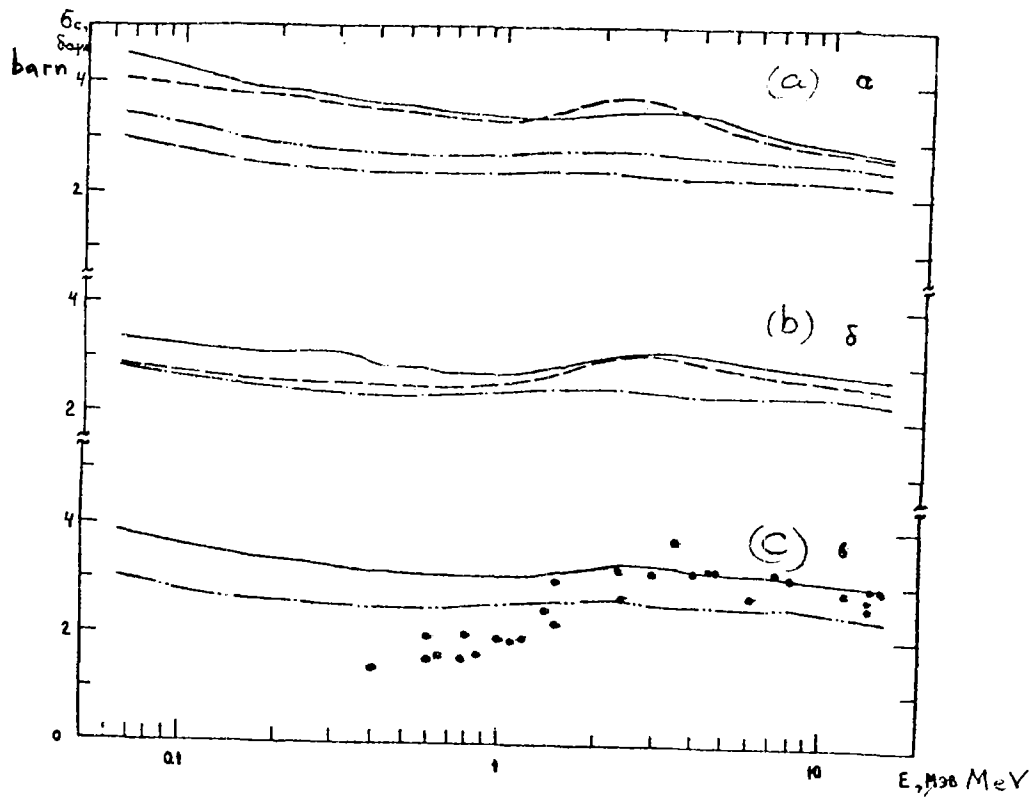
Fig. 2   Cross-sections for the formation of a compound nucleus.
The notation is the same as in Fig. 1.   The experimental
points represent the total inelastic interaction cross-
section.
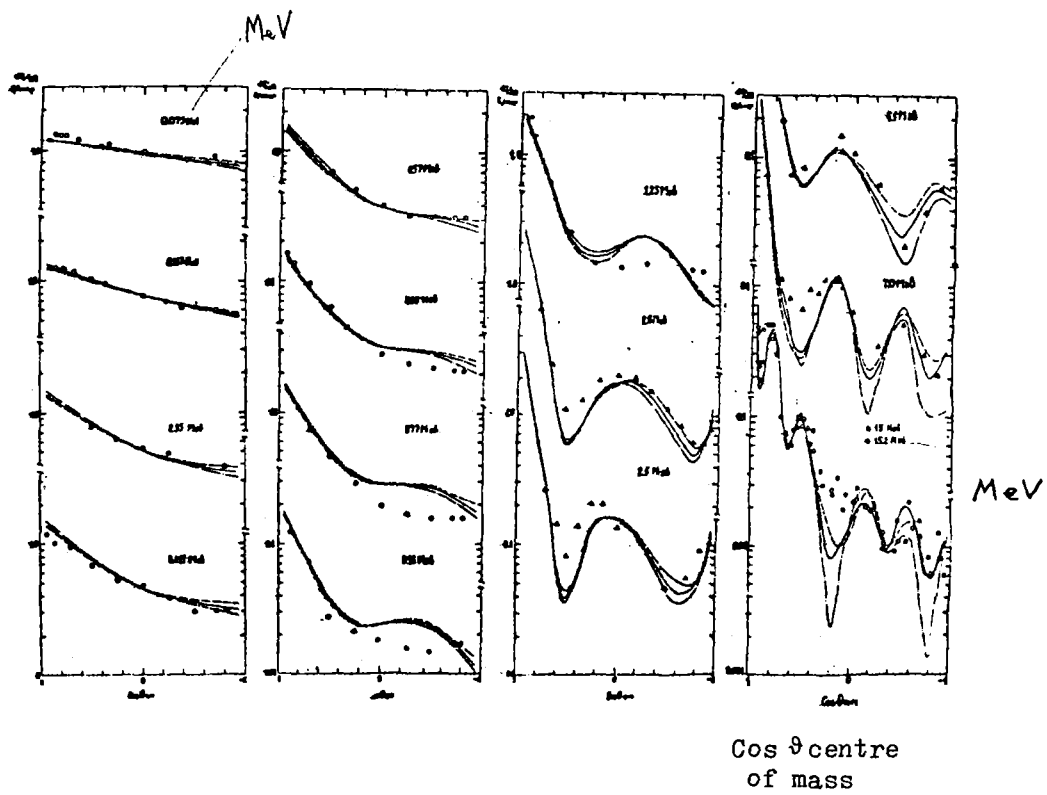
Fig. 3 Angular distributions of elastically scattered neutrons.
The theoretical curves are given for the No. II group
of parameters with combined (————), volume (— — —)
and surface (— · —) absorption.
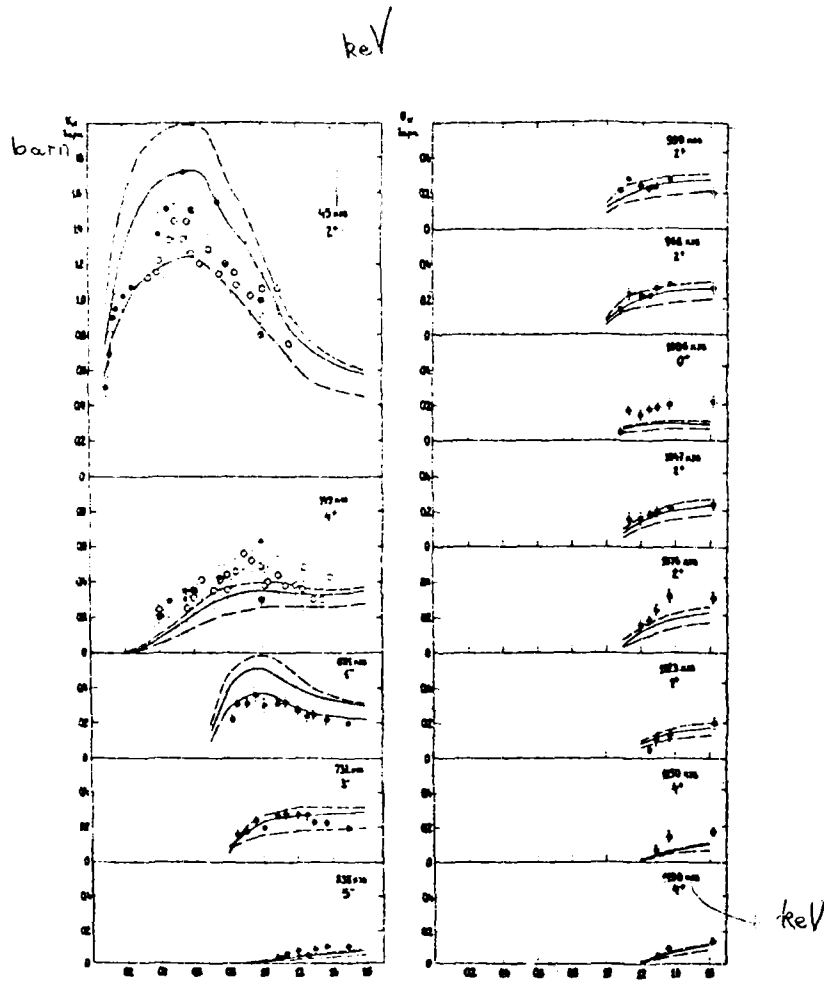
Fig. 4 Excitation functions of various ^{238}U levels. The notation for the theoretical curves is the same as in Fig. 3.

REFERENCES

_[1_]_ FERNBACH, S., SERBER, K., TAYLOR, T.B., Phys. Rev., 75 (1949) 1352.

_[2_]_ FESHBACH, H., PORTER, C.E., WEISSKOPF, V.F., Phys. Rev., 95 (1954) 448.

_[3_]_ HAUSER, W., FESHBACH, H., Phys. Rev., 87 (1952) 366.

_[4_]_ ERMAGAMBETOV, S.B. et al., Jadernaja fizika 8 (1968) 704.

_[5_]_ JOMES, L.S., Phys. Rev., 116 (1959) 1226.

_[6_]_ ANIKIN, G.V., ALEXANDROV, Yu.A., SOLDATOV, A.S., Intern. Conf. Nucl. Struct. (Antwerp, 1965).

_[7_]_ PEREY, F.G.J., BUCK, B., Nucl. Phys., 32 (1962) 353.

_[8_]_ HODGSON, P.E., Optičeskaja model'uprugogo rassejanija (Optical model of elastic scattering), Atomizdat (1966).

_[9_]_ AVERYANOV, I.K. et al., Jadernaja fizika 7 (1968) 1221.

_[10_]_ TAMURA, T., Rev. mod. Phys., 37 (1965) 679.

_[11_]_ AUERBACH, E.H., MOORE, S.O., Phys. Rev., 135, 4B (1964) 895.

_[12_]_ POPOV, V.I. et al., Bjul. inf. Centr. jad. Dannym, Atomizdat, Issue No. 4 (1967) 327.

_[13_]_ Neutron Cross-sections, BNL-325, v.3, Suppl. 2 (1935).

_[14_]_ Bjul. inf. Centr. jad. Dannym, Issue No. 1-4 (1964).

_[15_]_ KOLESOV, V.E., Bjul. inf. Centr. jad. Dannym, Moscow, Atomizdat, Issue No. 1 (1964) 402.

DIFFERENTIAL CROSS-SECTIONS FOR INELASTIC SCATTERING OF NEUTRONS BY Cr, Mn, Fe, Co, Ni, Cu, Y, Zr, Nb, W AND Bi NUCLEI

G.N. Lovchikova, O.A. Salnikov, G.V. Kotelnikova
A.M. Trufanov, N.I. Fetisov

Introduction

This paper supplies differential cross-sections for inelastic scattering of neutrons in the form of graphs and tables for an initial neutron energy of 14.36 MeV.

The differential cross-sections were measured at 30° intervals over the neutron scattering angle range 31°–151° with an uncertainty in the angle of $\Delta\vartheta = \pm 8^\circ$. The energy spread due to this uncertainty and to the thickness of the target was 0.14 MeV, so that the initial neutron energy was 14.36 ± 0.14 MeV.

The measurements were performed by the time-of-flight method in cylindrical geometry, the resolving time of the spectrometer was 5–8 nsec, the flight path was 2 m and the neutron recording threshold ~ 100 keV. The spectrometer is described in more detail in Ref. $\llcorner 1 \lrcorner$.

The differential cross-sections incorporate corrections for multiple scattering and neutron flux attenuation in the sample; these were calculated by the Monte Carlo method.

In analysing the results it is of interest to consider the angular distribution of scattered neutrons as a function not only of the scattering angle ϑ but also their energy, i.e. $\sigma(E_0, E, \vartheta)$. For this reason the experimentally obtained spectra of inelastically scattered neutrons at different scattering angles were split up into several energy intervals — from 0 to 3.0 MeV, from 3.0 to 4.2 MeV, from 4.2 to 5.4 MeV, from 5.4 to 6.4 MeV and from 6.4 to 14.4 MeV. Differential cross-sections were calculated for each energy interval. The method of measuring the spectra and the method of processing the results are described in Refs $\llcorner 1 \lrcorner$ and $\llcorner 2 \lrcorner$.

The data on the angular distributions of inelastic neutron scattering are given in the form of a series $\llcorner 3 \lrcorner$: $\sigma(\mu) = \frac{1}{4\pi} \sum_{l=0}^{\infty} a_l P_l(\mu)$, where a_l is the expansion coefficient, P_l is the Legendre polynomial of order l and μ is $\cos\vartheta$.

Three terms of the expansion were sufficient for representing the existing angular distributions. The curves drawn through the experimental points resulting from analytical expansion of the angular distributions in a Legendre polynomial series are shown in Figs 1-11.

Table 1 shows the Legendre polynomial expansion coefficients.

The differential cross-sections obtained by the authors are shown in Table 2. The errors indicated on the graphs and in the tables are the mean square statistical errors which do not include the error of the cross-section for scattering by carbon.

The uncertainty in the normalization of the spectra to scattering by carbon is 10%. Figs 12-14 compare the differential cross-sections for cobalt, zirconium and bismuth measured by other authors $\sqrt{4\_7}$ and the differential cross-sections obtained by the present authors for approximately the same energy ranges (denoted by black dots).

In conclusion the authors wish to thank M.D. Bityutskaya and E.S. Chernichenko for their help with the calculations and with the formulation of the data.

REFERENCES

$\sqrt{1\_7}$ SALNIKOV, O.A. et al., Preprint No. 216 of the Institute of Physics and Power Engineering (1970).

$\sqrt{2\_7}$ SALNIKOV, O.A. et al., in Nuclear Data for Reactors (Proc. Conf. Helsinki, 1970) 2 IAEA, Vienna (1970) 359.

$\sqrt{3\_7}$ NIKOLAEV, M.N., BAZAZYANTS, N.O., Bjul. inf. Centr. jad. Dannym. Atomizdat, Issue No. 4 (1967) 216.

$\sqrt{4\_7}$ GOLDBERG, M.D., MAY, V.M., STEHN, J.R., "Angular distributions in neutron-induced reactors" BNL-400 (1962)

Table 1

Coefficients for expanding the differential cross-sections in Legendre polynomial series

Element	Chromium			Manganese			Iron		
Energy range, MeV	a_0	a_1	a_2	a_0	a_1	a_2	a_0	a_1	a_2
3,0 + 4,2	0,188	0,0502	0,0132	0,203	0,0470	0,026	0,191	0,0442	0,0066
4,2 + 5,4	0,110	0,0374	0,0071	0,113	0,0241	0,019	0,117	0,0280	0,0044
5,4 + 6,4	0,069	0,0264	0,0043	0,068	0,0132	0,013	0,077	0,0178	0,0013
6,4 + 14,4	0,199	0,0877	0,0205	0,167	0,0223	0,045	0,230	0,0438	-0,0295
0 + 14,4	1,419	0,2460	0,0612	1,608	0,1395	0,146	1,614	0,2376	0,0071

Element	Cobalt			Nickel			Copper		
Energy range, MeV	a_0	a_1	a_2	a_0	a_1	a_2	a_0	a_1	a_2
3,0 + 4,2	0,215	0,0399	0,0211	0,128	0,0355	0,0138	0,2143	0,0538	0,0109
4,2 + 5,4	0,116	0,0238	0,0146	0,072	0,0214	0,0106	0,1237	0,0365	0,0049
5,4 + 6,4	0,069	0,0154	0,0110	0,045	0,0139	0,0081	0,0786	0,0269	0,0009
6,4 + 14,4	0,183	0,0521	0,0470	0,134	0,0445	0,0352	0,2269	0,1165	0,0028
0 + 14,4	1,772	0,1563	0,1391	1,056	0,1827	0,1409	1,9352	0,3361	-0,0139

Table 1 (continued)

Element / Energy range, MeV	Yttrium			Zirconium			Niobium		
	a_o	a_1	a_2	a_o	a_1	a_2	a_o	a_1	a_2
3,0 + 4,2	0,229	0,0573	0,0244	0,209	0,0314	0,0251	0,270	0,0489	-0,0005
4,2 + 5,4	0,120	0,0376	0,0083	0,101	0,0213	0,0133	0,130	0,0339	0,0030
5,4 + 6,4	0,071	0,0265	0,0046	0,059	0,0151	0,0082	0,071	0,0233	0,0033
6,4 + 14,4	0,163	0,0827	0,0079	0,155	0,0518	0,0079	0,155	0,0664	0,0126
0 + 14,4	2,577	0,3395	0,2785	2,298	0,2056	0,1296	2,738	0,2214	-0,1170

Element / Energy range, MeV	Tungsten			Bismuth		
	a_o	a_1	a_2	a_o	a_1	a_2
3,0 + 4,2	0,317	0,1211	0,0141	0,4114	0,0837	0,0573
4,2 + 5,4	0,152	0,0792	0,0189	0,1705	0,0512	0,0424
5,4 + 6,4	0,086	0,0529	0,0163	0,0842	0,0319	0,0304
6,4 + 14,4	0,208	0,1580	0,0665	0,1524	0,0632	0,0656
0 + 14,4	3,474	0,6463	- 0,0557	4,0039	0,3823	0,4103

Table 2

Differential cross-sections (n,n) + (n,2n) mb/sr

Chromium

θ \ ΔE	0 - 2,98	2,98-4,22	4,22-5,37	5,37-6,43	6,43-14,32
31°	67,5±1,4	18,5±0,9	11,1±0,9	7,1±0,8	19,7±2,3
61°	74,8±1,4	17,4±0,9	10,9±0,8	7,2±0,7	22,0±1,7
91°	68,1±1,3	14,4±0,8	8,4±0,7	5,3±0,6	14,9±1,4
121°	61,2±1,2	12,2±0,7	6,7±0,6	4,1±0,5	10,4±1,2
151°	63,5±1,3	12,4±0,7	6,7±0,6	4,1±0,5	11,7±1,2

Manganese

θ \ ΔE	0 - 2,98	2,98-4,22	4,22-5,37	5,37-6,43	6,43-14,32
31°	84,2±1,6	20,4±1,0	11,3±0,9	6,7±0,8	16,1±1,7
61°	91,1±1,6	18,0±0,8	10,1±0,7	6,1±0,6	14,7±1,2
91°	80,9±1,4	14,6±0,7	7,9±0,6	4,7±0,5	10,9±1,0
121°	79,9±1,4	14,4±0,7	7,9±0,6	4,8±0,5	12,2±1,0
151°	85,9±1,5	14,0±0,7	8,3±0,6	5,2±0,5	14,1±1,0

Iron

θ \ ΔE	0 - 2,98	2,98-4,22	4,22-5,37	5,37-6,43	6,43-14,32
31°	81,7±1,8	19,5±1,2	12,7±1,2	8,6±1,1	26,8±2,8
61°	84,7±1,7	15,6±0,9	9,0±0,8	5,7±0,7	16,3±1,6
91°	82,4±1,6	16,0±0,9	10,1±0,9	6,9±0,8	21,4±1,7
121°	68,4±1,4	13,1±0,8	8,2±0,7	5,5±0,7	18,4±1,5
151°	76,1±1,6	12,5±0,8	7,5±0,7	4,8±0,6	12,9±1,2

Cobalt

θ \ ΔE	0 - 2,98	2,98-4,22	4,22-5,37	5,37-6,43	6,43-14,32
31°	93,4±1,6	20,7±0,9	11,5±0,8	7,1±0,7	19,3±2,0
61°	102,0±1,6	18,9±0,8	10,1±0,7	6,2±0,6	17,2±1,4
91°	91,6±1,5	16,0±0,7	8,4±0,6	4,9±0,5	12,3±1,2
121°	89,4±1,4	15,5±0,7	8,3±0,6	4,9±0,5	11,9±1,0
151°	97,6±1,6	15,5±0,7	8,3±0,6	5,0±0,5	13,6±1,1

Nickel

θ \ ΔE	0 - 2,98	2,98-4,22	4,22-5,37	5,37-6,43	6,43-14,32
31°	60,3±1,1	13,8±0,7	8,1±0,6	5,1±0,6	15,2±1,9
61°	58,1±1,0	10,7±0,6	6,0±0,5	3,8±0,5	11,8±1,2
91°	48,8±0,9	9,8±0,5	5,6±0,5	3,6±0,4	10,1±1,0
121°	51,0±0,9	8,9±0,5	4,7±0,4	2,9±0,4	7,7±0,9
151°	52,8±1,0	8,3±0,5	4,8±0,4	3,1±0,4	9,8±0,9

Copper

θ \ ΔE	0 - 2,98	2,98-4,22	4,22-5,37	5,37-6,43	6,43-14,32
31°	97,2±1,7	21,0±1,1	12,3±1,0	7,9±1,0	24,7±2,9
61°	123,5±2,1	19,5±1,0	11,6±0,9	7,6±0,9	23,6±2,0
91°	103,6±1,8	16,6±0,8	9,5±0,7	6,1±0,6	17,9±1,4
121°	91,4±1,5	14,5±0,7	8,3±0,6	5,1±0,6	12,7±1,2
151°	98,8±1,7	14,0±0,7	7,6±0,6	4,4±0,6	10,4±1,3

Yttrium

θ \ ΔE	0-2,98	2,98-4,22	4,22-5,37	5,37-6,43	6,43-14,32
31°	163,4±3,5	24,2±1,7	13,6±1,6	8,6±1,5	25,7±4,7
61°	177,7±3,7	18,4±1,4	9,2±1,3	5,1±1,3	10,0±3,1
91°	147,2±3,2	18,8±1,3	10,3±1,2	6,2±1,1	15,0±2,7
121°	140,9±3,2	14,8±1,3	7,9±1,2	4,6±1,1	10,4±2,7
151°	169,4±4,0	15,7±1,4	7,3±1,3	3,8±1,2	6,5±2,9

Zirconium

θ \ ΔE	0 - 2,98	2,98-4,22	4,22-5,37	5,37-6,43	6,43-14,32
31°	143,4±2,6	20,5±1,?	10,4±1,1	6,3±1,0	17,9±3,2
61°	150,9±2,6	16,8±1,0	8,4±0,9	4,9±0,8	12,7±2,0
91°	138,0±2,5	16,1±1,0	7,9±0,9	4,6±0,8	13,6±2,0
121°	130,8±2,3	15,2±0,9	7,0±0,8	3,8±0,7	9,5±1,8
151°	142,5±2,4	15,6±0,9	7,3±0,8	4,1±0,7	9,3±1,6

Niobium

θ \ ΔE	0 - 2,98	2,98-4,22	4,22-5,37	5,37-6,43	6,43-14,32
31°	154,3±2,7	24,5±1,3	12,8±1,2	7,5±1,1	17,8±3,1
61°	187,3±3,0	23,6±1,2	11,4±1,0	6,4±0,9	14,4±2,1
91°	170,8±2,8	22,0±1,1	10,5±0,9	5,7±0,8	11,8±1,7
121°	159,1±2,7	18,6±1,0	8,6±0,8	4,6±0,8	9,6±1,7
151°	162,8±2,7	18,5±1,0	8,3±0,8	4,3±0,7	8,3±1,6

Tungsten

θ\ΔE	0 - 2,98	2,98-4,22	4,22-5,37	5,37-6,43	6,43-14,32
31°	216,5±4,3	34,7±2,3	18,7±2,1	11,5±2,0	32,2±5,9
61°	233,4±4,2	28,7±1,9	14,3±1,8	8,2±1,7	19,6±4,1
91°	224,8±4,1	25,7±1,8	11,9±1,6	6,7±1,5	16,2±3,5
121°	199,3±3,8	19,5±1,6	8,3±1,4	4,2±1,3	8,0±3,2
151°	194,5±3,8	17,7±1,5	7,7±1,3	4,1±1,3	9,5±3,0

Bismuth

θ\ΔE	0 - 2,98	2,98-4,22	4,22-5,37	5,37-6,43	6,43-14,32
31°	272,1±4,4	43,4±2,0	21,1±1,7	12,1±1,5	29,7±4,4
61°	254,7±4,0	32,7±1,6	12,7±1,3	5,4±1,2	4,8±2,9
91°	247,2±3,9	30,7±1,5	12,6±1,2	6,3±1,1	13,2±2,5
121°	245,1±3,8	30,5±1,4	11,9±1,1	5,6±1,0	10,1±2,3
151°	253,5±4,0	28,9±1,4	11,6±1,1	5,6±1,0	9,9±2,2

Key to graphs (pp 113-136)

Мэв = MeV

Лаб. = Lab.

мбарн/стерадиан = mbarn/sr

смещение нуля = Suppressed zero
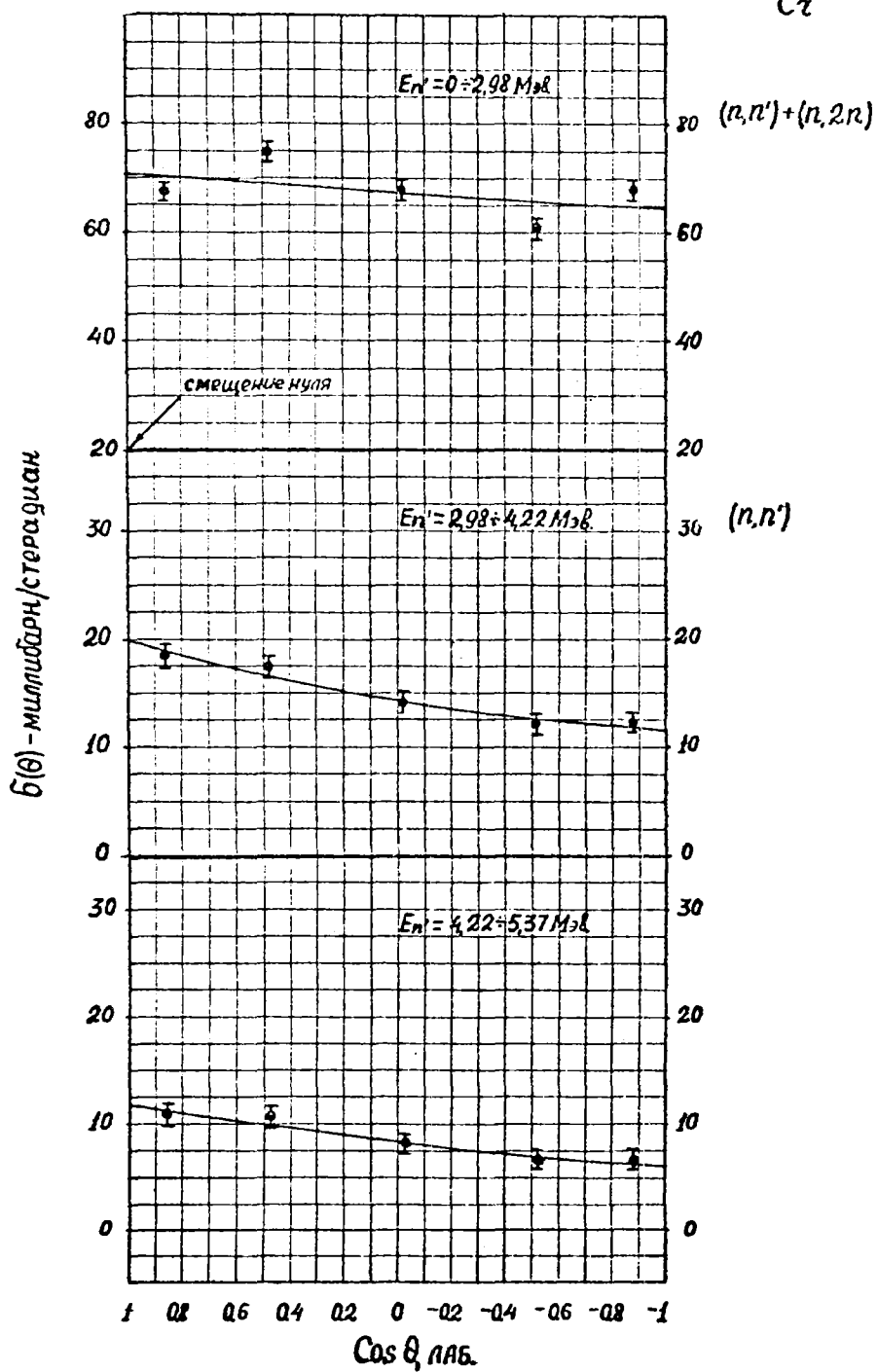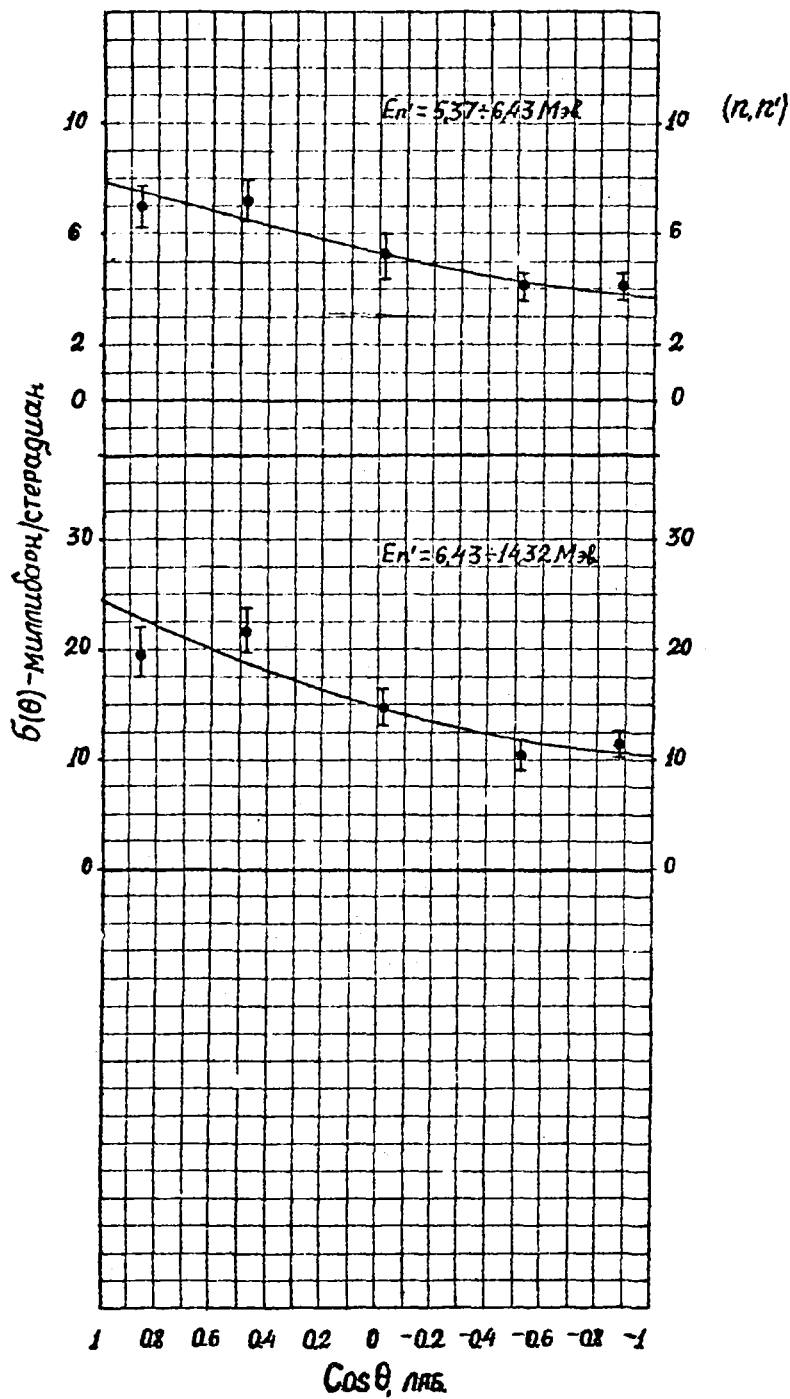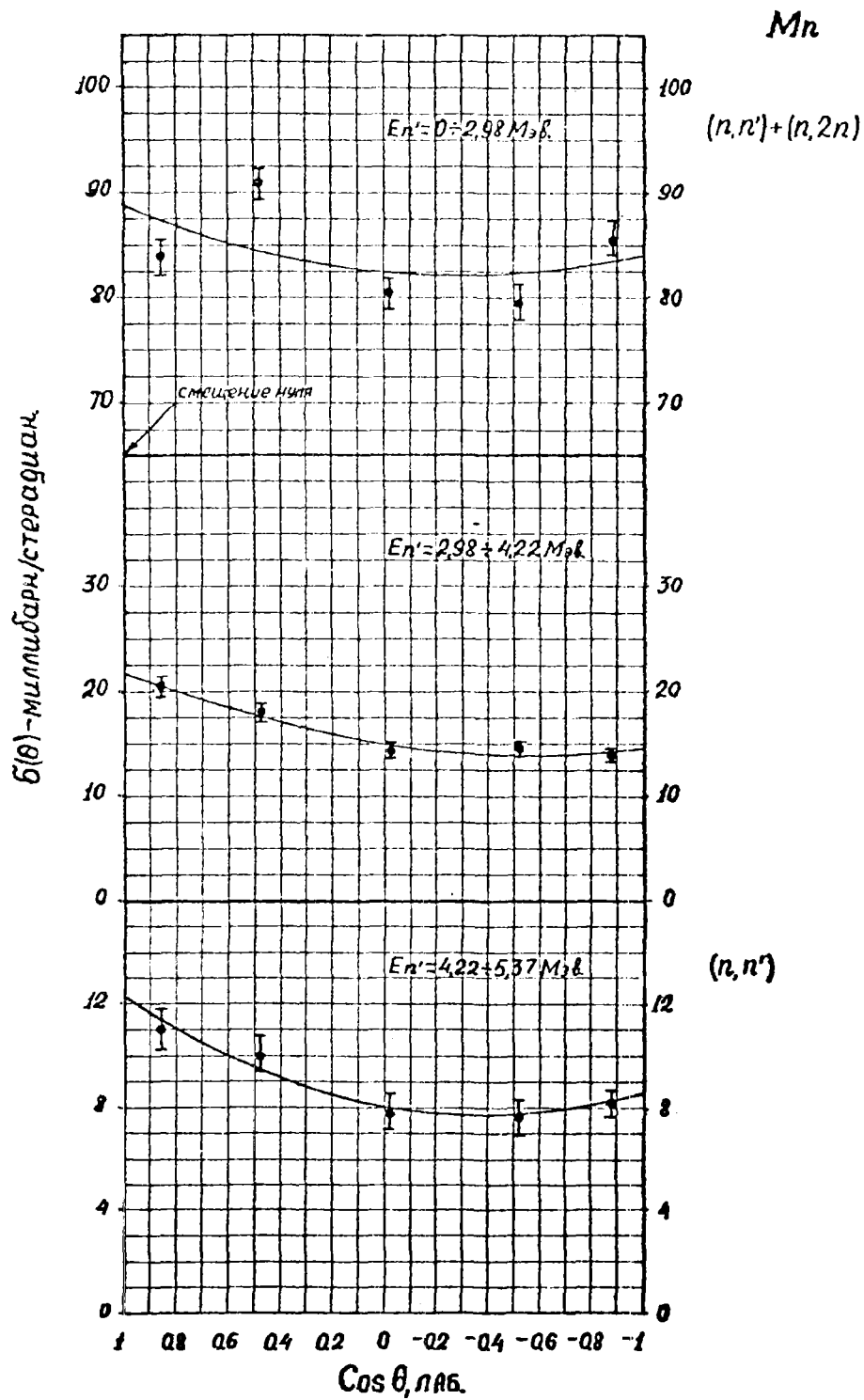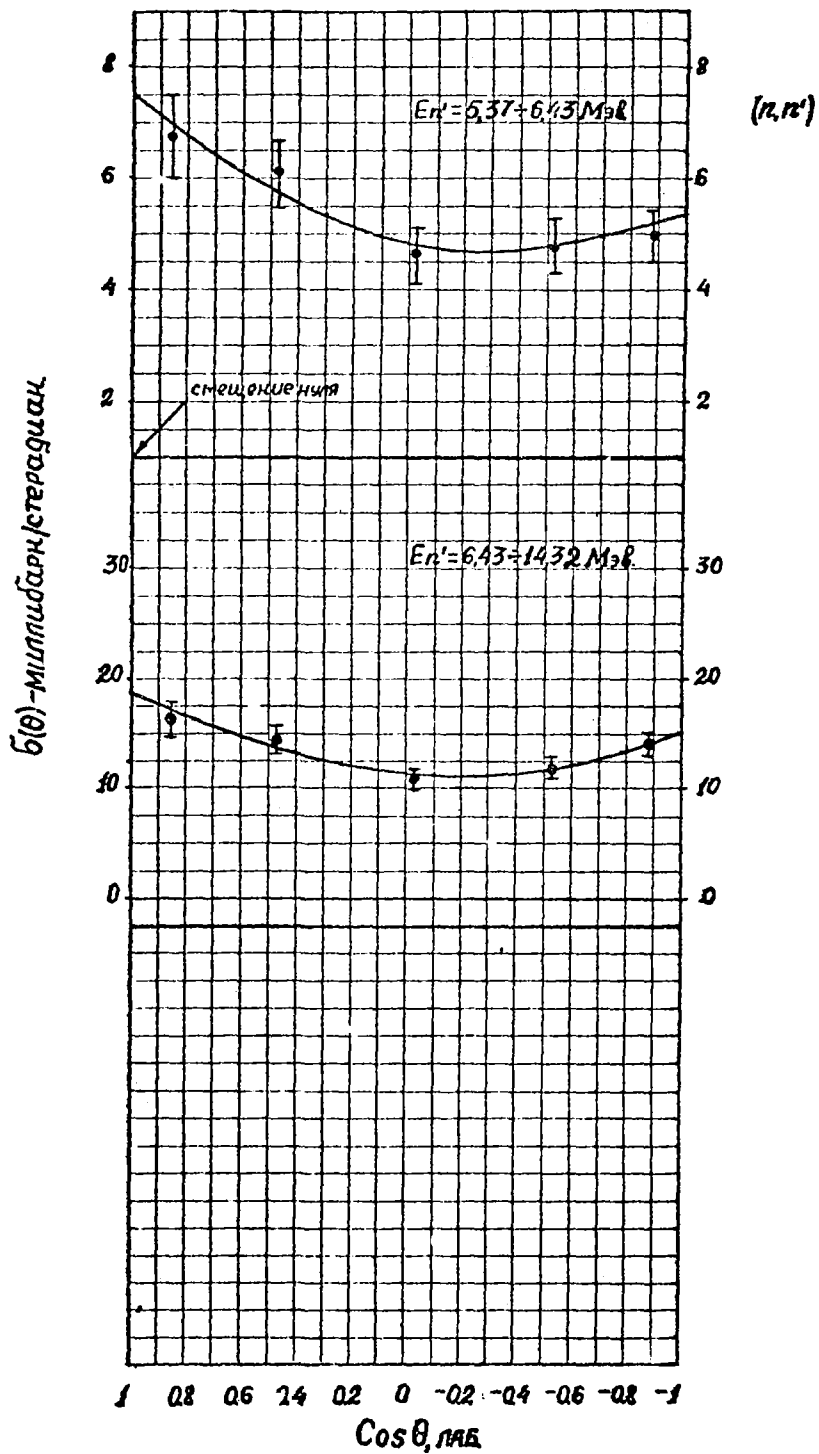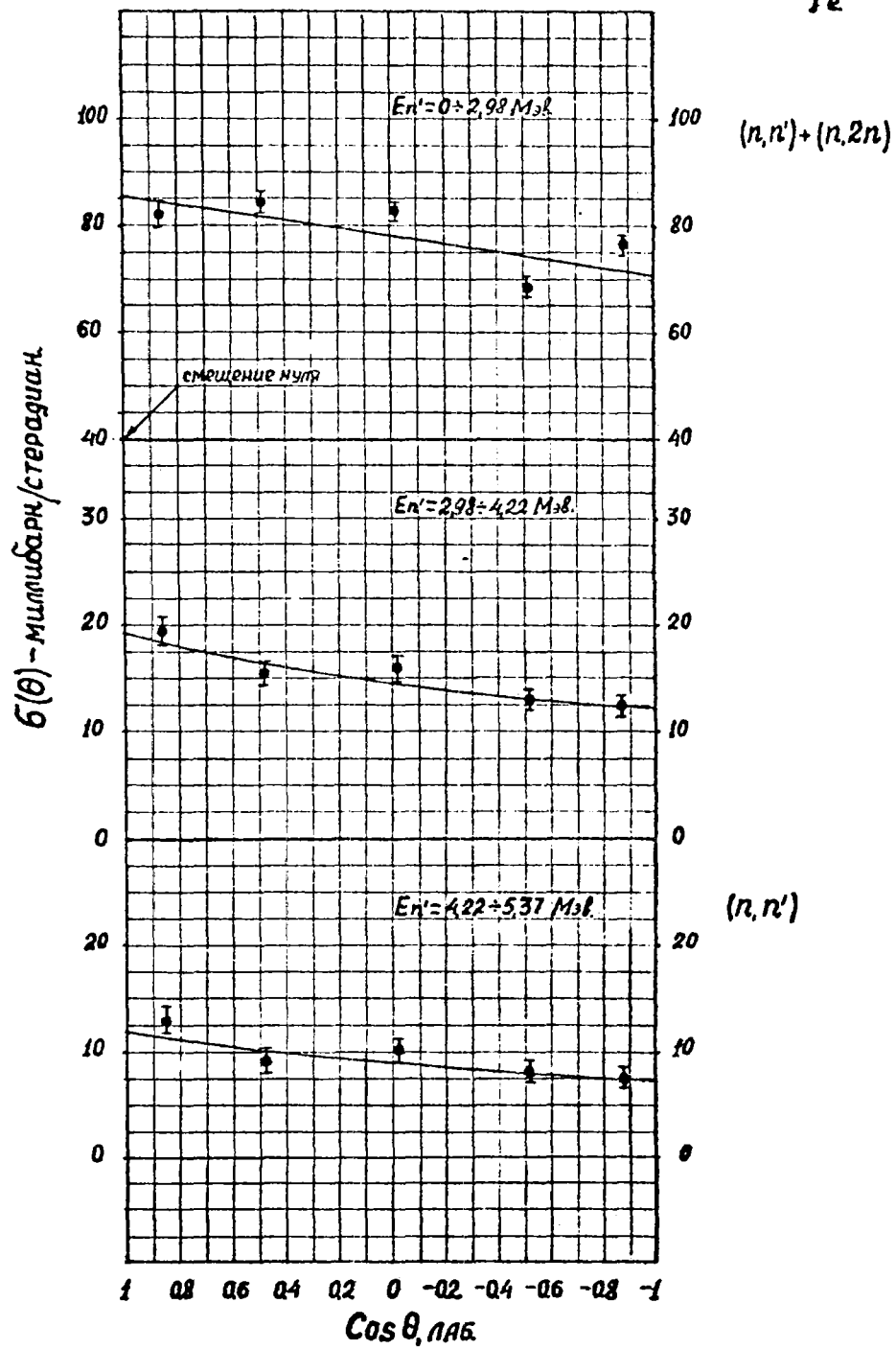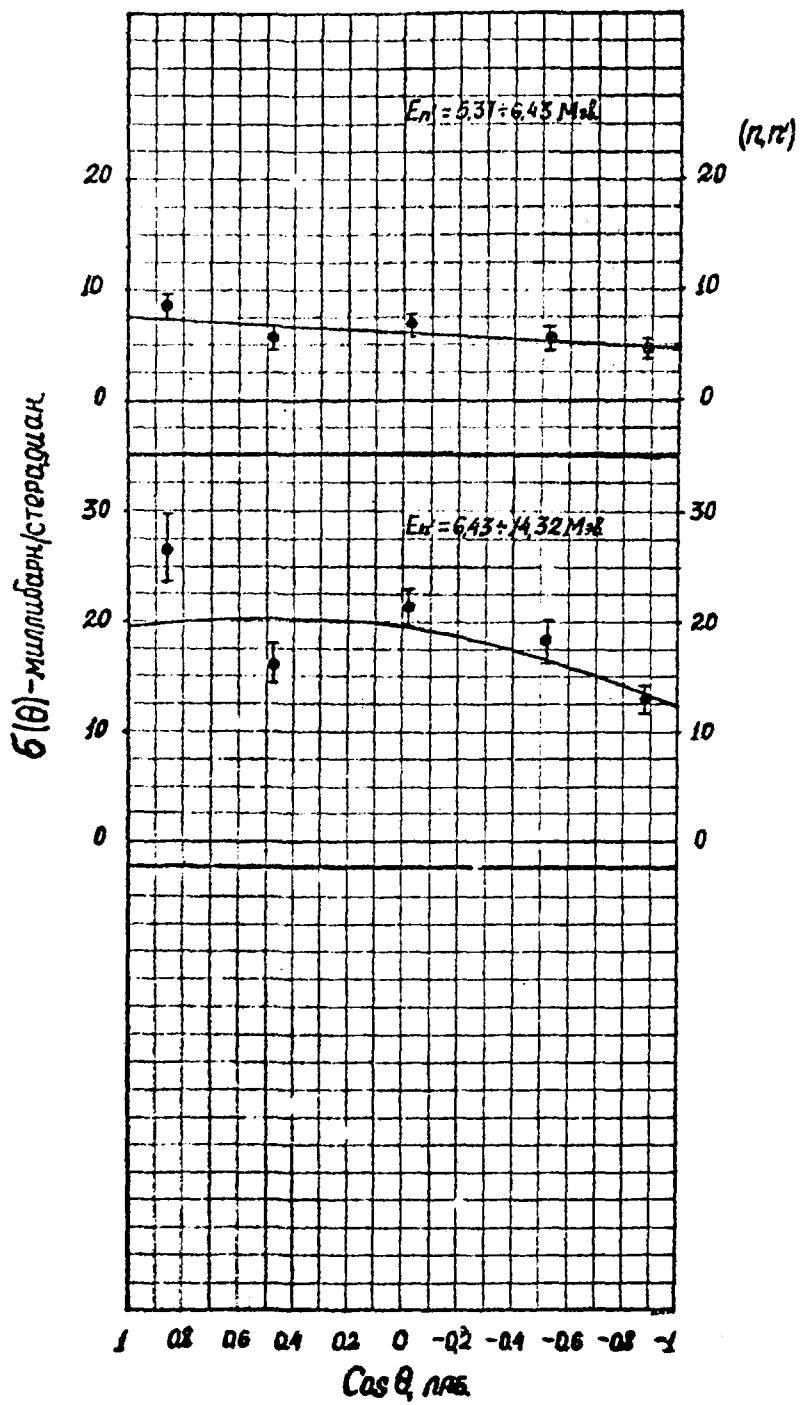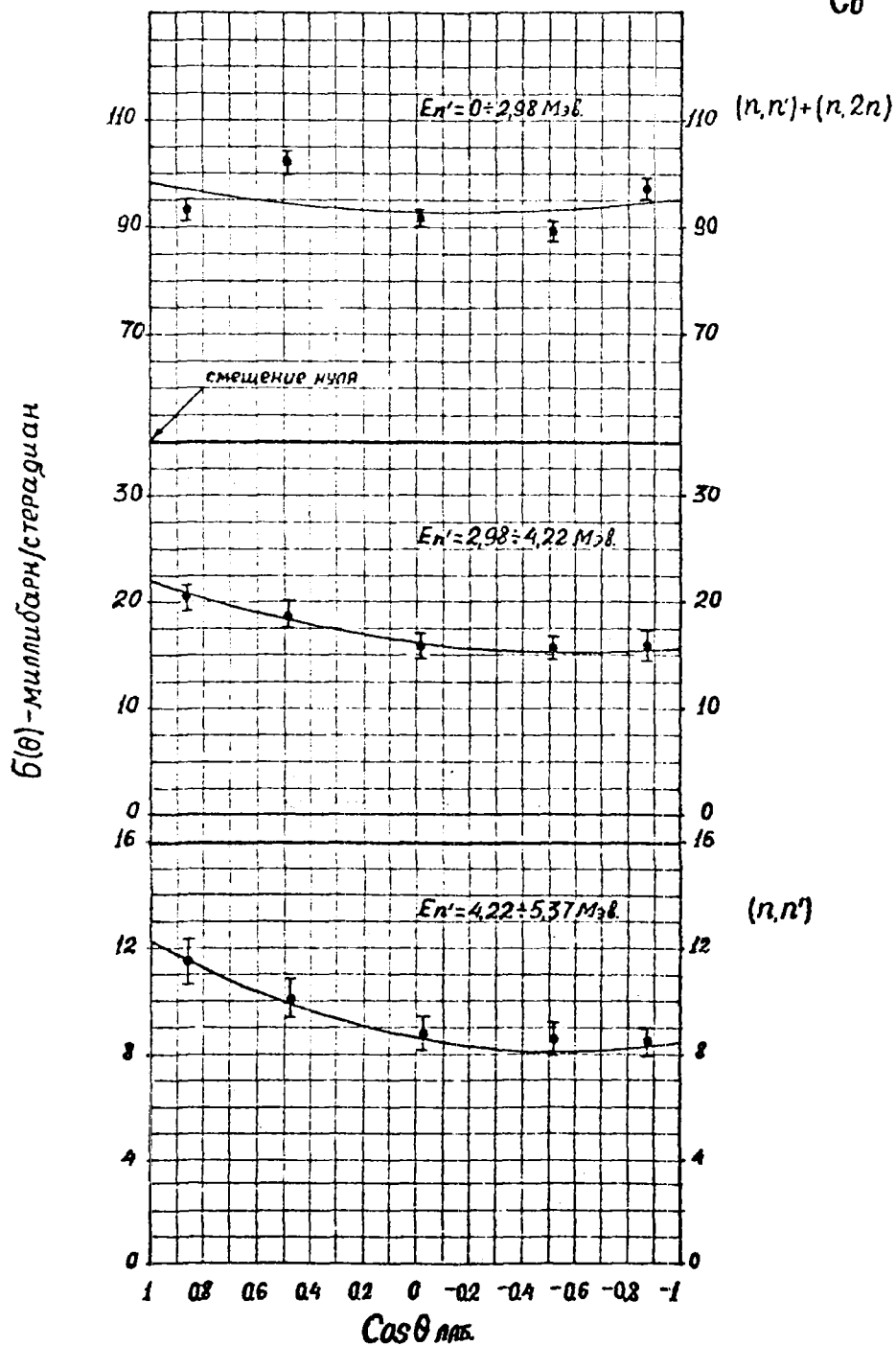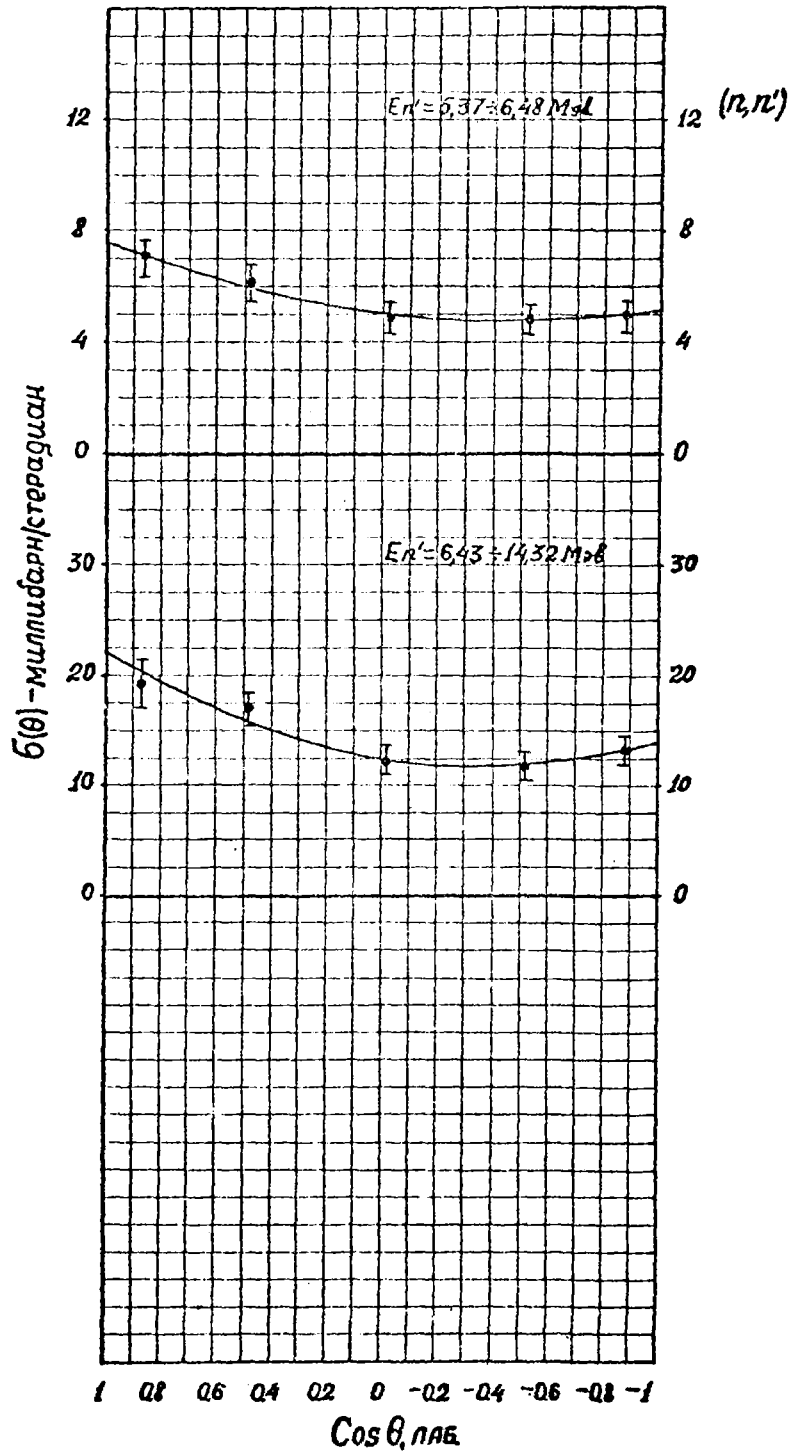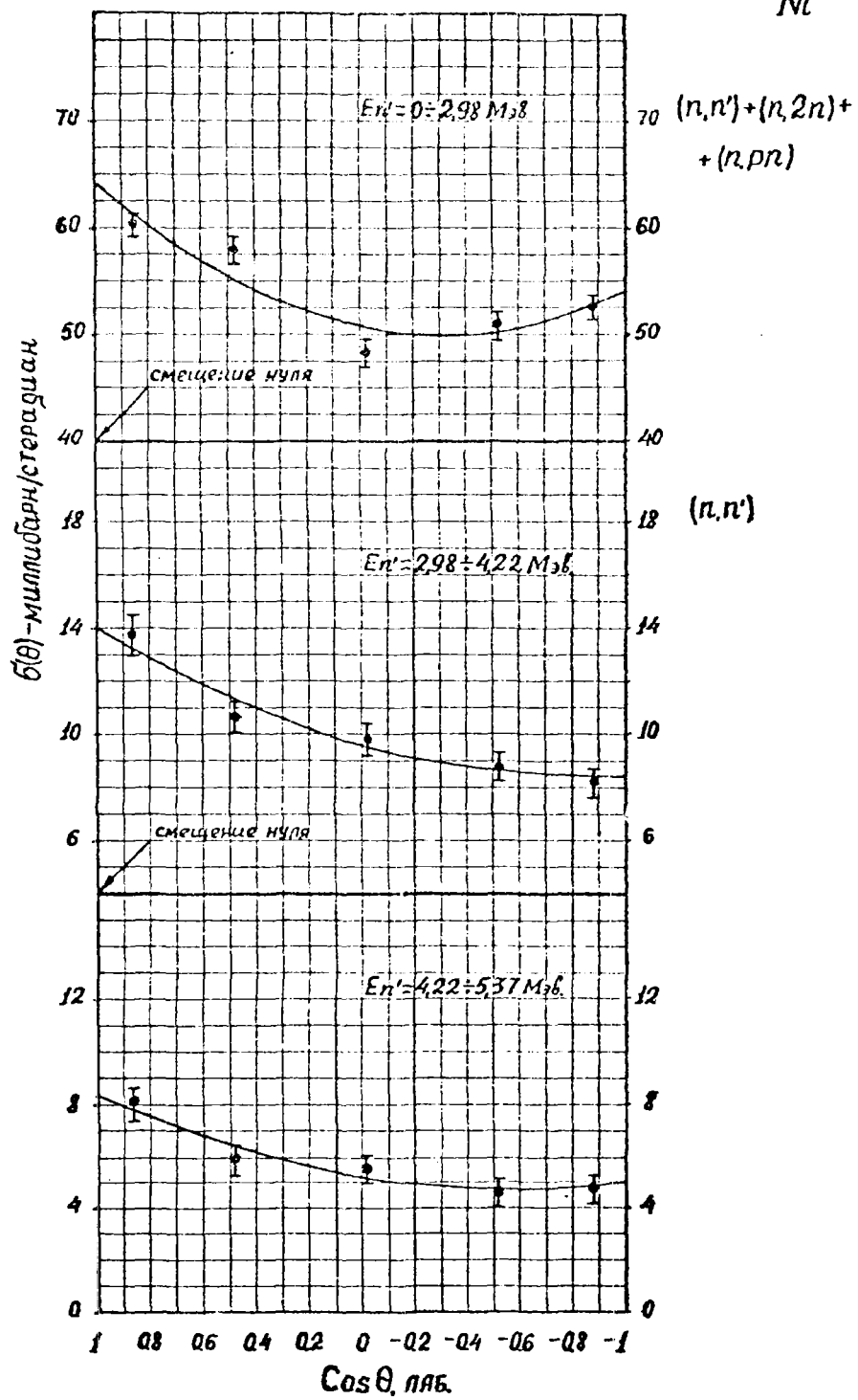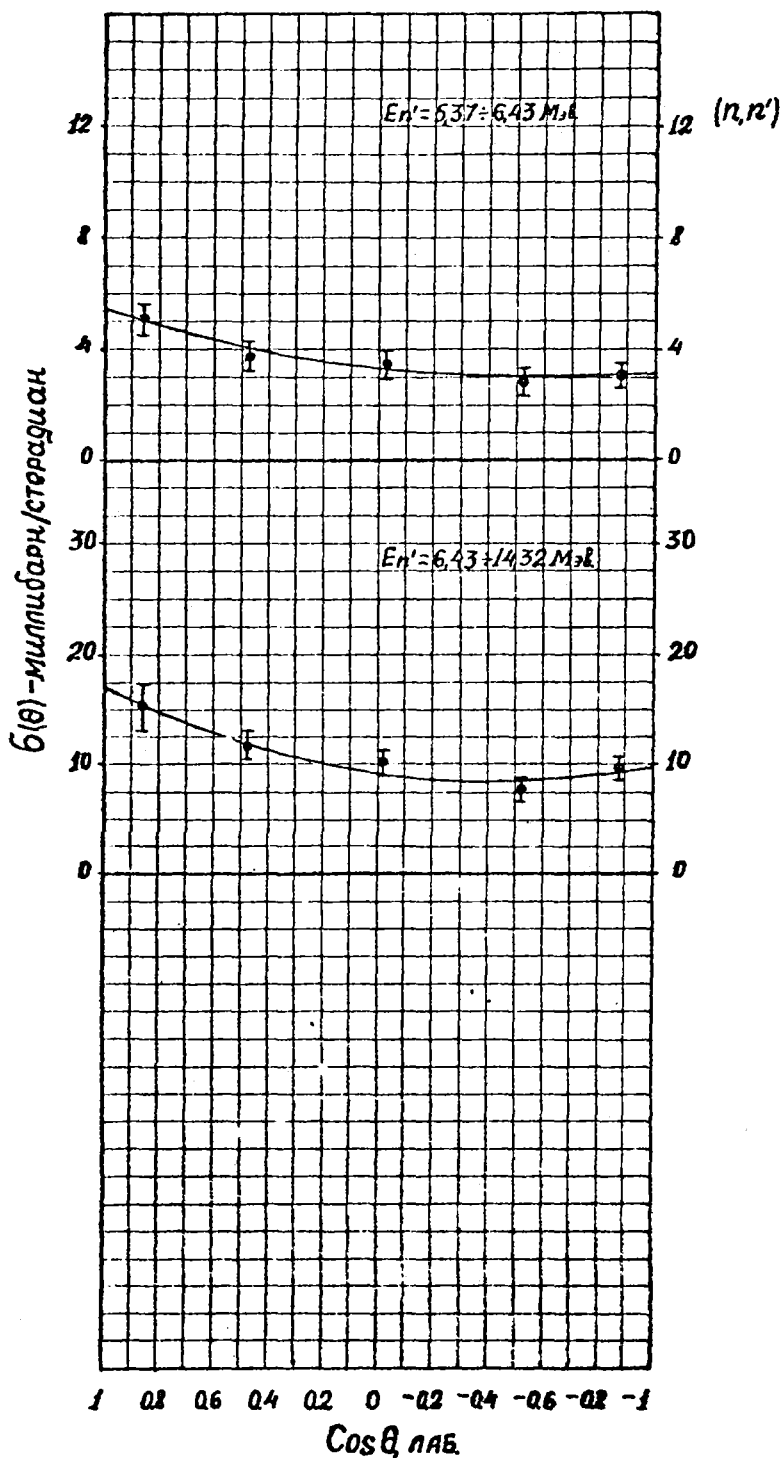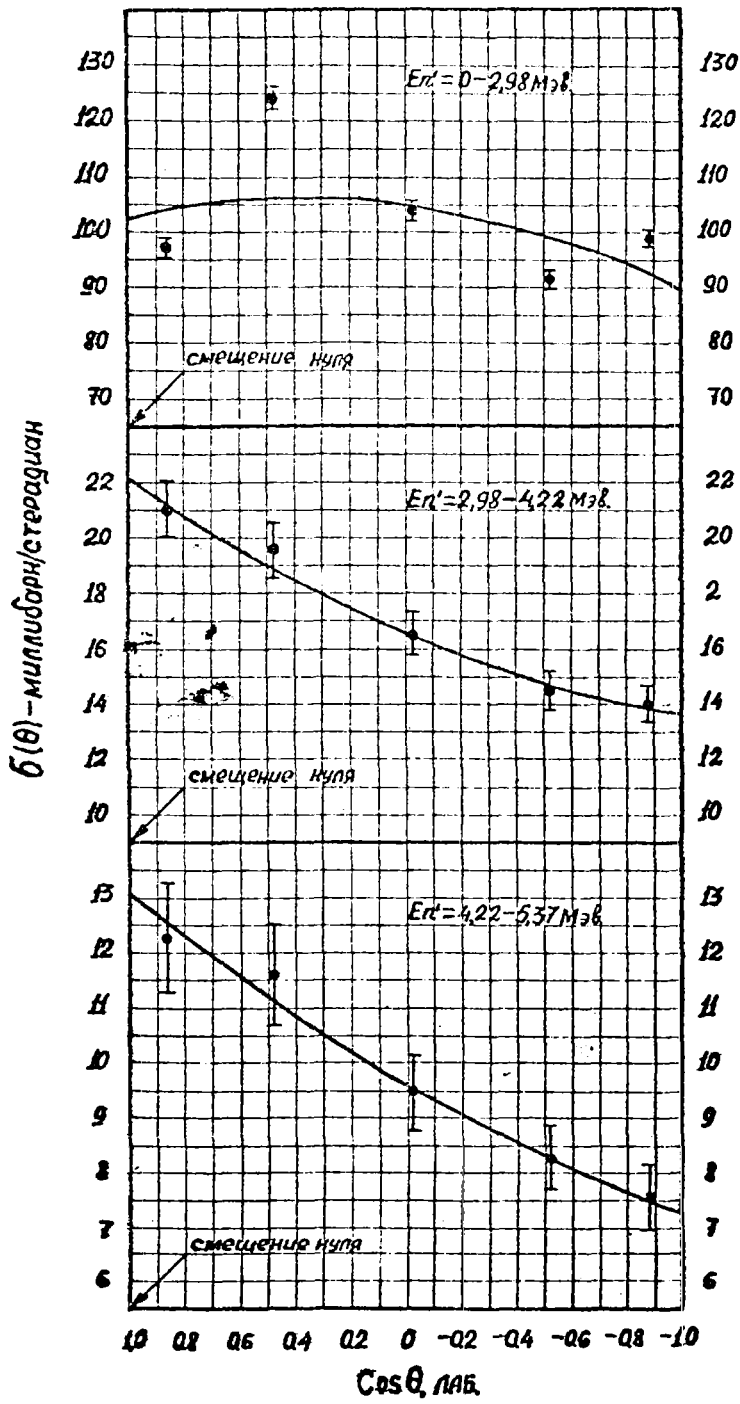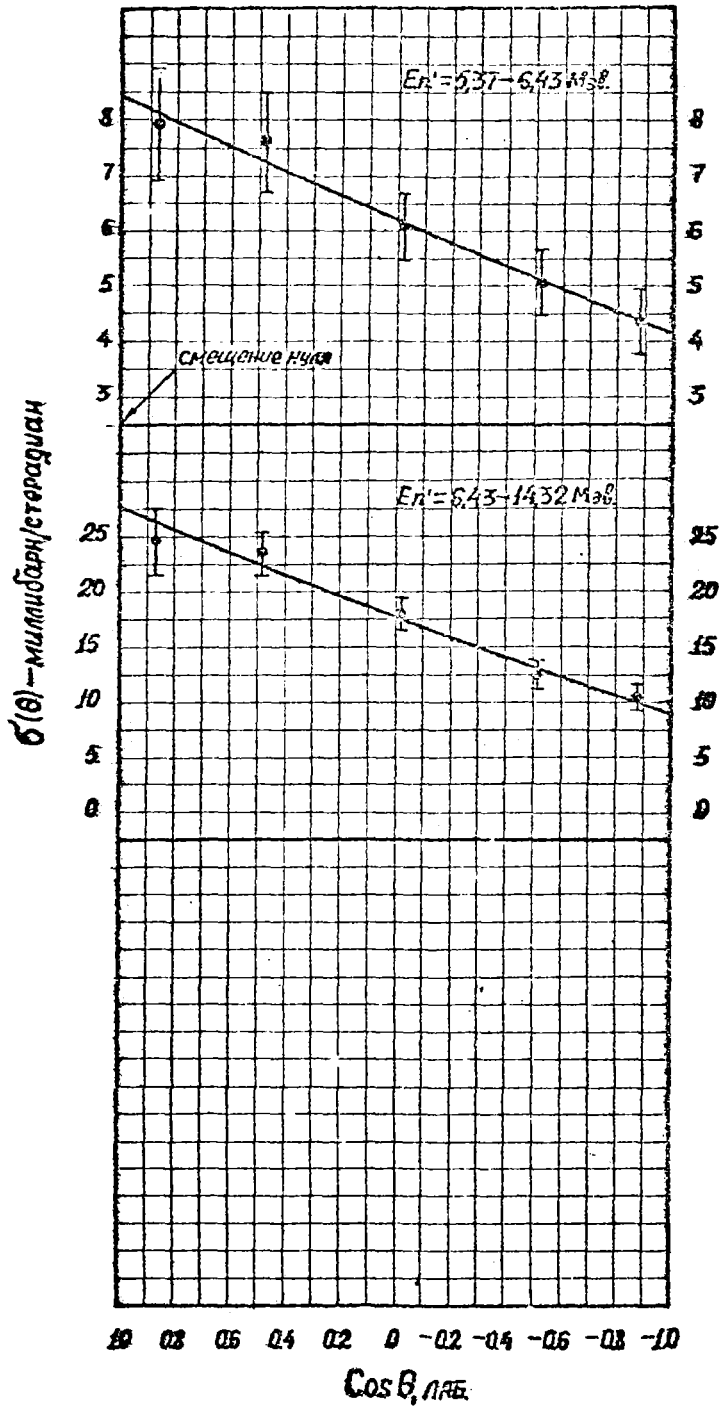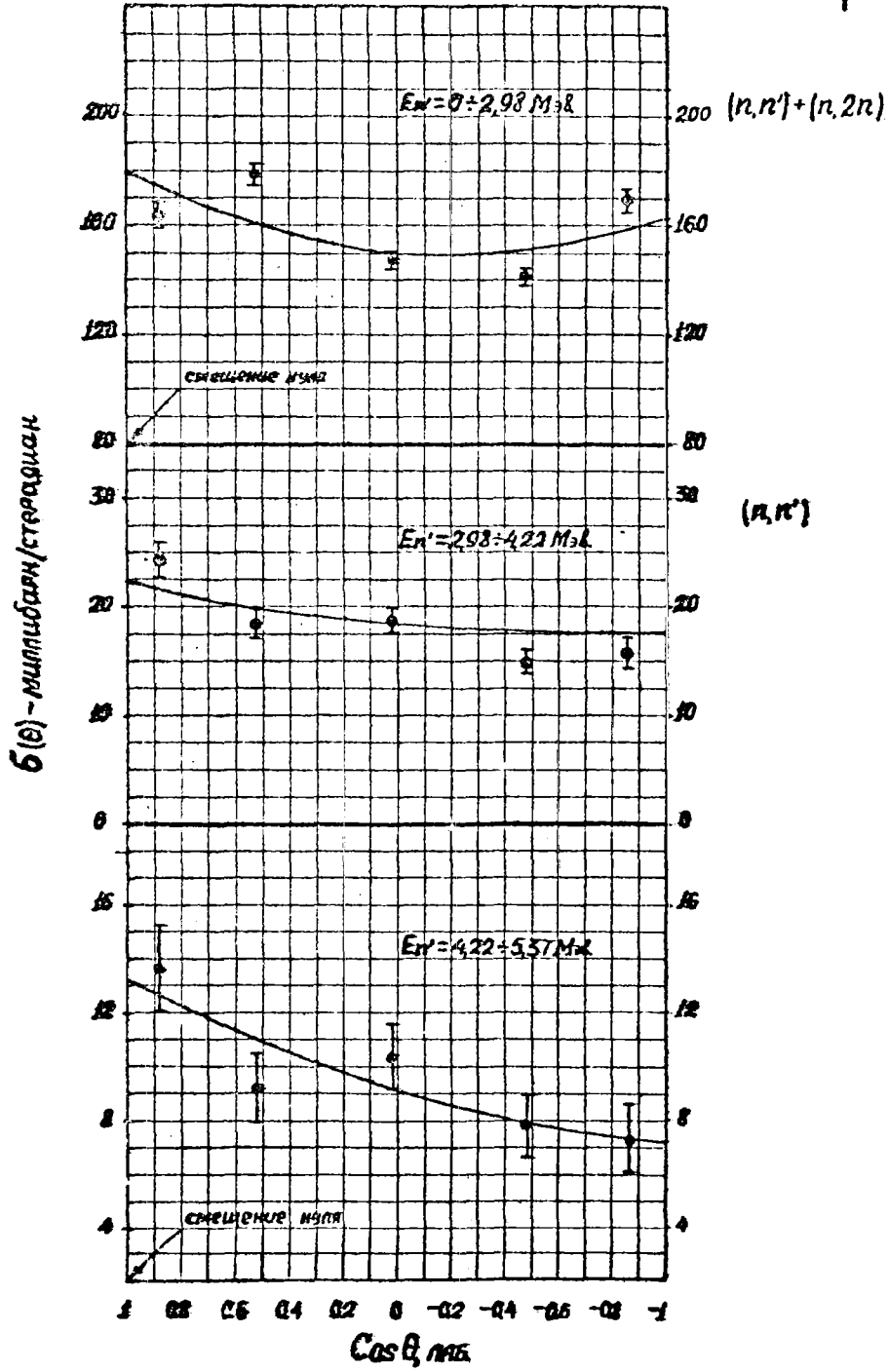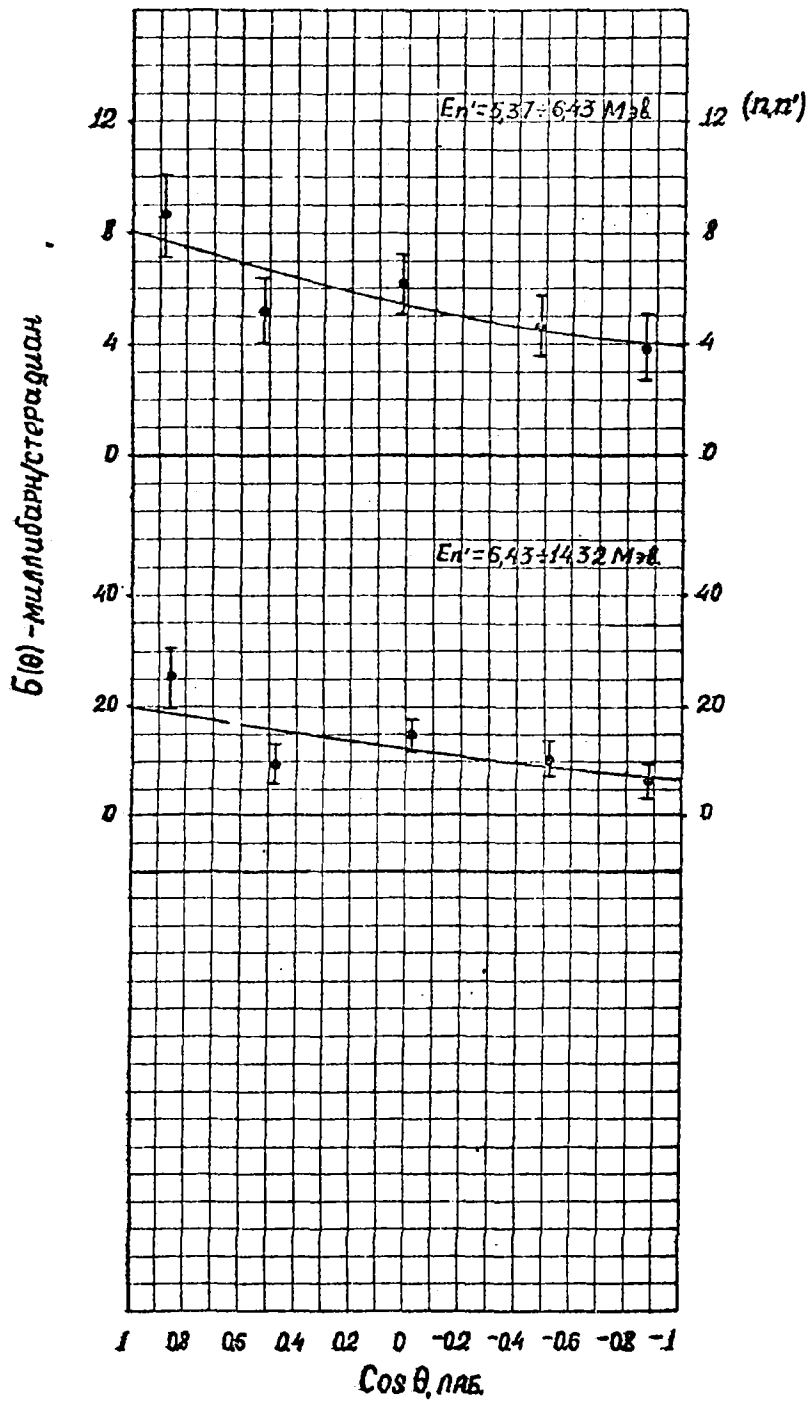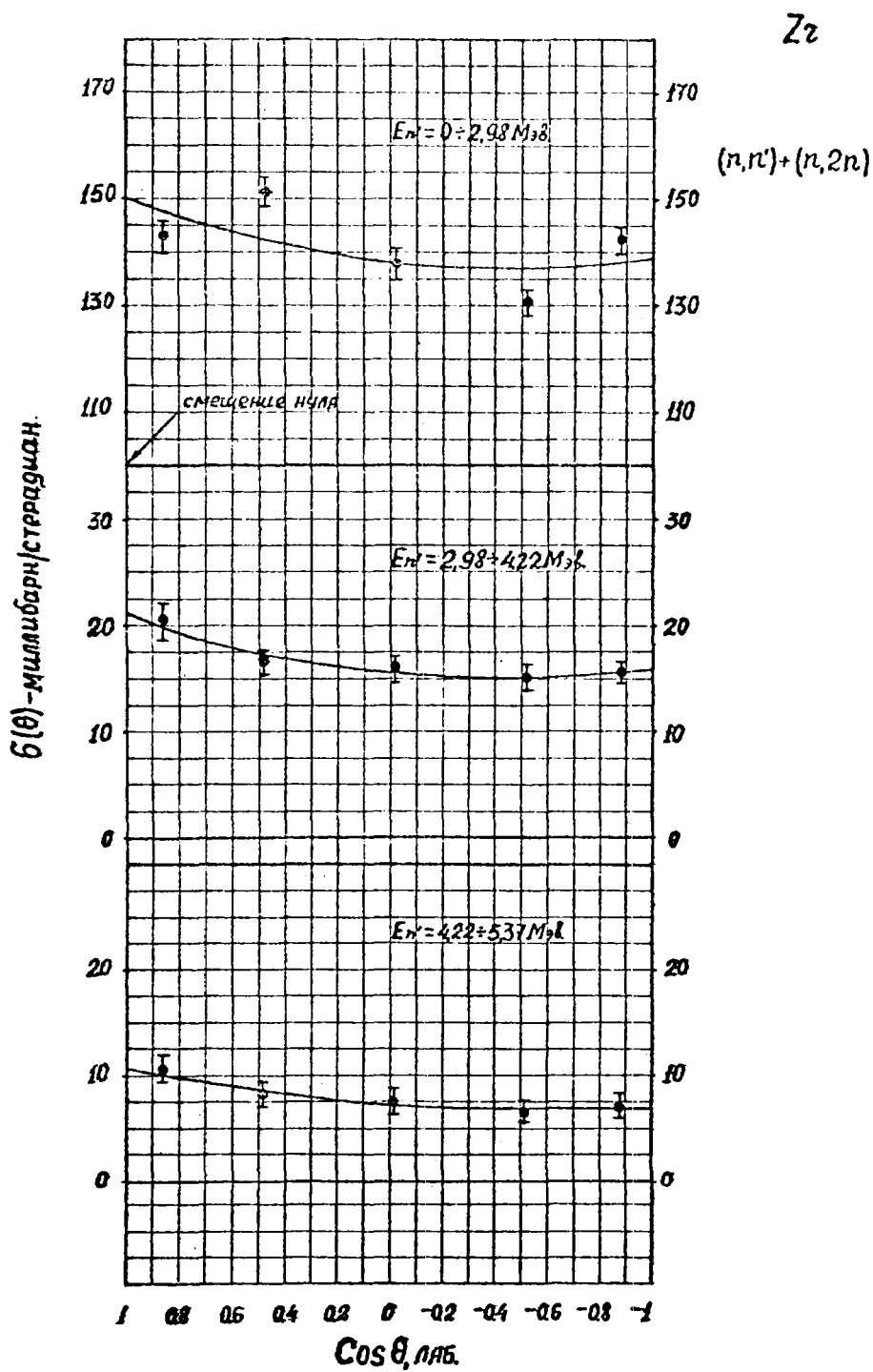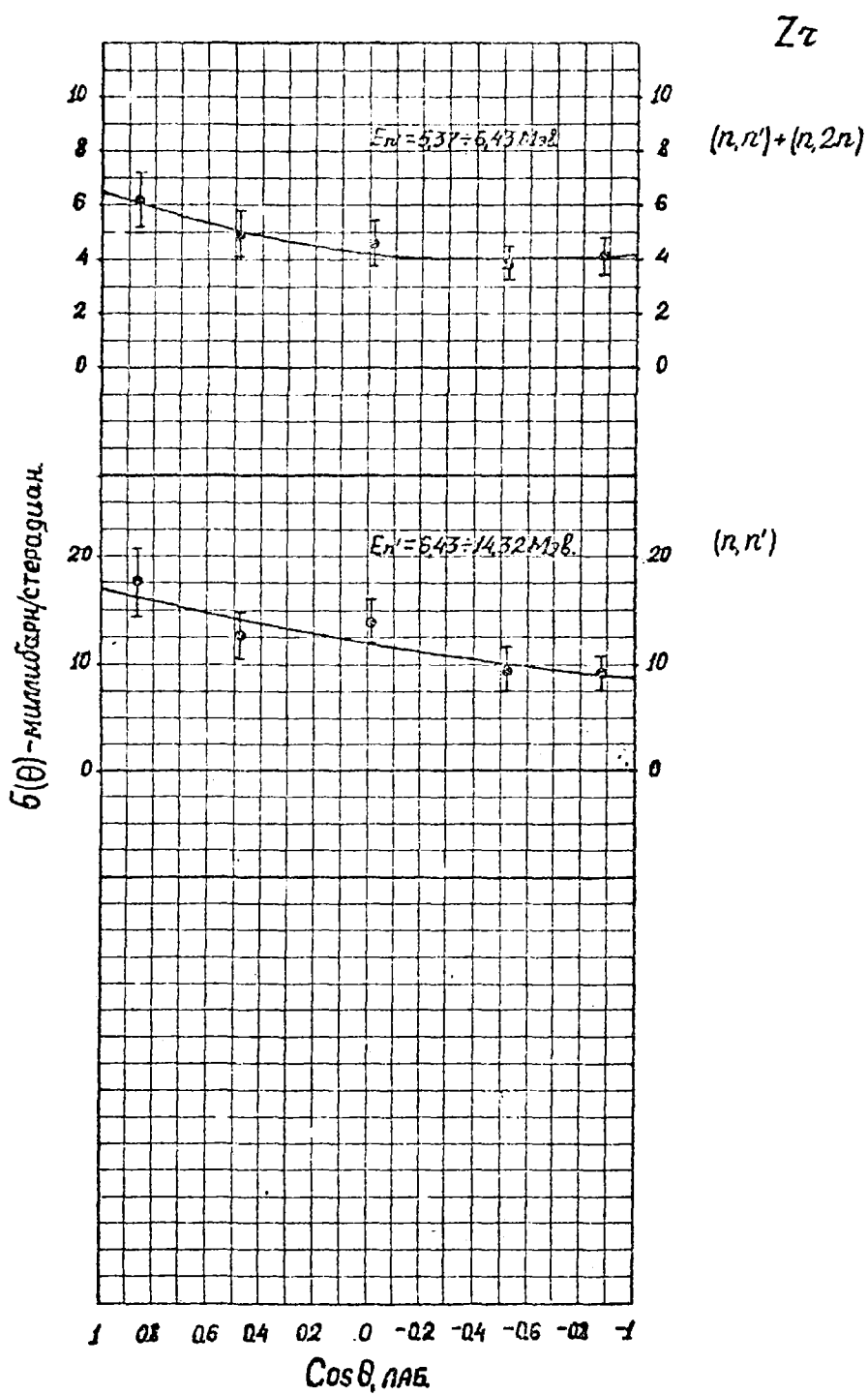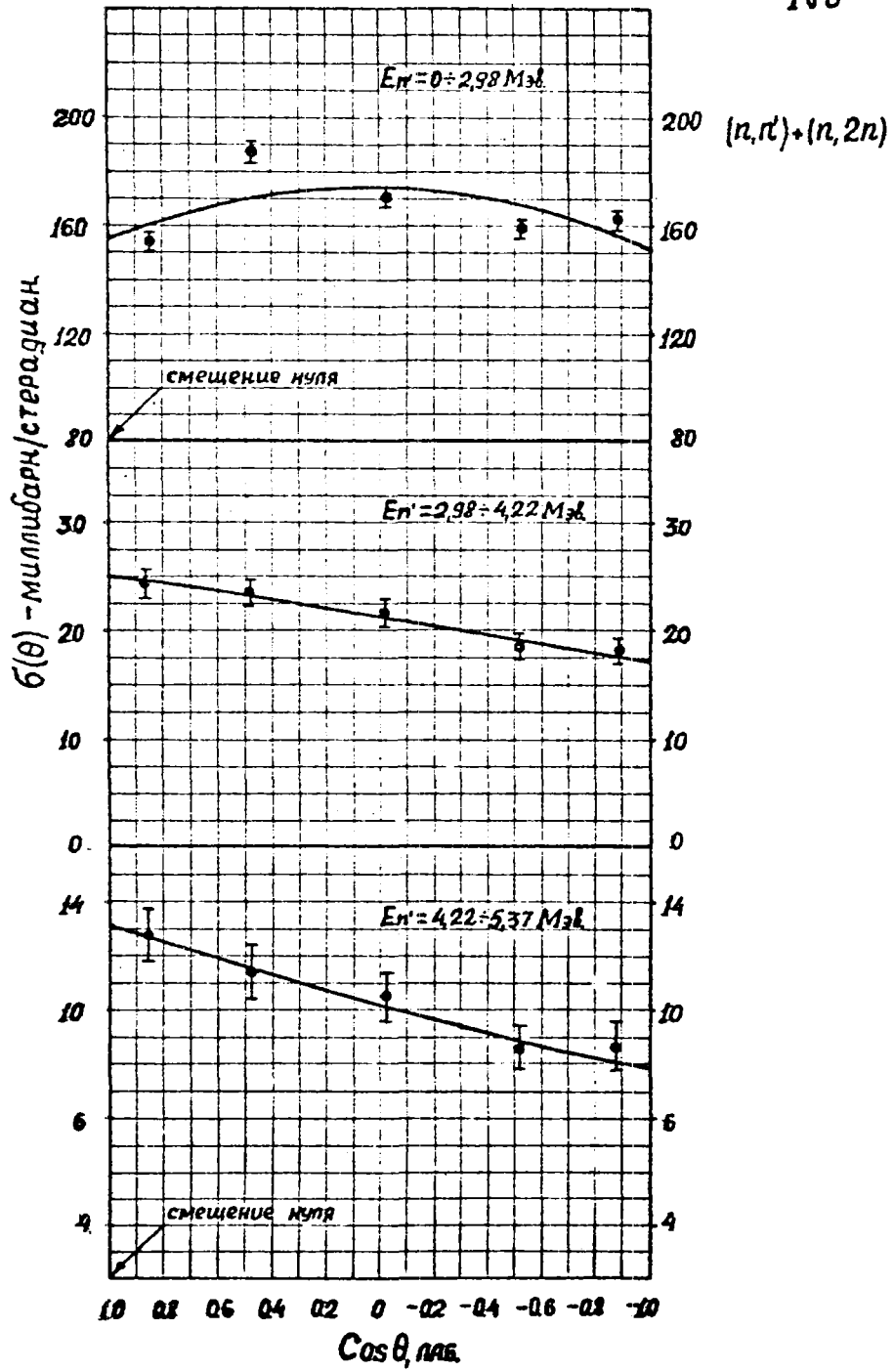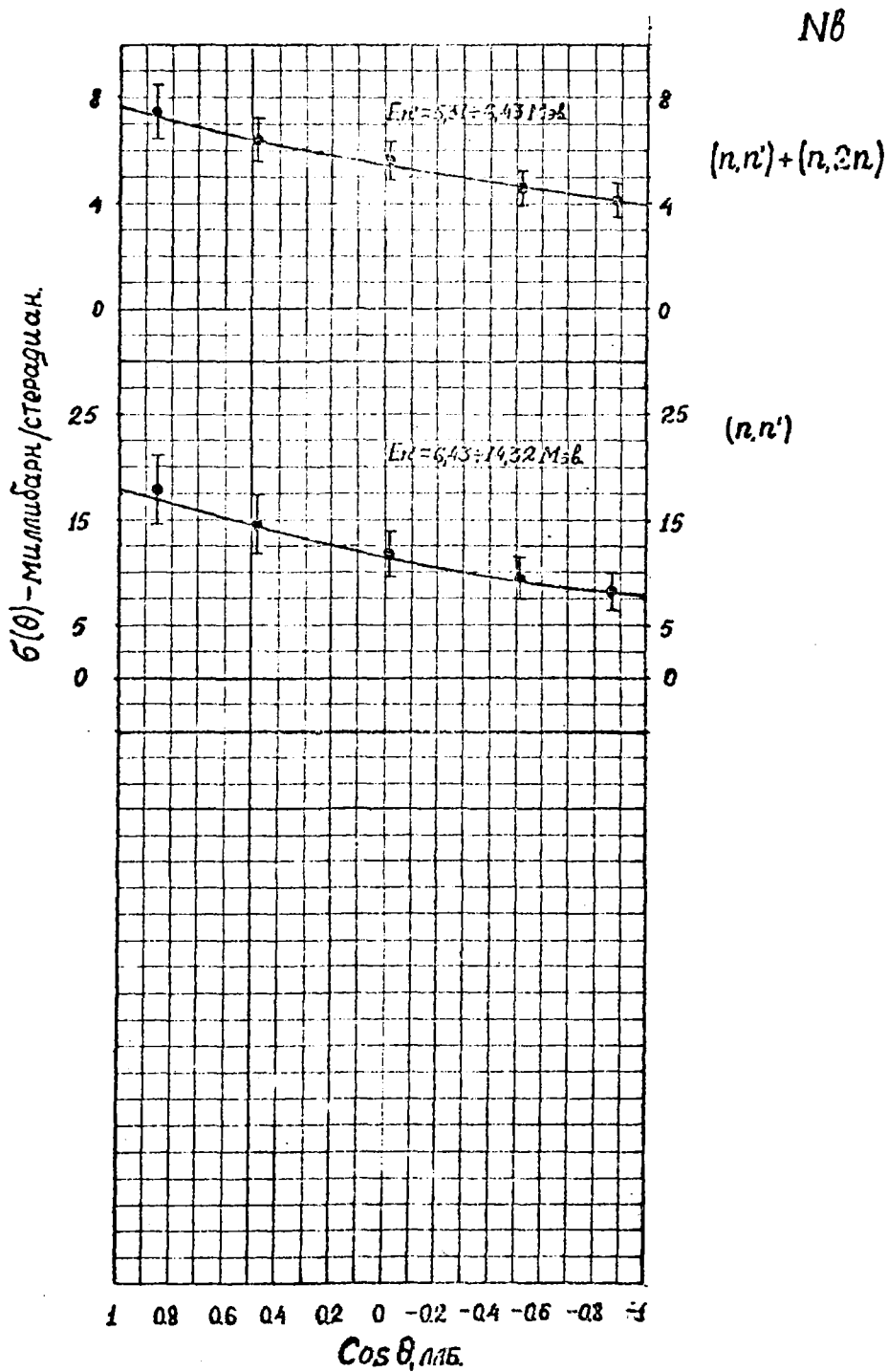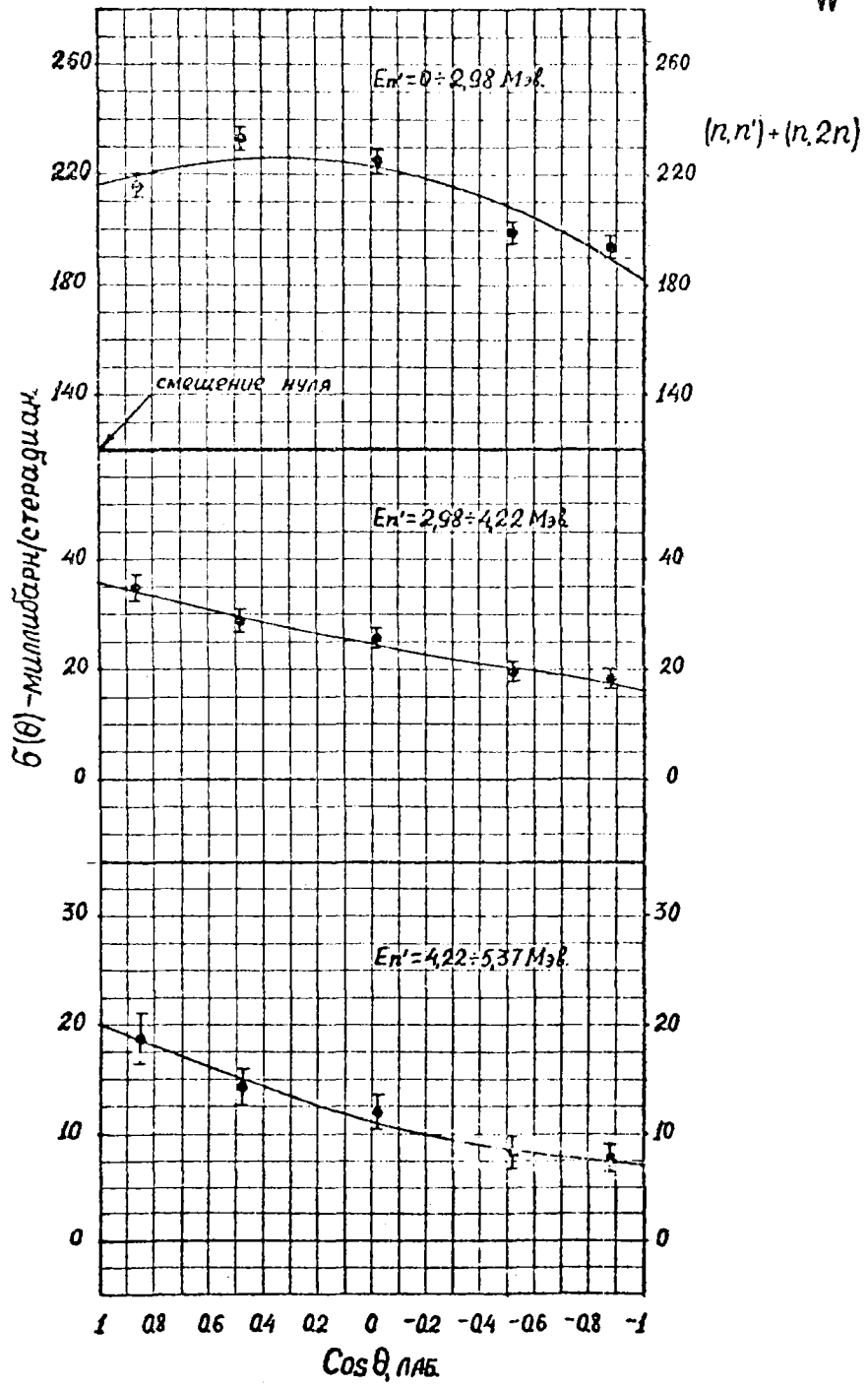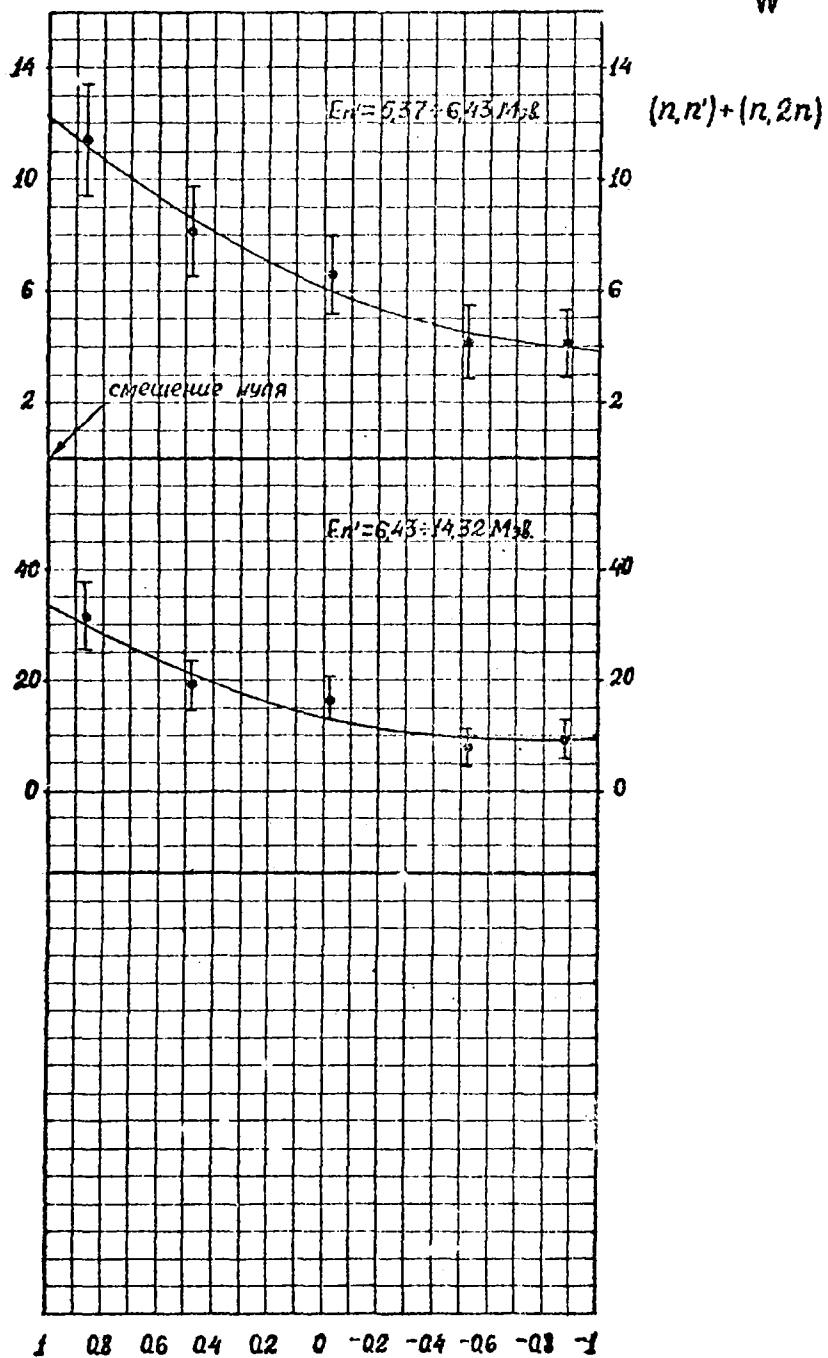
Fe

$(n,n') + (n,2n)$

$E_{n'} = 0 \div 2,98\ M_9 \theta.$

смещение нутр

$E_{n'} = 2,98 \div 4,22\ M_9 \theta.$

(n,n')

$E_{n'} = 4,22 \div 5,37\ M_9 \theta.$

$\delta(\theta)$ - миллибарн/стерадиан.

$\cos \theta$, ЛАБ.

Fe

Co

$E_{n'} = 0 \div 2,98 \, M_{2}l.$

$(n,n') + (n,2n)$

смещение нуля

$E_{n'} = 2,98 \div 4,22 \, M_{2}l.$

$E_{n'} = 4,22 \div 5,37 \, M_{2}l.$

(n,n')

$\delta(\theta)$ - миллибарн/стерадиан

$Cos\,\theta$ лаб.

$N\theta$

$(n,n')+(n,2n)$

(n,n')

Bi

(n,n') + (n,2n)

$_{27}Co$

$(n,n') + (n,2n)$

$_{40}Zr$

$(n,n') + (n,2n)$

14.1 Mev
$E_{n'} = 0.5 - 4.0$ Mev

(NOTE CHANGE OF SCALE)

14.1 Mev
$E_{n'} = 4.0 - 12.0$ Mev

15.2 Mev (SEE TEXT)

$\sigma(\theta)$ - MILLIBARNS/STERADIAN

$\cos \theta_{CM}$

$(n,n') + (n,2n)$

$_{83}Bi$

14 Mev
$E_{n'} = 0.5 - 4.0$ Mev

(NOTE CHANGE OF SCALE)

14 Mev
$E_{n'} = 4.0 - 12.0$ Mev

$\sigma(\theta)$ - MILLIBARNS/STERADIAN

$\cos \theta_{CM}$
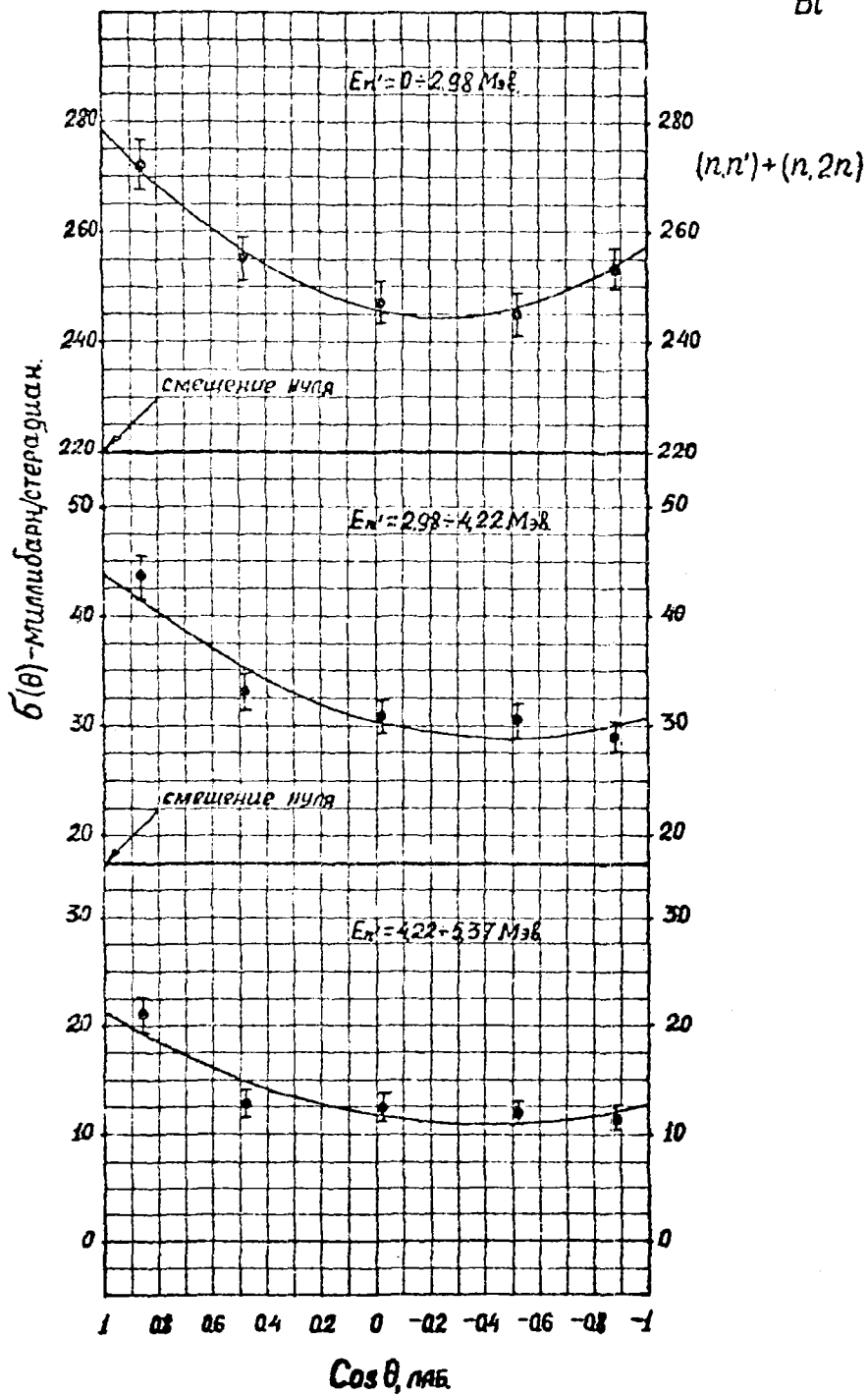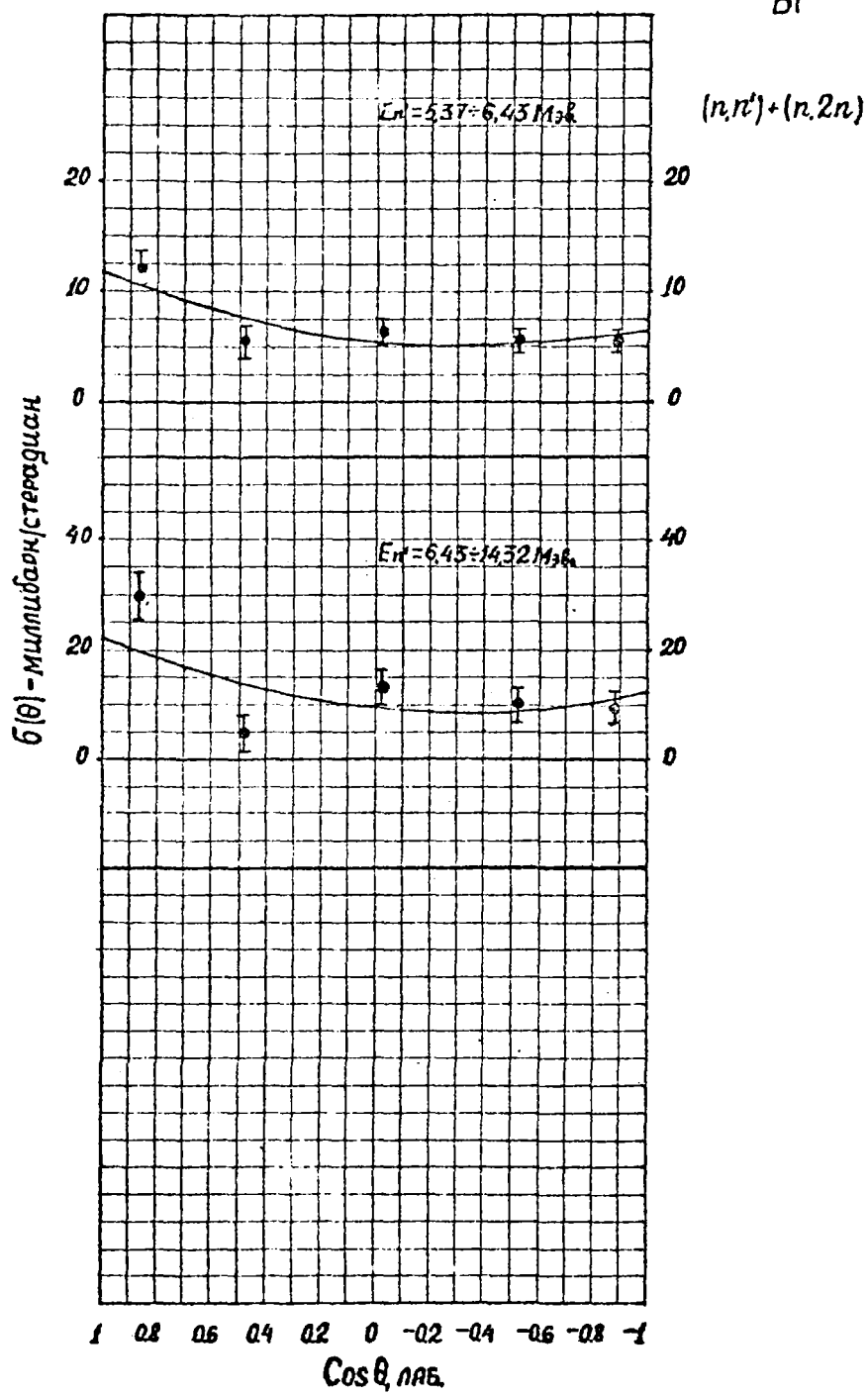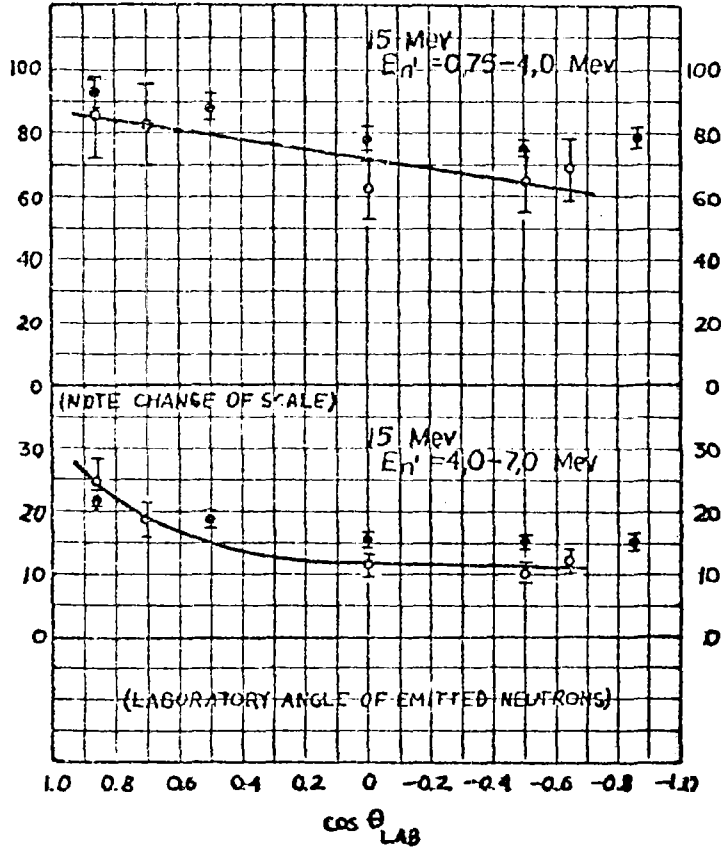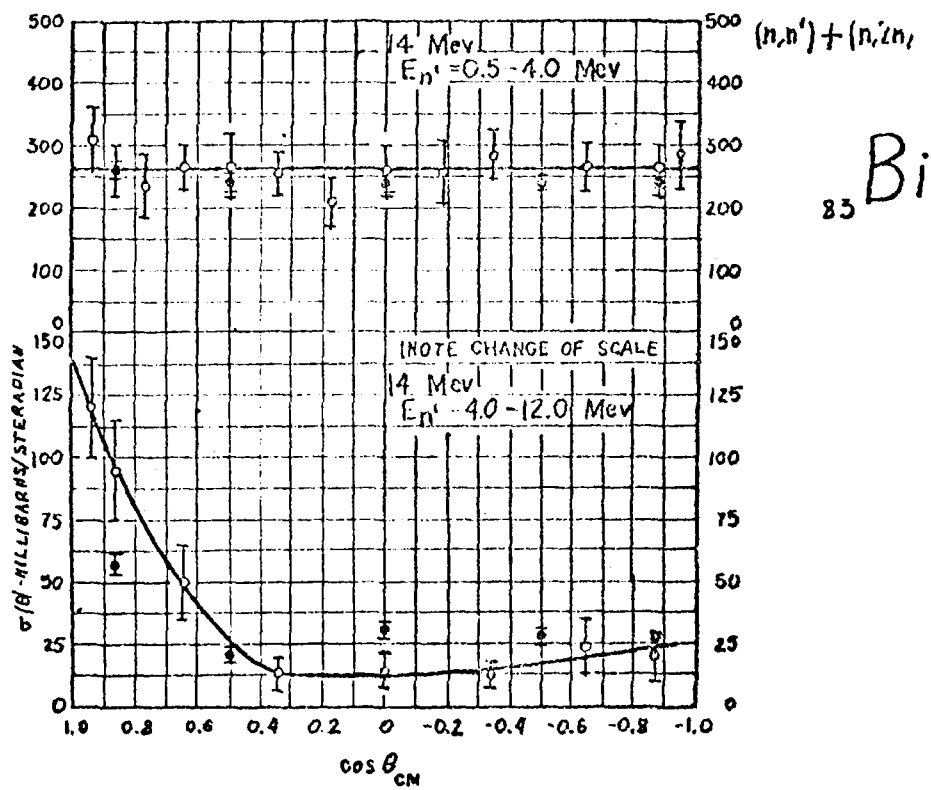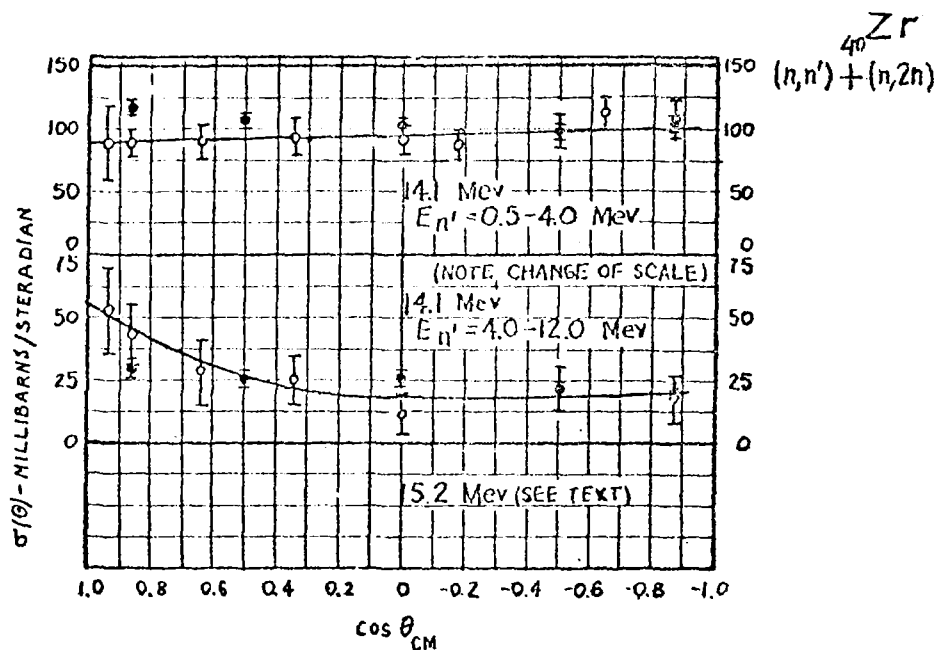
ENERGY SPECTRA OF INELASTICALLY SCATTERED NEUTRONS FOR Cr, Mn, Fe, Co, Ni, Cu, Y, Zr, Nb, W AND Bi

O.A. Salnikov, G.N. Lovchikova, G.V. Kotelnikova,
A.M. Trufanov, N.I. Fetisov

This paper supplies the energy spectra of inelastically scattered neutrons with initial energy of 14.4 MeV for scattering angles of 31°, 61°, 91°, 121° and 151° with angular resolution of $\pm 8^{\circ}$.

The spectra were measured by the time-of-flight method in cylindrical geometry. The resolving time of the spectrometer was 6-8 nsec, the analyser channel width 2.6 nsec, the flight path 2 m and the neutron recording threshold ~ 100 keV.

The measuring procedure is described in Refs $\boxed{1}$ and $\boxed{2}$. When the spectra were processed, corrections were made for counting losses due to the dead time of the spectrometer, the effect of the position of the collimator and the scatterer on the count of the monitor, for background due to cosmic rays and sample activation, and for multiple neutron scattering in the sample and attenuation of the direct flux. This correction was calculated by the Monte Carlo method using a programme developed in the Institute of Physics and Power Engineering. All the spectra were normalized to the same monitor count and were reduced to the same geometrical conditions for each element separately.

Since for all nuclei the primary neutron energy exceeds the neutron binding energy in the target nucleus, the measured spectra are in fact composite spectra of neutrons from the $(n,n') + (n,2n) + (n,pn)$ reaction. The data for the energy spectra are given in the form of graphs and tables. The errors of the different points in the energy spectra are mean square errors which take into account the statistical errors in the measurement of the spectra, errors in measuring the efficiency and the uncertainty of the flight path.

The spectra provided can be used for reactor shielding and core calcula-tions and for other practical purposes as well as for theoretical studies of nuclear properties.

In conclusion the authors wish to thank M.D. Bityutskaya and E.S. Chernichenko for performing numerous calculations and formulating the results.

Tables 1-11

Key: Хром   = Chromium

Марганец   = Manganese

Железо   = Iron

Кобальт   = Cobalt

Никель   = Nickel

Медь   = Copper

Иттрий   = Yttrium

Цирконий   = Zirconium

Ниобий   = Niobium

Вольфрам   = Tungsten

Висмут   = Bismuth

МэВ   = MeV

Усреднённый спектр = Average spectrum

TABLE I

ХРОМ

Таблица I

m.v. E, Мэв \ θ	31°	61°	91°	121°	151°	усреднённый спектр
1	2	3	4	5	6	7
0,102	4,26	7,01	12,97	10,00	6,66	8,53
0,136	6,30	11,12	17,77	14,56	13,21	12,60
0,182	8,82	18,22	24,44	20,07	19,17	18,14
0,221	11,93	23,57	30,82	25,73	24,34	23,28
0,241	13,50	25,95	33,56	28,11	26,82	25,59
0,285	15,67	30,51	38,13	31,04	30,60	29,19
0,292	17,94	35,19	42,68	34,25	34,41	32,90
0,323	21,21	41,73	48,66	39,92	38,81	38,07
0,360	24,40	49,75	53,12	43,40	45,22	43,18
0,403	28,90 ± 43,65	58,77 ± 16,30	58,65 ± 14,90	49,42 ± 16,13	52,51 ± 16,48	49,65 ± 10,81
0,455	34,41 ± 15,76	70,14 ± 12,10	64,71 ± 11,10	55,51 ± 11,08	51,13 ± 12,21	57,18 ± 5,62
0,518	41,14 ± 10,23	79,05 ± 9,93	71,56 ± 9,28	62,22 ± 9,17	71,61 ± 9,78	65,12 ± 4,33
0,594	50,51 ± 8,72	88,30 ± 8,89	77,74 ± 8,40	68,89 ± 8,16	84,14 ± 8,87	73,91 ± 3,85
0,639	52,61 ± 8,00	98,71 ± 8,62	84,79 ± 7,92	76,56 ± 7,56	98,48 ± 8,67	84,23 ± 3,65
0,808	79,40 ± 7,87	103,86 ± 8,62	92,04 ± 7,72	86,23 ± 7,39	106,99 ± 8,66	95,10 ± 3,61
0,901	95,30 ± 8,08	114,21 ± 8,67	97,26 ± 7,70	92,27 ± 7,39	111,74 ± 8,50	102,15 ± 3,61
1,162	102,23 ± 8,17	110,46 ± 8,30	97,88 ± 7,54	91,91 ± 7,14	106,00 ± 7,97	101,70 ± 3,50
1,308	101,61 ± 11,51	105,07 ± 10,63	96,31 ± 10,17	88,71 ± 9,86	99,77 ± 10,38	98,29 ± 4,70
1,365	100,49 ± 11,09	102,80 ± 10,18	95,20 ± 9,73	87,02 ± 9,50	97,40 ± 10,10	96,58 ± 4,53
1,426	98,80 ± 10,70	100,02 ± 9,84	93,33 ± 9,46	84,92 ± 9,17	94,06 ± 9,48	94,23 ± 4,36
1,491	96,61 ± 10,43	97,09 ± 9,54	90,91 ± 9,08	82,00 ± 8,73	90,86 ± 9,17	91,55 ± 4,20
1,550	94,95 ± 10,00	94,43 ± 9,14	88,65 ± 8,70	79,77 ± 8,24	87,63 ± 8,68	89,08 ± 4,01
1,635	92,83 ± 9,80	91,68 ± 8,85	85,98 ± 8,42	77,17 ± 7,95	84,53 ± 8,28	86,45 ± 3,88
1,715	90,47 ± 9,43	89,02 ± 8,59	83,22 ± 8,12	74,53 ± 7,61	81,32 ± 7,93	83,71 ± 2,74
1,801	87,85 ± 9,17	85,86 ± 8,32	79,94 ± 7,81	71,48 ± 7,29	77,87 ± 7,73	80,60 ± 3,61
1,893	85,19 ± 8,85	82,51 ± 8,02	76,56 ± 7,55	68,37 ± 7,04	74,05 ± 7,29	77,32 ± 3,47
1,993	82,29 ± 8,60	79,36 ± 7,73	73,17 ± 7,28	65,25 ± 6,75	70,25 ± 7,03	74,06 ± 3,35
2,101	78,94 ± 8,15	75,84 ± 7,39	69,38 ± 6,90	61,77 ± 6,38	66,07 ± 6,56	70,40 ± 3,18
2,218	75,31 ± 7,66	72,16 ± 7,06	65,33 ± 6,57	58,14 ± 6,11	61,81 ± 6,25	66,55 ± 3,04
2,346	71,72 ± 7,48	68,48 ± 6,74	61,45 ± 6,23	54,48 ± 5,76	57,53 ± 5,87	62,73 ± 2,88
2,484	67,99 ± 7,11	64,55 ± 6,40	57,28 ± 5,86	50,62 ± 5,41	53,20 ± 5,56	58,73 ± 2,72
2,635	64,13 ± 6,71	60,57 ± 6,08	53,13 ± 5,52	46,75 ± 5,06	48,81 ± 5,12	54,68 ± 2,56
2,801	60,14 ± 6,42	56,57 ± 5,77	49,02 ± 5,21	43,02 ± 4,77	44,53 ± 4,81	50,66 ± 2,43
2,982	56,32 ± 6,02	52,65 ± 5,46	45,19 ± 4,84	39,46 ± 4,44	40,53 ± 4,52	46,87 ± 2,27
3,182	52,51 ± 5,76	49,24 ± 5,16	41,53 ± 4,61	35,98 ± 4,18	36,78 ± 4,21	43,21 ± 2,15
3,403	48,46 ± 5,43	45,52 ± 4,89	37,84 ± 4,34	32,44 ± 3,90	32,97 ± 3,67	39,45 ± 2,02
3,647	44,10 ± 5,09	41,65 ± 4,60	34,14 ± 4,04	28,88 ± 3,60	29,25 ± 3,64	35,60 ± 1,89
3,919	39,82 ± 4,75	37,80 ± 4,32	30,57 ± 3,77	25,48 ± 3,34	25,65 ± 3,29	31,86 ± 1,76
4,222	35,54 ± 4,47	34,00 ± 4,05	27,10 ± 3,51	22,25 ± 3,09	22,30 ± 3,03	28,24 ± 1,64
4,562	31,44 ± 4,09	30,46 ± 3,74	23,76 ± 3,21	19,23 ± 2,81	19,22 ± 2,80	24,82 ± 1,50
4,946	27,50 ± 3,81	27,13 ± 3,50	20,71 ± 2,99	16,47 ± 2,57	16,48 ± 2,55	21,66 ± 1,40
5,379	23,74 ± 3,49	23,85 ± 3,23	17,82 ± 2,76	13,93 ± 2,37	14,02 ± 2,29	18,67 ± 1,28
5,872	20,35 ± 3,23	20,78 ± 2,97	15,22 ± 2,61	11,68 ± 2,16	11,85 ± 2,16	15,98 ± 1,18
6,437	17,19 ± 2,95	17,86 ± 2,73	12,83 ± 2,30	9,65 ± 1,98	9,91 ± 1,93	13,49 ± 1,08
7,067	14,29 ± 2,75	15,16 ± 2,49	10,62 ± 2,11	7,83 ± 1,82	8,20 ± 1,76	11,22 ± 0,99
7,842	11,61 ± 2,47	12,55 ± 2,25	8,65 ± 1,87	6,25 ± 1,62	6,69 ± 1,59	9,15 ± 0,89
8,725	9,27 ± 2,26	10,21 ± 2,00	6,96 ± 1,64	4,92 ± 1,46	5,40 ± 1,45	7,35 ± 0,80
9,767	7,30 ± 2,11	8,60 ± 1,75	5,37 ± 1,44	3,69 ± 1,26	4,41 ± 1,25	5,87 ± 0,71
11,008	5,46 ± 2,12	6,58 ± 1,49	4,34 ± 1,23	2,97 ± 1,11	3,43 ± 1,09	4,55 ± 0,65
12,503	4,22 ± 2,16	4,89 ± 1,30	3,38 ± 1,06	2,08 ± 0,93	2,62 ± 0,90	3,44 ± 0,60
14,328	3,13 ± 2,18	3,56 ± 1,20	2,46 ± 0,96	1,53 ± 0,83	1,94 ± 0,77	2,52 ± 0,67

TABLE 2

МАРГАНЕЦ

Таблица 2

Е, МэВ \ θ	31°	61°	91°	121°	151°	усреднённый спектр
1	2	3	4	5	6	7
0,102	0,10	10,49	7,66	10,08	14,23	8,51
0,136	0,10	13,76	12,32	14,65	19,94	12,15
0,182	0,10	20,63	19,42	21,43	27,08	17,85
0,221	2,74	28,18	26,16	28,31	34,74	24,03
0,241	4,02	31,73	28,66	31,33	38,86	26,92
0,265	7,97	37,47	33,73	36,48	44,67	32,07
0,292	12,77	42,37	38,45	41,79	49,55	36,98
0,323	19,13	49,59	43,82	46,99	56,11	43,13
0,360	26,54	57,02	51,51	53,67	66,10	52,97
0,403	40,47 ± 14,09	65,05 ± 13,82	57,65 ± 11,82	62,75 ± 12,61	75,66 ± 17,10	60,36 ± 6,26
0,455	39,43 ± 10,34	76,33 ± 10,65	64,96 ± 9,34	72,64 ± 10,57	87,02 ± 12,55	68,08 ± 4,80
0,519	44,46 ± 8,32	85,94 ± 8,98	72,46 ± 8,03	79,90 ± 8,76	99,79 ± 10,19	76,71 ± 3,97
0,594	56,71 ± 7,52	97,06 ± 8,37	79,14 ± 7,51	87,31 ± 7,90	105,70 ± 9,15	85,18 ± 3,62
0,689	67,63 ± 7,08	102,55 ± 7,59	83,70 ± 7,06	89,26 ± 7,31	103,19 ± 8,27	89,27 ± 3,35
0,808	77,56 ± 6,91	104,41 ± 7,73	88,92 ± 6,88	88,16 ± 6,83	100,90 ± 7,66	91,99 ± 3,22
0,961	89,36 ± 7,05	104,03 ± 7,85	92,18 ± 6,66	87,34 ± 6,56	101,74 ± 7,45	91,73 ± 3,17
1,152	95,99 ± 7,25	101,25 ± 7,27	92,10 ± 6,72	86,44 ± 6,35	100,74 ± 7,21	95,30 ± 3,12
1,308	97,69 ± 9,72	97,66 ± 8,92	90,20 ± 8,46	85,08 ± 8,25	96,79 ± 9,00	93,48 ± 3,97
1,365	97,78 ± 9,61	96,69 ± 8,57	89,48 ± 8,11	84,88 ± 8,09	94,40 ± 8,57	92,65 ± 3,85
1,426	97,19 ± 9,28	94,42 ± 8,25	87,72 ± 8,03	83,53 ± 7,85	91,52 ± 8,27	90,88 ± 3,73
1,491	96,17 ± 9,01	92,02 ± 8,09	85,72 ± 7,63	81,90 ± 7,55	86,95 ± 7,91	89,55 ± 3,59
1,560	95,18 ± 8,92	89,94 ± 7,82	83,67 ± 7,37	80,27 ± 7,29	83,34 ± 7,37	86,49 ± 3,47
1,635	93,62 ± 8,64	87,91 ± 7,58	81,48 ± 7,27	78,27 ± 7,02	79,92 ± 7,12	84,24 ± 3,37
1,715	91,77 ± 8,37	85,41 ± 7,38	79,02 ± 6,94	76,16 ± 6,76	76,54 ± 6,87	81,78 ± 3,28
1,801	89,36 ± 8,27	82,35 ± 7,15	75,90 ± 6,63	73,87 ± 6,54	72,51 ± 6,46	78,80 ± 3,15
1,893	86,66 ± 8,00	79,29 ± 6,90	72,79 ± 6,56	70,63 ± 6,36	68,32 ± 6,24	75,54 ± 3,06
1,993	83,39 ± 7,64	75,53 ± 6,63	68,97 ± 6,16	67,35 ± 6,02	63,90 ± 5,89	71,84 ± 2,90
2,101	78,46 ± 7,30	70,53 ± 6,25	63,89 ± 5,75	62,23 ± 5,67	58,75 ± 5,44	66,77 ± 2,73
2,218	76,00 ± 7,10	67,33 ± 5,98	60,57 ± 5,64	59,09 ± 5,45	55,54 ± 5,24	63,70 ± 2,64
2,346	71,15 ± 6,65	63,04 ± 5,70	55,99 ± 5,23	54,64 ± 5,09	50,94 ± 4,91	59,15 ± 2,48
2,484	66,66 ± 6,36	58,81 ± 5,38	51,48 ± 4,82	50,34 ± 4,75	46,95 ± 4,53	54,85 ± 2,33
2,635	62,23 ± 6,01	54,80 ± 5,06	47,35 ± 4,63	46,37 ± 4,44	43,25 ± 4,27	50,80 ± 2,20
2,801	57,33 ± 5,60	50,34 ± 4,76	42,96 ± 4,26	42,44 ± 4,14	39,65 ± 4,01	46,55 ± 2,05
2,982	52,18 ± 5,24	45,82 ± 4,44	38,51 ± 3,86	37,84 ± 3,79	35,57 ± 3,63	41,98 ± 1,89
3,182	47,66 ± 4,91	41,99 ± 4,11	34,68 ± 3,66	34,13 ± 3,51	32,55 ± 3,40	38,20 ± 1,77
3,403	42,66 ± 4,48	37,51 ± 3,81	30,34 ± 3,31	29,93 ± 3,19	29,04 ± 3,14	33,90 ± 1,62
3,647	37,08 ± 4,18	33,42 ± 3,53	26,75 ± 2,96	26,49 ± 2,92	25,93 ± 2,85	30,09 ± 1,49
3,919	33,26 ± 3,83	29,59 ± 3,22	23,34 ± 2,78	23,13 ± 2,65	23,13 ± 2,62	26,49 ± 1,36
4,222	29,44 ± 3,53	26,23 ± 3,00	20,72 ± 2,60	20,48 ± 2,44	20,99 ± 2,47	23,57 ± 1,27
4,562	25,52 ± 3,26	22,95 ± 2,78	17,84 ± 2,32	17,79 ± 2,24	18,62 ± 2,25	20,54 ± 1,16
4,945	21,51 ± 2,94	19,25 ± 2,42	15,04 ± 2,12	15,06 ± 2,00	15,95 ± 2,01	17,36 ± 1,04
5,379	18,50 ± 2,66	16,86 ± 2,27	12,99 ± 1,97	13,14 ± 1,85	14,14 ± 1,89	15,13 ± 0,96
5,872	15,18 ± 2,39	13,88 ± 2,03	10,55 ± 1,67	10,82 ± 1,63	11,78 ± 1,65	12,44 ± 0,85
6,437	12,65 ± 2,20	11,43 ± 1,78	8,55 ± 1,50	9,06 ± 1,47	9,66 ± 1,47	10,31 ± 0,76
7,087	10,34 ± 1,96	9,69 ± 1,66	7,12 ± 1,38	7,63 ± 1,34	8,48 ± 1,36	8,65 ± 0,69
7,842	8,65 ± 1,87	7,88 ± 1,52	5,92 ± 1,22	6,15 ± 1,19	7,14 ± 1,22	7,15 ± 0,54
8,725	6,39 ± 1,61	5,83 ± 1,26	4,49 ± 1,05	4,86 ± 1,04	5,61 ± 1,04	5,44 ± 0,54
9,707	4,78 ± 1,37	4,27 ± 1,02	3,35 ± 0,86	3,61 ± 0,84	4,35 ± 0,88	4,07 ± 0,45
11,008	3,32 ± 1,25	2,96 ± 0,77	2,26 ± 0,62	2,56 ± 0,64	2,99 ± 0,66	2,82 ± 0,37
12,503	1,81 ± 0,90	1,78 ± 0,55	1,12 ± 0,07	1,64 ± 0,45	1,94 ± 0,46	1,66 ± 0,27
14,328	1,09 ± 0,78	0,75 ± 0,32	0,50 ± 0,21	0,84 ± 0,29	1,23 ± 0,33	0,88 ± 0,19

TABLE 3

ХЕЛЕЗО

MeV θ / E, МэВ	31°		61°		91°		121°		151°		Усреднённый спектр	
1	2		3		4		5		6		7	
0,102	23,82		36,75		35,93		16,00		38,54		36,21	
0,136	33,55		56,86		50,13		22,17		52,98		41,93	
0,182	46,00		68,11		67,97		31,39		71,23		56,94	
0,221	56,14		84,55		65,97		42,49		87,62		70,95	
0,241	61,51		91,99		91,64		47,90		95,17		77,64	
0,265	68,14		103,00		102,41		55,53		108,76		86,98	
0,293	75,55		112,63		112,92		62,57		115,21		95,78	
0,323	84,58		130,97		127,04		72,64		130,92		109,19	
0,360	96,74		144,98		145,08		87,57		141,25		122,24	
0,403	105,35 ± 26,50		153,64 ± 20,64		137,46 ± 19,40		100,96 ± 17,21		144,42 ± 21,46		132,37 ± 9,51	
0,455	126,71 ± 20,34		166,10 ± 17,17		166,04 ± 16,83		119,22 ± 14,68		150,65 ± 16,85		146,68 ± 7,72	
0,516	138,15 ± 16,96		182,74 ± 15,95		176,38 ± 15,12		135,66 ± 13,19		159,12 ± 14,84		158,45 ± 6,82	
0,594	143,54 ± 15,26		162,13 ± 15,06		174,36 ± 14,26		144,83 ± 12,61		160,23 ± 13,86		161,01 ± 6,37	
0,689	150,24 ± 14,59		171,09 ± 1,04		167,91 ± 13,58		145,45 ± 12,20		156,94 ± 13,19		158,32 ± 6,05	
0,806	158,60 ± 14,48		164,33 ± 13,52		165,63 ± 13,40		145,74 ± 12,07		156,99 ± 13,04		158,52 ± 5,96	
0,951	165,17 ± 14,58		162,04 ± 13,58		163,08 ± 13,45		146,12 ± 12,23		157,37 ± 13,17		158,89 ± 6,01	
1,162	162,80 ± 14,60		156,11 ± 13,57		154,06 ± 13,15		139,82 ± 12,04		151,48 ± 13,03		153,25 ± 5,95	
1,306	158,49 ± 17,97		151,54 ± 15,07		145,60 ± 14,37		132,45 ± 13,59		142,94 ± 14,54		145,81 ± 6,79	
1,365	153,30 ± 17,44		149,05 ± 14,82		142,38 ± 14,07		128,48 ± 13,17		135,76 ± 14,17		142,39 ± 6,62	
1,426	149,27 ± 16,93		145,12 ± 14,46		138,57 ± 13,70		124,53 ± 12,86		124,19 ± 13,77		138,34 ± 6,44	
1,491	144,76 ± 16,36		140,73 ± 14,08		134,46 ± 13,33		120,21 ± 12,41		129,10 ± 13,25		133,86 ± 6,24	
1,550	140,43 ± 15,95		137,46 ± 13,84		130,58 ± 13,03		115,78 ± 11,97		124,06 ± 12,79		129,66 ± 6,07	
1,635	135,79 ± 15,50		132,95 ± 13,50		126,41 ± 12,72		110,97 ± 11,52		118,37 ± 12,32		124,90 ± 5,89	
1,715	131,19 ± 15,10		128,07 ± 13,19		122,22 ± 12,39		106,52 ± 11,18		112,99 ± 11,87		120,32 ± 5,73	
1,801	126,15 ± 14,68		123,60 ± 12,78		117,49 ± 12,06		101,90 ± 10,78		107,00 ± 11,36		115,23 ± 5,55	
1,893	121,01 ± 14,25		118,35 ± 12,45		112,52 ± 11,70		97,00 ± 10,44		100,74 ± 10,93		109,92 ± 5,38	
1,993	116,35 ± 13,83		112,92 ± 12,03		107,54 ± 11,32		92,29 ± 10,08		94,73 ± 10,42		104,77 ± 5,19	
2,101	111,24 ± 13,40		106,90 ± 11,56		102,13 ± 10,94		87,07 ± 9,65		88,50 ± 9,89		99,18 ± 4,99	
2,218	106,01 ± 12,94		100,86 ± 11,12		96,34 ± 10,50		81,82 ± 9,19		82,25 ± 9,40		93,41 ± 4,79	
2,346	100,76 ± 12,46		94,92 ± 10,62		91,12 ± 10,09		76,36 ± 8,75		76,31 ± 8,87		87,89 ± 4,59	
2,484	95,53 ± 11,98		88,27 ± 10,12		85,48 ± 9,65		71,14 ± 8,30		70,45 ± 8,33		82,17 ± 4,37	
2,635	90,30 ± 11,50		81,82 ± 9,60		79,72 ± 9,20		65,98 ± 7,86		64,79 ± 7,85		76,52 ± 4,15	
2,801	84,94 ± 10,99		75,09 ± 9,02		74,02 ± 8,72		60,93 ± 7,42		59,37 ± 7,34		70,85 ± 3,93	
2,982	80,23 ± 10,61		69,09 ± 8,51		68,50 ± 8,25		56,31 ± 7,01		54,82 ± 6,94		65,79 ± 3,74	
3,182	75,55 ± 10,18		63,34 ± 8,04		63,07 ± 7,84		51,95 ± 6,64		50,25 ± 6,54		60,69 ± 3,56	
3,403	70,64 ± 9,75		57,39 ± 7,52		58,39 ± 7,41		47,62 ± 6,26		45,93 ± 6,15		55,99 ± 3,36	
3,647	65,41 ± 9,31		51,58 ± 6,99		53,41 ± 6,97		43,37 ± 5,87		41,62 ± 5,73		51,08 ± 3,17	
3,919	60,11 ± 8,85		45,95 ± 6,47		46,62 ± 6,55		39,35 ± 5,50		37,41 ± 5,37		46,29 ± 2,98	
4,222	54,77 ± 8,33		40,74 ± 5,98		43,95 ± 6,12		35,50 ± 5,15		33,57 ± 4,96		41,67 ± 2,78	
4,502	49,73 ± 7,86		35,85 ± 5,50		39,36 ± 5,71		31,89 ± 4,78		29,55 ± 4,56		37,31 ± 2,59	
4,945	44,75 ± 7,36		31,10 ± 5,01		35,45 ± 5,32		28,53 ± 4,45		26,03 ± 4,22		33,18 ± 2,41	
5,379	39,65 ± 6,81		26,73 ± 4,54		31,52 ± 4,93		25,22 ± 4,09		22,68 ± 3,85		29,16 ± 2,21	
5,872	34,87 ± 6,30		22,81 ± 4,10		27,62 ± 4,50		22,17 ± 3,74		19,36 ± 3,45		25,37 ± 2,02	
6,437	30,28 ± 5,80		19,25 ± 3,70		23,95 ± 4,10		19,38 ± 3,43		16,26 ± 3,08		21,82 ± 1,84	
7,067	25,79 ± 5,27		16,17 ± 3,33		20,33 ± 3,65		16,71 ± 3,11		13,44 ± 2,74		18,49 ± 1,66	
7,842	21,34 ± 4,68		13,24 ± 2,95		16,89 ± 3,20		14,15 ± 2,73		10,85 ± 2,39		15,29 ± 1,47	
8,725	17,24 ± 4,14		10,65 ± 2,56		13,79 ± 2,76		11,73 ± 2,44		8,53 ± 2,05		12,39 ± 1,29	
9,767	14,32 ± 3,77		8,43 ± 2,19		11,65 ± 2,47		9,92 ± 2,19		6,85 ± 1,79		10,23 ± 1,15	
11,008	11,24 ± 3,56		6,59 ± 1,85		8,95 ± 2,04		7,37 ± 1,85		5,15 ± 1,47		7,98 ± 1,02	
12,503	5,66 ± 3,51		5,05 ± 1,62		6,97 ± 1,73		6,35 ± 1,59		3,65 ± 1,20		6,14 ± 0,93	
14,328	6,28 ± 3,31		3,77 ± 1,43		5,14 ± 1,46		4,66 ± 1,35		2,49 ± 0,98		4,51 ± 0,84	

TABLE 4

КОБАЛЬТ

Таблица 4

E, MeV / θ	31°	61°	91°	121°	151°	усреднённый спектр
1	2	3	4	5	6	7
0,102	16,14	32,61	29,84	28,24	34,70	28,30
0,156	22,?4	43,91	40,44	37,02	47,85	38,36
0,192	31,05	59,94	54,40	52,84	64,97	52,64
0,221	36,24	74,25	67,25	64,74	81,45	65,19
0,241	42,16	80,86	73,53	70,57	88,47	71,00
0,265	46,64	89,48	82,26	79,05	97,63	79,01
0,292	51,64	98,32	91,37	87,74	108,91	87,59
0,323	57,16	110,28	99,95	98,74	120,82	97,36
0,360	65,25	124,76	114,01	109,67	136,42	110,02
0,403	73,69 ± 18,22	142,76 ± 19,01	129,59 ± 19,42	123,93 ± 16,08	154,56 ± 20,36	124,91 ± 8,35
0,455	84,06 ± 13,52	155,89 ± 15,24	140,17 ± 15,11	141,97 ± 14,30	160,09 ± 15,94	116,04 ± 6,64
0,518	98,2 ± 11,??	163,60 ± 13,46	142,52 ± 12,47	153,88 ± 12,73	165,87 ± 13,75	144,64 ± 5,76
0,594	113,16 ± 10,89	169,12 ± 12,68	147,58 ± 11,55	162,42 ± 12,04	173,38 ± 12,99	153,13 ± 5,39
0,689	135,82 ± 10,98	174,30 ± 12,42	160,25 ± 11,58	165,16 ± 11,70	180,73 ± 12,80	163,25 ± 5,32
0,808	155,17 ± 11,44	181,28 ± 12,49	172,27 ± 11,90	165,36 ± 11,39	163,22 ± 12,03	171,56 ± 5,35
0,951	164,01 ± 11,64	182,71 ± 12,49	173,47 ± 11,87	163,52 ± 11,16	180,85 ± 10,35	172,67 ± 5,32
1,162	164,90 ± 13,61	175,86 ± 12,?7	165,47 ± 11,26	156,48 ± 10,73	172,96 ± 11,84	166,74 ± 5,15
1,308	165,65 ± 14,26	167,90 ± 13,64	154,81 ± 12,98	143,95 ± 12,25	165,43 ± 10,61	160,35 ± 5,97
1,365	162,63 ± 13,93	165,06 ± 13,18	151,16 ± 12,32	146,59 ± 11,98	161,75 ± 13,0.	157,50 ± 5,77
1,426	161,14 ± 13,48	161,31 ± 12,9?	147,00 ± 11,98	145,24 ± 11,69	157,46 ± 12,73	154,03 ± 5,62
1,491	158,07 ± 13,26	156,98 ± 12,??	143,31 ± 11,70	139,13 ± 11,23	152,52 ± 12,31	149,80 ± 5,47
1,560	156,37 ± 13,16	153,61 ± 12,34	138,34 ± 11,19	135,42 ± 10,88	147,39 ± 11,81	146,26 ± 5,31
1,635	154,40 ± 12,70	149,85 ± 11,96	134,02 ± 10,85	131,24 ± 10,51	142,35 ± 11,46	142,37 ± 5,15
1,715	151,23 ± 12,71	145,78 ± 11,75	129,60 ± 10,68	126,70 ± 10,19	126,54 ± 11,10	137,97 ± 5,06
1,801	147,01 ± 12,09	140,98 ± 11,25	124,07 ± 10,07	121,48 ± 9,73	130,45 ± 10,42	132,80 ± 4,80
1,893	142,28 ± 11,80	135,53 ± 11,02	118,71 ± 9,79	116,01 ± 9,41	123,63 ± 10,09	127,23 ± 4,67
1,993	137,17 ± 11,64	130,12 ± 10,72	113,14 ± 9,56	119,43 ± 9,09	116,90 ± 9,75	121,55 ± 4,56
2,101	130,93 ± 10,83	123,99 ± 10,08	107,18 ± 6,95	104,15 ± 6,46	109,66 ± 8,98	115,18 ± 4,25
2,218	123,88 ± 10,44	117,02 ± 9,75	100,61 ± 8,49	97,16 ± 8,10	101,51 ± 8,46	108,04 ± 4,05
2,346	116,68 ± 10,18	110,15 ± 9,37	94,11 ± 8,21	90,28 ± 7,66	93,61 ± 8,12	100,97 ± 3,91
2,484	109,00 ± 9,63	102,23 ± 8,73	86,85 ± 7,62	83,34 ± 7,13	85,82 ± 7,48	93,45 ± 3,65
2,635	100,35 ± 8,95	93,92 ± 8,18	79,73 ± 7,09	76,44 ± 6,71	78,22 ± 6,96	85,73 ± 3,41
2,801	91,74 ± 8,36	85,65 ± 7,66	72,48 ± 6,69	69,65 ± 6,21	70,88 ± 6,46	78,03 ± 3,18
2,982	83,84 ± 7,92	77,79 ± 7,07	65,95 ± 6,21	63,36 ± 5,76	64,18 ± 5,98	71,02 ± 2,96
3,182	76,30 ± 7,28	70,21 ± 6,56	59,04 ± 5,70	57,42 ± 5,38	57,73 ± 5,49	64,27 ± 2,74
3,403	68,70 ± 6,80	62,74 ± 6,10	53,31 ± 5,37	51,40 ± 4,96	51,45 ± 5,10	57,52 ± 2,55
3,647	60,97 ± 6,31	55,33 ± 5,53	46,86 ± 4,86	45,56 ± 4,52	45,22 ± 4,61	50,79 ± 2,35
3,919	53,74 ± 5,75	48,35 ± 5,05	40,85 ± 4,39	40,00 ± 4,17	39,50 ± 4,17	44,49 ± 2,12
4,222	47,00 ± 5,27	41,91 ± 4,65	35,24 ± 4,07	34,74 ± 3,78	34,21 ± 3,81	38,62 ± 1,95
4,562	40,85 ± 4,91	36,13 ± 4,20	30,10 ± 3,66	29,76 ± 3,39	29,43 ± 3,44	33,25 ± 1,77
4,945	35,35 ± 4,43	30,98 ± 3,81	25,55 ± 3,26	25,30 ± 3,08	25,24 ± 3,09	28,49 ± 1,60
5,379	30,03 ± 4,03	26,30 ± 3,52	21,38 ± 3,04	21,33 ± 2,79	21,37 ± 2,82	24,08 ± 1,46
5,872	25,36 ± 3,70	22,14 ± 3,16	17,73 ± 2,72	17,67 ± 2,46	17,98 ± 2,52	20,18 ± 1,32
6,437	21,19 ± 3,33	18,47 ± 2,84	14,52 ± 2,40	14,44 ± 2,23	14,97 ± 2,25	16,72 ± 1,18
7,087	17,47 ± 2,99	15,24 ± 2,60	11,73 ± 2,19	11,62 ± 1,98	12,31 ± 2,04	13,67 ± 1,07
7,842	14,13 ± 2,75	12,36 ± 2,29	9,29 ± 1,95	9,15 ± 1,74	9,92 ± 1,81	10,97 ± 0,95
8,725	11,22 ± 2,45	9,89 ± 2,00	7,21 ± 1,66	7,07 ± 1,54	7,88 ± 1,57	8,65 ± 0,84
9,767	8,93 ± 2,23	7,99 ± 1,77	5,56 ± 1,48	5,40 ± 1,35	6,28 ± 1,40	6,83 ± 0,75
11,008	6,99 ± 2,19	6,15 ± 1,50	4,23 ± 1,27	3,96 ± 1,11	4,87 ± 1,18	5,24 ± 0,67
12,503	5,15 ± 2,25	4,83 ± 1,31	3,06 ± 1,07	2,88 ± 0,95	3,63 ± 0,96	3,91 ± 0,62
14,328	3,96 ± 2,27	3,67 ± 1,21	2,24 ± 0,98	1,82 ± 0,82	2,73 ± 0,83	2,89 ± 0,59

TABLE 5

НИКЕЛЬ

Таблица 5

M_eV θ E, МэВ	31°	61°	91°	121°	151°	Усредненный спектр
1	2	3	4	5	6	7
0,102	6,42	22,15	16,27	17,17	14,48	15,30
0,136	10,18	31,04	22,77	24,59	20,74	21,93
0,163	14,92	44,02	30,33	33,49	30,35	30,62
0,221	20,65	54,36	38,85	41,66	40,20	39,14
0,241	22,04	52,36	42,76	45,53	44,14	42,87
0,265	25,56	67,62	47,57	50,82	56,17	48,35
0,292	29,99	73,75	52,52	55,74	56,03	54,02
0,323	35,84	62,76	56,60	61,28	65,17	60,81
0,360	54,84	95,49	65,96	71,50	75,50	70,17
0,403	55,44 ± 21,38	106,35 ± 19,29	74,54 ± 21,57	80,14 ± 18,56	86,43 ± 19,98	8,58 ± 9,03
0,455	63,45 ± 14,65	114,41 ± 14,59	84,87 ± 14,05	91,87 ± 13,74	99,45 ± 14,64	92,00 ± 6,43
0,518	85,57 ± 12,01	115,25 ± 11,97	96,78 ± 10,96	99,69 ± 11,27	111,67 ± 11,90	101,83 ± 5,20
0,594	92,95 ± 10,78	115,26 ± 10,52	101,76 ± 9,72	104,40 ± 9,87	119,13 ± 10,69	108,10 ± 4,62
0,689	118,14 ± 10,41	118,49 ± 9,82	105,63 ± 9,03	111,41 ± 9,31	127,52 ± 10,20	115,84 ± 4,37
0,803	131,80 ± 10,41	123,26 ± 9,49	107,93 ± 6,55	117,55 ± 9,04	135,35 ± 10,05	123,18 ± 4,26
0,961	140,32 ± 10,45	124,04 ± 9,25	105,60 ± 8,13	115,72 ± 8,64	132,82 ± 9,63	123,70 ± 4,14
1,162	136,43 ± 10,03	118,63 ± 8,75	95,54 ± 7,51	107,23 ± 7,97	118,39 ± 8,63	115,84 ± 3,85
1,308	129,60 ± 12,58	113,05 ± 10,86	93,53 ± 10,10	100,57 ± 10,18	107,07 ± 10,57	108,77 ± 4,87
1,565	126,49 ± 12,15	110,73 ± 10,50	91,66 ± 9,35	98,24 ± 9,90	105,04 ± 10,20	106,03 ± 4,63
1,426	122,77 ± 11,77	107,79 ± 10,08	89,34 ± 8,96	95,54 ± 9,53	98,91 ± 9,75	102,87 ± 4,50
1,491	118,48 ± 11,30	104,46 ± 9,77	87,02 ± 8,86	92,64 ± 9,04	94,89 ± 9,30	99,46 ± 4,33
1,560	115,27 ± 10,80	101,66 ± 9,44	84,97 ± 8,35	89,89 ± 8,71	90,44 ± 8,74	96,45 ± 4,13
1,635	111,56 ± 10,05	98,72 ± 9,12	82,72 ± 7,99	87,12 ± 8,34	86,51 ± 8,42	93,33 ± 4,00
1,715	107,92 ± 10,13	95,59 ± 8,64	80,51 ± 8,03	84,38 ± 8,05	82,74 ± 8,02	90,23 ± 3,87
1,861	103,50 ± 9,75	91,99 ± 6,56	77,93 ± 7,51	81,10 ± 7,55	76,51 ± 7,72	85,68 ± 3,69
1,893	99,76 ± 9,60	88,22 ± 6,24	74,95 ± 7,14	77,56 ± 7,44	74,18 ± 7,33	82,93 ± 3,63
1,993	95,95 ± 9,23	84,37 ± 7,96	72,20 ± 7,27	73,83 ± 7,19	70,19 ± 7,09	79,31 ± 3,48
2,101	91,67 ± 8,88	80,30 ± 7,68	68,97 ± 6,74	69,98 ± 6,70	65,94 ± 6,70	75,39 ± 3,30
2,218	87,19 ± 8,57	75,86 ± 7,31	65,29 ± 6,41	65,77 ± 6,48	61,27 ± 6,34	71,08 ± 3,16
2,346	82,77 ± 8,14	71,11 ± 6,97	61,76 ± 6,34	61,39 ± 6,17	56,76 ± 5,95	66,76 ± 3,02
2,484	78,12 ± 7,76	66,30 ± 6,63	57,93 ± 5,93	56,90 ± 5,80	52,24 ± 5,58	62,31 ± 2,85
2,635	73,15 ± 7,40	61,39 ± 6,26	53,93 ± 5,51	52,35 ± 5,48	47,83 ± 5,18	57,71 ± 2,69
2,801	68,12 ± 6,99	56,13 ± 5,88	49,90 ± 5,38	47,57 ± 5,06	43,46 ± 4,86	53,03 ± 2,54
2,982	63,37 ± 6,63	51,22 ± 5,56	45,92 ± 5,02	43,22 ± 4,73	39,45 ± 4,51	48,64 ± 2,39
3,182	58,74 ± 6,30	46,55 ± 5,22	42,12 ± 4,60	39,04 ± 4,47	35,77 ± 4,22	44,44 ± 2,24
3,403	53,79 ± 5,97	41,86 ± 4,87	38,24 ± 4,48	34,79 ± 4,11	32,36 ± 3,92	40,16 ± 2,11
3,647	48,46 ± 5,57	37,26 ± 4,57	34,35 ± 4,15	30,66 ± 3,77	28,60 ± 3,64	35,91 ± 1,96
3,919	43,39 ± 5,21	32,87 ± 4,25	30,66 ± 3,76	26,80 ± 3,52	25,62 ± 3,37	31,86 ± 1,82
4,222	38,41 ± 4,84	28,71 ± 3,92	26,95 ± 3,61	23,22 ± 3,21	22,67 ± 3,16	27,99 ± 1,70
4,562	33,69 ± 4,45	24,91 ± 3,66	23,56 ± 3,34	19,98 ± 2,93	20,09 ± 2,88	24,43 ± 1,56
4,945	29,33 ± 4,14	21,66 ± 3,38	20,49 ± 2,97	17,09 ± 2,71	17,55 ± 2,66	21,21 ± 1,44
5,379	25,40 ± 3,82	18,61 ± 3,11	17,64 ± 2,81	14,45 ± 2,49	15,29 ± 2,45	18,28 ± 1,33
5,872	21,83 ± 3,52	16,01 ± 2,86	15,13 ± 2,61	12,20 ± 2,27	13,26 ± 2,25	15,69 ± 1,23
6,437	18,55 ± 3,26	13,67 ± 2,66	12,82 ± 2,52	10,21 ± 2,12	11,40 ± 2,05	13,33 ± 1,13
7,067	15,57 ± 3,04	11,56 ± 2,45	10,69 ± 2,16	8,40 ± 1,92	9,72 ± 1,90	11,19 ± 1,04
7,842	12,85 ± 2,78	9,64 ± 2,23	8,72 ± 1,98	6,76 ± 1,72	8,13 ± 1,70	9,22 ± 0,95
8,725	10,44 ± 2,60	7,95 ± 1,98	7,10 ± 1,69	5,32 ± 1,56	6,67 ± 1,53	7,48 ± 0,85
9,767	8,37 ± 2,46	6,52 ± 1,72	5,70 ± 1,53	4,15 ± 1,39	5,62 ± 1,37	6,11 ± 0,78
11,008	6,66 ± 2,55	5,35 ± 1,53	4,37 ± 1,33	3,15 ± 1,17	4,39 ± 1,17	4,79 ± 0,73
12,503	5,16 ± 2,70	4,21 ± 1,35	3,11 ± 1,03	2,47 ± 1,00	3,44 ± 0,97	3,68 ± 0,70
14,328	3,91 ± 2,60	3,19 ± 1,23	2,35 ± 1,00	1,70 ± 0,88	2,59 ± 0,83	2,75 ± 0,65

TABLE 6

МЕДЬ   Таблица 6

θ MeV E,м	31°	θ MeV E,м	63°	93°	123°	153°	Усреднённый спектр
0,102	38,88	0,100	86,14	51,66	38,32	54,65	53,93
0,136	51,30	0,132	116,52	69,02	52,05	72,45	72,27
0,182	71,36	0,178	157,72	93,31	70,56	98,30	98,25
0,221	87,12	0,215	191,80	113,15	86,78	119,63	119,69
0,241	95,14	0,235	209,69	123,63	94,25	131,19	120,78
0,265	105,26	0,257	231,54	136,03	104,05	146,40	144,66
0,292	113,24	0,284	256,95	150,64	115,73	159,73	159,26
0,323	121,73	0,314	273,51	168,51	128,57	178,79	174,21
0,360	130,35	0,350	283,33	187,58	142,65	196,41	188,07
0,403	140,19	0,392	288,64	208,27	163,06	215,95	203,22
0,455	149,87 ± 20,30	0,443	287,71 ± 26,62	223,62 ± 21,72	186,63 ± 19,31	233,42 ± 21,22	216,25 ± 9,83
0,518	155,79 ± 16,80	0,503	277,75 ± 22,83	234,69 ± 19,92	205,78 ± 17,13	239,27 ± 18,66	222,66 ± 8,58
0,594	169,31 ± 15,34	0,578	269,08 ± 20,58	240,31 ± 19,10	214,45 ± 16,06	237,37 ± 17,27	226,10 ± 7,95
0,689	182,94 ± 14,71	0,670	266,60 ± 19,46	242,59 ± 18,64	216,02 ± 15,35	231,27 ± 16,33	227,85 ± 7,60
0,808	188,79 ± 14,31	0,785	261,45 ± 18,56	233,85 ± 17,72	208,96 ± 14,58	220,19 ± 15,23	222,85 ± 7,23
0,951	187,31 ± 13,74	0,934	246,51 ± 17,42	213,94 ± 16,27	195,27 ± 13,62	204,04 ± 14,18	209,41 ± 6,76
1,132	180,14 ± 13,12	1,130	221,45 ± 15,75	190,54 ± 14,67	176,39 ± 12,43	184,18 ± 12,89	190,54 ± 6,18
1,303	174,52 ± 16,65	1,271	203,94 ± 18,54	176,07 ± 16,23	163,39 ± 14,62	171,05 ± 15,08	177,50 ± 7,28
1,365	172,37 ± 16,25	1,327	198,16 ± 17,89	171,49 ± 15,72	158,53 ± 14,18	166,19 ± 14,56	173,35 ± 7,05
1,426	168,54 ± 15,74	1,386	191,35 ± 17,15	166,05 ± 15,00	153,00 ± 13,58	160,68 ± 14,11	167,32 ± 6,78
1,491	165,04 ± 15,27	1,449	184,26 ± 16,50	160,36 ± 14,47	147,21 ± 13,04	154,74 ± 13,47	162,32 ± 6,83
1,560	161,07 ± 14,80	1,517	177,71 ± 15,84	155,29 ± 13,92	141,47 ± 12,43	148,89 ± 12,94	156,80 ± 6,33
1,635	157,25 ± 14,47	1,589	171,79 ± 15,38	150,34 ± 13,56	136,07 ± 11,95	142,74 ± 12,36	151,64 ± 6,03
1,715	153,08 ± 14,02	1,667	165,38 ± 14,86	145,09 ± 13,04	130,78 ± 11,43	136,78 ± 11,94	146,22 ± 5,86
1,801	147,76 ± 13,66	1,751	153,16 ± 14,32	139,43 ± 12,64	125,19 ± 10,99	130,11 ± 11,38	140,13 ± 5,66
1,893	142,99 ± 13,35	1,841	150,53 ± 13,75	132,68 ± 12,10	118,71 ± 10,49	122,67 ± 10,89	133,53 ± 5,45
1,993	137,75 ± 12,90	1,938	143,31 ± 13,22	126,80 ± 11,66	112,66 ± 10,11	115,84 ± 10,36	127,27 ± 5,24
2,101	131,64 ± 12,44	2,043	135,96 ± 12,66	120,11 ± 11,12	106,45 ± 9,59	109,01 ± 9,88	120,63 ± 5,01

TABLE 6 (continued)

М Е Д Ь

M,V E ⟍ θ	31°	M,V $E,МэВ$	63°	93°	123°	153°	Усреднённый спектр
2,218	125,66 ± 12,04	2,157	123,68 ± 12,14	113,73 ± 10,64	100,32 ± 9,16	102,05 ± 9,34	114,09 ± 4,80
2,346	118,96 ± 11,45	2,281	121,04 ± 11,59	106,65 ± 10,06	93,95 ± 8,65	94,80 ± 8,87	107,06 ± 4,56
2,484	112,07 ± 10,98	2,416	113,24 ± 11,05	99,23 ± 9,57	87,59 ± 8,20	87,91 ± 8,33	100,01 ± 4,34
2,635	104,71 ± 10,45	2,563	104,99 ± 10,41	92,05 ± 8,96	81,33 ± 7,75	80,79 ± 7,81	92,75 ± 4,09
2,801	97,29 ± 9,90	2,724	97,11 ± 9,90	84,95 ± 8,45	74,66 ± 7,30	74,02 ± 7,28	85,61 ± 3,86
2,982	90,35 ± 9,40	2,900	89,53 ± 9,37	77,72 ± 7,84	68,25 ± 6,78	67,42 ± 6,87	78,65 ± 3,63
3,182	83,66 ± 9,02	3,095	82,13 ± 8,85	70,73 ± 7,35	62,32 ± 6,36	61,60 ± 6,38	71,97 ± 3,43
3,403	76,22 ± 8,45	3,310	74,76 ± 8,30	64,15 ± 6,83	56,37 ± 5,89	54,72 ± 5,95	65,24 ± 3,20
3,647	68,52 ± 7,95	3,548	67,84 ± 7,83	57,65 ± 6,36	50,56 ± 5,60	48,91 ± 5,50	58,76 ± 3,00
3,919	61,75 ± 7,49	3,812	60,78 ± 7,30	51,24 ± 5,86	45,08 ± 5,09	43,03 ± 5,10	52,37 ± 2,79
4,222	54,85 ± 7,00	4,108	53,93 ± 6,80	45,09 ± 5,39	39,55 ± 4,76	37,35 ± 4,68	46,16 ± 2,59
4,562	48,28 ± 6,50	4,439	47,79 ± 6,35	39,41 ± 4,93	34,51 ± 4,33	32,21 ± 4,30	40,44 ± 2,40
4,945	42,19 ± 6,14	4,812	41,76 ± 5,86	34,14 ± 4,50	29,72 ± 3,98	27,33 ± 3,90	35,03 ± 2,22
5,379	36,59 ± 5,70	5,235	36,33 ± 5,40	29,48 ± 4,11	25,21 ± 3,57	22,78 ± 3,55	30,09 ± 2,04
5,872	31,57 ± 5,33	5,715	31,68 ± 5,02	25,27 ± 3,76	21,23 ± 3,30	18,85 ± 3,26	25,73 ± 1,89
6,437	27,20 ± 5,04	6,266	27,23 ± 4,61	21,42 ± 3,40	17,65 ± 2,96	15,33 ± 2,98	21,77 ± 1,74
7,087	23,04 ± 4,72	6,900	23,17 ± 4,20	17,99 ± 3,01	14,42 ± 2,70	12,28 ± 2,70	18,18 ± 1,59
7,842	19,25 ± 4,39	7,636	19,35 ± 3,74	14,85 ± 2,72	11,48 ± 2,40	9,02 ± 2,45	14,91 ± 1,44
8,725	15,93 ± 4,13	8,497	16,20 ± 3,34	12,27 ± 2,38	9,09 ± 2,17	7,53 ± 2,22	12,20 ± 1,32
9,767	12,87 ± 3,82	9,513	13,06 ± 2,85	9,87 ± 2,03	6,96 ± 1,83	5,11 ± 1,94	9,57 ± 1,16
11,008	10,38 ± 3,76	10,725	10,47 ± 2,49	7,85 ± 1,74	5,11 ± 1,57	3,94 ± 1,64	7,55 ± 1,16
12,503	8,02 ± 3,76	12,184	8,04 ± 2,09	5,82 ± 1,43	3,58 ± 1,24	2,88 ± 1,38	5,67 ± 0,98
14,328	6,00 ± 3,44	13,966	5,84 ± 1,72	4,35 ± 1,19	2,34 ± 1,00	2,08 ± 1,18	4,12 ± 0,86

Таблица 7

E, МэВ	31°	61°	91°	121°	151°	Усреднённый спектр
1	2	3	4	5	6	7
0,102	14,28	26,23	18,58	18,10	48,17	25,0?
0,136	19,63	36,02	25,06	24,01	65,76	34,10
0,182	26,06	47,95	34,20	32,65	89,41	46,05
0,221	32,51	58,65	41,77	40,22	108,28	56,33
0,241	35,04	64,93	46,15	44,07	114,57	60,95
0,265	39,07	71,03	50,01	49,01	120,32	65,89
0,292	43,45	80,42	56,59	53,97	124,44	71,77
0,323	47,79	88,06	63,19	60,58	125,38	77,14
0,360	53,28	99,90	70,36	67,21	126,18	83,39
0,403	59,45 ± 16,93	108,25 ± 17,17	78,11 ± 15,88	75,50 ± 15,10	124,74 ± 20,84	89,21 ± 7,73
0,455	67,70 ± 13,03	122,19 ± 13,44	87,54 ± 12,59	85,76 ± 12,67	118,07 ± 15,16	96,25 ± 5,99
0,518	77,51 ± 10,46	126,76 ± 11,43	98,48 ± 10,15	87,91 ± 10,18	107,32 ± 11,84	99,59 ± 4,84
0,594	88,61 ± 9,26	120,82 ± 9,98	103,68 ± 9,06	90,76 ± 8,80	97,11 ± 9,81	100,20 ± 4,20
0,689	101,11 ± 8,86	113,26 ± 8,92	101,24 ± 8,19	92,95 ± 7,99	88,18 ± 8,44	99,35 ± 3,79
0,808	107,42 ± 8,51	106,59 ± 8,10	92,94 ± 7,28	90,98 ± 7,32	82,15 ± 7,39	96,02 ± 3,46
0,961	99,76 ± 7,70	96,14 ± 7,37	80,79 ± 6,31	82,65 ± 6,53	79,49 ± 6,75	88,17 ± 3,11
1,162	83,53 ± 6,58	84,93 ± 6,40	68,17 ± 5,42	70,83 ± 5,63	73,93 ± 6,05	76,29 ± 2,69
1,308	73,51 ± 8,51	75,42 ± 7,86	60,60 ± 7,14	62,75 ± 7,57	67,57 ± 8,42	67,97 ± 3,51
1,365	70,52 ± 8,19	71,78 ± 7,44	58,04 ± 6,73	59,73 ± 7,21	64,86 ± 8,03	64,99 ± 3,37
1,426	67,29 ± 7,73	67,87 ± 7,04	55,29 ± 6,37	56,47 ± 6,76	61,76 ± 7,56	61,74 ± 3,18
1,491	64,14 ± 7,36	63,94 ± 6,68	52,42 ± 5,98	53,12 ± 6,33	58,53 ± 7,08	58,43 ± 3,00
1,560	61,34 ± 7,04	60,14 ± 6,31	49,77 ± 5,69	50,02 ± 5,89	55,36 ± 6,70	55,33 ± 2,84
1,635	58,49 ± 6,70	55,31 ± 5,97	47,13 ± 5,39	46,85 ± 5,53	52,09 ± 6,31	52,18 ± 2,68
1,715	55,73 ± 6,40	52,74 ± 5,68	44,57 ± 5,10	43,74 ± 5,23	48,80 ± 5,95	49,12 ± 2,54
1,801	52,89 ± 6,13	49,08 ± 5,39	41,95 ± 4,86	40,55 ± 4,94	45,40 ± 5,64	45,97 ± 2,42
1,893	50,09 ± 5,84	45,60 ± 5,13	39,34 ± 4,67	37,40 ± 4,69	42,07 ± 5,33	42,90 ± 2,30
1,993	47,34 ± 5,57	42,27 ± 4,86	36,89 ± 4,42	34,48 ± 4,42	38,91 ± 5,02	39,38 ± 2,18
2,101	44,41 ± 5,31	38,85 ± 4,56	34,34 ± 4,18	31,56 ± 4,16	35,71 ± 4,75	36,97 ± 2,06

TABLE 7 (continued)

И Т Т Р И Й

E,МэВ \ θ	31°	61°	91°	121°	151°	Усреднённый спектр
1	2	3	4	5	6	7
2,218	41,33 ± 5,01	35,45 ± 4,28	31,82 ± 3,95	28,69 ± 3,90	32,59 ± 4,47	33,98 ± 1,94
2,346	38,33 ± 4,71	32,27 ± 4,02	29,44 ± 3,70	26,02 ± 3,65	29,62 ± 4,14	31,14 ± 1,81
2,484	35,29 ± 4,46	29,26 ± 3,76	27,15 ± 3,48	23,50 ± 3,40	26,75 ± 3,87	28,39 ± 1,70
2,635	32,28 ± 4,17	26,42 ± 3,53	24,92 ± 3,28	21,10 ± 3,17	23,94 ± 3,59	25,73 ± 1,59
2,801	29,35 ± 3,89	23,71 ± 3,31	22,76 ± 3,07	18,87 ± 2,95	21,25 ± 3,33	23,19 ± 1,48
2,982	25,66 ± 3,68	21,21 ± 3,11	20,75 ± 2,90	16,87 ± 2,77	18,85 ± 3,11	20,87 ± 1,40
3,182	24,19 ± 3,47	18,92 ± 2,93	18,84 ± 2,73	15,09 ± 2,59	16,60 ± 2,91	18,73 ± 1,31
3,403	21,78 ± 3,26	16,69 ± 2,76	16,92 ± 2,55	13,41 ± 2,44	14,42 ± 2,72	16,65 ± 1,23
3,647	19,41 ± 3,10	14,56 ± 2,61	15,06 ± 2,40	11,78 ± 2,29	12,38 ± 2,54	14,64 ± 1,16
3,919	17,20 ± 2,91	12,58 ± 2,45	13,27 ± 2,26	10,30 ± 2,16	10,50 ± 2,38	12,77 ± 1,09
4,222	15,08 ± 2,71	10,73 ± 2,30	11,60 ± 2,11	8,93 ± 2,01	8,78 ± 2,20	11,02 ± 1,02
4,562	13,14 ± 2,54	9,04 ± 2,15	10,04 ± 1,96	7,65 ± 1,88	7,24 ± 2,06	9,42 ± 0,95
4,945	11,41 ± 2,39	7,52 ± 2,01	8,57 ± 1,84	6,50 ± 1,76	5,89 ± 1,91	7,98 ± 0,89
5,379	9,84 ± 2,22	6,17 ± 1,88	7,21 ± 1,70	5,45 ± 1,64	4,71 ± 1,78	6,67 ± 0,83
5,872	8,46 ± 2,08	5,01 ± 1,75	6,02 ± 1,56	4,52 ± 1,53	3,72 ± 1,66	5,54 ± 0,77
6,437	7,19 ± 1,96	3,99 ± 1,63	4,95 ± 1,43	3,70 ± 1,43	2,87 ± 1,55	4,54 ± 0,72
7,087	6,04 ± 1,82	3,09 ± 1,51	3,99 ± 1,33	2,96 ± 1,33	2,15 ± 1,41	3,65 ± 0,67
7,842	4,95 ± 1,68	2,29 ± 1,37	3,13 ± 1,19	2,29 ± 1,21	1,56 ± 1,28	2,84 ± 0,60
8,725	4,01 ± 1,55	1,64 ± 1,21	2,42 ± 1,06	1,73 ± 1,08	1,09 ± 1,15	2,18 ± 0,54
9,767	3,24 ± 1,45	1,14 ± 1,05	1,79 ± 0,92	1,16 ± 0,95	0,68 ± 1,01	1,60 ± 0,49
11,008	2,65 ± 1,46	0,75 ± 0,91	1,32 ± 0,78	0,85 ± 0,82	0,43 ± 0,86	1,20 ± 0,44
12,503	1,99 ± 1,53	0,48 ± 0,83	1,00 ± 0,68	0,64 ± 0,70	0,27 ± 0,72	0,88 ± 0,42
14,328	1,52 ± 1,48	0,22 ± 0,77	0,74 ± 0,61	0,43 ± 0,62	0,12 ± 0,62	0,61 ± 0,39

TABLE 8

ЦИРКОНИЙ

MeV θ / E, Мэв	31°	61°	91°	121°	151°	Усреднённый спектр
1	2	3	4	5	6	7
0,102	18,28	25,90	26,19	24,05	29,97	24,88
0,136	26,28	37,54	37,05	33,93	41,69	35,30
0,182	35,85	50,26	50,99	44,80	55,51	47,48
0,221	44,00	61,56	62,57	54,81	67,94	58,18
0,241	48,09	68,25	69,25	60,91	75,40	64,38
0,265	54,27	76,50	76,40	66,08	83,28	71,30
0,292	60,48	85,36	87,07	74,32	93,25	80,10
0,323	66,66	94,38	96,41	82,65	101,84	88,39
0,360	74,61	105,62	107,43	92,56	114,11	98,87
0,403	83,67 ± 20,55	119,36 ± 18,72	118,87 ± 20,68	102,66 ± 15,26	126,96 ± 19,41	110,30 ± 8,51
0,455	97,03 ± 15,29	138,02 ± 14,76	129,17 ± 15,73	115,14 ± 13,60	137,32 ± 14,85	123,34 ± 6,64
0,518	108,49 ± 12,60	144,21 ± 12,65	133,86 ± 12,71	122,02 ± 12,00	136,95 ± 12,27	129,30 ± 5,56
0,594	116,30 ± 11,23	147,95 ± 11,62	136,25 ± 11,33	124,70 ± 10,63	135,08 ± 10,98	132,06 ± 4,99
0,689	120,47 ± 10,42	153,66 ± 11,22	135,36 ± 10,54	125,77 ± 9,90	133,26 ± 10,16	133,70 ± 4,67
0,808	126,09 ± 9,83	154,44 ± 10,88	131,13 ± 9,75	122,97 ± 9,22	130,08 ± 9,51	132,74 ± 4,41
0,961	129,97 ± 9,71	148,28 ± 10,33	126,41 ± 9,21	119,27 ± 8,73	126,52 ± 9,06	130,09 ± 4,21
1,162	130,71 ± 9,60	136,91 ± 9,55	120,56 ± 8,71	114,75 ± 8,28	121,77 ± 8,61	124,94 ± 4,00
1,308	127,56 ± 11,98	128,15 ± 10,95	114,47 ± 10,58	109,86 ± 10,32	117,12 ± 10,50	119,43 ± 4,86
1,365	125,51 ± 11,52	124,19 ± 10,44	111,52 ± 10,13	107,20 ± 9,90	114,78 ± 10,08	116,54 ± 4,66
1,426	122,52 ± 11,18	119,40 ± 10,00	107,77 ± 9,85	103,90 ± 9,57	111,83 ± 9,74	113,09 ± 4,51
1,491	118,43 ± 10,76	114,19 ± 9,65	103,38 ± 9,31	100,05 ± 9,06	107,90 ± 9,37	108,79 ± 4,31
1,560	114,27 ± 10,27	108,76 ± 9,18	98,87 ± 8,83	96,07 ± 8,64	104,00 ± 8,91	104,40 ± 4,11
1,635	109,73 ± 9,90	102,98 ± 8,70	93,92 ± 8,56	91,81 ± 8,25	99,49 ± 8,51	99,58 ± 3,93
1,715	104,93 ± 9,52	96,97 ± 8,31	93,85 ± 8,06	87,17 ± 7,84	94,48 ± 8,13	94,46 ± 3,75
1,801	99,27 ± 8,85	90,35 ± 7,83	83,36 ± 7,52	81,96 ± 7,38	88,77 ± 7,61	88,77 ± 3,51
1,896	93,13 ± 8,56	85,73 ± 7,40	77,67 ± 7,33	76,46 ± 7,01	82,85 ± 7,21	82,78 ± 3,36
1,993	86,95 ± 8,09	77,08 ± 6,96	71,97 ± 6,82	71,07 ± 6,65	76,68 ± 6,83	76,75 ± 3,17
2,101	80,42 ± 7,62	70,44 ± 6,45	65,96 ± 6,29	65,29 ± 6,18	70,15 ± 6,33	70,45 ± 2,95

TABLE 8 (continued)

Ц И Р К О Н И Й

Продолжение таблицы 8

E, Мэв	θ 31°		61°		91°		121°		151°		Усредненный спектр	
1	2		3		4		5		6		7	
2,218	73,69 ±	7,16	63,68 ±	5,98	59,94 ±	6,01	59,42 ±	5,79	63,49 ±	5,90	64,05 ±	2,76
2,346	67,07 ±	6,73	57,21 ±	5,58	54,25 ±	5,58	53,67 ±	5,38	57,05 ±	5,48	57,85 ±	2,58
2,494	60,48 ±	6,19	51,05 ±	5,14	48,67 ±	5,07	48,12 ±	4,94	50,73 ±	5,00	51,81 ±	2,36
2,635	54,13 ±	5,76	45,33 ±	4,70	43,34 ±	4,80	42,76 ±	4,57	44,72 ±	4,53	46,06 ±	2,19
2,801	48,08 ±	5,23	40,00 ±	4,38	38,38 ±	4,41	37,63 ±	4,18	39,04 ±	4,14	40,63 ±	2,01
2,932	42,68 ±	4,90	35,32 ±	4,04	33,91 ±	4,00	33,03 ±	3,85	34,03 ±	3,79	35,60 ±	1,85
3,182	37,70 ±	4,54	31,07 ±	3,71	29,81 ±	3,80	26,79 ±	3,56	29,50 ±	3,44	31,38 ±	1,71
3,403	32,97 ±	4,28	27,06 ±	3,47	25,91 ±	3,51	24,79 ±	3,26	25,38 ±	3,17	27,22 ±	1,59
3,647	28,56 ±	3,88	23,41 ±	3,20	22,26 ±	3,17	21,02 ±	2,97	21,55 ±	2,88	23,36 ±	1,45
3,919	24,56 ±	3,61	20,04 ±	2,96	19,01 ±	3,00	17,66 ±	2,74	18,17 ±	2,61	19,89 ±	1,34
4,222	21,01 ±	3,38	17,08 ±	2,75	16,13 ±	2,76	14,73 ±	2,51	15,23 ±	2,41	16,83 ±	1,24
4,562	17,90 ±	3,12	14,45 ±	2,55	13,60 ±	2,49	12,16 ±	2,29	12,70 ±	2,19	14,16 ±	1,14
4,945	15,18 ±	2,87	12,17 ±	2,34	11,46 ±	2,35	10,00 ±	2,12	10,53 ±	1,98	11,87 ±	1,05
5,379	12,82 ±	2,69	10,19 ±	2,19	9,59 ±	2,20	8,17 ±	1,95	8,66 ±	1,82	9,88 ±	0,98
5,872	10,60 ±	2,49	8,49 ±	2,05	8,01 ±	1,98	6,63 ±	1,80	7,08 ±	1,67	8,20 ±	0,90
6,437	9,04 ±	2,31	6,99 ±	1,87	6,66 ±	1,87	5,34 ±	1,67	5,72 ±	1,53	6,75 ±	0,83
7,087	7,48 ±	2,17	5,71 ±	1,74	5,52 ±	1,73	4,28 ±	1,53	4,54 ±	1,43	5,51 ±	0,77
7,842	6,10 ±	2,00	4,56 ±	1,60	4,53 ±	1,51	3,37 ±	1,39	3,51 ±	1,27	4,41 ±	0,70
8,725	4,92 ±	1,84	3,58 ±	1,41	3,69 ±	1,38	2,63 ±	1,25	2,66 ±	1,12	3,49 ±	0,63
9,767	3,99 ±	1,77	2,66 ±	1,23	2,99 ±	1,23	1,93 ±	1,11	2,01 ±	0,99	2,72 ±	0,58
11,018	3,10 ±	1,79	2,09 ±	1,05	2,42 ±	1,03	1,60 ±	0,95	1,42 ±	0,85	2,13 ±	0,53
12,503	2,51 ±	1,88	1,62 ±	0,95	1,98 ±	0,92	1,22 ±	0,82	1,01 ±	0,70	1,66 ±	0,50
14,328	1,83 ±	1,86	1,22 ±	0,89	1,66 ±	0,65	0,89 ±	0,75	0,64 ±	0,60	1,26 ±	0,48

TABLE 9

Н И О Б И Й

Таблица 9

MeV θ / E, МэВ	31°	61°	91°	121°	151°	Усреднённый спектр
1	2	3	4	5	6	7
0.102	26.36	54.87	45.50	73.46	63.29	52.70
0.136	37.06	77.59	64.39	102.33	87.59	73.79
0.162	51.34	111.68	88.64	136.73	119.71	101.66
0.221	65.14	126.61	111.39	167.42	149.45	124.00
0.241	72.56	138.92	122.19	170.04	166.81	135.30
0.265	82.14	154.59	137.99	165.70	179.43	147.97
0.292	92.37	167.91	154.81	191.05	190.20	159.27
0.323	107.81	176.72	173.07	193.71	197.24	168.93
0.360	118.61	192.51	191.30	195.36	202.52	180.14
0.403	135.17 ± 20.93	202.60 ± 21.39	206.06 ± 21.43	195.73 ± 21.35	206.06 ± 22.12	185.78 ± 9.59
0.455	160.14 ± 17.14	213.28 ± 18.15	213.69 ± 17.86	193.55 ± 17.20	207.58 ± 17.88	193.09 ± 7.89
0.518	176.78 ± 15.31	230.90 ± 16.99	214.50 ± 15.63	191.85 ± 15.06	206.90 ± 15.77	204.19 ± 7.07
0.594	178.90 ± 13.98	239.60 ± 16.58	211.34 ± 14.79	190.94 ± 13.94	201.07 ± 14.48	203.77 ± 6.61
0.689	168.74 ± 12.91	235.75 ± 16.04	226.64 ± 14.13	183.17 ± 12.96	192.57 ± 13.51	197.57 ± 6.24
0.806	163.81 ± 12.14	222.53 ± 15.00	197.32 ± 13.37	170.99 ± 11.95	179.67 ± 12.46	186.86 ± 5.82
0.951	160.67 ± 11.63	204.96 ± 13.92	183.68 ± 12.52	159.96 ± 11.18	166.34 ± 11.55	175.12 ± 5.45
1.152	158.10 ± 11.38	187.47 ± 12.88	169.30 ± 11.67	149.98 ± 10.51	154.93 ± 10.82	163.96 ± 5.13
1.308	155.07 ± 14.23	178.46 ± 14.49	160.83 ± 13.41	144.17 ± 12.63	147.15 ± 12.87	156.73 ± 6.05
1.365	153.95 ± 14.04	173.04 ± 13.98	157.07 ± 12.92	141.15 ± 12.31	144.17 ± 12.49	153.88 ± 5.89
1.426	150.04 ± 13.50	166.73 ± 13.57	152.59 ± 12.48	137.34 ± 11.87	140.46 ± 12.10	149.43 ± 5.69
1.491	146.45 ± 13.01	159.46 ± 12.97	147.11 ± 11.96	132.99 ± 11.40	135.63 ± 11.59	144.33 ± 5.46
1.560	142.98 ± 12.81	154.43 ± 12.58	141.96 ± 11.58	128.60 ± 10.93	131.15 ± 11.11	139.82 ± 5.29
1.635	138.49 ± 12.35	148.75 ± 12.13	136.71 ± 11.15	123.23 ± 10.43	127.07 ± 10.79	134.85 ± 5.09
1.715	132.30 ± 11.81	142.92 ± 11.71	131.12 ± 10.71	118.48 ± 10.05	121.94 ± 10.39	129.51 ± 4.90
1.801	127.44 ± 11.51	135.77 ± 11.23	123.71 ± 10.21	112.41 ± 9.62	115.61 ± 9.90	122.99 ± 4.70
1.893	121.06 ± 11.01	127.90 ± 10.70	117.10 ± 9.81	105.65 ± 9.16	108.86 ± 9.44	116.11 ± 4.49
1.993	114.18 ± 10.39	120.48 ± 10.20	110.55 ± 9.73	95.44 ± 8.73	102.23 ± 8.96	109.37 ± 4.27
2.101	106.72 ± 9.93	112.03 ± 9.60	102.77 ± 8.77	92.20 ± 8.22	94.43 ± 8.38	101.63 ± 4.02

TABLE 9 (continued)

Н И О Б И Й

E, МэВ / θ	31°	61°	91°	121°	151°	Усреднённый спектр
1	2	3	4	5	6	7
2,218	99,09 ± 9,40	103,46 ± 9,01	94,77 ± 8,20	84,73 ± 7,67	86,86 ± 7,86	93,79 ± 3,78
2,346	90,92 ± 8,66	94,50 ± 8,39	87,30 ± 7,70	77,49 ± 7,15	79,38 ± 7,32	85,92 ± 3,51
2,484	83,51 ± 8,23	86,10 ± 7,80	79,24 ± 7,11	70,26 ± 6,65	71,87 ± 6,74	78,20 ± 3,25
2,635	76,15 ± 7,67	77,89 ± 7,24	71,52 ± 6,58	63,13 ± 6,16	63,59 ± 6,14	70,46 ± 3,03
2,801	68,15 ± 7,10	69,06 ± 6,61	64,26 ± 6,07	56,13 ± 5,65	56,44 ± 5,65	62,81 ± 2,78
2,982	61,63 ± 6,59	61,34 ± 6,09	57,10 ± 5,56	49,19 ± 5,15	49,70 ± 5,15	55,79 ± 2,56
3,182	54,76 ± 6,10	54,22 ± 5,61	50,61 ± 5,13	43,24 ± 4,73	43,36 ± 4,71	49,24 ± 2,36
3,403	48,75 ± 5,62	47,24 ± 5,15	43,68 ± 4,66	37,59 ± 4,33	37,23 ± 4,29	42,94 ± 2,16
3,647	42,71 ± 5,26	40,73 ± 4,70	38,09 ± 4,27	32,85 ± 3,95	31,75 ± 3,88	37,06 ± 1,98
3,919	37,12 ± 4,87	35,00 ± 4,32	32,47 ± 3,86	27,04 ± 3,59	26,58 ± 3,54	31,64 ± 1,82
4,222	31,97 ± 4,46	29,41 ± 3,92	27,37 ± 3,52	22,57 ± 3,29	21,98 ± 3,21	26,06 ± 1,66
4,562	27,35 ± 4,13	24,63 ± 3,61	22,77 ± 3,18	18,85 ± 3,01	18,06 ± 2,91	22,20 ± 1,52
4,945	23,36 ± 3,91	20,50 ± 3,31	18,82 ± 2,90	15,36 ± 2,73	14,59 ± 2,64	18,51 ± 1,40
5,379	19,49 ± 3,49	16,89 ± 3,06	15,22 ± 2,62	12,31 ± 2,49	11,63 ± 2,44	15,12 ± 1,27
5,872	16,12 ± 3,24	13,80 ± 2,83	12,20 ± 2,39	9,85 ± 2,29	9,19 ± 2,20	12,23 ± 1,17
6,437	13,16 ± 3,03	11,06 ± 2,55	9,67 ± 2,17	7,78 ± 2,08	7,13 ± 2,01	9,78 ± 1,07
7,087	10,56 ± 2,73	8,74 ± 2,34	7,55 ± 1,98	6,05 ± 1,89	5,44 ± 1,84	7,67 ± 0,97
7,842	8,28 ± 2,55	6,75 ± 2,15	5,73 ± 1,77	4,60 ± 1,72	4,06 ± 1,65	5,83 ± 0,89
8,725	6,38 ± 2,37	5,13 ± 1,87	4,25 ± 1,55	3,44 ± 1,52	2,98 ± 1,49	4,43 ± 0,80
9,767	4,92 ± 2,12	3,94 ± 1,61	3,07 ± 1,34	2,51 ± 1,31	2,16 ± 1,30	3,32 ± 0,70
11,008	3,58 ± 2,09	2,81 ± 1,55	2,12 ± 1,10	1,73 ± 1,10	1,47 ± 1,07	2,33 ± 0,62
12,503	2,41 ± 2,17	1,85 ± 1,14	1,45 ± 0,90	1,21 ± 0,89	0,91 ± 0,85	1,56 ± 0,57
14,328	1,51 ± 2,01	1,14 ± 0,98	0,86 ± 0,74	0,73 ± 0,73	0,52 ± 0,67	0,95 ± 0,51

TABLE 10

В О Л Ь Ф Р А М Таблица 10

Мэв E, Мэв	31°	61°	91°	121°	151°	Усреднённый спектр
1	2	3	4	5	5	5
0,102	17,09	22,70	24,76	23,43	23,08	22,19
0,136	24,26	31,71	36,14	31,82	32,35	31,25
0,182	32,57	43,54	48,20	43,38	43,45	42,23
0,221	40,35	53,07	59,73	53,54	54,86	52,31
0,241	44,75	58,99	66,53	58,45	60,66	57,88
0,265	50,18	65,89	73,98	65,87	67,57	64,70
0,292	55,29	73,96	82,17	72,51	74,66	71,72
0,323	61,63	81,38	91,63	81,06	83,04	79,76
0,360	70,59	93,16	104,59	92,34	95,01	91,14
0,403	79,22 ± 19,09	105,37 ± 14,99	117,28 ± 18,89	101,37 ± 17,69	108,45 ± 18,54	102,34 ± 8,00
0,455	93,03 ± 14,72	121,97 ± 13,20	130,13 ± 14,72	109,49 ± 13,59	120,15 ± 14,16	114,95 ± 6,30
0,518	107,99 ± 12,35	143,46 ± 12,52	142,03 ± 12,47	116,23 ± 11,49	135,98 ± 12,27	129,15 ± 5,46
0,594	122,23 ± 11,40	157,56 ± 12,07	153,73 ± 11,87	126,09 ± 10,59	148,74 ± 11,67	141,67 ± 5,15
0,689	133,59 ± 11,12	168,27 ± 12,10	159,84 ± 11,60	137,18 ± 10,43	154,67 ± 11,34	150,71 ± 5,06
0,808	140,03 ± 10,86	168,69 ± 11,83	156,66 ± 11,10	143,25 ± 10,35	150,41 ± 10,75	151,81 ± 4,91
0,961	142,02 ± 10,63	159,67 ± 11,23	148,56 ± 10,51	141,89 ± 10,09	137,23 ± 9,82	145,88 ± 4,68
1,162	137,90 ± 10,28	146,26 ± 10,41	138,06 ± 9,87	131,53 ± 9,42	121,17 ± 8,80	134,98 ± 4,37
1,308	131,58 ± 13,52	136,71 ± 12,57	129,66 ± 12,07	121,16 ± 11,60	110,61 ± 11,14	125,94 ± 5,46
1,365	126,56 ± 13,02	132,83 ± 12,05	126,00 ± 11,63	117,18 ± 11,33	106,41 ± 10,75	122,19 ± 5,27
1,436	124,59 ± 12,58	128,07 ± 11,67	121,44 ± 11,12	111,93 ± 10,85	101,85 ± 10,16	117,58 ± 5,05
1,491	120,16 ± 12,11	122,72 ± 11,21	116,56 ± 10,67	106,45 ± 10,28	96,65 ± 9,78	112,51 ± 4,84
1,560	115,61 ± 11,70	117,49 ± 10,75	111,70 ± 10,25	100,93 ± 9,70	92,21 ± 9,23	107,59 ± 4,63
1,635	110,72 ± 11,30	112,07 ± 10,36	106,43 ± 9,80	95,28 ± 9,24	87,25 ± 8,80	102,35 ± 4,44
1,715	105,77 ± 10,90	106,39 ± 9,97	100,88 ± 9,38	89,74 ± 8,77	82,00 ± 8,38	96,95 ± 4,25
1,801	99,89 ± 10,41	99,93 ± 9,49	94,98 ± 9,01	83,48 ± 8,36	76,20 ± 7,97	90,90 ± 4,06
1,893	93,91 ± 9,96	93,33 ± 9,06	88,48 ± 8,56	77,38 ± 7,90	70,31 ± 7,47	84,68 ± 3,86
1,993	87,93 ± 9,48	86,57 ± 8,62	82,08 ± 8,15	71,32 ± 7,50	64,63 ± 7,13	78,50 ± 3,67
2,101	82,16 ± 9,01	79,52 ± 8,06	75,47 ± 7,66	64,95 ± 7,02	58,83 ± 6,66	72,18 ± 3,45
2,218	76,12 ± 8,55	72,20 ± 7,54	68,67 ± 7,19	58,40 ± 6,59	52,93 ± 6,22	65,68 ± 3,25
2,346	70,22 ± 8,07	65,31 ± 7,00	62,18 ± 6,67	52,07 ± 6,04	47,44 ± 5,80	59,45 ± 3,02
2,484	64,47 ± 7,58	58,73 ± 6,53	55,73 ± 6,20	46,05 ± 5,66	41,99 ± 5,38	53,39 ± 2,82

TABLE 10 (continued)

ВОЛЬФРАМ

$\frac{\theta}{E, \text{МэВ}}$	31°	61°	91°	121°	151°	Усреднённый спектр
I	2	3	4	5	6	7
2,635	58,78 ± 7,14	52,49 ± 6,05	49,74 ± 5,76	40,46 ± 5,20	36,84 ± 4,94	47,66 ± 2,62
2,801	53,14 ± 6,68	46,63 ± 5,63	43,78 ± 5,36	35,18 ± 4,81	31,99 ± 4,61	42,14 ± 2,44
2,982	47,93 ± 6,22	41,39 ± 5,22	38,30 ± 4,92	30,43 ± 4,45	27,58 ± 4,21	37,13 ± 2,26
3,182	43,04 ± 5,85	36,43 ± 4,88	33,28 ± 4,59	26,03 ± 4,11	23,53 ± 3,89	32,46 ± 2,11
3,403	36,19 ± 5,47	31,79 ± 4,56	28,63 ± 4,21	21,97 ± 3,74	19,89 ± 3,57	28,09 ± 1,95
3,647	33,60 ± 5,08	27,48 ± 4,24	24,37 ± 3,90	18,35 ± 3,48	16,64 ± 3,33	24,09 ± 1,81
3,919	29,38 ± 4,77	23,59 ± 3,94	20,58 ± 3,58	15,15 ± 3,18	13,79 ± 3,04	20,50 ± 1,68
4,222	25,55 ± 4,45	20,10 ± 3,68	17,21 ± 3,33	12,40 ± 2,98	11,33 ± 2,84	17,32 ± 1,56
4,562	22,06 ± 4,10	16,97 ± 3,40	14,26 ± 3,07	10,03 ± 2,76	9,24 ± 2,58	14,51 ± 1,44
4,945	18,94 ± 3,82	14,27 ± 3,32	11,81 ± 2,89	8,05 ± 2,54	7,51 ± 2,42	12,12 ± 1,35
5,379	16,11 ± 3,54	11,86 ± 3,00	9,70 ± 2,67	6,39 ± 2,36	6,06 ± 2,25	10,02 ± 1,25
5,872	13,66 ± 3,29	9,79 ± 2,79	7,91 ± 2,49	5,02 ± 2,20	4,89 ± 2,13	8,25 ± 1,17
6,437	11,44 ± 3,07	7,93 ± 2,57	6,41 ± 2,28	3,88 ± 2,04	3,90 ± 1,95	6,71 ± 1,08
7,087	9,47 ± 2,84	6,34 ± 2,38	5,11 ± 2,12	2,96 ± 1,90	3,07 ± 1,81	5,39 ± 1,00
7,842	7,68 ± 2,59	4,95 ± 2,16	3,99 ± 1,89	2,19 ± 1,73	2,36 ± 1,63	4,23 ± 0,91
8,725	6,14 ± 2,40	3,79 ± 1,96	3,08 ± 1,71	1,58 ± 1,55	1,78 ± 1,47	3,27 ± 0,82
9,767	4,93 ± 2,27	2,89 ± 1,71	2,35 ± 1,50	1,10 ± 1,36	1,40 ± 1,29	2,54 ± 0,74
11,008	3,91 ± 2,24	2,17 ± 1,46	1,95 ± 1,32	0,83 ± 1,20	1,09 ± 1,13	1,99 ± 0,68
12,503	2,90 ± 2,30	1,57 ± 1,31	1,38 ± 1,12	0,45 ± 1,01	0,76 ± 0,92	1,41 ± 0,63
14,328	2,28 ± 2,24	1,07 ± 1,23	0,90 ± 1,00	0,27 ± 0,89	0,55 ± 0,78	1,01 ± 0,59

TABLE 11

В И С М У Т

θ МэV / E, МэВ	31°	61°	91°	121°	151°	Усреднённый спектр
1	2	3	4	5	6	7
0,102	20,49	27,83	24,58	21,41	19,87	22,83
0,136	28,10	37,15	33,73	30,57	30,97	32,10
0,182	36,79	50,31	45,03	38,70	42,12	42,59
0,221	44,42	60,22	54,74	47,34	54,42	52,23
0,241	49,34	66,32	60,70	52,78	60,04	57,34
0,265	55,37	74,07	66,68	57,69	66,78	64,12
0,292	60,32	81,29	73,83	63,69	76,88	71,20
0,323	66,37	89,03	79,93	69,16	87,00	78,42
0,360	74,15	99,19	92,65	78,05	97,47	88,30
0,403	83,60 ± 25,47	111,68 ± 17,44	102,08 ± 18,28	86,90 ± 14,26	115,88 ± 21,83	100,03 ± 8,87
0,455	94,29 ± 17,24	126,46 ± 14,89	117,00 ± 14,76	98,62 ± 11,28	129,41 ± 16,24	113,16 ± 6,71
0,518	108,80 ± 13,24	139,92 ± 13,31	128,84 ± 12,43	113,70 ± 10,70	139,43 ± 13,40	126,14 ± 5,66
0,594	126,82 ± 12,11	146,85 ± 12,12	140,64 ± 11,74	129,42 ± 10,67	148,84 ± 12,30	138,51 ± 5,28
0,689	142,96 ± 11,77	154,01 ± 11,65	150,22 ± 11,36	144,26 ± 10,88	155,89 ± 11,78	149,47 ± 5,14
0,808	160,77 ± 11,94	161,39 ± 11,55	157,76 ± 11,25	155,86 ± 11,01	159,98 ± 11,46	159,15 ± 5,12
0,961	177,99 ± 12,53	167,49 ± 11,66	161,96 ± 11,28	165,09 ± 11,34	166,67 ± 11,58	167,84 ± 5,22
1,162	188,43 ± 13,01	169,78 ± 11,69	165,35 ± 11,37	169,79 ± 11,57	173,78 ± 11,89	173,43 ± 5,33
1,308	188,64 ± 15,22	167,13 ± 13,36	164,70 ± 13,37	169,70 ± 13,22	173,94 ± 13,80	172,62 ± 6,17
1,365	187,26 ± 14,84	165,10 ± 13,10	163,23 ± 12,74	166,95 ± 12,96	172,10 ± 13,48	170,93 ± 6,01
1,426	184,20 ± 14,56	161,70 ± 12,60	160,48 ± 12,47	163,90 ± 12,72	168,83 ± 13,16	167,83 ± 5,87
1,491	180,20 ± 14,18	157,40 ± 12,28	156,86 ± 12,30	159,99 ± 12,27	164,40 ± 12,69	163,77 ± 5,71
1,560	175,74 ± 13,67	152,97 ± 12,02	152,59 ± 11,72	155,78 ± 11,88	159,11 ± 12,21	159,24 ± 5,51
1,635	170,13 ± 13,38	147,63 ± 11,43	147,40 ± 11,35	150,45 ± 11,48	152,76 ± 11,80	153,67 ± 5,32
1,715	163,94 ± 12,85	141,70 ± 11,13	141,41 ± 11,09	144,17 ± 11,04	145,57 ± 11,28	147,36 ± 5,14
1,801	156,01 ± 12,23	134,64 ± 10,61	134,28 ± 10,34	136,74 ± 10,45	137,22 ± 10,68	139,72 ± 4,86
1,893	147,37 ± 11,80	126,85 ± 9,96	126,25 ± 9,84	128,27 ± 9,91	127,86 ± 10,08	131,32 ± 4,62
1,993	138,29 ± 11,02	118,67 ± 9,53	117,72 ± 9,47	119,46 ± 9,41	118,12 ± 9,42	122,45 ± 4,38
2,101	128,31 ± 10,41	109,86 ± 8,92	108,35 ± 8,69	109,82 ± 8,54	107,94 ± 8,70	112,86 ± 4,06

TABLE 11(continued)

В И С М У Т

E, МэВ \ θ	31°	61°	91°	121°	151°	Усреднённый спектр
1	2	3	4	5	6	7
2,218	117,81 ± 9,73	100,44 ± 8,24	98,39 ± 7,99	99,47 ± 8,00	97,31 ± 8,01	102,88 ± 3,78
2,346	107,53 ± 9,02	91,03 ± 7,64	88,50 ± 7,46	89,33 ± 7,38	86,92 ± 7,29	92,66 ± 3,47
2,484	97,22 ± 8,30	81,77 ± 7,06	78,75 ± 6,72	79,34 ± 6,61	76,73 ± 6,56	82,76 ± 3,16
2,635	87,05 ± 7,60	72,58 ± 6,37	69,21 ± 6,01	69,75 ± 5,99	67,00 ± 5,91	73,12 ± 2,86
2,801	77,21 ± 6,96	63,54 ± 5,73	60,22 ± 5,52	60,54 ± 5,35	57,88 ± 5,30	63,88 ± 2,59
2,982	68,26 ± 6,30	55,22 ± 5,26	51,99 ± 4,92	52,18 ± 4,77	49,65 ± 4,70	55,46 ± 2,33
3,182	59,96 ± 5,75	47,43 ± 4,68	44,49 ± 4,33	44,55 ± 4,29	42,19 ± 4,21	47,73 ± 2,09
3,403	52,20 ± 5,25	40,08 ± 4,19	37,54 ± 4,01	37,43 ± 3,79	35,34 ± 3,76	40,52 ± 1,89
3,647	44,93 ± 4,75	33,26 ± 3,82	31,18 ± 3,55	30,81 ± 3,32	29,12 ± 3,31	35,86 ± 1,69
3,919	38,29 ± 4,30	27,11 ± 3,39	25,58 ± 3,10	25,00 ± 2,97	23,76 ± 2,94	27,95 ± 1,51
4,222	32,42 ± 3,93	21,74 ± 3,01	20,71 ± 2,90	20,04 ± 2,64	19,19 ± 2,67	22,82 ± 1,37
4,562	27,21 ± 3,56	17,00 ± 2,79	16,56 ± 2,59	15,81 ± 2,33	15,31 ± 2,36	18,38 ± 1,23
4,945	22,73 ± 3,24	13,02 ± 2,51	12,12 ± 2,28	12,32 ± 2,11	12,09 ± 2,15	14,65 ± 1,11
5,379	18,80 ± 2,99	9,65 ± 2,27	10,30 ± 2,17	9,46 ± 1,91	9,40 ± 1,96	11,52 ± 1,02
5,872	15,51 ± 2,75	6,94 ± 2,16	8,04 ± 1,99	7,19 ± 1,72	7,21 ± 1,77	8,98 ± 0,94
6,437	12,63 ± 2,50	4,78 ± 1,97	6,18 ± 1,75	5,37 ± 1,60	5,45 ± 1,61	6,88 ± 0,85
7,087	10,14 ± 2,34	3,14 ± 1,77	4,70 ± 1,68	3,97 ± 1,47	4,04 ± 1,50	5,20 ± 0,79
7,842	7,93 ± 2,12	1,94 ± 1,68	3,53 ± 1,52	2,88 ± 1,32	2,91 ± 1,34	3,84 ± 0,72
8,725	6,13 ± 1,93	1,09 ± 1,50	2,64 ± 1,28	2,07 ± 1,18	2,07 ± 1,19	2,80 ± 0,64
9,767	4,78 ± 1,81		1,98 ± 1,17	1,33 ± 1,06	1,50 ± 1,05	1,93 ± 0,58
11,008	3,71 ± 1,82		1,58 ± 1,01	1,02 ± 0,89	1,01 ± 0,87	1,46 ± 0,53
12,503	2,69 ± 1,85		1,19 ± 0,84	0,81 ± 0,75	0,61 ± 0,72	1,06 ± 0,50
14,328	1,90 ± 1,79		0,86 ± 0,77	0,69 ± 0,67	0,39 ± 0,63	0,77 ± 0,47

Figs 1-55

	Рис.	= Fig.
Key:	отн. единицы	= Relative units
	Мэв	= MeV
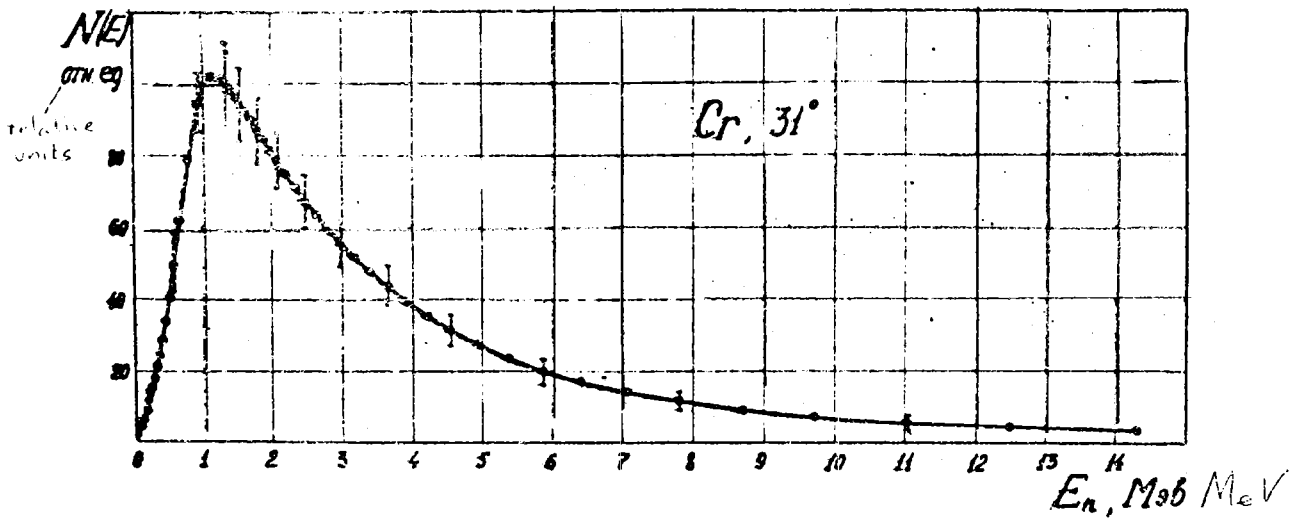
Рис. I.
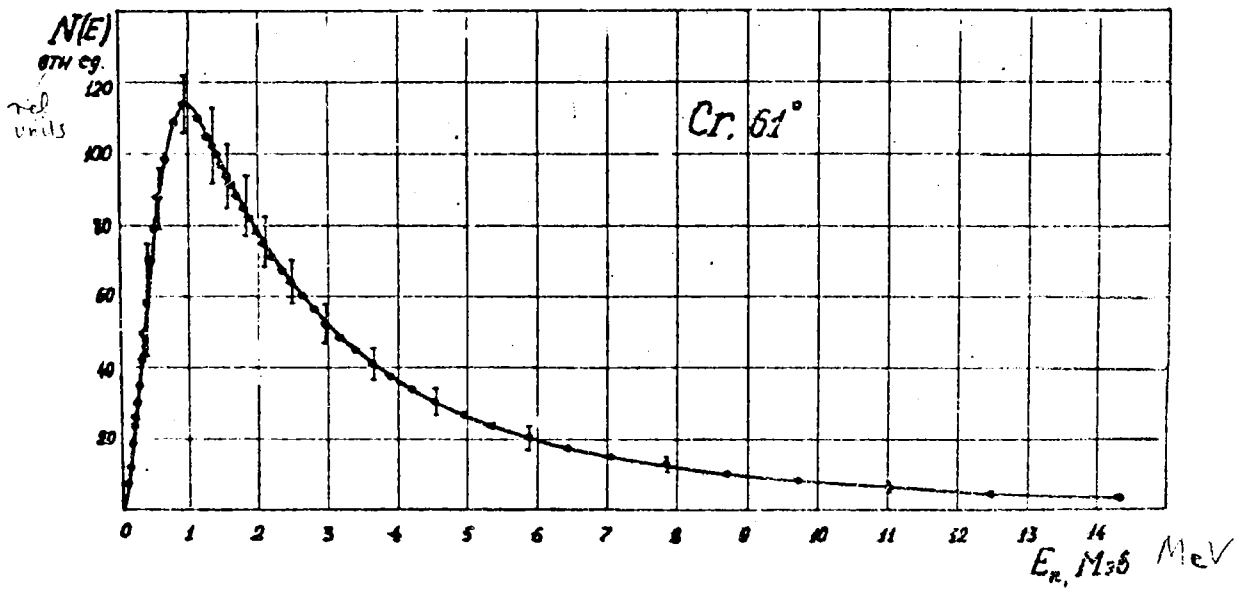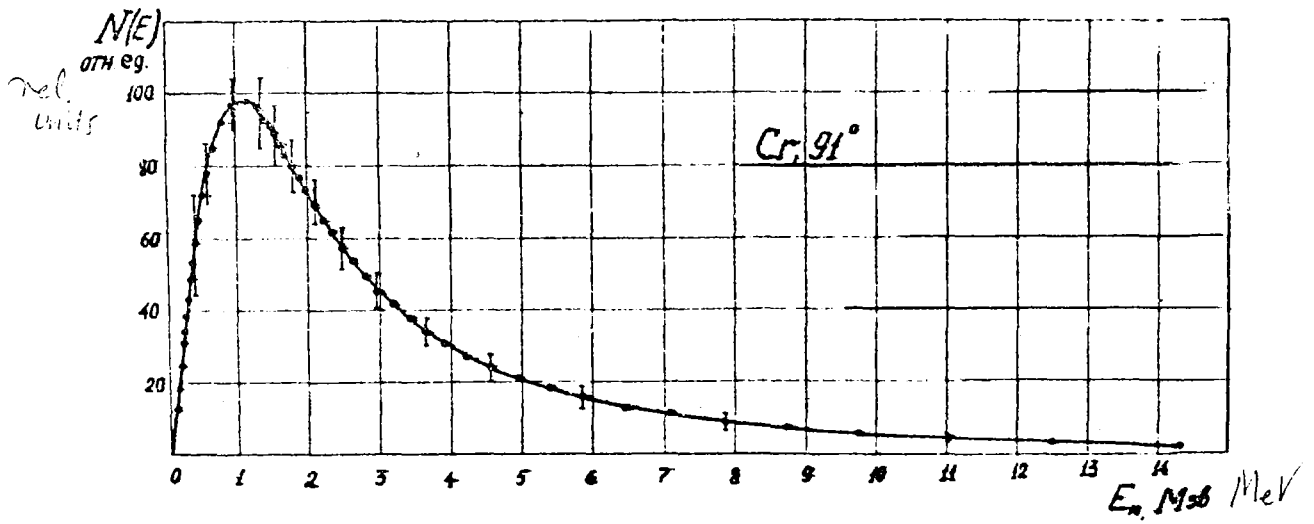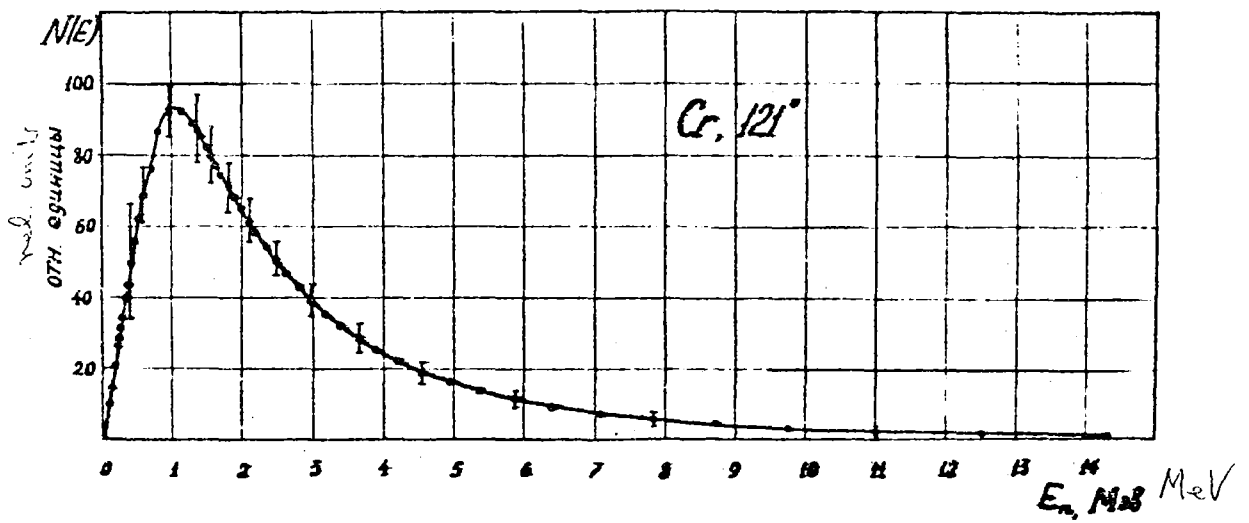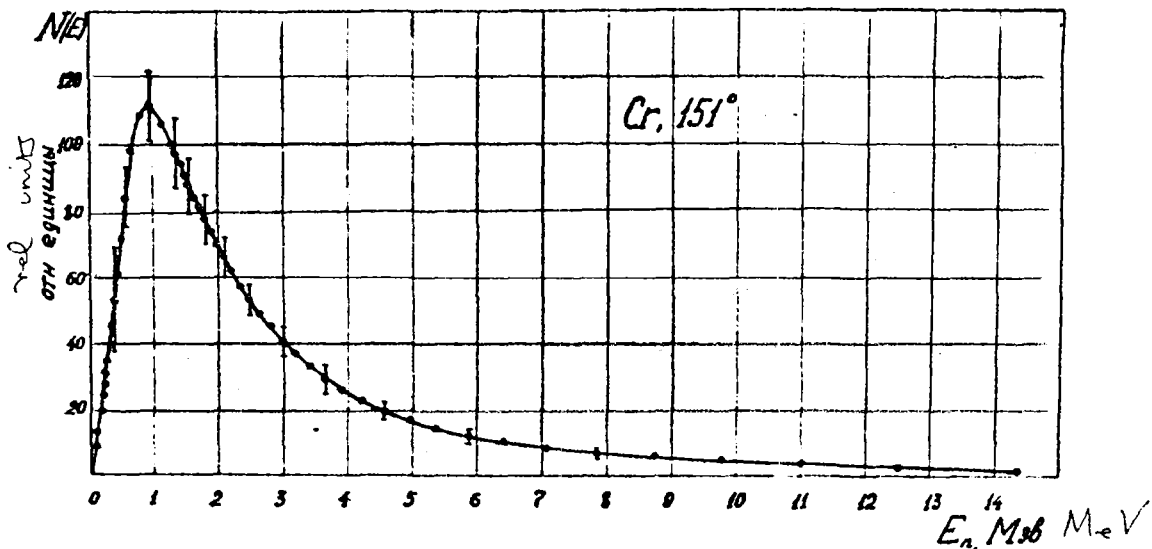
Рис. 2.

Рис. 3.

Рис. 4.

Рис. 5.
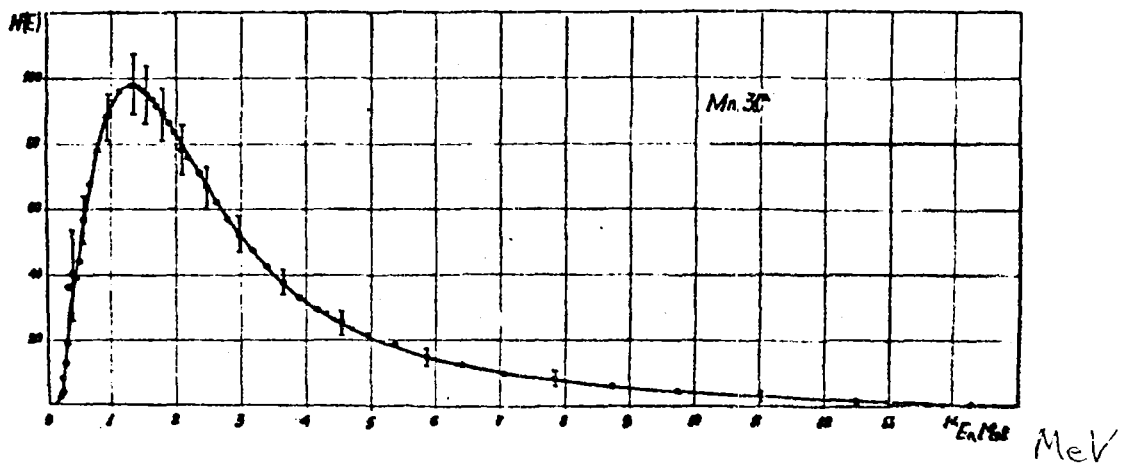
Рис. 6.
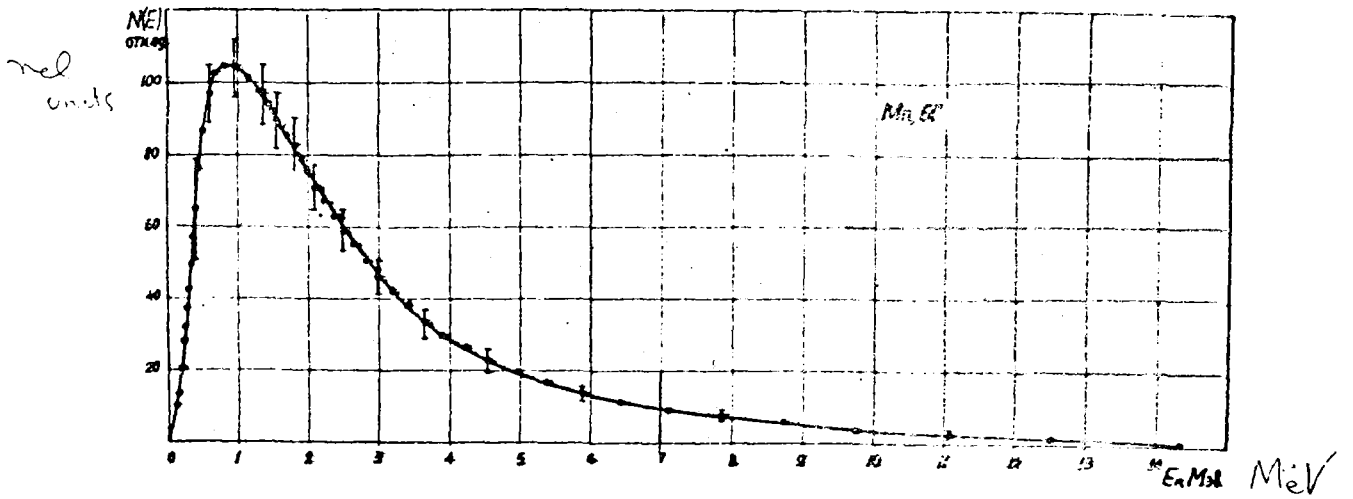
Рис. 7.
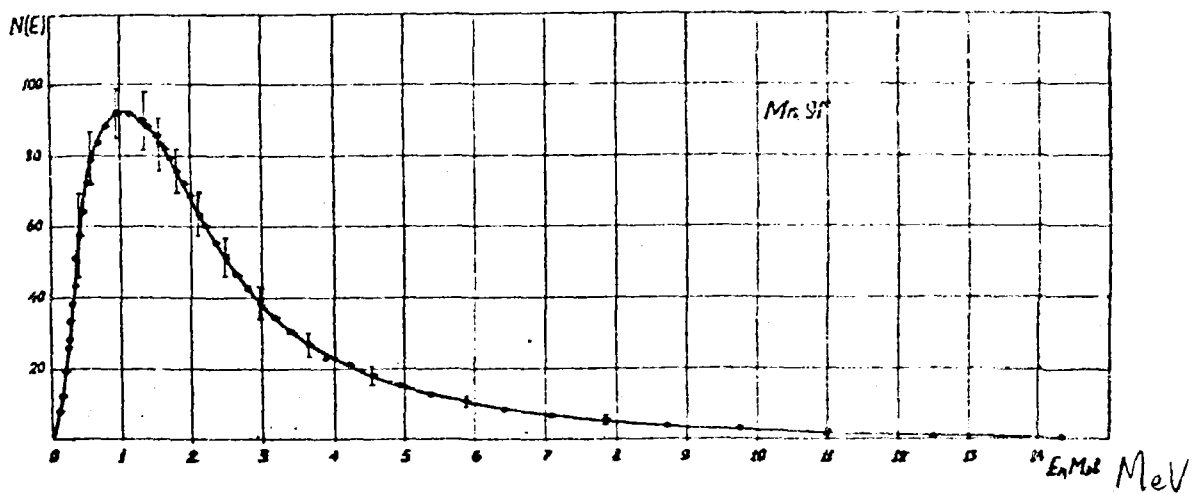
Рис. 8.
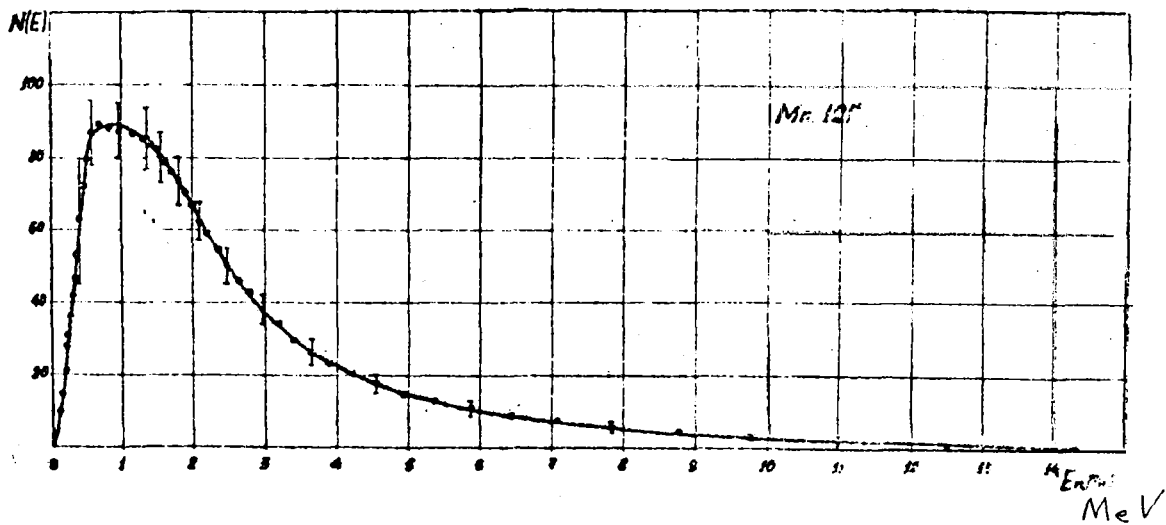
Рис. 9.

Рис. 10.

Рис. II.

Рис. I2.

Рис. 13.

Рис. 14.

Рис. I5.

Рис. I6.

Рис. I7.

Рис. 18.

Рис. I9.

Рис. 20.

Рис. 2I.
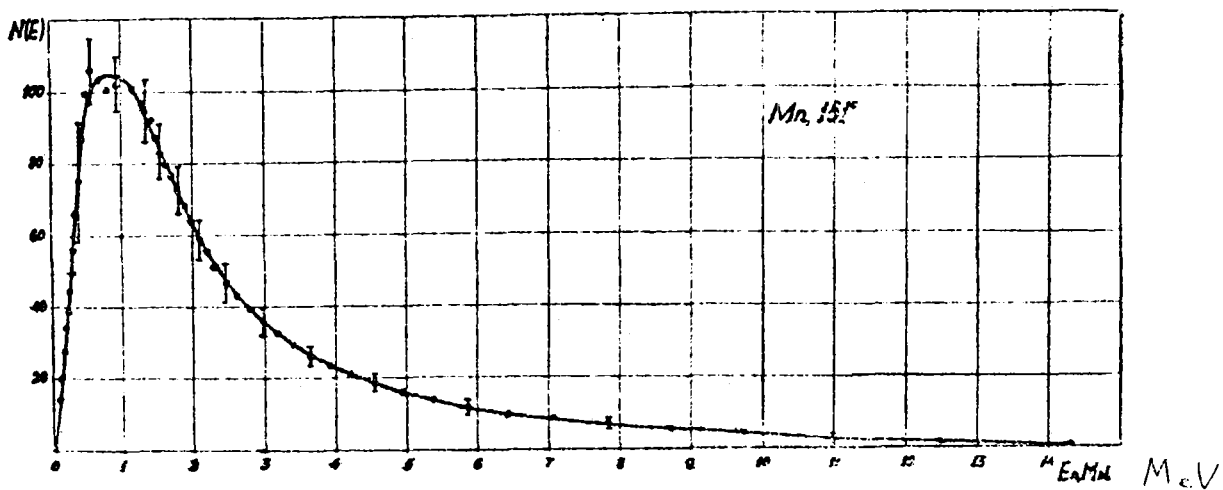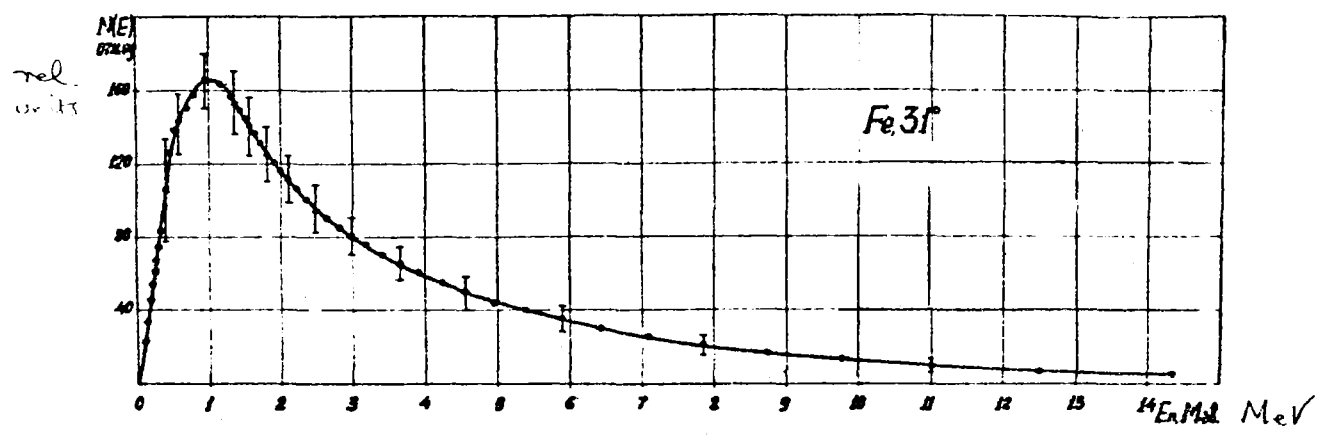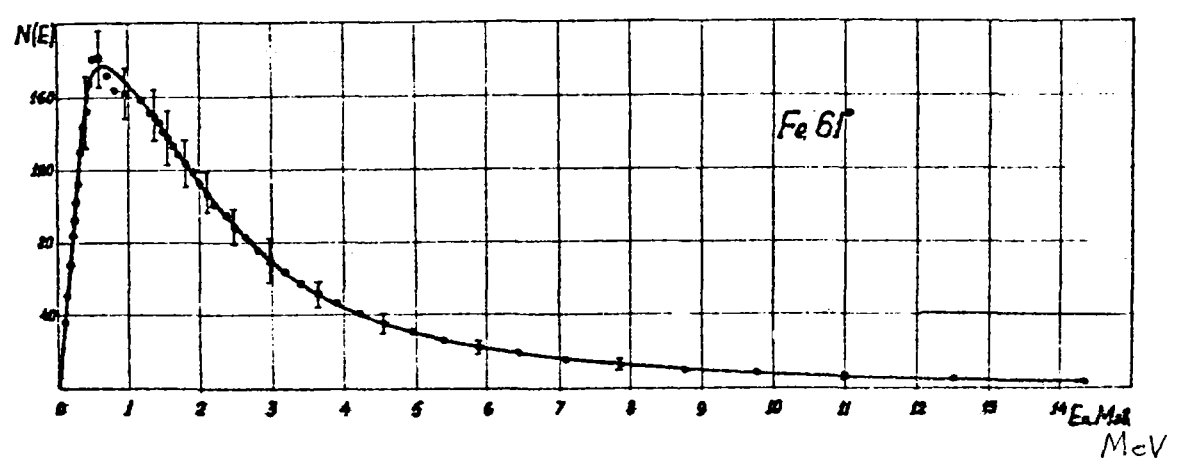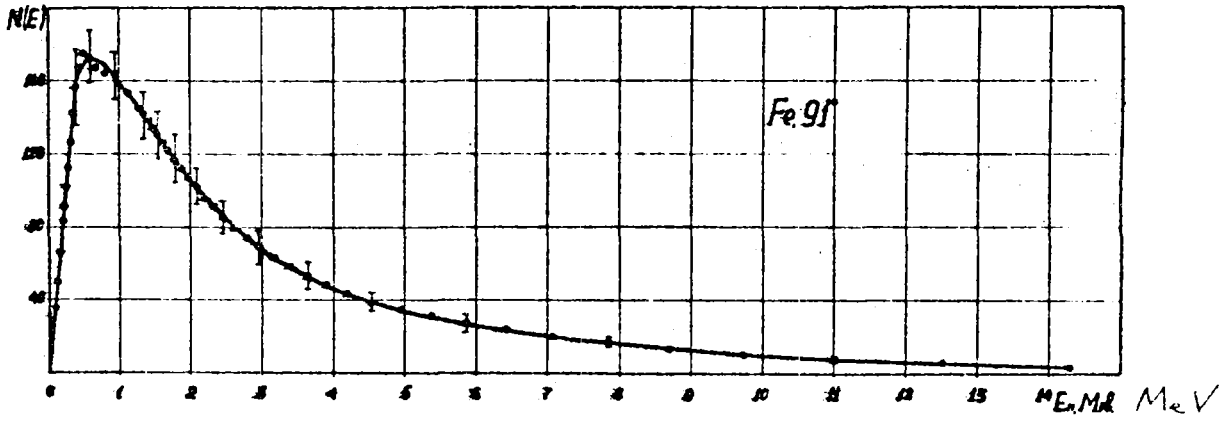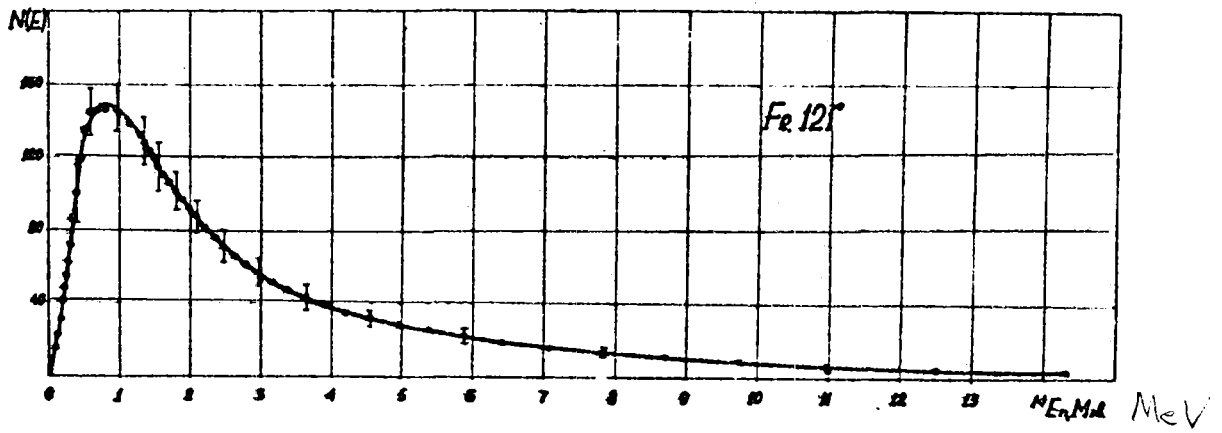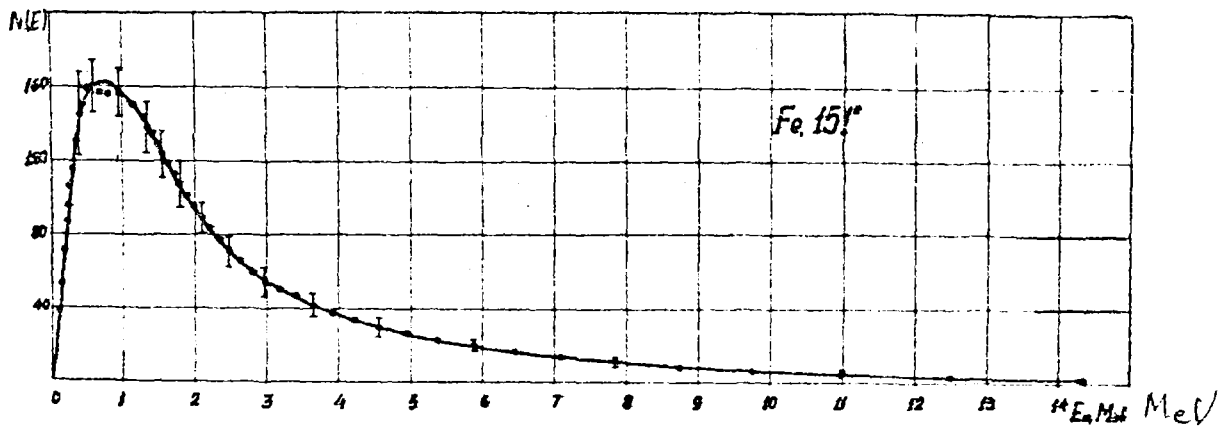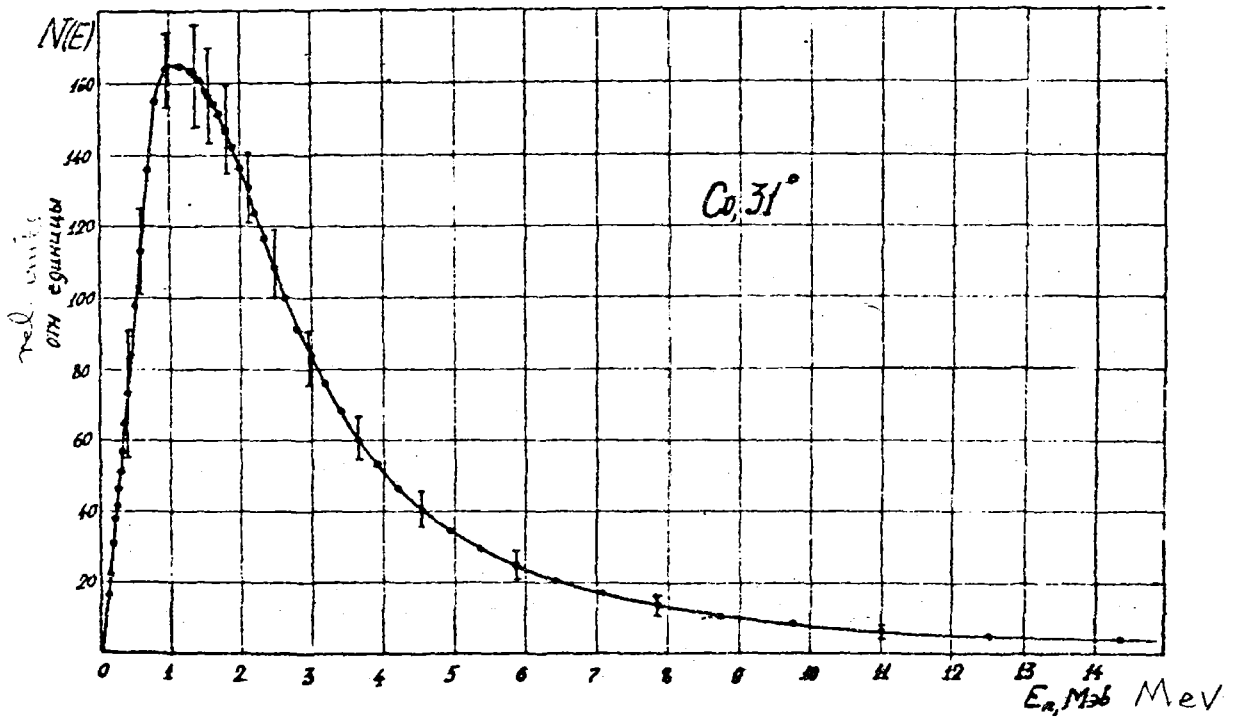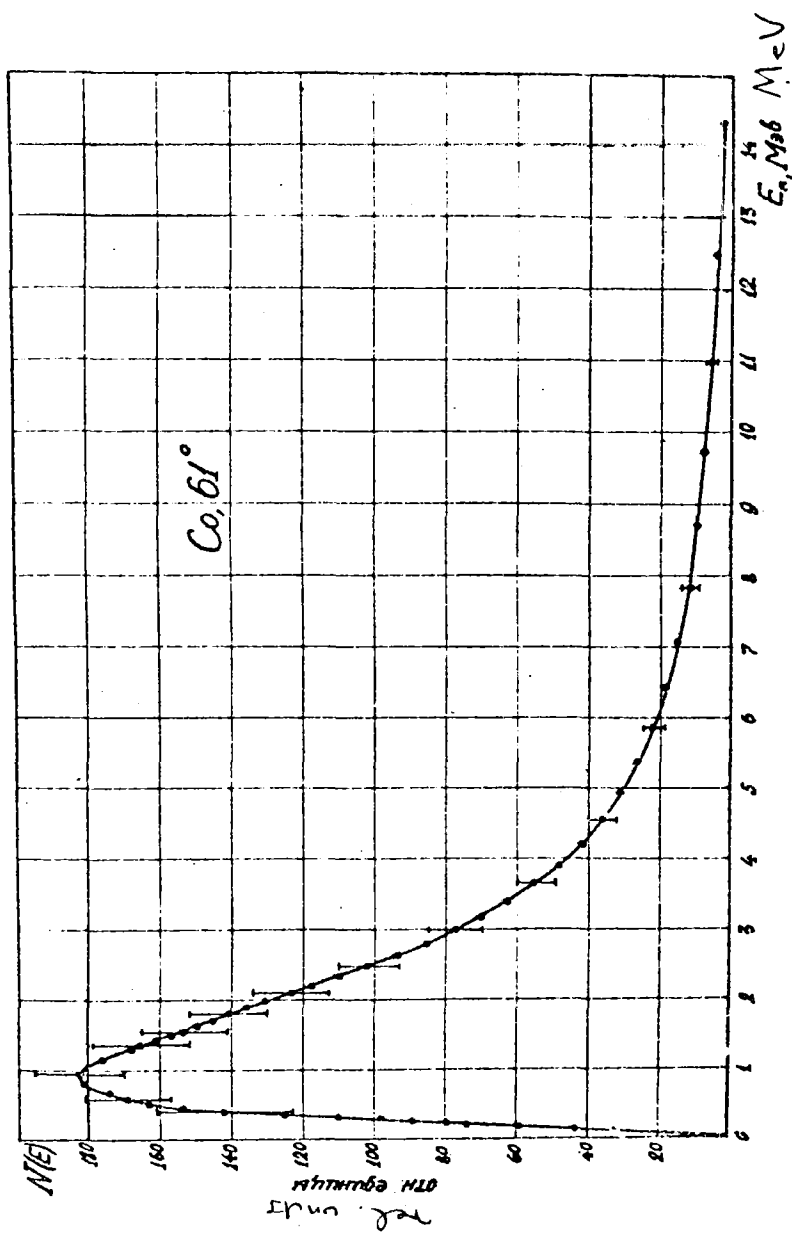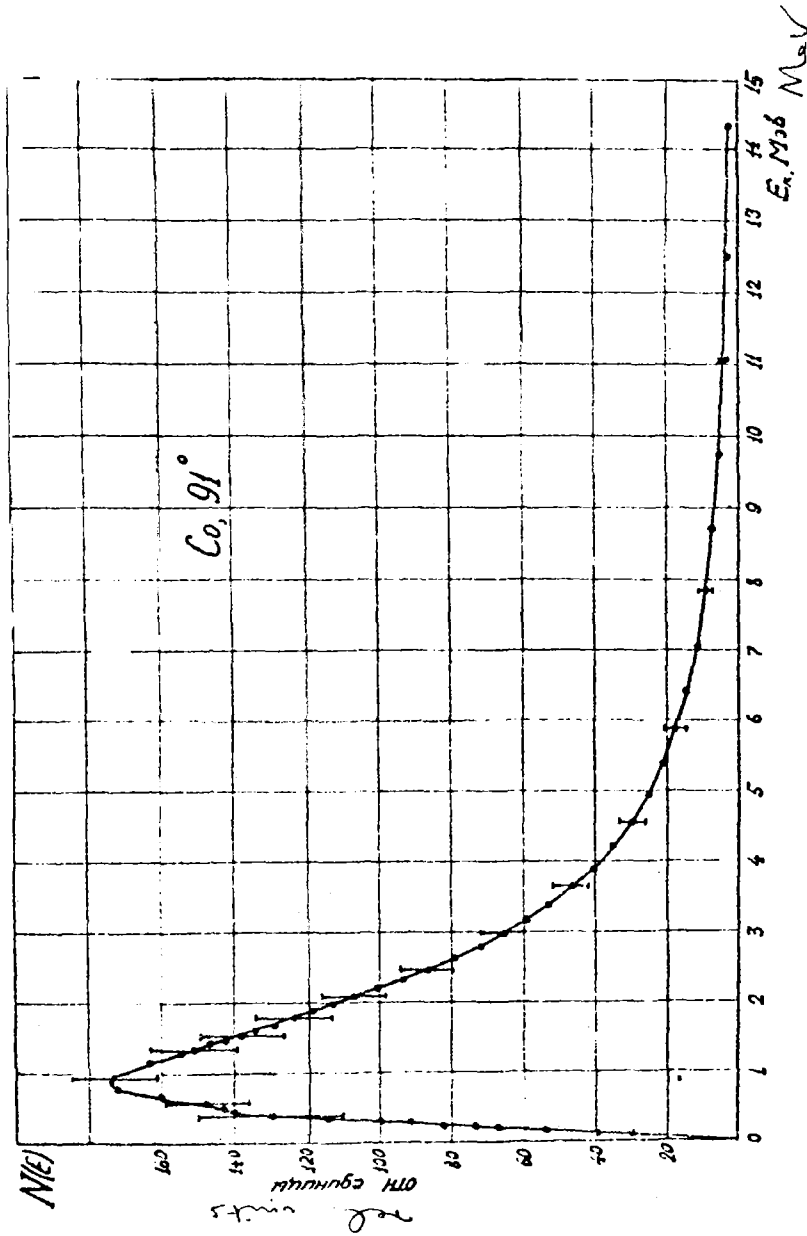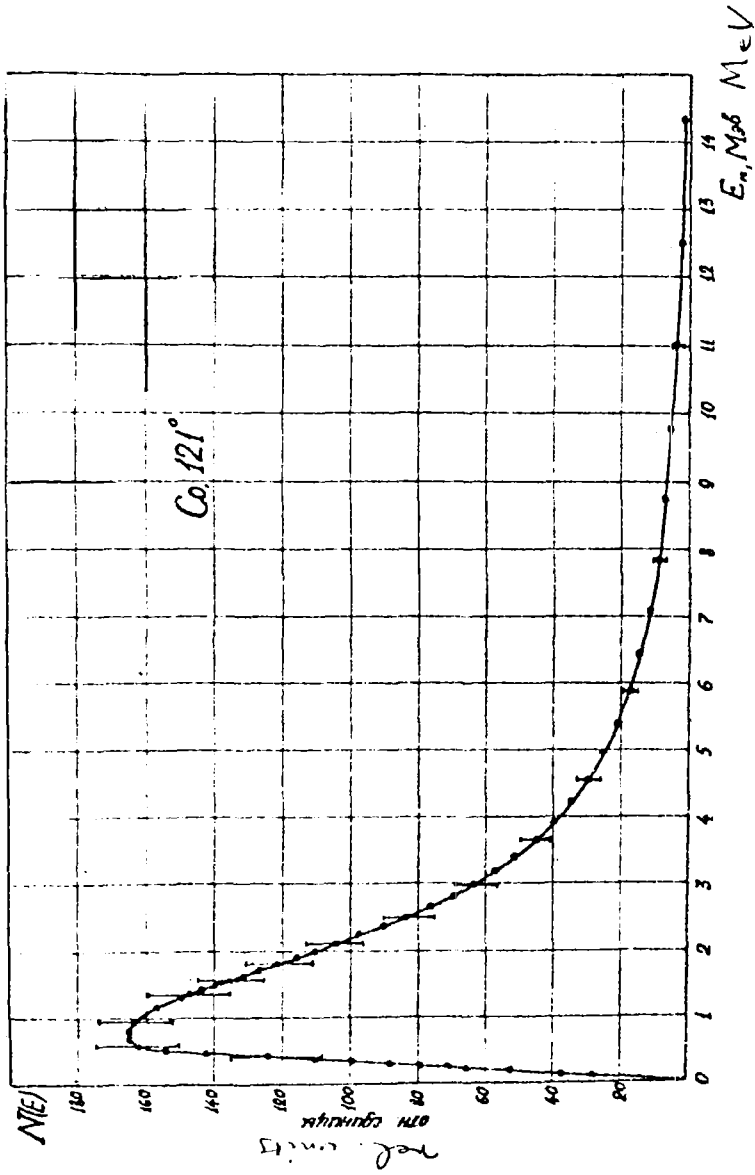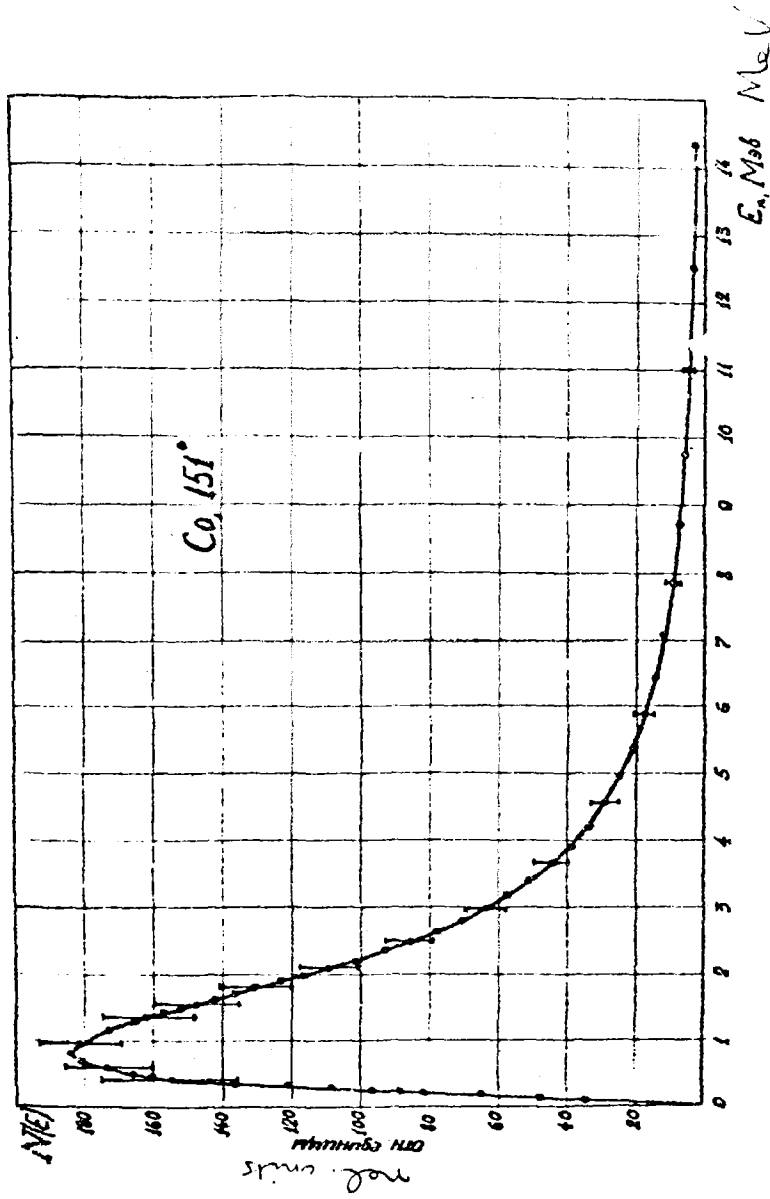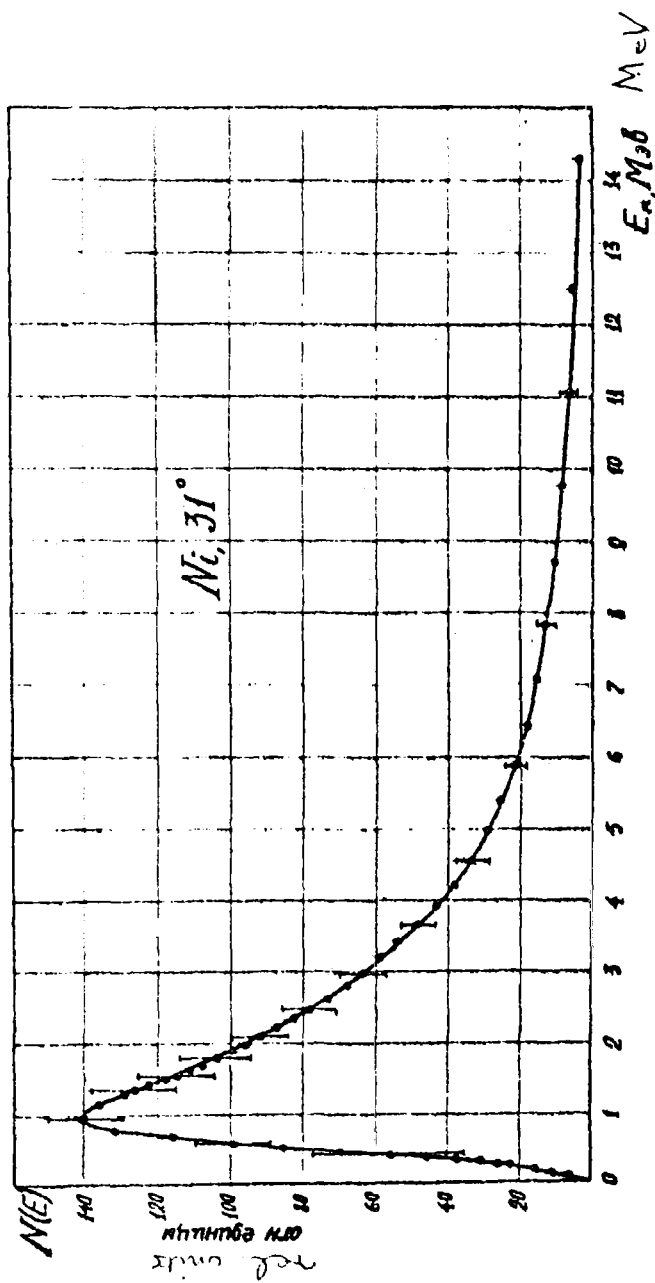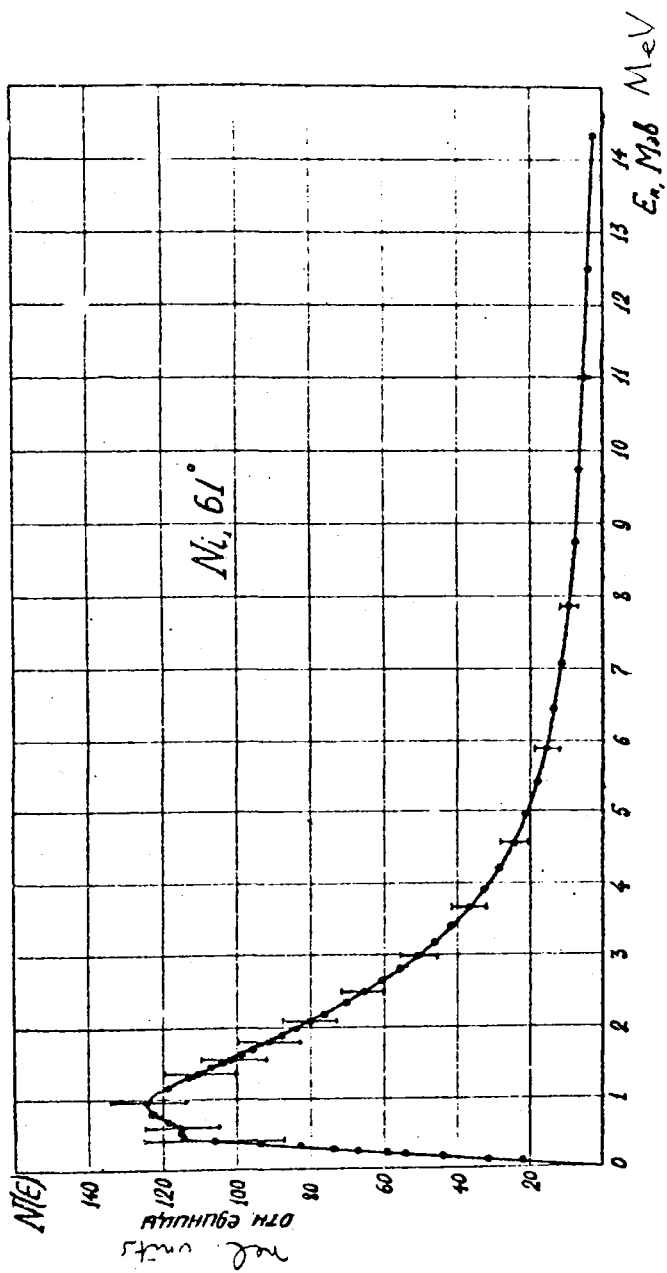
Рис. 22.
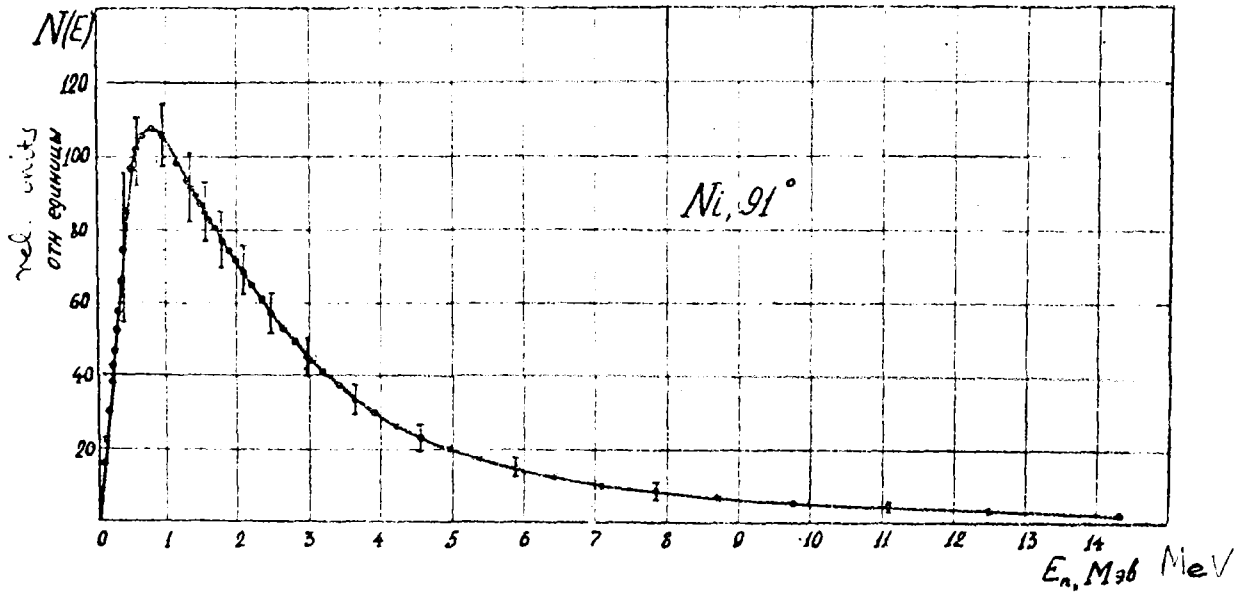
Рис. 23.
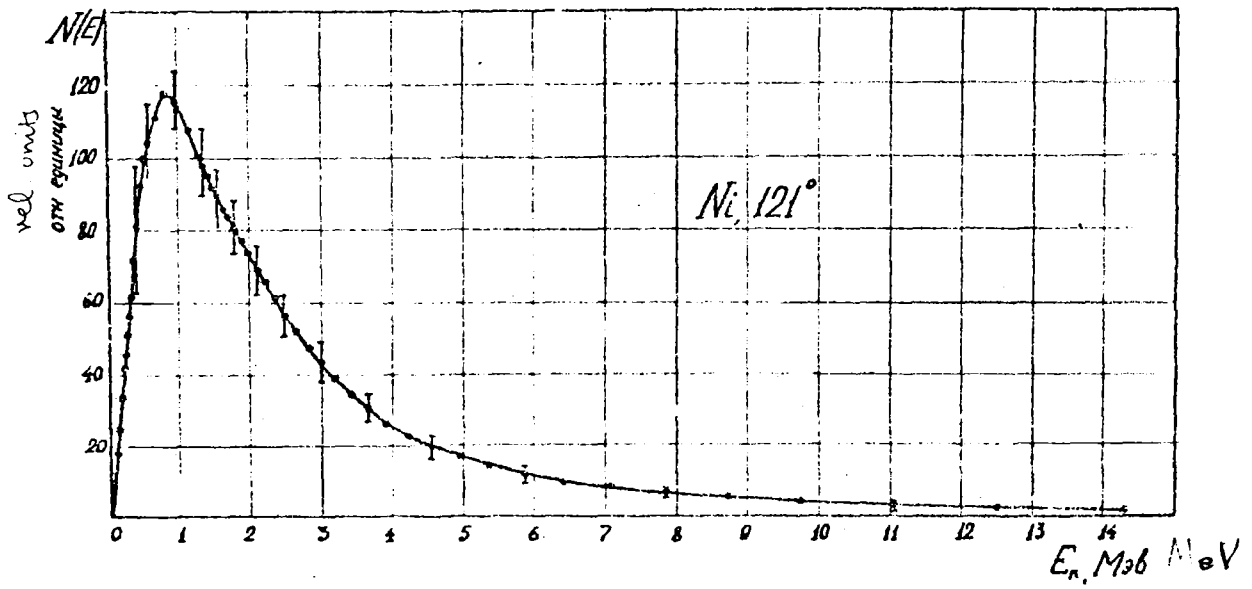
Рис. 24.
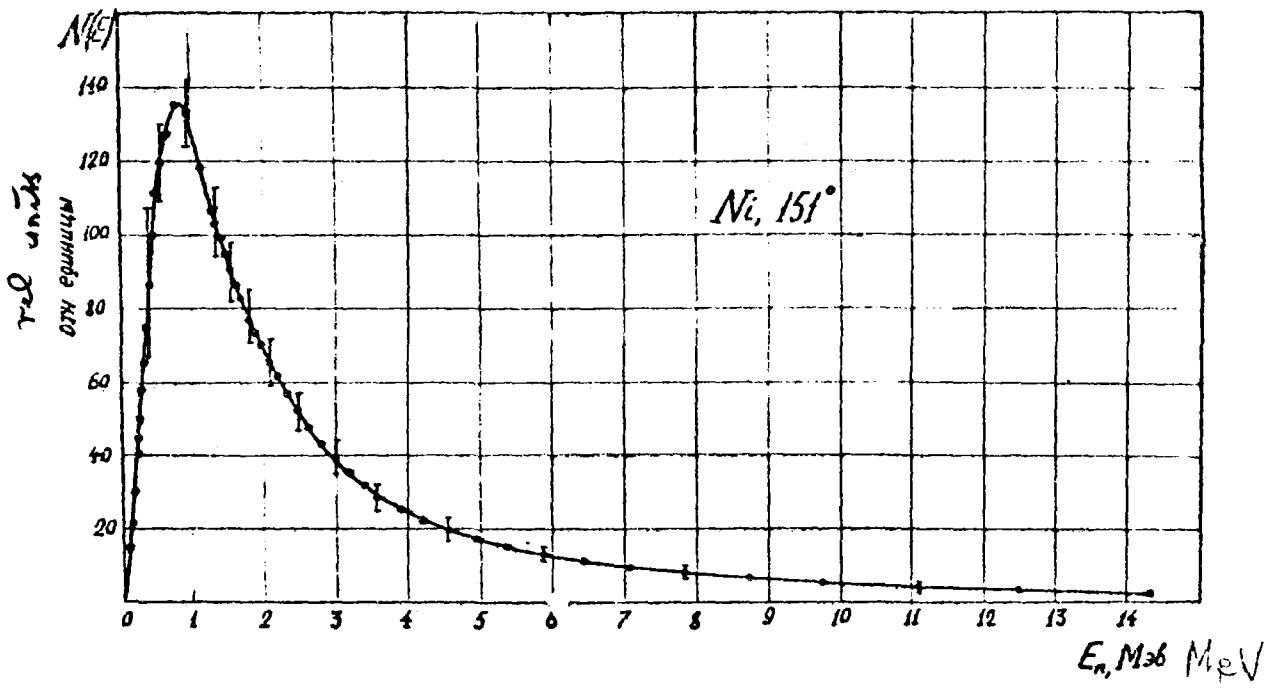
Рис. 25.
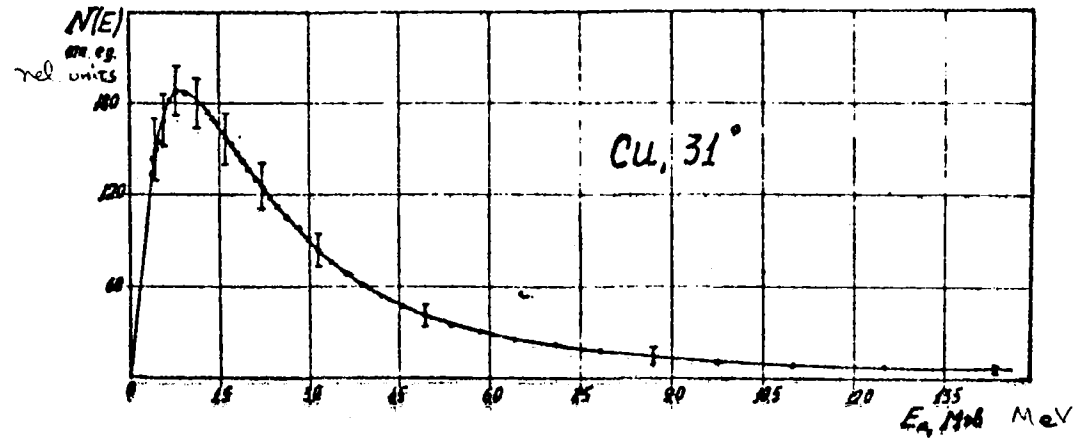
Рис. 26.
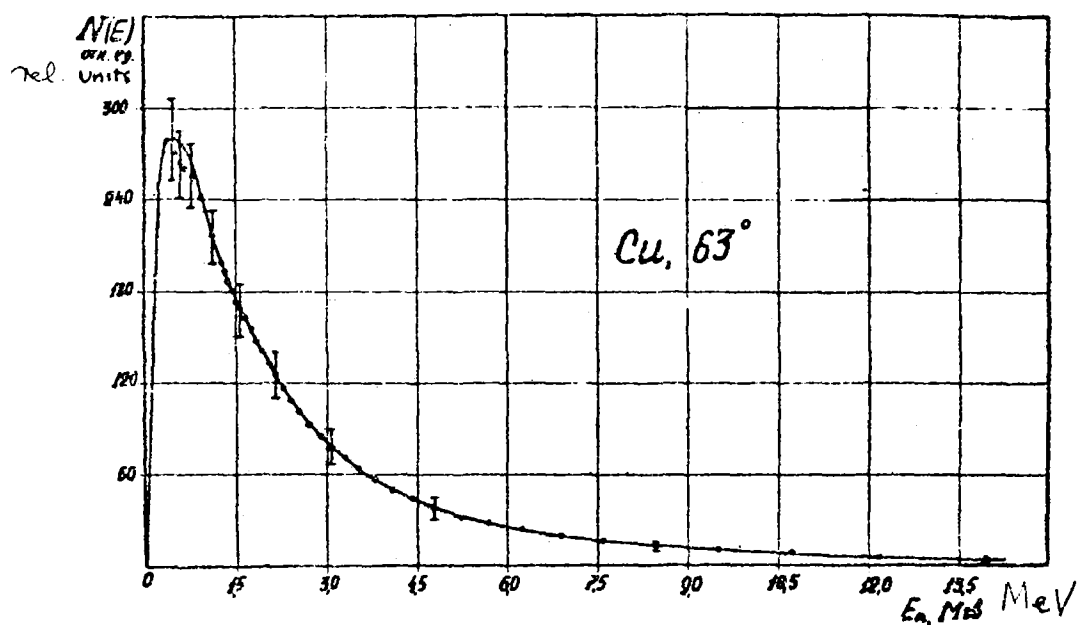
Рис. 27.
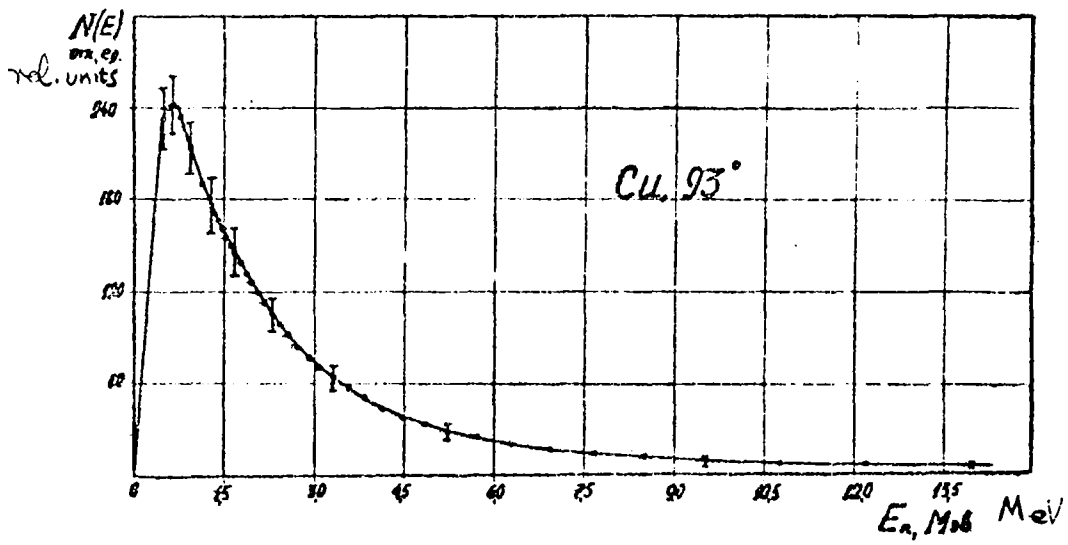
Fig 28
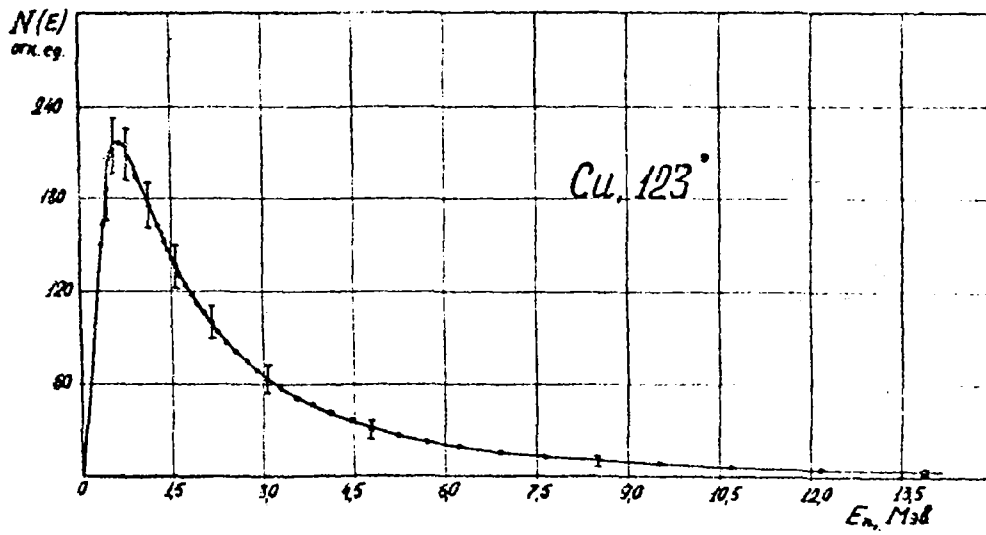
Рис. 29.
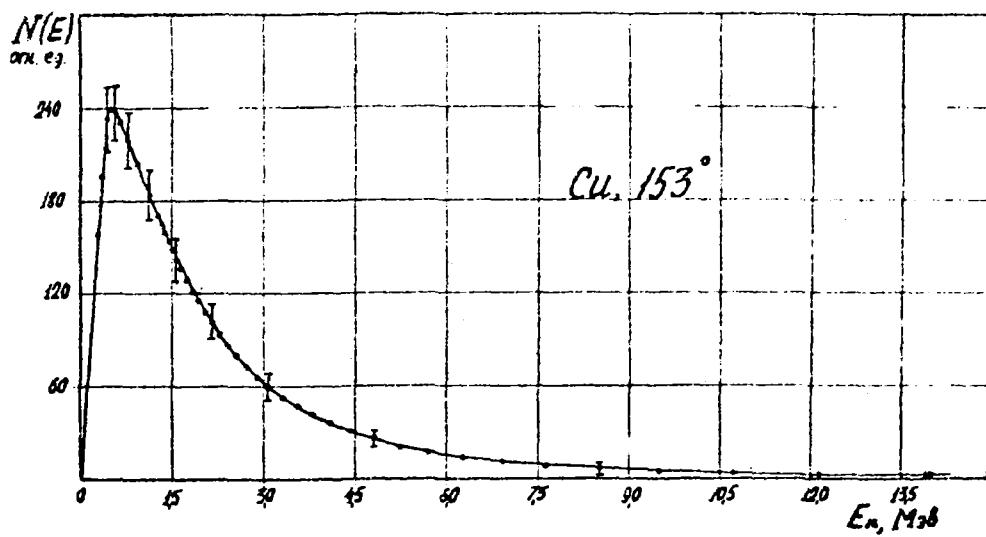
Рис. 30.
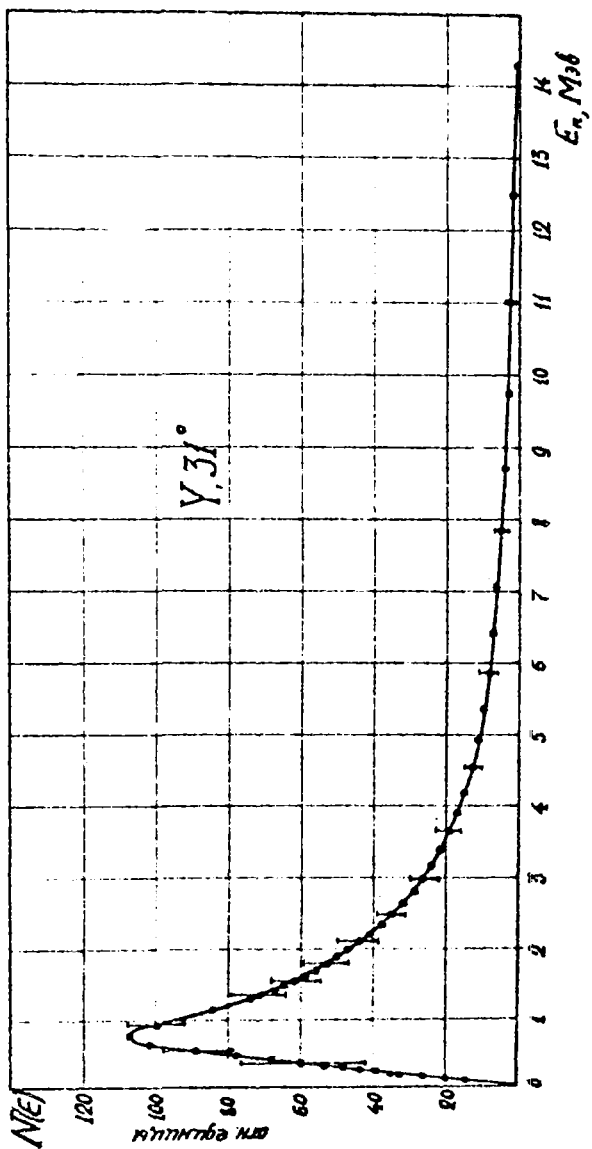
Рис. 31.
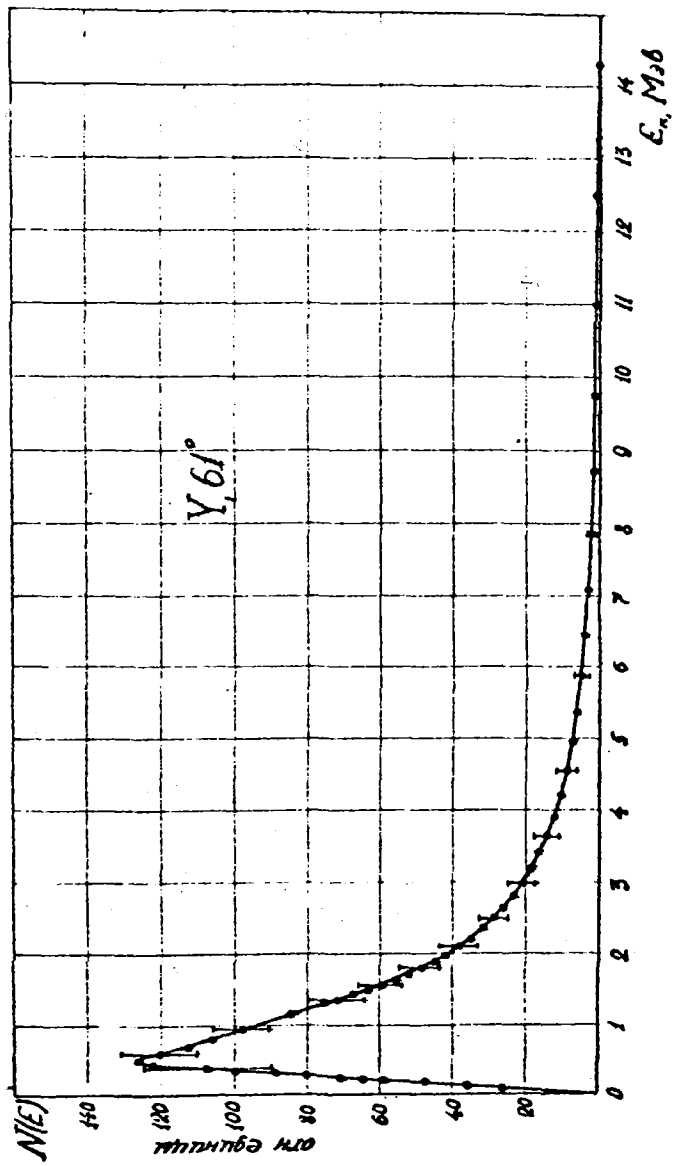
Рис. 32.
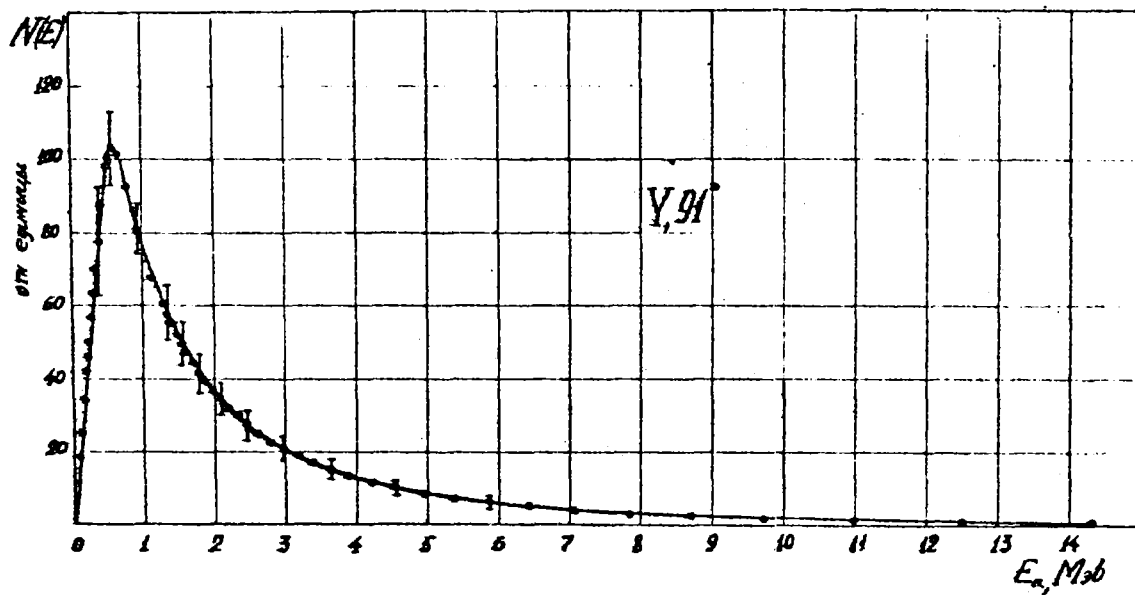
Рис. 33.
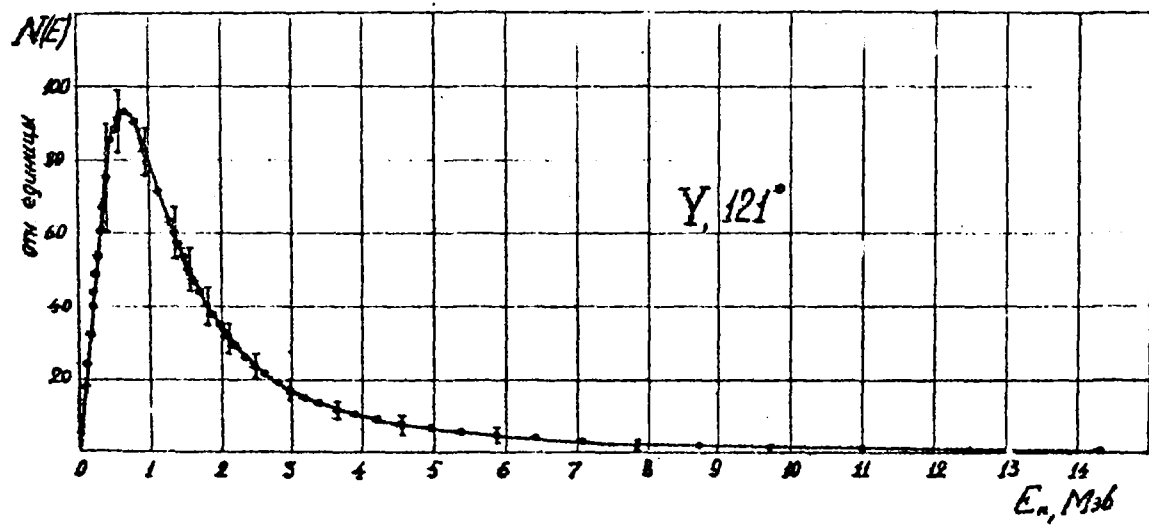
Рис. 34.
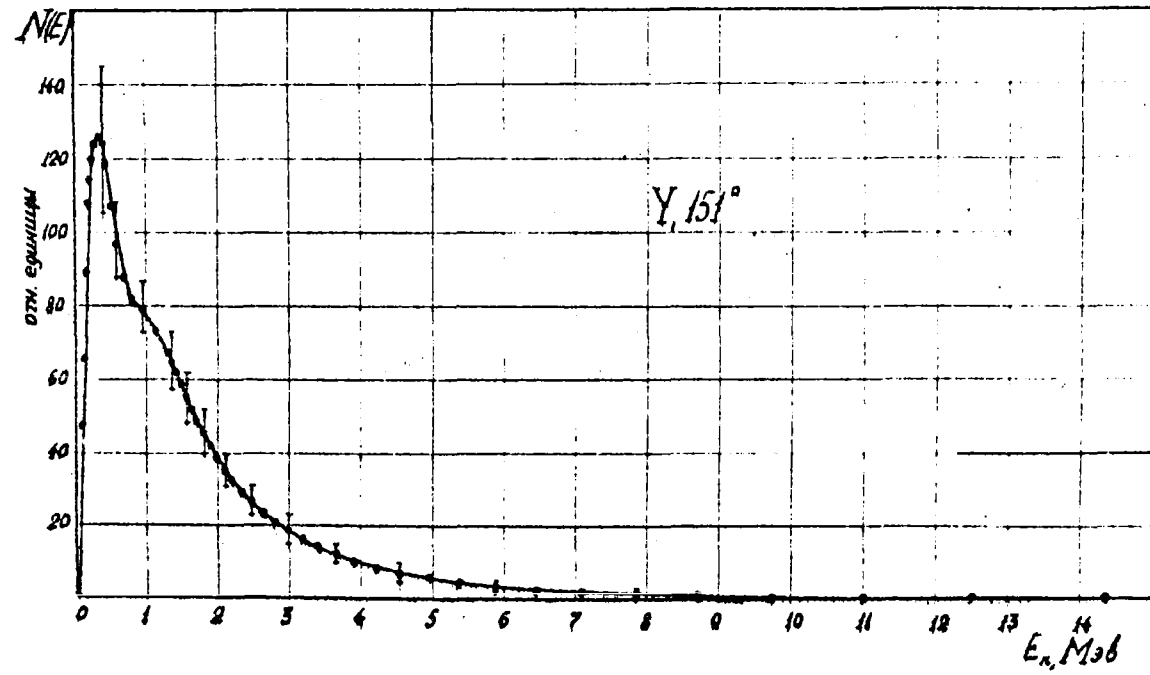
Рис. 35.
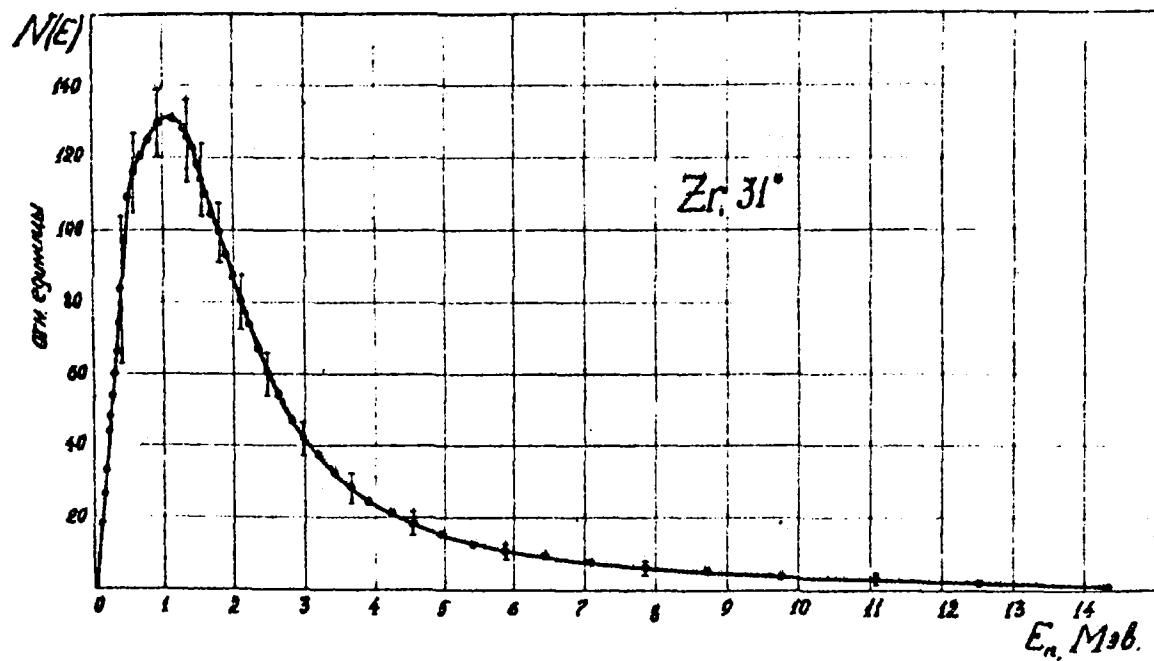
Рис. 36.

Рис. 37.

Рис. 38.

Рис. 39.

Рис. 40.
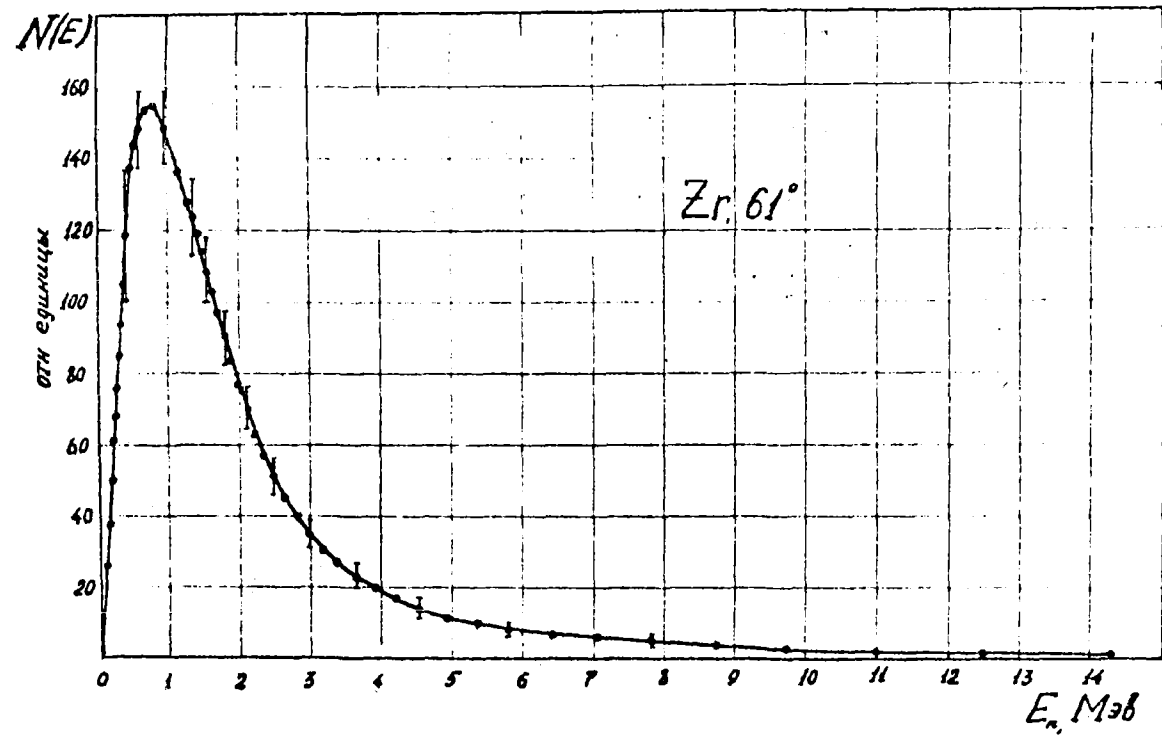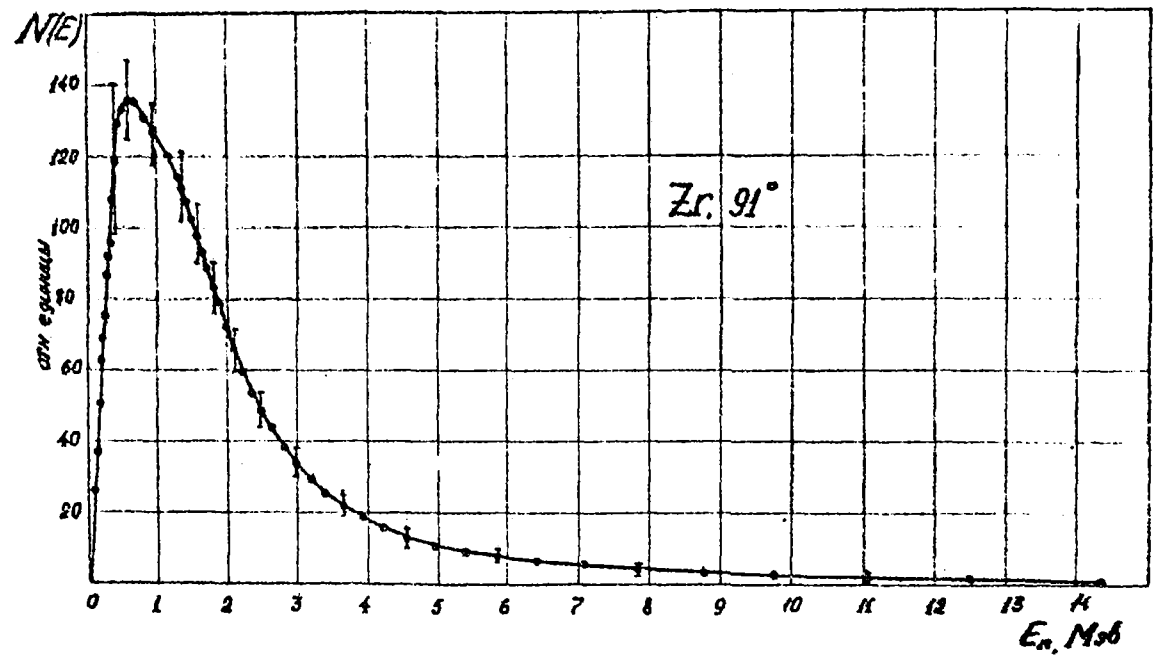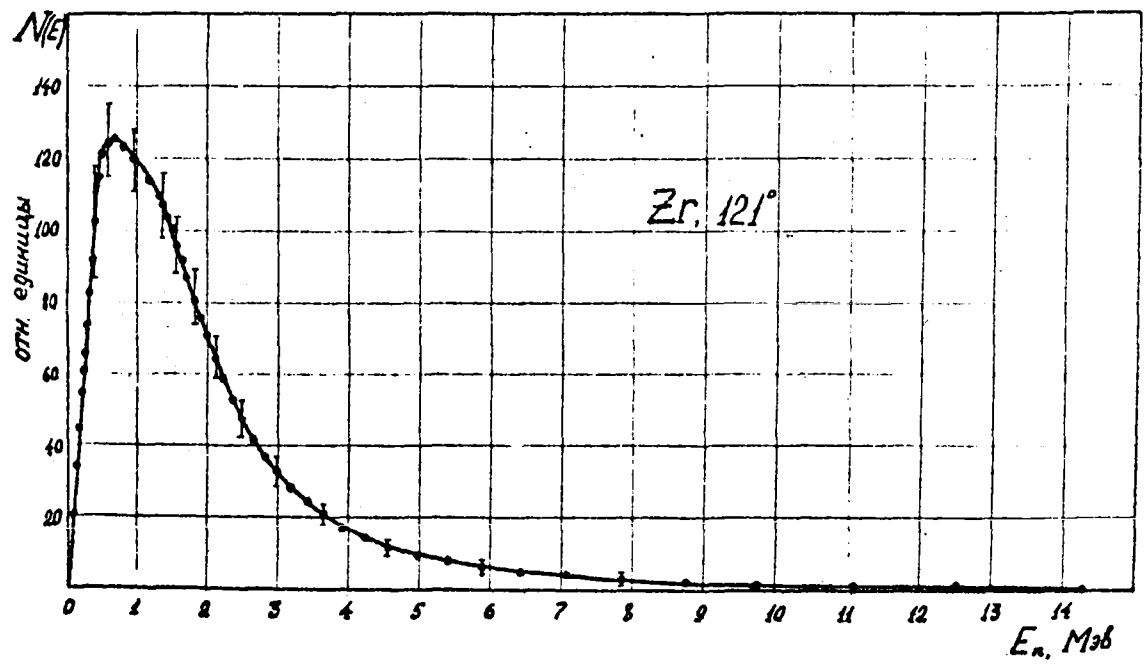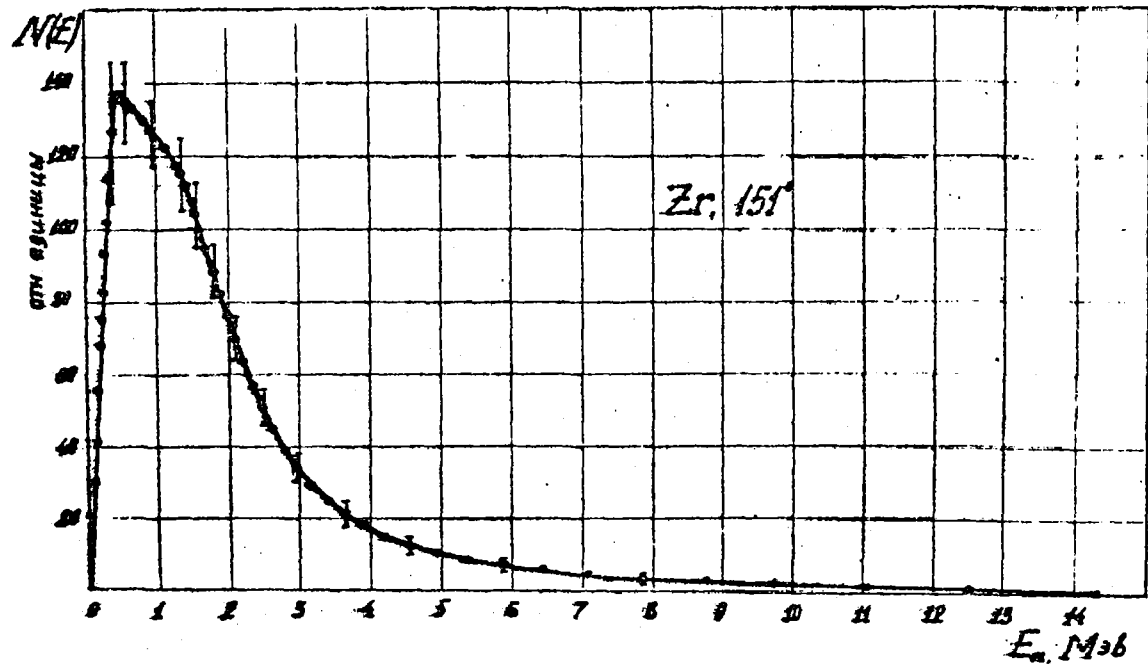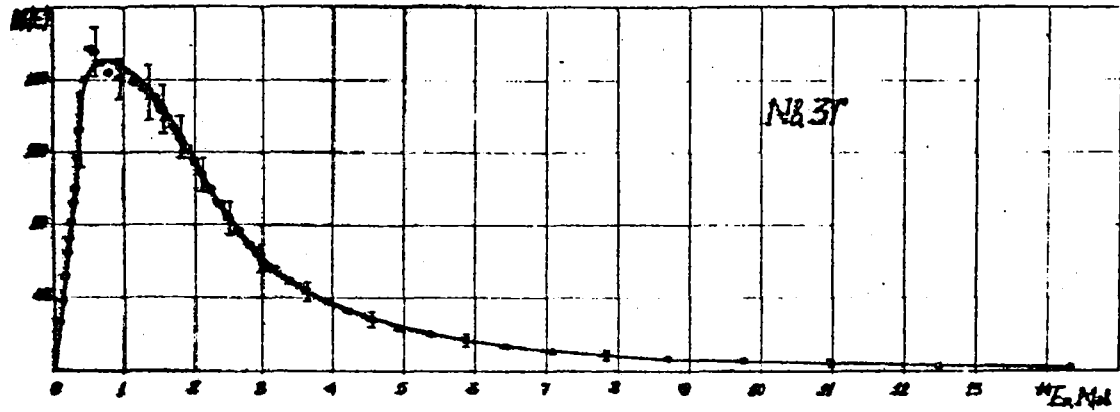
Рис. 4I.
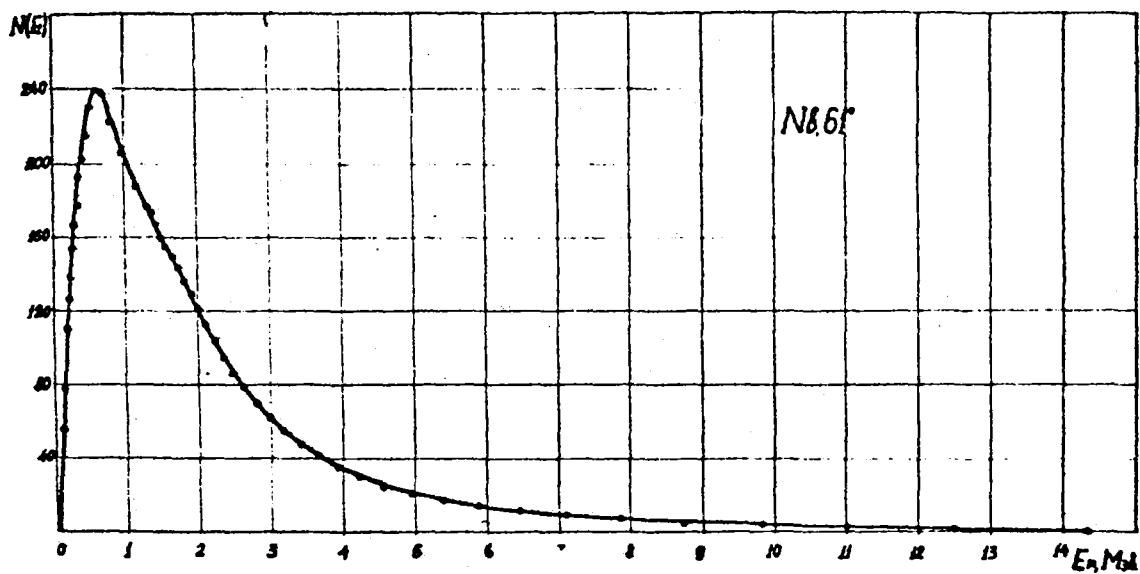
Рис. 42.
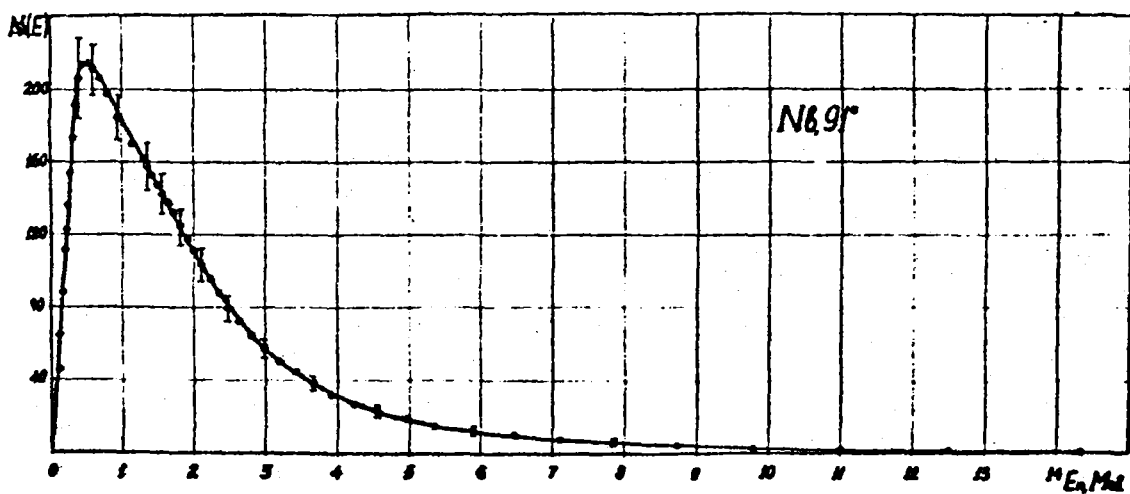
Рис. 43.
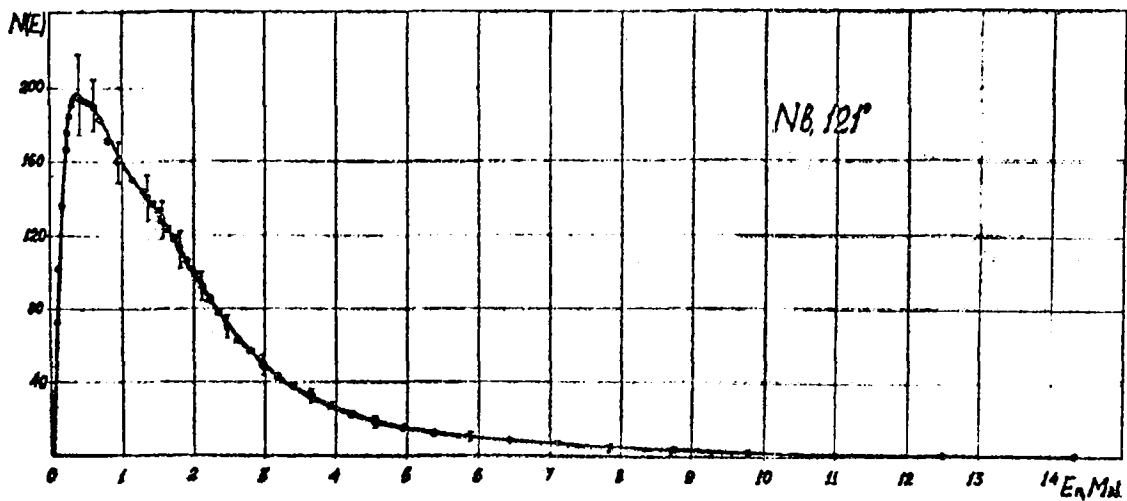
Рис. 44.
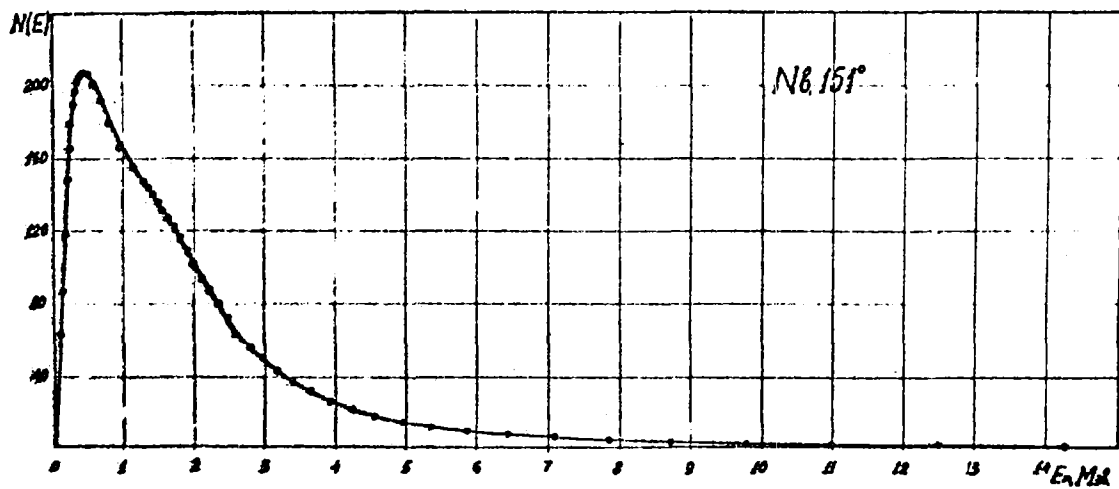
Рис. 45.
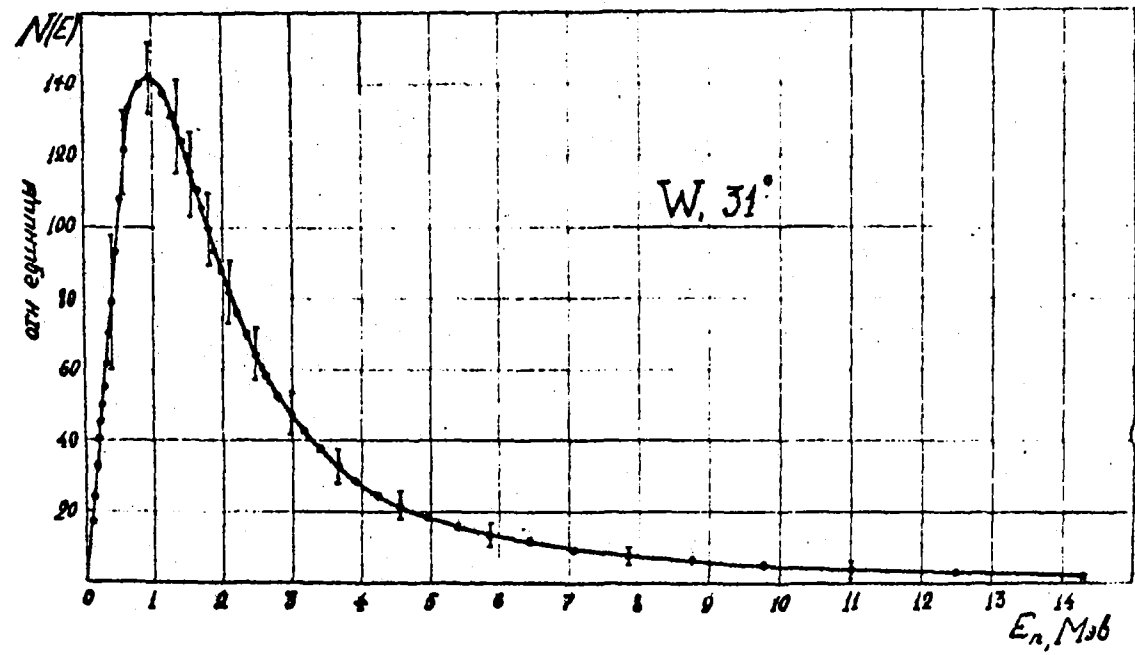
Рис. 46.
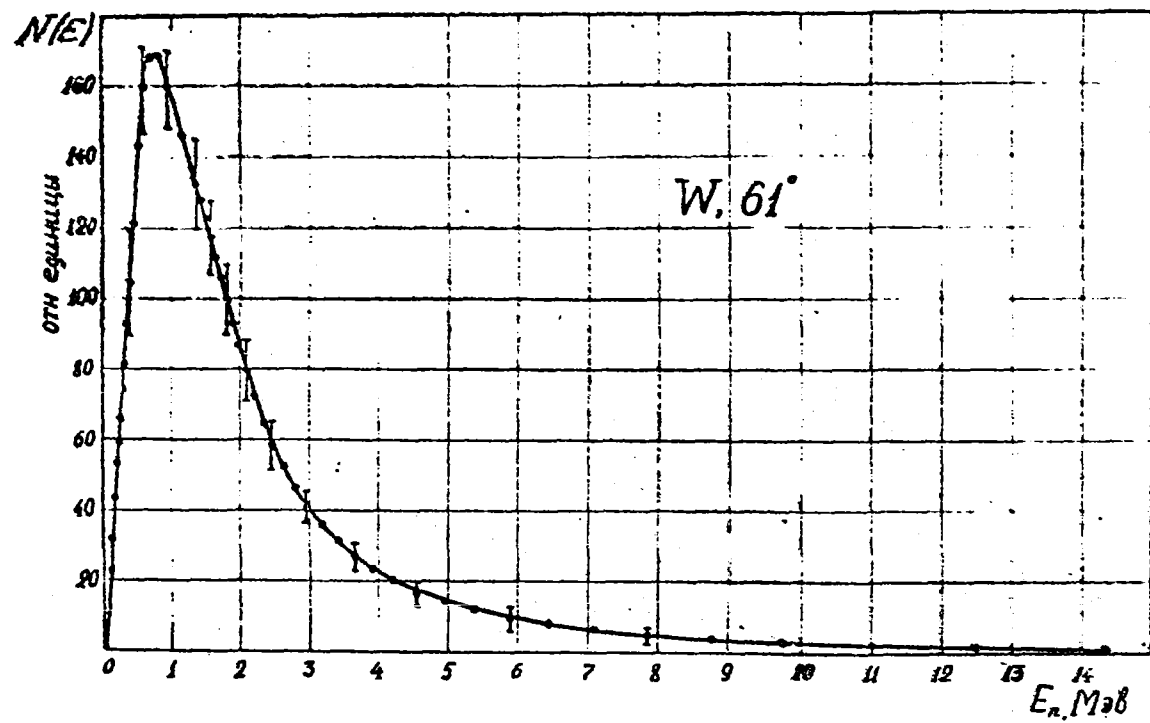
Рис. 47.
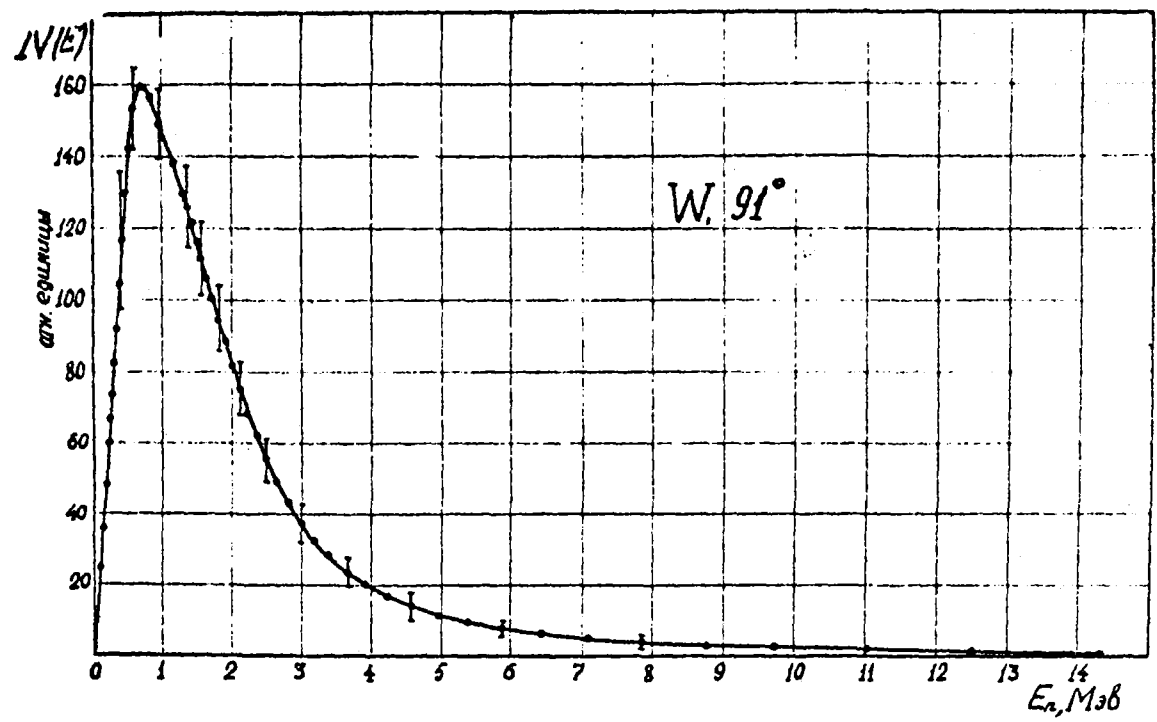
Рис. 48.
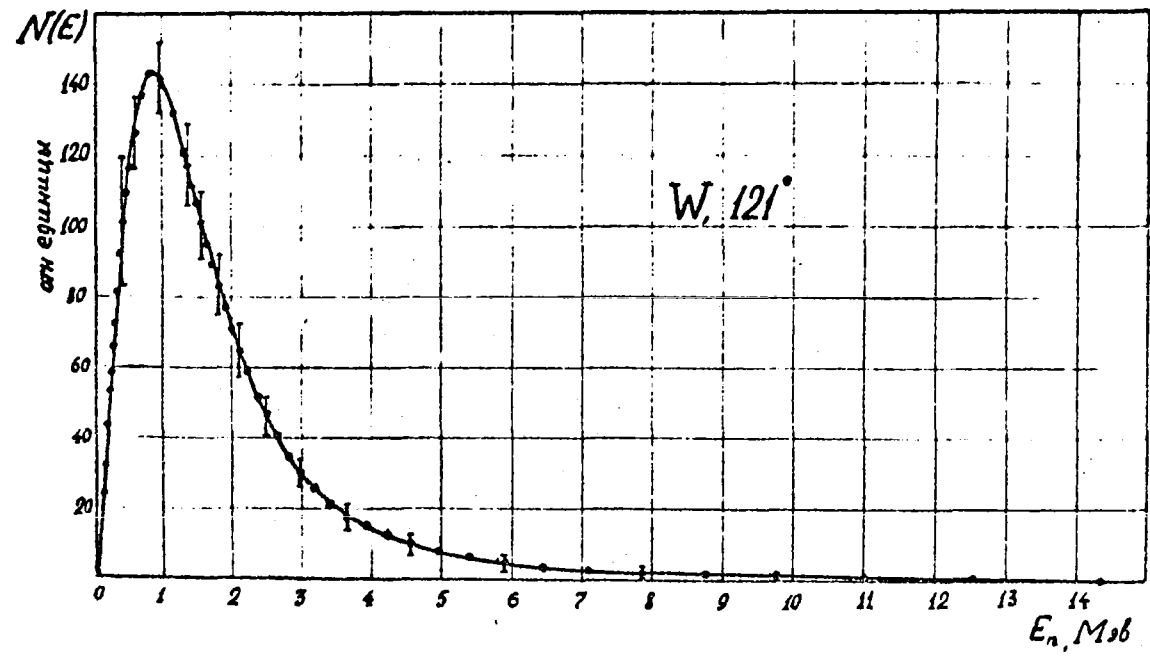
Рис. 49.
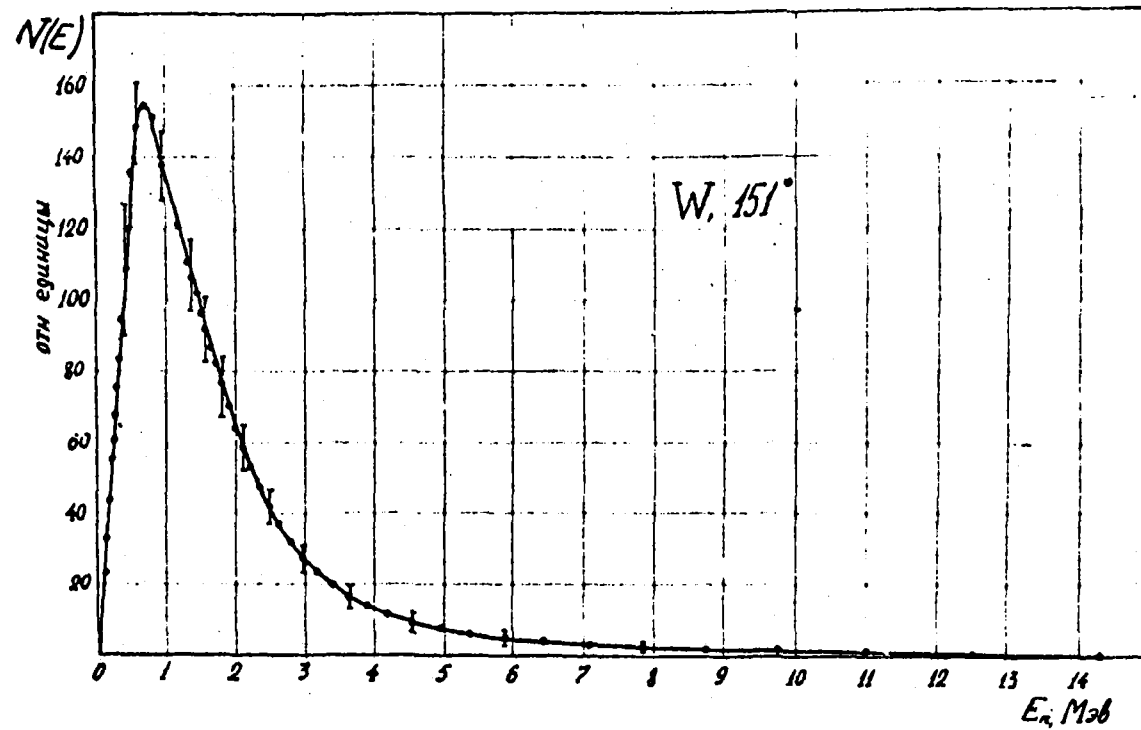
Рис. 50.
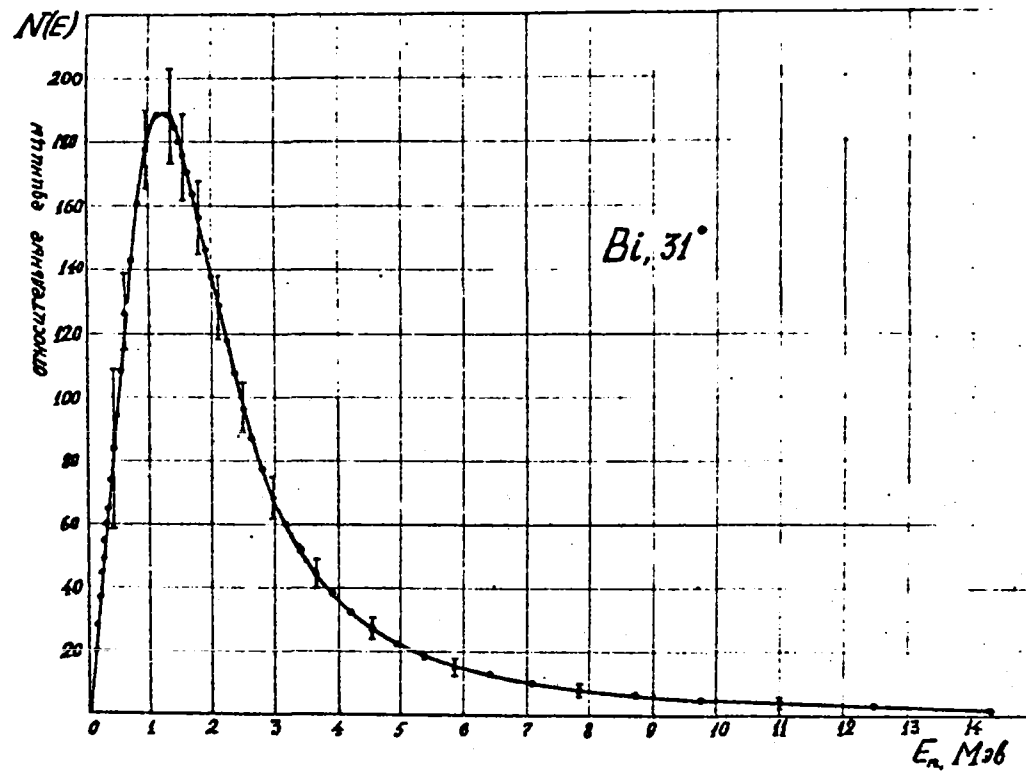
Рис. 51.
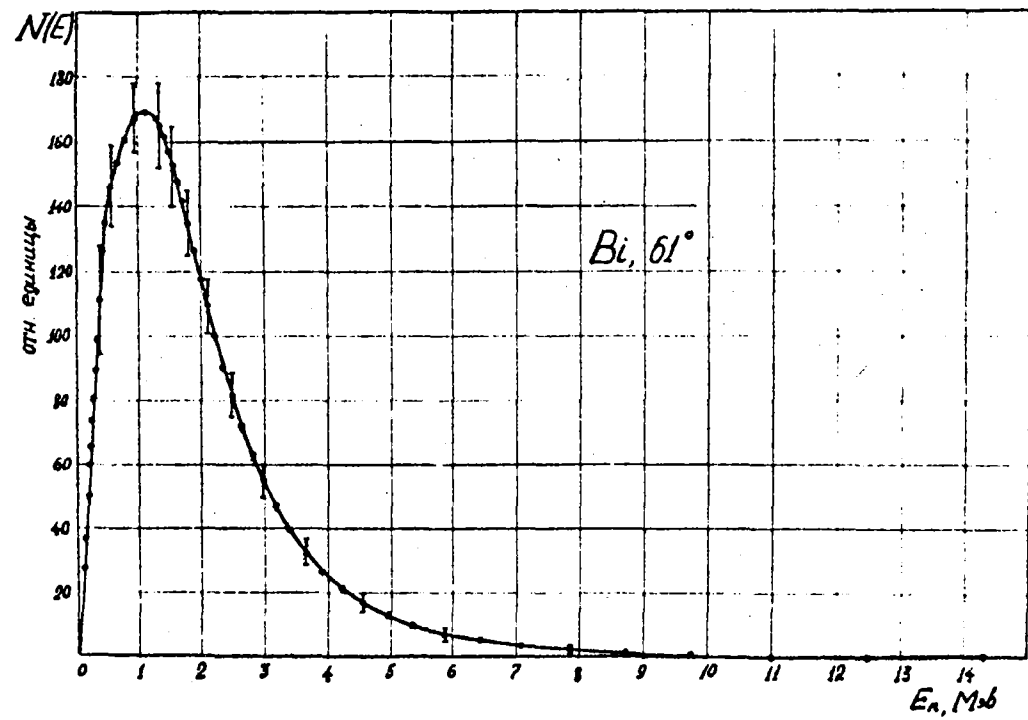
Рис. 52.
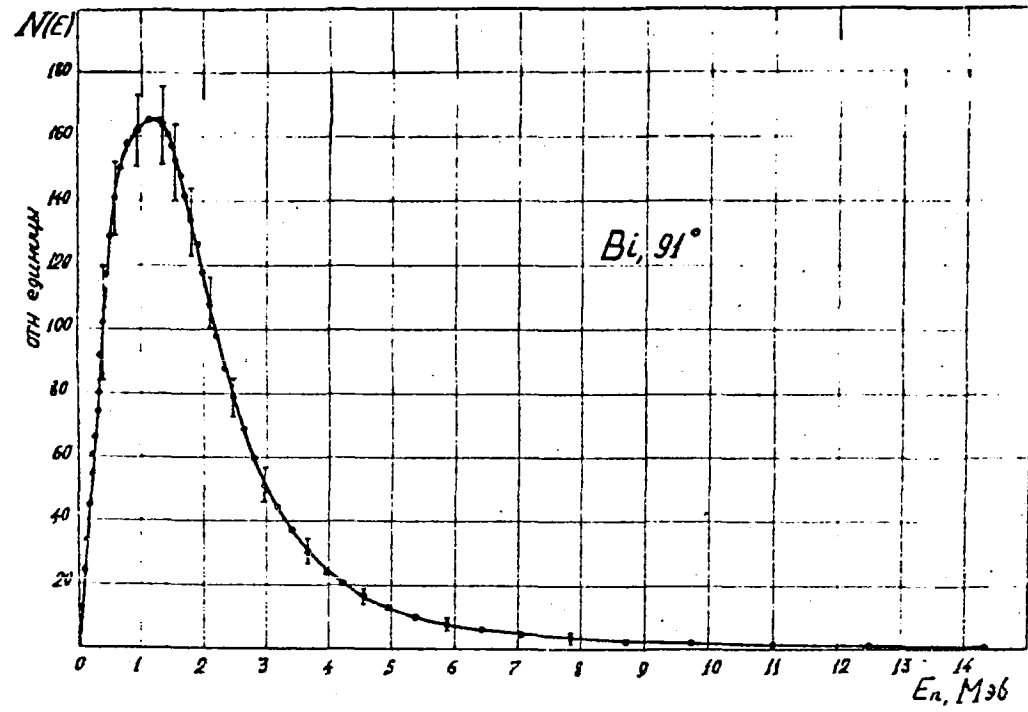
Рис. 53.
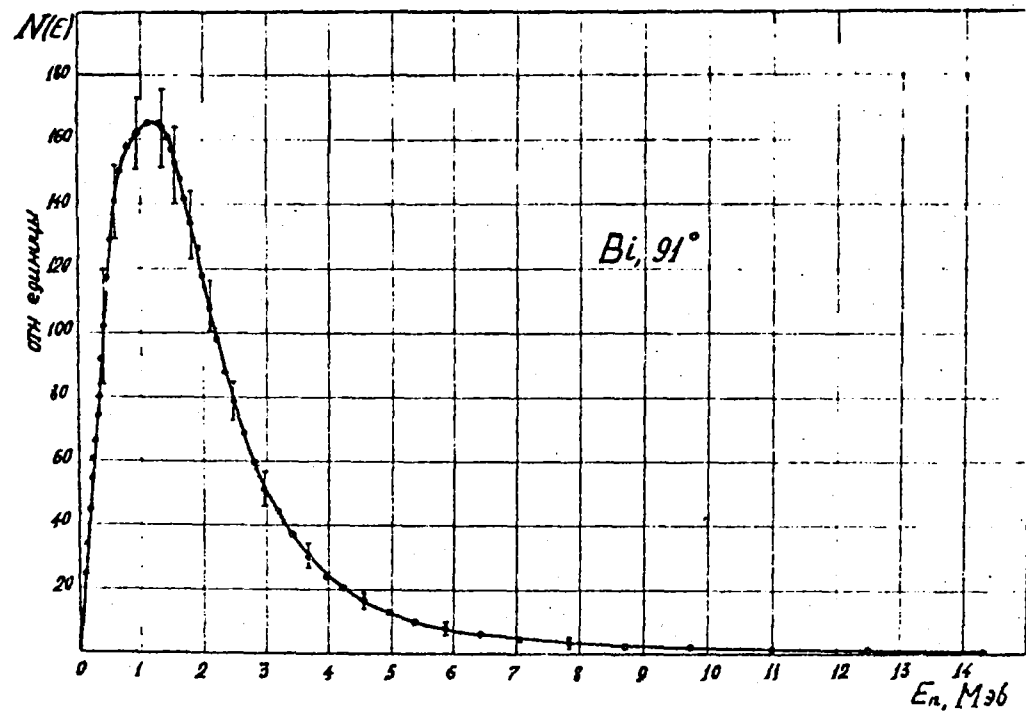
Рис. 53.
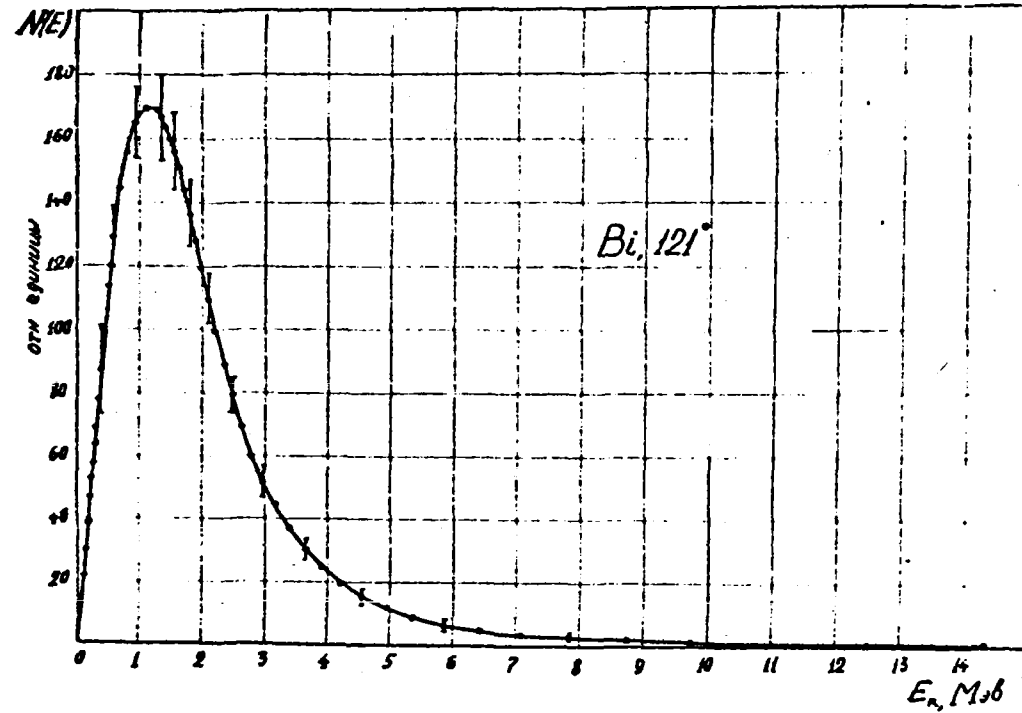
Рис. 54.
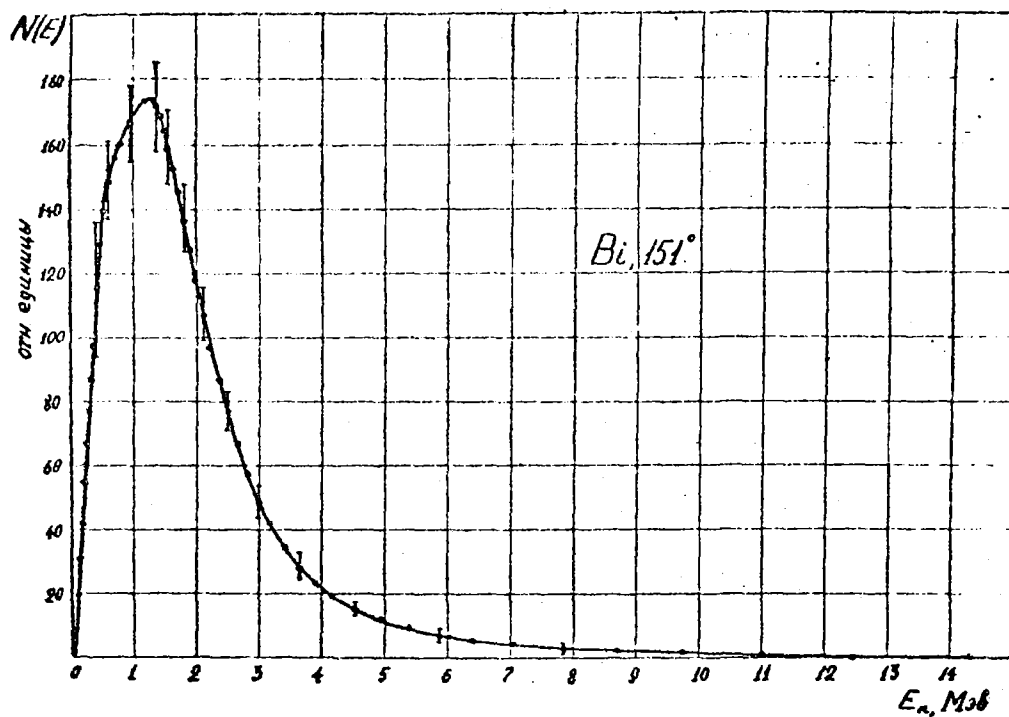
Fig. 55

REFERENCES

[1]   SALNIKOV, O.A. et al., Preprint No. 216 of the Institute of Physics and Power Engineering (1970).

[2]   SALNIKOV, O.A. et al., in Nuclear Data for Reactors (Proc. Conf. Helsinki, 1970) 2 IAEA Vienna (1970) 359.

ISOMER RATIOS AND GAMMA SPECTRA IN THE RADIATIVE CAPTURE OF THERMAL NEUTRONS

A.G. Dovbenko, A.V. Ignatyuk, V.A. Tolstikov

Introduction

Present investigations of the mechanism of neutron radiative capture by nuclei involve, essentially, the interpretation of three groups of experimental data: total radiative capture cross-sections, cross-sections for the formation of the isomeric state in radiative capture, and spectra of the cascade gamma rays produced. Wide use is made of statistical models of nuclear reactions to describe these data theoretically. If the total radiative capture cross-sections are investigated with such a model, it is possible to obtain data on the level density of the compound nucleus formed with excitation energy close to or above the neutron binding energy $/1\_/$, and the cross-section for the formation of isomeric states provides a basis for studying the relationship between level density and angular momentum $/2\_/$. A statistical description of the gamma spectra produced in radiative capture provides a means of studying the level density for excitation energies considerably below the neutron binding energy $/3\_/$. It emerges that the shape of the spectrum is sensitive even to the discrete primary low-excited nuclear levels $/4\_/$.

Investigation of the gamm spectra of radiative capture provides the most complete information on the radiative capture mechanism and, in the case of many nuclei, the difference in the shape of the gamma spectrum from the results of calculating spectra with the statistical model has served as a basis for developing new models of direct $/5\_/$ and semi-direct (or collective) $/6\_/$ capture mechanisms. It is clear that for these nuclei the total radiative capture cross-sections and the cross-sections for the formation of the isomeric states should also be described by a direct or collective capture model. However, the results of numerous investigations have so far been very inconsistent. The radiative capture cross-sections, the absolute values of the radiation widths and the isomeric ratios at neutron energies of not more than a few MeV are reasonably well described by the statistical model over practically the whole mass range of stable nuclei $/7, 8\_/$ investigated, whereas the gamma spectra of many nuclei are harder than predicted by the statistical model $/9\_/$.

To get a consistent explanation of the above experimental data we must determine to what extent the discrepancies in the gamma spectra can be accounted for by the parameters of the statistical model and establish the contribution of the direct process to the radiative capture cross-section for neutrons in the intermediate energy range.

In this study a statistical model is used to calculate the gamma spectra associated with thermal neutron capture, and also to calculate the ratios of the level populations in the ground and long-lived isomeric states formed as a result of these gamma transitions. Unlike earlier authors $\sqrt{3}$, 4$\underline{7}$, in calculating the spectra we took account of the dependence of level density on angular momentum. We also investigated the effect on the shape of the spectrum and on the isomeric ratios of different theories concerning the energy dependence of the excited state density and the dependence of the gamma transition probability on energy and on the angular momentum transmitted.

1. Basic relations

For describing multistage decay of an excited nucleus via gamma-ray emission it is convenient to use the method developed in Ref. $\sqrt{3}\underline{7}$. Let us consider this process, taking into account the effect of angular momentum on the probability of radiative transitions. We shall denote with y_k (E,J,t) the population after emission of the kth gamma quantum of a state with energy E and spin J at instant t. The variation of population with time is described in Bohr's classical model of compound nucleus decay $\sqrt{10}\underline{7}$ by the kinetic equation

$$\frac{\partial y_k(E,J,t)}{\partial t} = \sum_{J'} \int_E^{E_0} y_{k-1}(E',J',t) \Gamma_{\mu}(E',J' \longrightarrow E,J) dE' - y_k(E,J,t) \Gamma_{\mu}(E,J) \tag{1}$$

where $\Gamma_\gamma(E,J)$ is the total radiative decay width of the state (E,J) and $\Gamma_\gamma(E',J' \rightarrow E,J)$ is the width of radiative transition from the state (E',J') to the state (E,J), E_0 being the maximum excitation energy.

The initial condition for equation (1) is written

$$y_k(E,J,0) = \delta_{k0} y_0(E,J), \tag{2}$$

where $y_0(E,J)$ is the population of the state (E,J) at the initial moment of time. When a thermal neutron is captured the nucleus has an excitation energy $E_0 = B_n$ and momentum $J_0 = |I \pm 1/2|$, where B_n is the neutron binding energy and I is the target nucleus spin. It is then convenient to write

$$y_0(E, J) = \delta_{JJ_0} \delta(E - E_0) \tag{2a}$$

Integrating Eq. (1) with respect to time, we obtain

$$y_k(E, J, \infty) - y_k(E, J, 0) = \sum_{J'} \int_E^{E_0} dE' \Gamma_p(E' J' \to E J) \int_0^\infty dt\, y_{k-1}(E', J', t) -$$
$$- \Gamma_p(E, J) \int_0^\infty dt\, y_k(E, J, t) \tag{3}$$

We then determine

$$W_k(E, J) = \Gamma_p(E, J) \int_0^\infty dt\, y_k(E, J, t),$$

$$S(E' J' \to E J) = \frac{\Gamma_p(E' J' \to E J)}{\Gamma_p(E', J')} \tag{4}$$

Here $W_k(E,J)$ is the relative probability that in the gamma decay process the excited nucleus was in the state (E,J) after emission of the kth gamma quantum and $S(E',J' \to E,J)$ gives the relative probability of radiative transition to the state (E,J).

Since any excited state will decay in an infinite period of time, we have $y(E,J,\infty) = 0$ and equation (3) can be re-written in the form

$$W_k(E, J) = \sum_{J'} \int_E^{E_0} dE'\, S(E' J' \to E J)\, W_{k-1}(E' J') + y_k(E, J, 0) \tag{5}$$

If there is an isomeric state in the system its population may be defined as

$$W(E_m, J_m) = \sum_{k=0}^\infty W_k(E_m, J_m) \tag{6}$$

The isomeric ratio describes the relative probability of formation of a nucleus in the isomeric state and is usually determined experimentally as

$$\eta = \frac{\sigma_m}{\sigma_m + \sigma_g},$$

where σ_m and σ_g are the cross-sections for formation of the isomeric and ground states in the given reaction. On the basis of the above relations the isomeric ratio is determined as follows:

$$\eta = \frac{W(E_m, J_m)}{W(E_g, J_g) + W(E_m, J_m)} = W(E_m, J_m),$$ (7)

where the initial condition (2a) is explicitly taken into account.

Since $\Gamma_\gamma(E, J \rightarrow E - \varepsilon\gamma, J')$ determines the probability of emission of a gamma quantum with energy $\varepsilon\gamma$ during the transition from the state (E, J) to the state $(E - \varepsilon\gamma, J')$, the number of gamma quanta emitted at instant t from the state (E, J) may be written as

$$n_\gamma^{(E, J)}(\varepsilon_\gamma, t) = \sum_{J'} \Gamma_\gamma(E, J \longrightarrow E - \varepsilon_\gamma, J') \sum_{\kappa=0}^{\infty} y_\kappa(E, J, t)$$ (8)

The number of gamma quanta with energy $\varepsilon\gamma$ emitted during decay of the state (E, J) may thus be written

$$n_\gamma^{(E, J)}(\varepsilon_\gamma) = \sum_{J'} \Gamma_\gamma(E, J \longrightarrow E - \varepsilon_\gamma, J') \int_{\kappa=0}^{\infty} dt \sum_{\kappa=0}^{\infty} y_\kappa(E, J, t) =$$
$$= \sum_{J'} S(E, J \longrightarrow E - \varepsilon_\gamma, J') \sum_{\kappa=0}^{\infty} W_\kappa(E, J)$$ (9)

For the total number of gamma rays with energy $\varepsilon\gamma$ we obtain

$$n_\gamma(\varepsilon_\gamma) = \sum_{J, J'} \int_{\varepsilon_\gamma}^{E_0} dE \, S(E, J \longrightarrow E - \varepsilon_\gamma, J') W(E, J)$$ (10)

The gamma-ray spectrum will now be defined as

$$I(\varepsilon_\gamma) = \frac{\varepsilon_\gamma \, n_\gamma(\varepsilon_\gamma)}{\int_0^{E_0} n_\gamma(\varepsilon_\gamma) \, d\varepsilon_\gamma}$$ (11)

On the basis of the initial condition selected in expression (2a) above, we have

$$E_0 = \int_0^{E_0} I(\varepsilon_\gamma) \, d\varepsilon_\gamma$$ (12)

The total number of gamma quanta emitted is given by the formula

$$n_{\gamma} = \int_{0}^{\mathcal{E}_{0}} n_{\gamma}(\mathcal{E}_{\gamma}) \, d\mathcal{E}_{\gamma} \tag{13}$$

The above relations make use of the underlying assumption of Bohr's compound nucleus model that the mode of decay of the excited state is independent of its mode of formation. In this case the correlations of the gamma quanta must be determined solely by conservation of angular momentum and there should be no other correlations. The presence of such correlations would mean that the whole approach was incorrect.

In the statistical model the widths are expressed in terms of the density of the final nuclear states and to describe this it is normal to use the Fermi gas model $/10\_7$. This method was used to calculate the gamma-ray spectra (neglecting angular momentum) in Refs $/3\_7$ and $/4\_7$ and to calculate the isomeric ratios in Refs $/11-13\_7$. Below we shall show that existing data on radiation widths and level densities are not accurate enough.

For analysing isomeric ratios it is common to use the highly simplified description of Huizenga and Vandenbosch $/2\_7$ in which only a small number of cascades is considered ($\sim$ 3-4) and the isomeric ratio is determined simply by the spin dependence of the level density. The simplicity of this approach is of course very attractive but the results of Refs $/11-13\_7$ show that the accuracy is not good enough for a reliable quantitative analysis of experimental data.

2. Description of mean radiation widths

Let us now consider existing information on radiation width characteristics. Simple relationships for the widths of gamma transitions of different multipolarity from state i to state j were obtained by Weisskopf on the basis of single-particle estimates $/10\_7$. Comparison of these estimates with existing data for light nuclei has shown that on average they are valid, although there are fairly large discrepancies in individual transitions $/14\_7$. If the states of the excited nucleus have sufficient density, we are interested mainly in the value of the radiation width averaged over a large number of possible transitions. For mean widths of different multipolarity we have

$$\Gamma_{\gamma ij}(E1) = \frac{6.8 \cdot 10^{-2}}{D_o} \cdot A^{2/3} \varepsilon_\gamma^3 \rho_i^{-1}$$

$$\Gamma_{\gamma ij}(E2) = \frac{4.9 \cdot 10^{-8}}{D_o} A^{4/3} \varepsilon_\gamma^5 \rho_i^{-1} \tag{14}$$

$$\Gamma_{\gamma ij}(M1) = \frac{2.1 \cdot 10^{-2}}{D_o} \varepsilon_\gamma^3 \cdot \rho_i^{-1}$$

where A is the mass number, $\varepsilon\gamma$ is the gamma-ray energy, ϱ_i is the density of the initial states with given spin and parity and D_o characterizes the mean distance between degenerate single-particle levels (sub-shells). The numerical values of the constants were obtained by Wilkinson $\underline{/14\_/}$ and correspond to the measurement of Γ_γ in eV, ε_γ and D_o in MeV, and ϱ_i in MeV^{-1}. Initially, Weisskopf estimated D_o at ~ 0.5 MeV but the value now used is D_o ~ 15 MeV. It is often included in a constant whose value is found by fitting to experimental data $\underline{/8,9\_/}$.

Recently, another approach has been evolved for calculating Γ_γ based on the principle of a detailed balance linking the direct (n,γ) and the inverse (γ,n) reactions. Here it is assumed that the behaviour of the E1 transitions in the nucleus formed as a result of the (n,γ) reaction is governed by the same physical processes as the giant dipole resonance in photonuclear reactions. Approximating the photoabsorption cross-section by means of Lorentz's formula on the assumption that its validity extends to energies of 6-8 MeV — which are of interest from the point of view of the gamma radiation emitted during neutron capture — Axel $\underline{/15\_/}$ obtained an expression for the width $\Gamma_{\gamma o}$ of E1 transitions to the ground state:

$$\Gamma_{\gamma oi} = 1.13 \cdot 10^6 A \frac{\varepsilon_\gamma^4 \cdot \Gamma_g^2}{(\varepsilon_\gamma^2 - \varepsilon_g^2)^2 + \varepsilon_\gamma^2 \Gamma_g^2} \cdot \rho_i^{-1} \tag{15}$$

where εg is the energy of the giant resonance and Γg is its width. To obtain a relation for evaluating a large number of nuclei, Axel $\underline{/15\_/}$ recommended Γg = 5 MeV and εg = 80.$A^{-1/3}$. Then for gamma quanta with energies of 6-8 MeV expression (15) takes the simple form

$$\Gamma_{\gamma oi} = 6.1 \cdot 10^{-15} \varepsilon_\gamma^5 A^{8/3} \rho_i^{-1} \tag{16}$$

where $\Gamma_{\gamma oi}$ and $D_i = \frac{1}{\varrho_i}$ are in the same units and $\varepsilon\gamma$ is in MeV. Note once

again that expressions (15) and (16) were obtained only for transitions to
the ground state. Therefore their use for calculating the radiation widths
of transitions to excited states rests on the assumption that the shape of
the photoabsorption energy dependence is determined solely by the gamma quanta
energy and is independent of whether the nucleus is in the ground or the
excited state.

Note also that even the experimental data on the width of the transition
to the ground state relate only to the 15-20 MeV region in the photoabsorption
cross-section where a giant dipole resonance exists, and that there are
practically no experimental data for the 6-10 MeV region, so that extrapolation
of expression (15) to lower gamma transition energies also requires verifica-
tion.

One of the ways of experimentally verifying the dependence of $\Gamma\gamma$ on the
energy of the gamma quanta emitted is to analyse the gamma spectra resulting
from radiative capture of neutrons with energies in a range ΔE which
contains a sufficiently large group of resonances ("average capture"). Now,
thanks to the development of a new technique - Ge-Li gamma detectors - it has
become possible to obtain neutron capture gamma spectra with very good
resolution, by dividing the high energy part of the spectrum into separate
lines.

In an experiment of this type the intensities of the gamma lines in the
high energy part of the spectrum are proportional to the radiation widths
$\Gamma\gamma,i,j$ in the sense defined above, and one can obtain the dependence of the
radiation width on gamma-ray energy. The results of these investigations
are given in Fig. 1 $\boxed{16\,}$, which shows the radiation widths $\Gamma\gamma,i,j$ of the
high energy part of the capture gamma spectrum for the isotopes ^{156}Gd and
^{158}Gd. The results of the experiment are compared with the energy dependence
of $\Gamma\gamma ij$ according to Weisskopf $(\sim \varepsilon_\gamma^3)$ $\boxed{10\,}$, Axel $\boxed{15\,}$ and with the
dependence $\sim \varepsilon_\gamma^5$. It can be seen that the values obtained for $\Gamma\gamma ij$
in the 6.5-8.5 MeV energy range do not agree with the energy dependence cal-
culated according to Weisskopf. The experimental dependence is more
sharply defined than ε_γ^3 and can be described approximately by both ε_γ^5 and
expression (15). It is impossible, however, to draw any more definite
conclusions, since the experimental data were obtained for a limited energy
range and their accuracy is insufficient. Analysis of the spectra for other
nuclei such as ^{182}Ta, ^{184}W, ^{190}Os and ^{196}Pt also shows that the dependence of
$\Gamma\gamma ij$ on ε_γ is in any case more sharply defined that ε_γ^3 $\boxed{16\,}$.

Considerably less study has been devoted to the mean widths of the Ml
and E2 transitions. Recently obtained experimental data $/\overline{16}/$ have shown
that the mean widths of Ml transitions for gamma-ray energy about equal to
the neutron binding energy are an order of magnitude less than the widths of
the El transitions. Such a relationship is in quantitative agreement with
an estimate of the widths based on expression (14). It is not clear, however,
to what extent the result obtained depends on the energy range considered. If
it contains a giant Ml resonance, the mean radiative widths of the magnetic
transitions in this energy range may be comparable with the mean widths of the
electric dipole transitions. Bollinger $/\overline{16}/$ attempted to analyse the
effect of the giant Ml resonance by studying capture gamma-ray spectra from
the reactions $^{117}Sn(n,\gamma)^{118}Sn$ and $^{119}Sn(n,\gamma)^{120}Sn$. The energy dependence
of the widths which he obtained is shown in Fig. 2. Owing to the paucity
of experimental data available it is impossible to establish definitely whether
there is a giant resonance in the intermediate neutrons of Ml transitions, but
it appears that the transition intensity in the 6-9 MeV energy range fluctuates
rather strongly.

From expression (14) one would expect electric quadrupole transitions to
be considerably weaker than dipole transitions, so that their contribution to
the mean radiation width would be negligible. But here too it is not certain
whether this relationship holds for low-energy transitions. The collective
characteristics of the lower excited states may be such that quadrupole
transitions are amplified, and this must be allowed for in calculating the
mean radiation widths of nuclei in the low excitation energy range.

For calculating thermal capture gamma-ray spectra $/\overline{3, 4}/$ and the
corresponding total radiation widths $/\overline{8}/$, it is usually assumed that the
nucleus decays only by way of electric dipole transitions. In calculating
the isomeric ratios $/\overline{2, 11, 12}/$ a small contribution of other transitions
is admitted only at very low excitation energies. This brief examination
of the data on mean radiation widths indicates that the assumption that El
transitions dominate throughout the excitation energy range may not be correct;
at any rate it is not possible at the moment to assess the accuracy of this
approximation.

If the number of excited states involved in the decay process is large
enough, the spectral density of the gamma quanta will be proportional to
the number of states:

$$\Gamma_\gamma (E_\gamma) = \Gamma_{\gamma ij} (E_\gamma) \rho (u, I, \pi) \tag{17}$$

Here $\Gamma_{ij}(\varepsilon\gamma)$ coincides with the widths defined above - see expression (14) - and $\varrho(u,I,\pi)$ is the density of final states with excitation energy $u = E-\varepsilon\gamma$, the corresponding momentum I and parity π.

Since the relationships given above for the population of states and gamma-ray spectra contain the relative decay probability

$$ S\left(E, \mathcal{I}' \longrightarrow E, \mathcal{I}\right) = \frac{\Gamma_r(E,\mathcal{I}' \to E,\mathcal{I})}{\Gamma_r(E, \mathcal{I})} , \tag{18} $$

the results of the spectrum calculations do not depend on the constants used in expression (14), and are influenced only by the energy dependence of $\varrho(u,J)$ and $\Gamma_{\gamma ij}(\varepsilon\gamma)$. Levels of different parity are distributed on average with equal probability $\underline{/17\underline{/}}$ so that even in deriving the basic relationships we did not classify the transitions according to parity. Below we shall consider only dipole transitions and ignore the quadrupole contribution. The energy dependence in expression (18) should then be determined as a composite energy dependence of E1 and M1 transitions with allowance for their relative intensity.

3. Density of excited nuclear states

A description of the mean radiation width relying on the statistical approach (17) requires us to know the density of the excited nuclear states over the whole range of excitation energies and angular momenta investigated. Since there are no direct experimental data for this wide range, it is necessary when calculating to employ various model-based estimates of level density which are fitted to existing experimental data only at certain points.

It is most common in such calculations to use simple analytical relationships for level density obtained with the Fermi gas model $\underline{/17\underline{/}}$:

$$ \rho(u,\mathcal{I}) = \frac{2\mathcal{I}+1}{2\sqrt{2\pi}\,\sigma^3}\, exp\left\{-\frac{(\mathcal{I}+\frac{1}{2})^2}{2\sigma^2}\right\}\, \rho(u), \tag{19} $$

$$ \rho(u) = \frac{\sqrt{\pi}}{12\,a^{1/4}u^{5/4}}\, exp\left\{2\sqrt{au}\right\} \tag{20} $$

The basic parameters of this model are the level density parameters, a, and the spin dependence parameter

$$ \sigma^2 = \mathcal{F}\sqrt{\frac{u}{a}} = \frac{6}{\pi^2}\,\overline{m}^2\,\sqrt{au} \tag{21} $$

Since this parameter depends on the excitation energy u, it is more convenient to use the moment of inertia $F = \frac{6}{\pi^2} a < m^2>$ as a parameter, or even $<m^2> -$ the mean square of the projection of the single-particle moment of states close to the Fermi energy.

For u in these expressions we use the effective excitation energy, defined as

$$\mathcal{U} = E - \delta, \text{ where } \delta = \begin{cases} 0 & \text{for odd-odd nuclei} \\ \Delta_N \text{ or } \Delta_z & \text{for odd nuclei} \\ \Delta_N + \Delta_z & \text{for even-even nuclei} \end{cases} \qquad (22)$$

This way of determining the effective excitation energy corresponds to the phenomenological calculation of residual interactions in nuclei with different parity of the nucleon number. The pairing parameters Δ are determined here on the basis of the even-odd nuclear mass differences $/18, 19/$.

For a large number of nuclei the level density parameter, a, was found by analysing experimental data on neutron resonance density $/8, 19, 20/$. Selection of the parameter $<m^2>$ involves some uncertainty which leads to inconsistency in the parameter a derived by different authors. Thus the authors of Refs $/8, 19/$ used a value of $<m^2> = 0.146 A^{2/3}$ whereas in later investigations the value employed is $<m^2> = 0.24 A^{2/3}$ $/20/$. The latter value corresponds better to the theoretical determination of $<m^2>$ $/21/$.

The chief merit of the Fermi gas model is the simplicity of the results it yields — see expressions (19), (20) and (21). However, existing theory on the structure of the excited nucleus raises doubts as to the suitability of such a simple model for describing level density in a wide excitation energy range. A lot of experimental data are in direct contradition to Fermi gas model results $/22/$. To describe a large set of nuclear characteristics it is more logical to use a superfluid nuclear model based on the fundamental relations of the theory of superconductivity $/22/$. The expression for level density obtained with this approach is more complex. The following relation was used in this investigation:

$$\rho(\mathcal{U}) = \left[(2\pi)^3 f_{zz} f_{NN} (f_{\beta\rho}^{(z)} + f_{\beta\beta}^{(N)}) \right]^{-1/2} exp \left\{ S_z + S_N \right\} \qquad (23)$$

S_z is nuclear entropy, determined for protons as

$$S_z = 2 g_z \beta \Delta_z \sum_{n=1}^{\infty} (-)^{n+1} K_z (n \beta \Delta_z) \qquad (24)$$

where $K_\nu(x)$ is the Macdonald function. The pre-exponential functions are:

$$f_{zz} = g_z \int_0^\infty dx \left\{ \frac{1}{2 \, ch^2 \left(\frac{\beta \sqrt{x^2 + \Delta_z^2}}{2} \right)} + \frac{\Delta_z^2 \, t \, h^2 \frac{\beta \sqrt{x^2 + \Delta_z^2}}{2}}{\sqrt{x^2 + \Delta_z^2}} \right\},$$ (25)

$$f_{\beta\beta} = g_z \int_0^\infty dx \left\{ \frac{x^2 - \Delta_z^2}{2 \, ch^2 \frac{\beta \sqrt{x^2 + \Delta_z^2}}{2}} + \frac{\Delta_z^2 (x^2 - \Delta_z^2)}{\sqrt{x^2 + \Delta_z^2}} th \frac{\beta \sqrt{x^2 + \Delta_z^2}}{2} \right\}$$

Relations (24) and (25) take a similar form for neutrons, it being necessary only to replace the parameters g_z and Δ_z by g_N and Δ_N. The parameter Δ defines the effect of pair correlations and is obtained by solving the equation

$$ln \frac{\Delta_z}{\Delta_{oz}} = 2 \sum_{n=1}^\infty (-)^{n+1} n\beta \Delta_z K_2 (n \beta \Delta_z) \quad \text{when } \beta > \beta_{kp}^{(z)}$$ (26)

$$\Delta_z = 0 \qquad\qquad \text{when } \beta \leq \beta_{kp}^{(z)}$$

where $\beta_{kp}^{(z)} = 1.76/\Delta_{oz}$. A similar equation is written for Δ_N.

The above expressions are functions of the thermodynamic temperature $t = \beta^{-1}$. For a given excitation energy u, the temperature t is the solution of the equation

$$u = \frac{t}{2} (S_N + S_z) + \frac{1}{4} g_z (\Delta_{oz}^2 - \Delta_z^2) + \frac{1}{4} g_N (\Delta_{oN}^2 - \Delta_N^2)$$ (27)

The dependence of the thermodynamic functions on temperature for this model is shown in Fig. 3.

Thus in the superfluid nuclear model the level density energy dependence is determined by four parameters: the density of single-particle proton states g_z and neutron states g_N and the pair correlation parameters Δ_{oz} and Δ_{oN}. These parameters are equivalent to the parameters a and b in the Fermi gas model. If it is assumed that $\Delta_{oz} = \Delta_{oN} = \Delta_o$ and $g_z = g_N = g/2$, the level density in Eq. (23) will be a function of only two parameters. This reduction in the number of parameters considerably simplifies their determination in analyses of experimental data; however, theoretical determination of the parameters Δ_{oz} and Δ_{oN} shows that they almost always differ /23_7. It should be noted that in the superfluid nuclear model Δ_o does not vanish

for an odd number of protons or neutrons, and the observed even-odd differences in the excited state densities are associated with the difference of $1/4g\Delta_o^2$ for even and odd nuclei [22].

The dependence of level density on angular momentum in the superfluid model is similar to relation (19) in the Fermi gas model except that the spin dependence parameter takes a different form:

$$\sigma^2 = t \, (\mathcal{F}_Z + \mathcal{F}_N) \tag{28}$$

The moment of inertia is determined as

$$\mathcal{F}_Z = 2\overline{m}_Z^2 \sum_{n=1}^{\infty} (-)^{n+1} \beta n \Delta K_1(\beta n \Delta) \quad \text{when } \beta > \beta_{KP}^{(Z)} \tag{29}$$

$$\mathcal{F}_Z = \overline{m}_Z^2 \, g_Z \quad\quad\quad \text{when } \beta \leq \beta_{KP}^{(Z)}$$

The expression for F_N is similar.

In the general case $\overline{m}_Z^2 \neq \overline{m}_N^2$, but this difference has very little effect on the calculation of the level density spin dependence. To reduce the number of parameters in the calculation, it was assumed that $\overline{m}_Z^2 = \overline{m}_N^2 = 0.25 \, A^{2/3}$, where the numerical value of the coefficient is obtained from calculations on the single-particle spectrum of the shell model [21].

For near magic nuclei the level density energy dependence is more complex and cannot be described by any of the above models for constant values of the level density parameter, a (or g) [22]. For such nuclei it is accordingly best to make direct use of level density calculations on a given spectrum of single-particle states of the shell model. The results of these calculations provide a fairly good description of the experimental data on the excited state densities of magic nuclei in the barium-cerium range (A ~ 140) and in the lead range [24].

Calculations of the low energy part of the spectrum of cascade gamma radiation are considerably affected by the discrete character of the spectrum of the primary excited nuclear states [4]. If an experimental scheme of the primary nuclear levels exists, it is convenient, when calculating the radiation widths to separate out the transitions to explicit low-lying states or, what amounts to the same thing, to represent the level densities in the low energy region in the form

$$\rho(u, J) = \sum_i \delta(u - \varepsilon_i) \delta_{J J_i} \, , \tag{30}$$

where E_i and J_i are the energy and spin of the ith excited level.

This method of determining the density also enables allowance to be made for the probability of radiative transition to the ground state and for the effects of an energy gap in the spectrum of excited states of even-even nuclei.

4. Results of calculations

For calculating gamma-ray spectra and the relative population of the isomeric levels it is necessary to determine the population of excited states resulting from transitions with a given number of gamma quanta - see Eq. (5). This was found by successive calculation of the probabilities of transitions in each cascade, but for these calculations it is particularly important to choose the optimum number of cascades. This problem can be avoided by summing Eq. (5) in terms of the possible cascades and reducing the solution of the resulting integral equation to a system of differential equations $\boxed{3, 4\,}$. However, this approach is convenient only for a fairly simple energy dependence of the radiation width ($\sim \varepsilon_\gamma^3$); and since the behaviour of the radiation width can be more complex, we preferred the method of successive cascade analysis for calculating the spectra. Comparison of the results of those calculations with the results of solution of the differential equations in Refs $\boxed{3, 4\,}$ showed that the optimum number of cascades is $\sim$ 50 and that the calculations are not sensitive to any further increase in the number of cascades.

Troubetskoy and Strutinsky $\boxed{3, 4\,}$ have shown that the low energy part of the gamma-ray spectrum cannot be obtained with a continuous level distribution function (level density) close to the ground state and that it is necessary to allow explicitly for the discrete character of the spectrum of the primary excited nuclear states - see Eq. (30). In our calculations in the low excitation energy range we therefore used discrete levels, the energy and angular momentum of which were selected in accordance with Refs $\boxed{25\,}$ and $\boxed{26\,}$. This choice of levels also removes to some extent the indeterminacy associated with the use of the level density formulae - expressions (19)-(27) - in the low excitation energy range. If excited states arose (not the observed isomeric states) which could not decay via dipole transitions, we then took into account transitions of higher multipolarity. The consideration of the latter was analogous to the assumptions concerning gamma transitions of the final cascade used by Huizenga and Vandenbosch $\boxed{2\,}$ for investigating the isomeric ratios. These transitions have practically no effect on the gamma-ray spectra calculations and usually

have very little effect on the calculation of the population of the isomeric states. They are mainly required for correct normalization of the isomeric ratio — see Eq. (7).

Let us now see how our calculations are affected by differences in the energy characteristics of the excited state density and in the energy dependence of the radiation width.

Fig. 4a shows the experimental gamma-ray spectrum for thermal neutron capture by a Hf nucleus [26] and the results of calculating the spectrum of the ^{177}Hf(n,γ)^{178}Hf reaction for thermal capture to a state with momentum $J_0 = 3$. The spectra resulting from the formation of a compound nucleus with momentum $J_0 = 4$ differ only marginally from those given in the figure. Fig. 4b shows the excited state density used in the calculations; the broken line shows the boundary below which the discrete level scheme was used. The Fermi gas model parameters were taken from Ref. [20] and correspond to experimental data on neutron resonance density. The parameters of the super-fluid nuclear model were selected so that the density of the nuclear states in this model at an excitation energy equal to the neutron binding energy was the same as the neutron resonance density. This was achieved by selecting the quantity $g = g_Z = g_N$ with parameters Δ_{oN} and Δ_{oZ} taken from Ref. [23]. The results of the calculations are also greatly affected by the choice of different relations for the radiation widths — see expressions (14) and (15) — and by the difference in the level density characteristics. The Fermi gas model with the usual radiation width dependence ($\sim \varepsilon^{2\ell+1}$) gives spectra which are too soft. This conclusion is not in contradiction with the calculations in Refs [3] and [4], since they employ a level density which is too low in the high excitation energy range. Use of the Lorentz radiation width relation — Eq. (15) — improves the agreement with experimental data and it can be seen that with suitable choice of level density it is possible to achieve quite a good description of the experimental conditions; the level density curve should then fall between the curves given in Fig. 4b. When allowance is made for discrete levels in the range $\varepsilon\gamma \sim 1.2$ MeV, lines are obtained in positions corresponding to the experimental ones, but their intensity is 3-4 times higher. The Lorentz relation also gives intense lines in the high gamma-ray energy range which are not present in the experi-mental data. Since our calculations have an average statistical character they cannot be claimed to describe the separate lines, the intensity of which depends considerably on the structure of the wave functions of the initial and final states of the corresponding transitions. The integral spectral characteristics obtained in the calculations, the mean number of gamma quanta per capture and the isomeric ratio for the 8^- state, are given in Table 1.

Table 1

	$\mathcal{J}_0$	Fermi gas model		Superfluid nuclear model		Experiment
		$\Gamma_\gamma \sim (14)$	$\Gamma_\gamma \sim (15)$	$\Gamma_\gamma \sim (14)$	$\Gamma_\gamma \sim (15)$	
n_γ	3	3,5	3,0	3,1	2,5	$3,8 \div 4,7$ [28]
	4	3,6	3,1	3,2	2,6	
η	3	0,012	0,0065	0,013	0,0049	0.0037 [29]
	4	0,0017	0.00033	0,0012	0,00014	

The mean number of quanta is calculated from a spectrum with $\varepsilon_\gamma \geqslant 0.1$ MeV, i.e. the contribution of very soft gamma rays is not allowed for. A corrected value for gamma peak intensity is used for calculating the mean number of gamma quanta with $\varepsilon_\gamma \sim 1.2$ MeV. This correction has a value $\Delta n_\gamma = 0.4-0.6$ in the different variants of the calculations. The calculations performed give the correct order of magnitude of the isomeric ratio.

The isomeric ratios provide a means of studying the behaviour of the level density spin dependence, but such a study is very much limited by the fact that we can observe the population of only two states. The information would be more complete if the population of a larger number of states were investigated for a given nucleus. A method for the experimental derivation of this information was considered in Ref. [27]. The mean population of low-lying states with different spin was derived from the gamma peak intensity; the relative populations obtained for radiative capture of a thermal neutron by a ^{164}Dy nucleus are shown in Fig. 5a [27]. Fig. 5b shows the total gamma-ray spectrum for this reaction [26]. With relations (5)-(7) it is possible to calculate the population of these states and Fig. 5 compares the results of the calculation with experimental data. Only the results of the Fermi gas model calculations are shown, because for this nucleus the spectra calculated with the level density - Eq. (23) - are considerably at variance with experiment. As with the reaction ^{177}Hf$(n,\gamma)^{178}$Hf, considered above, the use of the Lorentz relation for the radiation width gives too high values for the intensity of the gamma lines in the high energy part of the spectrum. Fig. 5b shows how variation of the level density parameter, a, affects the results.

Fig. 6 shows the relative populations of low-lying discrete levels in the reaction $^{176}Lu(n,\gamma)^{177}Lu$ for a thermal neutron $\boxed{27}$. As in the case of Dy, the gamma-ray spectrum of ^{177}Lu is best described by the Fermi gas model, so the results of calculating the relative population of the states are given only for this model. The distributions indicate how the choice of momentum of the initial state affects the calculation of the relative population, and it may be concluded that in the case of thermal neutron capture the state with momentum $J_o = 13/2$ is to be preferred.

5. Discussion of results

The calculations have shown that allowance for the effect of angular momentum on the radiative transition probability produces a spectrum of cascade gamma quanta softer than the spectrum obtained in calculations not allowing for this effect $\boxed{3, 4}$. The spectra of intermediate and heavy nuclei (far from the magic numbers) calculated with a radiation width energy dependence of $\sim \varepsilon_\gamma^3$ and with level density according to the Fermi gas model, are usually much softer than the experimental spectra. Using the Lorentz curve to describe the radiation width gives harder spectra which describe the main part of the spectrum quite satisfactorily. However, in the case of discrete low-excited states this dependence usually gives unduly high values for the intensity of high-energy gamma transitions.

For even-even nuclei the agreement of the theoretical spectra with the experimental is better if the level density energy dependence obtained with the superfluid nuclear model is used. This model is much more consistent than the Fermi gas model in describing a wide range of experimental data $\boxed{22}$. However, before it can be used widely for calculations of this kind, it is necessary to have a more clearly defined selection of model parameters for a wide range of nuclei.

With allowance made for the discrete structure of the low-excited states, the calculations describe sufficiently well the mean population of levels with different spin. The spin dependence parameter employed, $<m^2> = 0.25 A 2/3$ corresponds to the solid-state value of the moment of inertia $\boxed{21}$. The integral characteristics of the radiative capture spectra for thermal neutrons — the mean number of gamma quanta and the isomeric ratio — are less sensitive to the choice of model parameters than the shape of the spectrum, and therefore a good description of these does not always serve to verify the adequacy of the model employed.

It should be noted in connection with the statistical description of gamma-ray spectra considered in this paper that correct choice of the radiation width and level density parameters does not produce the hard spectra observed for nuclei with near-magic proton or neutron numbers. The best example of this is provided by the spectra for thermal neutron capture by nuclei in the Au-Pb range $\underline{/}26\underline{\rfloor}$. The impossibility of describing them statistically has already been discussed $\underline{/}9\underline{\rfloor}$ and the above method should not be used for describing the isomeric ratios in the case of these nuclei.
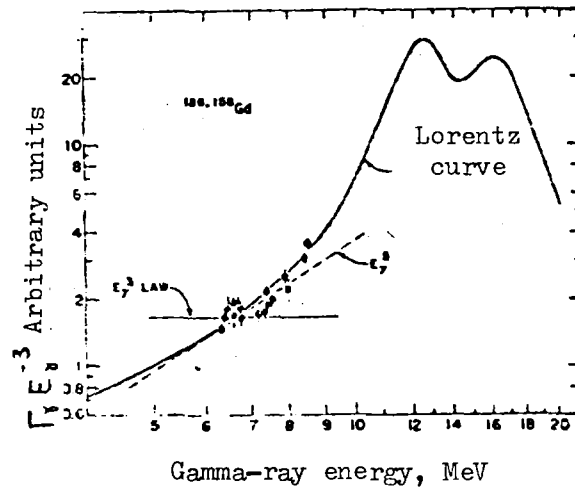
Fig. 1   Gamma energy versus mean width of electric dipole transitions
for ^{156}Gd and ^{158}Gd nuclei $\boxed{16}$.
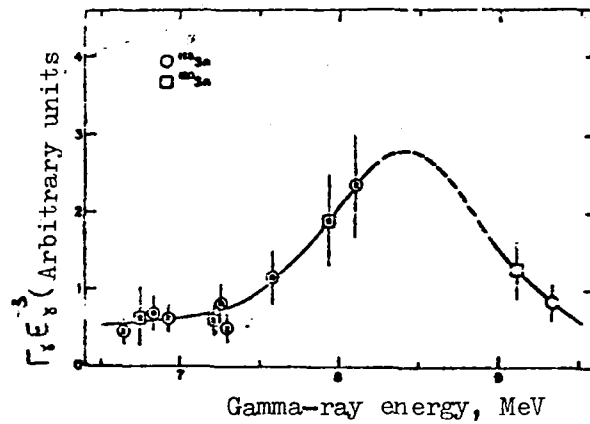
Fig. 2   Gamma energy versus mean width of magnetic dipole transitions
for ^{118}Sn and ^{120}Sn nuclei $\boxed{16}$.

Pre-exponential
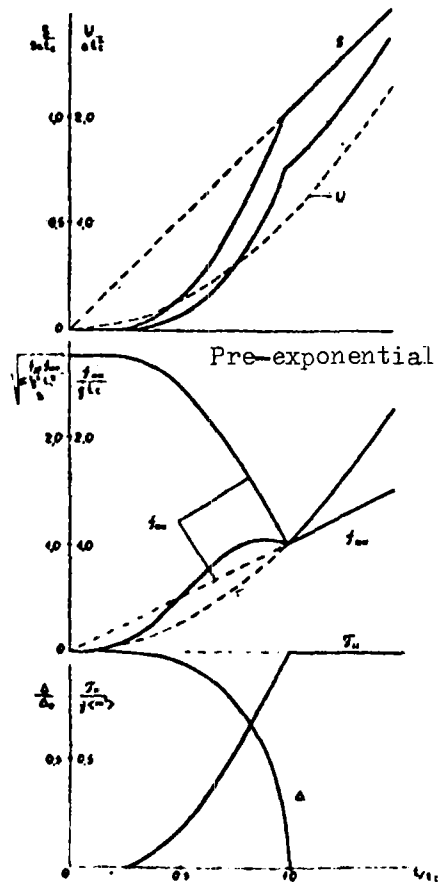
Fig. 3   Temperature dependence of the thermodynamic functions
of the superfluid nuclear model.   The broken line shows
the behaviour of the Fermi gas model level density
(Eq. (19)).
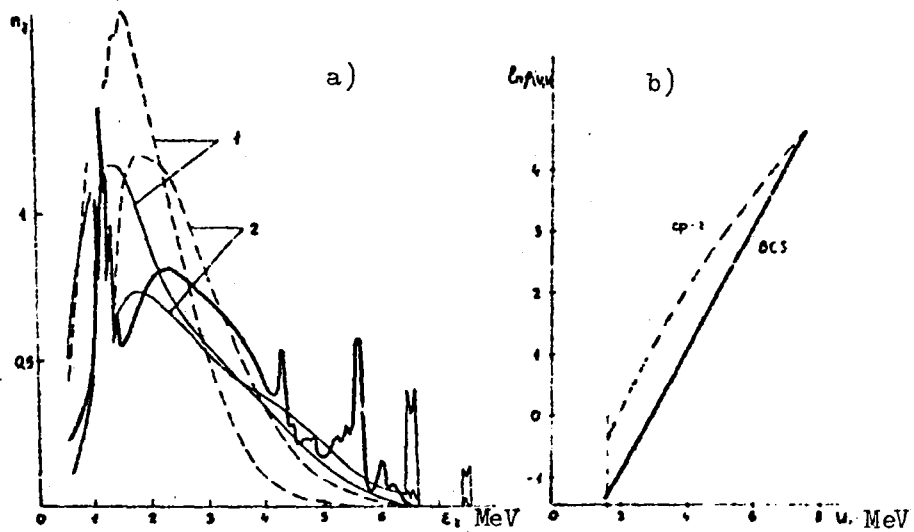
Fig. 4   (a) Gamma cascade spectra for thermal neutron capture. The
             experimental spectrum was obtained for a natural mixture
             of Hf isotopes $\sqrt{26\,\rfloor}$; the calculated results are for
             the reaction ^{177}Hf(n,γ). The solid line shows the
             results of calculations with level density according to
             the superfluid nuclear model – Eq. (23); the broken line
             shows the results obtained using the Fermi gas model –
             Eq. (20).
             1 = Energy versus radiation width – Eq. (14);
             2 = Curve of Eq. (15).

        (b) The excited state density used in the calculations.
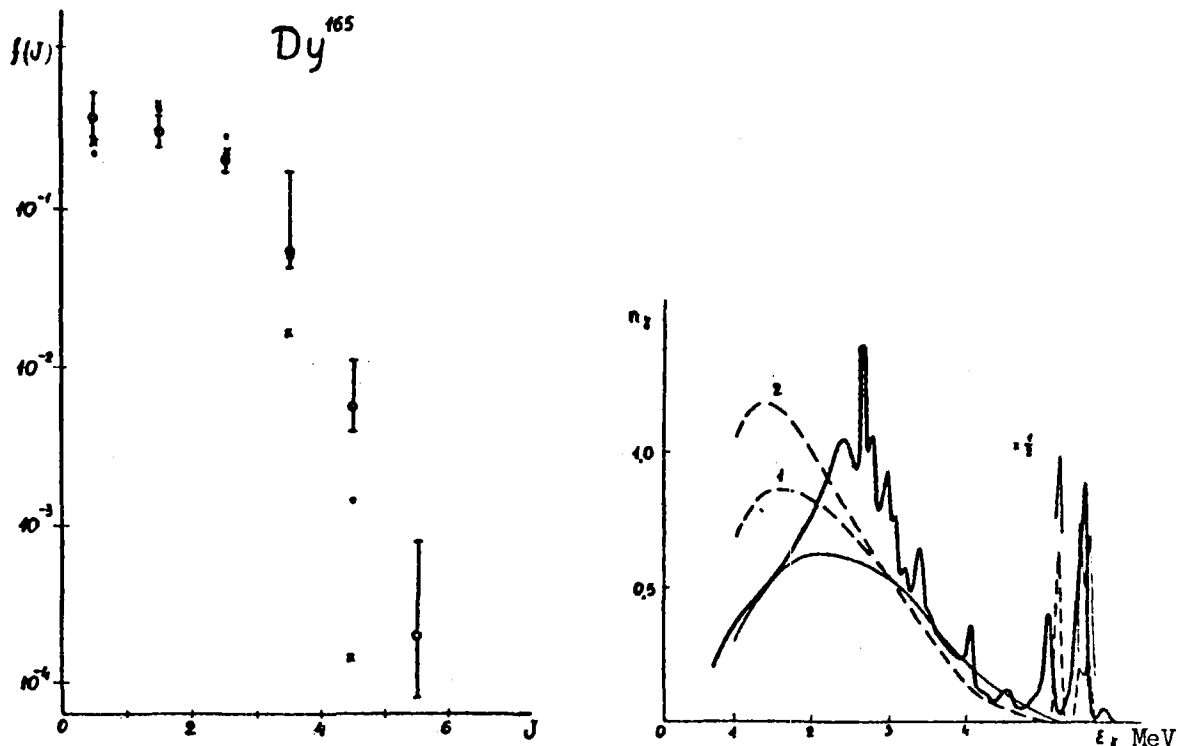
Fig. 5   (a)   Relative populations of low-lying states of a ^{165}Dy
nucleus Ͻ are experimental data, • are calculations in
the Fermi gas model with radiation width according to
Eq. (14), x are the same with radiative width according
to Eq. (15).

(b)   Gamma-ray spectra.   The notation is the same as in
Fig. 4a.
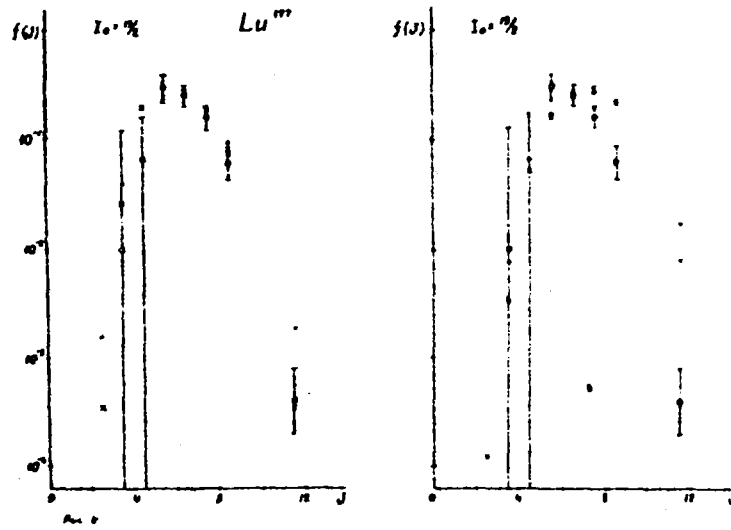
Fig. 6   Relative populations of low-lying states of ^{177}Lu.
Notation is the same as in Fig. 5a.

REFERENCES

[1]   MARGOLIS, B., Phys. Rev., 88 (1952) 327.

       LANE, A.M., LYNN, J.E., Proc. Phys. Soc., 70A (1957) 38.

[2]   HUIZENGA, J.P., VANDENBOSCH, R., Phys. Rev., 120 (1960) 1305;

       120 (1960) 1313.

[3]   STRUTINSKY, V.M. et al., Zh. eksp. teor. Fiz. 38 (1960) 598.

[4]   TROUBETZKOY, E.S., Phys. Rev., 122 (1961) 212.

       KOSORUKOV, A.L., STRUTINSKY, V.M., Jadernaja Fizika 2 (1965) 657.

[5]   SHUTKO, A.V., ZARETSKY, D.F., Zh. eksp. teor. Fiz. 29 (1955) 866.

       LANE, A.M., LYNN, J.E., Nucl. Phys., 11 (1959) 625; 11 (1959) 646.

[6]   BROWN, J., Nucl. Phys., 57 (1964) 339.

[7]   BENZI, V., Fundamentals in nuclear theory, Vienna (1967) 243.

[8]   MALYSHEV, A.V., Plotnost'urovnej i struktura atomnyh jader (Level
       density and the structure of atomic nuclei) Atomizdat (1969).
       ZAKHAROVA, S.I. et al., in "Nuclear data for reactors" (Proc.
       Conf. Helsinki 1970) 2 IAEA, Vienna (1970) 909.

[9]   DEMIDOV, A.M., Lectures of the summer school on nuclear
       spectroscopy, Obninsk (1966) 313.

[10]   BLATT, J., WEISSKOPF, V., Teoretičeskaja jadernaja fizika
       (Theoretical nuclear physics) Moscow (1954).

[11]   PÖNITZ, W., Z. Phys., 197 (1966) 262.

[12]   SPERBER, D., Nucl. Phys., A 90 (1967) 665.

[13]   MALYSHEV, A.V., Jadernaya Fizika 6 (1967), Issue No. 6, 1174.

[14]   WILKINSON, D.H., Nuclear Spectroscopy, Academic Press, Part B
       (1960).

[15]   AXEL, P., Phys. Rev., 126 (1962) 671.

[16]   BOLLINGER, L.M., Nuclear Structure, Vienna (1968).

[17]   BETHE, G., Fizika jadra (Nuclear physics) Gostekhizdat (1948)
       Vol. 3.

       ERICSON, T., Ach. Phys., 9 (1960) 425.

_[18_] NEMIROVSKY, P.E., ADAMCHUK, Y.V., Nucl. Phys., 39 (1962) 553.

_[19_] GILBERT, A., CAMERON, A., Can. J. Phys., 43 (1965) 1446.

_[20_] FACCHINI, U., SAETTA-MENICHELLA, E., Energia Nucl., 15 (1968) 54.

_[21_] IGNATYUK, A.V., STAVINSKY, V.S., Jadernaja Fizika 11 (1970) 1213.

_[22_] IGNATYUK, A.V., et al., in "Nuclear Data for Reactors" (Proc. Conf. Helsinki 1970) 2 IAEA, Vienna (1970) 885.

_[23_] MALOV, L.A. et al., Jadernaja Fizika 6 (1967) 1186.
VDOVIN, A.I. et al., Preprint No. P4-5125 of the Joint Institute for Nuclear Research, Dubna (1970).

_[24_] IGNATYUK, A.V. et al., Jadernaja Fizika 11 (1970) 1012.

_[25_] DZHELEPOV, B.S. et al., Shemy raspada radioaktivnyh jader c A >100 (Decay schemes of radioactive nuclei with A >100) Moscow, Izdat. Akad. Nauk SSSR (1963).

_[26_] GROSHEV, L.V. et al., Nuclear Data, 5 A, No. 1-4 (1968-1969).

_[27_] SCHULT, O.W. et al., Z. Phys., 185 (1965) 295.

_[28_] KERKEMESHI, I., KISHI, D., Jadernaja Fizika 10 (1969) 907.

_[29_] Neutron cross-sections, BNL-325, Supp. 2, v.2C (1966).

CROSS-SECTIONS FOR THE RADIATIVE CAPTURE OF NEUTRONS
BY SILVER, ^{197}Au, ^{232}Th AND ^{238}U NUCLEI

Yu.Ya. Stavissky, V.A. Tolstikov, V.B. Chelnokov,
A.E. Samsonov, A.A. Bergman

Introduction

The cross-sections for the radiative capture of neutrons by silver, ^{197}Au, ^{232}Th and ^{238}U nuclei are of interest for nuclear theory and reactor design.

This paper presents the results of measurements of the average cross-sections for the radiative capture of neutrons by Ag, ^{197}Au, ^{232}Th and ^{238}U nuclei in the energy range below 50 keV, performed with a neutron spectrometer on the basis of the slowing down time in lead $/$1, 2$/$.

The energy dependence of the cross-sections was normalized with respect to the resolved low-order resonances and also to the thermal cross-sections from measurements in a graphite prism placed close to the lead moderator $/$3$/$.

The data obtained here are compared with the results of other authors.

Measuring procedure

In the channel of the lead moderator the count of prompt gamma rays from radiative capture in each sample was measured against the slowing-down time $J_\gamma(t)$ and the neutron density $J_B(t)$, using a detector with an efficiency proportional to ~ $1/v$ (BF_3 - counter). Then, as shown in Ref. $/$7$/$, we have

$$\sigma_c(E) = \frac{J_\gamma(t)}{J_B(t)} \cdot \frac{(t + 0.3)}{K_x} \tag{1}$$

where $\sigma_c(E)$ is the cross-section for radiative capture by nuclei of the sample, and $K_x(\pi, M, \varepsilon_c)$ is the normalizing factor depending on the effective thickness of the sample $\bar{n}$, the monitor count M and the efficiency of recording a capture event ε_c.

The mean neutron energy E (keV) and the slowing-down time t (μsec) are related by the empirical expression $/$2$/$

$$E = \frac{183}{(t + 0.3)^2} \tag{2}$$

Detector

A gas proportional counter was used for detecting the prompt capture gamma rays. By surrounding its walls with lead (with total thickness $d > Re$, where Re is the path of a secondary electron formed by a gamma quantum) and filling it to a high pressure (10 atm + 4% CO_2) it is possible to obtain an approximately linear dependence of gamma-ray recording efficiency $\varepsilon\gamma$ on gamma energy $E\gamma$:

$$\varepsilon_\gamma \simeq const. E_\gamma \tag{3}$$

In this case the recording efficiency for a radiative capture event ε_c is determined solely by the total gamma-ray cascade energy, i.e. the neutron binding energy in the nucleus B_n (since the neutron kinetic energy may be neglected):

$$\varepsilon_c \simeq const. B_n \tag{3a}$$

and is unaffected by variations in the gamma-ray spectrum from resonance to resonance $\boxed{5\_7}$.

The accuracy of expression (3a) can be estimated from measurements on the proportional gamma counter with different samples. Since the normalizing factor K_x, calculated from resonances with known parameters or from the thermal cross-section $\boxed{3, 7\_7}$ and referred to the sample thickness $\bar{n}$ and the neutron flux, depends only on the capture event recording efficiency ε_c, it is possible to determine the function $\varepsilon_c(B_n)$.

The values of the normalizing factors obtained by measurements with the gamma counter for different samples are shown in Fig. 1. Processing the results by the least squares method gives a value $K_x/\bar{n} \times B_n = 0.945 \pm 0.037$, whence it follows that expression (3a) is fulfilled for the gamma detector used in the measurements with an accuracy of $\pm$ 4%.

Measurements and processing of results

The measurements were performed at a neutron burst frequency $f = 625$ and 312.5 Hz. The neutron burst time was set at the lowest value ($\sim$ 0.5 msec) in those measurements in which it was important to obtain the energy dependence of the cross-sections in the keV energy range (with small slowing-down times).

The amplification circuit of the gamma counter includes an antisaturation UIS-2 amplifier with a "Siren" amplifier discriminator. The time dependence of the detector count was investigated on the 256-channel analyser of the Measuring and Recording Centre at the Lebedev Physics Institute $\diagup 6\diagup$.

During the measurements of capture in the sample and the gamma background of the spectrometer (without sample), the activation of the detector was maintained at saturation (counter irradiated for ~ 10 min before the start of each series) so that it could be discounted in the processing of the results. The capture measurements were alternated with measurements of the natural gamma background of the samples (thorium and uranium) on the deactivated counter. The contribution of the natural background, which was constant at equal intervals over the whole time range, was allowed for by simple subtraction. The activation of the sample was determined from the ratios of the number of counts recorded with a sample in the gamma counter and the number recorded with the boron detector (with no activation) in the analyser channels corresponding to the energy range in which the investigated cross-section approximately follows the $1/v$ law:

$$\frac{J_{\gamma}' - a}{J_{B}'} = \frac{J_{\gamma}'' - a}{J_{B}''} = \text{const} \tag{4}$$

whence it is not difficult to obtain an expression that will give the correction for activation:

$$a = J_{\gamma}' - J_{B}' \cdot \frac{J_{\gamma}' - J_{\gamma}''}{J_{B}' - J_{B}''} \tag{5}$$

The estimation of the other corrections and possible measuring errors, performed in accordance with Ref. $\diagup 7\diagup$, results in a slight error (less than 1-1.5%) in the cross-sections investigated.

The energy dependence of the cross-sections was normalized to resolved resonances with known parameters $\diagup 7\diagup$ and to thermal capture cross-sections obtained from measurements in the graphite prism placed close   to the main prism of the lead moderator $\diagup 3\diagup$. In addition, measurements with a gamma detector for which expressions (3) and (3a) are satisfied make it possible to normalize with respect to measurements on samples with well-established radiative capture cross-sections. Then, if the investigated sample and the standard sample have the same geometry, we find

$$K_x = K_{st} \frac{\bar{n}_x \cdot M_x \cdot \varepsilon_c^x}{\bar{n}_{st} \cdot M_{st} \cdot \varepsilon_c^{st}} = K_{st} \frac{\bar{n}_x \cdot M_x \cdot B_n^x}{\bar{n}_{st} \cdot M_{st} \cdot B_n^{st}} \qquad (6)$$

where K_x, $\bar{n}_x$, M_x, ε_c^x and B_n^x are respectively the normalizing factor, the sample thickness, the monitor count, the recording efficiency for capture events and the nuclear binding energy of the sample; and K_{st}, $\bar{n}_{st}$, M_{st}, ε_c^{st} and B_n^{st} are the same quantities for the standard sample. The values of the normalizing factors obtained in measurements with the samples investigated are listed in Table 1. The errors quoted are mainly statistical but are also due in part to uncertainties in the resonance parameters employed [4].

Results and discussion

Silver. The energy dependence of the cross-section for radiative capture by silver nuclei was measured with samples of the natural isotopic mixture in two effective thicknesses (4.3×10^{21} and 2.2×10^{21} at/cm^2). The results are given in Fig. 2.

The data obtained here are in agreement with the results of previous measurements with a slowing-down time spectrometer [7] (normalized to the resonance at $E_0 = 5.19$ eV). Agreement with the other data presented in Fig. 2 is good within the limits of measuring error.

Gold-197. The energy dependence of the cross-section for radiative capture by ^{197}Au nuclei was measured with samples of two effective thicknesses (1.8×10^{21} and 6.0×10^{20} at/cm^2). The results of the measurements are shown in Fig. 3.

The data obtained here are also in agreement with earlier measurements made with a slowing-down time spectrometer [45] (normalized to the resonance at $E_0 = 4.9$ eV). Agreement with the data of other authors obtained mainly by the time-of-flight method is good.

Thorium-232. $\sigma_c(E)$ for ^{232}Th nuclei was measured with samples of ThO$_2$ in three effective thicknesses (9.6×10^{21}, 4.0×10^{21} and 1.0×10^{21} at/cm^2). The results of the measurements are given in Fig. 4 and compared with data of other authors.

The data from Refs [8] and [14-20] are given in their original form whereas the data from Refs [10-13] have been renormalized as described below. Note that the numerical data of Refs [8] and [17-20] were not available to us, the corresponding data being derived from the graphs in those publications.

Macklin and co-workers $/13_/$ measured the cross-section for ^{232}Th by the activation method. In calculating the cross-section from the experimental data the authors used K = 0.9 as the gamma quantum yield per decay event for gamma quanta with E_γ = 311 keV. However, according to the decay scheme of ^{233}Pa $/22_/$, only K_1 = 0.36 beta decays would give quanta with an energy of 311 keV; K_2 = 0.59 beta decays will give quanta with E_γ = 311 keV in a cascade with quanta of lower energy. Obviously, then, only $K_2/2$ quanta will reach the crystal unaccompanied by a cascade quantum and will be recorded at the 311 keV photopeak. The other half will be recorded in the aggregate peak of the cascade. However, because the soft quanta will be absorbed very efficiently in the sample and the crystal container, there will be an additional fraction of 311 keV gamma rays recorded in the 311 keV photopeak. Thus the true fraction K of gamma quanta per beta decay lies between the values $K_1 + K_2/2$ and $K_1 + K_2$. For making estimates it is natural to take K = $(K_1 + 3/4\ K_2) \pm K_2/4$; the corrected cross-section then becomes 560 ± 150 mb.

The data of Ref. $/10_/$ were renormalized using an σ_c ^{127}I for fast neutrons based on the curve from the atlas $/23_/$. Also, the latest recommended value of σ_c^{Th} ^{127}I = 6.2 b was used instead of 5.66 $/23_/$.

In Ref. $/12_/$ the σ_c ^{232}Th curve was measured in relation to the cross-section of the ^{10}B(n,α) reaction. The results have been re-evaluated by us and adjusted to give σ_c (24 keV) = 615 mb $/16_/$.

The results in Ref. $/11_/$ have been renormalized with allowance for the new fission cross-sections from Ref. $/21_/$.

Our data in the energy range above ~ 5 keV agree within the limits of measuring error with the data of most other authors. In this range and also in the range below ~ 5 keV there is, however, significant disagreement with the data of Refs $/17_/$ and $/20_/$. It is difficult to pinpoint the causes of this disagreement without having detailed information on these particular studies. However, it should be noted that when comparing the data of different authors it is essential to allow for differences in resolution and sample thickness (blocking effect).

Uranium-238. The energy dependence of the cross-section for radiative capture by ^{238}U nuclei was measured with U_3O_8 samples of three effective thicknesses (7.1×10^{21}, 3.9×10^{21} and 1.3×10^{21} at/cm^2). The results of the measurements are shown in Fig. 5.

Preliminary data on the cross-sections for radiative capture of neutrons in ^{238}U were published earlier $\left[\,24\,\right]$. Here these data are given in definitive form after more precise definition of a number of experimental constants associated with the normalization of the cross-section energy dependence.

In Fig. 5 our data are compared with the results of other authors, which are presented in their original form apart from Ref. $\left[\,12\,\right]$, where, at the suggestion of one of the authors, the data were renormalized to σ_c (23.5 keV) = 439 mb.

In comparing our data with the data of Ref. $\left[\,20\,\right]$ one should remember that the latter were obtained with a ^{238}U specimen thinner than ours $(\bar{n} = 1.3 \times 10^{21} \text{ at/cm}^2)$, so that the blocking effect should be comparatively slight.

Table 1

Normalizing factors obtained in measurements with the
samples under investigation

Sample	Method	K_x
Silver	^{109}Ag resonance $E_o = 5.19$ eV	
	Thermal cross-section b	
Gold-197	^{197}Au resonance $E_o = 4.906$ eV	
	Thermal cross-section b	
Thorium-232	^{232}Th resonances eV	
	With respect to gold-197	
Uranium-238	^{238}U resonance eV	
	With respect to gold-197	

Table 2

Numerical cross-sections for radiative capture
of neutrons by Ag nuclei ($\sigma_c(E)$)

E, eV	σ_c, barn
43600	0,78 ± 0,09.
34600	0,84 ± 0,09
28200	0,94 ± 0,09
23200	0,99 ± 0,08
19800	1,05 ± 0,08
16800	1,10 ± 0,08
13500	1,21 ± 0,08
11000	1,28 ± 0,08
8850	1,35 ± 0,08
7200	1,42 ± 0,09
5950	1,47 ± 0,09
5000	1,61 ± 0,10
4150	1,63 ± 0,10
3600	1,78 ± 0,11
2900	1,88 ± 0,11
2450	2,05 ± 0,12
1950	2,25 ± 0,13
1550	2,49 ± 0,15
1300	2,90 ± 0,17
1100	3,09 ± 0,18

Table 3

Numerical cross-sections for radiative capture of neutrons
by ^{197}Au nuclei $(\sigma_c(E))$

E, eV	σ_c, barn
43600	0,45 ± 0,05
34600	0,52 ± 0,05
28200	0,61 ± 0,05
23200	0,73 ± 0,05
19800	0,82 ± 0,05
16800	0,92 ± 0,06
15100	0,96 ± 0,06
13100	1,03 ± 0,06
11250	1,12 ± 0,07
9800	1,24 ± 0,07
7900	1,45 ± 0,09
6400	1,68 ± 0,10
5800	1,92 ± 0,12
4900	2,11 ± 0,13
4000	2,35 ± 0,14
3600	2,56 ± 0,16
3200	2,77 ± 0,17
2750	3,12 ± 0,19
2400	3,42 ± 0,21
2200	3,64 ± 0,22
1920	3,98 ± 0,24
1780	4,34 ± 0,26
1550	4,93 ± 0,30
1350	5,51 ± 0,34
1130	6,02 ± 0,36

Table 4

Numerical cross-sections for radiative capture of neutrons
by ^{232}Th nuclei ($\sigma_c(E)$)

E, eV	σ_c, barn
34600	0,50 ± 0,06
23200	0,63 ± 0,05
17300	0,73 ± 0,05
13100	0,85 ± 0,06
9350	0,96 ± 0,06
7600	1,00 ± 0,06
6200	1,05 ± 0,07
5000	1,14 ± 0,08
4100	1,23 ± 0,09
3300	1,34 ± 0,10
2700	1,47 ± 0,11
2300	1,66 ± 0,13
1750	1,82 ± 0,14
1350	1,90 ± 0,15
1130	1,95 ± 0,15

Table 5

Numerical cross-sections for radiative capture of neutrons
by ^{238}U nuclei ($\sigma_c(E)$)

E, eV	σ_c, barn
30500	$0,41 \pm 0,05$
25100	$0,45 \pm 0,04$
21000	$0,50 \pm 0,04$
17900	$0,58 \pm 0,04$
15400	$0,59 \pm 0,04$
13800	$0,64 \pm 0,04$
11700	$0,65 \pm 0,04$
10370	$0,69 \pm 0,05$
9200	$0,69 \pm 0,05$
7470	$0,74 \pm 0,06$
6160	$0,82 \pm 0,06$
5170	$0,87 \pm 0,07$
4480	$0,90 \pm 0,07$
3820	$0,96 \pm 0,07$
3410	$1,05 \pm 0,08$
2990	$1,11 \pm 0,08$
2640	$1,14 \pm 0,08$
2350	$1,20 \pm 0,09$
2100	$1,23 \pm 0,09$
1720	$1,30 \pm 0,09$
1430	$1,44 \pm 0,11$
1200	$1,64 \pm 0,13$
1110	$1,78 \pm 0,14$
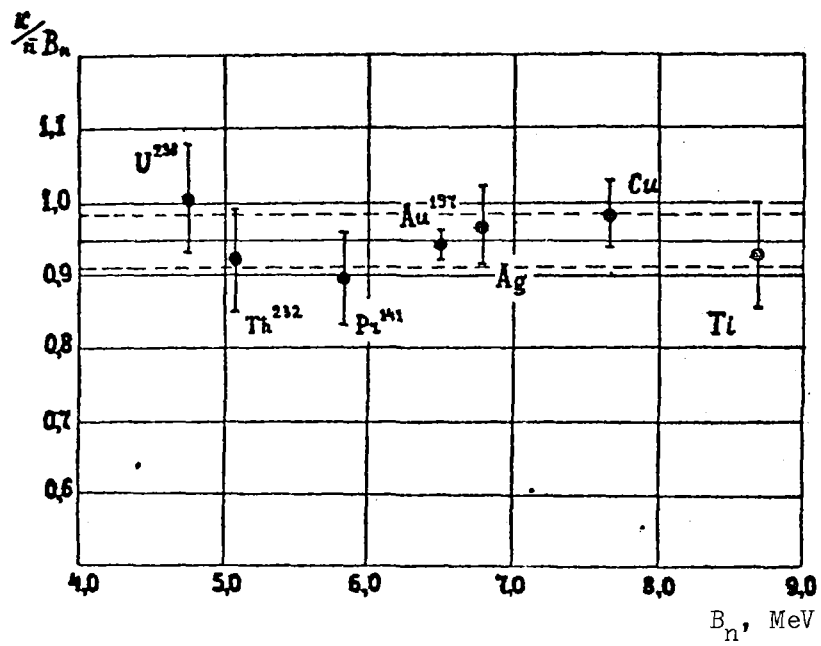
<u>Fig. 1</u>   Reduced normalizing factor versus B_n for different
samples (measurements with a proportional gamma
counter).
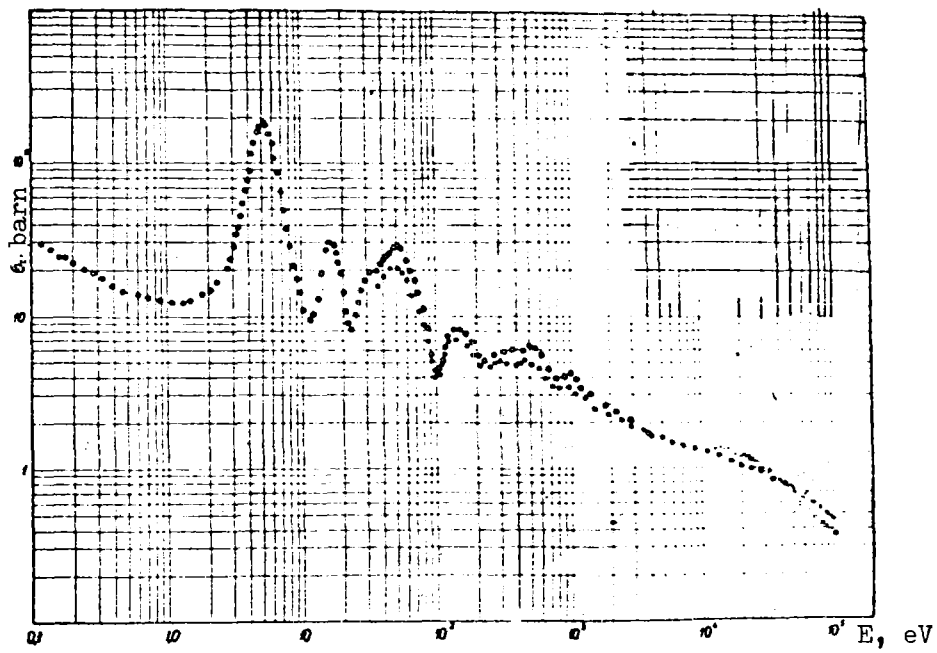
Fig. 2   Energy dependence of the cross-section for radiative
capture of neutrons by silver nuclei.

● $\bar{n}$ = 4,3.10^{21}ат/см^{2} ⎱
O $\bar{n}$ = 2,2.10^{21}ат/см^{2} ⎰ data of this investigation

◊ - [16] ;   □ - [43] ; ⊙ - [44] ; ▧ - [36] ;
          Δ - [26]
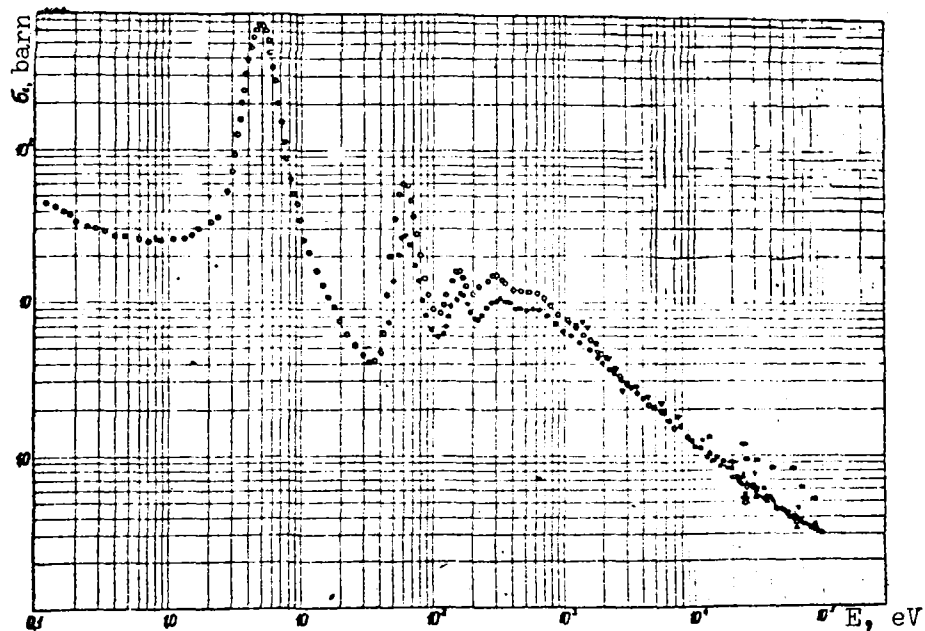
Fig. 3   Energy dependence of the cross-section for radiative
capture of neutrons by gold-197 nuclei.

● = $1,8.10^{21}$ат/см^2 ⎤
O = $6,0.10^{20}$ат/см^2 ⎦ data of this investigation

▭ - [32] , ◊ - [33] , ▢ - [34] , △ - [35] , ⬠ - [13] ,
⬠ - [36] , ⬠ - [37] , ◇ - [14] , ⬠ - [38] , ⊙ - [39] ,
■ - [16] , ▲ - [40] , ▬ - [11] , ▼ - [41] , ▽ - [42] .
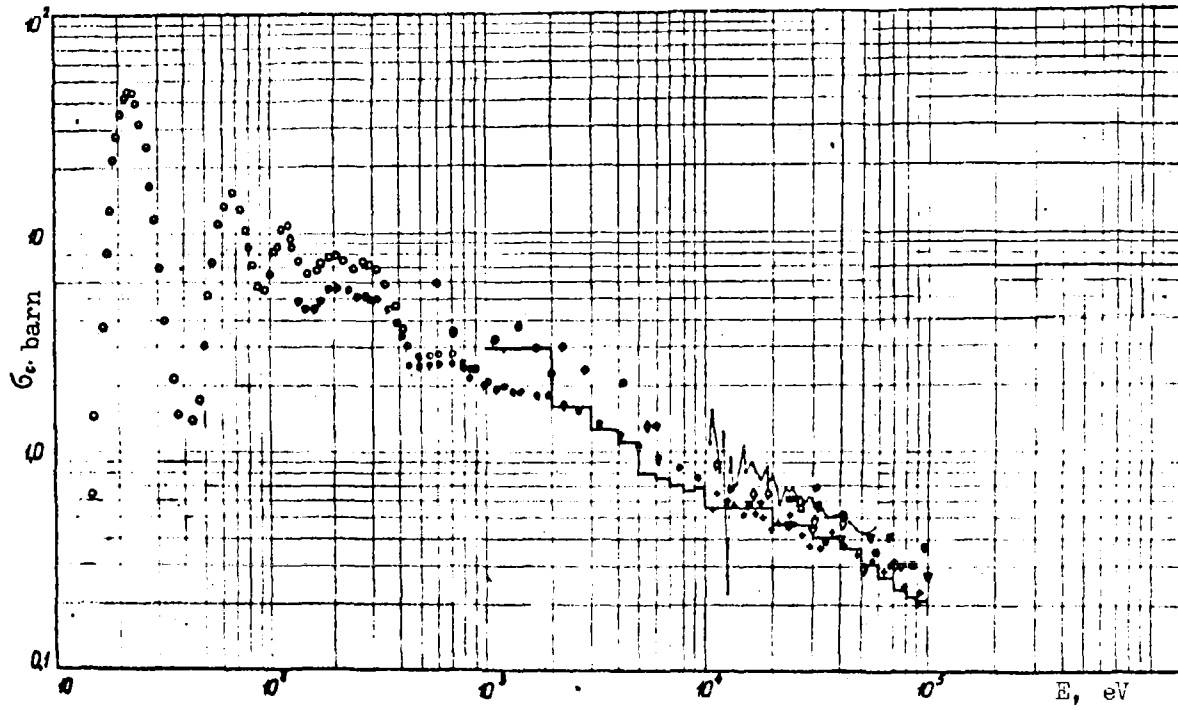
Fig. 4   Energy dependence of the cross-section for radiative capture
of neutrons by thorium-232 nuclei.

$\bullet$ = 9,6.10^{21} ат/см^2
$\mathbb{O}$ = 4,0.10^{21} ат/см^2 this investigation
$\bigcirc$ = 1,0.10^{21} ат/см^2

$\blacksquare$ - [8] , ∇ - [10] , $\bullet$ - [11] , $\Diamond$ - [12] , $\square$ - [13] ,
$\blacksquare\hspace{-2pt}\square$ - [14] , $\bullet$ - [15] , $\square$ - [16] , $\bullet$ - [17] , + - [18] ,
x - [19] , $\mathfrak{r}$ - [20] .
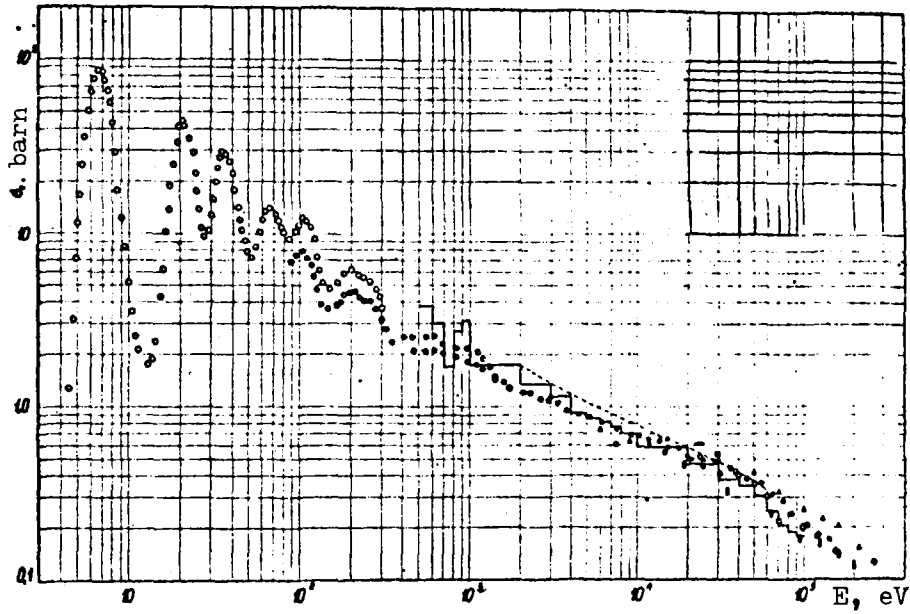
Fig. 5. Energy dependence of the cross-section
for radiative capture of neutrons by
uranium-238 nuclei.

$\bullet = 7,1.10^{21}$ ат/см^2

$\mathbb{O} = 3,9.10^{21}$ ат/см^2 this investigation

$\mathrm{O} = 1,3.10^{21}$ ат/см^2

$\blacktriangleleft$ - [13] , $\square$ - [12] , $\blacktriangle$ - [25] , Γ - [20] , $\mathbb{I}$ - [26] ,

$\blacksquare$ - [27] , $\diamondsuit$ - [28] , $\ominus$ - [29] , $\sim$ - [30] .

REFERENCES

[1] BERGMAN, A.A. et al., Int. Conf. peaceful uses of atom. energy (Proc. Conf. Geneva, 1955) 4, UN, New York (1956) 135.

[2] SHAPIRO, F.L., Trudy FIAN SSSR (Lebedev Physics Institute, Acad. Sc.) 24 (1964) 3.

[3] BERGMAN, A.A. et al., Atomn. Energ., in press (1971).

[4] HUGHES, D.J., MAGURNO, B.A., BRUSSEL, U.K., Neutron cross-sections, Suppl. to BNL-325, Second ed., 1960.

[5] MOXON, U.C., RAE, E.R., RIEHS, P., STEIN, W.E., THOMAS, B., Gamma-ray spectra from neutron resonance capture, UK/USSR Seminar, Paper UK/22 June, 1968.

[6] SHTRANIKH, I.V., et al., Trudy FIAN SSSR (Lebedev Physics Institute, Acad. Sc.) 42, (1968) 69.

[7] POPOV, Yu.P., Trudy FIAN SSSR (Lebedev Physics Institute, Acad. Sc.) 24 (1964) 111.

[8] Los Alamos data 1952 (see [9]).

[9] STEHN, J.R. et al., Neutron cross-sections, vol. III, Sigma Centre, BNL 1965 Suppl. to BNL-325.

[10] STAVISSKY, Yu.Ya. et al., Atomn. Energ. 10 (1961) 508.

[11] MISKEL, J.A., MARSH, K.V., LINDNER, M., NAGLE, R.J., Phys. Rev. 128 (1962) 2717.

[12] TOLSTIKOV, V.A. et al., Atomn. Energ. 15 (1963) 414.

[13] MACKLIN, R.L., LAZAR, N.H., LYON, W.S., Phys. Rev. 107 (1957) 504.

[14] CHAUBEY, A.K., SEHGAL, M.L., Nucl. Phys 66 (1965) 267.

[15] SCHUMAN, R.P., Wash-1127, 1969.

[16] BELANOVA, T.S. et al., Atomn. Energ. 19 (1965) 3.

[17] BLOCK, R.C., SLAUGHTER, G.G., ORNL-2910 (1960) 35.

[18] MOXON, M.C., CHAFFEY, C.M. (see [9]).

[19] MACKLIN, R.L., GIBBONS, J.H., 1964 (see [2]).

/ 20_7   MOXON, M.C., The measurement of average neutron capture cross-
         sections in the mass region above 100 dissertation, London
         University, 1968.

/ 21_7   HART, W., AHS B(5), R 124 (1967).

/ 22_7   DZHELEPOV, B.S. et al., Shemy raspada radioaktivnyh jader (Decay
         schemes of radioactive nuclei) Moscow-Leningrad (1963).

/ 23_7   GOLDBERG, M.D., MUGHABGHAL, S.F. et al., Neutron cross-sections
         BNL-325, 2 Supplement N2, v.IIB, 5/1966.

/ 24_7   BERGMAN, A.A., et al., in Nuclear data for reactors (Proc. Conf.
         Helsinki 1970) 2 IAEA, Vienna (1970) 51.

/ 25_7   BIBPUCH, E.G., WESTON, L.W., NEWSON, H.W. Annals,Phys. 10 (1960) 455.

RADIATIVE CAPTURE OF NEUTRONS BY ^{238}U IN THE BR-5 REACTOR CORE SPECTRUM (URANIUM CARBIDE VARIANT)

V.I. Ivanov, V.A. Tolstikov

Introduction

The cross-sections for radiative capture of neutrons in ^{238}U are very important for fast reactor calculations because radiative capture in ^{238}U is one of the factors that determine the breeding of nuclear fuel in fast power reactors.

A number of authors have performed critical analyses of experimental data on $\sigma_{n,\gamma}$ for ^{238}U over a wide range of neutron energies. Taking these analyses as a basis and using theoretical calculations in the low neutron energy range, it has been possible to obtain recommended curves of average radiative capture cross-sections for ^{238}U over the eV to 15 MeV energy range. The recommended data have been used to establish a system of multigroup constants for radiative capture in ^{238}U which may be used for reactor calculations.

In order to check and correct the systems of multigroup constants, measurements of $\sigma_{n,\gamma}$ for ^{238}U have been made in known (or at any rate comparatively well known) broad neutron spectra.

In this investigation measurements were performed in the core spectrum of the BR-5 reactor, fuelled with 90% enriched ^{235}U in carbide form.

Experimental set-up

For the experiment one of the fuel assemblies in the first complete row of the reactor core (4.6 cm from its vertical axis) was replaced by an experimental assembly in the form of a hexahedral cassette which, instead of fuel elements, supported a stainless steel can containing spectrometric samples of ^{238}U. The samples covered the region from the lower boundary of the core to the steel reflector formed by the tops of the assemblies.

Fig. 1 shows schematically the position of the samples inside the reactor as well as some of its structural features.

Irradiation was carried out for about somewhat over a day (1.008×10^5 sec) at nominal reactor power. The flux at the centre of the reactor was taken to be $(5.61 \pm 0.65) \times 10^{14}$ n/cm^2 sec*/.

---

*/ See Appendix.

Calculations allowing for neutron flux distribution showed that sample No. 1 located 4.7 cm from the core centre received an integral flux of $5.48 \pm 0.63 \times 10^{15}$ n/cm^2, and sample No. 2 (r = 5.6 cm) a flux of $5.41 \pm 0.62 \times 10^{15}$ n/cm^2. After irradiation the experimental assembly was cut up by remote handling in the hot cell and the uranium samples were removed for measurement.

Measuring procedure

The alpha activity of the unirradiated and the irradiated samples was investigated with a semiconductor alpha-spectrometer incorporating a surface-barrier silicon detector with a working surface of about 2 cm^2 and resolution of about 40 keV.

Results of the measurements

After a few small experimental corrections, the radiative capture cross-sections may be calculated from the formula

$$\sigma_{n,\gamma} = \frac{1}{(\varphi \cdot t)} \cdot \frac{T_{\frac{1}{2}}^{239_{Pu}}}{T_{\frac{1}{2}}^{238_{U}}} \cdot \left(\frac{A^{239_{Pu}}}{A^{238_{U}}} \right) \tag{1}$$

where $T_{\frac{1}{2}}^{239_{Pu}}$ is the half-life of ^{239}Pu equal to 2.44×10^4 yr $\left[1 \right]$, and $T_{\frac{1}{2}}^{238_{U}}$ is the half-life of ^{238}U equal to 4.51×10^5 yr $\left[1 \right]$. These are mean values based on data in Ref. $\left[1 \right]$; φt is the integrated neutron flux, which for sample No. 1 was $5.48 \pm 0.63 \times 10^{-19}$ n/cm^2 and for sample No. 2 was $5.41 \pm 0.62 \times 10^{13}$ n/cm^2; and $A^{239_{Pu}}/A^{238_{U}}$ is the experimentally determined ratio of the alpha activities for ^{239}Pu and ^{238}U, equal to 1.641 ± 0.029 for sample No. 1 and 1.649 ± 0.031 for sample No. 2.

Substituting these constants in formula (1) we obtain

$$\sigma_{n,\gamma}^{238_{U}} = 162 \pm 19 \text{ mb for sample No. 1 } (r = 4.7 \text{ cm})$$

$$\sigma_{n,\gamma}^{238_{U}} = 165 \pm 20 \text{ mb for sample No. 2 } (r = 5.6 \text{ cm})$$

The error in the cross-section is determined by (a) the uncertainty in the half-lives of ^{239}Pu and ^{238}U, which does not exceed $\pm 0.5\%$, (b) the error in the determination of the integrated flux, equal to 11.6% (see Appendix) and (c) the error in measurements of $A^{239_{Pu}}/A^{238_{U}}$ — the ratio of the alpha activities of plutonium and uranium — which does not exceed $\pm 1.5\%$.

The total error in the determination of $\sigma_{n,\gamma}$ for ^{238}U is $\pm$ 12%. Fig. 2 shows the distribution of the numbers of neutron captures $(\sigma_{n,\gamma}\varphi)_z/(\sigma_{n,\gamma}\varphi)_o$ over the core of the BR-5 reactor.

Comparison of the experimental results with theory

Ref. $\boxed{2}$ provides theoretical values of neutron spectra for various distances from the reactor centre.

Averaging the recommended group constants for $\sigma_{n,\gamma}$ of ^{238}U $\boxed{3}$ over the neutron spectrum, we obtain 136.3, 138.4, 136 and 136.9 mb for r = 0.9, 3.2, 4.6 and 6.1 cm from the reactor centre.

As indicated above, the measurements gave values of 161 and 164 mb for distances of r = 4.7 and 5.6 cm respectively. Thus the results of calculation and experiment differ by 15%, although they agree within the error limits.

APPENDIX

Neutron flux in reactor centre

As a result of the appearance of new experimental data we have revised the multigroup constants for the fission cross-sections of ^{235}U and ^{239}Pu which were used previously $\boxed{2}$ as reference values in the experimental determination of the neutron flux in the reactor centre.

The experiment to determine the neutron flux in the reactor centre was based on an average fission cross-section for ^{239}Pu of 1.79 b. This value was obtained by averaging the 26 group constants for the ^{239}Pu fission cross-section $\boxed{4}$ over the theoretical neutron spectrum in the reactor centre $\boxed{2}$.

The revision of the constants resulted in a value for the average ^{239}Pu fission cross-section in the reactor centre of 1.67 b. Allowing for this, and using the experimental data of Ref. $\boxed{2}$, we found φ_{max} = 5.61 $\pm$ 0.65 x 10^{14} n/cm^2 sec for the flux in the core centre.

REFERENCES

$\int 1\overline{J}$ GORBACHEV, V.M. et al., Osnovnye harakteristiki izotopov
tjaželyh élementov (The principal characteristics of the isotopes
of heavy elements) Atomizdat, Moscow (1970).

$\int 2\overline{J}$ ARISTARKHOV, N.A. et al., Voprosy fisiki jadernyh reaktorov
(Problems of reactor physics) Issue No. 1, Trudy FEI (Proc. Institute
of Physics and Power Engineering) Obninsk (1968).

$\int 3\overline{J}$ ABAGYAN et al., in Nuclear data for reactors (Proc. Conf. Helsinki
1970) 2 IAEA Vienna (1970) 667.

$\int 4\overline{J}$ ABAGYAN, L.P. et al., Gruppovye konstanty dlja rasčeta jadernyh
reaktorov (Group constants for calculating nuclear reactors) Atomizdat,
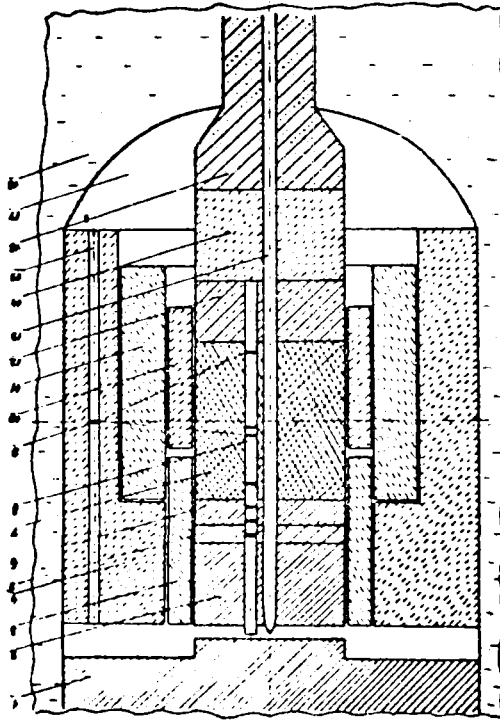Moscow (1964).

Fig. 1   Schematic arrangement of ^{238}U samples in the BR-5 reactor
and some design features of the reactor

1 = Top cover — biological shield;   2 = Steel reflector formed by tops of
fuel assemblies;   3 = Part of fixed nickel reflector;   4 = Fixed nickel
reflector;   5 = Space inside fuel assembly;   6 = Steel end reflector;
7 = Core;   8 = Experimental assembly;   9 = ^{238}U samples;   10 = Movable
compensating cylinder;   11 = Shield compensator;   12 = Part of bottom
reflector with the shafts of the fuel assemblies;   13 = Central bypass
channel;   14 = Bottom reflector;   15 = OK-50 channel (irradiation channel)
at r = 430 mm from centre of reactor;   16 = Central pipe with sodium
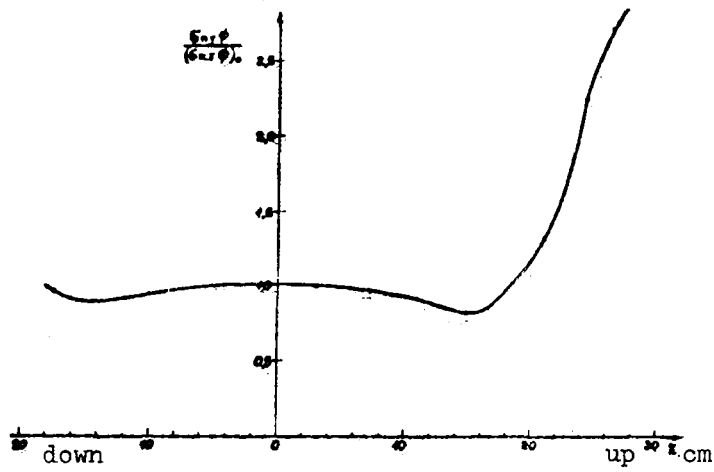coolant;   17 = Space for dropping control elements;   18 = Water tank of
biological shield.

Fig. 2   Capture distribution in ^{238}U along the vertical at a distance
r = 4.6 cm from axis of BR-5 reactor (relative trend)

MEAN RADIATION WIDTHS OF NEUTRON RESONANCES

S.M. Zakharova

This contribution is a supplement to Ref. $\boxed{Z-70}$ and contains (see Table 1) experimental data on the radiation widths of neutron resonances published in the period from January to September 1970. The averaging was performed on the same assumptions as were made in Ref. $\boxed{Z-70}$, i.e. if the discrepancy between different published results does not go beyond the limits of the indicated experimental errors, then

$$\overline{\Gamma_\gamma} = \frac{\sum_{i=1}^{n} \Gamma_{\gamma i} \cdot \frac{1}{(\Delta \Gamma_{\gamma i})^2}}{\sum_{i=1}^{n} \frac{1}{(\Delta \Gamma_{\gamma i})^2}} \qquad \text{and} \qquad \overline{\Delta \Gamma_\gamma} = \frac{1}{\sqrt{\sum_{i=1}^{n} \frac{1}{(\Delta \Gamma_{\gamma i})^2}}} \tag{1}$$

whereas in all other cases

$$\overline{\Gamma_\gamma} = \frac{\sum_{i=1}^{n} \Gamma_{\gamma i}}{n} \qquad \text{and} \qquad \overline{\Delta \Gamma_\gamma} = \sqrt{\frac{\sum_{i=1}^{n} (\overline{\Gamma_\gamma} - \Gamma_{\gamma i})^2}{n-1}} \tag{2}$$

where n is the number of references if we have the mean radiation width of a given resonance, or the number of resonances if we have the mean radiation width of a given isotope. Table 1 contains only those resonances for which new data have appeared. The mean radiation widths Γ_γ^{res} of the remaining resonances used for obtaining the mean radiation widths of the isotopes (see table column headed Remarks) may be found in Ref. $\boxed{Z-70}$. The notation used in Table 1 is the same as in Ref. $\boxed{Z-70}$. The mean radiation widths obtained with formula (2) are indicated with an asterisk.

REFERENCES

$\boxed{A-70}$ ASGHAR, M. et al., Nucl. Phys. A145, 2 (1970) 549.

$\boxed{K-69-1}$ KING, T., BLOCK, R., Nucl. Phys. A138, 3 (1969) 556.

$\boxed{F-70}$ FRIESENHAHN, S. et al., Nucl. Phys. A146, 2 (1970) 337.

$\boxed{M-69-4}$ MOORING, F., Phys. Rev. 178, 4 (1969) 1612.

$\boxed{M-70}$ MATEICIC, V. et al., J. Nucl. Energy 24, 5 (1970) 245.

$\boxed{N-70}$ NAKAJIAMA et al., Nucl. Sci. Technol. (Tokyo) 7, 1 (1970) 7.

$\boxed{W-70}$ WATANABE, T., REEDER, S., Nucl. Science Engng. 41, 2 (1970) 188.

$\boxed{Z-70}$ ZAKHAROVA, S.M. et al., Sistematika srednih radiacionnyh
Širin nejtronnyh rezonansov (The systematics of the mean
radiation widths of neutron resonances) Bjul. inf. Centr jad.
Dannym, Issue No. 7, Appendix (1970).

Note: For remaining references contained in Table 1 consult
Ref. $\boxed{Z-70}$.

Table 1

Key:

изотоп	= Isotope
МВ	= mV
эв	= eV
рез	= res
Работа	= Ref.
Примечания	= Remarks
При усреднении учтены резонансы	= Averaging with resonances
КЭВ	= keV
Мэв	= MeV
метод площади	= Area method
метод формы	= Shape method
Щ-66	= ShCh-66
принято, что	= Assuming
от	= of
Продолжение	= (continued)
без учёта	= omitting
При усреднении этот резонанс не учтён	= This resonance omitted from averaging

Table 1

изотоп	$\overline{\Gamma_\gamma}$ мв.	$\overline{\Delta\Gamma_\gamma}$ мв	ℓ	n	E_o эв	ℓ	J	$\Gamma_\gamma^{рез}$ мв	$\Delta\Gamma_\gamma^{рез}$ мв	Работа	$\overline{\Gamma_\gamma^{рез}}$ мв	$\overline{\Delta\Gamma_\gamma^{рез}}$ мв	Примечания
$_5\text{B}^{10}$ $I=\frac{3}{2}$	112 *	124	2	2									При усреднении учтены резонансы: $E_o=20,8$ кэв ; $E_o=1,28$ Мэв
					$20,8.10^3$	2	3	25	8	И-69-4	25	8	
$_{27}\text{Co}^{59}$ $I=7/2$	510 *	228		12									При усреднении учтены резонансы: $E_o=132$ эв ; 4,327кэв ; 5,021 кэв ; 6,359 кэв ; 8,047 кэв ; 8,75 кэв ; 9,70 кэв ; 10,69 кэв ; 11,83 кэв ; 13,26 кэв; 15,64 кэв; 16,89 кэв .
					132		4	500 670 470 440 400 480 850	150 40 40	Н -52 В -60 С -62 Q -66 С -65 W -69 N -70	544 *	160	
$_{43}\text{Tc}^{99}$ $I=9/2$	112 *	32		4	5,6			134 135	4	W -70	134	4	метод площади метод формы
					20,3			140 150	7	W -70	140	7	метод площади метод формы
					39,9			71	13	W -70	71	13	
					56,9			104	13	W -70	104	13	
$_{48}\text{Cd}^{111}$ $I=1/2$	115 *	38		8									При усреднении учтены резонансы : $E_o=27,7$ эв; 99,6 эв; 137,6 эв; 164,2 эв; 233,8 эв; 356,5 эв; 389,5 эв; 578 эв.
					164,2		1	104 132	12 ~26	Ш₃-66 К -69-1	109	11	Принято,что $\Delta\Gamma_\gamma\sim20\%$ от Γ_γ.

Table 1 contin'd

Изотоп	Г$_\gamma$ мв	ΔГ$_\gamma$ мв	ℓ	n	E$_o$ эв	ℓ	J	рез Г$_\gamma$ мв	рез ΔГ$_\gamma$ мв	Работа	рез Г$_\gamma$ мв	рез ΔГ$_\gamma$ мв	Примечания
$^{113}_{48}$Cd I=1/2	117*	14		15									При усреднении учтены резонансы: E$_o$= 0,178 эв; 18,5 эв; 64 эв; 84,9 эв; 108,5 эв; 193,2 эв; 215,4 эв; 232 эв; 261,5 эв; 270 эв; 415,8 эв; 433,8 эв; 503 эв; 527 эв; 552 эв.
					193,2		0	112	18	Ш$_\gamma$ – 66	122	15	
								149	~30	К –69 – I			Принято, что ΔГ$_\gamma$ ~20% от Г$_\gamma$.
					215,4		I	114	20	Ш$_\gamma$ – 66	118	16	
								125	~25	К –69 – I			Принято,что ΔГ$_\gamma$~ 20% от Г$_\gamma$.
					232		I	155	~30	К –69 – I	155	~30	Принято,что ΔГ$_\gamma$~ 20% от Г$_\gamma$.
$^{114}_{48}$Cd I=0	123*	53	I								123*	53	
					120,2		I/2	110	~10	{ S – 57-I / G – 66			
								200	31	S – 57-2			
								100	20	G – 66			
								82	~17	К – 69-I			Принято,что ΔГ$_\gamma$~ 20% от Г$_\gamma$.
$^{121}_{51}$Sb I=5/2	88,1	3		10							70*	14	При усреднении учтены резонансы: E$_o$ = 6,24 эв; 15,4 эв; 29,7 эв; 53,5 эв; 64,5 эв; 73,8 эв; 126,8 эв; 144,3 и 149,9 эв; 167,1 эв.
					6,24		3	60	20	Р –55– I			
								61	9	S –57			
								90	4	В –63			
								~58	~10	А –68			
								79	9	М –70			

Table 1 continued

Изотоп	Γ_γ мв.	$\Delta\Gamma_\gamma$ мв.	ℓ	n	E_0 вв.	ℓ	Э	рез Γ_γ мв.	рез $\Delta\Gamma_\gamma$ мв.	Работа	рез Γ_γ	рез $\Delta\Gamma_\gamma$ мв.	Примечания
$^{155}_{64}Gd$ $I=3/2$	115 *	22		39	0,0268		2				108	I	
								108	I	M – 60			
								108		A – 70			
					2,008		I				110	I	
								110	5	G –66			
								113	40	S –57–3 / G –66			
								110	I	M –60			
								110		A –70			
					2,568		2				III	I	
								III	4	G –66			
								III	I	M –60			
								III		A –70			
					3,616						130	17	
								130	17	F –70			
					6,300		2				109	6	
								106	20	S –57–3 / G –66			
								120	13	K –69			
								108	10	Э –69			
								107,5	9,8	F –70			
								90	~33	A –70			
					7,750		2				117 *	27	Принято, что $\Delta\Gamma_\gamma = \Delta\Gamma$.
								142	58	S –57–3 / G –66			
								85	16	K –69			
								140	20	Э –69			
								127	4	F –70			
								93	~20	A –70			Принято, что $\Delta\Gamma_\gamma = \Delta\Gamma$.
					10,01		2				III	8	
								115	20	F –70			
								110	~9	A –70			Принято, что $\Delta\Gamma_\gamma = \Delta\Gamma$.
					11,53		I				116	I	
								125	23	F –70			
								116	~I	A –70			Принято, что $\Delta\Gamma_\gamma = \Delta\Gamma$.
					11,99		2				105	7	
								137	120	S –57–3 / G –66			
								112	II	F –70			
								100	~10	A –70			Принято, что $\Delta\Gamma_\gamma = \Delta\Gamma$.

Table 1 continued

изотоп	$\Gamma_т$ мв : $\Delta\Gamma_\sigma$ мв	ℓ	n	В озв.	ℓ	J	рез $\Gamma_т$ мв : рез $\Delta\Gamma_т$ мв : Работа	рез $\Gamma_т$ мв : рез $\Delta\Gamma_\sigma$ мв.	Примечания
Gd^{155} 64 (продолжение)				14,51		I	97　60 {S - 57 -3 / G - 66} ; III　10 F - 70 ; 95　~10 A - 70	103　7	Принято, что $\Delta\Gamma_т = \Delta\Gamma$.
				17,77		2	120　25 F -70 ; 114　~46 A -70	119　22	Принято, что $\Delta\Gamma_т = \Delta\Gamma$.
				19,92		2	91　25 {S -57-3 / G -66} ; 110　16 K -69 ; 108　16 F -70 ; 119　~29 A -70	108　10	Принято, что $\Delta\Gamma_т = \Delta\Gamma$.
				21,02		2	62　45 {S -57-3 / G -66} ; 75　19 K -69 ; 101　6 F -70 ; 84　~24 A - 70	97　6	Принято, что $\Delta\Gamma_т = \Delta\Gamma$.
				23,45		2	108　31 {S -57-3 / G -66} ; 167　14 F -70 ; 105　~15 A -70	127*　35	Принято, что $\Delta\Gamma_т = \Delta\Gamma$.
				27,56		I	126　~20 A -70	126　20	Принято, что $\Delta\Gamma_т = \Delta\Gamma$.
				29,58		2	124　61 K -69 ; 90　22 F -70 ; 128　~26 A - 70	107　16	Принято, что $\Delta\Gamma_т = \Delta\Gamma$.
				30,10		2	87　39 K -69 ; 105　11 F -70 ; 182　~60 A -70	125*　50	Принято, что $\Delta\Gamma_т = \Delta\Gamma$.
				31,72		2	73　57 F -70 ; 138　~21 A -70	130　20	Принято, что $\Delta\Gamma_т = \Delta\Gamma$.
				34,83		I	152　~24 A -70	152　24	Принято, что $\Delta\Gamma_т = \Delta\Gamma$.

изотоп	$\overline{\Gamma_{MB}}$: $\overline{\Delta\Gamma\,MB}$		ℓ	$\cap$	E_0 эв	ℓ	J	$\Gamma_\gamma^{рез}$ мв. : $\Delta\Gamma_\gamma^{рез}$ мв	Работа	$\Gamma_6^{рез}$ мв. : $\Delta\Gamma_\gamma^{рез}$ мв	Примечания
Gd^{155}_{64} (продол-жение)					35,48		2	118 ~24	A - 70	118 24	Принято, что $\Delta\Gamma_\gamma = \Delta\Gamma$.
					37,10		I	86 15 / 143 18 / 121 ~25	K - 69 / F - 70 / A - 70	117* 29	Принято, что $\Delta\Gamma_\gamma = \Delta\Gamma$.
					39,02		2	118 ~26	A - 70	118 26	Принято, что $\Delta\Gamma_\gamma = \Delta\Gamma$.
					43,92			136 9	F - 70	136 9	
					46,82			100 39 / 84 12	K - 69 / F - 70	85 12	
					51,41		I	100 56 / 138 ~50	K - 69 / A - 70	121 37	Принято, что $\Delta\Gamma_\gamma = \Delta\Gamma$.
					52,17		I	130 ~40	A - 70	130 40	Принято, что $\Delta\Gamma_\gamma = \Delta\Gamma$.
					53,68		2	72 10 / 141 ~25	F - 70 / A - 70	106* 49	Принято, что $\Delta\Gamma_\gamma = \Delta\Gamma$.
					56,17		2	61 55 / 131 ~19	F - 70 / A - 70	96* 50	Принято, что $\Delta\Gamma_\gamma = \Delta\Gamma$.
					59,48		2	129 ~20	A - 70	129 20	Принято, что $\Delta\Gamma_\gamma = \Delta\Gamma$.
					62,74		2	82 11 / 129 ~25	F - 70 / A - 70	106* 33	Принято, что $\Delta\Gamma_\gamma = \Delta\Gamma$.
					69,50		I	151 36 / 186 ~90	F - 70 / A - 70	156 33	Принято, что $\Delta\Gamma_\gamma = \Delta\Gamma$.
					78,80			47 23	F - 70	47 23	
					84,27		2	140 ~49	A - 70	140 49	Принято, что $\Delta\Gamma_\gamma = \Delta\Gamma$.
					112,4			84 10	F - 70	84 10	

Table 1 continued

изотоп	рез Г_γ мв.	рез Г_т мв	ℓ	n	E_o эб.	ℓ	Э	рез Г_т мв	рез ΔГ_т мв	Работа	рез Г_т мв	рез ΔГ_т мв	Примечания
Gd^{155} 64(продолжение)					113,8			67	12	F - 70	67	12	
					116,6			116	94	F - 70	116	94	
					123,4			159	65	F - 70	159	65	
					126,1			152	131	F - 70	152	131	
					173,6			110	29	F - 70	110	29	
Gd^{157} 64	109	21		27									
I=3/2					0,0314		2	100	30	L - 56	106	1	
								106	1	M - 60			
								107	~10	A - 70			Принято,что ΔГ_т = ΔГ.
					2,825		2	97	1	M - 60	97	1	
								97	~10	A - 70			Принято,что ΔГ_т = ΔГ.
					16,85		2	85	16	S - 57- 3	103*	25	Г_γ =78± 4 мв без учёта Э -69 ; M-69-2 ; A -70 ;
										G - 66			
								81	10	K - 69			
								120	20	Э - 69			
								130	20	M - 69 -2			
								77	5	F - 70			
								128	~30	A - 70			Принято,что ΔГ_т = ΔГ.
					20,56		2	83	20	K - 69	100*	26	Г_γ = 88 ±5мв без учёта A -70
								88	5	F - 70			
								130	~38	A - 70			Принято,что ΔГ_т =ΔГ.
					21,66			147	65	F - 70	147	65	
					23,33			121	31	F - 70	121	31	
					25,40		I	75	13	K - 69	82	9	
								79	23	F - 70			
								94	~16	A - 70			Принято,что ΔГ_т = ΔГ

Table 1 continued

изотоп	$\overline{\Gamma_\gamma}$ мв	$\overline{\Delta\Gamma_{\gamma}}$ мв	ℓ	n	E_o эв	ℓ	$Ј$	$\overline{\Gamma^{рез}_{\gamma}}$ мв	$\overline{\Delta\Gamma^{рез}_{\gamma}}$ мв	Работа	$\overline{\Gamma^{рез}_{\gamma}}$ мв	$\overline{\Delta\Gamma^{рез}}$ мв	Примечания
Gd^{157}_{64} $I=3/2$ (продолжение)					44,20		2 2	89 110 91 110	19 20 8 ~14	K -69 M -69-2 F -70 A -70	96	6	Принято, что ΔГ_γ= ΔГ.
					48,72		2	86 82 90 100 87 ~117	34 12 30 10 4 ~15	{G - 66, S - 57-3} K - 69 J - 69 M - 69-2 F - 70 A - 70	94*	13	Принято, что ΔГ_γ = ΔГ
					58,31		I	79 ~104 ~134	12 5 ~28	K - 69 F - 70 A - 70	106*	28	Принято, что ΔГ_γ = ΔГ.
					66,57		I	67 ~128	12 ~17	F - 70 A - 70	98*	43	Принято, что ΔГ_γ = ΔГ.
					81,58		I	108	~35	A - 70	108	35	
					87,20		2	173 113 136	65 33 ~17	K - 69 F - 70 A - 70	133	15	Принято, что ΔГ_γ = ΔГ.
					96,59		2	81 103 ~137	26 31 ~17	K - 69 F - 70 A - 70	107*	28	Принято, что ΔГ_γ = ΔГ.
					100,2		I	89 79 ~98	19 ~19 ~23	K - 69 F - 70 A - 70	88	12	Принято, что ΔГ_γ = ΔГ
					104,9		2	66 ~102	~9 ~24	F - 70 A - 70	84*	26	

Table 1 continued

изотоп	$\overline{\Gamma_{n}}$	$\Delta\overline{\Gamma_{n6}}$	ℓ	n	$E_{0\,эb}$	ℓ	$\exists$	$\Gamma_{\gamma\,мб}^{рез.}$	$\Delta\Gamma_{\gamma\,мб}^{рез.}$	Работа	$\overline{\Gamma_{\gamma\,мб}^{рез}}$	$\overline{\Delta\Gamma_{\gamma\,мб}^{рез}}$	Примечания
Gd_{64}^{157} (про - должение)					110,5		(2)				87	9	
								83	21	К — 69			
								87	10	F — 70			
								~ 117	~ 45	А — 70			Принято, что $\Delta\Gamma_{\gamma}=\Delta\Gamma$.
					115,4						121	11	
								130	75	К — 69			
								113	56	F — 70			
								121	~ 23	А — 70			Принято, что $\Delta\Gamma_{\gamma}=\Delta\Gamma$.
					120,9		I				91	6	
								91	6	F — 70			
								104	~ 44	А — 70			Принято, что $\Delta\Gamma_{\gamma}=\Delta\Gamma$.
					138,70		2				86	19	
								86	~ 19	А — 70			Принято, что $\Delta\Gamma_{\gamma}=\Delta\Gamma$.
					143,7		2				90	6	
								88	10	F — 70			
								111	~ 29	А — 70			Принято, что $\Delta\Gamma_{\gamma}=\Delta\Gamma$.
					149,07		I				140	29	
								140	~ 29	А — 70			Принято, что $\Delta\Gamma_{\gamma}=\Delta\Gamma$.
					156,6		(2)				122	28	
								87	70	F — 70			
								129	~ 30	А — 70			Принято, что $\Delta\Gamma_{\gamma}=\Delta\Gamma$.
					164,9		2				108	55	
								69	31	F — 70			
								147	~ 33	А — 70			Принято, что $\Delta\Gamma_{\gamma}=\Delta\Gamma$.
					172,26		I				271	109	
								271	~ 109	А —70			При усреднении этот резонано не учтён
					179,33		2				145	45	
								145	~ 45	А — 70			Принято, что $\Delta\Gamma_{\gamma}=\Delta\Gamma$.
					184,93		2				113	44	
								113	~ 44	А — 70			Принято, что $\Delta\Gamma_{\gamma}=\Delta\Gamma$.
					208,9		2				160	74	
								160	~ 74	А — 70			Принято, что $\Delta\Gamma_{\gamma}=\Delta\Gamma$.

GAMMA RAYS FROM RADIOACTIVE CAPTURE OF FAST NEUTRONS IN Fe, Ni AND Cu

A.T. Bakov, O.A. Shcherbakov

The radiative capture of neutrons is one of the main processes involved in the interaction of neutrons with nuclei in the reactor spectrum region. For estimating the energy release in core structural materials, calculating the composition and size of the shielding and so on, it is often necessary to have a detailed knowledge of the capture gamma ray spectrum and its dependence on neutron energy. At present there exist "group spectra" of gamma rays from the radiative capture of thermal neutrons $/1/$, which are usually used for such calculations. But, as was pointed out long ago and has been stated again more recently in a number of publications $/2, 3/$, the gamma-ray spectra associated with radiative capture depend on the energy of the absorbed neutrons.

In this study we measured the energy spectra of gamma rays from radiative capture of fast neutrons by Fe, Ni and Cu nuclei. For each element samples of the natural isotopic mixture were used. The neutrons were produced by the $T(p,n)^3He$ reaction in a Van de Graaff accelerator. The measurements were performed in annular geometry at kinetic incident neutron energies in the ranges 150-370, 360-560 and 580-840 keV.

The gamma-ray detector was a single-crystal scintillation spectrometer with stilbene crystal ($\phi = 50$, h = 45 mm). The measured pulse distributions were processed by the smoothing differentiation method. After averaging the results of several measurements and subtracting the background, the gamma-ray energy spectra were corrected with the aid of a 90th order correction matrix (energy step 100 keV) and corrections were made for self-absorption of gamma rays in the sample.

Table 1 shows the gamma-ray yields per 100 captures in 500-keV wide energy intervals, calculated by the formula

$$Y_{\Delta E} = 100 \frac{\int_{Ei}^{E_{i+1}} \varphi(E_\gamma) dE_\gamma}{\int_{0}^{} \varphi(E_\gamma) E_\gamma dE_\gamma} (\bar{B}_n + \bar{E}_n)$$

where $\Delta E = E_{i+1} - E_i$, $\varphi(E_\gamma)$ is the capture gamma-ray energy spectrum, $\bar{B}_n$ is the mean neutron binding energy and $\bar{E}_n$ is the mean neutron kinetic energy.

In calculating $\bar{B}_n$ we assumed that the contribution of the individual isotopes to the mean binding energy would be proportional to their fraction in the natural isotopic composition of the element. The last two columns of Table 1 show the number of gamma quanta per 100 captures and the energy spread of captured neutrons due to the thickness of the target and the geometry of the experiment.

For the "smooth" kind of spectra shown in Table 1 an important factor is the error associated with differentiation of the pulse distributions. The error is below 15% except for those spectra marked with an asterisk, where it is 25-30%.

For comparison Table 2 presents data on capture gamma-ray yields from Ref. $\int 3\underline{J}$. Comparison of the gamma-ray spectra given in Tables 1 and 2 for the various neutron energies shows satisfactory agreement when allowance is made for measuring errors.

The authors wish to thank Yu.A. Kazansky for his constant interest in the work and the valuable advice he rendered during the discussion of the results.

Table 1 and Table 2

Key:

Элемент	= Element
Мэв	= MeV
кэв	= keV

TABLE 1

Эле-мент	$E_б$, Мэв																		V	$E_н$, кэв
	1,0–1,5	1,5–2,0	2,0–2,5	2,5–3,0	3,0–3,5	3,5–4,0	4,0–4,5	4,5–5,0	5,0–5,5	5,5–6,0	6,0–6,5	6,5–7,0	7,0–7,5	7,5–8,0	8,0–8,5	8,5–9,0	9,0–9,5	9,5–10,0		
Cu	13	13,5	14,6	15,7	16,0	14,8	15,4	12,8	12,5	10,4	10,9	10,7	9,6	8,0	1,4	0	0	0	187	150÷370
	13,0	13,6	14,5	15,8	16,1	15,0	15,2	13,8	12,5	9,9	9,9	10,5	9,3	7,7	4,2	1,0	0	0	189	360÷560
	17,4	16,2	16,7	18,8	17,0	15,0	15,1	14,6	12,5	11,0	9,4	10,5	8,9	7,7	4,5	1,3	0	0	213	580÷840
Fe	17,1	16,7	13,8	11,9	11,7	11,0	10,2	12,1	9,7	8,7	11,7	4,0	12,3	18,8	5,7	0,6	2,4	0,52	183	150÷370
	20,0	16,8	14,6	13,2	11,5	12,1	12,0	9,8	11,0	9,1	7,9	5,7	9,2	15,4	9,4	2,6	0,7	0,8	187	360÷560
	22,2	13,6	15,0	12,3	9,4	9,2	12,7	9,4	11,9	7,7	10,6	3,0	13,7	9,2	12,2	3,9	1,2	0,8	189	580÷840
Ni	19,8	15,1	13,5	10,4	10,1	9,1	7,6	7,6	9,3	10,0	8,8	6,7	9,6	8,2	13,5	14,2	5,2	0,3	182	150÷370
	20,4	18,7	14,3	12,4	10,6	11,0	8,3	8,7	9,1	10,2	8,1	7,6	7,4	8,6	11,1	13,0	7,2	1,3	192	360÷560
	28,7		19,2		18,6		15,8		16,8		23,4		15,4		24,7		13,0		178	580÷840

TABLE 2

	E_γ , Мэв											
	4,8-5,2	5,2-5,6	5,6-6,0	6,0-6,4	6,4-6,8	6,8-7,2	7,2-7,6	7,6-8,0	8,0-8,4	8,4-8,8	8,8-9,2	$E_н$, кэв
Cu	6,6	7	6,9	8,5	3,9	9,3	5,5	12,8	-	-	-	15 ÷ 300
	-	-	-	3	6	7	8	24	8	9	II	10 ÷ 20
Ni	-	-	-	4	6	7	9	10	17	10	II	55 ÷ 75
	-	-	-	4	7	8	9	II	9	II	12	265÷335

REFERENCES

[1]   TROUBETZKOY, E., GOLDSTEIN, H., Nucleonics 18 (1960) 17.

[2]   BERGQVIST, I., STARFELT, N., Nucl. Phys. 39 (1962) 353.

[3]   BERGQVIST, I., STARFELT, N., Ark. Fys. 23 (1963) 435.

[4]   DVUKHSHERSTNOV, V.G. et al., Pribory Tekh. Eksp. 4 (1969) 39.

ANGULAR DISTRIBUTIONS OF PHOTONEUTRONS IN THE INTERACTION OF 23-MeV ELECTRONS WITH COPPER, TUNGSTEN AND LEAD TARGETS

V.P. Kovalev, V.P. Kharin, V.V. Gordeev

Using the LUE-25 linear electron accelerator and targets of copper, tungsten and lead, measurements were made of the angular distributions of photoneutrons in relation to target thickness and diameter.

The experiments were performed with a straight 23-MeV electron beam directed at the centre of the target. The targets were placed 20 cm from the output window of the accelerator. The threshold reaction $^{31}P(n,p)^{31}Si$ was used for detecting neutrons. The experimental set-up was similar to that used in Ref. $/ 1 /$.

The angular distributions of photoneutrons for lead targets are shown in Fig. 1. The thickness of the lead targets varied from 11 to 53 mm and the diameter from 30 to 80 mm. Statistical measuring errors were less than 3%. The forward shift of the angular distributions is due to inelastic loss of neutron energy with increasing target thickness $/ 2 /$. Similar results were obtained for the copper and tungsten targets. The table shows the results for copper and tungsten targets of various dimensions. The data were normalized at $\varphi = 90°$.

REFERENCES

$/ 1 /$ KOVALEV, V.P. et al., Bjul. inf. Centr jad. Dannym, Issue No. 6 (1969) 393.

$/ 2 /$ KOVALEV, V.P. et al., Bjul. inf. Centr jad. Dannym, Issue No. 6 (1969) 398.

Angular distributions of photoneutrons
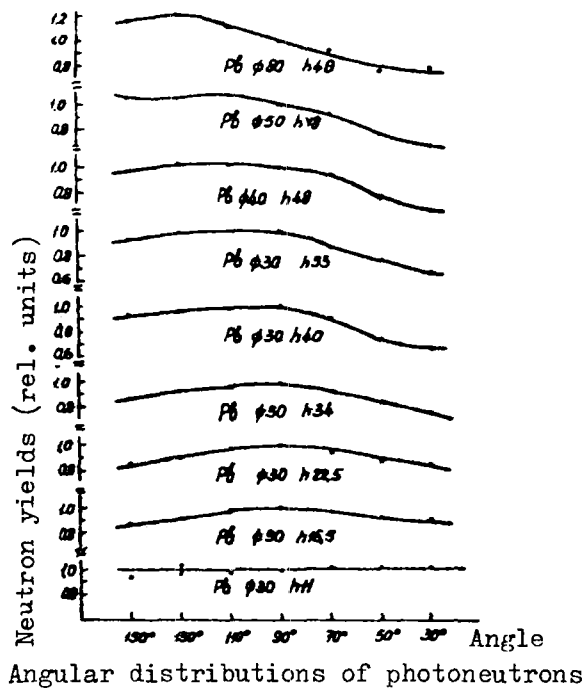
Fig. 1 Angular distributions of photoneutrons for a lead target as a function of diameter (ϕ - mm) and thickness (h - mm)

Table 1

Title: Angular distributions of photoneutrons in relation to
         diameter and thickness of copper and tungsten targets.
         Primary electron energy 23 MeV.

Key:

Материал мишени	= Target material
Диаметр мишени	= Target diameter ϕ(mm)
Толщина	= Thickness h (mm)
Угол	= Angle
Вольфрам	= Tungsten
Медь	= Copper

TABLE 1

Материал мишени	Диаметр мишени φ(мм)	угол h(мм)°	30°	50°	70°	90°	110°	130°	150°
Вольфром	40	3.3	1.23	1.32	1.28	1.00	1.29	1.30	1.25
	–"–	6.64	1.20	1.20	1.11	1.00	1.19	1.20	1.12
	–"–	10	1.07	1.19	1.16	1.00	1.13	1.17	1.06
	–"–	13.3	0.99	1.01	0.98	1.00	1.00	1.00	0.97
	–"–	24	0.73	0.79	0.94	1.00	1.00	0.99	0.92
Медь	40	15	1.16	1.08	1.04	1.00	1.01	1.06	1.17
	–"–	30	0.90	0.91	0.98	1.00	0.97	0.95	1.00
	–"–	45	0.72	0.87	0.95	1.00	0.97	0.93	0.91
	–"–	50	0.65	0.81	0.92	1.00	0.99	0.95	0.99
	–"–	75	0.59	0.73	0.93	1.00	1.05	0.95	0.89
	–"–	100	0.55	0.71	0.82	1.00	1.04	1.02	1.01
	50	–·–	0.47	0.70	0.84	1.00	1.01	1.12	1.16
	80	–"–	0.52	0.73	0.92	1.00	1.05	1.23	1.21
	100	–·–	0.51	0.62	0.87	1.00	1.00	1.28	1.50
	135	–·–	0.69	0.70	0.82	1.00	1.09	1.62	1.80

PHOTONEUTRON YIELDS AS A FUNCTION OF THE DIAMETER AND THICKNESS OF COPPER, TUNGSTEN AND LEAD TARGETS

V.P. Kovalev, V.P. Kharin, V.V. Gordeev

The results of this study are an extension of investigations aimed at developing a pulsed photoneutron source with isotropic distribution on the basis of a linear electron accelerator $\boxed{1}$.

To this end photoneutron yields were investigated experimentally as a function of the diameter and thickness of copper, lead and tungsten targets at an electron energy of 23 MeV.

The total photoneutron yield was measured from neutron stopping in a paraffin sphere 30 cm in diameter. A thin indium foil at the centre of the sphere served as slow neutron detector. The experiments were performed with a straight electron beam directed at the centre of the target. The targets were placed 20 cm away from the output window of the accelerator. The neutron detector was situated at an angle of 90° to the direction of the incident electron beam.

The experimental results are given in the figures in the form of relative yields of photoneutrons from copper, tungsten and lead as a function of the thickness (Fig. 1) and the diameter (Fig. 2) of the targets.

The statistical measuring error was less than 2%.

REFERENCES

$\boxed{1}$ KOVALEV, V.P., KHARIN, V.P., GORDEEV, V.V., FILIPENOK, S.P., Bjul. inf. Centr jad. Dannym, Issue No. 6 (1969) 393.
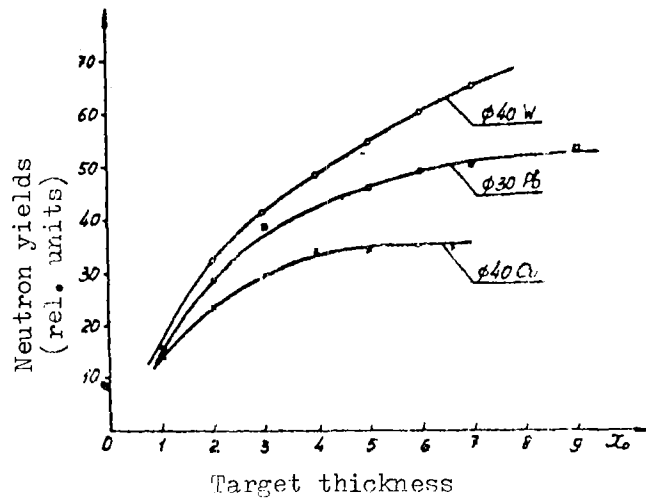
Fig. 1   Neutron yields versus thickness of copper, tungsten
          and lead targets:

          XXX = Cu target, diameter 40 mm

          OOO = W target, diameter 30 mm

          ⬜⬜⬜= Pb target, diameter 40 mm
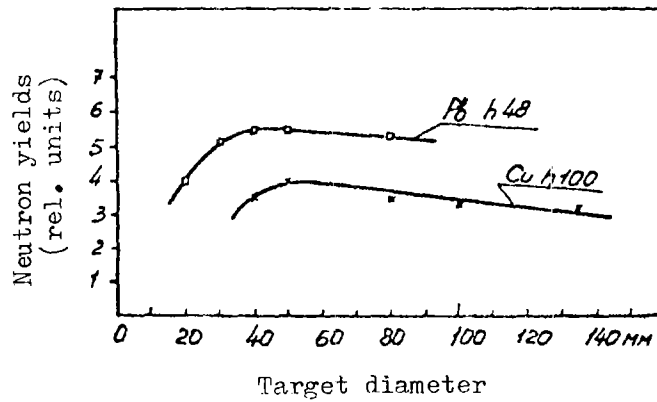
Fig. 2   Neutron yields versus diameter of copper and lead
          targets:

          XXX = Cu target 100 mm thick
          ⬜⬜⬜= Pb target 48 mm thick

ABSOLUTE YIELDS OF THE REACTIONS ^{12}C(γ,n) AND ^{16}O(γ,n)

V.P. Kovalev, S.P. Kapchigashev

The activation method was used to measure the yields of (γ,n) reactions from carbon and oxygen at maximum bremsstrahlung beam energies of 22 and 24 MeV. The bremsstrahlung source was a tungsten target 6 mm thick. The distance from the target to the samples was 25 cm. The current supplied to the target was 3-5 μA. The samples used were thin Plexiglas ($C_5H_8O_2$) and distilled water. The irradiation time was 10 min. The induced activity of the samples was measured with a scintillation gamma spectrometer, in order to separate the annihilation gamma quanta with energy 0.511 MeV.

The data obtained were normalized to the known yield of the ^{63}Cu(γ,n)^{62}Cu reaction [1].

The yield of the (γ,n) reaction for the element under investigation, $\sigma_x(E\gamma m)$, was determined from the formula

$$\sigma_x(E\gamma m) = \sigma_{Cu}(E\gamma m) \cdot \frac{n_{Cu} N(0) \epsilon_{\beta}^{Cu} (1-\ell^{-heuto})}{n_x N_{Cu}(0) \epsilon_{\beta}^{x} (1-\ell^{-hxto})}$$

where n_x and n_{Cu} are the nuclear densities of the sample and of copper, respectively; $N_x(0)$ and $N_{Cu}(0)$ are the counting rates at the moment of termination of irradiation; t_o is the irradiation time, and ϵ_{β}^{x} and ϵ_{β}^{Cu} are the respective output efficiencies of gamma quanta with energy 0.511 MeV resulting from β+ decay.

The results of the measurements together with the data of other authors are presented in Table 1.

From the table it can be seen that the yields of the (γ,n) reactions from carbon at E = 22 MeV and E = 24 MeV are in good agreement with the data of Price, Haslam and co-workers, and are 4.5 times lower than the values obtained by Montalbetti and co-workers. For the yield of the (γ,n) reaction from oxygen our data are in satisfactory agreement with the data of other authors apart from Price and Thorson. Note the paucity of data on the yield of photoneutrons from ^{12}C and ^{16}O for bremsstrahlung with a maximum energy of 24 MeV.

REFERENCE

[1]   ROALSVIG, J.P. et al., Can. J. Phys. <u>39</u>, 5 (1961) 643.

Table 1

Title: Absolute yields of the reactions $^{12}C(\gamma,n)^{11}C$ and $^{16}O(\gamma,n)^{15}O$

Key:

$$\frac{\text{нейтроны}}{\text{в единицах моль-рентген}} = \text{in} \frac{neutrons}{mole\text{-}roentgen}$$

Элементы	= Elements
Результаты данной работы	= Present work
Прайс	= Price (1950)
Хаслам и др./1951/	= Haslam et al. (1951)
Монталбетти и др.	= Montalbetti et al. (1953)
Натанс и Халперн	= Nathans and Halpern (1954)
Барбер и др.	= Barber et al. (1955)
Кук	= Cook (1957)
Торсон	= Thorson (1957)
Хаслам и др.	= Haslam et al. (1961)
Литература	= Literature
См. ссылку	= See Ref.

TABLE 1

Абсолютные выходы $C^{12}/р,n$ / C и $O^{16}/р,n/O^{15}$ - реакций

нейтроны

в единицах моль-рентген

Элементы	C^{12}			O^{16}			Литература
$E_{\gamma m}$, Мэв	22	23	24	22	23	24	
Результаты данной работы	$0,6.10^4$	–	$4,5.10^4$	$1,72.10^4$	–	1.10^5	См. ссылку
Прейс (1950)	$0,67.10^4$	–	–	$0,67.10^4$	–	–	1
Хеслам и др.(1951)	$0,75.10^4$	–	$4,35.10^4$	$1,68.10^4$	–	$4,53.10^4$	-"-
Монталбетти и др.(1953)	$2,7.10^4$	–	–	$3,2.10^4$	–	–	-"-
Нэтэнс и Хэлперн(1954)	–	–	–	$3,2.10^4$	–	–	-"-
Барбер и др.(1955)	–	–	–	$2,3.10^4$	–	–	-"-
Кук (1957)	–	–	–	$1,5.10^4$	–	–	-"-
Торсон (1957)	–	–	–	$0,76.10^4$	–	–	-"-
Хеслам и др.(1961)	$1,15.10^4$	$2,77.10^4$		$2,37.10^4$	–	–	-"-

REACTIONS INVOLVING LIGHT NUCLEI AND CAUSED BY CHARGED PARTICLES ARISING FROM 14.6 MeV NEUTRON INTERACTIONS

B.L. Lebedev, F. Nasyrov

Calculations and measurements were performed to establish the yields and cross-sections of the $^{11}B(p,n)^{11}C$, $^{10}B(p,\alpha)^{7}Be$, $^{16}O(p,\alpha)^{13}N$, $^{18}O(p,n)^{18}F$, $^{13}C(p,n)^{13}N$, $^{12}C(d,n)^{13}N$ and $^{7}Li(p,n)^{7}Be$ reactions in H_3BO_3, $H_3{}^{10}BO_3$, $(C_2H_4)_n$, $(C_2D_4)_n$, LiOH and $(COOH)_2 \cdot 2H_2O$ induced by recoil protons and deuterons produced in the elastic scattering of 14.6 MeV neutrons. Experiments were performed to determine the yields of the $^{16}O(t,n)^{18}F$ reaction in H_3BO_3, $H_3{}^{10}BO_3$ and LiOH induced by tritons resulting from the interaction of neutrons with boron and lithium nuclei.

The irradiation of various materials with neutrons induces various nuclear reactions, including reactions that give rise to charged particles such as protons, deuterons, tritons, alpha particles, etc. The charged particles in turn cause secondary reactions in various elements. These secondary reactions are thus a source of varying degrees of radioactivity in reactor structural materials and neutron shield materials. For example ^{13}N and ^{18}F are formed in reactor cooling water through the reactions $^{16}O(p,n)^{13}N$ and $^{18}O(p,n)^{18}F$ $/\overline{1-3}/$, and ^{7}Be is formed in boron shielding through the $^{10}B(p,\alpha)^{7}Be$ reaction. Moreover, reactions induced by secondary charged particles are used to obtain radioactive isotopes in reactors $/\overline{4-8}/$. Naude and Peisach $/\overline{9}/$ measured the cross-sections of a number of reactions in boron, carbon, nitrogen and oxygen, caused by recoil protons and deuterons arising from the interactions of 14.5 MeV neutrons.

Here we have calculated and measured the yields and the cross-sections of reactions induced by secondary charged particles in certain reactor and biological shield materials, following irradiation with 14.6-MeV neutrons; the materials in question were polyethylene – $(C_2H_4)_n$, deutero-polyethylene – $(C_2D_4)_n$, boric acid in the natural isotopic mixture – H_3BO_3, boric acid 85% enriched in ^{10}B–$H_3{}^{10}BO_3$, lithium hydroxide – LiOH and oxalic acid $(COOH)_2 \cdot 2H_2O$.

Calculation of the yields and cross-sections of secondary reactions

The number of reactions in one gram of a substance due to secondary charged particles arising from the interaction of monoenergetic neutrons with that substance is given by

$$Q = n_i n \, \sigma_n N \cdot \int_0^{E_{max}} \varphi(E)dE \int_0^E \frac{\sigma(E')}{\left|\frac{dE'}{d\xi}\right|} dE' \tag{1}$$

where n is the number of nuclei of the element in which fast charged particles are formed by interaction with neutrons, n_i is the number of nuclei of the element in which reactions are induced by secondary charged particles, σ_n is the cross-section for the formation of charged particles, N is the neutron flux per unit area, $\varphi(E)$ is the secondary charged particle spectrum, $\sigma(E)$ is the cross-section for the reaction induced by the charged particles, and $\frac{dE}{d\xi}$ is the energy lost by a charged particle along its track, in $MeV/g/cm^2$.

Changing the order of integration in Eq. (1), we find

$$Q = n_i n \sigma_n N \cdot \int_0^{E_{max}} \frac{\sigma(E)P(E)}{\left|\frac{dE}{d\xi}\right|} dE, \tag{2}$$

where

$$P(E) = \int_E^{E_{max}} \varphi(E)dE \tag{3}$$

is the probability that a charged particle will be formed with energy greater than E, i.e. the integral secondary charged particle spectrum. From Eq. (2) it follows that the mean cross-section for secondary charged particles is

$$\bar{\sigma} = \frac{Q}{n_i n \sigma_n N \cdot \int_0^{E_{max}} \frac{P(E)}{\left|\frac{dE}{d\xi}\right|} dE} \tag{4}$$

Here we have calculated the yields and cross-sections of a number of secondary reactions induced by recoil protons and deuterons resulting from the irradiation of the substances under study with 14.6-MeV neutrons. The differential and integral recoil proton spectra were calculated on the assumption of isotropic scattering of neutrons by protons, and the recoil deuteron spectra were calculated from the differential cross-sections for neutron scattering by deuterons supplied in Ref. $\boxed{10}$.

The integral recoil proton and deuteron spectra are shown in Fig. 1. The cross-sections for neutron scattering by protons and deuterons were taken to be 0.67 b $\boxed{11}$ and 0.61 b $\boxed{10}$ respectively. The slowing-down capacities of the investigated substances for recoil protons and deuterons were calculated from the proton and deuteron ranges in different elements $\boxed{12, 13}$. The yields and the cross-sections of secondary reactions induced by protons and deuterons, calculated according to formulae (1) and (4), are shown in Table 1. Only recoil protons and deuterons produced by elastic neutron scattering were taken into account, since the number produced by other mechanisms is negligible in the substances with which we are concerned here. The last column of the table shows the sources of the excitation functions for charged particle reactions used in the calculations.

Measurement of the yields and cross-sections of secondary reactions

The measurements were performed by the activation method. We studied the reactions $^{16}O(p,\alpha)^{13}N$, $^{18}O(p,n)^{18}F$, $^{11}B(p,n)^{11}C$, $^{10}B(p,\alpha)^{7}Be$, $^{7}Li(p,n)^{7}Be$, $^{13}C(p,n)^{13}N$ and $^{12}C(d,n)^{13}N$ induced by recoil protons and deuterons in materials irradiated with neutrons of energy 14.6 ± 0.2 MeV. In addition, we were able to determine the yields of the $^{16}O(t,n)^{18}F$ reaction in H_3BO_3, $H_3^{10}BO_3$ and LiOH induced by tritons from neutron interactions with ^{10}B, ^{11}B and ^{7}Li nuclei.

Neutrons were obtained in the $T(d,n)^{4}He$ reaction with a low voltage generator which accelerates deuterons to an energy of 120 keV. The samples were in the form of tablets 25 mm in diameter and 5-10 mm thick. For irradiation they were set at 0° to the deuteron beam at a distance of 15 mm from the target.

After irradiation the activity induced in the specimens was recorded by a single-crystal scintillation spectrometer with a NaI(Tl) crystal 80 x 80 mm in diameter and an AI-256 multichannel analyser. The yield of the reactions producing ^{13}N, ^{11}C and ^{18}F was determined from the counting rate of pulses in the photopeak from 0.511 MeV gamma quanta accompanying the decay of these nuclei, and the yield of the $^{10}B(p,\alpha)^{7}Be$ and $^{7}Li(p,n)^{7}Be$ reactions was determined from the counting rate of pulses from 0.480 MeV gamma quanta accompanying the decay of ^{7}Be.

The absolute yields of the secondary reactions were determined by comparison with the yield of a reaction having a well-known cross-section,

viz. the $^{65}Cu(n,2n)^{64}Cu$ reaction: the cross-section for this was taken as 970 mb $\underline{/11\underline{/}}$. The data on gamma quanta yield per disintegration, gamma quanta energy and half-lives were taken from Ref. $\underline{/14\underline{/}}$.

Table 1 shows the measured secondary reaction yields compared with the theoretical values. It can be seen that there is good agreement. An exception is the formation of ^{18}F in H_3BO_3, $H_3^{10}BO_3$ and LiOH, where the experimental yields considerably exceed the theoretical. We believe this is due to the contribution of the $^{16}O(t,n)^{18}F$ reaction with tritons produced in neutron interactions with ^{11}B, ^{10}B and ^7Li. The table also includes the experimental values of the average cross-sections for recoil protons and deuterons, determined from the experimental yields by means of Eq. (4). Some of these cross-sections are compared with the results of Naude and Peisach $\underline{/9\underline{/}}$ and it can be seen that their values are higher than ours. This is due partially to the fact that we averaged over the range from 0 to E_{max} whereas Naude and Peisach averaged from the threshold energy E_{thr} to E_{max}. The disagreement is also explained to some extent by the fact that they used different standard reactions, and the difference in neutron fluxes to the samples determined with these reactions was as much as 40%. In view of this it can be considered that our results are in agreement with the results of Ref. $\underline{/9\underline{/}}$.

From our results it will be seen that in certain materials containing boron and lithium which are not activated directly by neutrons it is possible for short-lived and indeed long-lived activity to arise through the formation of ^7Be in reactions induced by secondary charged particles, and this must be taken into account in the design of biological shields.

Table 1

Yields and cross-sections of secondary reactions

REACTION	SAMPLE	η_N $(\cdot10^{-7} \frac{1}{g \cdot n/cm})$ THEORETICAL	EXPERIMENTAL	$\bar{\sigma}$ (mb) THEORETICAL	EXPERIMENTAL	REF. 9	LITERATURE REFERENCE
$O^{15}(p,\alpha)N^{13}$	H_3BO_3	9,7	II,9±I,0	I7,2	2I±2,0	28±9	[I5]
	$H_3B^{18}O_3$	9,8	I0,7±I,0	I7,2	I8,6±2,0		-"-
	$LiOH$	6,3	II,I±I,0	20,0	22,7±2,0		-"-
	$(COOH)_2 \cdot 2H_2O$	I0,7	9,0±I,5	I5,5	I8,4±3,0		-"-
$O^{18}(p,n)F^{18}$	$(COOH)_2 \cdot 2H_2O$	0,25	0,30±0,006	2I0	252 ± 42		[I6],[I7]
	H_3BO_3	0,27		232			-"-
	$H_3B^{10}O_3$	0,27		232			-"-
	$LiOH$	0,24	- -	280			-"-
$O^{16}(t,n)F^{18}+$	H_3BO_3		0,77±0,I0				
$+O^{n}(p,n)F^{18}$	$H_3B^{10}O_3$		I,9 ±0,2				
	$LiOH$		5,9 ±0,6				
$O^{18}(t,n)F^{18}$	H_3BO_3		0,5 ±0,I				
	$H_3B^{10}O_3$		I,6 ±0,2				
	$LiOH$		5,6 ±0,6				
$B^{11}(p,n)C^{11}$	H_3BO_3	I5,9	I3,7±2,0	I05	90±I3	I60±50	[I6],[I8]
		28		I85			[I9],[20]
	$H_3B^{10}O_3$	3,0	2,7±0,5	I02	95±I4		[I6],[I8]
		5,3	- -	I80			[I9] [20]
$C^{13}(p,n)N^{13}$	$(C_2H_4)_n$		2,7±0,3		I20±I2	250±I00	
$C^{12}(d,n)N^{13}$	$(C_2D_4)_n$	42,7	63±6	I8,I	26,6±2,5		[2I]
$B^{10}(p,\alpha)Be^{7}$	H_3BO_3	3,6	6,I±0,9	97	I63±25		[22]
		8,8	- - -	238			[I9]
	$H_3B^{10}O_3$	I5,7	27,9±2,5	87	I55±I5		[22]
		38,6		2I2			[I9]
$Li^{7}(p,n)Be^{7}$	$LiOH$	8I,0	62,6±5,0	2I2	I65±I5		[I9],[23]

Fig. 1   Integral spectra of recoil protons (1) and deuterons (2)
produced in elastic scattering of 14.6-MeV neutrons

REFERENCES

/ 1 7   RUSSEL, J., RIDER, B., Trans. Am. Nucl. Soc., 1 (1958) 36.

/ 2 7   BALCARCZYK, L., KIM, K.H., LANZEL, E., Nucleonik, 4 (1962) 105.

/ 3 7   NIKOLOV, K., KULIEV, I., Atomn. Energ. 25 3 (1968).

/ 4 7   RUDENKO, I.P., SEVASTYANOV, A.I., Atomn. Energ. 18 (1965) 649.

/ 5 7   ROY, J.C., HOUTON, J.J., Can. J. Phys., 39 (1961) 1528.

/ 6 7   GLICKSTEIN, S., WINTER, R., Nucl. Instrum. Meth. 9 (1960) 226.

/ 7 7   ROY, J.C., BRESESTY, M., HOUTON, J.J., Can. J. Phys. 38 (1960) 1428.

/ 8 7   LEVIN, V.I. et al., Atomn. Energ. 24 3 (1968).

/ 9 7   NAUDE, W.J., PEISACH, M., J. Nucl. Eng. 21 (1967) 893.

/ 10 7   ALLRED, J.C., ARMSTRONG, A.H., ROSEN, L., Phys. Rev., 91 (1953) 90.

/ 11 7   Neutron cross-sections, BNL-325, Suppl. No. 2, v.1 (1964),
         Suppl. No. 2, v.2A (1966).

/ 12 7   WHAILING, W., in "Handbuch der Physik", Band XXXIY, Berlin-
         Göttingen-Heidelberg, (1958).

/ 13 7   NIJGH, G.J., WAPSTRA, A.H., VAN LIESHOUT, R., "Nuclear Spectroscopy
         Tables", Amsterdam, 1959.

/ 14 7   LEDERER, C.M., HOLANDER, J.M., PERLMAN, S., "Tables of Isotopes",
         New York, London, 1968.

/ 15 7   WHITEHEAD, A.B., FASTER, J.B., Can. J. Phys., 36 (1958) 1276.

/ 16 7   BLASER, J.P., BOEHM, F., SCHERRER, P., Helv. Phys. Acta, 24
         (1951) 473.

/ 17 7   YUNG SU TSAI, Bull. Am. Phys. Soc., 1 (1957) 327.

/ 18 7   FURUCAVE, M. et al., J. Phys. Soc. Japan, 15 (1960) 2167.

/ 19 7   KALININ, S.P. et al., Atomn. Energ. 2 (1957) 171.

/ 20 7   LEGGE, G.J.F., BUBB, I.F., Nucl. Phys., 26 (1961) 613.

/ 21 7   BRILL, O.D., SUMKIN, L.V., Atomn. Energ. 7 4 (1959).

/ 22 7   JENKIN, J., EARWAKER, L., TITTERTON, E., Nucl. Phys., 50 (1964) 516.

/ 23 7   Fizika bystryh nejtronov (Fast neutron physics) Vol. 1
         (MARION, J. and FOWLER, J., Eds) Atomizdat (1963).

KINEMATIC ANALYSIS AND TABLES OF NEUTRON ENERGY AND ENERGY SPREAD VALUES FOR (p,n) REACTIONS

G.A. Borisov, R.D. Vasilev, V.F. Shevchenko

The (p,n) reactions produced with electrostatic accelerators are widely used as sources of monoenergetic neutrons. To make practical use of such sources, it is necessary to know how neutron energy varies with the proton escape angle and proton energy and also to know the factors causing neutron energy spread. These questions are the subject of Refs $/$1-9$/$, in which neutron energies and energy spreads were determined with kinematic equations. The results of the calculations are presented in the form of tables and graphs.

To assist with the calibration of different types of neutron detectors for monoenergetic neutrons and the measurement of cross-sections, the authors of this article have compiled energy tables for neutrons produced in the $^3T(p,n)^3He$, $^7Li(p,n)^7Be$, $^{45}Sc(p,n)^{45}Ti$, $^{51}V(p,n)^{51}Cr$ and $^{65}Cu(p,n)^{65}Zn$ reactions. In addition, a quantitative assessment was made of the factors responsible for the neutron energy spread, principal among these being uncertainties in the proton energy values and the target thickness, as well as the Doppler effect due to thermal motion of the target atoms. The authors also estimated the effect on neutron energy of the uncertainty in the masses of the particles involved in the reaction and in the reaction energy Q. The results obtained differ from those published earlier in that they supply more detailed neutron energy data for the above reactions in the proton energy range from the corresponding thresholds to approximately 3 MeV together with additional information on how the Doppler effect influences the neutron energy spread at various target temperatures, as well as data from a comparison of neutron energies obtained using a relativistic equation, two non-relativistic approximations and one classical approximation. The calculations were performed using more accurately defined values for particle mass and Q $/$10, 11$/$. In this abridged report only those results will be presented which are not reproduced in the literature or which differ from published data.

The neutron energies presented in Tables 2 and 3 were calculated with the relativistic equation (34) described in Ref. $/$5$/$. Apart from the data given in the tables, neutron energy values were calculated on the basis of two non-relativistic and one classical approximation in accordance with formulae (38) and (55) also from Ref. $/$5$/$. Comparison of the results shows that the relativistic equation should be used for calculating the energies of neutrons

from the $^3T(p,n)^3He$ and $^7Li(p,n)^7Be$ reactions, because if the calculation is done with the non-relativistic or classical approximation there is a difference in neutron energy values of the order of 0.1% which can reach several per cent in the near-threshold proton energy range. This difference is negligible (about 100 eV) for the $^{45}Sc(p,n)^{45}Ti$, $^{51}V(p,n)^{51}Cr$ and $^{65}Cu(p,n)^{65}Zn$ reactions.

A quantitative assessment of the factors responsible for the neutron energy spread was carried out by the method described in Ref. $[5]$. The results of evaluations for neutron escape angles of 0°, 60° and 120° in the laboratory system of co-ordinates are presented in Table 4. The spread in neutron energies, ΔE_1 and ΔE_2, is due to the energy spread in the beam or target and to the Doppler effect, respectively. ΔE_1 was determined from the relation $\Delta E_1 = f(E + \Delta E) - f(E - \Delta E)$, where E is proton energy and ΔE is the proton energy increment, taken to be 0.5 keV. ΔE_2 was calculated from the formula $\Delta E_2 = 2(E_{3\,max} - E_3)$ $[5]$, where $E_{3\,max}$ is the maximum neutron energy allowing for the Doppler effect and E_3 is neutron energy without allowance for the Doppler effect. The values of $\Delta E_2'$ and $\Delta E_2''$ given in Table 4 relate to target temperatures of ~ 20 and $\sim 200^\circ C$ respectively. From Table 4 it is clear that the energy spread of protons in the beam or target has the most significant effect on the energy distribution of the neutrons.

The effect of the uncertainty in the values of Q, conditionally taken to be 1 keV and leading to the uncertainty in the neutron energy values ΔE_3, was estimated from the formulae supplied in Ref. $[6]$. The resulting data are listed in Table 4 and can be used for correcting the neutron energy values in Tables 1, 2 and 3 in the event of more accurate values of Q becoming available. The uncertainty in neutron energy resulting from the uncertainty in the masses is about 0.01‰.

<u>Table 1</u>

Title: Neutron energy T_n (keV) for angle ϑ (degrees) and proton energy T_p (keV) in the laboratory system of co—ordinates

Key:

    МэВ   = MeV
    кэВ   = keV

<u>Table 2</u>

Title: As above.

Key: As above.

<u>Table 3</u>

Title: As above.

Key: As above.

<u>Table 4</u>

No caption.

TABLE 1

Энергия нейтронов T_n (кэв) для угла Θ (град) и энергия протонов T_p (кэв) в лабораторной системе координат

Θ	T_p 1147,4	1150	1155	1160	1165	1170	1175	1180	1185	1190
0	288,19	291,45	297,65	303,81	309,94	316,03	322,09	328,11	334,11	340,08
10	279,50	282,74	288,90	295,02	301,11	307,15	313,17	319,15	325,10	331,03
20	254,47	257,66	263,70	269,71	275,67	281,60	287,49	293,34	299,16	304,96
30	216,13	219,23	225,10	230,92	236,70	242,43	248,12	253,77	259,39	264,97
40	169,11	172,09	177,74	183,33	188,87	194,34	199,77	205,16	210,50	215,80
50	119,06	121,93	127,34	132,66	137,90	143,08	148,19	153,25	158,26	163,23
60	72,04	74,79	79,93	84,95	89,86	94,67	99,41	104,08	108,68	113,23
70	33,71	36,35	41,18	45,80	50,26	54,60	58,84	63,00	67,09	71,11
80	8,69	11,16	15,41	19,32	23,04	26,64	30,15	33,59	36,97	40,31
90		1,30	3,80	6,29	8,78	11,28	13,77	16,27	18,76	21,25
100		0,15	0,94	2,05	3,35	4,77	6,29	7,88	9,52	11,20
110		0,05	0,35	0,86	1,54	2,33	3,22	4,20	5,25	6,35
120		0,02	0,18	0,47	0,86	1,34	1,91	2,54	3,24	3,99
130		0,01	0,11	0,30	0,56	0,89	1,28	1,73	2,22	2,77
140		0,01	0,08	0,22	0,41	0,65	0,95	1,29	1,67	2,09
150		0,01	0,06	0,17	0,33	0,52	0,76	1,04	1,36	1,70
160		0,01	0,05	0,15	0,28	0,45	0,66	0,90	1,18	1,48
170		0,01	0,05	0,13	0,26	0,41	0,61	0,83	1,08	1,36
180		0,01	0,05	0,13	0,25	0,40	0,59	0,81	1,05	1,33

M_p = 938, 25921 Мэв; $M_{тт}$ = 2808, 88257 Мэв : M_n = 939, 55274 Мэв; $M_{не}$ = 2808, 35298 Мэв; Q = - 0,76384 Мэв.

TABLE 2

Энергия нейтронов Тн (кэв) для угла Θ (град) и энергия протонов Тр (кэв) в лабораторной системе координат

Θ \ Тр	1920	1922	1925	1930	1935	1940	1945	1950	1955	1960
0	121,30	124,41	129,00	136,50	143,84	151,03	158,10	165,06	171,93	178,71
10	117,64	120,75	125,33	132,81	140,13	147,30	154,34	161,28	168,11	174,86
20	107,11	110,21	114,76	122,19	129,44	136,54	143,50	150,35	157,10	163,76
30	90,97	94,05	98,56	105,90	113,04	120,01	126,83	133,54	140,14	146,65
40	71,18	74,23	78,68	85,88	92,84	99,62	106,25	112,74	119,12	125,41
50	50,12	53,13	57,50	64,49	71,20	77,70	84,04	90,23	96,31	102,29
60	30,32	33,29	37,52	44,19	50,53	56,63	62,55	68,34	74,01	79,58
70	14,19	17,08	21,05	27,18	32,93	38,46	43,81	49,05	54,18	59,24
80	3,66	6,31	9,72	14,89	19,77	24,49	29,10	33,64	38,12	42,55
90		1,50	3,75	7,49	11,23	14,98	18,72	22,46	26,20	29,95
100		0,36	1,45	3,77	6,38	9,16	12,04	15,00	18,01	21,08
110		0,13	0,67	2,06	3,83	5,83	8,00	10,29	12,67	15,14
120		0,07	0,37	1,27	2,50	3,96	5,60	7,38	9,28	11,27
130		0,04	0,24	0,87	1,77	2,89	4,17	5,59	7,13	8,77
140		0,03	0,18	0,65	1,36	2,25	3,30	4,47	5,76	7,15
150		0,02	0,14	0,53	1,12	1,87	2,76	3,78	4,90	6,12
160		0,02	0,12	0,46	0,97	1,64	2,44	3,36	4,37	5,48
170		0,02	0,11	0,42	0,90	1,52	2,27	3,13	4,08	5,12
180		0,02	0,11	0,41	0,88	1,48	2,22	3,06	3,99	5,02

M_p = 938, 25921 Мэв; M_{T_U} = 6534, 76171 Мэв; M_n = 939, 55274 Мэв; $M_{T_{Be}}$ = 6535, 11530 Мэв;

Q = - 1,64406 Мэв

TABLE 3

Энергия нейтронов T$_n$ (кэв) для угла θ (град) и энергии протонов
T$_p$ (кэв) в лабораторной системе
координат

θ \ T$_p$	0°	10°	20°	30°	40°	50°
2906	5,18	5,01	4,52	3,78	2,86	1,88
2950	60,39	60,06	59,08	57,52	55,46	53,02
3000	115,50	115,06	113,76	111,67	108,88	105,54
3050	168,98	168,45	166,90	164,39	161,03	156,99
3100	221,66	221,06	219,28	216,41	212,57	207,93
3150	273,85	273,18	271,20	268,00	263,72	258,54
3200	325,69	324,96	322,80	319,31	314,62	308,93
3250	377,29	376,50	374,17	370,39	365,32	359,17
3300	428,70	427,86	425,36	421,31	415,88	409,28
3400	531,08	530,14	527,33	522,78	516,66	509,22
1566	3,94	3,87	3,65	3,32	2,90	2,43
1600	43,86	43,68	43,16	42,32	41,21	39,88
1650	97,18	96,92	96,16	94,94	93,30	91,32
1700	149,24	148,93	147,99	146,47	144,42	141,95
1750	200,76	200,39	199,29	197,51	195,13	192,22
1800	251,95	251,53	250,29	248,28	245,58	242,29
1850	302,93	302,46	301,09	298,86	295,87	292,21
1900	353,75	353,25	351,75	349,31	346,04	342,04
1950	404,46	403,91	402,29	399,66	396,12	391,79
2000	455,08	454,49	452,75	449,93	446,13	441,49
2166	3,08	2,96	2,78	2,50	2,15	1,77
2170	8,61	8,53	8,28	7,90	7,40	6,82
2180	20,61	20,49	20,15	19,60	18,88	18,02
2190	31,90	31,76	31,35	30,68	29,80	28,75
2200	42,91	42,75	42,28	41,52	40,51	39,29
2220	64,47	64,28	63,71	62,79	61,56	60,08
2240	85,69	85,47	84,82	83,76	82,35	80,64
2260	106,70	106,45	105,73	104,55	102,98	101,07
2280	127,56	127,29	126,50	125,22	123,50	121,41
2300	148,32	148,03	147,17	145,79	143,93	141,67

(Row labels at left: $^{45}Sc(p,n)^{45}Ti$, $^{51}V(p,n)^{51}Cr$, $^{65}Cu(p,n)^{65}Zn$)

M$_p$ = 938, 25921 Мэв; M$_n$ = 939,55274 Мэв; M$_{45Sc}$ =41875, 5934 Мэв

M$_{45Ti}$= 41877, 1410 Мэв; Q$_{Sc(p,n)}$= -2,841 Мэв; M$_{51V}$ = 47453, 3423 Мэв;.

M$_{51Cr}$= 47453, 5830 Мэв; Q$_{V(p,n)}$= -1,5341 Мэв; M$_{65Cu}$=60479, 0120 Мэв;

M$_{65Zn}$ = 60479, 8500 Мэв; Q$_{Cu(p,n)}$ = -2,1318 Мэв.

TABLE 4

Ep	0°					60°					120°				
	E_n	ΔE_1	$\Delta E_2'$	$\Delta E_2''$	ΔE_3	E_n	ΔE_1	$\Delta E_2'$	E_2''	ΔE_3	E_n	ΔE_1	$\Delta E_2'$	$\Delta E_2''$	ΔE_3
1881	37,87	7,09	1,87	2,40	6,45	0,00	0,00	0,00	0,00	0,00	0,00	0,00	0,00	0,00	0,00
1900	84,47	1,87	0,55	0,70	2,10	0,00	0,00	0,00	0,00	0,00	0,00	0,00	0,00	0,00	0,00
1920	121,24	1,56	0,43	0,56	1,74	30,32	1,52	0,54	0,70	1,74	0,00	0,00	0,00	0,00	0,01
2000	230,52	1,25	0,31	0,40	1,39	121,95	1,02	0,36	0,46	1,17	29,42	0,49	0,21	0,27	0,58
2500	786,65	1,06	0,19	0,24	1,13	586,38	0,90	0,33	0,42	1,00	321,61	0,62	0,34	0,44	0,74
1020	75,74	7,20	2,34	2,99	8,36	0,00	0,00	0,00	0,00	0,00	0,00	0,00	0,00	0,00	0,00
1160	303,77	1,22	0,29	0,36	1,47	84,95	0,99	0,50	0,65	1,39	0,47	0,07	0,03	0,06	0,10
1200	351,90	1,18	0,26	0,33	1,39	122,20	0,89	0,44	0,56	1,23	5,64	0,17	0,11	0,14	0,27
2000	1202,50	1,02	0,13	0,17	1,11	727,61	0,72	0,43	0,55	0,95	246,65	0,34	0,33	0,42	0,55
2500	1711,32	1,01	0,11	0,14	1,08	1098,02	0,72	0,47	0,60	0,92	418,49	0,34	0,42	0,53	0,57
2908	8,67	1,60	0,25	0,32	1,62	4,10	1,35	0,22	0,28	1,37	0,71	0,56	0,10	0,12	0,58
2910	11,72	1,46	0,23	0,29	1,49	6,68	1,23	0,20	0,26	1,26	1,96	0,70	0,11	0,14	0,69
3000	115,49	1,08	0,15	0,19	1,10	101,79	1,02	0,16	0,21	1,04	79,00	0,89	0,16	0,21	0,92
1568	6,83	1,36	0,14	0,18	1,46	4,46	1,16	0,13	0,17	1,24	1,81	0,75	0,09	0,11	0,72
1600	43,85	1,10	0,10	0,13	1,11	38,38	1,03	0,11	0,14	1,05	29,37	0,89	0,11	0,14	0,92
1700	149,24	1,04	0,09	0,11	1,05	139,13	1,00	0,10	0,13	1,02	120,90	1,12	0,13	0,16	0,95
2167	4,56	1,47	0,16	0,21	1,52	2,73	1,25	0,14	0,18	1,30	0,69	0,69	0,08	0,11	0,67
2168	5,97	1,38	0,15	0,20	1,39	3,89	1,19	0,14	0,17	1,20	1,59	0,75	0,09	0,12	0,77
2190	31,90	1,11	0,12	0,15	1,13	27,57	1,04	0,12	0,15	1,06	20,57	0,90	0,11	0,14	0,91

Row group labels (left margin, rotated): $^7Li(p,n)^7Be$; $^3T(p,n)^3He$; $^{55}Sc...$; $^{...}V(p,n)^{...}Cr$; $^{63}Cu(p,n)^{63}Zn$

REFERENCES

[1] McKIBBEN, J.L., Phys. Rev., 70 (1946) 101.

[2] HANSON, O.A., TASCHEK, R.F., WILLIAMS, J.H., Rev. Mod. Phys. 21 (1949) 635.

[3] LANGSDORF, A.S., MONAHAN, J.E., REARDON, W.A., Argonne Nat. Lab. Report ANL-5219 (1954).

[4] FOWLER, J.L., BROLLEY, J.E., Rev. Mod. Phys., 28 (1956) 103.

[5] MONAGHAN, J., in Fizika bystryh nejtronov (Fast neutron physics) (MARION, J., FOWLER, J., Eds) Atomizdat, Moscow (1963).

[6] MARION, J., in Fizika bystryh nejtronov (Fast neutron physics) (MARION, J., FOWLER, J., Eds) Atomizdat, Moscow (1963).

[7] GIBBONS, J., NEWSON, G., in Fizika bystryh nejtronov (Fast neutron physics) (MARION, J., FOWLER, J., Eds) Atomizdat, Moscow (1963).

[8] COPPOLA, M., KNITTER, H.H., Kerntechnik, 10 (1967) 459.

[9] WINTER, J., Nucl. Instrum. Meth. 59 (1968) 167.

[10] TAYLOR, B.N., PARKER, W.H., LANGENBERG, D.N., Rev. Mod. Phys., 41 (1969) 375.

[11] MATTAUCH, J.H.E., THIELE, W., WAPSTRA, A.H., Nucl. Phys., 67, 1 (1965).

RECOIL PROTON SPECTRA IN A HYDROGEN-FILLED
PROPORTIONAL COUNTER

A.N. Davletshin, V.A. Tolstikov

Measurement of monoenergetic neutron fluxes by the recoil proton method
involves determining the quantity N_{int}, the number of interactions of incident
neutrons with a known number of hydrogen nuclei. The recoil protons arising
from elastic scattering of neutrons by hydrogen nuclei have a rectangular
energy spectrum in the range $0-E_n$, where E_n is the incident neutron energy.
Since the detector recording the recoil proton energy has finite geometry
and the electronic equipment has a certain energy threshold, it is not
possible to measure the recoil proton energy spectrum without distortion.
For this reason N_{int} can be determined only by comparing experimental results
with a theoretical recoil proton spectrum. The accuracy of the value of
N_{int} obtained in this way depends upon how well the experimental conditions
are allowed for in the calculations.

Figure 1 shows a typical experimental set up for measuring a mono-
energetic neutron flux. A proportional counter filled with hydrogenous gas
is irradiated by a plane-parallel neutron beam. It is assumed that the
ionization produced by a recoil proton in the gas of the counter is proportional
to the energy lost. The differential spectrum of the recoil proton energy
losses (hereafter called recoil proton spectrum) is determined experimentally
in the sensitive volume of the counter. The shape of this spectrum is
governed both by the recoil protons produced in the sensitive volume of the
counter with length H and diameter 2R and by the protons escaping from the
insensitive volume at the front with a length equal to the maximum range of
a recoil proton, i.e. of a proton with energy $E_p = E_n$. Some recoil protons
will lose part of their energy in the wall of the counter or in the gas
outside the sensitive volume.

Thus, the problem is to calculate the differential recoil proton
spectrum $\varphi(x)$ formed in the counter and the quantity K_H, which will enable
us to determine the spectrum of recoil protons produced in the sensitive
volume of the counter, for which the number of hydrogen nuclei is known.
Here and below $x = E_p/E_n$, i.e. the recoil proton energy in incident neutron
energy units, whilst the index 1 denotes normalization to 1.

Clearly,

$$K_H = 1 + \frac{N_1}{N_V} \tag{1}$$

where N_1 is the number of tracks of recoil protons escaping from region 1 (Fig. 1) in the sensitive volume and N_V is the number of tracks of recoil protons formed in the sensitive volume (regions 2, 3 and 4).

We can then write

$$N_{int} = \frac{N_{cou}(x)}{\varepsilon_V(x)} \tag{2}$$

where $N_{cou}(x)$ is the number of recoil protons recorded with energy $> x$;

$$\varepsilon_V(x) = K_H \cdot \varepsilon_1(x) \tag{3}$$

$$\varepsilon_1(x) = \int_x^1 Q_1(x)\,dx \tag{4}$$

Several publications describe the results of calculations of $Q_V(x) = K_H \cdot Q_1(x)$ performed by the analytical method $\underline{/}$1-3$\underline{/}$ and the Monte Carlo method $\underline{/}$4$\underline{/}$. All these calculations were done on the following assumptions:

(1) Neutron trajectories parallel to counter axis;

(2) Interaction density constant over counter volume.

The range-energy relationship is given either in the form of a table of average ranges $\underline{/}$2, 4$\underline{/}$ or by the approximate formula $R = c \times E^{3/2}$, where c is a constant $\underline{/}$1, 3$\underline{/}$. The calculations performed by the analytical method are notable for the limitations imposed on the maximum range of recoil protons; the most rigorous limitations are imposed in Refs $\underline{/}$1, 2$\underline{/}$, which have $R(E_n) < 2R$, whilst Ref. $\underline{/}$3$\underline{/}$ has $R(E_n) \leqslant 6R$. These calculations will be compared below.

In order to increase the accuracy of neutron flux measurements, it is necessary to calculate recoil proton spectra with more careful allowance for the conditions under which they are recorded. This makes it possible to assess the quality of data from earlier calculations as well as their range of applicability – and hence the reliability of cross-sections obtained with them.

The recoil proton spectra were calculated here on the following assumptions:

(1) Neutron trajectories parallel to counter axis;

(2) Density of interactions between neutrons and hydrogen nuclei in the sensitive volume of the counter inversely proportional to $(R_u + Z)^2$, where R_u is the distance from the neutron source to the point $Z = 0$ with Z varying in the range $0-H+q$ (Fig. 1);

(3) Incident neutron energy equally distributed over the range from $E_n - \Delta E$ to $E_n + \Delta E$;

(4) The energy recorded by the counter is a random value distributed according to the normal law with parameters EQ and $\sigma(EQ)$, where EQ is the energy lost by a recoil proton in the sensitive volume, calculated on the basis of the geometrical conditions of track formation and the range—energy relationship:

$\sigma(EQ) = \dfrac{\eta(E_p)}{2.36} \cdot Ep.$ It was assumed also that the dependence of the counter resolution on recoil proton energy $\eta(E_p)$ is described by the formula

$$\eta(E_p) = \frac{A}{\sqrt{E_p}} \qquad (5)$$

where the constant A is determined by experiment.

The calculation was done by the Monte Carlo method.   The programme was compiled so that by appropriate selection of the values of R_u, ΔE and A it would be possible to exclude the effect of any one of these factors on the results of the calculation.   Likewise, it is possible to analyse separately the effect of any of assumptions Nos 2-4 on the shape of the calculated spectrum.   In particular, by putting $R_u = \infty$, $\Delta E = 0$ and $A = 0$, we obtain a recoil proton spectrum calculated on the same assumptions as in Refs $\boxed{1-4\,}$.

Fig. 2 shows the recoil proton spectra, $\varrho_v(x)$, calculated by the methods described in Refs $\boxed{1-3\,}$ and with our programme using the Monte Carlo method (this of course agrees with the calculation performed with the programme described in Ref. $\boxed{4\,}$).   On the whole the spectra are in quite good agreement except for the earlier work $\boxed{1\,}$.   If we take as our standard the

spectrum calculated by the Monte Carlo method, the spectrum calculated according to Ref. $\boxed{2}$ is lower in the centre and higher at the ends than the Monte Carlo spectrum. With the spectrum calculated by the method described in Ref. $\boxed{3}$ we find the reverse situation.

A more accurate impression of the differences between these calculations is gained by comparing $\varepsilon_v(x)$ for the different spectra. These quantities and their values in relation to $\varepsilon_v(0.6)$ for the Monte Carlo spectrum are given in the table: also given are the corresponding values of K_H and $\varepsilon_1(0.6)$.

Thus we can see from the foregoing discussion that the differences in $\varepsilon_v(x)$ calculated by the various methods depend both on the shape of the spectrum (the trend of $\varepsilon_1(x)$) and on K_H. The closer the calculation conditions are to the limitations imposed on a particular analytical method, the more the shape of the "analytical" spectrum obtained by that method will differ from the Monte Carlo spectrum. The difference in the values of K_H largely depends on the form of the range-energy relationship used in the calculation. Since an experimental range-energy relationship was used in Ref. $\boxed{2}$ and an approximate empirical formula $R(E) = c \times E_p^n$ where $n = 3/2$ in Ref. $\boxed{3}$, we may expect that the K_H calculated in Ref. $\boxed{3}$ will be higher than the true values, since $n \sim 1$ for low energy protons entering the sensitive volume of the counter from the frontal volume. These conclusions are confirmed by the results shown in the table. The calculation conditions are close to the limit for Ref. $\boxed{2}$; accordingly the essential difference in $\varepsilon_v(x)$ is attributable to the difference in $\varepsilon_1(x)$, and the values of K_H are approximately the same. For the counter involved (see caption to Fig. 2) the calculation of the spectrum at $E_n = 900$ keV will be the limiting case for the method according to Ref. $\boxed{3}$, and the following results are obtained: $\varepsilon_1(0.6) = 0.1077$, $K_H = 1.140$. Calculation by the Monte Carlo method gives $\varepsilon_1(0.6) = 0.0874$, $K_H = 1.069$. In this case the difference in $\varepsilon_v(x)$ is due to the significant difference in the values of $\varepsilon_1(x)$ and K_H.

Thus, the analytical methods of calculating recoil proton spectra described in Refs $\boxed{2, 3}$ give approximately equal results for conditions not close to the limitations imposed. But, since the limitations imposed in Ref. $\boxed{3}$ are less rigorous and the results are obtained in the form of an analytical formula and not as tables, as in Ref. $\boxed{2}$, they should be preferred in cases where the experimental conditions approximate the assumptions made in the calculation.

As remarked above, our programme enables spectra to be calculated with more detailed allowance for experimental conditions. Fig. 3 shows the results of calculating a recoil proton spectrum, $\varrho_1(x)$, with allowance for the point neutron source, the spread of incident neutron energy around the mean value and the energy resolution of the proportional counter. For comparison Fig. 3 also shows a spectrum calculated with the same assumptions as in Ref. $\underline{/4\underline{/}}$. Calculations with separate allowance for each of the above factors show that the differences in the spectra for $x < \dfrac{E_n - \Delta E}{E_n}$ or $x < \dfrac{E_n - 3\sigma(E_n)}{E_n}$ are caused by variations in the density of the interactions in the sensitive volume of the counter. Thus, if the experiment and the corresponding calculation are performed in conditions where R_u does not satisfy the condition $R_u \gg H$, the results of the calculation will differ greatly from the case where $R_u = \infty$. For $R_u = \infty$ we have $\varepsilon_1(0.6) = 0.265$; $K_H = 1.040$, and for $R_u = 6$ cm, $\varepsilon_1(0.6) = 0.284$, $K_H = 1.297$. The corresponding difference in the values of N_{int} is 25%. If $R_u \gg H$, the spectra will coincide at the recoil proton energies indicated above and the N_{int} calculated from them will agree to within the limits of error.

It is well known that for the kind of target normally used the neutron energy spread is comparable with the mean energy at neutron energies below 100 keV; moreover, the resolution of the proportional counter at such recoil proton energies has a strong effect on the spectrum shape. Under these experimental conditions the polychromaticity of the neutron source and the counter resolution will affect the shape of the recoil proton spectrum over the whole recoil proton energy range. Therefore, these factors must be allowed for in the calculation of the spectra if distortion is to be avoided. But it should be remembered that in this energy range there will be a greater error in the calculation than at energies above 100 keV, since the range-energy relationship and the dependence of the resolution on proton energy are less accurately known.

Method of calculation	$\varepsilon_v(0.6)$	Rel. value $\varepsilon_v(0.6)$	Standardization coeff. K_H	$\varepsilon_1(0.6)$
$\underline{/1\underline{/}}$	0.322	1.16	1.045	0.308
$\underline{/2\underline{/}}$	0.263	0.95	1.045	0.252
$\underline{/3\underline{/}}$	0.278	1.01	1.049	0.265
Monte Carlo	0.276	1	1.040	0.266

REFERENCES

[1]   ROSSI, B.B., STAUB, H.H., Ionization chambers and counters, 1949.

[2]   SKYRME, T.H.R., TUNNIDIFFE, P.R., WARD, A.C., Rev. Scien. Instrum. 22, 2 5/1959, 204–209.

[3]   REMBSER, J., Nucleonik, 1, 5, 4/1959, 167–171.

[4]   PARKER, J.B., WHITE, P.H., WEBSTER, R.J., Nucl. Instrum. Meth., 23, 1, 5/1963, 61–68.
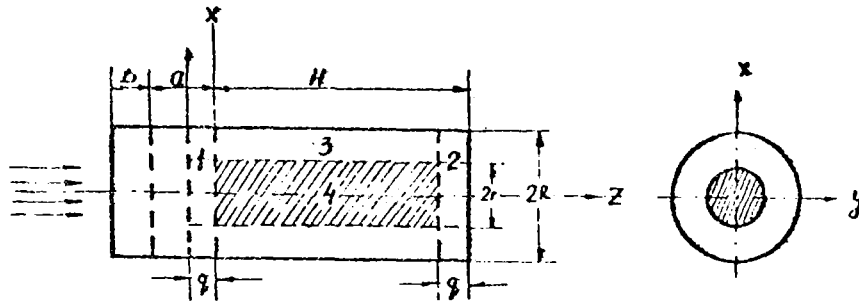
<u>Fig. 1</u>   Scheme of cylindrical recoil proton counter

<u>Fig. 2</u>   Recoil proton spectra calculated by various

methods (counter filled with hydrogen)

E_n = 500 keV, H = 21 cm, R = 1.55 cm,

p = 1 atm.abs., R (500 keV) = 3.05 cm,

1 - $\boxed{3}$, 2 - Monte Carlo method,

3 - $\boxed{2}$, 4 - $\boxed{1}$.
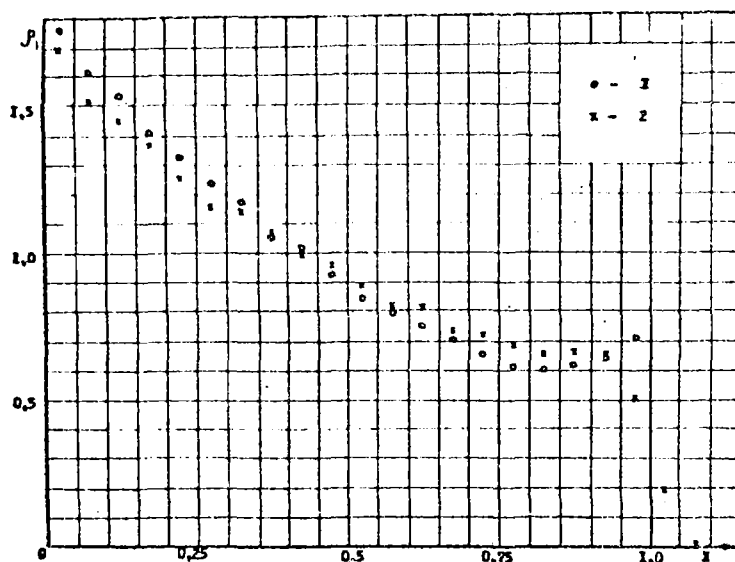
Fig. 3. Differential recoil proton spectra calculated
by the Monte Carlo method (counter filled with
hydrogen)

E_n = 500 keV, H = 21 cm, R = 1.55 cm,

p = 1 atm.abs., R (500 keV) = 3.05 cm,

1 - R_u = ∞ , ΔE = 0, A = 0($\eta(E_p)$ = 0),

2 - R_u = 6 cm, ΔE = 25 keV, $\eta(E_p$ = 764 keV) = 4.5%

MAXIMUM RESOLVING POWER OF IONIZING RADIATION DETECTORS

I.V. Gordeev, Yu.S. Gerasimov, V.A. Koshelev

In order to assess the maximum resolving power of various types of ionizing radiation detectors, it is necessary to know the Fano factor $\boxed{1, 2}$. The Fano factor may be written

$$F = \frac{<(I-\bar{I})^2>}{\bar{I}} ,$$

where quantum-mechanical and statistical averaging is performed (I is ionization in each collision event).

To obtain a correct result, it is necessary to know the cross-sections of all processes occurring when a particle passes through a substance (ionization, excitation, charge exchange, elastic scattering) as well as the energy transmitted in each collision event (the energy transmitted and the square of the energy transmitted averaged over the cross-section of a given process).

We calculated the Fano factor for the scattering of hydrogen protons and atoms by hydrogen atoms. For these processes the calculation is simple and reliable and is of practical value for investigations of neutrons passing through organic substances and biological tissues and also for work involving hydrogen-filled chambers. The results show that the Fano factor for the passage of heavy particles through a substance may considerably exceed the Fano factor for the passage of electrons through the same substance . The higher the ratio of the mass of the incident particle to the mass of an atom of the substance, the higher the Fano factor. This "unusual" result is largely due to the contribution of elastic scattering to the Fano factor. This contribution is negligible for electron scattering but is considerable when heavy particles are involved.

At comparatively low energies an appreciable contribution is also made by the charge exchange process. Consequently the resolving power of an instrument may be considerably lower in the case of ionization caused by heavy particles than it is in the case of ionization caused by electrons.

The contribution due to elastic scattering and ionization was calculated theoretically in the Boron approximation, which is valid at proton energies above 25 keV. This was done because there is still an almost complete lack of data on the cross-sections for elastic scattering by hydrogen and on the energy distribution of secondary electrons formed as a result of ionization.

Mainly experimental data were used for the remaining processes, supplemented where necessary by theoretical data.

The results of the calculations are given in the form of tables and graphs. Stopping powers and ion-formation energies $\mathcal{E}$ were also calculated.

REFERENCES

[1]   FANO, U., Phys. Rev., 72 (1947) 26.

[2]   DIRNLEY, D., NORTHROP, D., Poluprovodnikovye sčetčiki jadernyh izlučenij (Semiconductor radiation counters) Mir Press, Moscow (1966).

Table 1

Mean energy of ion-formation during passage of electrons and
protons through helium

	I	1,055	1,217	1,27	1,35	1,4142	1,49	1,72	1,922	2,008	2,46	2,84	4,48	6,35
E_e(eV)	13,5	15	20	21,8	24,5	27,2	30	40	50	54,5	81,7	108	272	544,6
E_p(keV)	25	27,5	36,7	40	43,9	50	55,1	73,4	91,8	100	150	200	500	1000
	-	-	-	-		62,4	49,8	29,1	32,4	34,6	37,3	40,1	42,1	42,2
	27,9	26,7	28,2	28,5	28,9	29,3	29,6	30,2	31,4	32,3	37,8	39,2	41,5	41,7

$^v\!/v_o$ is the ratio of the incident particle velocity to the velocity of a Bohr
electron, $v_o = 2.1877 \times 10^8$ cm/sec.

E_e is the incident electron energy in eV; E_p is the incident proton energy
in keV.

ω_e and ω_p are the differential energies of ion-formation for incident electrons
and protons respectively, expressed in eV per ion pair.

Table 2

Differential Fano factor, F_{dif}, for passage of electrons and protons through helium

v/v_0	0,448	0,635	0,778	0,896	I	1,22	1,27	1,36	1,414	1,49	1,92	2,008	3,17	4,48	5,31	6,35
E_e (eV)	–	–	–	–	–	–	–	25	27,32	30	50	54,46	136,1	272,3	381,2	544,6
E_p (keV)	5	I0	I5	20	25	36,72	40	45,9	50	55,08	9I,8	I00	250	500	700	I000
(diff.)	0,44	0,52	0,57	0,53	0,5	0,45	0,415	0,38	0,27	0,26	0,31	0,35	0,62	0,71	0,75	0,8
(diff.)	–	–	–	–	–	–	–	I	0,82	0,53	0,25	0,31	0,32	0,35	0,38	0,4
	–	–	–	–	–	–	–	0,38	0,33	0,49	I,2I	I,13	I,94	2,03	I,97	2,0

v/v_0, E_e and E_p are the same as in Table 1.

F_e and F_p are the differential Fano factors for incident electrons and protons respectively (dimensionless quantities)

ACTIVATION DETECTORS FOR NEUTRON DETECTION
(Review)

R.D. Vasilev, E.A. Grigorev, V.P. Yaryna

In the All-Union Scientific Research Institute for Physico-Technical and Radiotechnical Measurements a programme has started to select, process and standardize nuclear physics constants for measurements of neutron field characteristics by the activation method. This survey, which marks the first step towards fulfilling this task, is devoted to selecting the most up-to-date data on isotopes widely used for neutron-activation measurements, and is designed to supplement and improve on earlier surveys $\llbracket 7$, 16, 27, 29, 49, 50 $\rrbracket$.

1. Resonance detectors

Table 1 contains a list of isotopes suitable for use as resonance detectors for neutrons on the basis of the (n,γ) reaction. Columns 2-4 of the table show the chemical symbol of the isotope, its percentage concentration in the natural mixture and the activation reaction. Data on the use of these reactions for recording neutrons are contained in Refs $\llbracket 3$, 7, 16, 17, 19, 29, 60 $\rrbracket$; in particular, for ^{164}Dy and ^{37}Cl, see Ref. $\llbracket 27 \rrbracket$, for P see Ref. $\llbracket 55 \rrbracket$, for Lu see Ref. $\llbracket 31 \rrbracket$, for Rh see Ref. $\llbracket 23 \rrbracket$, for ^{50}Cr see Ref. $\llbracket 26 \rrbracket$ and for ^{63}Cu and F see Ref. $\llbracket 25 \rrbracket$. $T_{\frac{1}{2}}$ (col. 5) is the half-life of the product nucleus resulting from the activation reaction. The half-life data are taken mainly from Refs $\llbracket 8$, 15 $\rrbracket$; otherwise the source is indicated beside the half-life in the table. $\lambda \llbracket sec^{-1} \rrbracket$ is the decay constant, calculated from the half-life (in seconds) with the formula

$$\lambda = \frac{0.693}{T_{\frac{1}{2}}} \tag{1}$$

$E_0 \llbracket eV \rrbracket$ (col. 6) is the energy of the fundamental resonance of the reaction. For ^{164}Dy and ^{31}P the first resonance of the activation reaction lies above 100 keV, so they may be used as detectors with a cross-section subject to the $1/v$ law. The data are taken mainly from Refs $\llbracket 1$, 2, 16 $\rrbracket$.

σ_{act} is the cross-section for the (n,γ) reaction induced by thermal neutrons. The data are taken mainly from Ref. $\llbracket 1 \rrbracket$.

$J_R \llbracket barns \rrbracket$ (col. 8) is the resonance integral of the activation reaction determined by the formula

$$J_R = \int_{0.55}^{\infty} \sigma(E)\frac{dE}{E} \tag{2}$$

The data were selected from Refs $\boxed{16, 18, 22, 23, 27, 29, 30\_}$; the resonance integral of the $^{197}Au(n,\gamma)$ reaction (1550 b) was taken as the standard.

E_β MeV (%) (col. 9) is the beta particle energy from decay of the radioactive product; the figure in brackets shows the external yield of particles with that energy as a percentage of the number of disintegrations.

E_γ MeV(%) (col. 10) is the gamma energy and the external yield of gamma rays with that energy as a percentage of the number of disintegrations. The decay data were selected from Refs $\boxed{3, 5, 7, 8, 10, 12, 14, 15\_}$.

Information on associated reactions occurring simultaneously with the basic reaction in detectors consisting of natural isotopic mixtures is given in column 11. This column also indicates certain decay characteristics as well as the thermal neutron reaction cross-section or the resonance integral.

2. Resonance parameters

Table 2 contains information on the parameters of the fundamental and neighbouring resonances for the most widely used detectors. Columns 2 and 3 show the chemical symbol of the isotope-detector and E_R (eV) — the energies of the fundamental (see column 6, Table 1) and neighbouring resonances of the (n,γ) reaction. Column 4 shows the spin of the ground state of the target nucleus (I) and column 5 shows the total momentum of the compound nucleus (J). Sufficient data are supplied for calculating the statistical factor g:

$$g = \frac{2J+1}{2(2I+1)} \tag{3}$$

Γ, eV (col. 6) is the total resonance width, Γ_γ, eV (col. 7) the width for gamma-ray escape, Γ_n, eV (col. 8) the width for neutron escape, and σ_0, barn (col. 9) the experimentally measured total cross-section at the resonance.

The table was compiled mainly on the basis of data from Ref. $\boxed{1\_}$. In the case of ^{197}Au a careful analysis of the contributions made by the various resonances to the activation process has been performed by Brisbois $\boxed{38\_}$. The diversity of the data on Γ_γ for ^{23}Na has been

analysed in Ref. $\boxed{35\_}$. The first reliable data on Γ_n for ^{37}Cl are given in Ref. $\boxed{40\_}$. The data on Γ_γ for ^{37}Cl are very approximate $\boxed{28\_}$, although it had already been concluded in Ref. $\boxed{3\_}$ that the 25.5 keV resonance made the primary contribution to activation. The bibliography includes references to investigations of the resonances of Rh $\boxed{41\_}$; ^{63}Cu and ^{65}Cu $\boxed{34\_}$; Mg, Fe and S $\boxed{36\_}$; and Dy $\boxed{37\_}$.

3. Threshold detectors

Table 3 contains a list of isotopes used as fast neutron detectors on the basis of threshold reactions of the (n,f), (n,n'), (n,p), (n,α) and $(n,2n)$ types.

Columns 2-4 show the chemical symbol of the isotope, its percentage concentration in the natural mixture and the activation reaction.

Data on the use of these reactions for recording neutrons are contained in Refs $\boxed{45, 49, 50, 52, 54, 57\_}$ for ^{115}In, ^{32}S, ^{58}Ni, ^{24}Mg, ^{27}Al, ^{56}Fe, ^{31}P and ^{64}Zn, in Refs $\boxed{49, 51\_}$ for ^{237}Np, ^{232}Th and ^{238}U, in Refs $\boxed{26, 53, 70\_}$ for ^{54}Fe, in Ref. $\boxed{55\_}$ for ^{103}Rh, in Refs $\boxed{52, 57, 63\_}$ for Ti, in Refs $\boxed{56, 62\_}$ for ^{35}Cl, in Ref. $\boxed{45\_}$ for ^{28}Si, in Ref. $\boxed{57\_}$ for ^{63}Cu, in Ref. $\boxed{50\_}$ for ^{65}Cu and in Ref. $\boxed{45\_}$ for F and I.

$T_{\frac{1}{2}}$ (col. 5) is the half-life of the product nucleus resulting from the activation reaction. The data are taken mainly from Refs $\boxed{8\text{-}15\_}$.

$\lambda \boxed{\text{sec}^{-1}\_}$ is the decay constant calculated from the half-life in seconds using formula (1).

E_{eff}, MeV (col. 6) and σ_{eff}, mbarn (col. 7) are the effective reaction threshold and the effective cross-section at the threshold, which are related by the expression

$$\int_0^\infty \sigma(E)\varphi(E)dE = \sigma_{eff}\int_{E_{eff}}^\infty \varphi(E)dE \tag{4}$$

where $\sigma(E)$ is the activation cross-section and $\varphi(E)$ is the differential neutron spectrum.

The shape of the neutron spectrum and the criteria for choosing E_{eff} and σ_{eff} are described in the original sources and will not be repeated here; all the recommended values of E_{eff} and σ_{eff} satisfy the ^{235}U fission spectrum with an error not exceeding 10%. The source from which the values of E_{eff} and σ_{eff} were derived is indicated in the table. $\bar\sigma$ mbarn (col. 8) is the mean cross-section in the fission spectrum, determined by the relation

$$\int_0^\infty \sigma(E)\varphi(E)dE = \overline{\sigma} \int_0^\infty \varphi(E)dE \qquad (5)$$

E_β,MeV (%) (col. 9) is the beta particle energy from decay of the radioactive product; the external yield of particles with that energy is shown in brackets as a percentage of the number of disintegrations.

E_γ,MeV (%) (col. 10) is the energy and external yield of gamma rays as a percentage of the number of disintegrations. The decay data were derived from Refs $\underline{/}$3, 5, 7, 8, 10, 12, 14, 15$\underline{/}$.

Information on the associated reactions occurring simultaneously with the basic reaction in detectors consisting of the natural isotopic mixtures is given in column 11.

Column 12 gives the reference from which the energy dependence of the activation reaction cross-section is taken.

REFERENCES

General

$\underline{/}$1$\underline{/}$ Neutron cross-sections, BNL-325, Suppl. 2 (1966).

$\underline{/}$2$\underline{/}$ GORDEEV, I.V. et al., Jaderno Fiziŝeskie konstanty (Nuclear physics constants) Gosatomizdat (1963).

$\underline{/}$3$\underline{/}$ BECKURTS, K., WIRTZ, K., Nejtronnaja Fizika (Neutron physics) Atomizdat (1968).

$\underline{/}$4$\underline{/}$ MARION, J., FOWLER, J., Fizika bystryh nejtronov (Fast neutron physics), 1, 2, Gosatomizdat (1963), Atomizdat (1966).

$\underline{/}$5$\underline{/}$ ALIEV, A.I. et al., Jaderno-fiziŝeskie konstanty dlja nejtronnogo activacionnogo analiza (Nuclear physics constants for neutron activation analysis) Handbook, Atomizdat (1969).

$\underline{/}$6$\underline{/}$ BOWENS, G., GIBBONS, D., Radioactivacionnyj analiz (Radioactivation analysis) Atomizdat (1968).

$\underline{/}$7$\underline{/}$ LAMBERIEUX, J., in Neutron dosimetry (Proc. Symp. Harwell, 1962) 2 IAEA Vienna (1963) 157.

Decay of radioactive nuclei

$\underline{/}$8$\underline{/}$ DZHELEPOV, B.S., PEKER, L.K., Shemy raspada radioaktivnyh jader (Decay schemes of radioactive nuclei) Nauka Press (1966).

$\underline{/}$9$\underline{/}$ SALMAN, L., Gamma-ray spectroscopy applied to radioactive analysis, AERE (1959).

_/10_/   GUSEV, N.G. et al., Radioaktivnye izotopy kak gamma-izlučateli (Radioactive isotopes as gamma emitters) Atomizdat (1964).

_/11_/   STROMINGER, D. et al., Table of isotopes, Rev. Mod. Phys., 30, (1963) 585-940.

_/12_/   SHUMAN, R., EANDC(US)111 (1968) 68.

_/13_/   EIDENS, J., et al., EANDC(E)115 (1968) 50-57.

_/14_/   Set of calibrated solid gamma sources, Recommended nuclear data, IAEA, Vienna (1969).

_/15_/   LEDERER, C., HOLLANDER, J., PELMAN, J., Table of isotopes, Sixth Edition, N-Y, Wiley (1967).

Thermal activation
Resonance integral

_/16_/   STANFORD, G., PWR React. Technol. 9 (1966) 2.

_/17_/   FASTRUP, B., OLSEN, J., in Neutron dosimetry (Proc. Symp. Harwell, 1962) 1, IAEA Vienna (1963) 227.

_/18_/   DRAKE, M., Nucleonics, 24, 8 (1966) 108-111.

_/19_/   STARODUBTSEV, S.V., WEINSTEIN, G.N., Dozimetrija intensivnyh potokov ioniŝirujuŝĉih izlučenij (Dosimetry of intensive sources of ionizing radiation) FAN, Tashkent (1969) 87.

_/20_/   GOLUBEV, V.I. et al., Atomn. Energ. 2 6 (1961) 522.

_/21_/   FABRY, A. et al., EANDC(E)115 (1968) 196.

_/22_/   SHER, R., Neutron cross-section and technology, 1 Washington (1968) 257.

_/23_/   SHNEIDER, E., EANDC(E)89, (1968) 43.

_/24_/   CRANSTON, F. et al., EANDC(US)91 (1966) 82.

_/25_/   KONIJN, J., in Neutron Dosimetry (Proc. Symp. Harwell, 1962) 1, IAEA, Vienna (1963) 425.

_/26_/   MOTEFF, J., in Neutron Dosimetry (Proc. Symp. Harwell, 1962) 1, IAEA, Vienna (1963) 461.

_/27_/   AVAEV, V.N., EGOROV, Yu.A., Voprosy dozimetrii i zaŝĉity ot izlučenija (Questions of dosimetry and radiation protection) 4 Atomizdat (1965).

/28_7   TROSHIN, V.S., Dissertation, Moscow Engineering Physics Institute
         (1970).

/29_7   SCHUMANN, P., ALBERT, D., Kernenergie 8 2 (1965) 88.

/30_7   KÖHLER, W. et al., ATKE, 11-55 (1966) 321.

/31_7   CHIDLEY, B. et al., Nuclear Sci. Eng., 16 (1963) 39.

/32_7   KORPIUM, P., et al., BNL-719 (1962) 401.

/33_7   BRUNNER, J., WIDDER, F., Nuclear data for reactors, 1, IAEA,
         Vienna (1967) 61.

Resonance parameters

/34_7   ALVES, R. et al., EANDC(E)89 (1968) 210.

/35_7   FRIESENHAHN, S. et al., Neutron cross-section and technology,
         2, Washington (1968) 695.

/36_7   TATARZUK, J. et al., EANDC(US)191 (1968) 153.

/37_7   VERTEBNY, V.P., Bjul. inf. Centr jad. Dannym, Issue No. 4 (1967) 7.

/38_7   BRISBOIS, J., in Neutron Dosimetry (Proc. Symp. Harwell, 1962)
         I, IAEA, Vienna (1963) 181.

/39_7   HOCKENBURY, R., Phys. Rev., 178 (1969) 1746.

/40_7   MORGENSTERN, J., Nucl. Phys., A123, 3 (1969) 561

/41_7   KING, T., BLOCK, R., EANDC(US)105 (1968) 122.

/42_7   ZAKHAROVA, S., MALYSHEV, A., Bjul. inf. Centr jad. Dannym, Issue No. 1
         (1964) 18.

/43_7   ABAGYAN, L.P., ZAKHAROVA, S., Bjul. inf. Centr jad. Dannym, Issue
         No. 2 (1965) 167.

/44_7   ABAGYAN, L.P., ZAKHAROVA, S., Bjul. inf. Centr jad. Dannym, Issue
         No. 4 (1967) 234.

/45_7   KORMUSHKIN, Yu. et al., Bjul. inf. Centr jad. Dannym, Issue No. 4
         (1967) 286.

/46_7   SLUCHEVSKAYA, V., Bjul. inf. Centr jad. Dannym, Issue No. 4 (1967) 112.

/47_7   SLUCHEVSKAYA, V., Bjul. inf. Centr jad. Dannym, Issue No. 5 (1968) 81.

/48_7   BORISOV, G. et al., Rekomendacii po vyboru effektivnyh porogov i
         sečenij (Recommendations on the choice of effective thresholds and
         cross-sections) Izmeritelnaja tehnika, in press.

/49_7   ROMANKO, J., DUNGAN, W., Neutron dosimetry, 1, IAEA, Vienna (1963) 153.

/50_7   GROSS, W., in Neutron Dosimetry (Proc. Symp. Harwell, 1962) 1,
         IAEA, Vienna (1963) 389.

/51_7   BRESESTI, et al., Neutron Dosimetry (Proc. Symp. Harwell, 1962) 1
         IAEA, Vienna (1963) 27.

/52_7   ZIJP, W.L., in Neutron Dosimetry (Proc. Symp. Harwell, 1962), 1
         IAEA, Vienna (1963) 589.

/53_7   PASSELL, T.O., in Neutron Dosimetry (Proc. Symp. Harwell, 1962) 1
         IAEA, Vienna (1963) 501.

/54_7   DIERCKX, R., in Neutron Dosimetry (Proc. Symp. Harwell, 1962) 1
         IAEA, Vienna (1963) 330.

/55_7   TREBILCOCK, R.J., in Neutron Dosimetry (Proc. Symp. Harwell, 1962) 1
         IAEA, Vienna (1963) 565.

/56_7   CASARELLI, G., in Neutron Dosimetry (Proc. Symp. Harwell, 1962) 2
         IAEA, Vienna (1963) 41.

/57_7   NILSSON, R., in Neutron Dosimetry (Proc. Symp. Harwell, 1962) 2
         IAEA, Vienna (1963) 276.

/58_7   MENLOVE,H. et al., EANDC(US)91 (1966) 102.

/59_7   BORMAN, M., LAMERS, B., EANDC(E)115 (1966) 69.

/60_7   DILG, W., VONACH, H., EANDC(E)89, (1968) 35.

/61_7   BORMANN, M. et al., EANDC(E)89 (1968) 43.

/62_7   SHCHRODER, J., EANDC(US)104 (1967) 119.

/63_7   RAU, G., EANDC(E)89 (1968) 41.

/64_7   BUTLER, J., SANTRY, D., Neutron cross-section and technology, 2
         Washington (1968) 803.

/65_7   McELROY, W. et al., Neutron cross-section and technology, 1
         Washington (1968) 235.

/66_7   KANDA, Y., NAKASIMA, R., Neutron cross-section and technology, 1
         Washington (1968) 193.

/67_7   SANTRY, D., BUTLER, J., Can. J. Phys. 44 (1966) 1183.

/68_7   BUTLER, J., SANTRY, D., Can. J. Phys., 41 (1963) 372.

$\sqrt{}$69$\underline{}$$\overline{}$ LISKIEN, M., PAULSEN, A., EUR-119e (1963).

$\sqrt{}$70$\underline{}$$\overline{}$ FRANSIS, W., et al., in Nuclear data for reactors (Proc. Conf. Paris, 1966) 2, IAEA, Vienna (1967) 267.

Table 1

Resonance detectors

Key:

Изотоп	= Isotope
Содержание %	= Concentration %
Реакция	= Reaction
сек	= Sec
эв	= eV
барн	= barn
Мэв	= MeV
Сопутствующие реакции	= Accompanying reactions

Footnote to Table 1:

*/ At the 1.46 eV resonance only 79% of neutron captures result in activity with $T_{\frac{1}{2}}$ = 54 min $\underline{/}3\underline{/}$.

Table 2

Resonance parameters

Key:

Изотоп	= Isotope
эв	= eV
барн	= barn

Table 3

Threshold detectors

Key:

Изотоп	= Isotope
Содержание изотоп.%	= Concentration %
Реакция	= Reaction
сек	= sec
эв	= eV

Мэв = MeV

эфф = eff

мбарн = mbarn

⌠Сопутствующие = Accompanying reactions
⌡реакции
Литература = Reference

см. = see

Translator's note: the key to Russian abbreviations in columns 5 and 11
of Tables 1 and 3 is as follows:

ч or час = h

ДН   or дн = d

б = b

мбарн = mb

акт = act

лет = yr

содерж = content

сек = sec

м or мин = min

Table 1

Резонансные детекторы

№	Изотоп	Содержание %	Реакция	$T_{1/2}$ λ сек$^{-1}$	E_0 эв	σ акт барн	J_R барн	E_β Мэв (%)	E_γ Мэв (%)	Сопутствующие реакции $T_{1/2}$; E_β Мэв(%); E_γ Мэв(%)
1	2	3	4	5	6	7	8	9	10	11
1	$^{164}_{66}Dy$	28,18	$^{164}Dy(n,\gamma)^{165}Dy$ $^{165}Ho^\beta$	140±5 мин. 8.25·10^{-5}	$\frac{1}{v}$	800±100	377	0.29(2) 1.19(13) 1.26(85)	0.095(14)	1) 0,052% $^{156}Dy(n,\gamma)^{157}Dy$; 8,2час; $\varepsilon(100)$ E_γ 0,327 (98). 2) 0,09% $^{158}Dy(n,\gamma)^{159}Dy$; 139дн; $\varepsilon(100)$; E_γ 0,058 (3,57) σ акт 90б.
2	$^{31}_{15}P$	100	$^{31}P(n,\gamma)^{32}P$ $^{32}S^\beta$	14.50±0.04дн. 5.532·10^{-7}	$\frac{1}{v}$	0.19±0.01	0.092	1.707(100)	–	$^{31}P(n,p)^{31}Si$; 2,64час; E_β 1,48(100) σ 30 мбарн.
3	$^{176}_{71}Lu$	2,60	$^{176}Lu(n,\gamma)^{177}Lu$ $^{177}Hf^\beta$	6.75±0.05дн. 1.188·10^{-6}	0.142±0.005	2100±150	978	0.176(1) 0.384(3) 0.497(90)	0.208(1) 0.113(3.2)	97,40% $^{175}Lu(n,\gamma)^{176m}Lu$; 3,7час; E_β 1,1(6,5) 1,2(93,5); E_γ 0,09(6,5) J_R 476б.
4	$^{103}_{45}Rh$	100	$^{103}Rh(n,\gamma)^{104m}Rh$ $^{104}Pd^\beta$	4.41±0.02мин. 2.619·10^{-3}	1,257±0.002	11±1	83	1.88(1,85) 2,44(98)	0.556(1,9) 0.051(100)	$^{103}Rh(n,n')^{103m}Rh$; 57,5мин; E_γ 0,02(100); σ 1,09б.
5	$^{115}_{49}In$	95,77	$^{115}In(n,\gamma)^{116m}In$ $^{116}Sn^\beta$	54.0±0.5мин. 2.139·10^{-4}	1.451±0.02	198±3	3440	0.60(8) 0.87(36) 1.00(56)	2.12(17) 1.77(2) 1.29(80) 0.13+1,52(210)	4,23% $^{113}In(n,\gamma)^{114m}In$; 50дн; E_γ 0,192; J_R 1050 б.
6	$^{175}_{71}Lu$	97,40	$^{175}Lu(n,\gamma)^{176m}Lu$ $^{176}Hf^\beta$	3.69±0.04час. 5.217·10^{-5}	2.61±0.01	16.4±0.9	476	1.1(6.5) 1.2(93.5)	0.09(6.5)	2,60 $^{176}Lu(n,\gamma)^{177}Lu$; 6,8дн; E_β 0,176(1); 0,384(3) 0,497(90); E_γ 0,208(1) 0,113(3,2); J_R 978б.
7	$^{165}_{67}Ho$	100	$^{165}Ho(n,\gamma)^{166m}Ho$ $^{166}Er^\beta$	26.9±0.1час 7.156·10^{-6}	3.92±0.01	64±6	860	0.38(1) 1.77(47) 185(52)	1.61(1.7) 1,53(33) 1.37(9) 0.08(48)	

1	2	3	4	5	6	7	8		10	11
8	$^{197}_{79}Au$	100	$^{197}Au(n,\gamma)^{198}Au$ β ^{198}Hg	2.695$\pm$0.002дн 4.906$\pm$0.010 2.976·10^{-6}	98.8$\pm$0.3	1550	0.295(1) 0.957(99)		0.412(95.7)	$^{197}Au(n,\gamma)^{198}Au; 3,14дн;$ $E_\beta 0,25(24) 0,3(69) 0,46(7);$ $E_\gamma 0,2(11) 0,156(47); \sigma_{akt}26000б.$
9	$^{109}_{47}Ag$	48,65	$^{109}Ag(n,\gamma)^{110m}Ag$ β ^{110}Cd	252.5$\pm$1,5дн 3.177·10^{-8}	5.20$\pm$0.01	3.2$\pm$0.4	1240	0.087(64) 0.53(36)	1.506(14) 1.476(5) 0.116÷1.38(295)	$51,35\% ^{107}Ag(n,\gamma)^{108}Ag; 2,4 мин;$ $E_\beta 1,77(97); E_\gamma 0,632(1,9);$ $\sigma_R 87,2б.$
10	$^{152}_{62}Sm$	26,63	$^{152}Sm(n,\gamma)^{153}Sm$ β ^{153}Eu	47.1$\pm$0.1час 4.087·10^{-6}	8.03$\pm$0.01	210$\pm$10	3163	0.645(40) 0.720(36) 0.825(22)	0.1(34) 0.07(8)	1)3,16\% $^{144}Sm(n,\gamma)^{145}Sm; 340дн; E(100);$ $E_\gamma 0,061(15).$ 2)22,53\% $^{154}Sm(n,\gamma)^{155}Sm; 23,5мин.$ $E_\beta 1,8(100); E_\gamma 0,246(6,3)0,105(74)$ $б_{akt} 5,5б.$
11	$^{186}_{74}W$	28,41	$^{186}W(n,\gamma)^{187}W$ β ^{187}Re	24.04$\pm$0.09час 8.007·10^{-6}	18.84$\pm$0.02	38$\pm$2	484	0.866(0.82) 622(80) 1.304(20)	0.775(4.75) 0.687(31,4)	1)30,6\% $W(n,\gamma)^{185}W; 74,5дн.;$ $E_\beta 0,425(100).$ 2)0,14\% $^{180}W(n,\gamma)^{181}W; 140дн;$ $E(100); E_\gamma 0,152 0,136$
12	$^{123}_{51}Sb$	42,75	$^{123}Sb(n,\gamma)^{124}Sb$ β ^{124}Te	60.4$\pm$0.2дн 1,328.10^{-7}	21.6$\pm$0.2	2,5$\pm$0,5	138	1,68(79) 2.39(21)	2.088(6,5) 1.69(50) 0.6÷1.4	57,25 $^{121}Sb(n,\gamma)^{122}Sb; 2,8дн;$ $E_\beta 0,74(4) 1,4(63) 1,97(30);$ $E(3); E_\gamma 1,14(1) 0,69(3,5)0,57(6,25);$ $\sigma_R 143б.$
13	$^{75}_{33}As$	100	$^{75}As(n,\gamma)^{76}As$ β ^{76}Se	26.8$\pm$0.1час 7.183·10^{-6}	47.0$\pm$0.2	51$\pm$0.2	40.3	1,76(12) 2.41(32) 2.96(55) 0.56(38)	2,64÷1.49(0,64) 1.21(5,8) 0.65(6,3)	
14	$^{139}_{57}La$	99,91	$^{139}La(n,\gamma)^{140}La$ β ^{140}Ce	40,22$\pm$0.02ч. 4.786·10^{-6}	72.4$\pm$0.6	8,2$\pm$0.8	14.1	1.27÷1.71(76) 2.2(24)	2.5(3,5) 1,6(96) 0.32÷0.92(100)	
15	$^{198}_{78}Pt$	7,21	$^{198}Pt(n,\gamma)^{199}Pt$ β ^{199}Au	30$\pm$3 мин. 3.8·10^{-4}	95.8$\pm$0.3	3.9$\pm$0.8	53	0.8÷1.7(100)	0.96÷0.07	1)0,012\% $^{190}Pt(n,\gamma)^{191}Pt; 18час; E(100);$ $E_\gamma 0,04÷0,62.$ 2)0,78\% $^{192}Pt(n,\gamma)$ $^{193m}Pt; 4,5дн.; E_\gamma 0,135.$ 3)26,4\% $^{196}Pt(n,\gamma)^{197}Pt; 18час;$ $E_\beta 0,47÷0,67(100); E_\gamma 0,279(77).$

:I	2	3	4	5	6	7	8	9	IO	II
16 $^{59}_{27}Co$	100	$^{59}Co(n,\gamma)^{60}Co$ $^{60}Ni\,\beta$	5.28±0.01лет 4.17·10⁻⁹	132±I	37.2±0.6	74.6	0.318(100)	1.33(100) 1.17(100)	—	
17 $^{55}_{26}Mn$	100	$^{55}Mn(n,\gamma)^{56}Mn$ $^{56}Fe\,\beta$	2.576±0.002час 7.472·10⁻⁵	337±I	13.3±0.1	I4	0.75(I6) 1.05(24) 2.86(60)	2,12(15) 1.81(24) 0.845(99)	—	
18 $^{63}_{29}Cu$	69,1	$^{63}Cu(n,\gamma)^{64}Cu$ $^{64}Ni\,^{64}Zn\,\beta$	12.88±0.08час 1.495·10⁻⁵	577±I	4.51±0.23	4.68	0.573(38) 0.656(19) (43)	1.34(0.05) 0.511(38)	30,9% $^{65}Cu(n,\gamma)^{66}Cu$; 5,15мин; E_β 1,65(9) 2,63(91)· E_γ 1,037(9) 0,83(0,25); J_R 2,42 δ.
19 $^{130}_{52}Te$	34,49	$^{130}Te(n,\gamma)^{131m}Te$ $^{131}J\,\beta$	1.2 дн. 6.7·10⁻⁶	1500±500	0.04±0.01	—	0.2+2.46 (82)	1.22(13) 1,14(17) 0.85(32.5) 0.78(65)	1)18,71 $^{126}Te(n,\gamma)^{127}Te$; 105дн/9,3час; E_β 0,695; 0,217(?) E_γ 0,418(0,8); 0,088(1,81); 2)31,79 $^{128}Te(n,\gamma)^{129/125m}Te$; 72мин/33,5дн; E_β 1,29+ 1,45(100); E_γ 1,09(10) 0,46(15) 0,027(3,76); 3)34,49 $^{130}Te(n,\gamma)^{131}Te$; 24,8мин; E_β 1,36-2,1(??) E_γ 0,149± 0,92.
20 $^{23}_{11}Na$	100	$^{23}Na(n,\gamma)^{24}Na$ $^{24}Mg\,\beta$	15.05±0.05час 1.279·10⁻⁵	2900±50	0.531±0.008	0.30	1,4(100)	2.76(100) 1.37(100)	—
21 $^{51}_{23}V$	99,76	$^{51}V(n,\gamma)^{52}V$ $^{52}Cr\,\beta$	3.76±0.02мин. 3.07·10⁻³	4162±7	1.9±0.3	2.15	2.73(100)	1.44(100)	—
22 $^{50}_{24}Cr$	4,31	$^{50}Cr(n,\gamma)^{51}Cr$ $^{51}V\,\xi$	27.8±0.1дн 2.885·10⁻⁷	5500±500	14.6±1,5	7.11	ξ≤0.76(100)	0.325(9.8)	2,38% $^{54}Cr(n,\gamma)^{55}Cr$; 3,5мин; E_β 2,85 (100).
23 $^{37}_{17}Cl$	24,6	$^{37}Cl(n,\gamma)^{38}Cl$ $^{38}Ar\,\beta$	37.29±0.04мин 3.097·10⁻⁴	25500±500	0.56±0.12	—	1.11(31) 2.77(16) 4.81(53)	2.19(47) 1.64(31)	1)75,4% $^{35}Cl(n,\gamma)^{36}Cl$; 3·10⁵лет; E_β 0,714(98,3). E 1,16(1,7); $\sigma_{акт}$ 30 δ. 2)$^{35}Cl(n,p)^{35}S$; 87дн; E_β 0,167(100); $\sigma_{акт}$ 0,19δ 3)$^{35}Cl(n,d)^{32}P$; 14,5дн; E_β 1,7(100); $\sigma_{акт}$ 0,06 мδ
24 $^{19}_{9}F$	100	$^{19}F(n,\gamma)^{20}F$ $^{20}Na\,\beta$	11.2±0.1сек 6.18·10⁻²	27000±1000	0.009±0.002	2.3	5.42(100)	1.63(100)	$^{19}F(n,p)^{19}O$; 29сек; 3,26(59) 4,6 (41); E_γ 1,36(55) 0,198(97).

*) Примечание. В резонансе 1.46 эв только 79% захватов нейтронов приводит к активности с $T_{1/2}$ =54 мин [3].

Table 2

Параметры резонансов

№ п/п	Изотоп	E_a эб	I	J	Γ эб	Γ_γ эб	Γ_n эб	δ_o δ арн
1	2	3	4	5	6	7	8	9
1	$^{115}_{49}In$	1.457		5	$(75\pm2)\cdot10^{-3}$	$(72\pm2)\cdot10^{-3}$	$(3.04\pm0.05)10^{-3}$	38500 ± 1000
		3.86	9/2	4	$(81\pm4)\cdot10^{-3}$	$(81\pm4)\cdot10^{-3}$	$(0.354\pm0.015)\cdot10^{-3}$	480
		9.12		5	$(82\pm40)10^{-3}$	$(80\pm40)10^{-3}$	$(1.57\pm0.16)10^{-3}$	780
2	$^{197}_{79}Au$	4.906		2	0.140 ± 0.03	0.124 ± 0.003	0.0156 ± 0.0004	37000 ± 500
		58.1		I	0.115 ± 0.015	$;0.112\pm0.015$	$=(2.3\pm0.14)10^{-3}$	-
		60.3	3/2	2	0.206 ± 0.020	0.130 ± 0.020	0.076 ± 0.005	$\delta_o\Gamma^2=450\pm130$
		78.7		I	0.157 ± 0.015	0.140 ± 0.015	0.0167 ± 0.0008	$\delta_o\Gamma^2=32\pm8$
3	$^{109}_{47}Ag$	5.20		I	0.153 ± 0.003	0.140 ± 0.003	0.0125 ± 0.0001	34000 ± 1000
		30.5	I/2	I	0.132 ± 0.013	0.125 ± 0.013	$(8.0\pm0.3)10^{-3}$	3530 ± 640
		40.2		I	0.142 ± 0.019	0.137 ± 0.019	$(5.0\pm0.4)10^{-3}$	$\delta_o\Gamma^2=34\pm10$
4	$^{152}_{62}Sm$	8.03	0		0.201 ± 0.008	0.071 ± 0.010	0.130 ± 0.005	210000 ± 2000
5	$^{186}_{74}W$	18.84			0.369 ± 0.007	0.052 ± 0.006	0.317 ± 0.005	$\delta_o\Gamma_\gamma=(7\pm1)10^3$
		171.5	0		0.092 ± 0.020	0.065 ± 0.020	0.027 ± 0.003	4500 ± 1200
		219			0.602 ± 0.040	0.062 ± 0.006	0.540 ± 0.040	$\delta_o\Gamma_\gamma=450\pm50$
6	$^{139}_{57}La$	72.4	7/2		0.150 ± 0.030	$0,120\pm0.030$	0.030 ± 0.003	
7	$^{59}_{27}Co$	132	7/2	4	5.57 ± 0.10	0.45 ± 0.05	5.12 ± 0.04	9700 ± 1800
8	$^{55}_{25}Mn$	337		2	22.5 ± 1.0	0.5 ± 0.1	22 ± 1	$\delta_o\Gamma^2=(3.0\pm0.6)10^6$
		1098	5/2	3			14.6 ± 0.7	$\delta_o\Gamma^2=(2.8\pm0.7)10^4$
		2375		3			400 ± 10	-
9	$^{63}_{29}Cu$	577		2	1.41 ± 0.05	0.55 ± 0.07	0.86 ± 0.03	1550
		2060	3/2	I	43.8 ± 2.0	0.4	43.5 ± 2.0	626
		2660		2	4.7		4.5 ± 0.5	
10	$^{23}_{11}Na$	2900		I		0.35 ± 0.04	424 ± 13	
		54000	3/2	2	1400 ± 200		$g\Gamma_n=750\pm40$	
11	$^{50}_{24}Cr$	5500				2.9 ± 0.9	1600 ± 200	473
		28700	0				510 ± 50	
		38700					1820 ± 460	
12	$^{37}_{17}Cl$	8700				0.5	$g\Gamma_n=40\pm7$	
		25500	3/2	I		~25	$g\Gamma_n=250\pm15$	
		47000		2		~14	$g\Gamma_n=236\pm12$	

Table 3

Пороговые детекторы

№ №	Изо-топ	Содер-жание изо-топ %	Реакция	$T_{1/2}$ λ сек$^{-1}$	$E_{эфф}$ М эв	$\delta_{эфф}$ мбарн	$\sum$ мбарн	E_ρ Мэб(%); E_f Мэб(%)		Сопутствующие реакции; $T_{1/2}$; E_β Мэб(%); E_f Мэб(%)	Лите-ратура
1	2	3	4	5	6	7	8	9	10	11	12
I	$^{237}_{73}Np$		$^{237}Np(n,f)$	–	0.65	1420 [48]	1100 [3]				[I]
2	$^{103}_{45}Rh$	100	$^{103}Rh(n,n')^{103m}Rh$	57,5±0.5м					0.040(0.6)	$^{103}Rh(n,f)^{104m}Rh; 4,41 мин, E_\rho 1,38 (1,35)$ $2,44(38,15)E_f 0,556(1,35)0,051(100)$	64.
			^{103}Rh	2.009·10^{-4}	0.80	950 [48]	1093 [3]	–	0.020(100)	$^{103}Rh(n,2n)^{102}Rh; 102 дн. E_\rho 1,15(20);$ $6(30). E_f 0,418÷1,1$	
8	$^{115}_{49}In$	95,72	$^{115}In(n,n')^{115m}In$	4.4±0.4 час					0.335(50)	$^{115}In(n,\gamma)^{116m}In; 64 мин; E_f 2,12÷0,8(30)$ $^{115}In(n,d)^{112}Ag; 3,2 час; E_\beta 1,0÷4,1(100);$ $E_f 1,62(15) 1,39(35)0,6(13(40)).$ $^{115}In(n,p)^{115}Cd; 53 час; E_\beta 0,19÷1,12(100);$ $E_f 0,523(25) 0,335(52) 0,26(1,5)$ $^{115}In(n,\gamma)^{114m}In; 50 дн; E_f 0,72(3,5)$ $0,556(3,5)0,192(18,2)$	58
			^{115}In	4.375·10^{-5}	I.15	302 [48]	174 [54]	0.96(5)			
4	$^{238}_{92}U$	99,3	$^{238}_{92}U(n,f)$	–	I.60	608 [48]	310 [3]				I
5	$^{232}_{90}Th$	100	$^{232}_{90}Th$	–	I.60	145 [48]	28 [3]				I
6	$^{199}_{80}Hg$	16,84	$^{199}Hg(n,n')^{199m}Hg$	42±I мин.					0.375(15)	$^{196}Hg(n,\gamma)^{197m/197}Hg; 24 час/65 час; \delta(100);$ $E_f 0,19; 0,077; 0,165; 0,13; одер. 0,146 %$ $24,80 \% ^{202}Hg(n,\gamma)^{203}Hg; 46,9 дн. E_\beta 0,21(100);$	
			^{199}Hg	2.750·10^{-4}	I.9	120 [45]		–	0.158(33)	$E_f 0,279(1,1,5)$ $6,85 \% ^{204}Hg(n,\gamma)^{205}Hg; 5,1 мин; E_\rho 1,66(100)$ $23,13 \% ^{201}Hg(n,p)^{200}Au; 48 мин, E_\beta 0,65(24)$ $1,31(6) 2,23(70); E_f 1,22(23) 0,37(29)$	
7	$^{31}_{15}P$	100	$^{31}P(n,p)^{31}Si$	2.64±0.02 ч					0.22(0.01) 1,26(0.07)	$^{31}P(n,\gamma)^{32}P; 14,50 дн; E_\beta 1,707(100)$ $^{31}P(n,d)^{28}Al; 2,3 мин; E_\beta 2,865(100);$	1,69
			^{31}P	7.292·10^{-5}	2,55	122 [48]	30.5 [43]	1,48(100)		$E_f 1,79(100)$	

1	2	3	4	5	6	7	8	9	10	11	12

8 $^{64}_{30}Zn$ 48,89 $^{64}Zn(n,p)^{64}Cu$
0.57(38)
12.88±0.08ч. 1.34(0.6)
^{64}Ni ^{64}Zn
2.60 129 27 +0.66(19)
1.495·10⁻⁶ [48] [44] (43) 0.511(38) I

1) $^{64}Zn(n,p)^{64}Zn$; 246, 4дн; E_β 0,325(15); б(94,5);
E_γ 1,119(43); 0,511(3)
2) 18,56% $^{64}Zn(n,\gamma)^{65}Zn$; 51 мин; E_β 0,914(100)
3) $^{64}Zn(n,p)^{64}Cu$; 12 сек; E_β 3,0 (100)
4) 27,81% $^{64}Zn(n,p)^{64}Cu$; 5,1 мин; E_β 1,65(8)2,63(84)
E_γ 1,05(9)

9 $^{61}_{28}Ni$ 67,76 $^{61}Ni(n,p)^{61}Co$
71.3±0.2дн +0.484(14,5) 0.805(100)
^{61}Co
2.70 430 105
1.125·10⁻¹ [48] [49] (85.5) 0.511(29) 1,65,69

9) 1,19% $^{61}Zn(n,p)^{61}Cu$;6 час; E_β 0,57(33)0,31(67);
E_γ 0,13(23)0,9
1) $^{61}Ni(n,\gamma)^{61}Ni$; 10⁴ лет; б(100)
2) 66% $^{61}Ni(n,p)^{61}Ni$; 12,5 мин; E_β 0,067(100)
3) 1,16% $^{61}Ni(n,p)^{61}Ni$; 2,57 час; E_β 0,6÷2,1(100)
E_γ 1,49(11)1,12(18)0,36(11)
4) 26,16% $^{61}Ni(n,p)^{61}Co$; 5, 28 мин; E_β 0,31(11)(100),E_γ (33(100)
1,17(100)

10 $^{32}_{16}S$ 95,018 $^{32}S(n,p)^{32}P$
14.50±0.04дн
^{32}P
5.532·10⁻⁷ 2.65 252 60 1.707(100) — 1,69

1) 0,214% $^{32}S(n,\gamma)^{35}S$; 87дн; E_β 0,167(100)
2) $^{32}S(n,\alpha)^{32}Si$; 2,62 час; E_β 1,48(100); E_γ 1,26(100)
3) 0,75% $^{33}S(n,p)^{33}P$; 25, 1дн; E_β 0,248(100)
4) 0,017% $^{36}S(n,\gamma)^{37}S$; 5 мин; E_β 4,6(90),4,7(10)
E_γ 3,09(90)

11 $^{54}_{26}Fe$ 5,84 $^{54}Fe(n,p)^{54}Mn$
313.5±0.7дн
^{54}Cr
2.558·10⁻⁸ 3.00 372 60 0.528(100) 0.835(100) 1,65

1) $^{54}Fe(n,\gamma)^{55}Fe$; 2,6 мин; б 0,22(100)
2) 0,33% $^{57}Fe(n,\gamma)^{58}Fe$; 46,5 дн; E_β 0,27(14)0,46(86);
E_γ 1,99(44)1,1(56)0,192(2,5)
3) 91,68% $^{56}Fe(n,p)^{56}Mn$; 2,576 час; E_β 0,33÷2,86(100);
E_γ 2,12(15)1,81(23)0,845(99)
4) $^{54}Fe(n,\alpha)^{51}Cr$; 27,8 дн; б (100); E_γ 0,32(9)

12 $^{35}_{17}Cl$ 75,4 $^{35}Cl(n,\alpha)^{32}P$
14.50±0.04дн 3.70 190 24 1.707(100) —
^{32}S
5.532·10⁻⁷ [48]

1) $^{35}Cl(n,\gamma)^{36}Cl$; 3·10⁵ лет; E_β 0,714(98,3); б(47)
2) $^{35}Cl(n,p)^{35}S$; 87дн; E_β 0,167(100)
3) 24,6% $^{37}Cl(n,\gamma)^{38}Cl$; 37,5 мин; E_β 1,11(31)
4,77(16)4,81(53); E_γ 2,19(47)1,64(31)
4) $^{37}Cl(n,p)^{37}S$; 5 мин; E_β 1,6(90)4,7(10)E_γ 3,09(90)

13 $^{27}_{13}Al$ 100 $^{27}Al(n,p)^{27}Mg$
9.54±0.08м.
1.59(42) 0.837(70)
^{27}Al
4.50 48 2.9
1.210·10⁻⁸ [48] [43] 1.75(58) 1.02(30) 1,65

1) $^{27}Al(n,\gamma)^{28}Al$; 2, 31 мин; E_β 2,86(100);
E_γ 1,79(100)
2) $^{27}Al(n,\alpha)^{24}Na$; 15, 05 час; E_β 1,41(100);
E_γ 2,76(100)1,37(100)

1	2	3	4	5	6	7	8	9	10	11	12

14 $^{28}_{14}Si$ 92,27 $^{28}Si(n,p)^{28}Al$ 2,31±0.01мин.

5.50 125 4.0 2.865(100) I.79(100)

^{29}Si 5.0·10⁻³ [48] [43]

Column 11:
1) 4,68% $^{29}Si(n,p)^{29}Al$; 6,7 мин; E_β 1,6(4) 2,7(96); E_γ 2,43(6,2) 1,28(93,8).
2) 3,05% $^{30}Si(n,r)^{31}Si$; 2,62 час; E_β 1,48(100); E_γ 1,26(0,07)
3) $^{30}Si(n,\alpha)^{27}Al(g; 9,5 мин; E_\beta 1,59(4a) 1,81(56); E_\gamma 1,02(30) 0,8 1(70)$

Column 12: I,69

15 $^{46}_{22}Ti$ 7,93 $^{46}Ti(n,p)^{46}Sc$ 84.2±0.2дн

5.5 12.6 0.357(100)

^{46}Ti 9.526·10⁻⁷ [52] [63]

I.118(100)
0.892(100)

Column 11:
1) 5,35% $^{50}Ti(n,r)^{51}Ti; 5,8 мин; E_\beta (5(5,5) 2,13(94,5); E_\gamma 0,93(4,2)0,605(1,4)0,393(96)$
2) 7,28% $^{47}Ti(n,p)^{47}Sc; 3,43 дн; E_\beta 0,44(57)0,6(43) E_\gamma 0,16(57)$
3) 5,51% $^{48}Ti(n,p)^{48}Sc; 57 мин; E_\beta 2,05(100).$
4) 73,94% $^{48}Ti(n,p)^{48}Sc; 1,82 ч; E_\beta 0,64(100) E_\gamma 1,32(100)1,04(100)0,984(100).$

16 $^{90}_{40}Zr$ 51,46 $^{90}Zr(n,p)^{90}Y$ 64.3±0.4час.

6.20 15,5 [48]

2.273(100)
I.75(0.016)

^{90}Zr 2.994·10⁻⁶

Column 11:
1) 17,40% $^{94}Zr(n,r)^{95}Zr; 65 дн; E_\beta 0,36÷(13100) E_\gamma 0,756; 0,723$
2) 2,80% $^{96}Zr(n,r)^{97}Zr; 17 час; E_\beta 0,45; 1,9; E_\gamma 0,58÷1,77; 0,75(96)$
3) 11,23% $^{91}Zr(n,p)^{91}Y; 58,8 дн; E_\beta 1,58(100); E_\gamma 1,2(0,3)$
4) 17,11% $^{92}Zr(n,p)^{92}Y; 3,53 час; E_\beta 1,2÷3,6(100) E_\gamma 0,94(33)0,55(11).$

17 $^{65}_{29}Cu$ 80,9 $^{65}Cu(n,p)^{65}Ni$ 2,564±0.008ч.

0.523 0.6(29) I.49(11)
[44] 1.01(14) I.12(19)
2,1(57) 0.36(11)

^{65}Cu 7.357·10⁻⁵

Column 11:
1) $^{65}Cu(n,r)^{66}Cu; 5,1 мин; E_\beta 1,65(9)2,63(91); E_\gamma 1,05(9).$
2) 59,1% $^{63}Cu(n,r)^{64}Cu; 12,8 час; E_\beta 0,57(38); E_\beta·0,66(19); E_\gamma 1,34(0,6)0,511(38)$
3) $^{63}Cu(n,p)^{63}Ni; 125 лет. E_\beta 0,067(100)$
4) $^{63}Cu(n,\alpha)^{60}Co; 5,2 года; E_\beta 0,318(100); E_\gamma 1,33(100)1,17(100)$
5) $^{65}Cu(n,2n)^{64}Cu; 12,8 час; см №15$
6) $^{63}Cu(n,2n)^{62}Cu; 9,1 мин; см №18$

Column 12: I,67

18 $^{56}_{26}Fe$ 91,68 $^{56}Fe(n,p)^{56}Mn$ 2,576±0.002ч.

6.60 60 0.92
[48] [54]

0.75(15) 2,12(15)
1.05(24) I.81(23)
2.86(60)
0.33(1) 0.845(99)

^{56}Fe 7.472·10⁻⁵

Column 11: см №11

Column 12: I,66

19 $^{48}_{22}Ti$ 73,94 $^{48}Ti(n,p)^{48}Sc$ I.83±0.04дн

7.0 50 0.50 0.640(100)
[45] [52]

^{48}Ti 4.383·10⁻⁶

I.32(100)
I.04(100)
0.984(100)

Column 11: см №15

1	2	3	4	5	6	7	8	9	10	11	12
								0.33(I)	2,12(I5)	1) $^{59}Co(n,d)^{60}Co$; 5,28 лет; E_β 0,318(100); E_γ 1,33(100) 1,17(100)	
20	$^{59}_{27}Co$ 100	$^{59}Co(n,d)^{56}Mn$	2,576±0.002ч					0.75(I5)	1.81(23)	2) $^{59}Co(n,p)^{59}Fe$; 45,5дн; E_β 0,271(46)0,462(54);	I
	.27	β↓		7.10	13.8			1.05(24)		E_γ 1,29 (74)1,1(56) 0,192(2,5).	
		^{56}Fe 7.472·10⁻⁵			[48]			2.86(60)	0.845(99)	3) $^{59}Co(n,2n)^{58}Co$; 71,3дн; E_β 0,485(14,5); δ(85,5); E_γ 0,805(100)0,511(29)	
21	$^{24}_{12}Mg$ 78,6	$^{24}Mg(n,p)^{24}Na$	15.05±0.05ч						2.76(100)	11,1% $^{26}Mg(n,\gamma)^{27}Mg$; 9,5мин;E_β 1,59(42)	1,68
		β↓		7.15	128	1.3	1.4(100)		1.37(100)	1,75(58); E_γ 1,02(30)0,837(70)	
		^{24}Mg 1.279·10⁻⁵			[48]	[50]					
22	$^{27}_{13}Al$ 100	$^{27}Al(n,p)^{24}Na$	15.05±0.05ч.						2.76(100)	1) $^{27}Al(n,\gamma)^{28}Al$; 2,31 мин; E_β 2,85(100) E_γ 1,79(100)	1,58,65,
		β↓		7.45	82.5	0.61	1.4(100)			2) $^{27}Al(n,p)^{27}Mg$; 9,5мин; E_β 1,59(42)1,75(58); E_γ 1,02(30)0,837(70)	68
		^{24}Mg 1.279·10⁻⁵			[48]	[3]			1.37(100)		
23	$^{203}_{81}Tl$ 29,50	$^{203}Tl(n,2n)^{202}Tl$	12.0±0.1дн						0.965(0,5)	1) $^{203}Tl(n,\gamma)^{204}Tl$; 3,78 лет; E_β 0,76(98)(β-δ); E_γ - нет	I
		ε↓ 6.68·10⁻⁷		9.90	1224	4.0		ε (100)	0.523(3.9)	2) 70,50 $^{205}Tl(n,\gamma)^{206}Tl$; 4,26 мин; E_β 1,57(100)	
		^{202}Hg			[48]	[47]			0.440(95)	3) $^{203}Tl(n,2n)^{202}Tl$; 3,78 лет;E_β 0,76(97); δ(3)	
								0.39(6)	0.86(0.8)	1) $^{127}J(n,\gamma)^{128}J$; 25 мин; E_β 1,67(16)2,0(77); E_γ 0,53(1,7)0,45(17)	
24	$^{127}_{53}J$ 100	$^{127}J(n,2n)^{126}J$	13.1±0.5дн					0.87(29)	0.75(3.6)	2) $^{127}J(n,p)^{127m/127}Te$; 105дн/9,35час; E_β 0,70; E_γ 0,418; 0,033	I
		β⁺↓		11.0	1000	1.7	1,25(9)		0.65(33)	3) $^{127}J(n,d)^{124}Sb$; 60дн; 0÷2,39(100); E_γ 2,09(6,5)1,69(50)0÷1,45(133)	
		^{126}Te ^{126}Xe 6.12·10⁻⁷			[48]	[47]	ε,β⁺(5I)		0.511(5)		
									0.38(31)		
								0.57(38)	1.34(0.6)		
25	$^{65}_{29}Cu$ 80,9	$^{65}Cu(n,2n)^{64}Cu$	12.88±0.08ч	11.2	608	0.31	β⁺(19)		0.511(38)	см. N 17	
		β⁻↓ β⁺↓ 1.495·10⁻⁵			[48]	[3]	δ (43)				1,66,67
		^{64}Ni ^{64}Zn									

1	2	3	4	5	6	7	8	9	10	11	12
26	$^{55}_{25}Mn$	100	$^{55}Mn(n,2n)^{54}Mn$ 2.558·10⁻⁸	313,5±0.7 дн	11.7	740 [48]	0.13 [47]	ε 0.528(100)	0.835(100)	1) $^{55}Mn(n,p)^{54}Mn$; 2,576 сек ; E_β 0,33÷1,8(100); E_γ 2,12(15) 1,81(13) 0,845(99). 2) $^{55}Mn(n,p)^{55}Cr$; 3,5 мин ; E_β 2,85(100).	1,58
27	$^{19}_{9}F$	100	$^{19}F(n,2n)^{18}F$ β⁺↓ ^{18}O 1.053·10⁻⁴	109.72±0.08м	12.8	50 [48]		β⁺ (97) ε (3)	0.511(194)	$^{19}F(n,p)^{19}O$; 11,56 сек ; E_β 5.42(100); E_γ 1,63 (100)	58
28	$^{63}_{29}Cu$	69,1	$^{63}Cu(n,2n)^{62}Cu$ β⁺↓ ^{62}Ni 1.17·10⁻³	9.9±0.2 мин.	12.9	526 [48]	0.073 [3]	β⁺ 2.91(100)	0.511(196)	см. N17	1,66

Chapter II. REACTOR CONSTANTS AND PARAMETERS

NEUTRON FLUX RELAXATION LENGTHS AND RETHERMALIZATION LENGTHS
IN GRAPHITE AND WATER (RESULTS OF A STUDY OF NEUTRON
THERMALIZATION EXPERIMENTS)

G.Ya. Trukhanov, Yu.A. Safin

Introduction

For a number of years investigations have been carried out in the I.V.
Kurchatov Atomic Energy Institute on neutron thermalization in a graphite-
water system with a large temperature gradient over a wide range of graphite
temperatures from 133 to 823°K.

Reports on these investigations containing preliminary analyses of the
experimental data have been presented at IAEA conferences $\lfloor 1, 2 \rfloor$. More
recently publications have appeared $\lfloor 3-7 \rfloor$ giving a detailed analysis of the
experimental data obtained in both the low and the high graphite temperature
ranges.

In this article the data of Refs $\lfloor 3-7 \rfloor$ on neutron relaxation and re-
thermalization lengths in graphite and water are combined and generalized,
and a detailed comparison is made with the results of other authors $\lfloor 11, 12 \rfloor$.

A short description is given of the experimental set-up and the method
used to derive the primary relaxation length and the rethermalization lengths
from the experimental data.

2. Experimental section

The experimental equipment consisted of a graphite prism measuring
100 x 100 x 59.5 cm^3 with a water tank adjacent to one of its sides
(100 x 100 cm^2) (Fig. 1). In the initial series of measurements (series A/1/)
an oblong tank measuring 175 x 175 x 50 cm^3 was used but in subsequent
measurements (series B/2/) this was replaced by a cylinder 38 cm in diameter.

The graphite was heated electrically by elements positioned on the five
faces of the graphite prism. Stainless steel pipes for circulating the
coolant were installed in the same plane as the heating elements. In order
to obtain a low graphite temperature (133°K), liquid nitrogen was used.

The graphite prism and the water tank were separated by a heat shield
consisting of two stainless steel foils 100 microns thick and one aluminium
foil 200 microns thick. The other four faces of the graphite prism were
insulated with a 20-cm thick layer of ultra light-weight chamotte, which

in turn was covered with a layer of boron carbide. The prism was then enclosed in an aluminium tank.

The water moderated and cooled WWR-2 reactor was used as the external neutron source. The reactor provided a means of obtaining a wide (50 x 50 cm) beam of thermal neutrons. One of the faces of the graphite prism was placed close to the reactor core. The thermal neutron spectrum measured on this face (with a near-Maxwellian distribution) and the spectrum temperature depend on both the reactor power and the graphite temperature. Neutron beams were extracted from various points of the graphite with the aid of a continuous channel 17 mm in diameter passing through the centre of the prism along the axis of symmetry of the system and filled with graphite inserts of different length. The neutron beam was extracted from the water via a movable aluminium tube closed at the end, having a diameter of 14 mm. The neutron spectra in the beams extracted from different points in the graphite and the water were measured by the time-of-flight method.

The measurements were performed with a mechanical chopper having one plane-parallel slit 5 mm wide and a 160-channel time analyser. The 150 mm-diameter rotor of the mechanical chopper was made from glass-fibre-reinforced plastic containing boron. The neutron detector employed was an end-window proportional counter filled with enriched BF_3 gas. The resolution in the time-of-flight measurements was 20 μsec/m.

The graphite and water temperatures at which measurements were carried out are indicated in Table 1. The temperature nonuniformity was 7% in the graphite and 3% in the water.

Experiments at identical graphite and water temperature were carried out for checking purposes.

The neutron spectrum was calculated from the counting rate in the channels of the time analyser, using a familiar relation $\boxed{8}$ which takes into account the rotor transmission function*/, counter efficiency**/, the dependence of the effective flight path on neutron energy (by displacement of the effective neutron recording centre in the counter), the dependence of neutron absorption and scattering in air between the end of the tube and the detector, and the neutron background.

No corrections were made for selector resolution in the thermal range or for neutron counting losses, since they were less than the statistical measuring error.

---

*/ The effect due to penetration of the wall of the rotor slit was taken into account.

**/ The counter efficiency was determined experimentally.

Neutron spectra consisting of a vector neutron flux $\varphi(z,v,1)$ were measured at the following distances from the temperature jump:

(a) In graphite: 0; 0.5; 1.0; 2; 4.5; 9.5; 19.5; 29.5; 39.5; 49.5; 59.5 cm;

(b) In water: 0; 0.1; 0.2; 0.3; 0.5; 0.7; 1; 1.5; 2; 3; 5 and 7.5 cm.

By way of example[***] Fig. 2 shows the spectra of the vector flux $\varphi(z,v,1)$ in graphite and water at different distances from the thermal barrier (graphite temperature $594^{\circ}K$, water temperature $302^{\circ}K$).

The experimental spectra were used to obtain the mean values $\bar{v}$, $\overline{v^2}$ and $\overline{1/v}$ averaged over the neutron density $v^{-1}\varphi(z,v,1)$ and the corresponding temperatures of the neutron gas (see for example Ref. $\underline{/7\underline{7}}$). In addition, by fitting the Maxwellian curve to the experimental distribution of $v\cdot\varphi(z,v,1)$ in the region of the distribution peak, a neutron gas temperature $T = \frac{m}{4k}(\frac{1}{1/v_m})^2$ was obtained, where $\frac{1}{v_m}$ is the inverse velocity corresponding to the most probable velocity in the $v\cdot\varphi(v,z,1)$ distribution. Figs 3–6 show the spatial distribution of this temperature at various graphite and water temperatures. In addition, the integral thermal neutron density in water was measured by the activation method in the series B experiments. Figs 7–9 show the results of these measurements at different graphite and water temperatures in semilogarithmic scale.

3. Method of obtaining neutron flux relaxation
   lengths from experimental data

The results of the experiments (spatial trend of neutron gas temperature and integral thermal neutron density) enable us to estimate the neutron flux relaxation length in water. The neutron flux relaxation lengths are by definition equal to the reciprocals of the discrete eigenvalues of problems arising in the separation of the variables in the kinetic equation. They are determined solely by the properties of the medium, irrespective of the nature of the sources. This means that they contain information on the scattering law of the medium and that, being derived from experimental data, they can be useful for checking theoretical models of the scattering kernel. On the other hand, knowledge of some of the primary neutron flux relaxation lengths and the corresponding eigenfunctions makes it possible in some cases to construct approximate solutions of the kinetic equation with a fair degree of accuracy.

[***] For detailed information on the space–energy neutron distribution in this system see Refs $\underline{/6}$, $7\underline{7}$.

As shown in Ref. $\boxed{3\_7}$, which explains the meaning of the relaxation lengths obtained by various methods of solving the kinetic equation, the diffusion length L_o, which is the reciprocal of the zero-eth discrete eigenvalue x_o and the first relaxation length $L_1 = x_1^{-1}$ (and in certain cases also $L_2 = x_2^{-1}$) can be obtained by analysing the asymptotic behaviour of the density or any other integral quantities (such as mean neutron velocity or neutron gas temperature). We shall demonstrate this using the example of the integral neutron density and the neutron gas temperature, confining ourselves to the plane case and the condition that there are only two discrete relaxation lengths, L_o and L_1. The consideration is based on Ref. $\boxed{3\_7}$. In our assumptions, the asymptotic part of the vector neutron flux (for $Z > 1/x^*$) where $x^* = \min[\Sigma_t(E)]$ is the boundary between the continuous and discrete parts of the spectrum of eigenvalues of the kinetic equation, $\Sigma_t(E)$ being the total cross-section for neutron interaction with the substance) can be represented in the form

$$\Psi(z,\mu,E) = \sum_{n=0;1} C_n \cdot f_n(\mu,E) \cdot exp\left(-\frac{z}{L_n}\right) \qquad (1)$$

Here $f_n(\mu,E)$ $(n = 0;1)$ are eigenfunctions corresponding to the discrete eigenvalues x_o and x_1, and $C_n(n = 0;1)$ are expansion coefficients.

For the neutron integral density we have

$$n(z) \approx \sum_{n=0;1} P_n \cdot exp\left(-\frac{z}{L_n}\right) \quad (z > \frac{1}{x^*}) \qquad (2)$$

where P_n are the corresponding angle and energy integrals[*/] in Eq. (1).

Hence it follows that, if we describe the experimental neutron density $n_{exp}(Z)$ by the asymptotic part $(Z > \frac{1}{x^*})$ with an expression like Eq. (2), it is in fact possible to obtain the fundamental relaxation length L_o and the primary relaxation length L_1 provided the experimental conditions correspond to those with which formula (2) was obtained.

---

* The eigenfunctions $f_o(\mu,E)$ and $f_1(\mu,E)$ are solutions of the sourceless kinetic energy equation (sourceless also at infinity). This means that $f_o(\mu,E)$ and $f_1(\mu,E)$ do not contain a $\frac{1}{E}$ term. Therefore the upper limit in the energy integration of these functions can be taken as infinite.

*/ See footnote above.

Let us now find the asymptotic expression for neutron gas temperature. Using the same assumptions made when obtaining formula (2), we obtain for $z > \frac{1}{x^*}$:

$$T(z,\mu) = \frac{\int E^{1/2} \cdot \varphi(z,\mu,E) \, dE}{\int E^{-1/2} \cdot \varphi(z,\mu,E) \, dE} = \frac{\bar{E}_0(\mu) + C(\mu) \cdot \bar{E}_1(\mu) \cdot exp(-z/L_2)}{1 + C(\mu) exp(-z/L_2)} \qquad (3)$$

$$C(\mu) = \frac{C_1 \cdot \int f_1(\mu,E) E^{-1/2} dE}{C_0 \cdot \int f_0(\mu,E) \cdot E^{-1/2} dE} ; \quad \bar{E}_n = \frac{\int f_n(\mu,E) \cdot E^{1/2} dE}{\int f_n(\mu,E) E^{-1/2} dE} \qquad (4)$$

where $\qquad L_2^{-1} = L_1^{-1} - L_0^{-1} \qquad (n=0;1) \qquad (5)$

Expression (3) can be converted to

$$T(z,\mu) \approx T_2 + (T_1 - T_2) \frac{g}{b + exp\left(\frac{z}{L_2}\right)} \qquad (6)$$

where $\quad T_2 = \bar{E}_0(\mu) \; ; \; b = C(\mu) \; ; \; (T_1 - T_2) \cdot g = \left[\bar{E}_1(\mu) - \bar{E}_0(\mu)\right] \cdot C(\mu) \qquad$ (6a)

When $z > L_r$ we obtain the relation

$$T(z,\mu) \approx T_2 + (T_1 - T_2) g \cdot exp\left(-\frac{z}{L_2}\right) \qquad (7)$$

which coincides with the familiar asymptotic expression for neutron gas temperature, $T(z) = T_\infty + (T_0 - T_\infty) exp\left(\frac{z}{L_r}\right)$, if L_r is taken to represent the so-called neutron gas temperature relaxation length (see, for example, Ref. [2]).

Approximating the asymptotic behaviour of the experimental neutron gas temperature with formula (6) or (7) will give a relaxation length L_r, which is related to the neutron flux relaxation lengths by expression (5), provided the experimental conditions correspond to those under which expressions (6) or (7) were obtained.

Thus, if the diffusion length L_0 is known, the primary neutron flux relaxation length can be obtained from the neutron gas temperature relaxation length with the formula

$$L_1 = \frac{L_0 L_2}{L_0 + L_2} \qquad (8)$$

Note that in formula (4) the neutron gas temperature is determined as proportional to the mean square of the neutron velocity. However, the neutron gas temperature is often determined as being proportional to the square of the mean velocity $\overline{\mathcal{V}(z,\mu)}(T_r \sim \overline{\mathcal{V}}^2)$, or inversely proportional to the square of the mean inverse neutron velocity $\left(\overline{\dfrac{1}{\mathcal{V}}}\right)$, $\left(T_{1/r} \sim \left(\dfrac{1}{\mathcal{V}}\right)^{-2}\right)$. In these cases it is necessary, using formulae similar to Eqs (6) or (7), to analyse

$$\sqrt{T_r\,(z,\mu)} \sim \overline{\mathcal{V}(z,\mu)} \quad \text{and} \quad \cfrac{1}{\sqrt{T_{1/r}\,(z,\mu)}} \sim \left(\overline{\cfrac{1}{\mathcal{V}(z,\mu)}}\right) \qquad (8a)$$

respectively with the asymptotic form.

All the calculations performed above can easily be generalized to the case where there are more than two discrete eigenvalues. Obviously the procedure for obtaining the lengths L_0 and L_1 will be the same (provided L_1 is considerably greater than L_2) in an analysis of the region where $Z > L_2$. However, the problem of establishing succeeding neutron flux relaxation lengths is much more complicated because higher eigenvalues, if they exist, are usually similar to each other and difficult to separate.

4. Method of obtaining neutron rethermalization lengths from experimental data

In accordance with the conventional terminology $\underline{/}1$, 9, $11\underline{\,/}$, rethermalization length is the name given to one of the two relaxation lengths of the method of overlapping groups in the P_1 approximation. The second of these is called the diffusion length. The difference between these relaxation lengths and the true neutron flux relaxation lengths considered above, as shown in Refs $\underline{/}4$, $5\underline{\,/}$, is that they may be used to try to describe the neutron flux over the whole range of variation of the spatial variable with uniform accuracy, whereas the true relaxation lengths give the correct asymptotic behaviour of the neutron flux. We shall demonstrate this using the equations of the method of overlapping groups in the P_1 approximation for a two-region plane infinite system. In accordance with the basic assumption of the method of overlapping groups, the neutron flux $\psi(z,v)$ at any point Z for either of the regions of the two-region plane system is represented as

$$\psi(z,r) = \sum_{\ell=1,2} \psi_\ell(z) \cdot \chi_\ell(r) \qquad (9)$$

where $\chi_1(v)$ and $\chi_2(v)$ are trial functions representing a neutron spectrum in an infinite medium filled with the substance of the given region. In the P_1 approximation the weighting functions $\Psi_1(Z)$ and $\Psi_2(Z)$ satisfy the familiar system of equations given in Ref. [1, 9]:

$$\mathcal{D}_1 \Delta \Psi_1(z) - \left(\Sigma_{a1} + \Sigma_R^{1 \to 2}\right)\Psi_1(z) + \Sigma_R^{2 \to 1}\Psi_2(z) = -S_1(z)$$

$$\mathcal{D}_2 \Delta \Psi_2(z) - \left(\Sigma_{a2} + \Sigma_R^{2 \to 1}\right)\Psi_2(z) + \Sigma_R^{1 \to 2}\Psi_1(z) = -S_2(z) \tag{10}$$

where the notation of the physical quantities is that conventionally employed.

The fundamental difference between Eq. (9) and Eq. (1) is that instead of the eigenfunctions and the eigenlengths for the given medium Eq. (9) contains certain other functions and lengths. It is clear that, when the trial functions $\chi_{\ell}(v)$ badly reproduce the eigenfunctions of the problem, formula (9) will give an unreliable asymptotic representation of the neutron flux. However, formula (9) is not designed to give the correct asymptotic form. It is arrived at describing with uniform accuracy the neutron spectrum over the whole range of variation of Z.

This means that the relaxation lengths of the method of overlapping groups are not universal. Their degree of universality is evidently directly related to their proximity to the true relaxation lengths. Thus the relaxation lengths of the method of overlapping groups, including the rethermalization length, are of interest for the following reasons: firstly, they are a kind of approximation to the corresponding true relaxation lengths; secondly, they can be used in conjunction with the method of overlapping groups for solving reactor problems; and, thirdly, they are a certain integral characteristic of the experiment.

The relaxation lengths of the method of overlapping groups (diffusion length and rethermalization length) are characteristic numbers in a system of conventional uniform differential equations with constant coefficients [10]. They can be found if the parameters $D_\ell, \Sigma_{a\ell} (\ell=1,2)$ and the rethermalization cross-sections $\Sigma_R^{1 \to 2}$ and $\Sigma_R^{2 \to 1}$ are known. Obviously these relaxation lengths will depend not only on the properties of the medium but also on the form of the trial functions.

In the particular case where one of the rethermalization cross-sections may be neglected (in the first region $\Sigma_R^{1 \to 2} \simeq 0$, this means that the trial function $\chi_1(v)$ has a near-Maxwellian distribution with the temperature

of the first region; in the second region, $\Sigma_R^{2 \to 1} = 0$, it means that the trial function $\chi_2(v)$ has a near-Maxwellian distribution with the temperature of the second region), we obtain for the first region

$$L_{D_1} = \sqrt{\frac{D_1}{\Sigma_{a_1}}} \quad \text{and} \quad L_{rt}^{2 \to 1} = \sqrt{\frac{D_2}{\Sigma_R^{2 \to 1} + \Sigma_{a_2}}} \quad (11)$$

and for the second region

$$L_{D_2} = \sqrt{\frac{D_2}{\Sigma_{a_2}}} \quad \text{and} \quad L_{rt}^{1 \to 2} = \sqrt{\frac{D_1}{\Sigma_R^{1 \to 2} + \Sigma_{a_1}}} \quad (12)$$

where L_{D1} and L_{D2} are the diffusion lengths and $L_{rt}^{2 \to 1}$ and $L_{rt}^{1 \to 2}$ are the rethermalization lengths.

The rethermalization length can also be derived from the neutron gas temperature distribution, using expressions (6) and (7), if the following conditions are observed.

A relationship such as Eq. (6) for neutron gas temperature is obtained with the method of overlapping groups when in the system of equations in expression (10) the source terms S_1 and S_2 for one of the regions can be equated to zero and, consequently, the solution of the system within the limits of that region can be put in the form of the sum of two exponents (with coefficients), one of which contains as parameter the diffusion length L_D and the other the rethermalization length L_{rt}. The neutron gas temperature relaxation length, L_r, obtained with the method of overlapping groups is associated with the diffusion length L_D and the rethermalization length L_{rt} by a relation similar to Eq. (5):

$$L_r^{-1} = L_{rt}^{-1} - L_D^{-1} \quad (5a)$$

Thus with Eq. (6) it is indeed possible to derive the rethermalization length from the experimental neutron gas temperature distribution, provided our assumptions regarding the thermal neutron source correspond to the experimental conditions. It should be borne in mind, however, that Eq. (6) must be used over the whole range of variation of the spatial variable Z (note that in the case of the true relaxation lengths formula (6) is fulfilled only when $Z > 1/x^*$). A relation such as Eq. (7) for the neutron gas temperature is obtained with the method of overlapping groups in the case where,

for the system of equations in expression (10), apart from the source terms S_1 and S_2 being equated to zero, it is assumed that the diffusion coefficients and absorption cross-sections have no energy dependence, i.e. when $D_1 = D_2$ and $\Sigma_{a1} = \Sigma_{a2}$. If these assumptions correspond to the experimental conditions, formula (7) may be used to obtain the rethermalization length from the experimental neutron gas temperature. In this case the parameter minimization range should coincide with the whole range of variation of the spatial variable.

5. Results

5.1. Relaxation lengths in water

Using the method described in section 3, we analysed the asymptotic part of the spatial distribution of the integral thermal neutron density (Figs 7-9) and the asymptotic behaviour of the experimental neutron gas temperature in water (Figs 3-6).

The behaviour of the integral thermal neutron density was analysed as follows: on the basis of Eq. (2) the asymptotic part of the neutron density was described by a function $n(z) = P_0 e^{-z/L_0} + P_1 e^{-z}$. The fundamental length L_0 and the corresponding weight P_0 were determined by graph (Fig. 7). Then $P_0 \cdot exp(-z/L_0)$ was subtracted from the initial curve (the curve of $n(z) - P_0 exp(-z/L_0)$ is given in the same figure under the curve of $n(Z)$) and the first relaxation length L_1 was evaluated in the same way. The results of the analysis are given in Table 2.

No temperature dependence of the fundamental relaxation length L_0 in the 300-343°K water temperature range was detected within the limits of experimental error. The fact that the value obtained is on average somewhat higher than the values supplied by other authors (see, for example, Ref. [16]), is apparently due to the contribution of epithermal neutrons slowing down in water with a length of about 2 cm [2].

Table 2 also shows relaxation lengths L_r obtained by analysing the asymptotic behaviour of the neutron gas temperature in water with the method described in section 3. The parameters g, b and $1/L_r$ were determined by minimizing the corresponding functionals by the method of successive approximations, using the "Tempel-3" and "Tempel-2" programmes [10] based on formulae (6) and (7). The minimization[*] was done in the range $Z = 0.7-8$ cm (here Z is the distance from the thermal barrier in water).

---

[*] For the case where the graphite temperature was 133°K and water temperature 297°K, minimization was performed in the range $Z = 0.5-2.1$ cm.

The primary neutron flux relaxation lengths L_1 were determined from the relaxation lengths L_r with aid of relation (5)[*]/.

The mean value of the first relaxation length in water, L_1, based on activation measurements, is ~ 0.44 cm, whilst the mean lengths derived with formulae (6) and (7) for the asymptotic part of the neutron gas temperature are ~ 0.32 and ~ 0.40 cm respectively.

The relaxation lengths L_1 derived from activation measurements are less reliable because the graph subtraction process involves large errors. The disagreement with the relaxation lengths obtained with formulae (6) and (7) is quite considerable. However, it should be noted that formula (6) is preferable to formula (7) for analysing experiments in the asymptotic part, because it begins to describe the asymptotic part of the experimental curve at lower values of Z than formula (7). In our case this is important because there are very few points in the asymptotic part.

The values obtained for L_1 are much lower than the maximum possible value for water of $\frac{1}{x^*}$ = 0.74 cm. On the one hand this may mean that only a fundamental relaxation length exists in water and the values of L_1 obtained are the result of an attempt to describe a continuous spectrum of eigenvalues with one discrete eigenvalue. On the other hand, the fact that they all fall into a definite range (0.27–0.42 cm) within the error limits may indicate that a quasi-discrete relaxation length exists in the range of the continuous spectrum for water, much as quasi-discrete damping constants can exist in the non-steady-state thermalization problem (see, for example, Refs $/$13, 14$/$. Unfortunately, no final conclusion can be drawn as to the existence of L_1 in water on the basis of this experiment, because there are not enough Z points in the asymptotic part.

5.2. Rethermalization lengths in graphite and water

The rethermalization lengths in graphite and water were obtained by analysing the spatial dependence of the neutron gas temperature using the method described in section 4.

The parameters g, b and $\frac{1}{L_r}$ were determined by minimizing the corresponding functionals by the method of successive approximations, using the "Tempel-3" programme $/$10$/$ based on formula (6). Minimization was done in the range Z = 0–3 cm for water and Z = 0–29.5 cm for graphite (here Z is the distance from the thermal barrier). The rethermalization lengths L_{rt}

---

[*]/   In the analysis of the series B experiments the relaxation lengths in water were obtained on the assumption that the dimensions of the system were infinite in the transverse direction. Numerical evaluations of the effect of two-dimensionality indicate that the corrections to the relaxation lengths are only fractions of a per cent and may be neglected.

for graphite and water were calculated from relaxation lengths obtained with the method of overlapping groups, using Eq. (5a). The results obtained for graphite are given in Table 3 and for water in Table 4.

It can be seen that the neutron rethermalization length in graphite depends strongly on the graphite temperature. This reflects the chemical bond effects in graphite. The results agree well with Bennett's results $\boxed{11}$, which indicates that the rethermalization length in graphite approximates the true primary relaxation length.

The rethermalization characteristics of water were calculated with the "Emodis" programme $\boxed{10}$. The differential scattering cross-sections for water were calculated with the Nelkin model $\boxed{15}$ using G.F. Liman's "PRADIS" programme. The results of the calculations are given in Table 5.

The neutron rethermalization lengths in water obtained here by analysing the experimental curve of neutron gas temperature and those obtained in Refs $\boxed{11, 12}$ are at variance, coming within the range 0.26–0.57 cm. No specific dependence on the temperature of the neighbouring region was observed. The neutron rethermalization lengths in water obtained with the aid of the Nelkin model do depend on the temperature of the neighbouring region, though only very slightly.

The reason for the disagreement, in our opinion, may lie in the fact that the rethermalization lengths were obtained with constants $D(E), \Sigma_a(E)$, $\Sigma_s(E)$ and $\mu(E)$ derived from independent experiments and averaged over the trial functions of both regions. This means that the rethermalization lengths depend directly on the choice of initial constants and the form of the trial functions.

In addition, the disagreement of the rethermalization lengths in water indicates that a neutron physics characteristic of water such as the re-thermalization length is not universal. This disagreement, and also the fact that all the rethermalization lengths are much lower than the limiting value for the true discrete relaxation lengths in water ($\sim$ 0.74 cm), may be taken as additional evidence of there being no primary relaxation length in water.

Table 1

Key:

Серия А/1= series A/1/
Серия Б/2= series B/2/

Table 2

Neutron flux relaxation lengths in water

Key:

Номер эксперимента	= Number of experiment
По какой формуле вычислено	= Formula employed
Длины релаксации, см	= relaxation lengths, cm

Table 3

Rethermalization lengths in graphite

Table 4

Rethermalization lengths in water

Table 5

Retheralization properties of water (Nelkin model$\underline{*/}$)

$\underline{*/}$ Scattering by oxygen was taken into account in accordance with the gas model (the mass of the nucleus was assumed to be 16).

Table 1

	Серия А/I/				Серия Б/2/				
T_c , °К	443	594	725	823	133	133	303	359	443
T_{H_2O} , °К	298	302	305	305	297	343	303	304	294

Неравномерность температуры по объему графита составляла 7°, а воды 3°.

Эксперименты при одинаковой температуре графита и воды были проведены с целью контроля.

Table 2

Длины релаксации потока нейтронов в воде

По какой формуле вычислено	Длины релаксации, см $T_c, °K$ / $T_{H_2O}, °K$	Номер эксперимента					
		I	2	3	4	5	6
	$T_c, °K$	I33	I33	443	594	725	823
	$T_{H_2O}, °K$	297	343	298	302	305	305
(2)	L_0	3,0 ± 0,I5	3,04±0,I5	3,2±0,2	-	-	-
	L_1	0,45± 0,I5	0,43±0,I5	-	-	-	-
(6)	L_2	0,29± 0,03	0,30±0,03	0,37±0,04	0,43±0,04	0,36±0,04	0,40±0,04
	L_1	0,27± 0,03	0,27±0,03	0,33±0,03	0,37±0,04	0,32±0,04	0,35±0,03
(7)	L_2	0,40± 0,04	0,45±0,05	0,50±0,05	0,47±0,05	0,50±0,05	0,48±0,05
	L_1	0,35± 0,04	0,39±0,04	0,42±0,04	0,40±0,04	0,42±0,04	0,41±0,04

Table 3

Длины ретермализации в графите

	I	2	3	4	5	6
T_c, °K	I33	I33	443	594	725	823
T_{H_2O}, °K	297	343	298	302	305	305
T_1, °K	I55	I55	454	596	726	830
L_z, см	18 ± 3	15,6±3,2	7,4±0,7	6,3±0,6	5,I±0,5	4,9±0,5
L_{zt}, см	I0 ± I	9,2±I,I	5,6±0,6	4,9±0,5	4,I±0,4	4,0±0,4
$L_{zt}[11]$, см	–	9,6±0,5*)		4,2±0,2**)	3,5±0,2***)	3,5±0,2****)

x) T_c = I44°K, T_{H_2O} = 283°K

xx) T_c = 523°K, T_{H_2O} = 299°K

xxx) T_c = 690°K, T_{H_2O} = 308°K

xxxx) T_c = 828°K, T_{H_2O} = 315°K

Table 4
Длины ретермализации в воде

	I	2	3	4	5	6
T_c, °К	I33	I33	443	594	725	823
T_{H_2O}, °К	297	343	298	302	305	305
T_2, °К	307	356	303	3I0	3I0	3I5
L_τ, см	0,30±0,03	0,47±0,05	0,52±0,05	0,44 ± 0,04	0,45 ± 0,04	0,48 ± 0,05
$L_{\tau t}$, см	0,26±0,03	0,4I±0,04	0,44±0,04	0,38 ± 0,04	0,39 ± 0,04	0,4I ± 0,04
$L_{\tau t}[H]$, см	-	-	0,35±0,04*)	0,36 ± 0,04**)	0,55 ± 0,05***)	-

ж) $T_{H_2O} = 292$°К, $T_c = 4I0$°К
жж) $T_{H_2O} = 293$°К, $T_c = 558$°К
жжж) $T_{H_2O} = 295$°К, $T_c = 720$°К

Table 5
Ретермализационные свойства воды (модель Нелкина*)

T_I, °К	T_2, °К	T_{H_2O}, °К	L_{D2}, см	D_1, см	Σ_{s1}, см⁻¹	$\Sigma_R^{1\to2}$, см⁻¹	$L_{\tau t}$, см
I55	307	297	3,00	0,I23	3,73	0,735	0,339
I55	356	343	3,I2	0,II9	3,74	0,82I	0,374
380	310	304	2,99	0,I87	2,82	0,689	0,5I4
453	305	300	2,83	0,I89	2,72	0,765	0,49I
596	310	300	2,85	0,20I	2,54	0,748	0,5I4
725	310	300	2,85	0,2II	2,4I	0,724	0,534
883	310	300	2,85	0,2I7	2,35	0,7I0	0,547

* Рассеяние на кислороде учтено по газовой модели (масса ядра полагалась равной I6).
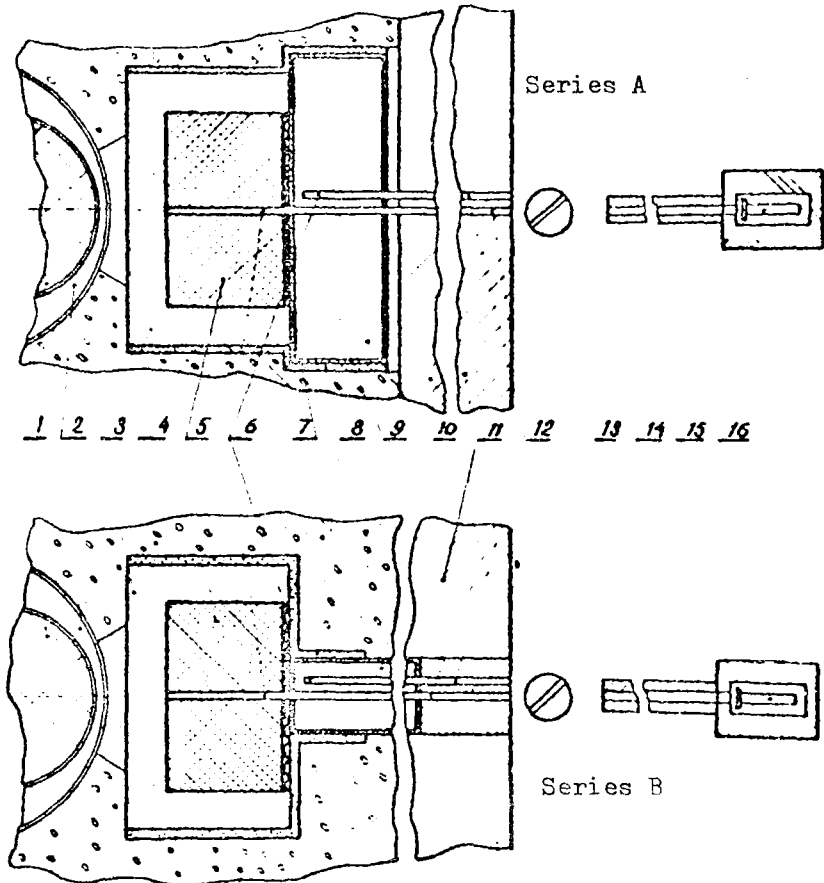
Fig. 1.   Scheme of experimental rig

1 = Core of WWR-2 reactor, 2 = Reflector, 3 = Thermal insulation,

4 = Reactor shield, 5 = Graphite, 6 = Channels for extracting beam,

7 = Heat shields, 8 = Cadmium plus boron carbide, 9 = Aluminium tank,

10 = Water, 11 = Movable shield of WWR-2 reactor, 12 = Collimators,

13 = Mechanical chopper, 14 = Vacuum pipe, 15 = Detector shield,

16 = Detector.
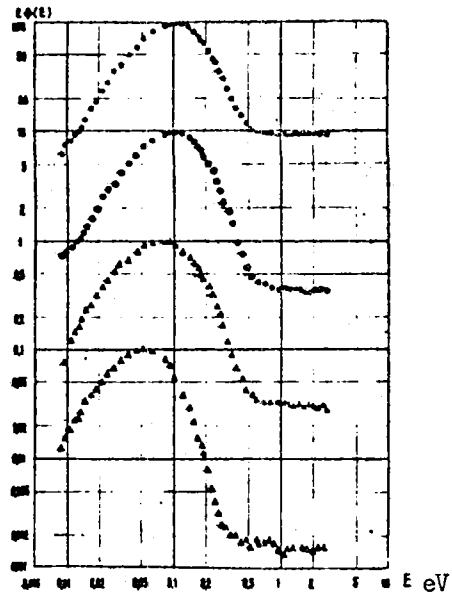
Fig. 2. Neutron spectra in graphite (at a distance of 29.5 cm (●);
4.5 cm (●) from the thermal barrier) and in water (at a
distance 0.2 cm (▲) and 3.0 cm (▲) from the thermal barrier)
at a graphite temperature of 594°K and a water temperature
of 302°K.
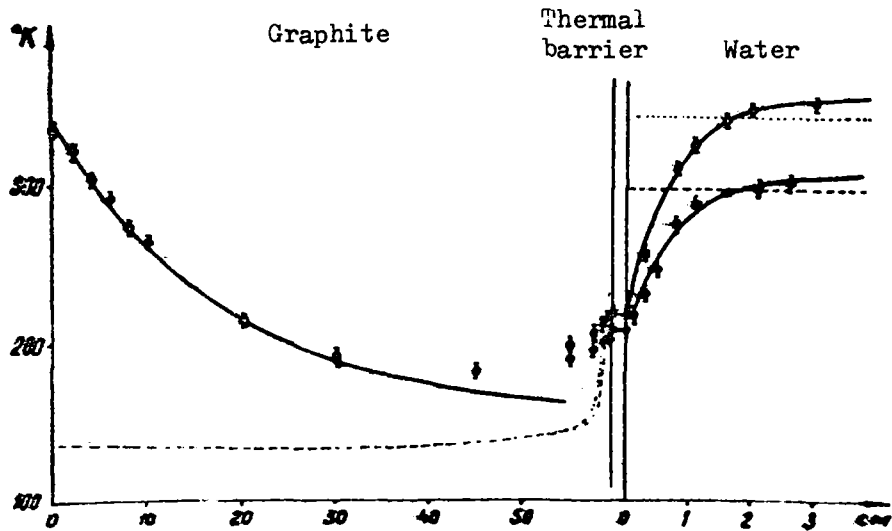
Fig. 3. Neutron temperature distribution in graphite and water at a
graphite temperature of $133°K$ and water temperature of $297°K$
and $343°K$.

●	= neutron temperature	)	
— — —	= temperature of the medium	)	Water temperature $297°K$
O	= neutron temperature	)	
— — —	= temperature of the medium	)	Water temperature $343°K$
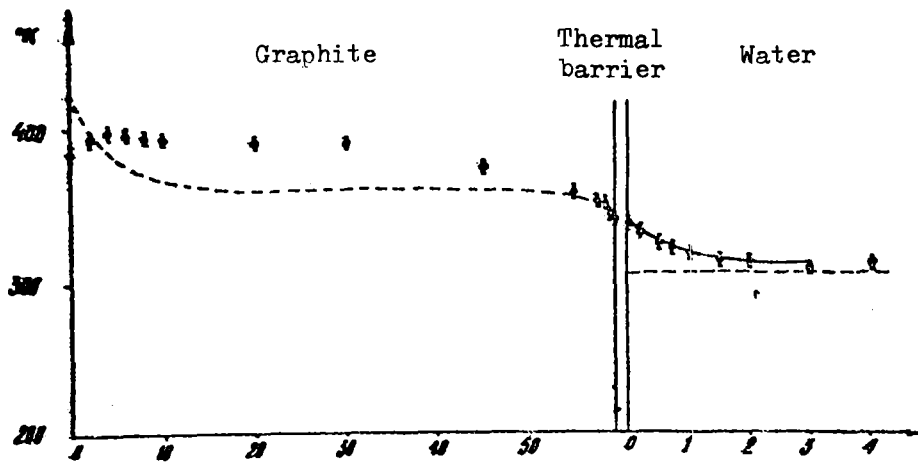
Fig. 4. Neutron temperature distribution in graphite and water at a graphite temperature of 359°K and a water temperature of 304°K.

O   = neutron temperature

— — — = temperature of the medium
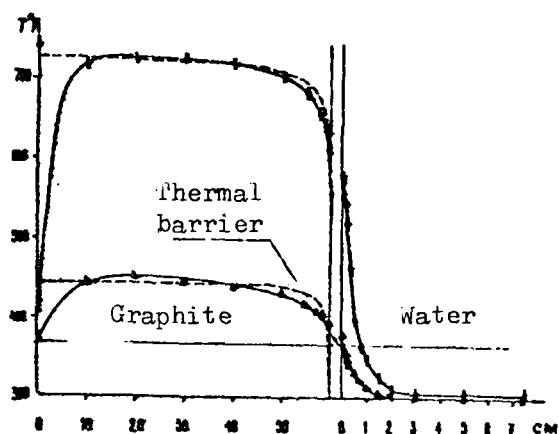
Fig. 5. Neutron temperature distribution in graphite and water at a graphite temperature of $443^{\circ}K$ and a water temperature of $298^{\circ}K$ ($\blacktriangle$ = neutron temperature, — — — = temperature of the medium) and at a graphite temperature of $725^{\circ}K$ and a water temperature of $305^{\circ}K$ (ϕ = neutron temperature, — — — = temperature of the medium).

Fig. 6. Neutron temperature distribution in graphite and water at a graphite temperature of $594^{\circ}K$ and a water temperature of $302^{\circ}K$ (ϕ = neutron temperature, — — — = temperature of the medium) and at a graphite temperature of $823^{\circ}K$ and a water temperature of $305^{\circ}K$ ($\blacktriangledown$ = neutron temperature, — — — = temperature of the medium).
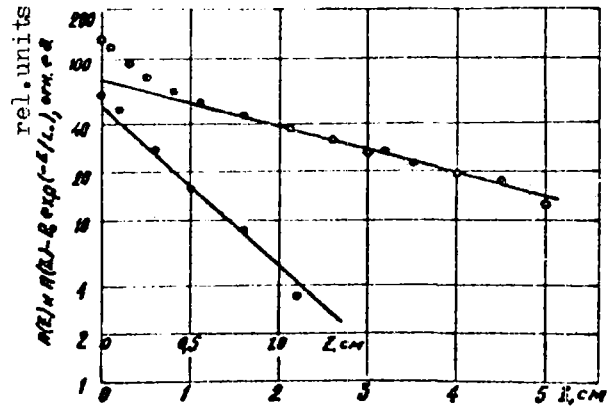
Fig. 7. Intergral thermal neutron density in water at a graphite temperature of $133^{\circ}K$ and a water temperature of $297^{\circ}K$ (O = integral thermal neutron density, ● = integral thermal neutron density after deduction of the term $P_{o} \ell^{-Z/L_{o}}$).
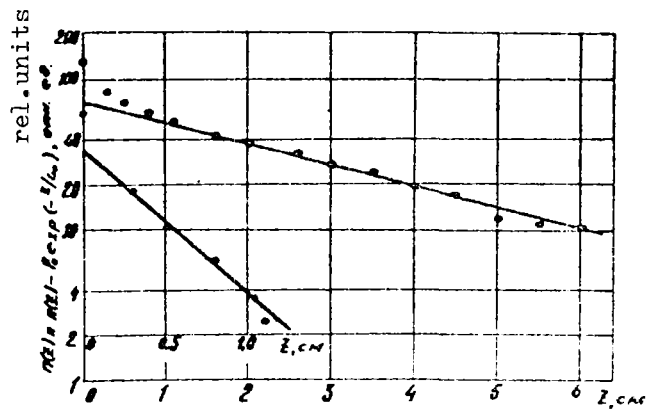
Fig. 8. Integral thermal neutron density in water at a graphite temperature of $133^{\circ}K$ and a water temperature of $343^{\circ}K$. Notation same as Fig. 7.
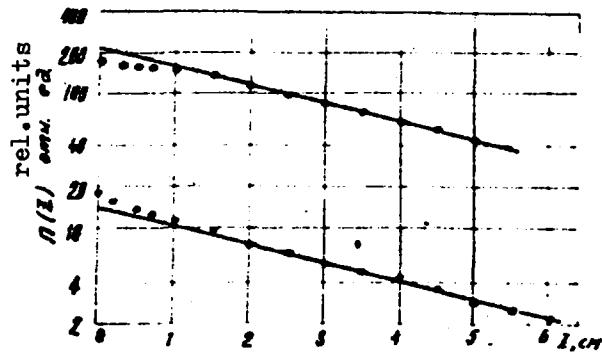
Fig. 9. Integral thermal neutron flux in water

O = graphite temperature 443°K, water temperature 294°K

● = graphite temperature 359°K, water temperature 304°K

REFERENCES

_[1]_ MAIOROV, L.V. et al., in Pulsed Neutron Research (Proc. Symp. Karlsruhe, 1965) 1, IAEA, Vienna (1965) 657.

_[2]_ ABDULAEV, Kh.Sh. et al., in Neutron Thermalization and Reactor Spectra (Proc. Conf. Ann Arbor, 1967) 2, IAEA, Vienna (1968) 233.

_[3]_ ABDULAEV, Kh.Sh. et al., Dliny relaksacii v vode (Relaxation lengths in water) Kurchatov Atomic Energy Institute Preprint, IAE-1612, Moscow (1968).

_[4]_ ABDULAEV, Kh.Sh. et al., Atomn. Energ. 26 6 (1969) 537.

_[5]_ ABDULAEV, Kh.Sh. et al., Atomn. Energ. 26 6 (1969) 538.

_[6]_ ABDULAEV, Kh.Sh. et al., Atomn. Energ. 27 2 (1969) 116.

_[7]_ MOSTOVOY, V.I. et al., Analiz éksperimentov po termalizacii nejtronov (Analysis of neutron thermalization experiments) Kurchatov Atomic Energy Institute Preprint IAE-2027, Moscow (1970).

_[8]_ MOSTOVOY, V.I. et al., Int. Conf. peaceful Uses atom. Energy (Proc. Conf. Geneva, 1958) 16, UN, Geneva (1958) 254.

_[9]_ LINDENMEIER, S.U., in Termalizacija nejtronov (Neutron thermalization), Atomizdat, Moscow (1964) 252.

_[10]_ TRUKHANOV, G.Ya., Programmy raščeta dlin relaksacii potoka nejtronov i dlin retermalizacii na osnove éksperimental'nyh dannyh (Programmes for calculating neutron flux relaxation lengths and rethermalization lengths from experimental data) Kurchatov Atomic Energy Institute preprint, IAE-1973, Moscow (1970).

_[11]_ BENNETT, R.A., "Nucl. Sci. Engng.", 17 (1963) 191.

_[12]_ RASTAS, A., SAASTAMIONEN, J., "Nucl. Sci. Engng.", 36 (1969) 351.

_[13]_ CORNGOLD, N., in Pulsed Neutron Research (Proc. Symp. Karlsruhe 1965) 1, IAEA, Vienna (1965) 199.

_[14]_ KAZARNOVSKY, M.V. et al., in Neutron Thermalization and Reactor Spectra (Proc. Symp. Ann Arbor, 1967) 2, IAEA Vienna (1968) 331.

_[15]_ NELKIN, M., "Phys. Rev." 119 (1960) 741.

_[16]_ "Reactor Physics Constants", ANL-5800 (1967) 111.

RESONANCE INTEGRALS OF ELEMENTS WITH Z $\geqslant$ 90

Yu.P. Elagin

A resonance integral is the name usually given to the quantity

$$ I = \int_{E_H}^{\infty} \sigma(E) \frac{dE}{E} \tag{1} $$

i.e. the cross-section integrated over the Fermi slowing-down spectrum. The lower limit E_H is usually the effective cadmium cut-off.

Resonance integrals of fission, radiative capture and absorption are distinguished by the form of the cross-section under the integral in formula (1). A number of publications supply data on activation resonance integrals. In principle, the activation integral should coincide numerically with the capture integral, but often these values are identified separately in accordance with the method of measurement. Normally the mechanism of only one disintegration is analysed in activation measurement and the resultant activity may or may not be proportional to the total absorption cross-section.

Near an isolated resonance the cross-section of, say, radiative capture $\sigma_\gamma(E)$ is described by the Breit-Wigner formula:

$$ \sigma_\gamma(E) = \sigma_0 \frac{\Gamma_\gamma}{\Gamma} \sqrt{\frac{E_0}{E}} \left[1 + \left(\frac{E - E_0}{\frac{\Gamma}{2}} \right)^2 \right]^{-1} \tag{2} $$

where $\sigma_0 = 4\pi\lambda_0^2 g \frac{\Gamma_n}{\Gamma}$ is the total maximum cross-section in the resonance, E and E_0 are the incident neutron and resonance energies respectively, Γ is the total resonance width, Γ_n and Γ_γ are the partial widths for emission of a neutron and a gamma quantum, $2\pi\lambda_0$ is the neutron wavelength at the resonance energy and g is the statistical weight of the level. If the conditions $E_0 \gg kT$ and $E \gg \Gamma$ are fulfilled and if it is assumed that $\sqrt{\frac{E_0}{E}} \sim 1$

in the resonance region, we obtain

$$I_\gamma = 4120 \, g \, \frac{\Gamma_n \, \Gamma_\gamma}{E_o^2 \, \Gamma} \tag{3}$$

It is usually assumed that the total capture resonance integral I_γ is described sufficiently accurately by the expression

$$I_\gamma \approx \sum_i I_\gamma^{(i)} + I_\gamma^{\frac{1}{v}} \tag{4}$$

where all the resonances i are summed and

$$I_\gamma^{\frac{1}{v}} = \frac{\sigma_\gamma \, (2200 \, {}^M/cc\hbar)}{2} \tag{5}$$

The resonance integrals of fission and absorption can be represented in a form similar to Eq. (4).

Note that the $I^{1/v}$ component of the integral is sometimes omitted from the resonance integrals supplied by investigators.

The table below lists the resonance integrals of infinite dilution for isotopes with $Z \geqslant 90$. The data are arranged as follows:

(1) The first column indicates the type of resonance integral –

> abs = absorption
> fiss = fission
> act = activation
> capt = radiative capture

If it is known that a particular experimental value does not contain the $I^{1/v}$ term, this is indicated with an asterisk.

(2) The second column shows the value and the associated error (in barns) obtained by the author(s).

(3) The third column shows the cut-off E_H. The value of E_H is given in tenths of electron-volts. The symbol TP corresponds to the thermal spectrum.

(4) The fourth column indicates the method used to obtain the resonance integral, and the following abbreviations are used:

ACT — activation method

TOF — time—of—flight

BUR — burn—up in reactor

GAM — total gamma radiation of fission products

ION — ionization chamber

MSA — mass spectrographic analysis of fission products

OSC — oscillator method

EST — estimated from known data

CAL — calculated from resonance parameters

REA — reactivity method: variations in reactivity

REC — recommended value

FIS — fission counter

COM — comparison (back to back)

THE — theoretical estimate

(5) The fifth column shows the normalization standard employed. In most measuring procedures the values obtained are normalized to some standard. The most generally used standards are the isotopes ^{197}Au and ^{59}Co. The values adopted for the resonance integrals of these isotopes have varied to some extent with time. The brackets contain the value of the integral (in barns) used by the author(s).

(6) The sixth column gives the reference to the publication from which the data were obtained. The following abbreviations were employed:

AE — Aktiebolaget atomenergi, report series	Sweden
AECL — Atomic Ener. of Canada Limited, C.R., rep. ser.	Canada
AEEW — Winfrith report series	UK
ANL — Argonne National Lab. report series	USA
ANS — Trans. American Nucl. Soc.	USA
AT — Atomn. Energ.	USSR
BAP — Bull. American Phys. Soc.	USA
BAPS — Bull. American Phys. Soc.	USA
BICJD — Bjul. inf. centr jad Dannym	USSR
BNL — Brookhaven National Lab. report series	USA

CEA/R — Centre d'étude nucléaires, Saclay, rep. ser.   France

CYP — Canadian Journal of Physics   Canada

CRC — Nat. Res. Coun. of Canada, C.R. rep. ser.   Canada

CRRP — Chalk River report series   Canada

DP — Du Pointde Memours Co. Savannah

    — river lab. reports   USA

GA — General Atomic Div., General Dynamic Corp. rep. ser.   USA

IN — Reports Idaho op-office, AEC   UK

JNE — Journ. Nuclear Energy   Netherlands

NP — Nuclear Physics   USA

NSE — Nuclear Science and Engineering   Japan

NST — Nuclear Science and Technology

Nucl — Nucleonics   USA

ORNL — Oak Ridge Nat. Lab. report series   USA

PR — Physical Review   USA

WAPD/T — Westinghouse, Atomic Power Div. rep. ser.   USA

WASH — AEC, Washington reports to the NCSAG   UK

PrNE — Progress in nuclear energy, London

55 Geneva.   International Conference on the Peaceful Uses of
          Atomic Energy (Proc. Conf. Geneva, 1955) UN, New York (1956).

58 Geneva.   International Conference on the Peaceful Uses of
          Atomic Energy (Proc. Conf. Geneva, 1958) UN, Geneva (1958).

66 Paris.   Nuclear Data for Reactors (Proc. Conf. Paris, 1966)
          IAEA Vienna (1967).

66 San Diego.   Reactor Physics in the Resonance and Thermal Regions
          (Proc. Nat. topical Meeting, Am. Nucl. Soc., San Diego, 1966)
          Goodjohn, A.J., Ed., MIT Press, Cambridge, Mass. (1966).

68 Washington.   Neutron Cross-Sections and Technology (Proc. Conf.
          Washington, D.C., 1968) Goldman, D.T., Ed., Gov.
          Printing Office, NBS Spec. Publication No. 299,
          Washington (1968).

(7)   The seventh column indicates the laboratory where the results
were obtained, and the following abbreviations are used:

AE-AB — Atomenergi, Studsvik, Stockholm   Sweden

ANL — Argonne National Laboratory   USA

BET — Westinghouse, Bettis Atomic Power Lab., Pittsburgh   USA

BNL — Brookhaven National Laboratory   USA

BNW — Battelle-Northwest, Richland, Wash.   USA

CRC — Chalk River, Ontario   Canada

FAR — Fontenay-aux-Roses, Seine   France

GA — General Atomic, San Diego, California   USA

GEL — B.C.M.N. EURATOM, Geel   Belgium

HAR – AERE, Harwell   UK

Hanf – Hanford Laboratories   USA

JAE – Japan Atomic Energy Research Inst.   Japan

KAP – Knolls Atomic Power Lab., New York   USA

KFK – Kernforschungszentrum, Karlsruhe   FRG

LRL – Lawrence Radiation Lab., Livermore   USA

MTR – Phillips Petroleum Co. Idaho Falls   USA

ORL – Oak Ridge National Laboratory   USA

SRL – Savannah River Laboratory   USA

SWD – AB Atomenergi, Stockholm   Sweden

WES – Westinghouse Research, Pittsburgh   USA

WIN – AEE, Winfrith   UK

(8) The eighth column gives the date (year) of publication.

To determine the resonance integral (see formula (1)), the microscopic cross-section is integrated over the 1/E flux. However, very few experimental systems have exactly this spectrum. Sometimes investigators make corrections to the measured values to allow for spectra deviating from the 1/E law. In our table the resonance integrals are given as obtained and published by the authors without any assessment of their reliability.

Table

Resonance integrals of isotopes with $Z \geqslant 90$

Key:

Ак	=	ACT
ВП	=	TOF
Вж	=	BUR
Га	=	GAM
ИК	=	ION
МС	=	MSA
Ос	=	OSC
Оц	=	EST
РП	=	CAL
Ре	=	REA
Рк	=	REC
СД	=	FIS
Ср	=	COM
Те	=	THE

мин	=	min
АЭ	=	AT
Женева	=	Geneva
Сан-Диего	=	San Diego
Вашинг	=	Washing.
Париж	=	Paris
БИЦЯД	=	BICJD
БИЦЯД5	=	BWDC

Table

Резонансные интегралы изотопов с   90.

1	2	3	4	5	6	7	8
Th							
abs	84±4	5	Oc	B	CEA/R-2486	FAR	64
Th - 229							
fiss	240				*АЭ* 8,47		60
Th -230							
capt	996±40	5	Ак	Co(74)	CJP 40,194	CRC	62
abs	1020±30	0,5			PR 176,1421	ANL	68
Th- 232							
act	69,8		Oc	Au(1558)	PrNE 1,179	ORL	56
act	67±5	5	Ак	Au	JNE 2,243	ORL	56
act	67±3	5	Ак	Au, In	2,22		57
act	61,8±12,0		Pe	Li(32,2)	3,507		57
abs	93		РП		NSE 4,649	AI	58
abs	85±10	5	Оп		NSE 6,100	ORL	59
abs	106±10		Oc	Au(1513)	JNE 12,32	HAR	60
act	85±10	5	Ак	Au(1565)	JNE 11,95	ORL	60
act	83±6	3,5	Ак	Au(1510)	AEEW 163	WIN	62
act	84±5		Ак	Au(1561)	GA -3069	GA	62
act	82,7±1,8	5	Ак	Au(1462)	NSE 19,244	KFK	64
abs	87±4		Oc	Au(1540)	CEA -2486	FAR	64
abs	81,2±3,4	5	Pe	Au(1579)	NSE 21,406	MTR	65
abs	82,5±1,7	5		Au	NSE 22,121	BET	65
capt	79±4		РП		NP 76,196	HAR	66
abs	84	5	Рк		Nucl 24,108	GA	66
abs	86±5	5			PR 155,1330	BNL	67
Th - 233							
capt	500±150	3				ORL	58
capt	400±100	5	Оп		NSE 6,100	ORL	59
act	400±100	5	Ак	Au(1565)	JNE 11,95	ORL	60
Pa - 231							
abs	1200	1			BAPS 4,414	MTR	59
abs	1200±200				WASH 1029	MTR	60
abs	1560±55	1	РП		NSE 12,243	MTR	62
abs	480	5	Рк		Nucl 24,108	GA	66
Pa- 233							
abs	1072	3	Рк		58 Женева	ORL	58
abs	1200±400	5	Оп		NSE 6,100	ORL	59
act	470±90	5	Ак	Co(75)	CJP 38,751	CRC	60
(— I,2мин)							

1	2	3	4	5	6	7	8
act	460±100 (−6,7тыс.)	5	Ак	Co(75)	CJP 38,751	CRC	60
act	930±135	5	Ак	Co(75)	CJP 38,751	CRC	60
abs	920±90	2	МС	Co(75)	ORNL −3320	ORL	62
capt	820	5	Рк		Nucl 24,108	GA	66
capt	842±35	5	Ак	Co(72)	NSE 29,408	BET	67
abs	901±45	4			NSE 28,133	MTR	67
U							
abs	224±40	5	Рк	Li(32,2)	ЛЭ 3,507		57
U − 232							
abs	280±15	5	МС	Co(75)	NSE 21,257	ORL	65
fiss	320	5	Рк		Nucl 24,108	GA	66
abs	540	5	Рк		Nucl 24,108	GA	66
capt	220	5	Рк		Nucl 24,108	GA	66
U − 233							
fiss	833		Рк		58 Женева	ORL	55
fiss	900±100	5	Оц		NSE 6,100	ORL	59
fiss	865±40		Ак	Co(75)	NSE 17,144	ORL	63
fiss	761±17			Au,B,In,Li	CRRP −1183	CRC	64
fiss	743±24		Га	Au(1535)	AECL −1910	CRC	64
fiss	753±36		Га	In(2790)	AECL −1910	CRC	64
fiss	820±65	5	МС	Au(1555)	ANS 7,272	KAP	64
fiss	798±26	5	Га	Au(1553)	NSE 22,121	BET	65
fiss	764±44	5	Ак	Co(72,5)	66 Сан-Диего	KAP	66
fiss	780	5	Рк		Nucl 24,108	GA	66
fiss	735±15	5			ANS 10,220	ORL	67
fiss	771±49	5	Ак	Co(72)	NSE 29,1	BET	67
fiss	850±90	5			АЭ 28,359		70
abs	927±30				PG Colmb ЗАЭ	MTR	57
abs	1200±200	5	Оц		NSE 6,100	ORL	59
abs	917	5	Рк		Nucl 24,108	GA	66
act	147±7				AENDC(US)28L		62
capt	300±100	5	Оц		NSE 6,100	ORL	59
capt	147±5		МС	Co(75)	WASH −1033	ORL	61
capt	147±7		МС	Co(75)	NSE 17,144	ORL	63
capt	138±10	5	МС	Au(1555)	ANS 7,272	KAP	64
capt	135±7	5	МС	Co(72,3)	66 Сан-Диего	KAP	66
capt	137	5	Рк		Nucl 24,108	GA	66
capt	140±13	5	Мс	Au(1555)	ANS 10,220	ORL	67
capt	135±8	5	Ак	Co(72)	NSE 29,1	BET	67
U − 234							
abs	710	3			BAP 1 187к6	BNL	56

1	2	3	4	5	6	7	8
capt	700±100	5	Оц		NSE 6,100	ORL	59
abs	665	5	Рк		Nucl 24,108	GA	66
capt	700	5,5	Рк		BNL 982,22	BNL	66
U - 235							
fiss	271		Ак	Au(1558)	55 Женева	ANL	55
fiss	292	4			WASH -192		57
fiss	300±50	5	Оц		NSE 6,100	ORL	59
fiss	276±11	5	Га	Au(1535)	NSE 9,341	BET	61
fiss	263±12	6	Га	Au(1535)	DP -817	SRL	63
fiss	272±8	4,5	Га	Au(1535)	CRRP -1183	CRC	64
fiss	298±14	4,5	Га	In(2790)	CRRP -1183	CRC	64
fiss	275±9		Га	Au	EANDC(E)33L	SWD	64
fiss	274±10				BNL 325 Sup2		64
fiss	288±18	3,9	Ак	Au(1553)	ANS 7,78	KAP	64
fiss	292	4,1	Оц		GA -5944	GA	64
fiss	279±8	5	Га	Au(1550)	AE 181	AE	65
fiss	269±16	5	Ак	Co(72,5)	66 Сан-Диего	KAP	66
fiss	280	5	Рк		Nucl 24,108	GA	66
fiss	275±16	5		Co	NSE 29,1	BET	67
fiss	222,0±2,0	62	Ср		68 Вашинг.,475	GEL	68
fiss	258	5	СД		NSE 35,350	LRL	69
fiss	274±11	5			АЭ 28,359		70
abs	450±100	5	Оц		NSE 6,100	ORL	59
abs	445	4,1	Оц		GA -5944	GA	64
abs	420	5	Рк		Nucl 24,108	GA	66
abs	380				68 Вашинг.,127	SRL	68
act	271±25				ANL -5800	ANL	58
capt	150±50	5	Оц		NSE 6,100	ORL	59
capt	144±5		МС	Au(1535)	EANDC(can)20L	CRC	63
capt	148±7	3,9	МС	Au(1535)	ANS 7,78	KAP	64
capt	133+7	5	МС	Co(72,5)	66 Сан-Диего	KAP	66
capt	140	5	Рк		Nucl 24,108	GA	66
capt	143±7	5			66 Париж 2,17	CRC	66
capt	136±8	5			NSE 29,1	BET	67
capt	134±8	1,8			АЭ 24,351		68
U - 236							
abs	310				BAP -1,187 K6	BNL	56
act	400				WASH -191	ORL	56
act	350				ANL -5800	ANL	58
act	350±40			Au	58 Женева	ORL	58
act	257±22	5	Ак	Co(48,6)	JNB 7,81	CRC	58
capt	400±100	5	Оц		NSE 6,100	ORL	59

1	2	3	4	5	6	7	8
capt	381	5	Ак	Au(1558)	WASH 1041	MTR	62
capt	320	5	Рк		Nucl 24,108	GA	66
capt	400±40	5,5	Рк		BNL 982,22	BNL	66
capt	350±25	5			GA 9057	GA	68
capt	417±25	5	Ак		NSB 32,265	SRL	68
abs	400±40				68 Вашинг. I27I	SRL	68
capt	350±25	5			NP A141, 577		70
capt	300	5	РП		БИЦЯД 5, I59		68
U - 237							
abs	290				68 Вашинг.,I27I	SRL	68
U - 238							
abs	276±12	5			PR 99,10	BNL	55
act	281±20	5	МС	Au(1558)	JNE 2,243	ORL	56
act	279±20				PR 105,661	ANL	57
abs	224±40		Ос	Li(71)	АЭ 3,507		57
abs	269		РП		NSB 4,649	AI	58
act	280±15	5	Од		NSB 5,100	ORL	59
abs	285±25		Ос	Au(1513)	JNEA 12,32	HAR	60
act	282±8	5	Ак	Au(1535)	NSB 14,358	WES	62
abs	280±10	6,2		Au	DP -817	SRL	63
act	277±10	5,5	Га	Au(1535)	ANS 7,27	SRL	64
capt	280±12		Рк		BNL325 Sup 2	BNL	66
capt	278	5	Рк		Nucl 24,108	GA	66
abs	270			Au(1579)	NSB 25,12		66
Np - 237							
abs	870±130		Ос	Au(1510)	58 Женева	HAR	58
abs		27			АЭ 6,569		59
abs	945±130		Ос	Au(1513)	JNEA 12,32	HAR	60
capt	500	5,5	.Рк		BNL 982,22	BNL	66
abs	905	5		Au(1558)	ANS 10,259	MTR	67
abs	850				68 Вашинг.,I27I	SRL	68
abs	900±30	5	Ре	Au	IN -1195	MTR	68
capt	715±5	5	РП		БИЦЯД 5, I59		68
Np - 238							
abs	1500±500				68 Вашинг.,I27I	SRL	68
Np - 239							
abs	415	5	Рк		Nucl 24,108	GA	66
Pu - 238							
capt	3260±280	5	МС	Co(36,4)	CJP 35,147	CRC	57
fiss	25±5	6			58 Женева	CRC	58
fiss	25	5,5	Рк		BNL 982,22	BNL	66
capt	150	5,5	Рк		BNL 982,22	BNL	66

1	2	3	4	5	6		7	8
abs	168±15	5			NSE	30,355	MTR	67
abs	169				68 Вашинг.,1271		SRL	68
	Pu - 239							
fiss	2000±200	5	Оц		NSE	6,100	ORL	59
fiss	327±22	5	СД	Au(1535)	NSE	9,341	BET	61
fiss	324±9	4,5	СД	Au	CRRP	1183	CRC	64
fiss	319±12	5			EANDC(E)33L		SWD	64
fiss	314±9		СД	Au(1535)	AECL	1910	CRC	64
fiss	385±18			In, Li	AECL	1910	CRC	64
fiss	301±10	5	СД	Au(1550)	AE	-181	AE	65
fiss	333±15		Рк		BNL 325 Sup 2		BNL	66
fiss	288	5	Рк		Nucl	24,108	GA	66
fiss	365±26	5		Au	NST	4,43L	JAE	67
fiss	330±30	5			АЭ,	24,351		68
fiss	330±30	5			АЭ,	28,359		70
abs	460±23				АЭ	1,27(No.3)		56
abs	3500±500	1,5	Оц		NSE	6,100	ORL	59
abs	472	5	Рк		Nucl	24,108	GA	66
capt	656±26	5			CRC	-633	CRC	56
capt	1500±300	5	Оц		NSE	6,100	ORL	59
capt	184	5	Рк		Nucl	24,108	GA	66
fiss	Pu - 540 $^{184}_{5±6}$				58 Женева			5B
abs	11000±2800	5	Ос	Li(32,2)	55 Женева		CRC	55
abs	9000±3000		Ак		АЭ I № 3			56
act	8700±800		Ак		CRC	-633	CRC	56
abs	10000±2800	2	Ос		АЭ 2, 240			57
abs	11300±1000		Ос	Au(1510)	58 Женева		HAR	58
capt	9000±1500	1,5	Оц		NSE	6,100	ORL	59
abs	8700±800				NSE	5,32	BNW	59
capt	8700±550	5	Ак	Au(1525)	CJP	38,57	CRC	60
abs	8270±500		Ос	Au(1513)	AEEW-R 115		HAR	62
abs	8620±700		Pe		NSE	17,144	Hanf	63
abs	8280	5	Рк		Nucl	24,108	GA	66
capt	8000	5,5	Рк		BNL	982,22	BNL	66
capt	8035	5	РП		БИЦЯД 5,159			68
	Pu - 241							
fiss	1800±300	1,5	Оц		NSE	6,100	ORL	59
fiss	557±33	5	СД	Au(1535)	NSE	9,341	BET	61
fiss	541±14	4,5	СД	Au	CRRP	-1183	CRC	64
fiss	573	5	Рк		Nucl	24,108	GA	66
fiss	545	5,5	Рк		BNL	982,22	BNL	66
fiss	550±40	5			АЭ	28,359		70

1	2	3	4	5	6	7	8
abs	2800±500	1,5	Оц		NSE 6,100	ORL	59
abs	712	5	Рк		Nucl 24,108	GA	66
abs	1389±15				WASH-1136,43		69
capt	1000±300	1,5	Оц		NSE 6,100	ORL	59
capt	139	5	Рк		Nucl 24,108	GA	66
capt	260	5,5	Рк		BNL 982,22	BNL	66

Pu - 242

1	2	3	4	5	6	7	8
fiss	0,6				ANS 10,228	BNL	67
abs	1275±30	5	МС	Co(48,6)	CJP 35,147	CRC	57
capt	1300±20	1,5	Оц		NSE 6,100	BNL	59
capt	1050±150	5		Co	PR 114,505	ANL	59
abs	1280±60		Ак	Co(75)	ORLN-3679,13	ORL	64
capt	1100	5	Рк		Nucl 24,108	GA	66
capt	1150	5,5	Рк		BNL 982,22	BNL	66
act	1180	9,2	Ак	Co(75)	68 Вашинг.,1279	SRL	68
capt	1061	5	РП		БИЦЯД 5, 159		68

Pu - 244

1	2	3	4	5	6	7	8
capt	35±7			Au(1558)	WASH 1136,51	MTR	69

Am - 241

1	2	3	4	5	6	7	8
fiss	8,5	5,5	Те		BNL 982,22	BNL	66
fiss	21±2	5		Au	АЭ 23,316		67
fiss	21±2	5			АЭ 28,359		70
act	900		Ак	Au(1558)	WASH 1053,76	MTR	64
capt	1600	5,5	Те		BNL 982,22	BNL	66
capt	1470±135	5·	РП		PR 114,505	ANL	59
capt	2100±200 (→16 час)	5		Au	АЭ 23,316		67
capt	300±30 (→152 ч.)	5		Au	АЭ 23,316		67
capt	850±60 (→16 час)	5		Co(74,6)	WASH 1136,53	MTR	69
capt	250±40 (→152 ч.)	5		Co(74,6)	WASH 1136,53	MTR	69
capt	1472	5	РП		БИЦЯД,5, 159		68

Am - 242

1	2	3	4	5	6	7	8
fiss	< 300	5		Au	АЭ 23,316		67

Am - 242^m

1	2	3	4	5	6	7	8
abs	7000±2000	5		Co(74,6)	WASH 1136,53	MTR	69
fiss	1570	5			PR 166,1219	LRL	68
fiss	1570±110	5			NSE 32,131	LRL	68

Am - 243

1	2	3	4	5	6	7	8
fiss	1,5		Те		ANS 10,228	BNL	67

1	2	3	4	5	6	7	8
abs	2290±50	5	Ак	Au(1558)	CJP 35,147	CRC	57
abs	1470±135				58 Женева	ANL	58
capt	1400	5,5			BNL 982,22	BNL	66
capt	1400		Te		ANS 10,228	BNL	67
capt	2300±200	5		Au	АЭ 23,316		67
	111(←10)	5		Au, Co	IN -1126	MTR	67
capt	2160	5		Au, Co	IN -1126	MTR	67
	(←оба изомера)						
Cm - 242							
act	2250	8,3	Ак	Co(75)	68 Вашинг.,1279	SRL	68
abs	1470				68 Вашинг.,1285	SRL	68
capt	1335	5	РП		БИЦЯД 5, 159		68
Cm - 242							
capt	150±40	5		Co	WASH 1136,53	MTR	69
	(←32 ч.)						
Cm - 244							
fiss	72		Te		ANS 10,228	BNL	67
capt	650	5,5			BNL 982,22	BNL	66
capt	650		Te		ANS 10,228	BNL	67
act	700	8,3		Co	68 Вашинг.,1279	SRL	68
capt	625	5	РП		БИЦЯД 5, 159		68
capt	650±50	5		Co(74,6)	WASH 1136,54	MTR	69
abs	621				68 Вашинг.,1285	SRL	68
Cm - 245							
fiss	345		Te		ANS 10,228	BNL	67
capt	133		Te		ANS 10,228	BNL	67
act	260			Co	68 Вашинг.,1279	SRL	68
abs	680±30			Co(74,6)	WASH 1136,54	MTR	69
Cm - 246							
fiss	18		Te		ANS 10,228	BNL	67
abs	2800		Te		ANS 10,228	BNL	67
capt	140				BNL 325 Sup 2	BNL	65
act	260			Co(75)	68 Вашинг.,1279	SRL	68
capt	110±40	5		Co(74,6)	WASH 1136,54	MTR	69
Cm - 247							
fiss	492		Te		ANS 10,228	BNL	67
capt	200		Te		ANS 10,228	BNL	67
Cm - 248							
fiss	0,2		Te		ANS 10,228	BNL	67
capt	600		Te		ANS 10,228	BNL	67
act	350±40		Ак	Mn(13,1)	ORNL 3832	ORL	65
Bk - 249							
fiss	5		Te		ANS 10,228	BNL	67

1		2	3	4	5	6	7	8
capt	1850			Te		ANS 10,228	BNL	67
act	1240		5,5		Co(75)	68 Вашинг.,1279	SRL	68
	Cf - 250							
fiss	85			Te		ANS 10,228	BNL	67
capt	940			Te		ANS 10,228	BNL	67
act	5300				Co(75)	68 Вашинг.,1279	SRL	68
	Cf - 251							
fiss	445			Te		ANS 10,228	BNL	67
capt	172			Te		ANS 10,228	BNL	67
act	980				Co(75)	68 Вашинг.,1279	SRL	68
	Cf - 252							
fiss	5			Te		ANS 10,228	BNL	67
capt	1800			Te		ANS 10,228	BNL	67
act	42		9,2		Co(75)	68 Вашинг.,1279	SRL	68
act	43,5±3		5			NSE 27,228	ORL	69
capt	44					ORNL 4428	ORL	69
	Cf - 253							
fiss	198			Te		ANS 10,228	BNL	67
capt	540			Te		ANS 10,228	BNL	67
	Cf - 254							
fiss	28			Te		ANS 10,228	BNL	67
capt	1650			Te		ANS 10,228	BNL	67
capt	1650					ORNL -4428	ORL	69
	Es - 253							
act	3600		5,5		Co(75)	68 Вашинг.,1279	SRL	68

USE OF THE ITERATION METHOD FOR RAPID UNFOLDING OF
A SPECTRUM OF ARBITRARY FORM

V.S. Troshin, E.A. Kramer-Ageev, R.D. Vasilev

E.I. Grigorev, G.B. Tarnovsky, V.P. Yaryna

Work is being carried out in the All-Union Scientific Research Institute of Physico-Technical and Radiotechnical Measurements aimed at standardizing the methods and equipment used for neutron measurements, and the Institute is now preparing, in conjunction with the Moscow Engineering-Physics Institute, to issue instructions for unfolding fast neutron reactor spectra from measurements of induced activity in threshold detectors. These instructions are centred around a rapid method for unfolding fast neutron spectra $/\!\!-1\!\!\_/$, using the effective threshold cross-sections.

The effective threshold cross-section calculated for different types of spectra are given in Refs $/\!\!-2\!\!-5\!\!\_/$. Ref. $/\!\!-5\!\!\_/$ recommends optimum values of the effective threshold (E_{eff}) and the effective threshold cross-section (σ_{eff}) for a group of spectra comprising the fission neutron spectrum and fission neutron spectra after passage of neutrons through layers of polyethylene, carbon, iron, lead and nickel. The values obtained agree with EURATOM recommendations $/\!\!-4\!\!\_/$.

When unfolding neutron spectra not included in the above group, errors may arise due to differences between the recommended effective threshold cross-sections and the cross-sections corresponding to the spectrum being constructed. To increase the accuracy of unfolding such spectra, we propose a method of iterative refinement of the results of the unfolding which involves redetermining the values of σ_{eff} for constant values of E_{eff}. This method of iterative refinement simplifies the calculation compared with the method employed in Ref. $/\!\!-6\!\!\_/$, in which the effective reaction threshold is redetermined for each iteration.

The unfolding of a spectrum by the rapid iterative method is done in the following sequence:

(1) The neutron spectrum is unfolded by the method described in
Ref. $/\!\!-1\!\!\_/$, using the effective threshold cross-sections
supplied in Refs $/\!\!-1, 5\!\!\_/$ (zero approximation).

(2) Using the exponential form of the spectrum obtained in the zero approximation $[f^0(E)]$ and the well-known dependence of reaction cross-section on energy $[G_i(E)]$, we calculate the activation integrals R_i^o for the ith reaction:

$$R_i^o = \int_0^\infty G_i(E) \cdot f^0(E)dE \approx \sum_{k=1}^n f^0(E_k) \cdot \int_{E_k}^{E_{k+1}} G_i(E) \cdot e^{-\mu_k^o(E-E_k)} \cdot dE \ , \qquad (1)$$

where $f^0(E_k)$ is the differential flux density at the lower boundary of the kth interval, and the coefficient μ_k^o is calculated from the formula

$$\mu_k^o = \frac{1}{E_{k+1} - E_k} \cdot \ell n \frac{f^0(E_k)}{f^0(E_{k+1})} \ . \qquad (2)$$

For convenience we have tabulated the values of the integrals

$$J_i(\mu_k) = \int_{E_k}^{E_{k+1}} G_i(E) \cdot e^{-\mu_k(E-E_k)} \cdot dE \qquad (3)$$

for $-2 \leqslant \mu_k \leqslant 2$ for the intervals 0.5-1.5; 1.5-2.5; ....; 9.5-10.5 and 10.5-17 MeV. The dependence of J_i on μ_k is given in Figs 1-12, and the following numerical key has been adopted for the reactions:

$1 - ^{237}Np(n,f)$; $2 - ^{103}Rh(n,n')$; $3 - ^{115}In(n,n')$; $4 - ^{238}U(n,f)$;
$5 - ^{232}Th(n,f)$; $6 - ^{31}P(n,p)$; $7 - ^{64}Zn(n,p)$; $8 - ^{32}S(n,p)$;
$9 - ^{58}Ni(n,p)$; $10 - ^{54}Fe(n,p)$; $11 - ^{35}Cl(n,\alpha)$; $12 - ^{27}Al(n,p)$;
$13 - ^{28}Si(n,p)$; $14 - ^{90}Zr(n,p)$; $15 - ^{56}Fe(n,p)$; $16 - ^{59}Co(n,\alpha)$;
$17 - ^{24}Mg(n,p)$; $18 - ^{27}Al(n,\alpha)$; $19 - ^{203}Tl(n,2n)$; $20 - ^{127}J(n,2n)$;
$21 - ^{65}Cu(n,2n)$; $22 - ^{55}Mn(n,2n)$; $23 - ^{19}F(n,2n)$; $24 - ^{63}Cu(n,2n)$.

For the reactions $^{237}Np(n,f)$, $^{103}Rh(n,n')$ and $^{15}In(n,n')$, the contribution of neutrons with energy less than 0.5 MeV was taken into account when calculating the integral $J(\mu)$ in the range 0.5-1.5 MeV. For the remaining reactions this contribution is negligible.

(3) The effective threshold cross-sections are derived from the calculated activation integrals in a first approximation:

$$\overline{\sigma}_{i\ \text{eff}} = \frac{R_i''}{\phi^o(E_{i\ \text{eff}})}, \qquad (4)$$

where $\phi^o(E_{i\ \text{eff}})$ is the integral flux density of neutrons with energy above $E_{i\ \text{eff}}$, obtained in the zero approximation.

(4) The integral neutron flux densities are determined in a first approximation, using the experimental values of the activation integrals and the effective threshold cross-sections obtained in a first approximation:

$$\phi^1(E_{i\ \text{eff}}) = \frac{R_{i\ \text{exp}}}{\sigma_i^1\ \text{eff}} \qquad (5)$$

and the spectrum is unfolded in a first approximation [1].

The iteration process is repeated until the differential flux densities in the centres of the energy intervals obtained in two successive approximations agree to within ~15% (this figure is accounted for by the errors in the method used and the calculations).

By way of example Fig. 13 shows a spectrum unfolded on the basis of two iterations which differ considerably from the fission spectrum.

REFERENCES

[1] TROSHIN, V.S. et al., Atomn. Energ. 29 (1970) 37.

[2] KHARIZOMENOV, Yu.V. et al., Bjul. inf. Centr jad. Dannym, Issue No. 3 (1966).

[3] KORMUSHKIN, Yu.P. et al., Bjul. inf. Centr jad. Dannym, Issue No. 4 (1967).

[4] ZEIP, W.L., RCN-Int-64-036.

[5] BORISOV, G.A. et al., Izmerit. Tekh. (in press) Rekomendacii po vyboru effektivnyh porogov i sečenij (Recommendations for selection of effective thresholds and cross-sections).

[6] BRESESTI, M. et al., in Neutron Dosimetry, (Proc. Conf. Harwell, 1962) 1, IAEA Vienna (1963) 27.

Fig. 1

Fig. 2

Fig. 3

Fig. 4

4.5-5.5
MeV

Рис. 5.

Fig. 5

Fig. 6

Рис. 7.

Fig. 7

Гис. 8.

Fig. 8

Рис. 9.

Fig. 9

Рис. 10.

Fig. 10

Рис. II.
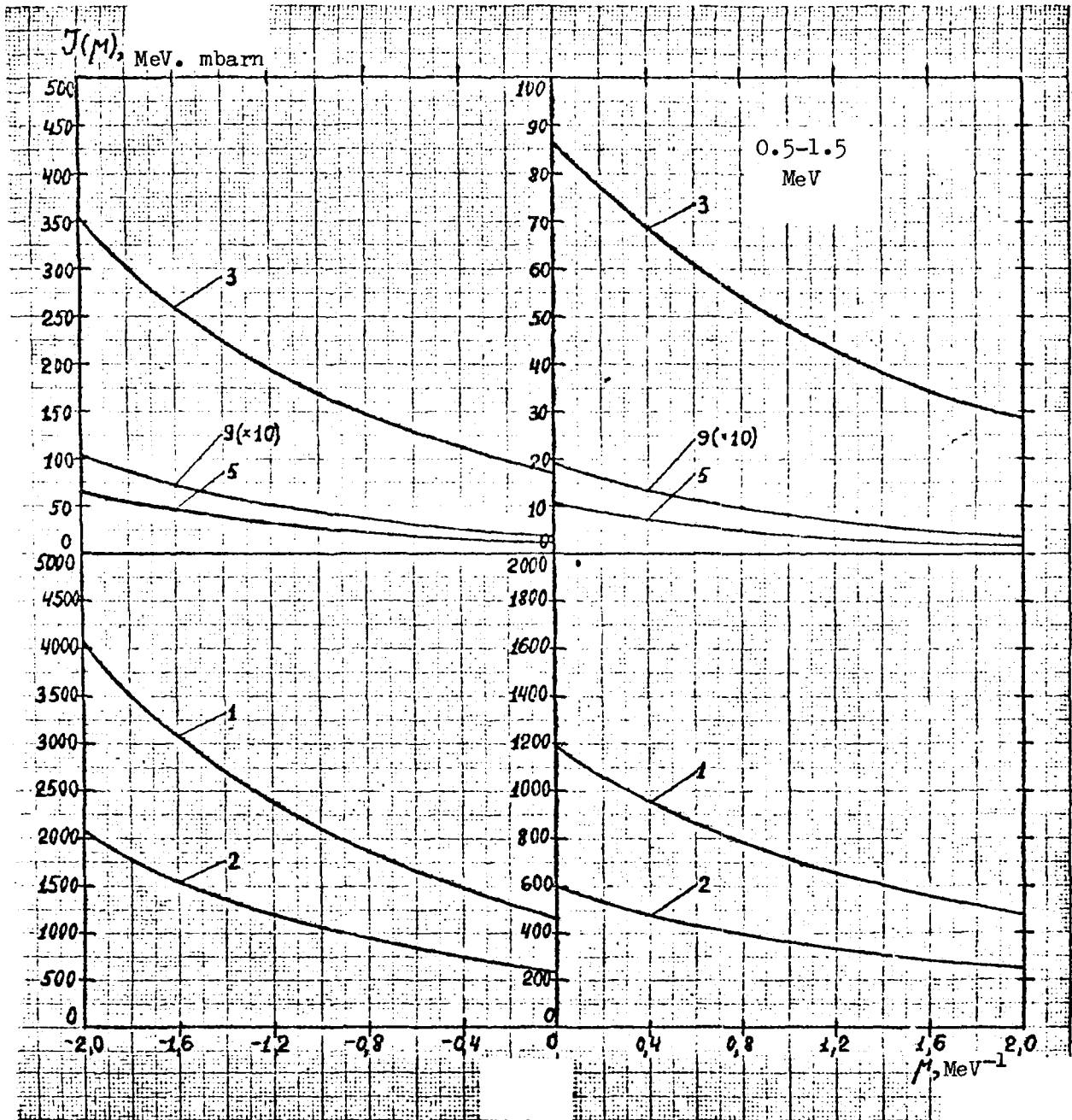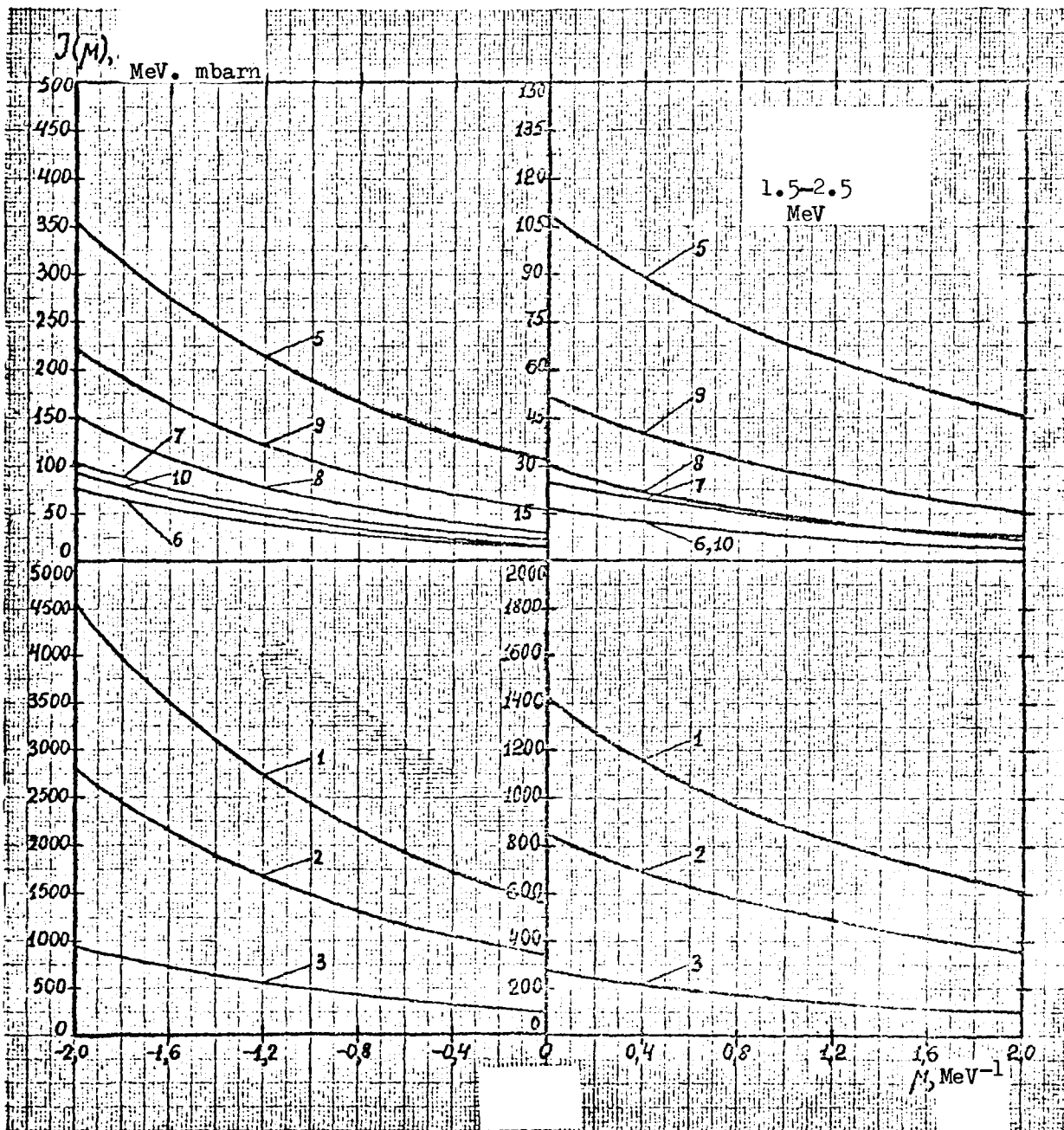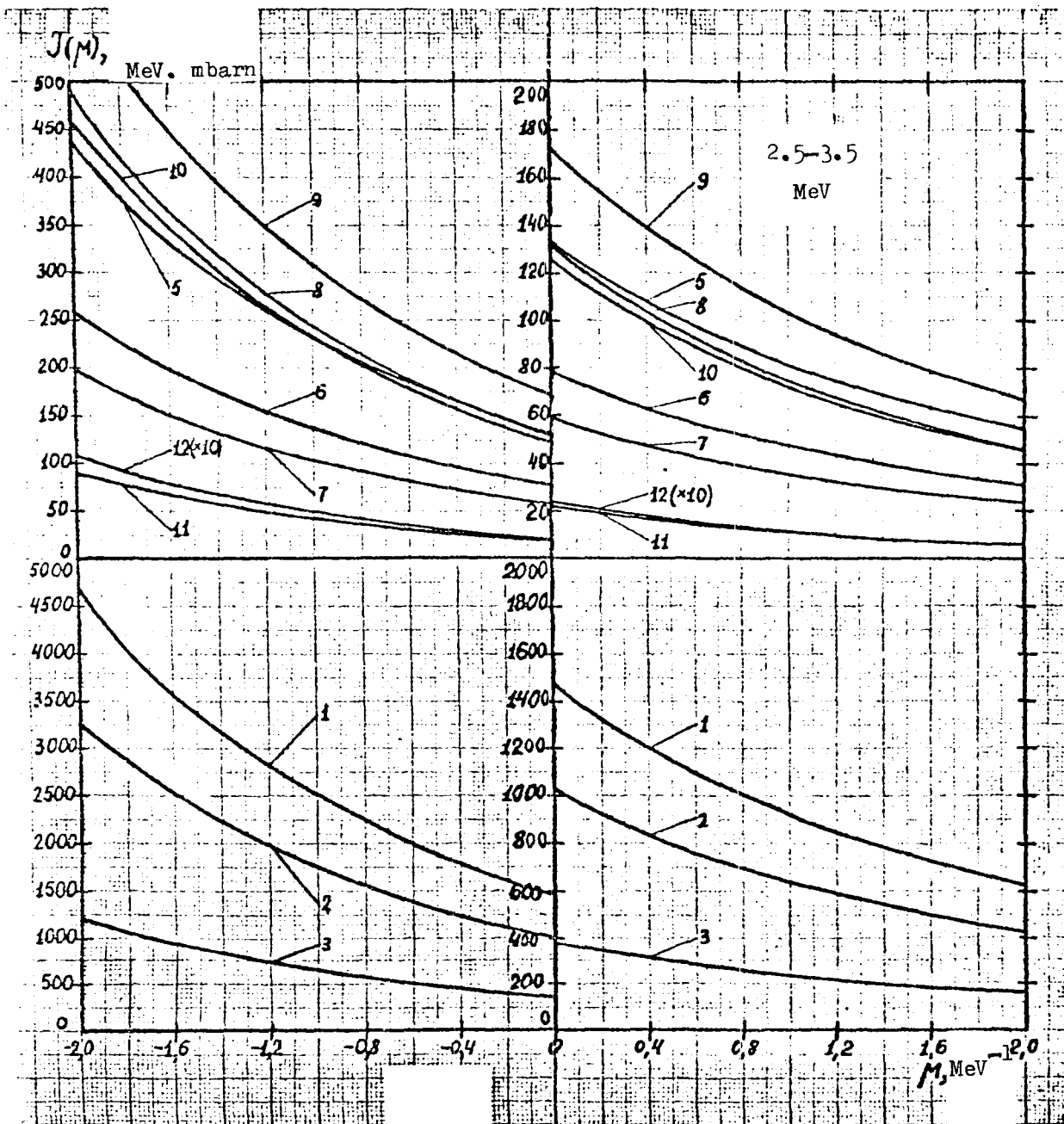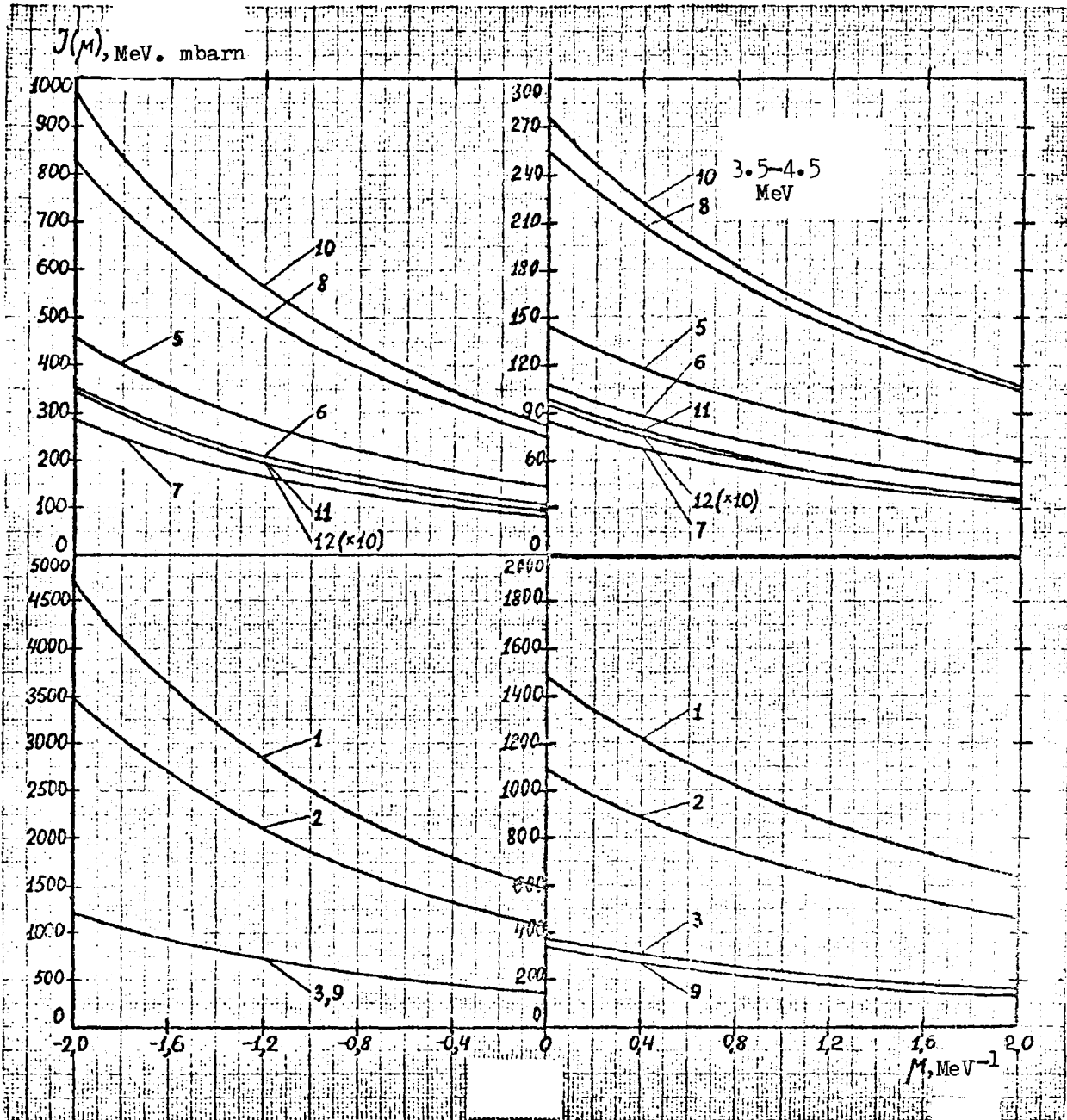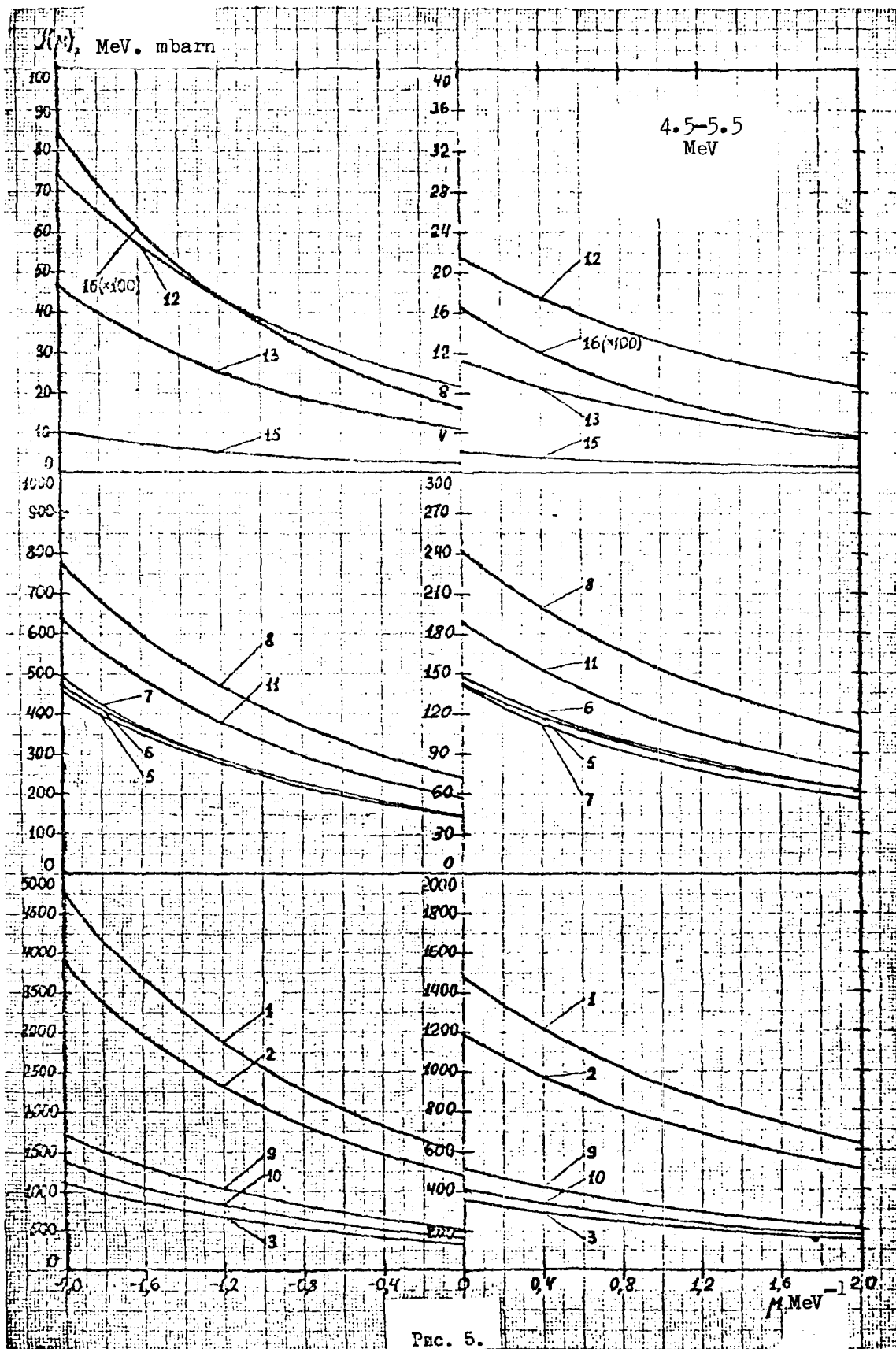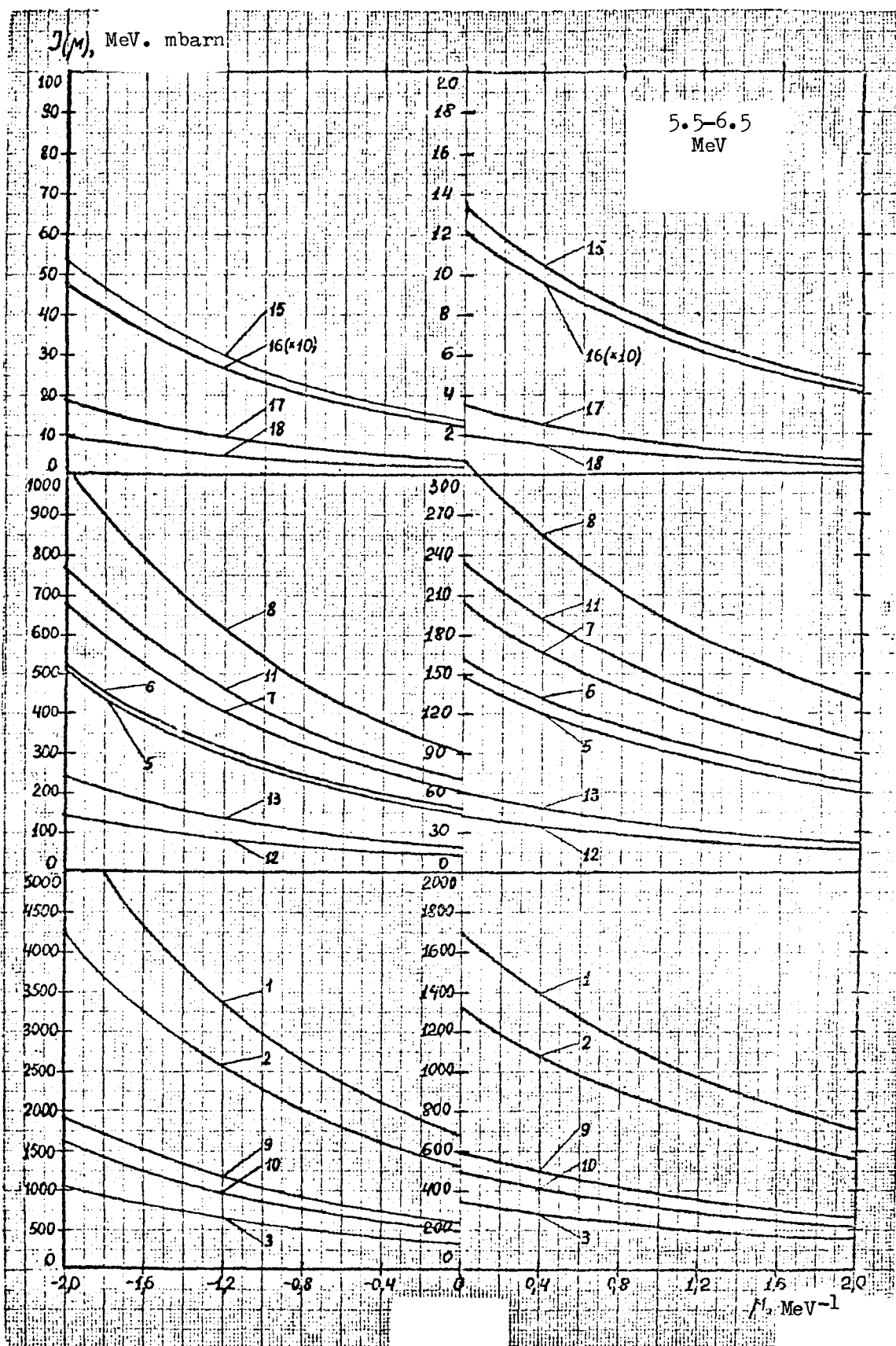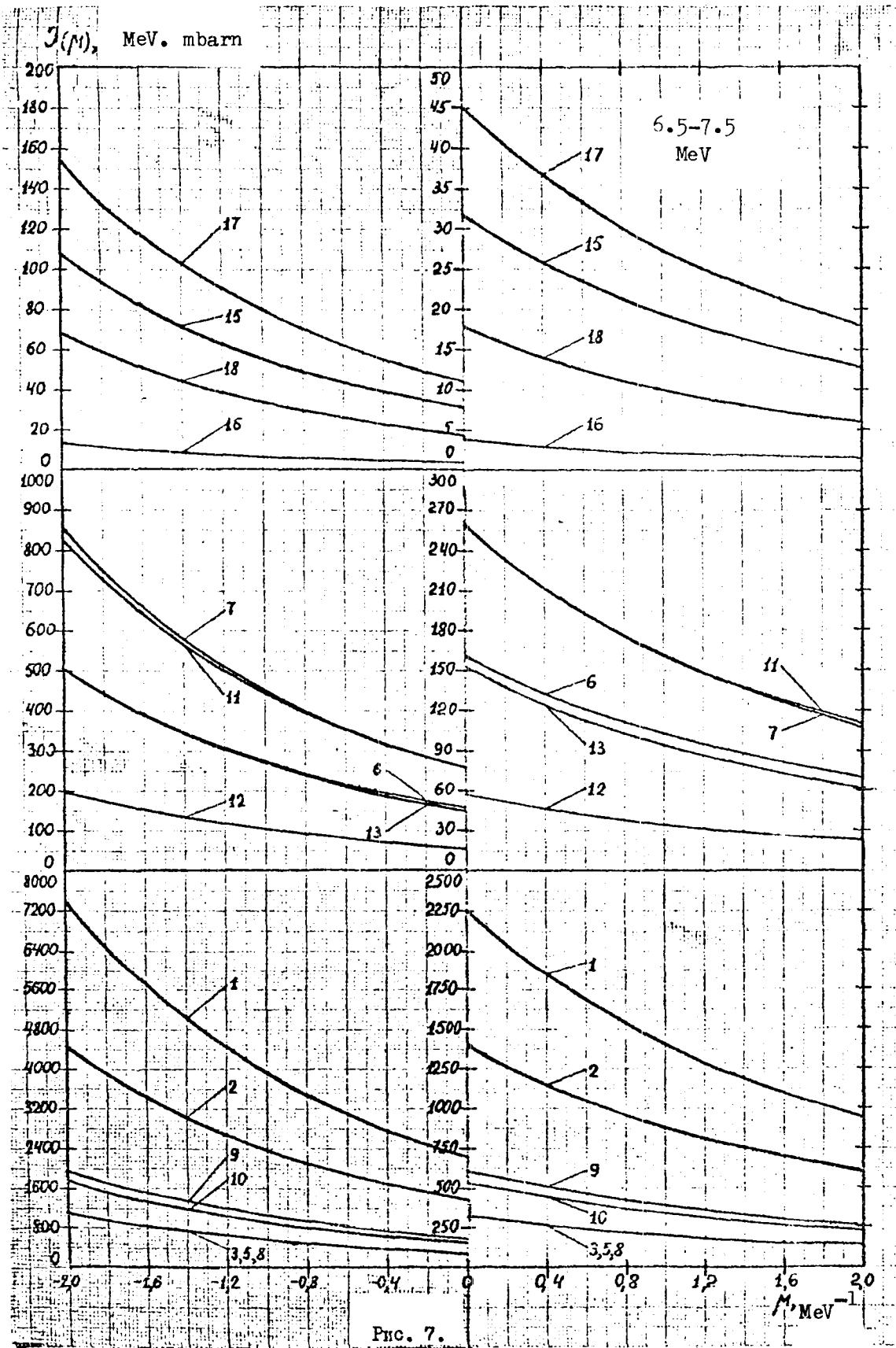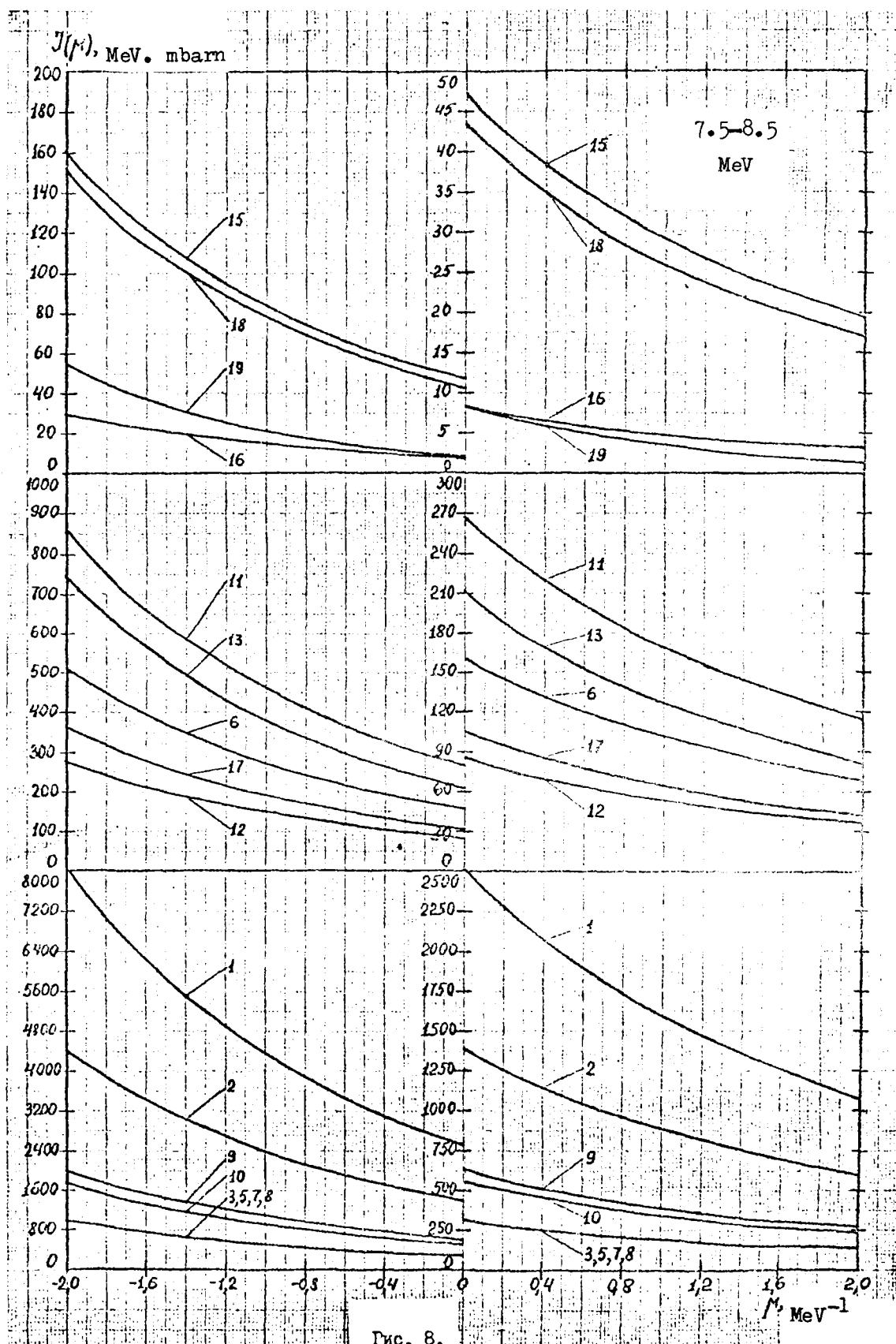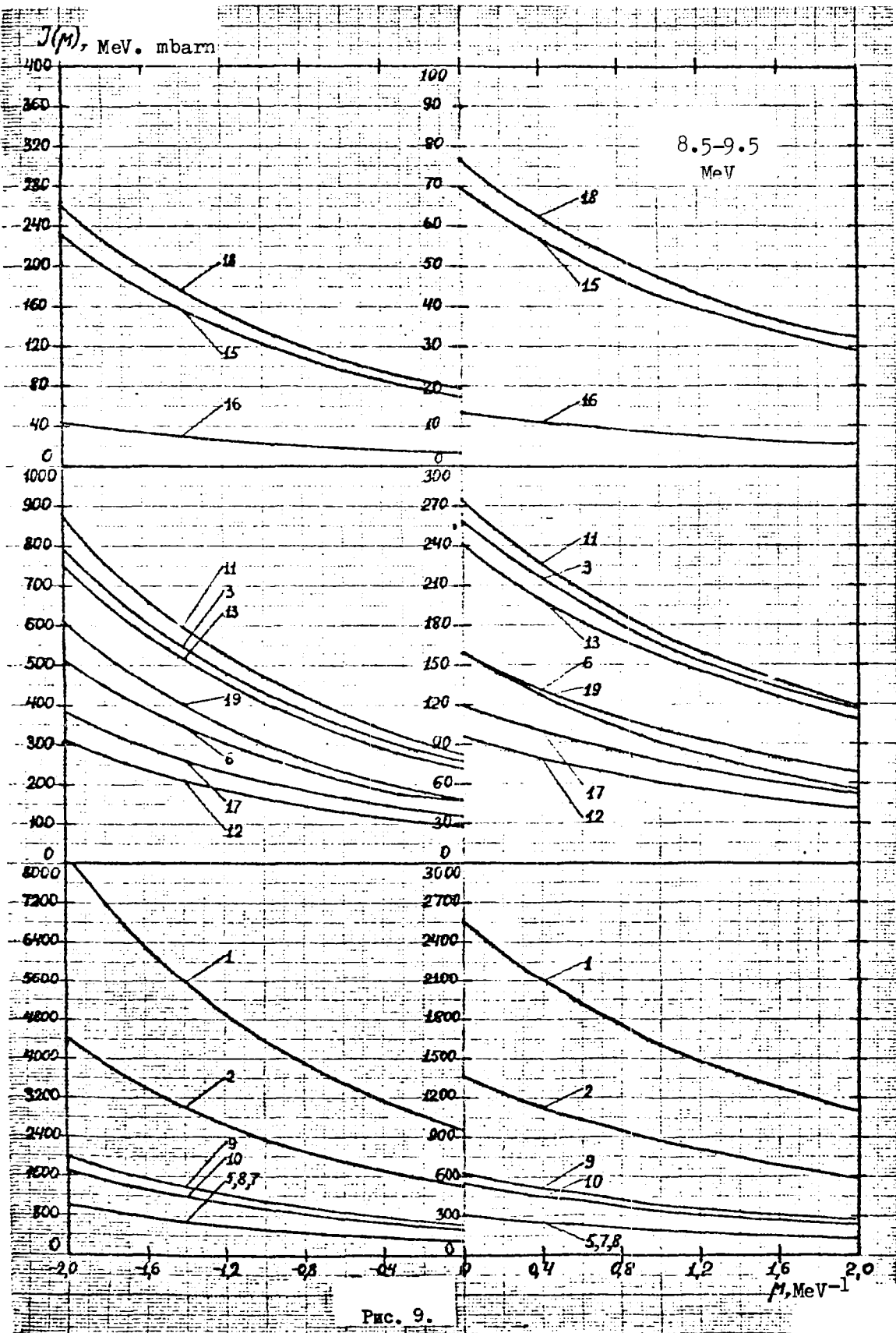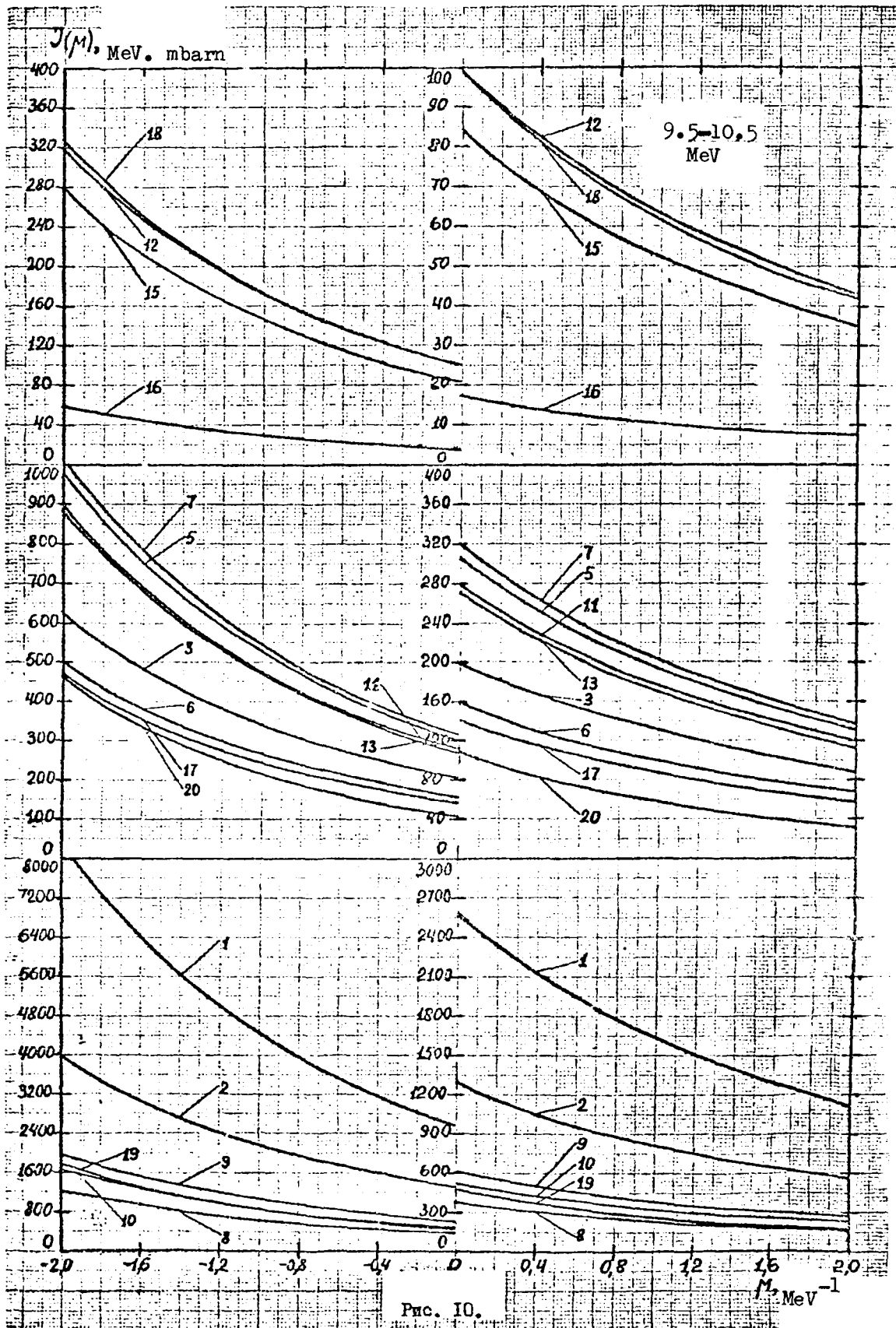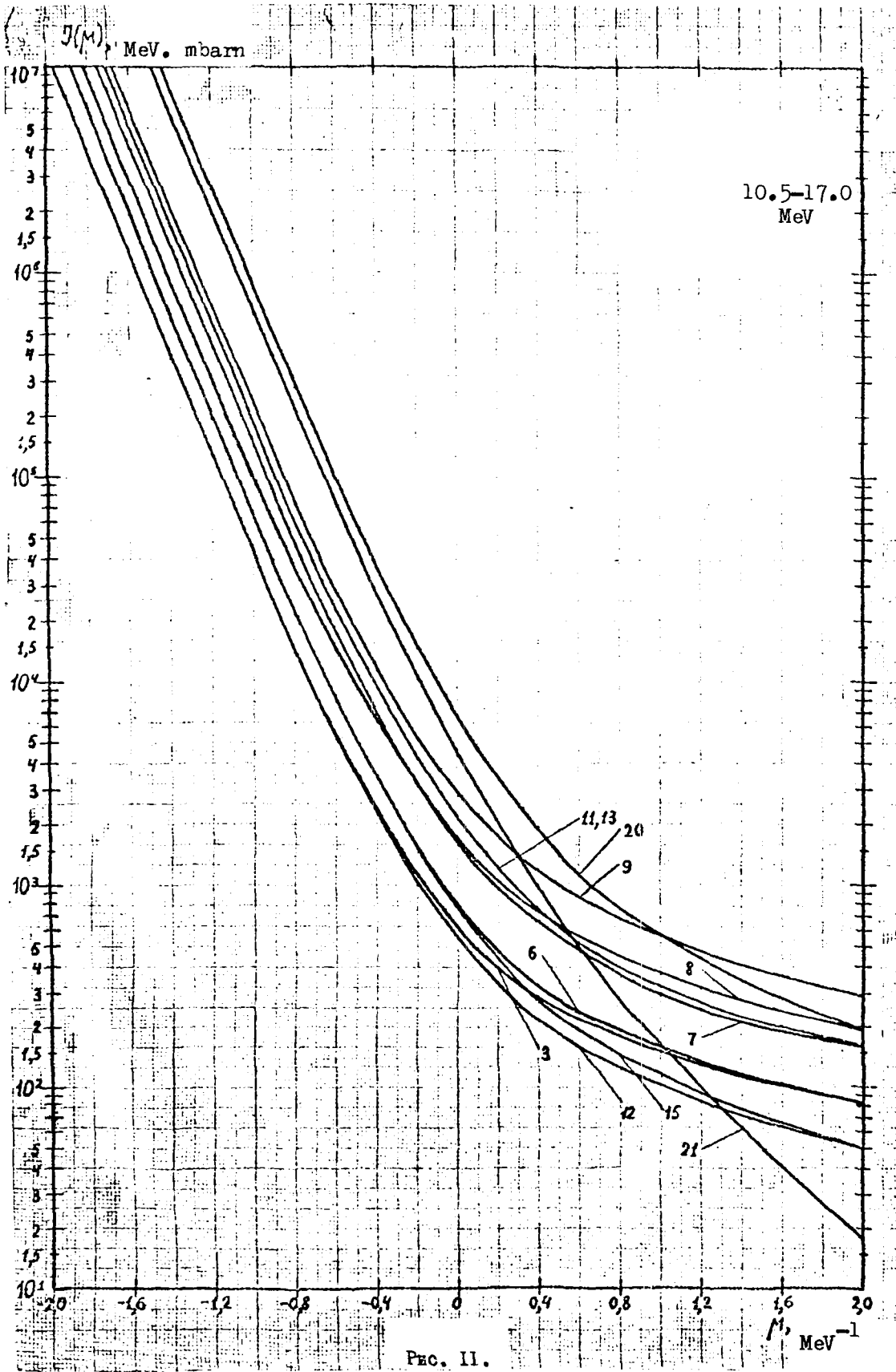
Fig. 11
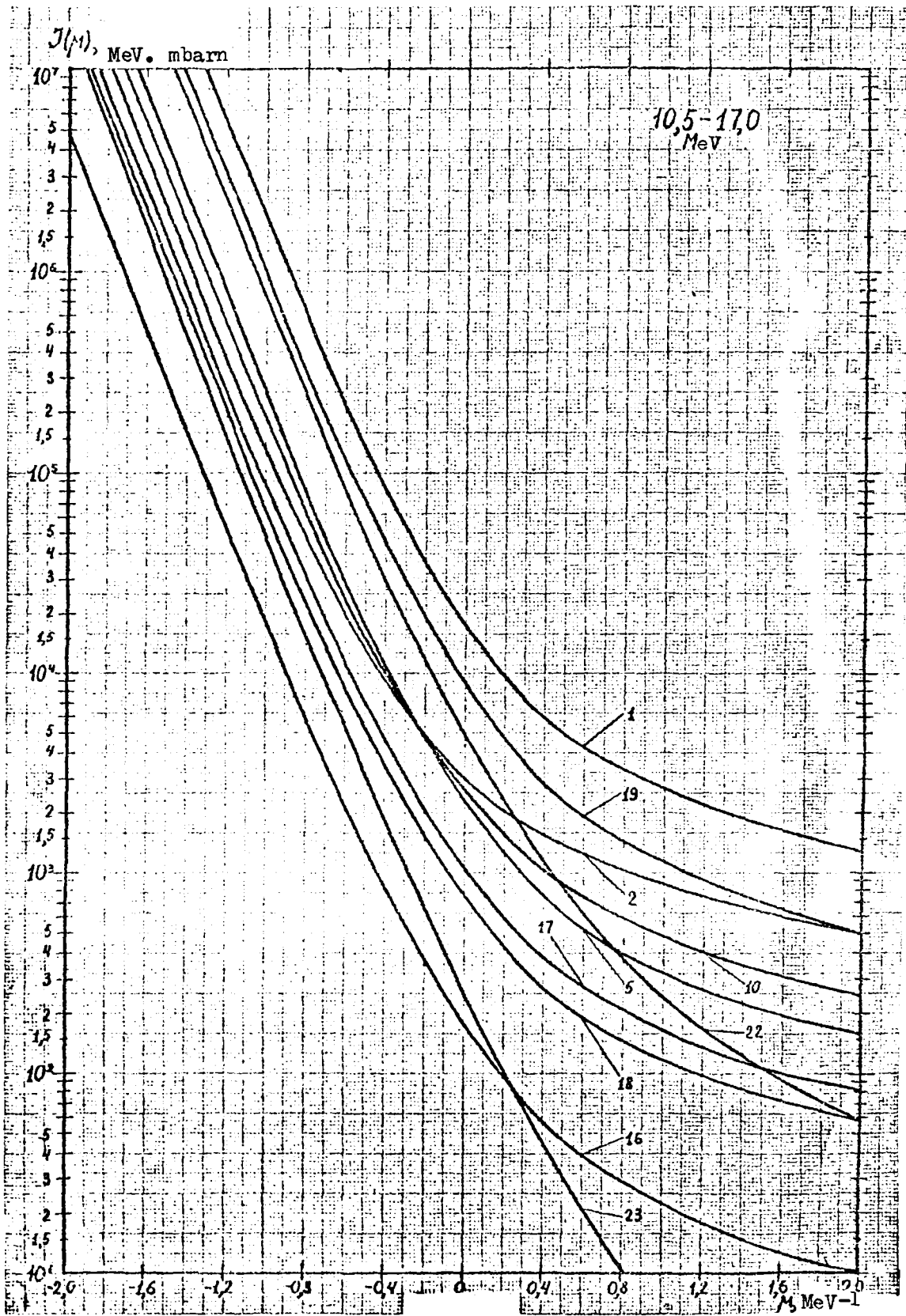
Fig. 12
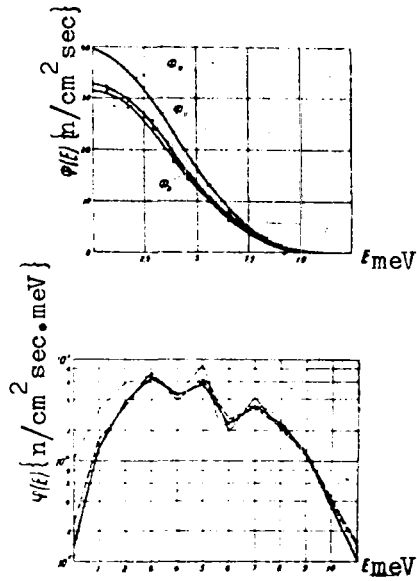
Fig. 13   Results of unfolding a spectrum similar to the spectrum
from a Po-Be source by the rapid method using two iterations.

(a) Integral spectra

O,△,□ are the integral neutron flux densities in the
first, second and third approximations respectively.

Φ_o, Φ_1, Φ_2 are the zero, first and second approximations
respectively.

(b) Differential spectra

_____ = initial spectrum

_ • _ • _ = unfolded spectrum - zero approximation

_ _ _ _ _ _ = unfolded spectrum - first approximation

_____ = unfolded spectrum - second approximation

NEUTRON SPECTRUM CALCULATIONS IN THE P_1 APPROXIMATION

V.S. Shulepin

In Ref. $\boxed{1}$ a system of equations was obtained for calculating the neutron spectrum in any region of a reactor in the P_1 approximation. From these results, the following algebraic equations can be written for determining the slowing-down spectrum:

$$
\left.
\begin{aligned}
\widetilde{\varphi}_1^j + \Sigma_{oy}^j\, \varphi_o^j &= \sum_{\ell=1}^{j-1} \Sigma_o^{\ell \to j}\, \varphi_o^\ell + S_v^j + S_s^j \ , \\
\tfrac{1}{3} L^j\, \varphi_o^j + \Sigma_{1y}^j\, \widetilde{\varphi}_1^j &= \sum_{\ell=1}^{j-1} \Sigma_1^{\ell \to j}\, \widetilde{\varphi}_1^\ell \ ,
\end{aligned}
\right\}
\tag{1}
$$

where

$$
\varphi_o^j = \int \varphi_o^j\,(\vec{z})\,d\nu \ , \qquad \widetilde{\varphi}_1^j = \int d\omega\, \widetilde{\varphi}_1^j\,(\vec{z})\,d\nu
\tag{1a}
$$

(The integrals are taken over the volume of the region);

$\varphi_o^j(\vec{r})$, $\varphi_1^j(\vec{r})$ are the coefficients for expanding a flux of neutrons of the jth energy group $\vec{\varphi}^j(\vec{r},\vec{\Omega})$ in a Legendre polynomial series relative to the angular variable $\boxed{2}$;

Σ_{oy}^j, Σ_{1y}^j are the group removal cross-sections;

$\Sigma_o^{\ell \to j}$, $\Sigma_1^{\ell \to j}$ are the cross-sections for transition from group ℓ to group j;

S_v^j, S_s^j are the volume and surface sources of the region respectively; and

L_v^j is the leakage parameter.

The various possible ways of selecting the quantities S_v^j, S_s^j and L^j are discussed in Ref. $\boxed{1}$.

In this paper we derive a formula with which the desired quantities φ_o^j may be written concisely. Let us determine $\widetilde{\varphi}_1^j$ from the first equation of the system in expression (1) above and $\widetilde{\varphi}_1^\ell$ from similar equations, and then substitute these expressions in the second equation, so that we have:

$$
\begin{aligned}
\tfrac{1}{3} L^j\, \varphi_o^j + \Sigma_{1y}^j\left[\sum_{\ell=1}^{j-1} \Sigma_o^{\ell \to j}\, \varphi_o^\ell - \Sigma_{oy}^j\, \varphi_o^j + S_v^j + S_s^j \right] = \\
= \sum_{\ell=1}^{j-1} \Sigma_1^{\ell \to j}\left[\sum_{\kappa=1}^{\ell-1} \Sigma_o^{\kappa \to \ell}\, \varphi_o^\kappa - \Sigma_{oy}^\ell\, \varphi_o^\ell + S_v^\ell + S_s^\ell \right]
\end{aligned}
\tag{2}
$$

The latter equation may be written as follows:

$$\frac{1}{3} \frac{L^j}{\Sigma^j_{ty}} \varphi^j_o - \Sigma^j_{oy} \varphi^j_o + \sum_{\ell=1}^{j-1} (\Sigma^{\ell+j}_{\cdot o} + \Lambda^\ell_j) \varphi^\ell_o +$$

$$+ S^j_v + S^j_s - \frac{1}{\Sigma^j_{ty}} \sum_{\ell=1}^{j-1} (S^\ell_v + S^\ell_s) = 0 ,$$

(3)

where:

$$\Lambda^\ell_j = \frac{\Sigma^\ell_{oy} \Sigma^{\ell+j}_{\cdot t} - \sum_{m=\ell+1}^{j-1} \Sigma^{m-j}_{\cdot t} \Sigma^{\ell-m}_{\cdot o}}{\Sigma^j_{ty}}$$

$$1 \leqslant \ell \leqslant j - 1 , \qquad \ell + 1 \leqslant m \leqslant j - 1 ,$$

Note that $\Sigma^{p \to q}_o = \Sigma^{p \to q}_1 = 0$ when $p \geqslant q$. It will be seen that equations (2) and (3) are completely equivalent for any j. The final expression for φ^j_o takes the form:

$$\varphi^j_o = \frac{S^j_v + S^j_s - \sum_{\ell=1}^{j-1} \left[\frac{\Sigma^j_t}{\Sigma_{ty}} (S^\ell_v + S^\ell_s) - (\Sigma^{\ell+j}_{\cdot o} + \Lambda^\ell_j) \varphi^\ell_o \right]}{-\frac{1}{3} \frac{L^j}{\Sigma^j_{ty}} + \Sigma^j_{oy}}$$

(4)

All values of φ^j_o can be calculated successively (j = 1, 2, ...) with formula (4).

REFERENCES

[1]   PERKINS, S., Nucl. Sci. Engng., 24 (1966) 284.

[2]   MARCHUK, G.I., Metody rasčeta jadernyh reaktorov (Methods of calculating nuclear reactors) Gosatomizdat, Moscow (1961).

CALCULATION OF BOUNDARY CONDITIONS FOR A "BLACK" ROD

P.E. Bulavin

In Ref. $\boxed{1}$ the neutron balance method $\boxed{2}$ was used to obtain the following expression for the effective boundary conditions for a "black" rod situated in a non-absorbing infinite medium:

$$\beta = 4/3 - a\,\mathcal{P}(a) \,, \tag{1}$$

where

$$\mathcal{P}(a) = \frac{4}{\pi}\int_0^{\pi/2}\cos\psi\,d\psi\int_0^{\pi/2}\sin^2\nu\,d\nu\int_0^{\infty}e^{-\xi}\,\ell_n\sqrt{1+\frac{2\xi\sin\nu\cos\psi}{a}+\frac{\xi^2\sin^2\nu}{a^2}}\,d\xi \,(\tag{2}$$

$$a = z_0\Sigma_s \,,$$

r_0 = the radius of the absorbing rod and Σ_s = the macroscopic scattering cross-section of the medium.

However, the expression for the function $\mathcal{P}(a)$ can be greatly simplified by integrating analytically over the angles ψ and v. In fact let us differentiate $\mathcal{P}(a)$ with respect to the parameter a. The following expression is then obtained for the function $W(a) = a\,\dfrac{d\mathcal{P}(a)}{da}$

$$W(a) = \frac{2}{\pi}\int_0^{\pi/2}\cos\psi\,d\psi\int_0^{\pi/2}\sin^2\nu\,d\nu\int_0^{\infty}e^{-\xi}\frac{\frac{2\sin\nu\cos\psi}{a}\xi+\frac{2\sin^2\nu}{a^2}\xi^2}{1+\frac{2\sin\nu\cos\psi}{a}\xi+\frac{\sin^2\nu}{a^2}\xi^2}\,d\xi \tag{3}$$

The expression for the function W(a) may now be integrated over the angle ψ , as a result of which we obtain

$$W(a) = \frac{2}{\pi}\int_0^{\pi/2}\sin^2\nu\,d\nu\int_0^{\infty}e^{-\xi}\left[\left(\frac{a}{\xi\sin\nu}+\frac{\xi\sin\nu}{a}\right)\arctan\frac{\xi\sin\nu}{a}-\frac{1}{2}\frac{\xi\sin\nu}{a}\right]d\xi \tag{4}$$

Integrating expression (4) over the angle v, we obtain

$$W(a) = \frac{2}{3}\int_0^{\infty}e^{-\xi}\left[\frac{\left(\frac{\xi}{a}+\frac{a}{\xi}\right)^2}{\sqrt{1+\xi^2/a^2}}-\frac{a^2}{\xi^2}-\frac{\xi}{a}-\frac{3}{2}\right]d\xi \,. \tag{5}$$

or, substituting ax for ξ , we obtain

$$W(a) = \frac{2}{3} a \int_0^\infty e^{-ax} \left[\frac{(x + 1/x)^2}{\sqrt{1 + x^2}} - 1/x^2 - x - \frac{3}{2} \right] dx \tag{6}$$

Dividing Eq. (6) by a, integrating the result over a and applying the condition $\varphi(\infty) = 0$, we obtain

$$\varphi(a) = \frac{2}{3} \int_0^\infty \frac{e^{-ax}}{x} \left[\frac{3}{2} + x + 1/x^2 - \frac{(x + 1/x)^2}{\sqrt{1 + x^2}} \right] dx \tag{7}$$

or, substituting ξ/a for x, we obtain:

$$\varphi(a) = \frac{2}{3} \int_0^\infty \frac{e^{-\xi}}{\xi} \left[\frac{3}{2} + \frac{\xi}{a} + \frac{a^2}{\xi^2} - \frac{(\frac{\xi}{a} + \frac{a}{\xi})^2}{\sqrt{1 + \xi^2/a^2}} \right] d\xi \tag{8}$$

When a tends to 0, the limit W(0) = -1 is obtained from formula (5) whence follows the logarithmic character of the function φ (a):

$$\varphi(a) = -\ln 2a \, , \quad a \ll 1. \tag{9}$$

When a $\gg$ 1, by expanding the expression in square brackets in Eq. (8) into a power series of ξ/a and confining ourselves to two terms of the series, we obtain

$$\varphi(a) = \frac{2}{3a} - \frac{1}{4a^2} \, , \quad a \gg 1 \tag{10}$$

The results of calculating the functions φ(a) and W(a) from formulae (7) and (6) on the "Nairi" computer are presented in Table 1.

The accuracy of the calculations is estimated at not less than $\pm$ 0.0001 for the function φ (a) and $\pm$ 0.0005 for the function W(a) when a < 0.1. When a $\geq$ 0.1 there is an accuracy of $\pm$ 1 in the last significant figure.

The calculations of the function φ(a) differ considerably from the results given in Ref. [1] for small values of a (maximum deviation 12.6% for a = 0.025).

Table 1

Values of the functions $\varphi(a)$ and $W(a)$

α	0,025	0,05	0,075	0,1	0,2	0,3	0,4	0,5	0,6	0,7	0,8
$\varphi(a)$	3,0258	2,4099	2,0682	1,8372	1,3279	1,0670	0,9008	0,7833	0,6949	0,6255	0,5694
$W(a)$	-0,9099	-0,8628	-0,8216	-0,7851	-0,6797	-0,6058	-0,5492	-0,5037	-0,4660	-0,4341	-0,4066

α	0,9	1	2	3	4	5	6	7	8	9	10
$\varphi(a)$	0,5229	0,4837	0,2788	0,1965	0,1518	0,1237	0,1043	0,09023	0,07948	0,07102	0,06419
$W(a)$	-0,3826	-0,3614	-0,2342	-0,1737	-0,1381	-0,1145	-0,09784	-0,08538	-0,7573	-0,06803	-0,06175

REFERENCES

_[1_]   MARCHUK, G.I., Cislennye metody rasčeta jadernyh reactorov
         (Numerical methods of calculating nuclear reactors)
         Atomizdat (1958).

_[2_]   BAT, G.A., ZARETSKY, D.F., Atomn. Energ. 4 (1958) 510.

_[3_]   ZARETSKY, D.F., ODINTSOV, V.D., Effektivnye graničnye uslovija
         dlja "seryh" tel (Effective boundary conditions for "grey" bodies)
         in Int. Conf. peaceful Uses atom. Energy (Proc. Conf. Geneva, 1955)
         5 UN, New York (1956) 525.

_[4_]   ISAKOVA, L.Ya., Atomn. Energ. 25 (1968) 229.

CHAPTER III

RADIATION SHIELDING CHARACTERISTICS AND PARAMETERS
RADIATION AND NUCLEAR SAFETY

SPATIAL–ENERGY DISTRIBUTION OF FAST NEUTRONS IN TWO–LAYER
IRON–WATER SHIELDING

A.I. Ganshin, S.F. Degtyarev, V.P. Polivansky, A.P. Suvorov,
V.V. Tarasov, V.K. Tikhonov, S.G. Tsypin, A.I. Shulgin

Fairly extensive theoretical and experimental data are already available
on fast neutron transport in homogeneous shielding layers of varying thickness
$\underline{/1\,\underline{/}}$. However, this question has been far less well investigated in the case
of inhomogeneous shields $\underline{/2, 3, 4\,\underline{/}}$.

Here the authors report on a study of the space–energy distribution
of a flux of fast neutrons with energy $E > 0.4$ MeV in barrier geometry in
two–layer iron–water shielding. The thickness of the first layer, made of
iron, was 20 cm in the first case and 35 cm in the second. The thickness
of the adjacent water shield was 15 cm in both cases. The source used
was a plane collimated neutron beam with a reactor spectrum $\underline{/5\,\underline{/}}$. The
transverse dimensions of the shielding layers and the beam were ~ 70 cm.
The neutrons were detected by means of a single–crystal scintillation
spectrometer with a stilbene crystal 3 cm in diameter and 2 cm high, with
gamma–background discrimination based on de–excitation time $\underline{/6\,\underline{/}}$. The
signal and the background were recorded with the shielding layers in place,
and the intensity of the incident neutron beam was measured with the shielding
removed. The pulse height distributions were recorded with a "diaphragm"
256–channel analyser and were converted into energy spectra by differentiation;
the neutron recording efficiency and the light output of the stilbene crystal
were allowed for by the method described in Ref. $\underline{/7\,\underline{/}}$.

The penetration of fast neutrons in the shielding compositions described
above was calculated by the multigroup method of discrete ordinates in the
$2D_7P_7$ approximation $\underline{/1\,\underline{/}}$. The calculations were performed in plane
unidimensional geometry for a monodirectional neutron beam, using the POZ–1
programme $\underline{/8\,\underline{/}}$. The group constants used for iron and water were obtained

by averaging over the neutron spectra in an infinite homogeneous medium consisting of the appropriate material. These constants are given in Ref. $/\overline{1\_7}$. They were verified by calculation of the experimental data for fast neutron fields in extended iron-water shields $/\overline{1}$, 9_7. Fig. 1 shows experimental and theoretical data on the energy distributions of a fast neutron flux with energy E> 0.4 MeV behind the iron-water shields described above. (Geometrical attenuation of the beam has been omitted in the presentation of the experimental data.) The figure also shows experimental data on the energy spectrum of a monodirectional neutron beam impinging on the shields under investigation. By averaging these data within the group intervals we obtained the data on the incident beam spectrum on which our subsequent calculations were based.

For comparison Fig. 1 also shows the calculated energy spectrum of a neutron flux behind 15 cm of water $/\overline{1\_7}$ for the same incident beam spectrum together with similar data for layers of iron 20 and 35 cm thick $/\overline{9\_7}$. In the case of the 20 cm thick iron layer experimental data from Ref. $/\overline{9\_7}$ are also shown and these agree well with the calculated values. Note that Ref. $/\overline{9\_7}$ includes a comparison of theoretical and experimental results for neutron energy spectra behind 10 and 30 cm thick iron shields. Good agreement was also obtained in these cases.

From Fig. 1 we see that there is good agreement in the 1.4 to 6.5 MeV range between experimental and theoretical data on neutron spectra behind iron-water shields (the results agree within the limits of experimental error). However, a significant deviation (by more than a factor of 2) is observed for energies less than 1.4 MeV. This is partially attributable to the fact that the constants which we used for iron $/\overline{9\_7}$ and water $/\overline{10\_7}$ for neutrons with E < 1 MeV have not been proved experimentally. Another possible reason is that, strictly speaking, when calculating inhomogeneous shields consisting of thin layers (say, less than 4-5 free path lengths), one ought to use group constants obtained by averaging not over the spectra in an infinite homogeneous medium (as was done here) but over the integral neutron spectrum in each layer $/\overline{1\_7}$. For calculating these integral spectra it is necessary to allow for mutual effects of these layers. Unfortunately no algorithms have yet been devised to allow for this effect. An improvement can be obtained by using the results of an additional calculation with a large number of groups for averaging the cross-sections (this calculation may, of course, be done in a lower approximation).

Also, averaging over the neutron spectrum in an infinite homogeneous medium consisting of a homogeneous mixture of iron and water nuclei can be used as a simpler approximation in the above problem.

Analysis of the fast neutron spectra obtained behind iron-water shields shows competition between two trends: "softening" of the spectrum by the layer of iron (due to inelastic scattering by iron nuclei) and "hardening" of the spectrum by the succeeding mass of water (due to intense slowing-down of neutrons by hydrogen nuclei). These tendencies are also to be observed in monolayer shields. For example, a 20 cm iron layer increases the ratio of the neutron flux in the 0.4-1.4 MeV range to the flux with E> 1.4 MeV, $\frac{F(0.4-1.4 \text{ MeV})}{F(E > 1.4 \text{ MeV})}$, by approximately a factor of 10 compared with the incident beam spectrum shown in Fig. 1 (for which the ratio is ~ 1.5). At the same time this ratio decreases by almost a factor of 3 behind 15 cm of water with the same incident beam. The two shields together also reduce this ratio but to a lesser extent (by a factor of approximately 2.4). Thus, a mass of water situated behind a 20 cm thick iron layer reduces $\frac{F(0.4-1.4 \text{ MeV})}{F(E > 1.4 \text{ MeV})}$ by a factor of approximately 24.

The neutron spectrum behind a two-layer iron-water shield is, so to speak, half way between the spectrum in water and the spectrum in iron (at comparable distances). Note that this has already been demonstrated for water shields less than 20 cm thick in Ref. [3], where the authors investigated the space-energy distribution of fast neutrons from monoenergetic sources, D(d,n) and T(d,n) in metal-water shields.

Increasing the thickness of the iron layer causes its "softening" capacity to increase, so that at a thickness of 35 cm the ratio $\frac{F(0.4-1.4 \text{ MeV})}{F(E > 1.4 \text{ MeV})}$ is more than 20 times greater than in the incident beam spectrum. However, the attentuation of the beam of relatively "soft" neutrons is also enhanced.

It is interesting to note that the fast neutron spectrum behind a two-layer shield consisting of a layer of iron ~ 25-30 cm thick (20 cm according to experimental data, 35 cm according to calculations) and a somewhat thinner mass of water (~ 15 cm) is very similar in shape to the incident beam spectrum. Evidently, it would be possible to choose other iron-water combinations which would also maintain the shape of the incident beam spectrum. Clearly, if the iron layer thickness is increased, the thickness of the water layer must also be increased (but of course to a lesser extent).

One further conclusion to be drawn from an analysis of the above
spectra is that in two-layer iron-water shields a 15 cm thick water layer
is inadequate for a specific "water" spectrum to be established.   This
will begin to show up only when the thickness of the iron layer is
considerably less than 20 cm.

Fig.2 shows the spatial flux distributions of fast neutrons in the
two-layer iron-water shields described above for energies $E > 2.5$ MeV,
$E > 1.4$ MeV and 0.4 MeV $< E < 1.4$ MeV.

Of interest here is the dependence of the neutron distribution close
to the boundary of the iron layer on the material of the succeeding layer.
This dependence is particularly marked for neutrons with $E < 1.4$ MeV.

For comparison Fig. 2 also shows calculated neutron flux distributions
in water.   The attenuation effect of the water varies with its position.
For example, for a neutron flux with $E > 1.4$ MeV, the attenuation factor of
a 15 cm thick mass of water is ~ 6.6 when it is irradiated directly with a
unidirectional beam, ~ 15.5 when it is located behind a 20 cm layer of iron,
and ~ 19 when located behind a 35 cm iron layer.   This difference is due
primarily to the change in the angular distribution of the neutron flux on
passage through the iron layer and, secondly, to the resulting change in
the neutron energy spectrum.   The difference between the corresponding
attenuation values for neutrons with $E > 2.5$ MeV is slightly less: instead
of a factor of ~ 3, as in the case of neutrons with $E > 1.4$ MeV, it is
only ~ 1.6.   For neutrons in the range 0.4 MeV $< E < 1.4$ MeV the corresponding
attenuation factors calculated as ~20, ~230 and ~580.   This strong
dependence of attenuation on the position of the water layer is attributable
to the different degree of "softening" of the neutron spectrum in these
cases.

For comparison, Fig. 2 also shows experimental and theoretical data
on the dependence of a fast neutron flux with different energies behind
layers of iron on the thickness of these layers, t.   As can be seen, for
neutrons with $E < 2.5$ MeV the nature of this dependence can differ appreciably
from the spatial flux distribution $F_o(x)$ within iron layers that are backed
by a layer of water.

REFERENCES

/1_7   GERMOGENOVA, T.A. et al., Perenos bystryh nejtronov v ploskih
         zaŠčitah (Fast neutron transport in plane shields), Atomizdat (1971).

/2_7   GERMOGENOVA, T.A. et al., in Voprosy fiziki zaŠčity reaktorov
         (The physics of reactor shielding), Issue No. 2, Atomizdat (1966) 57.

/3_7   BRODER, D.L. et al., in Voprosy fiziki zaŠčity reaktorov (The physics
         of reactor shielding), Issue No. 2, Atomizdat (1966) 104.

/4_7   BARSOV, B.A. et al., in Voprosy fiziki zaŠčity reaktorov (The physics
         of reactor shielding), Issue No. 5, Atomizdat (1971).

/5_7   DEGTYAREV, S.F. et al., Atomn. Energ. 21 (1966) 392.

/6_7   DULIN, V.A. et al., Pribory Tekh. Eksp. No. 2 (1961) 35.

/7_7   KAZANSKY, Yu.A., Fizičeskie issledovanija zaŠčity reaktorov
         (Physical investigations of reactor shielding) (Tsypin, S.G., Ed.)
         Atomizdat (1966).

/8_7   GERMOGENOVA, T.A. et al., in Voprosy fiziki zaŠčity reaktorov
         (The physics of reactor shielding), Issue No. 2, Atomizdat (1966) 22.

/9_7   DEGTYAREV, S.F. et al., in Problemy zaŠčity ot pronikajuŠčih
         izlučenij reaktornyh ustanovok (Problems of shielding against
         penetrating radiations from reactor installations) COMECON Symposium,
         Melekess 5 (1969) 113.

/10_7   DEGTYAREV, S.F. et al., in Voprosy fiziki zaŠčity reaktorov
         (The physics of reactor shielding), Issue No. 3, Atomizdat (1969) 116.

Key:

$$\frac{\text{нейтрон}}{\text{см}^2 \text{ рт}} \qquad = n/cm^2 \text{ W}$$

Мэв $\qquad$ = MeV

Вода $\qquad$ = water

Железо $\qquad$ = iron

Fig. 1 $\qquad$ The energy dependence of the fast neutron flux in layers of iron and water

Lines indicate calculated data; points indicate experimental data

— — — — — — 15 cm water layer $[1]$

— — — , 20 cm iron layer $[9]$

——————, 20 cm iron layer + 15 cm of water

————•———— 35 cm iron layer

——————, 35 cm iron layer + 15 cm water

——————, Incident beam spectrum

Fig.
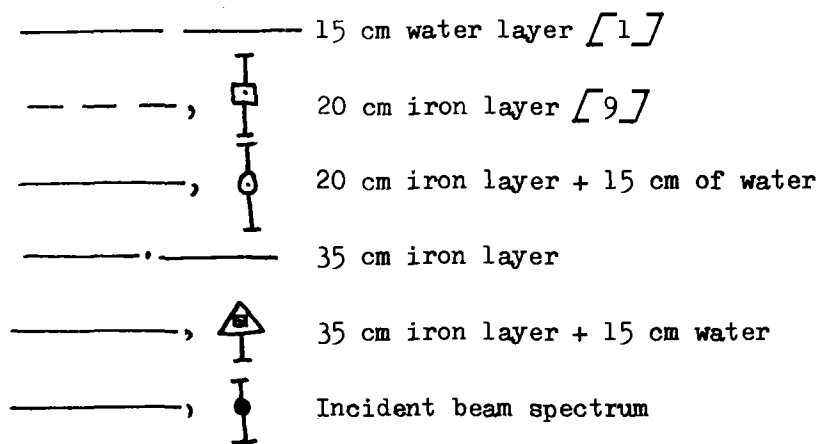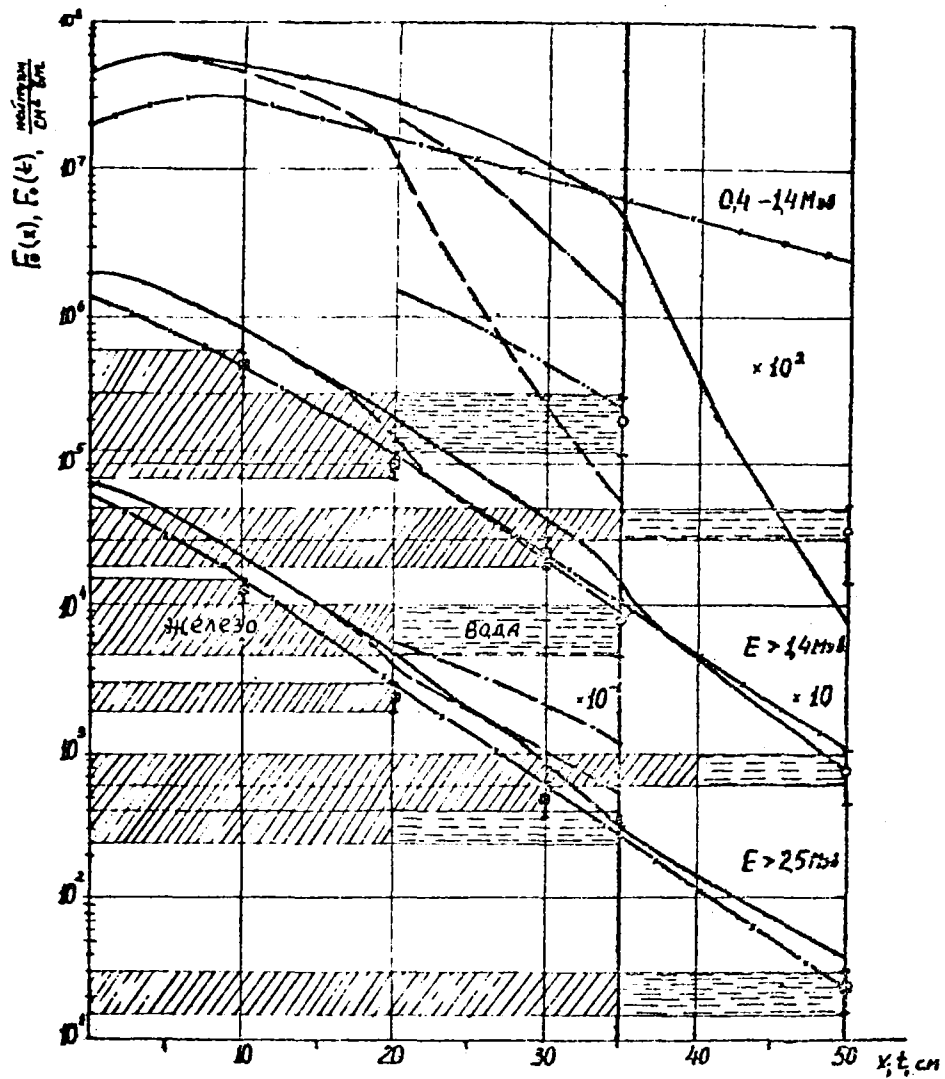
Рис. 1. Энергетические распределения потока быстрых нейтронов за слоями железа и воды.

Линии - расчет, точки - эксперимент:

———x——— - слой воды 15 см [1],

——─—, — - слой железа 20 см [9],

————, — - слой железа 20 см и воды 15 см,

——·—— - слой железа 35 см,

————, — - слой железа 35 см и воды 15 см,

————, — - спектр падающего пучка.

Fig. 2   ʼSpatial flux distributions of fast neutrons of various energies
          in iron-water shields irradiated by a plane unidirectional beam.

Results of calculations:

_____ = 2-layer shield, 35 cm Fe + 15 cm H_2O

_ _ _ _ _ = 2-layer shield, 20 cm Fe + 15 cm H_2O

_ • • _ = 15 cm layer of H_2O [1]

   ⊥̅
   ◯   = Results of neutron flux measurements behind
   ⊥   iron-water shields

For comparison, the figure also includes data on $F_0(t)$ — the
neutron flux behind an iron barrier as a function of the barrier
thickness t [9].

   ⊥   indicates experimental data
   ⬦
   ⊥

- x - indicates calculated data
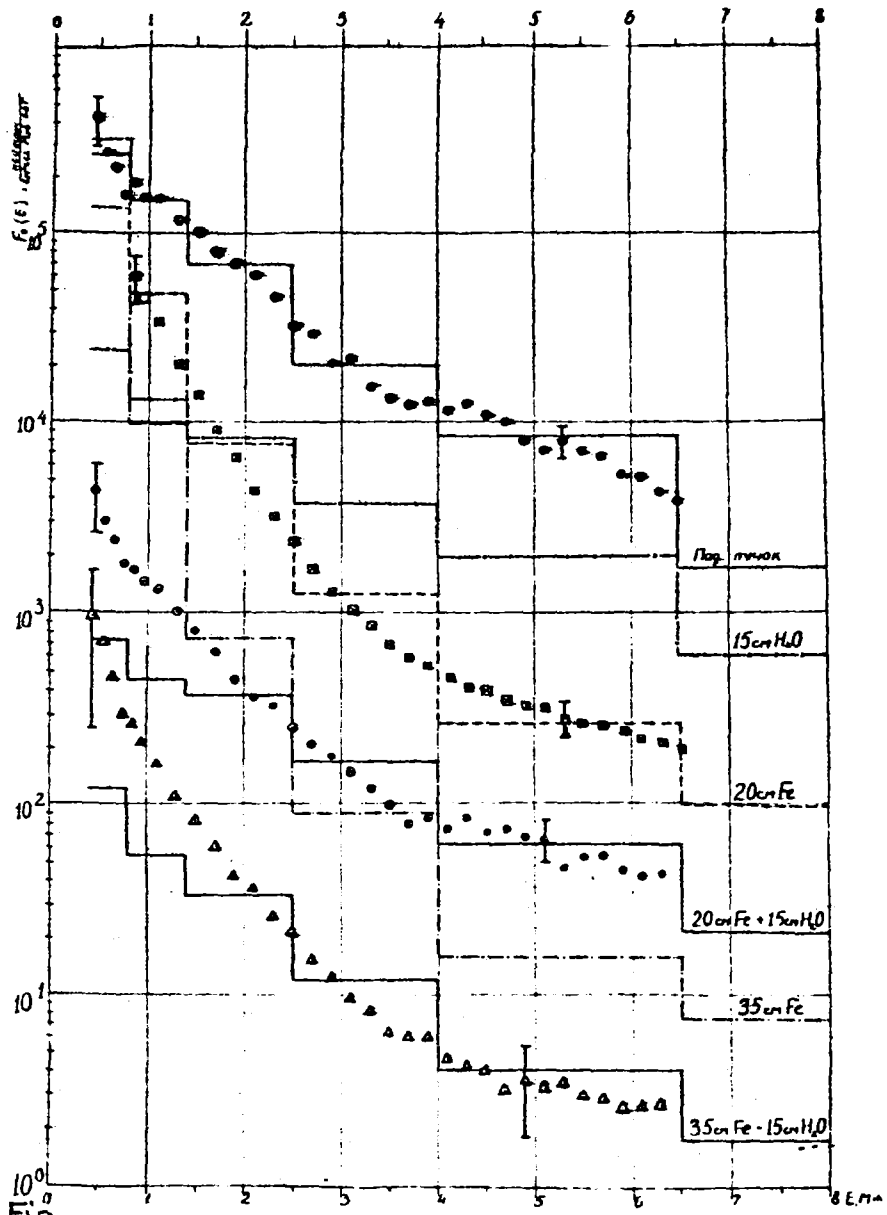
Рис. 2. Пространственные распределения потока быстрых нейтронов
различных энергий в железоводных защитах при их
облучении плоским мононаправленным пучком.

Результаты расчетов:

────────── - двухслойная защита 35 см + 15 см ,

── ── ── ── - двухслойная защита 20 см + 15 см ,

──∙── - слой воды 15 см I .

Ⴌ - результаты измерений потока нейтронов за железовод-
ными защитами.

Для сравнения приведены данные по зависимости $F_0(t)$ потока нейтро-
нов за барьером из железа от толщины t этого барьера [9]:

▉ - эксперимент, ──х── - расчет.

DIFFERENTIAL ALBEDOS OF FAST NEUTRONS FOR CARBON
AND BORON CARBIDE

T.A. Germogenova, V.A. Klimanov, M.G. Kobozev, V.P. Mashkovich,
E.I. Panfilova, O.G. Petrov, A.P. Suvorov

For solving many problems concerned with the physics of shielding,
dosimetry and radiation technology it is necessary to know the differential
characteristics of the back-scattered radiation field of unidirectional
neutron beams. This problem has in recent years attracted the attention
of a large number of investigators. A brief review of work on neutron back-
scattering is presented in Ref. $\boxed{1}$.

This paper reports calculated differential albedo characteristics of
plane unidirectional neutron beams impinging on plane barriers of various
thicknesses made of carbon and boron carbide. The calculations were
performed for plane unidimensional geometry by a special albedo method $\boxed{2}$
in the $2D_N P_N$ approximation of the discrete ordinates method $\boxed{3}$. We
used the group constants from Ref. $\boxed{4}$ together with a group with
$E > 10.5$ MeV supplemented by data on scattering anisotropy from Refs $\boxed{5, 6}$.

Tables 1-4 show the calculated differential flux albedo
$A(\Delta E_o, \vartheta_o; \Delta E, \vartheta, \varphi)$ of a plane unidirectional fast neutron beam. These values
characterize the probability of a neutron in the energy group ΔE_o, incident
on a scattering medium at angle ϑ_o, being reflected at a single solid angle,
described by the angle ϑ and the azimuthal angle φ, and thereby falling into
the group ΔE. The angles ϑ and ϑ_o are read off from the normal to the
surface of the scatterer, the azimuthal angle φ from the projection of the
beam direction onto the surface of the medium. The results are normalized
to an incident flux of intensity 10^4 n/cm^2. The calculations were performed
for nine groups of neutrons with energy $E > 0.1$ MeV in the $2D_7 P_7$ approximation.
It was found that for neutrons with $E > 4$ MeV the P_7-approximation of the
scattering angular distribution is inadequate for describing all the
irregularities of its angular dependence. In some cases the P_7-representation
of the scattering angular distribution for carbon and boron assumes negative
values for certain scattering angles and its use in albedo calculations
accordingly leads, for some values of ϑ, to physically meaningless negative
albedo values. Tables 1-4 show the albedo values only for neutrons with
$E_o < 4$ MeV. These values relate to layers of carbon 15 and 25 cm thick and

layers of boron carbide (density 1.3 g/cm^3) 5 and 10 cm thick. When calculating the differential angular albedos for neutrons with $E_0 > 4$ MeV it is necessary to use a higher approximation of the scattering angular distribution. From the data supplied in the above references it can be seen that a significant azimuthal dependence of the albedos exists only for neutrons with energy $E > 0.8$ MeV at large ϑ_0 and ϑ.

The theoretical data were verified experimentally with plane scatterers made of carbon 20 and 40 cm thick. The horizontal channel of the IRT-2000 reactor of the Moscow Engineering-Physics Institute was used as the neutron source. The neutron beam diameter where it intersected the surface of the scatterer at normal incidence was 7 cm. The fast neutron detector used was a scintillation counter based on a 5 x 30 mm ZnS crystal, having virtually constant sensitivity to fast neutrons with a recording threshold of $E_{thr} \simeq 1.0$ MeV $\llbracket 7 \rrbracket$. The detector was put 2.0 m from the scatterer. The scattering medium measured 1.8 m across. A special mechanical system was used to set the necessary angles of ϑ_0, ϑ and φ. The above experimental set-up enabled measurements to be made of the flux differential albedos of fast neutrons with a threshold energy $E_{thr} \simeq 1.0$ MeV. The theoretical values of this quantity were determined by integrating the data obtained during this investigation for separate monogroups of ΔE_0 with allowance for the energy distribution of reactor neutrons incident on the scatterer. The experimental values of the differential numerical albedo were obtained for the angles ϑ_0 and $\vartheta = 0-75^\circ$ and $\varphi = 0^\circ$ and 180°. The maximum disagreement between the theoretical and experimental values did not exceed 25%. The figure compares the theoretical and experimental data on the differential flux neutron albedo for a 25 cm layer of carbon.

Key for tables 1 through 4c

град = deg

Мэв = MeV

Table 1a

Differential albedos of neutrons for a 15 cm layer of carbon, ΔE_o = 2.5–4 MeV

Table 1b

Differential albedos of neutrons for a 15 cm layer of carbon, ΔE_o = 1.4–2.5 MeV

Table 1c

Differential albedos of neutrons for a 15 cm layer of carbon, ΔE_o = 0.8–1.4 MeV

Table 2a

Differential albedos of neutrons for a 25 cm layer of carbon, ΔE_o = 2.5–4 MeV

Table 2b

Differential albedos of neutrons for a 25 cm layer of carbon, ΔE_o = 1.4–2.5 MeV

Table 2c

Differential albedos of neutrons for a 25 cm layer of carbon, ΔE_o = 0.8–1.4 MeV

Table 3a

Differential albedos of neutrons for a 5 cm layer of boron carbide,
ΔE_o = 2.5–4 MeV

Table 3b

Differential albedos of neutrons for a 5 cm layer of boron carbide,
ΔE_o = 1.4–2.5 MeV

Table 3c

Differential albedos of neutrons for a 5 cm layer of boron carbide,
ΔE_o = 0.8–1.4 MeV

Table 4a

Differential albedos of neutrons for a 10 cm layer of boron carbide,
ΔE_o = 2.5–4 MeV

Table 4b

Differential albedos of neutrons for a 10 cm layer of boron carbide,
ΔE_o = 1.4–2.5 MeV

Table 4c

Differential albedos of neutrons for a 10 cm layer of boron carbide,
ΔE_o = 0.8–1.4 MeV

Table 1a

Дифференциальные альбедо нейтронов для слоя углерода 15 см, ΔE_0= 2,5 - 4 Мэв

θ, град	ΔЕ, Мэв	φ = 0°				φ= 90°				φ = 180°			
		θ=0°	30°	45°	75°	0°	30°	45°	75°	0°	30°	45°	75°
0	2,5 - 4,0	2322	2340	2493	3496	2322	2340	2493	3496	2322	2340	2487	3497
	1,4 - 2,5	11472	11014	10468	8000	11472	11014	10468	8000	11472	11014	10468	8000
	0,8 - 1,4	2362	2393	2428	2485	2362	2393	2428	2485	2362	2393	2428	2485
	0,4- 0,8	1361	1356	1347	1223	1361	1356	1347	1223	1361	1356	1347	1223
	0,2 - 0,4	651	644	634	549	651	644	634	549	651	644	634	549
30	2,5 - 4,0	2199	2482	2772	3135	2199	2306	2507	3424	2199	2334	2407	3131
	1,4 - 2,5	10340	8715	7820	5684	10384	10015	9576	7578	10426	11502	11739	10840
	0,8 - 1,4	2304	2350	2391	2472	2303	2334	2368	2428	2303	2318	2344	2380
	0,4 - 0,8	1319	1314	1306	1187	1319	1315	1306	1188	1319	1315	1307	1189
	0,2 - 0,4	630	624	614	532	630	624	614	532	630	624	614	532
45	2,5 - 4,0	2165	2555	2738	3085	2159	2310	2520	3317	2154	2218	2342	2849
	1,4 - 2,5	9089	7248	6402	4966	9143	8872	8547	7068	9197	10870	11520	11950
	0,8 - 1,4	2218	2269	2313	2407	2217	2247	2281	2344	2216	2285	2247	2276
	0,4- 0,8	1260	1256	1248	1136	1260	1257	1249	1138	1260	1257	1250	1140
	0,2 - 0,4	601	595	585	508	601	595	585	508	601	595	585	508
75	2,5 - 4,0	1749	1670	1783	4859	1750	1824	1917	2417	1750	1667	1647	2187
	1,4 - 2,5	4138	3154	2966	3459	4180	4196	4220	4391	4221	5978	7048	10950
	0,8 - 1,4	1496	1544	1584	1711	1495	1519	1546	1630	1495	1493	1507	1543
	0,4 - 0,8	814	812	808	747	814	813	809	749	814	813	810	751
	0,2 - 0,4	383	379	374	327	383	379	374	327	383	379	373	327

Table 1b

Дифференциальные альбедо нейтронов для слоя углерода 15 см, ΔE= 1,4 - 2,5 Мэв

θ₀, град	ΔE, Мэв	φ=0°				φ=90°				φ=180°			
		θ=0°	30°	45°	75°	0°	30°	45°	75°	0°	30°	45°	75°
0	1,4 - 2,5	3090	3540	3930	5170	3090	3540	3930	5170	3090	3540	3930	5170
	0,8 - 1,4	5670	5690	5710	5670	5670	5690	5710	5670	5670	5690	5710	5760
	0,4 - 0,8	2553	2552	2545	2378	2553	2552	2545	2378	2553	2552	2545	2378
	0,2 - 0,4	1206	1194	1176	1030	1206	1194	1176	1030	1206	1194	1176	1030
30	1,4 - 2,5	3343	3877	4166	6218	3327	3633	3919	5125	3311	3050	3251	4535
	0,8 - 1,4	5400	5297	5275	5218	5404	5431	5461	5484	5408	5579	5677	5830
	0,4 - 0,8	2453	2455	2451	2297	2453	2452	2447	2290	2453	2450	2443	2283
	0,2 - 0,4	1155	1144	1127	988	1155	1144	1127	988	1155	1144	1127	988
45	1,4 - 2,5	3416	3839	4207	6703	3404	3612	3831	5052	3391	2996	2982	4131
	0,8 - 1,4	5061	4928	4904	4834	5066	5102	5143	5238	5072	5303	5442	5747
	0,4 - 0,8	2318	2322	2319	2183	2318	2318	2313	2173	2318	2315	2308	2162
	0,2 - 0,4	1087	1077	1062	932	1087	1077	1062	932	1087	1077	1062	933
75	1,4 - 2,5	2600	3312	3874	6820	2587	2760	2920	4190	2576	2416	2387	2346
	0,8 - 1,4	3145	3053	3061	3166	3150	3209	3283	3642	3155	3412	3604	4349
	0,4 - 0,8	1456	1465	1470	1422	1456	1460	1463	1409	1456	1456	1456	1395
	0,2 - 0,4	663	658	650	578	663	658	650	578	663	658	650	579

Table 1c

Дифференциальные альбедо нейтронов для слоя углерода 15 см, $\Delta E_0 = 0,8 - 1,4$ Мэв

θ_0, град	ΔE, Мэв	$\varphi = 0^0$				$\varphi = 90^0$				$\varphi = 180^0$			
		$\theta = 0^0$	30^0	45^0	75^0	0^0	30^0	45^0	75^0	0^0	30^0	45^0	75^0
0	0,8 - 1,4	4100	4335	4640	6290	4100	4335	4640	6290	4100	4335	4640	6290
	0,4 - 0,8	6533	6590	6645	6657	6533	6590	6645	6657	6533	6590	6645	6657
	0,2 - 0,4	2716	2702	2678	2435	2716	2702	2678	2435	2716	2702	2678	2435
30	0,8 - 1,4	4083	4644	5125	7473	4075	4305	4600	6266	4064	3975	4094	5082
	0,4 - 0,8	6266	6306	6347	6311	6266	6321	6380	6430	6266	6327	6393	6510
	0,2 - 0,4	2585	2574	2553	2331	2585	2573	2551	2327	2585	2571	2549	2323
45	0,8 - 1,4	4030	4724	5280	7970	4016	4240	4524	6120	4003	3773	3810	4510
	0,4 - 0,8	5912	5940	5973	5940	5912	5970	6030	6130	5913	5982	6053	6235
	0,2 - 0,4	2417	2408	2390	2193	2417	2406	2387	2187	2417	2404	2385	2181
75	0,8 - 1,4	3170	3984	4610	8000	3150	3320	3540	4910	3135	2710	2610	2730
	0,4 - 0,8	3728	3720	3746	3810	3730	3790	3870	4210	3731	3840	3935	4350
	0,2 - 0,4	1431	1432	1430	1356	1431	1430	1426	1347	1431	1428	1422	1340

Дифференциальные альбедо нейтронов для слоя углерода 25 см, $\Delta E_0 = 2,5 - 4$ Мэв

θ₀ град	ΔE, Мэв	φ = 0°				φ = 90°				φ = 180°			
		θ = 0°	30°	45°	75°	0°	30°	45°	75°	0°	30°	45°	75°
0	2,5 - 4,0	2536	2541	2686	3590	2536	2541	2686	3590	2536	2541	2686	3590
	1,4 - 2,5	12510	11950	11310	8470	12510	11950	11310	8470	12510	11950	11310	8470
	0,8 - 1,4	3167	3173	3173	3033	3167	3173	3173	3033	3167	3173	3173	3033
	0,4 - 0,8	2040	2010	1970	1696	2040	2010	1970	1696	2040	2010	1970	1696
	0,2 - 0,4	1090	1066	1037	858	1090	1066	1037	858	1090	1066	1037	858
30	2,5 - 4,0	2388	2663	2940	3222	2388	2485	2672	3511	2388	2500	2560	3240
	1,4 - 2,5	11250	9560	8600	6164	11300	10880	10376	8065	11340	12330	12570	11340
	0,8 - 1,4	3033	3056	3066	2967	3033	3040	3042	2921	3033	3023	3017	2873
	0,4 - 0,8	1936	1910	1875	1617	1936	1911	1873	1618	1936	1911	1876	1619
	0,2 - 0,4	1031	1010	983	815	1031	1011	983	815	1031	1010	983	815
45	2,5 - 4,0	2377	2710	2880	3160	2321	2463	2660	3390	2512	2570	2857	3618
	1,4 - 2,5	9860	7960	7055	5374	9913	9600	9225	7484	9962	11630	12230	12320
	0,8 - 1,4	2858	2888	2904	2838	2858	2886	2871	2774	2858	2843	2836	2706
	0,4 - 0,8	1807	1784	1752	1516	1807	1785	1753	1518	1807	1735	1754	1519
	0,2 - 0,4	958	939	915	760	958	940	915	760	958	940	915	760
75	2,5 - 4,0	1798	1716	1826	4882	1799	1870	1960	2439	2370	2481	2692	3299
	1,4 - 2,5	4394	3393	3189	3600	4435	4440	4450	4533	4477	6230	7335	11090
	0,8 - 1,4	1757	1795	1822	1879	1756	1770	1784	1798	1755	1744	1744	1710
	0,4 - 0,8	1049	1038	1024	906	1049	1039	1025	908	1049	1040	1026	910
	0,2 - 0,4	542	532	520	437	542	533	520	437	542	533	520	437

Table 2b

Дифференциальные альбедо нейтронов для слоя углерода 25 см, $\Delta E_0 = 1,4 - 2,5$ Мэв

θ_0, град	ΔE, Мэв	$\varphi = 0°$				$\varphi = 90°$				$\varphi = 180°$			
		$\theta = 0°$	30°	45°	75°	0°	30°	45°	75°	0°	30°	45°	75°
0	1,4 - 2,5	3480	3935	4300	5410	3480	3935	4300	5410	3480	3935	4300	5410
	0,8 - 1,4	6350	6330	6310	6060	6350	6330	6310	6060	6350	6330	6310	6060
	0,4 - 0,8	3190	3170	3130	2800	3190	3170	3130	2800	3190	3170	3130	2800
	0,2 - 0,4	1652	1623	1584	1334	1652	1623	1584	1334	1652	1623	1584	1334
30	1,4 - 2,5	3700	4225	4500	6410	3682	3980	4245	5320	3420	3740	4330	5200
	0,8 - 1,4	6016	5880	5830	5580	6020	6018	6010	5840	6025	6170	6230	6190
	0,4 - 0,8	3040	3016	2980	2680	3038	3013	2977	2673	3038	3010	2973	2666
	0,2 - 0,4	1565	1538	1502	1267	1565	1538	1502	1267	1565	1538	1502	1267
45	1,4 - 2,5	3728	4144	4496	6870	3715	3915	4116	5220	3383	3570	4362	5014
	0,8 - 1,4	5600	5440	5380	5200	5606	5616	5625	5552	5611	5818	5925	6060
	0,4 - 0,8	2836	2819	2789	2521	2836	2815	2783	2511	2836	2811	2778	2500
	0,2 - 0,4	1452	1428	1395	1180	1452	1428	1395	1180	1452	1428	1395	1180
75	1,4 - 2,5	2708	3418	3975	6880	2696	2835	3020	4252	3290	3260	3860	4646
	0,8 - 1,4	3350	3250	3244	3285	3356	3406	3470	3760	3360	3610	3790	4470
	0,4 - 0,8	1670	1670	1663	1560	1670	1666	1657	1546	1670	1661	1650	1532
	0,2 - 0,4	820	808	792	683	820	808	792	683	820	808	793	683

Дифференциальные альбедо нейтронов для слоя углерода 25 см, $\Delta E_0 = 0,8 - 1,4$ Мэв

θ_0 град	ΔE, Мэв	$\varphi = 0°$				$\varphi = 90°$				$\varphi = 180°$			
		$\theta=0°$	30°	45°	75°	0°	30°	45°	75°	0°	30°	45°	75°
0	0,8 - 1,4	4370	4600	4890	6460	4370	4600	4890	6460	4370	4600	4890	6460
	0,4 - 0,8	6980	7010	7030	6910	6980	7010	7030	6910	6980	7010	7030	6910
	0,2 - 0,4	3080	3050	3000	2670	3080	3050	3000	2670	3080	3050	3000	2670
30	0,8 - 1,4	4330	4880	5340	7600	4319	4537	4814	6532	4300	4450	4850	6070
	0,4 - 0,8	6660	6680	6690	6540	6662	6695	6727	6657	6662	6700	6740	6737
	0,2 - 0,4	2910	2890	2850	2540	2914	2885	2844	2534	2914	2884	2842	2531
45	0,8 - 1,4	4239	4923	5460	8070	4226	4440	4710	6225	4206	4310	4815	5650
	0,4 - 0,8	6253	6260	6270	6140	6254	6290	6330	6320	6254	6300	6350	6430
	0,2 - 0,4	2700	2680	2645	2370	2702	2677	2642	2366	2701	2675	2639	2361
75	0,8 - 1,4	3240	4050	4670	8040	3223	3390	3600	4950	3970	3993	4320	4950
	0,4 - 0,8	3854	3840	3860	3880	3856	3910	3980	4270	3857	3960	4040	4420
	0,2 - 0,4	1542	1538	1529	1425	1542	1535	1525	1416	1542	1533	1521	1408

88

Table 3a

Дифференциальные альбедо нейтронов для слоя карбида бора 5 см, ΔE_0 = 2,5 - 4 Мэв

θ_0, град	ΔE, Мэв	$\varphi = 0°$				$\varphi = 90°$				$\varphi = 180°$			
		$\theta = 0°$	30°	45°	75°	0°	30°	45°	75°	0°	30°	45°	75°
0	2,5 - 4	2120	1800	1560	2060	2120	1800	1560	2060	2120	1800	1560	2060
	1,4 - 2,5	5320	5215	5090	4430	5320	5215	5090	4430	5320	5215	5090	4430
	0,8 - 1,4	1013	1030	1050	1150	1013	1030	1050	1150	1013	1030	1050	1150
	0,4 - 0,8	415	422	430	451	415	422	430	451	415	422	430	451
	0,2 - 0,4	188	189	190	185	188	189	190	185	188	189	190	185
30	2,5 - 4	1675	1261	1345	3030	1690	1510	1590	2120	1710	2145	2140	1710
	1,4 - 2,5	4920	4310	3980	3230	4940	4850	4750	4260	4950	5440	5630	5800
	0,8 - 1,4	992	990	1007	1135	993	1010	1031	1143	934	1033	1065	1183
	0,4 - 0,8	412	419	427	448	412	419	428	449	412	420	428	449
	0,2 - 0,4	186	186	187	181	186	187	188	183	186	188	189	186
45	2,5 - 4	1337	1239	1535	3450	1351	1283	1277	2190	1365	1970	2190	1940
	1,4 - 2,5	4460	3710	3370	2830	4480	4430	4360	4040	4510	5240	5590	6320
	0,8 - 1,4	964	960	979	1132	965	983	1007	1126	966	1014	1053	1189
	0,4 - 0,8	406	413	421	442	406	413	422	443	406	414	422	444
	0,2 - 0,4	182	182	182	177	182	183	185	180	182	185	186	184
75	2,5 - 4	1043	1610	1990	5090	1031	1129	1266	2230	1019	910	1121	2345
	1,4 - 2,5	2410	1880	1780	2170	2435	2470	2520	2820	2460	3350	3910	5990
	0,8 - 1,4	724	738	770	979	725	744	769	897	725	770	812	989
	0,4 - 0,8	318	324	331	352	318	325	332	354	318	325	333	356
	0,2 - 0,4	141	140	140	137	141	142	143	143	141	144	146	148

Table 3b

Дифференциальные альбедо нейтронов для слоя карбида бора 5 см, $\Delta E_0 = 1,4 - 2,5$ Мэв

θ_0, грэд	ΔE, Мэв	$\varphi = 0°$				$\varphi = 90°$				$\varphi = 180°$			
		$\theta = 0$	30°	45°	75°	0°	30°	45°	75°	0°	30°	45°	75°
0	1,4 - 2,5	2995	3285	3560	4610	2995	3285	3560	4610	2995	3285	3560	4610
	0,8 - 1,4	4490	4490	4520	4750	4480	4490	4520	4750	4480	4490	4520	4750
	0,4 - 0,8	1210	1235	1265	1365	1210	1235	1265	1365	1210	1235	1265	1365
	0,2 - 0,4	436	439	441	431	436	439	441	431	436	439	441	431
30	1,4 - 2,5	3093	3373	3547	4995	3086	3300	3516	4544	3079	3034	3234	4463
	0,8 - 1,4	4240	4064	4032	4268	4246	4272	4313	4613	4253	4512	4662	5141
	0,4 - 0,8	1177	1206	1238	1343	1177	1201	1231	1330	1176	1197	1224	1316
	0,2 - 0,4	423	426	428	419	423	426	429	419	423	426	429	419
45	1,4 - 2,5	3088	3269	3465	5248	3084	3241	3419	4456	3079	2980	3074	4273
	0,8 - 1,4	3959	3745	3715	3996	3967	4006	4062	4431	3976	4330	4543	5225
	0,4 - 0,8	1133	1164	1195	1301	1133	1157	1185	1282	1133	1150	1175	1263
	0,2 - 0,4	406	409	411	402	406	409	412	452	406	409	412	403
75	1,4 - 2,5	2308	2659	3031	5479	2305	2419	2574	3664	2302	2376	2468	3016
	0,8 - 1,4	2556	2405	2424	2689	2533	2600	2689	3235	2540	2898	3171	4338
	0,4 - 0,8	805	831	857	952	895	823	844	924	805	814	830	896
	0,2 - 0,4	281	283	285	281	281	284	286	282	281	284	286	283

Table 3c

Дифференциальные альбедо нейтронов для слоя карбида бора 5 см, $\Delta E_0 = 0{,}8 - 1{,}4$ Мэв

θ_0, град	ΔE, Мэв	$\varphi = 0°$				$\varphi = 90°$				$\varphi = 180°$			
		$\theta = 0°$	$30°$	$45°$	$75°$	$0°$	$30°$	$45°$	$75°$	$0°$	$30°$	$45°$	$75°$
0	0,8 - 1,4	3895	3890	3925	4900	3895	3890	3925	4900	3895	3890	3925	4900
	0,4 - 0,8	4750	4780	4815	4930	4750	4780	4815	4930	4750	4780	4815	4930
	0,2 - 0,4	1272	1285	1300	1310	1272	1285	1300	1310	1272	1285	1300	1310
30	0,8 - 1,4	3648	3598	3777	5739	3653	3683	3761	4857	3659	3896	4017	4518
	0,4 - 0,8	4525	4417	4402	4460	4530	4567	4613	4778	4535	4732	4855	5183
	0,2 - 0,4	1232	1248	1263	1279	1232	1244	1258	1270	1232	1241	1253	1260
45	0,8 - 1,4	3394	3481	3798	6126	3399	3467	3586	4791	3404	3702	3891	4464
	0,4 - 0,8	4254	4108	4085	4157	4260	4305	4360	4581	4260	4530	4696	5175
	0,2 - 0,4	1178	1195	1211	1230	1178	1190	1203	1217	1178	1185	1196	1203
75	0,8 - 1,4	2462	3055	3539	6098	2452	2586	2767	4024	2443	2405	2579	3611
	0,4 - 0,8	2742	2623	2622	2781	2748	2810	2888	3297	2754	3046	3260	4129
	0,2 - 0,4	805	820	833	865	804	814	825	848	804	808	816	829

Дифференциальные альбедо нейтронов для слоя карбида бора 10 см, $\Delta E_0 = 2,5 - 4$ Мэв

θ_0, град	ΔE, Мэв	$\varphi = 0^\circ$				$\varphi = 90^\circ$				$\varphi = 180^\circ$			
		$\theta = 0^\circ$	30°	45°	75°	0°	30°	45°	75°	0°	30°	45°	75°
0	2,5 – 4,0	2764	2405	2126	2485	2764	2405	2126	2485	2764	2405	2126	2485
	1,4 – 2,5	6975	6796	6574	5406	6975	6796	6574	5406	6975	6796	6574	5406
	0,8 – 1,4	1958	1962	1963	1900	1958	1962	1963	1900	1958	1962	1963	1900
	0,4 – 0,8	1015	1011	1004	912	1015	1011	1004	912	1015	1011	1004	912
	0,2 – 0,4	495	489	481	417	495	489	481	417	495	489	481	417
30	2,5 – 4,0	2241	1791	1875	3485	2260	2050	1913	2524	2279	2734	2704	2087
	1,4 – 2,5	6425	5698	5277	4089	6443	6298	6117	5160	6462	6949	7078	6755
	0,8 – 1,4	1884	1871	1870	1840	1884	1890	1894	1845	1885	1913	1927	1882
	0,4 – 0,8	981	977	970	883	981	977	971	884	981	978	971	885
	0,2 – 0,4	477	471	463	401	477	472	464	403	477	473	465	406
45	2,5 – 4,0	1826	1728	2043	3891	1842	1763	1748	2566	1857	2492	2705	2290
	1,4 – 2,5	5790	4924	4496	3601	5814	5707	5574	4857	5840	6601	6910	7206
	0,8 – 1,4	1786	1772	1776	1779	1787	1795	1802	1770	1788	1826	1847	1830
	0,4 – 0,8	934	930	924	844	934	931	925	846	934	932	926	847
	0,2 – 0,4	454	447	440	381	454	449	441	385	454	450	443	389
75	2,5 – 4,0	1256	1856	2248	5316	1243	1344	1483	2406	1231	1111	1323	2504
	1,4 – 2,5	2964	2391	2258	2517	2986	3010	3033	3182	3009	3921	4480	6391
	0,8 – 1,4	1146	1154	1178	1301	1146	1160	1175	1216	1147	1185	1217	1306
	0,4 – 0,8	601	600	599	563	601	601	600	564	601	602	601	566
	0,2 – 0,4	290	285	281	247	290	287	284	253	290	289	286	259

Table 4b

Дифференциальные альбедо нейтронов для слоя карбида бора 10 см, ΔE_0 = 1.4 - 2.5 Мэв

θ_0, град	ΔE, Мэв	$\varphi = 0°$				$\varphi = 90°$				$\varphi = 180°$			
		$\theta = 0°$	30°	45°	75°	0°	30°	45°	75°	0°	30°	45°	75°
0	1,4 - 2,5	3860	4144	4400	5184	3860	4144	4400	5184	3360	4144	4400	5184
	0,8 - 1,4	5850	5822	5791	5639	5850	5822	5791	5639	5850	5822	5791	5639
	0,4 - 0,8	2100	2103	2104	2006	2100	2103	2104	2006	2100	2103	2104	2006
	0,2 - 0,4	912	903	889	779	912	903	885	779	912	903	889	779
30	1,4 - 2,5	3902	4180	4330	5540	3695	4100	4294	5077	3890	3816	3934	4990
	0,8 - 1,4	5500	5376	5190	5080	5510	5500	5486	5432	5515	5750	5854	5970
	0,4 - 0,8	2010	2020	2022	1940	2010	2013	2015	1930	2010	2010	2010	1913
	0,2 - 0,4	869	861	848	744	869	861	848	744	869	861	848	745
45	1,4 - 2,5	3816	3990	4170	5740	3811	3960	4114	4934	3806	3680	3750	4744
	0,8 - 1,4	5084	4825	4747	4722	5093	5100	5112	5166	5103	5440	5614	5970
	0,4 - 0,8	1890	1903	1909	1843	1890	1895	1900	1823	1890	1888	1887	1804
	0,2 - 0,4	814	806	794	700	814	806	794	700	814	806	795	700
75	1,4 - 2,5	2600	2950	3318	5680	2595	2704	2851	3855	2592	2658	2740	3200
	0,8 - 1,4	3003	2865	2865	2990	3010	3065	3140	3550	3017	3370	3630	4655
	0,4 - 0,8	1168	1165	1197	1202	1168	1176	1183	1175	1168	1166	1169	1147
	0,2 - 0,4	484	480	475	425	484	480	476	426	484	488	476	427

Table 4c

Дифференциальные альбедо нейтронов для слоя карбида бора 10 см, $\Delta E_o = 0,8 - 1,4$ Мэв

θ_o, град	ΔE, Мэв	$\varphi = 0°$				$\varphi = 90°$				$\varphi = 180°$			
		$\theta = 0°$	30°	45°	75°	0°	30°	45°	75°	0°	30°	45°	75°
0	0,8 - 1,4	4680	4650	4646	5366	4680	4650	4646	5366	4680	4650	4646	5366
	0,4 - 0,8	5800	5790	5770	5560	5800	5790	5770	5560	5800	5790	5770	5569
	0,2 - 0,4	1890	1885	1870	1730	1890	1885	1870	1730	1890	1885	1870	1730
30	0,8 - 1,4	4360	4290	4440	6170	4367	4374	4420	5282	4373	4593	4680	4934
	0,4 - 0,8	5490	5340	5270	5030	5497	5495	5489	5353	5502	5664	5736	5759
	0,2 - 0,4	1806	1803	1793	1664	1806	1800	1787	1655	1805	1795	1782	1645
45	0,8 - 1,4	4020	4091	4388	6514	4025	4074	4167	5167	4030	4314	4478	4836
	0,4 - 0,8	5111	4926	4857	4665	5117	5127	5137	5090	5124	5359	5480	5686
	0,2 - 0,4	1694	1693	1686	1574	1693	1688	1679	1561	1694	1683	1671	1547
75	0,8 - 1,4	2697	3289	3766	6240	2687	2815	2990	4160	2677	2632	2800	3750
	0,4 - 0,8	3090	2954	2935	2980	3095	3143	3200	3500	3100	3380	3577	4330
	0,2 - 0,4	1034	1041	1043	1012	1034	1035	1034	995	1034	1029	1026	977
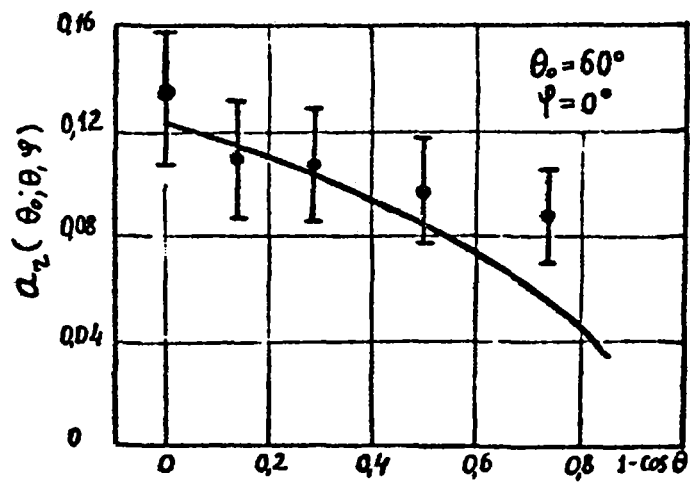
Fig. 1. Differential flux albedo of neutrons (with E_0, $E > 1$ MeV)
for a 25 cm layer of carbon at angles of $\vartheta_0 = 60^\circ$ and
$\varphi = 0^\circ$:

⊺ indicates experimental data

—— indicates calculated data.

REFERENCES

_[1_]   GERMOGENOVA, T.A. et al., in Problemy zaščity ot pronikajuščih
izlučenij reaktornih ustanovok (Problems of shielding against
penetrating radiations from reactor installations) COMECON
Symposium, Melekess 4 (1969) 35.

_[2_]   GERMOGENOVA, T.A. et al., in Voprosy fiziki zaščity reaktorov
(The physics of reactor shielding) Issue No. 2, Atomizdat (1966) 22.

_[3_]   GERMOGENOVA, T.A. et al., in Voprosy fiziki zaščity reaktorov
(The physics of reactor shielding) Issue No. 4, Atomizdat (1969) 7.

_[4_]   ABAGYAN, L.P. et al., Gruppovye konstanty dlja rasčeta jadernyh
reaktorov (Group constants for calculating nuclear reactors)
Atomizdat (1964).

_[5_]   NIKOLAEV, M.N. et al., Anizotropija rassejanija nejtronov
(Neutron scattering anistropy) Atomizdat (1971).

_[6_]   NIKOLAEV, M.N. et al., in Bjul. inf. Centr jad. Dannym, Issue No.1,
Atomizdat (1964) 308.

_[7_]   KAZANSKY, Yu.A. et al., Fizičeskie issledovanija zaščity
reaktorov (Physics investigations of reactor shielding) (Tsypin S.G.Ed.)
Atomizdat (1966).

PARAMETERS OF THE REFLECTION FROM IRON OF A FILTERED
FAST NEUTRON BEAM

I.V. Goryachev, A.P. Suvorov, L.A. Trykov

The use of the albedo concept for solving engineering physics problems such as the passage of neutrons through channels and slots in shields, the determination of the characteristics of scattered radiation fields in closed volumes, step-by-step calculation of radiation fields in separate zones of multi-layer shielding with the assignment of irradiation and reflection boundary conditions allowing for the effect of adjacent zones $\boxed{1, 2\,\boxed{}}$ and so on requires us to determine the reflection parameters of neutrons which have already passed through a certain mass of shielding material. The fact that many materials have a pronounced cross-section resonance structure leads to filtration of the source neutrons at the cross-section minima and to the associated effect of "filtered" neutrons interacting with the material of the reflecting layer. Thus it can be assumed, for example, that the albedo of a reactor spectrum beam for materials with a cross-section resonance structure will be very different from the albedo of a neutron beam transmitted through a layer of material similar to the material of the reflecting layer and depleted in resonance neutrons.

The aim of this investigation was to verify experimentally the lower albedo for iron associated with a filtered neutron beam, to establish the reflection parameters for the conditions in question, and also to develop methods of allowing for resonance self-shielding of cross-sections in multi-group calculations of neutron transmission through shielding.

The methods used for the experimental investigations were similar to those described in Ref. $\boxed{3\,\boxed{}}$. The neutron source was a zero-power research reactor with a 16 cm thick stainless steel reflector. The initial neutron beam leaving the surface of the reflector was filtered with an iron prism 27 cm thick, installed in a channel of the reactor's biological shield. The neutron detector employed was a single-crystal scintillation spectrometer with gamma discrimination based on de-excitation time $\boxed{3\,\boxed{}}$. The flux and dose albedos were determined from measurements of the neutron energy distributions. The specimen used for investigating the reflection characteristics was a 19.5 cm thick iron strip.

The differential flux albedos were calculated by a special method based on a kinetic equation in the $2D_7P_7$-approximation of the discrete ordinates method $/\overline{2}/$. The calculations were performed for seven energy groups with the ROZ-III programme, using the group constants employed for calculating the albedos in Ref. $/\overline{4}/$ multiplied by an additional blocking factor. This factor was determined as the ratio of the blocked total cross-section, obtained by measuring the transmission of a filtered beam in narrow geometry $/\overline{5}/$, to the total cross-section used in calculations for an unfiltered neutron beam $/\overline{4}/$. In the latter values, resonance self-shielding of the cross-sections was taken into account by an approximate "homogenization" method $/\overline{6}/$. However, the degree of self-shielding for an unfiltered beam is much less than for a filtered beam. Table 1 shows the blocked total cross-sections for a filtered beam and the corresponding values of the additional blocking factor f. The differential elastic and inelastic scattering cross-sections were multiplied by this factor, i.e. it was assumed that these cross-sections are shielded to exactly the same extent.

The nature of the experimental and theoretical results obtained is illustrated in Figs 1 and 2, which show the energy distributions of reflected neutrons for different incident beam angles γ both for a scalar flux (Fig. 1) and for an angular flux (Fig. 2).

The results indicate that the albedo of the prefiltered beam neutrons is the albedo of a beam with a "smooth" spectrum, i.e. with no pronounced reasonance structure. From Fig. 1 it can be seen that the reflected neutron intensity for a filtered beam in the energy range $E < 2.5-3$ MeV is several times lower than the intensity of neutrons reflected from an iron strip of the same thickness when its surface is irradiated with an unfiltered beam having a reactor spectrum. The normalization of the integral intensity was identical for both incident beams. The shape of the unfiltered beam spectrum and that of the filtered beam spectrum (smoothed by averaging over the resolution of the spectrometer - Fig. 1), differ somewhat. However, as the present authors have already established in previous investigations, slight variations in the shape of the incident beam spectrum cause only insignificant variations in the reflected neutron intensity. Therefore the difference observed between the reflected neutron intensities of the filtered and unfiltered beams is caused by the difference in the fine microstructure of their spectra and not by the difference in the smooth (averaged) shape of their spectra.

The data in Fig. 1 also indicate how the effect of the microstructure of the incident beam spectrum decreases as the angle at which the beam strikes the surface of the reflecting layer becomes larger. This is directly due to a reduction in the neutron cross-sections as a result of their self-shielding and to a corresponding increase in the probability of straight-line streaming and small-angle scattering.

This conclusion is also backed up by results of calculations of the integral flux albedos. To illustrate this, Table 2 shows the flux albedos of neutrons in the 0.4-1.4 MeV range (same energy range before and after reflection).

Fig. 2 shows the experimental and calculated energy distributions of an angular flux of reflected neutrons for different angles ψ with normal incidence of a filtered beam onto the iron strip. The angle ψ is measured from the normal.

Table 3 compares the differential angular albedos calculated for unfiltered $\boxed{7}$ and filtered neutron beams in the 0.4-1.4 MeV range (same range before and after reflection). Here we were considering a plane passing through the projection of the incident neutron beam direction onto the surface of the reflecting layer (i.e. with azimuthal angle $\varphi = 0^{o}$).

As can be seen, filtration of the beam considerably reduces the differential angular albedos as well (by factors of up to 2-3). However, the effect is much less for angles of ψ far from the normal. This is particularly true in the case of oblique beam incidence giving "sliding" reflection (such that the reflected beam direction deviates little from the direction of incidence).

Table 4 compares the theoretical and experimental values of the integral flux and dose albedos for unfiltered and filtered beams of fast neutrons with E>100 keV (for the experimental conditions described above) at different incident beam angles ψ.

Note that the data in Table 4 for the unfiltered beam relate to a strip 15 cm thick and the data for the filtered beam to a strip 19.5 cm thick. However, there should be very little difference between the fast neutron albedos of an unfiltered beam for these two thicknesses, particularly in the case of oblique beam incidence.

The large difference between the experimental and theoretical data
for the filtered beam (factors of 2-2.5) - far exceeding the very slight
difference observed in the case of the unfiltered beam (no more than 20-30%) -
is explained by the approximate nature of the assumptions made in deriving
the group constants for calculating the filtered beam albedos.   In the first
place, the values of the total cross-section $<\sigma>$ (Table 1) used in the
calculations do not, generally speaking, characterize the spectrum of
neutrons striking the reflecting layer, but represent rather the average
characteristics of the neutron spectrum in the filter.   Strictly speaking,
the total cross-section for such a calculation should be derived from an
analysis of the transmission curve at the very end of the filter.   Such
cross-sections would be smaller than those which were employed in the
calculation and, if they were used instead, beam filtration would be shown
to reduce the albedo values even more.   In the second place, the validity
of the assumption that the elastic and inelastic scattering cross-sections
have identical self-shielding has not been verified;   and, in the third place,
the assumption that there is no resonance self-shielding of the angular
distributions in neutron scattering is unjustified.   As shown in Ref. $\boxed{9}$
for neutrons with $E > 1.5$ MeV, and in Ref. $\boxed{10}$ for 1-2 MeV neutrons,
filtration of the beam has the effect of slightly increasing the anisotropy
in the case of scattering into the forward half-space and of increasing the
isotropism in the case of scattering at angles exceeding $90°$, compared with
the unfiltered beam.   None of these effects were allowed for in the above
calculation because the literature as yet offers no detailed data on the
effect of resonance self-shielding of the differential scattering cross-
sections.

Thus filtration gives a beam depleted in resonance neutrons and thereby
substantially reduces the albedo of an iron reflector 19.5 cm thick.   The
experimental data indicate a dose albedo lower by factors of 2.6-3 and a flux
albedo lower by factors of 2.8-3.6.   This albedo reducing effect is greater
with normal beam incidence and smaller with oblique incidence.   The albedo
versus angle of incidence curve is generally the same as for an unfiltered
beam.   However, in the large incident angle range the albedo is somewhat
higher for the filtered beam than would follow from the pattern established
for the unfiltered beam.   This is due to the increase in anisotropy occurring

with scattering into the forward half-space and to the increase in isotropy occurring with scattering at angles larger than 90°, which are characteristic of a filtered beam as mentioned above. This is also the reason why there is greater isotropism in the angular distribution of the reflected neutrons for a filtered beam than for an unfiltered beam.

It would also be of great practical interest to investigate the albedos of filtered beams for iron strips more than 20 cm thick. From the physics of the phenomena analysed here one would expect a much closer relationship between neutron albedo and strip thickness for filtered beams than for unfiltered beams.

It should be noted that in the case of neutron transmission through realistic shields (i.e. not in narrow beam geometry) consisting of materials with a pronounced resonance structure of the cross-sections, the flux also becomes depleted in resonance neutrons; but this depletion is of course less than in narrow beam geometry and the albedo reducing effect of beam filtration is correspondingly slighter. In other words, for the calculation of real shields the data presented here represent in a certain sense an upper limit on the effect (for ~ 20 cm thick iron strips). Nevertheless it is clear that when calculating neutron transmission through a channel in an iron shield for example, one should, generally speaking, use values for the albedos of the "inleakage" component which differ from the albedos of the "direct visibility" component.

REFERENCES

[1] GERMOGENOVA, T.A. et al., in Voprosy fiziki zaščity reaktorov (The physics of reactor shielding) Issue No. 4, Atomizdat (1969) 7.

[2] ORLOV, V.V. et al., in Voprosy fiziki zaščity reaktorov (The physics of reactor shielding) Issue No. 5, Atomizdat (1971).

[3] KUKHTEVICH, V.I. et al., Zaščita ot pronikajuščej radiacii atomnogo vzryva (Shielding against penetrating radiation from nuclear explosions) Atomizdat (1970).

[4] GERMOGENOVA, T.A. et al., Obratnoe rassejanie nejtronov (Neutron back-scattering) Atomizdat (1971).

[5] KUKHTEVICH, V.I. et al., in Problemy zaščity ot pronikajuščyh izlučenij reaktornyh ustanovok (Problems of shielding against penetrating radiations from reactor installations) Doklady SEV (Proc. COMECON Symposium) Melekess 5 (1969) 5.

_/6_/ ABAGYAN, L.P. et al., Gruppovye konstanty dlja rasčeta jadernyh
reaktorov (Group constants for calculating nuclear reactors)
Atomizdat (1964).

_/7_/ GERMOGENOVA, T.A. et al., in Bjul. inf. Centr jad. Dannym, Issue
No. 5 Atomizdat (1968) 339.

_/8_/ GORYACHEV, I.V. et al., in Voprosy fiziki zaščity reaktorov
(The physics of reactor shielding) Issue No. 3, Atomizdat (1969) 97.

_/9_/ SUVOROV, A.P. et al., Atomn. Energ. 18 (1965) 278.

_/10_/ GUSEINOV, A.G. et al., in Bjul. inf. Centr jad. Dannym, Issue No. 6
Atomizdat (1969) 407.

_/11_/ ZOLOTUKHIN, V.G. et al., Prohoždenie izlučenij čerez neodnorodnosti
v zaščite (The passage of radiation through non-uniform areas of
shields) Atomizdat (1968).

Table 1

Blocked total cross-sections <σ> and additional blocking
factors ƒ for neutrons of different energies

Key:

Номер группы   = number of group

Энергия, Мэв   = energy, MeV

барн   = barn

Table 2

Theoretical flux albedos of neutrons in the 0.4-1.4 MeV
range

Key:

град   = degrees

Нефильтров.⎫
        пучок⎬ = unfiltered beam $\boxed{7}$
Фильтров.   = filtered beam
    пучок

Table 3

Calculated differential angular albedos of neutrons
in the 0.4-1.4 MeV range (per steradian)

Key:

град   = degrees

Нефильтров.⎫
    пучок⎬ = unfiltered beam $\boxed{7}$
Фильтров.пучок = filtered beam

Table 4

Integral flux and dose albedos of fast neutrons
with E > 100 keV for an iron strip*/

Key:

град   = degrees   расчет   = calculation $\boxed{8}$

Нефильтров.⎫ = unfiltered beam   фильтров.пучок   = filtered beam
    пучок⎬
эксперимент = experiment $\boxed{8}$ эксперимент   = experiment

        расчет   = calculation

*/ Note: the figure above the line is the flux albedo and that below
the line is the dose albedo.

Table 1

Значения блокированного полного сечения
$<G>$ и фактора дополнительной блокировки
f для нейтронов различных энергий

Номер группы	Энергия, Мэв	$<G>$, барн	f
I	4 - 6,5	3,68	I,0
2	2,5 - 4	2,90	0,86
3	I,4 - 2,5	I,32	0,446
4	0,8 - I,4	0,65	0,29
5	0,4 - 0,8	0,55	0,204
6	0,2 - 0,4	0,44	0,I9I
7	0,I - 0,2	0,50	0,347

Table 2

Расчетные потоковые альбедо нейтронов с энергией
0,4 - I,4 Мэв

γ, град	Нефильтров. пучок [7]	фильтров. пучок
0	0,888	0,422
60	0,704	0,395

Table 3

Расчетные дифференциальные угловые альбедо нейтронов
с энергией 0,4 - 1,4 Мэв (на стерадиан)

γ, град	ψ, град	Нефильтров. пучок [7]	Фильтров. пучок
0	0	0,148	0,055
0	60	0,146	0,066
60	0	0,095	0,033
60	60	0,107	0,069

Table 4

Интегральные потоковые и дозовые альбедо быстрых нейтронов
с Е > 100 кэв для железной пластины [*)]

γ, град	Нефильтрованный пучок		Фильтрованный пучок	
	Эксперимент [8]	расчет [8]	эксперимент	расчет
0	0,77	1,06	0,21	0,51
	0,82	0,85	0,27	0,48
30	0,67	0,96	0,19	0,50
	0,73	0,75	0,25	0,47
50	0,58	0,79	0,183	0,46
	0,63	0,62	0,23	0,43
70	0,37	0,54	0,132	0,36
	0,40	0,40	0,153	0,34

*) ПРИМЕЧАНИЕ. Над чертой указано потоковое альбедо, под чертой - дозовое.
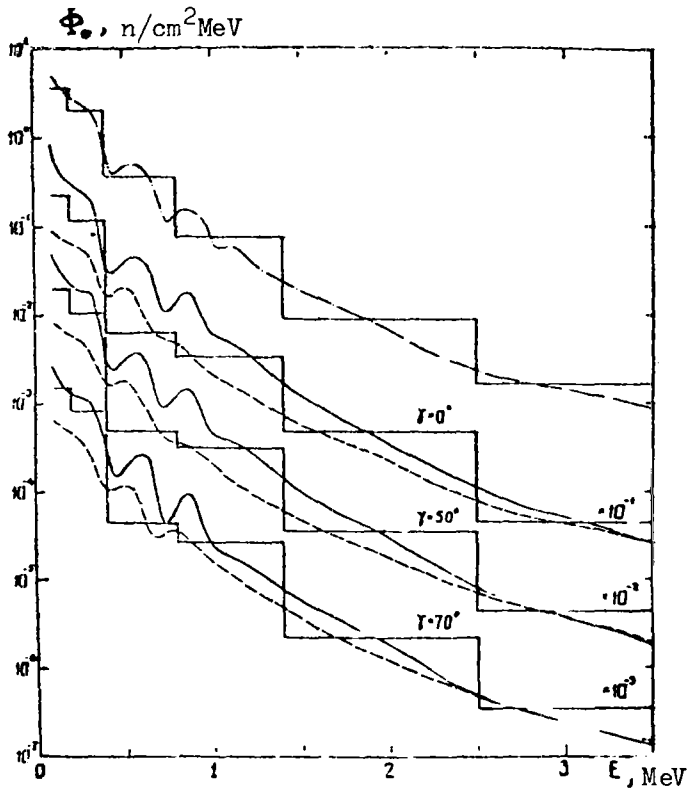
Fig. 1. Energy distributions of a scalar flux of neutrons reflected from an iron strip for different incident beam angles γ:

– – – – – filtered beam

――――― unfiltered beam

• ―――• filtered beam spectrum

The histograms show the calculated intensities of reflected neutrons for filtered beams.
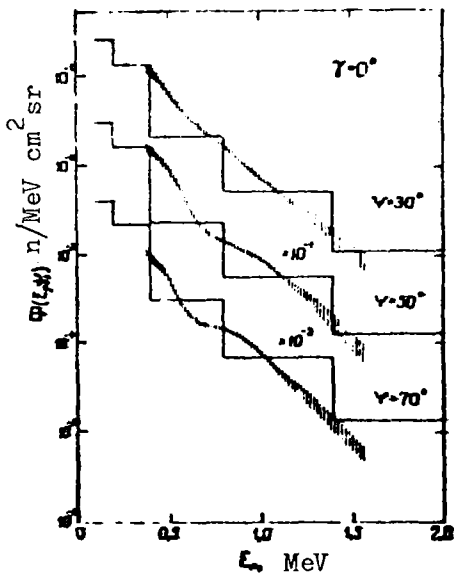
Fig. 2. Energy distributions of an angular flux of reflected neutrons for different angles ν with normal incidence of the filtered beam on the iron strip.

⌶ indicate experimental data; the histograms represent calculated values.

INVESTIGATION OF THE ERROR INVOLVED IN VARIOUS APPROXIMATIONS OF THE DISCRETE ORDINATES METHOD IN REACTOR SHIELDING CALCULATIONS

A.P. Suvorov, V.A. Utkin

The discrete ordinates method $/1-4/$ is being used more and more for calculating reactor shielding. When calculating with programmes based on this method, the work involved as well as the amount of computing time increase greatly with the number of the approximation; hence it is important to study the nature of the convergence of the solution to the accurate solution in relation to this number. This is particularly important for the solution of optimization problems, when it is necessary to calculate a large number of variants, and therefore undesirable to use a high order approximation.

Moreover, whilst the limitations of the computer memory quite often do not allow calculations of alternative compositions with a large number of spatial nodes $/3/$ in high approximations, this is quite feasible in the case of sufficiently low-order approximations. However, no detailed study has yet been made of the errors involved in these approximations of the discrete ordinates method or of the difference between the results obtained with them and reactor shielding calculations performed with higher approximations.

In this paper the authors compare the results of calculations in the different approximations of the discrete ordinates method for scalar and angular fast neutron fluxes in the heterogeneous iron-water shield of a water moderated and cooled reactor. The shield was a four-layer construction consisting of two layers of iron 10 cm thick alternating with two layers of water 30 cm thick (Fig. 1). The core composition was assumed to be similar to that of the reactor at the TES-3 nuclear power station $/5/$.

The calculations were performed for nine neutron groups in the 0.1-14 MeV range. The iron and water constants from Ref. $/3/$ used in the calculations were verified by calculations based on experimental data on fast neutron distributions in homogeneous shields consisting of water or iron $/3/$ and in heterogeneous shields of the same materials $/6/$.

The calculations were performed with the ROZ-2 programme $/7/$ in the $2D_NP_L$ approximation of the discrete ordinates method (the $2D_N$-approximation of the angular flux and the P_L-approximation of the scattering angular distribution) for different N and L. The $2D_N$ approximation of the

angular flux $\boxed{3}$ involves approximating the flux with values at the 2N
angular nodes, for which the binary Gaussian nodes (roots of the equation
$P_N(2\mu \overset{\pm}{} 1) = 0$ are chosen. The P_L-representation of the scattering angular
distribution means that the expansion of the angular distribution into
Legendre polynomials is restricted to the (L+1) - term (including the zero
term).

Since the ROZ-2 programme is intended for calculating neutron fields
(and gamma quanta) in non-fertile media only, the reactor shield calculation
is performed for a specific distribution of fission neutron sources in the
core. This distribution was obtained by a calculation with the reactor
programme in the P_1 approximation of the spherical harmonics method $\boxed{8}$,
using a 26-group system of constants (9). The presence of fertile material
in the core was taken into account, as suggested in Ref. $\boxed{10}$, by an
approximate method whereby it is assumed, in compiling the group constants
for uranium, that neutrons produced in the fission of nuclei by neutrons
of a given group either remain partially in that group or are produced with
lower energies.

The calculated spatial fast neutron flux distributions in the reactor
core and the iron-water shield performed in the $2D_{12}P_{12}$-approximation,
together with the virtually identical results of the calculation in the
$2D_7P_7$-approximation, are given in Fig. 1. These calculations of the scalar
neutron flux for a shield of this particular thickness may be regarded as
accurate for all practical purposes. This conclusion is confirmed by
comparing the results with calculations using the ROZ-5 programme $\boxed{11}$
which can be regarded as even more accurate, since in this case the $2D_{12}$-
approximation was used not only for the angular neutron flux but also for
the angular distribution of scattering by hydrogen nuclei $\boxed{7, 3}$ (the
P_{12}-approximation of the angular distribution was used for the other
elements). The adoption of this "discrete" specification of the scattering
angular distribution for hydrogen nuclei $\boxed{7, 11, 3}$ is justified in view
of the poor convergence of the P_L-representation of this angular distribution.
For example, even the P_{12}-representation often leads to negative values of
the angular distribution at many angles where arc cos $\mu_s > 50\%$ and sometimes
also at smaller angles.

Good agreement is found on comparing the calculations of the scalar
neutron flux with E > 2.5 MeV in the $2D_{12}$-approximation of the angular flux

and in the P_{12}-approximation of the scattering angular distribution for hydrogen nuclei, performed with the ROZ-2 programme, and in the $2D_{12}$-approximation, performed with the ROZ-5 programme. For the shielding composition with which we are concerned here the maximum difference in the neutron fluxes was less than 2% in the iron layers and less than 1% in the water layers.

Jumping ahead a little, it should be noted here that, although this difference is small, it is somewhat greater than the difference in the results of the $2D_{12}P_{12}$-calculations and the $2D_{N}P_{L}$-calculations for N, L ~ 5. Thus the difference between the algorithms used for solving the problem (matrix factorization in the ROZ-2 programme and the iteration method in the ROZ-5 programme) and between the respective programme codes had more effect on the attenuation values than a reduction in the order of the approximation.

In view of the closeness of the results of the different approximations there is no point in comparing the neutron flux distributions in the usual semilog graphs. Instead, the numerical results of the different approximations are compared in Tables 1-5. To facilitate comparison, the Tables include data on the discontinuity of the neutron flux values at the boundaries of the different layers compared with calculations using the $2D_{12}P_{12}$ (or $2D_{7}P_{7}$) approximation.

The following conclusions may be drawn from an analysis of Tables 1-5:

1. If the accuracy of the calculated scalar neutron flux (~ 20%) is considered adequate (this compares with the present accuracy of measuring neutron spectra), then for attenuations (a) of more than $10^{1}-10^{5}$ it is necessary to use the $2D_{N}P_{L}$-approximations with $N \geqslant 3$, $L \geqslant 2$, i.e. approximations of a higher order than $2D_{3}P_{2}$. Then with increasing N and L the error in the approximations decreases, and for approximations with N, $L \geqslant 5$ the error in the scalar flux calculations for attenuations of less than $10^{5}-10^{6}$ (due to the finiteness of the approximation) is virtually zero (the error due to inaccuracies in the constants and other factors is not considered here);

2. When N = 1 and 2, the solution of the problem is strongly dependent on the value of L. This is because the representation

of the scattering angular distribution of fast neutrons by its
values at only two or four angular points is - owing to the poor
convergence of the P_L-approximation of the angular distribution -
closely dependent on L.   As a result the data of the $2D_1P_L$- and
$2D_2P_L$-approximations may differ by several factors from the
accurate values;

3.   On the whole the error in the calculations increases
     systematically with flux attenuation, and in this case $2D_NP_N$-
     approximations at large distances from the core yields results
     which are too low rather than too high. The accuracy of the
     $2D_NP_N$ calculations is somewhat greater when N increases than
     when L increases;

4.   The error in the calculations has a relatively weak dependence
     on neutron energy.

Fig. 2 shows the results of calculations in the $2D_{12}P_{12}$-approximation
for an angular flux of neutrons escaping from the shielding composition
under consideration.   As can be seen, the angular distributions of these
neutrons are well spread out in the forward direction.   However, the form
of this spread is reproduced differently by different $2D_NP_L$-approximations.

Let us describe the degree of spread with the coefficient of non-
uniformity of the angular neutron flux distribution, which is the ratio
of the maximum angular flux (in the forward direction) to the mean angular
flux (i.e. averaged over all angles of neutron escape).   Table 6 shows
the values of this coefficient for different approximations.

It should be noted that, to obtain the coefficient of non-uniformity
of the angular flux, it is necessary to know the values of the flux at
$\mu = 1$, and these are not calculated in the $2D_NP_L$-approximation because the
only solutions of F considered are those at the Gaussian nodes μ_n.
Strictly speaking, to obtain the angular flux for other angles it would be
necessary to use the following interpolation formula:

$$F(\mu) = \sum_n F(\mu_n) L_n(\mu). \tag{1}$$

Here $L_n(\mu)$ are the Lagrangian interpolation factors.

$$L_n(\mu) = \frac{\prod_{n' \neq n} (\mu - \mu'_n)}{\prod_{n' \neq n} (\mu_n - \mu'_n)}. \tag{2}$$

To simplify our calculations the ordinary linear interpolation (with respect to μ) was used here in calculating F ($\mu = 1$).

The coefficient of non-uniformity of the angular flux, characterizing the degree of forward spread, also to a large extent characterizes the penetrating power of the flux over large distances. Judging from Table 6, the low order approximations systematically understate the values of this coefficient, but the characteristics of the angular flux approach the accurate solution fairly monotonically as the order of the approximation is increased. However, in this case we consider the most accurate results to be those obtained in the calculation using the ROZ–5 programme mentioned above, i.e. in the $2D_{12}$–approximation of the angular distribution of scattering by hydrogen nuclei.

Table 6 shows that the error in the approximations can increase considerably for the attenuation range beyond 10^5–10^6. Therefore the set of approximations capable of providing a satisfactory description of these attenuations must be reduced. This will obviously involve the use of approximations with $N \geqslant 5$, $L \geqslant 3$, i.e. approximations of a higher order than $2D_5P_3$. Special investigations will have to be carried out to establish more accurately the limits of applicability of the various approximations for describing the higher attenuations characteristic of biological shielding.

Note further $\lfloor 7 \rfloor$ that if there are any hydrogen–containing materials in the shield (as for example in our case), then, because of the bad convergence of the P_L–approximation of the "hydrogen" angular distribution mentioned above, calculations performed in the $2D_NP_L$–approximations will not give a very good description of the angular neutron flux travelling in the direction of the radiation source, i.e. when $\mu < 0$. The error of the low–order approximations is particularly large when the calculations give negative values of the angular flux for many different angles. However, when N and L are large enough the integral flux travelling back towards the source can often be described with relatively good accuracy even in cases where hydrogen is present $\lfloor 12 \rfloor$. But we will not consider this problem further here.

REFERENCES

[1] BELL, J. et al., Int. Conf. peaceful Uses atom. Energy (Proc. Conf. Geneva, 1964) Paper No. 261, UN, Geneva (1964).

[2] GERMOGENOVA, T.A. et al., in Voprosy fiziki zaščity reaktorov (The physics of reactor shielding) Issue No. 2, Atomizdat (1966) 22.

[3] GERMOGENOVA, T.A. et al., Perenos bystryh nejtronov v ploskih zaščitah (The transport of fast neutrons in plane shields) Atomizdat (1971).

[4] STEVENS, P.N., Nucl. Eng. Design, 13 (1970) 395.

[5] SINEV, N.M. et al., Atomn. Energ. 17 (1964) 448.

[6] GANSHIN, A.I. et al., this publication, beginning of Chapter III.

[7] GERMOGENOVA, T.A. et al., in Voprosy fiziki zaščity reaktorov (The physics of reactor shielding) Issue No. 4, Atomizdat (1969) 7.

[8] MARCHUK, G.I., Metody rasčeta jadernyh reaktorov (Methods of calculating nuclear reactors) Atomizdat (1961).

[9] ABAGYAN, L.P. et al., Gruppovye konstanty dlja rasčeta jadernyh reaktorov (Group constants for calculating nuclear reactors) Atomizdat (1964).

[10] SUVOROV, A.P. et al., Bjul inf. Centr. jad. Dannym, Issue No. 3 Atomizdat (1966) 513.

[11] GERMOGENOVA, T.A. et al., in Problemy zaščity ot pronikajuščih izlučenij reaktornyh ustanovok (Problems of shielding against penetrating radiations from reactor installations) COMECON Symposium, Melekess, 1 (1969) 157.

[12] GORYACHEV, I.V. et al., in Voprosy fiziki zaščity reaktorov (The physics of reactor shielding) Issue No. 4, Atomizdat (1969) 128.

Table 1

Differences in fast neutron fluxes calculated in the $2D_N P_L$- and $2D_{12}P_{12}$-approximations at the core boundary, %

Table 2

Differences in fast neutron fluxes calculated in the $2D_N P_L$- and $2D_{12}P_{12}$-approximations at a distance of 10 cm from the core, %

Table 3

Differences in fast neutron fluxes calculated in the $2D_N P_L$- and $2D_{12}P_{12}$-approximations at a distance of 40 cm from the core, %

Table 4

Differences in fast neutron fluxes calculated in the $2D_N P_L$- and $2D_{12}P_{12}$-approximations at a distance of 50 cm from the core, %

Table 5

Differences in fast neutron fluxes calculated in the $2D_N P_L$- and $2D_{12}P_{12}$-approximations at a distance of 80 cm from the core, %

Table 6

Coefficient of non-uniformity of the angular distribution of a neutron flux behind an iron-water shield 80 cm thick in the $2D_N P_L$-approximation

Key for the above tables:

МэВ = MeV

Table 1

Различие значений потока быстрых нейтронов, рассчитанных в $2D_N P_L$ и $2D_{12} P_{12}$ - приближениях, на границе активной зоны, %

E, Мэв	N\L	1	2	3	5	7
>2,5	1	1,35	6,27	4,22	22,8	31,6
	2	0,89	0,41	-0,40	-0,49	1,83
	3	0,57	-0,01	0,05	-0,04	-0,06
	5	0,60	0,01	0,10	0,02	0,01
	7	0,63	0,03	0,08	0,08	-
>1,4	1	-0,13	5,75	6,57	24,8	29,5
	2	0,26	-0,02	-0,32	-0,37	0,55
	3	0,98	0,30	0,04	0,02	-0,05
	5	0,75	0,26	0,04	$0,0^27$	0,02
	7	0,60	0,21	0,04	0,03	-
0,1 - 1,4	1	-3,09	7,86	8,48	24,4	31,7
	2	0,44	0,57	0,30	C,87	1,08
	3	0,39	0,12	0,11	0,10	0,07
	5	0,34	0,14	0,02	$0,0^26$	$0,0^28$
	7	0,26	0,16	0,01	$0,0^22$	-

Table 2

Различие значений потока быстрых нейтронов, рассчитанных в $2\mathcal{D}_N P_L$ - и $2\mathcal{D}_{12} P_{12}$ - приближениях, на расстоянии 10 см от активной зоны, %

E, Мэв	α	$N \backslash L$	I	2	3	5	7
> 2,5	9,3	I	-38,I	-28,6	32,5	I02	I50
		2	2,76	2,93	2,37	8,70	I7,0
		3	I,8I	0,74	-0,3I	-0,28	-0,I3
		5	I,89	0,60	-0,I2	$0{,}0^2 2$	-0,0I
		7	I,95	0,50	-0,05	$-0{,}0^3 6$	-
> I,4	6,8	I	-25,9	-I4,6	2I,8	76,0	I04
		2	2,I3	2,9I	I,I2	3,49	38,6
		3	2,49	0,04	-0,I6	-0,I6	-0,I6
		5	2,40	0,06	-0,03	$0{,}0^2 9$	$0{,}0^2 6$
		7	2,32	0,I0	0,02	$-0{,}0^2 3$	-
0,I-I,4	2,4	I	-4,00	I2,2	I5,6	47,7	68,5
		2	0,80	I,0I	0,33	0,04	4,33
		3	I,II	-0,02	-0,07	-0,06	0,0I
		5	I,II	0,05	$-0{,}0^2 8$	-0,0I	$-0{,}0^2 5$
		7	I,I0	0,II	$0{,}0^2 8$	$0{,}0^2 5$	-

Table 3

Различие значений потока быстрых нейтронов, рассчитанных в $2 \mathcal{D} \mathcal{N} P_{L}$ и $2 \mathcal{D}_{12} P_{12}$- приближениях, на расстоянии 40 см от активной зоны, %

E, Мэв	α	$\diagdown \begin{matrix} L \\ N \end{matrix}$	1	2	3	5	7
$> 2,5$	6.10^2	1	−93,8	−92,0	−55,0	4,85	81,6
		2	−24,2	−24,0	−9,0	17,9	42,0
		3	−18,9	−0,45	0,62	0,69	2,13
		5	−19,0	−0,69	0,19	0,01	0,02
		7	−19,1	−0,85	0,15	$−0,0^21$	−
$> 1,4$	$6,9.10^2$	1	−94,2	−92,4	−57,3	−2,46	55,8
		2	−26,0	−25,8	−97,7	−12,5	30,0
		3	−20,5	−0,29	0,55	0,61	1,44
		5	−20,6	−0,50	0,15	$0,0^24$	$0,0^35$
		7	−20,7	−0,72	0,13	$−0,0^22$	−
$0,1−1,4$	$8,6.10^2$	1	−94,4	−92,1	−60,0	−48,5	40,1
		2	−26,8	−26,3	−9,58	5,83	19,5
		3	−21,5	−0,16	0,44	0,48	0,93
		5	−21,6	−0,29	0,05	0,06	$0,0^26$
		7	−21,7	−0,48	0,04	0,01	−

Table 4

Различие значений потока быстрых нейтронов, рассчитанных
в $2D_N P_L$ - и $2D_{12} P_{11}$ - приближениях, на расстоянии
50 см от активной зоны, %

E, Мэв	α	$_N\backslash^L$	1	2	3	5	7
> 2,5	$3.3 \cdot 10^3$	1	-97,6	-96,7	-60,6	23,8	184
		2	-38,2	-38,1	-19,1	16,0	54,2
		3	-28,7	-1,25	0,21	0,27	-0,04
		5	-28,7	-1,38	0,20	0,01	-0,04
		7	-28,7	-1,41	0,19	$-0{,}0^2 2$	-
> 1,4	$3,0 \cdot 10^3$	1	-97,1	-95,8	-63,1	9,70	120
		2	-36,6	-36,6	-17,5	10,1	36,0
		3	-28,1	-1,23	0,37	0,19	1,54
		5	-28,1	-13,0	0,15	0,01	$-0{,}0^2 9$
		7	-28,1	-13,3	0,14	$-0{,}0^2 3$	-
0,1-1,4	$1,7 \cdot 10^3$	1	-95,2	-92,8	-60,3	-74,2	81,0
		2	-29,8	-9,43	-5,56	6,15	25,7
		3	-23,6	-0,23	0,29	0,33	1,07
		5	-23,5	0,33	0,05	-0,02	-0,11
		7	-23,7	0,40	0,03	$-0{,}0^2 3$	-

Table 5

Различие значений потока быстрых нейтронов, рассчитанных в $2 D_N P_L$ - и $2 D_{12} P_{12}$ - приближениях, на расстоянии 80 см от активной зоны, %

E, Мэв	α	L / N	1	2	3	5	7
>2,5	$1,5 \cdot 10^5$	1	-99,7	-99,6	-84,8	-34,2	115
		2	-59,7	-59,6	-35,5	28,3	96,6
		3	-48,5	-6,44	-2,13	-1,65	6,73
		5	-48,3	-6,39	-0,14	-0,06	0,05
		7	-47,9	-6,36	-0,21	-0,05	-
>1,4	$2,5 \cdot 10^5$	1	-99,7	-99,6	-85,1	-36,9	93,5
		2	-59,6	-59,5	-35,0	22,5	82,5
		3	-48,6	-5,89	-2,08	-1,61	5,48
		5	-48,3	-6,05	-0,08	-0,04	0,04
		7	-48,1	-6,22	-0,13	-0,03	-
0,1-1,4	$8,9 \cdot 10^5$	1	-99,7	-99,6	-98,6	31,0	23,6
		2	-56,6	-56,3	-31,9	7,52	43,7
		3	-46,6	-6,70	-1,68	-1,39	2,51
		5	-46,3	-6,36	-0,14	$0,0^2 8$	0,02
		7	-46,2	-5,92	-0,15	0,01	-

Table 6

Коэффициент неравномерности углового распределения
потока нейтронов за железо-водной защитой толщиной
80 см в $2 \mathcal{D}_N P_L$ - приближении

Е, Мэв	N	$L = 1$	$L = 2$	$L = 3$	$L = 5$	$L = 7$	$2\mathcal{D}_{12}$
>4	2	2,10	2,12	2,19	2,40	2,39	4,58
	3	2,69	2,96	3,20	3,24	3,30	
	5	3,06	3,62	4,09	4,25	4,26	
	7	3,42	4,29	4,41	4,53	4,54	
>2,5	2	2,03	2,03	2,15	2,27	2,28	4,28
	3	2,49	2,80	2,99	3,02	3,04	
	5	2,77	3,15	3,70	3.80	3,81	
	7	3,07	3,49	3,93	4,01	4,02	
>1,4	2	1,94	1,94	2,09	2,17	2,09	3,75
	3	2,33	2,64	2,81	2,83	2,84	
	5	2,56	2,93	3,39	3,45	3,46	
	7	2,79	3,23	3,57	3,62	3,62	
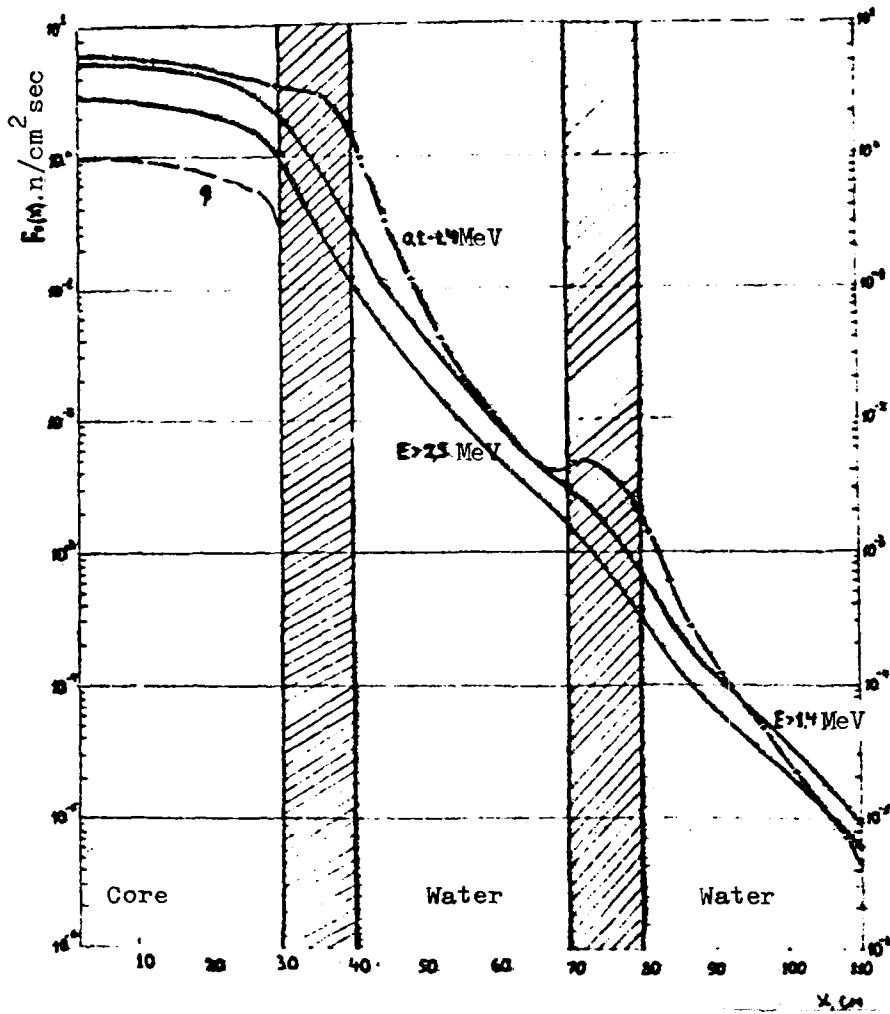
Fig. 1. Flux distribution of fast neutrons of different energies in
the iron—water shield of a water moderated and cooled reactor.
(Broken line = source intensity distribution; q = number of
fission neutrons per cm^3).
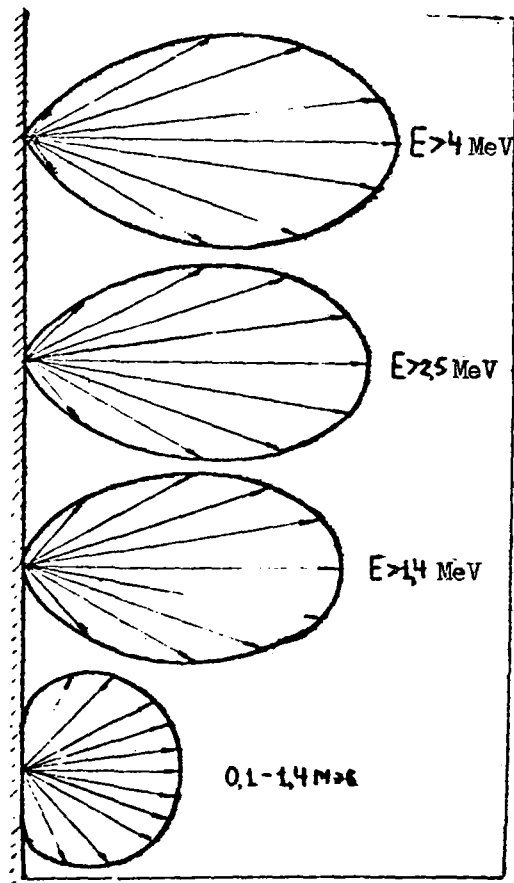
Fig. 2. Angular distributions of neutrons of different energy escaping from iron-water shield 80 cm thick.

BREMSSTRAHLUNG YIELDS OF ELECTRONS WITH AN END-POINT ENERGY
OF 22.5 MeV AS A FUNCTION OF THE ATOMIC NUMBER OF A TARGET
OF VARIABLE THICKNESS

V.P. Kovalev, V.P. Kharin, V.V. Gordeev

According to the theory of Bethe and Heitler $/1/$ radiative energy
losses for an "infinitely thin" target are proportional to Z^2 (Z being the
atomic number of the target). For the "thick" total absorption targets
and "medium" thickness targets used in practical applications, deviations
of the Bremsstrahlung yields from the Z^2 law may be expected owing to the
increase in non-radiative electron energy losses, absorption in the target
and multiple emission of photons by a single electron $/2/$. These
processes begin to appear at thicknesses as little as 0.1 Xo (Xo being the
radiation width). Buechner and co-workers $/3/$ analysed experimental
data on Bremsstrahlung yields for total absorption targets made of Al, Be,
Cu, Ag, W and Au $(E\gamma^{max} = 1.25 - 2.35$ MeV) in order to find the dependence
of the yield on Z. They showed that for targets whose thickness slightly
exceeds the electron range the Bremsstrahlung yield in the energy range
investigated increases linearly with increasing Z. For medium thickness
targets it can evidently be expected that the yield will vary as ~ Z^k,
where $1 < k < 2$.

In order to verify this assumption we used the LUE-25 linear accelerator
operating at an electron energy of 22.5 MeV to measure the forward
Bremsstrahlung yields in the 0-12° angle range for targets of Al, Ti, Cu,
Mo, Ta and W of various thicknesses. The experimental set-up and procedure
are described in Ref. $/5/$.

The experimental results are presented in Fig. 1 in the form of yields
relative to aluminium. The errors in measuring the yields were 6-9%.
The target thickness (t) is expressed as a fraction of the total electron
range (R). The curve for thin targets (t $\cong$ 0.02R) agrees with the Z^2
dependence and for thicker targets the above assumption is confirmed: the
Bremsstrahlung yield varies as Z^k, tending to the linear as the thickness
increases.
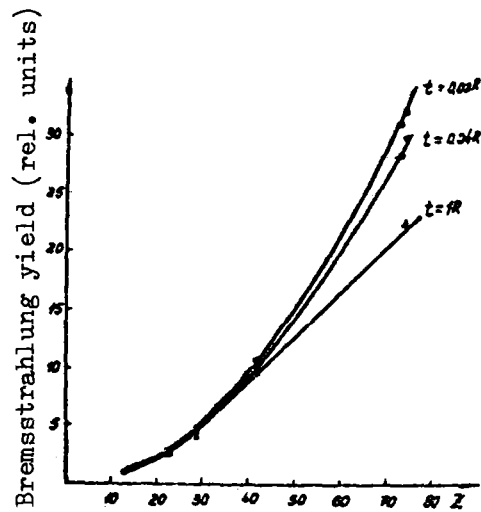
Fig. 1

REFERENCES

[1]   HEITLER, W., Kvantovaja teorija izlučenija (The quantum
       theory of radiation), Moscow, Inostrannaya Literatura (1956)
       (also 3rd Ed. London, Oxford, 1954).

[2]   WU, C.S., Phys. Rev., 59 6 (1941) 481.

[3]   BUECHNER, W.W., VAN DE GRAAFF, R.J., BURRILL, E.A., SPERDUTO, A.,
       Phys. Rev., 74 10 (1948) 1348.

[4]   ERMAKOV, V.I. et al., Atomn. Energ. 29 3 (1970) 206.

[5]   KOVALEV, V.P. et al., Atomn. Energ. (in press).

CALCULATION OF ATOMIC EXCITATION AND ELASTIC SCATTERING CROSS-SECTIONS NECESSARY FOR COMPUTING THE STOPPING POWER AND IONIZATION ENERGY OF A SUBSTANCE

Yu.S. Gerasimov, I.V. Gordeev

The stopping power and ionization energy of a substance exposed to a flux of charged particles (and neutrons) can be determined theoretically if the cross-sections of elastic scattering, excitation, ionization and charge exchange are known and, in the case of ionization and elastic scattering, the differential cross-sections as well $\boxed{1}$. For many substances these cross-sections are either not known or have been determined only at isolated points. The situation is particularly bad in the low energy range, but as it happens knowledge of the cross-sections at low incident particle energies is important for calculating the effects associated with secondary electrons.

A common method suitable for calculating the excitation cross-sections of any atomic substance is proposed here. The wave functions needed to calculate the matrix elements were found by two methods: the Bates-Damgaard method $\boxed{2}$ and a method taking into account the atomic potential (calculated by the Hartree-Fock method) in which the correct asymptotic form of the wave functions is conserved.

The cross-sections were calculated in parallel by three methods: the Born approximation, Ochkur's first exchange approximation and Ochkur's second exchange approximation.

In Ochkur's first approximation $\boxed{3}$, the scattering exchange amplitude $g(q)$ is expressed by the direct scattering amplitude $f(q)$ as follows:

$$f(q) = \frac{q^2}{K_a^2} \cdot f(q) \tag{1}$$

In Ochkur's second approximation $\boxed{4}$

$$f(q) = \frac{q^2}{K_a^2 + 2|E_b|} \cdot f(q) \tag{2}$$

in atomic units. Here q is the transmitted pulse, K_a is the initial pulse of the incident particle and E_b is the excitation energy in atomic units for the final state (reckoned from the ionization potential).

The calculations were performed for several elements of the first and second groups of the periodic table and, for checking purposes, for atomic hydrogen (for which the precise wave functions are known). The results show that the exchange term always has a large effect on the results in the range of low incident particle energies. As might be expected, Ochkur's second approximation gives better results than the first approximation. However, it is even more important to allow for the atomic potential distribution when calculating the wave functions, and to maintain their correct asymptotic form.

These wave functions not only give better agreement with experiment in the high energy range than the Bates-Damgaard wave functions $/ 2 /$, but also reduce the cross-section peak in the low energy range. These results make it possible to select a common method of calculating wave functions and cross-sections which is suitable for any atoms in the periodic table. The corresponding cross-sections will be used for calculating stopping power, ionizing energy, the Fano factor $/ 5 /$ and other atomic and nuclear constants.

The calculation was done on the BESM-6 computer.

Table 1

Cross-section for excitation of the 6p $^1P_1$ level of barium by electrons

Key:

Энергия электронов= Electron energy, eV
эв

Сечения возбуждения=Excitation cross-sections

"Сшиваемые"волновые= "Joined" wave functions
функции

"Асимптотические" = "Asymptotic" wave functions
волновые функции

Legend under table:

The Table shows cross-sections calculated in Ochkur's second exchange approximation. Electron energies are expressed in electron volts and the cross-sections in units of 10^{-16} cm^2.

The second column shows cross-sections calculated with the "joined" wave functions and the third column those calculated with the Bates-Damgaard "asymptotic" wave functions.

Table 1

Сечение возбуждения $6p\ ^1P_1$ уровня бария электронами

Энергия электро-нов, эв	Сечения возбуждения	$(10^{-16}$ см$^2)$
	"Сшиваемые" волновые функции	"Асимптотические" волновые функции
2,357	33,53	50,88
2,487	45,35	69,06
2,617	53,16	81,16
2,727	58,05	88,82
2,927	64,41	98,93
3,127	68,66	105,8
3,327	71,67	110,5
3,827	75,06	116,8
4,427	75,81 $= 7,581 \times 10^{-15}$	118,7 $= 1,187 \times 10^{-14}$
5,027	74,84	117,9
6,327	70,69	112,4
7,427	66,75	106,7
8,527	62,99	101,2
12,33	52,42	85,01
15,43	46,15	75,15
18,53	41,30	67,43
21,63	37,45	61,26
24,73	34,30	56,21
27,83	31,69	52,00
30,93	29,49	48,42
37,33	25,85	42,52
42,33	23,62	38,90
62,43	17,74	29,29
82,53	14,34	23,73
152,3	8,859	14,70
202,4	7,042	11,70
252,5	5,879 $\times 10^{-16}$	9,776 $\times 10^{-16}$

В таблице приведены сечения, вычисленные во 2-ом обменном приближении Очкура. Энергии электронов выражены в электронвольтах, сечения - в 10^{-16}см^2.

Во 2-ой колонке - сечения, вычисленные с помощью "сшиваемых" волновых функций, в 3-ей колонке - с помощью "асимптотических волновых функций Бэйтса и Демгаард.
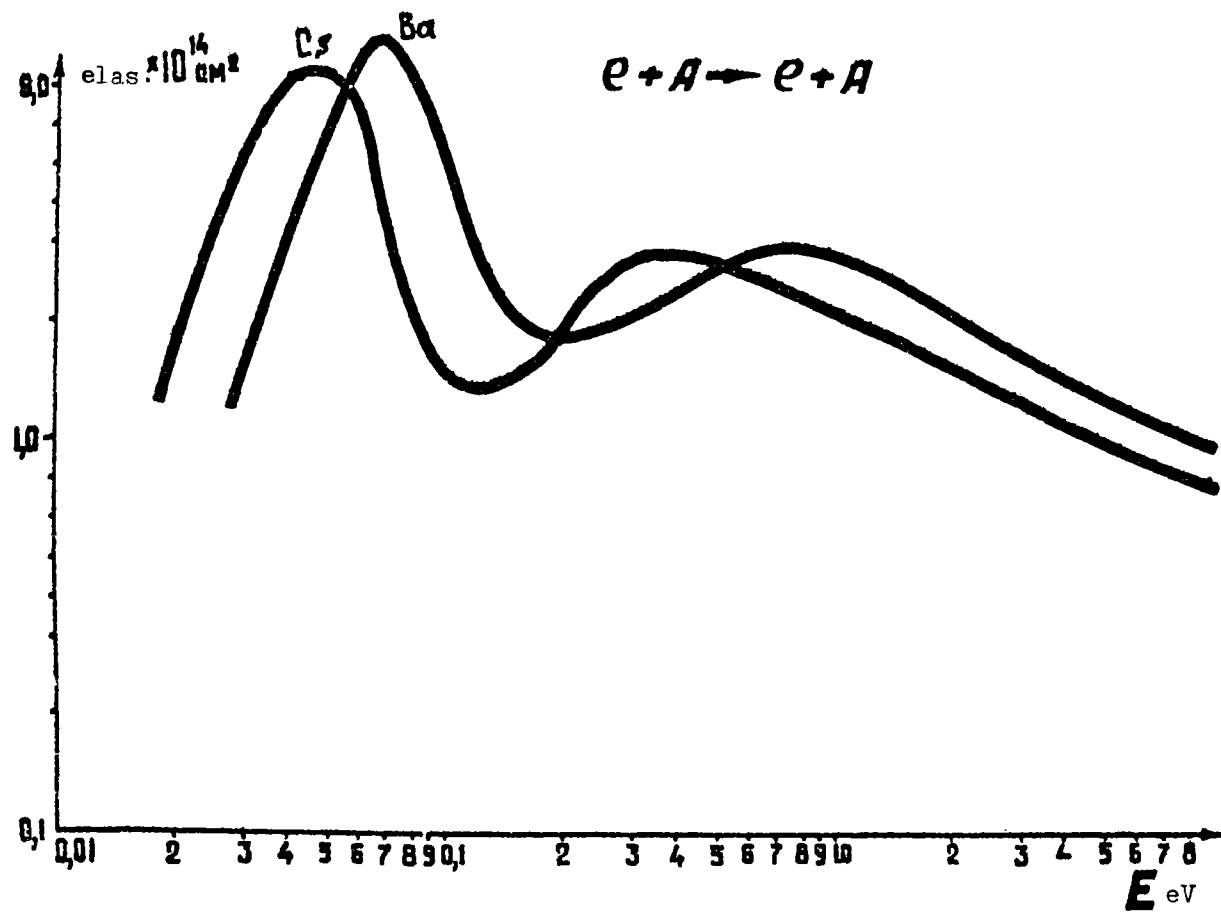
Fig. 1
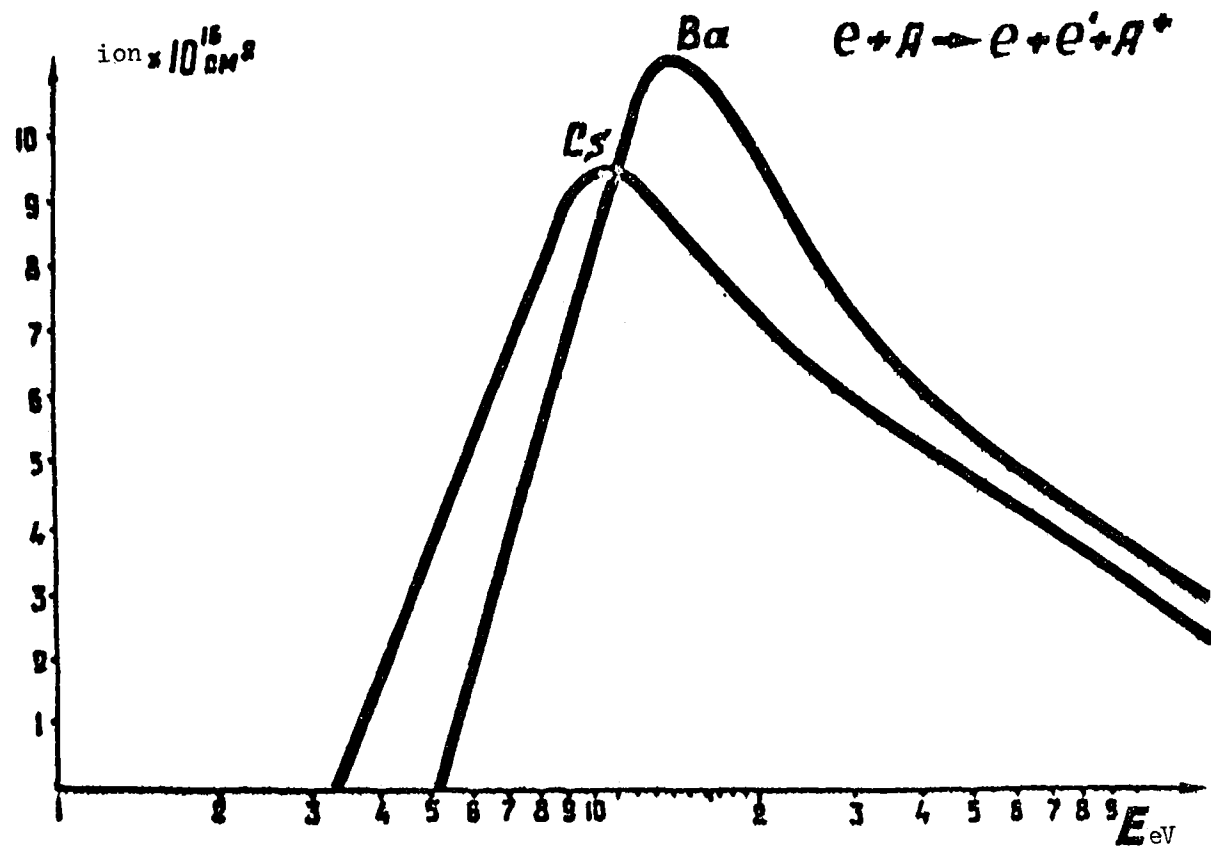
Fig. 2

REFERENCES

[1] BETHE, H., Annln. Phys. (Lpz.), 5 (1930) 325.

[2] BATES, D.R., DAMGAARD, A., Phil. Trans. Soc. London, A-242, (1949) 101.

[3] OCHKUR, V.I., Zh. eksp. teor. Fiz. 45 (1963) 734.

[4] OCHKUR, V.I., Abstracts of papers presented at the Fourth All-Union Conference on the Physics of Electron and Atom Collisions, Riga (1969).

[5] FANO, U., Phys. Rev., 72 (1947) 26.

CALCULATION OF TRANSITION PROBABILITIES AND ATOMIC EXCITATION FUNCTIONS NECESSARY FOR COMPUTING THE STOPPING POWER OF A SUBSTANCE

Yu.S. Gerasimov, I.V. Gordeev

As is well known, the excitation function for excitation of atomic levels by charged particles or neutrons is expressed by the "oscillator force" $\lfloor 1 \rfloor$, which is the square of the modulus of the matrix transition element multiplied by the transition energy expressed in rydberg (or by the neutron binding energy):

$$f_{ik} = \frac{E_k - E_i}{g_i \cdot Rh} \cdot \left| < \Psi_k | V | \Psi_i > \right|^2 \qquad (1)$$

where E_k and E_i are the initial and final transition energies, Ψ_i and Ψ_k are the initial and final atomic wave functions respectively, and V is the interaction potential.

For electromagnetic transitions in the dipole approximation we have

$$f_{ik} = \frac{1}{3 \cdot g_i} \cdot \frac{E_k - E_i}{Rh} \left| < \Psi_k | \vec{r} | \Psi_i > \right|^2 \qquad (2)$$

where g_i is the statistical weight of the initial state and $\vec{r}$ is the radius-vector.

The main difficulty in calculating excitation functions is to choose the correct wave functions of an atom of the target. The wave functions must have the correct asymptotic behaviour and must also be solutions of the equation for the atomic (or residual nuclear) core. The method of constructing wave functions is easier to check in the case of atomic interactions, since the atomic potential (the interaction potential for an atom and an incident particle) is either well known or can be calculated reliably.

The calculations were performed in the central-symmetrical field approximation. In this approximation an atom is represented in the form of a "core" whose potential has central symmetry and an external "optical" electron situated in the field of this potential $\lfloor 2 \rfloor$. The potential distribution was calculated by the Hartree-Fock method with complete allowance for exchange effects, spin-orbit coupling effects, relativistic corrections and other effects. However, the wave function obtained as the solution

of the Hartree–Fock equations $[2]$ was not used as the wave function of the "optical" electron. If the atomic energy levels are sufficiently well known, the wave functions can be obtained by a "semi–empirical" method $[3, 4]$ based on familiar atomic level theory. The desired wave functions are solutions of the equation for an electron located in the Hartree–Fock atomic potential, with the difference that the energy parameter, E, employed is not the Hartree–Fock level energy but the experimental value of this energy. Here, it is assumed that the correction to the level energy obtained from the Hartree–Fock approximation is in fact the best approximation of the wave function to its "true" value $[3, 4]$.

In the case of an atom this equation is written

$$\frac{d^2\psi}{d\tau^2} + \left[\frac{2Z(\tau)}{\tau} - 2\varepsilon - \frac{\ell(\ell+1)}{\tau^2}\right]\cdot\psi(\tau) = 0 \tag{3}$$

where $\psi(r)$ is the radial part of the wave function $[2]$, $\frac{2Z(\tau)}{\tau}$ is the atomic potential, 2ε is the level energy and ℓ is the orbital quantum number. Atomic units are used throughout $[2]$.

We must obtain solutions of equation (3) at the given potential, $V(\tau)=\frac{Z(\tau)}{\tau}$, and they must be solutions that exhibit the correct asymptotic behaviour. These solutions can be obtained by "asymptotic" methods $[5]$. In fact, Eq. (3) is similar to the Whittaker equation, but its solution, with an arbitrary function $Z(r)$, cannot be expressed as a single analytical formula apart from the case where $Z(r)$ = const. (when the solution is the Whittaker function) $[5]$. The asymptotic methods of solving the differential equations in the complex region give solutions in the vicinity of the singular points of the equation $[5]$ (in this case the singular points are the two points r_1 = 0 and r_2 = ∞), and thereby ensure the correct asymptotic behaviour of the solutions. But, since the asymptotic solutions are quite accurate even in regions far from the singular points $[5]$, the two solutions relating to the two singular points 0 and ∞ can be "joined" at an intermediate point namely the "boundary" of the atom, where the logarithmic derivatives $\frac{\varphi'}{\varphi}$ of the two solutions are equal. The complete solution of Eq. (3) is then

$$\psi(\tau) = N\cdot[C\cdot\varphi_1(\tau) + \varphi_2(\tau)] \tag{4}$$

where C is the coupling constant, N the normalizing factor and $\varphi_1(r)$ and $\varphi_2(r)$ the asymptotic wave functions.

This method was employed to calculate the wave functions and the "oscillator forces" for transitions in atoms of the first and second groups in the periodic table, using the atomic potential $V(r) = \frac{Z(r)}{r}$ calculated by the Hartree-Fock method. This potential, which is approximated by a smooth function composed of exponents, was introduced in Eq. (3).

It should be noted that the two wave functions $\varphi_1(r)$ and $\varphi_2(r)$ "joined" in Eq. (4) satisfy simultaneously both boundary conditions at the points $\varphi_1(r)$ and $\varphi_2(r)$, only their asymptotic behaviour being "incorrect" in the regions which do not correspond to them. $\varphi_1(r)$ behaves "incorrectly" when $r \to \infty$, and $\varphi_2(r)$ likewise when $r \to 0$. Therefore it was possible to check the correctness of the asymptotic behaviour of the wave function when $r \to \infty$ and the correct allowance for the atomic potential in the internal region.

For this reason the oscillator forces were calculated with three forms of the wave functions:

$$\psi(z) = N[c \cdot \psi_1(z) + \psi_2(z)] , \tag{4}$$

$$\psi_1(z) = N_1 \cdot \psi_1(z) , \tag{5}$$

$$\psi_2(z) = N_2 \cdot \psi_2(z) , \tag{6}$$

where N, N_1, N_2 are the respective normalizing factors, $\varphi_2(r)$ has the correct asymptotic behaviour when $r \to \infty$ and $\varphi_1(r)$ behaves correctly in the internal region of the atom. The wave function in Eq. (6) actually coincides with the Bates-Damgaard wave function.

Some of the results are given in the table in which the following notation is used: f is the oscillator force calculated with the aid of the "joined" wave function in Eq. (4), f_1 is the oscillator force calculated with the wave function in Eq. (5), f_2 is the oscillator force calculated with the Bates-Damgaard wave function in Eq. (6), and f_{exp} is an experimental value. The calculation was done on the BESM-4 computer. For hydrogen all three methods give practically identical results and agree with the experimental values. Differences exist only in the third or fourth significant figure.

The following conclusions may be drawn. For atomic calculations, at any rate, correct asymptotic behaviour of the wave function when $r \to \infty$ is extremely important. Wave functions with incorrect asymptotic behaviour are generally unsuitable for calculating physical quantities. However, allowance for the effect of the potential in the internal region of the atom is also important and will considerably improve the agreement with experiment, particularly in the case of excitation of the low-lying levels.
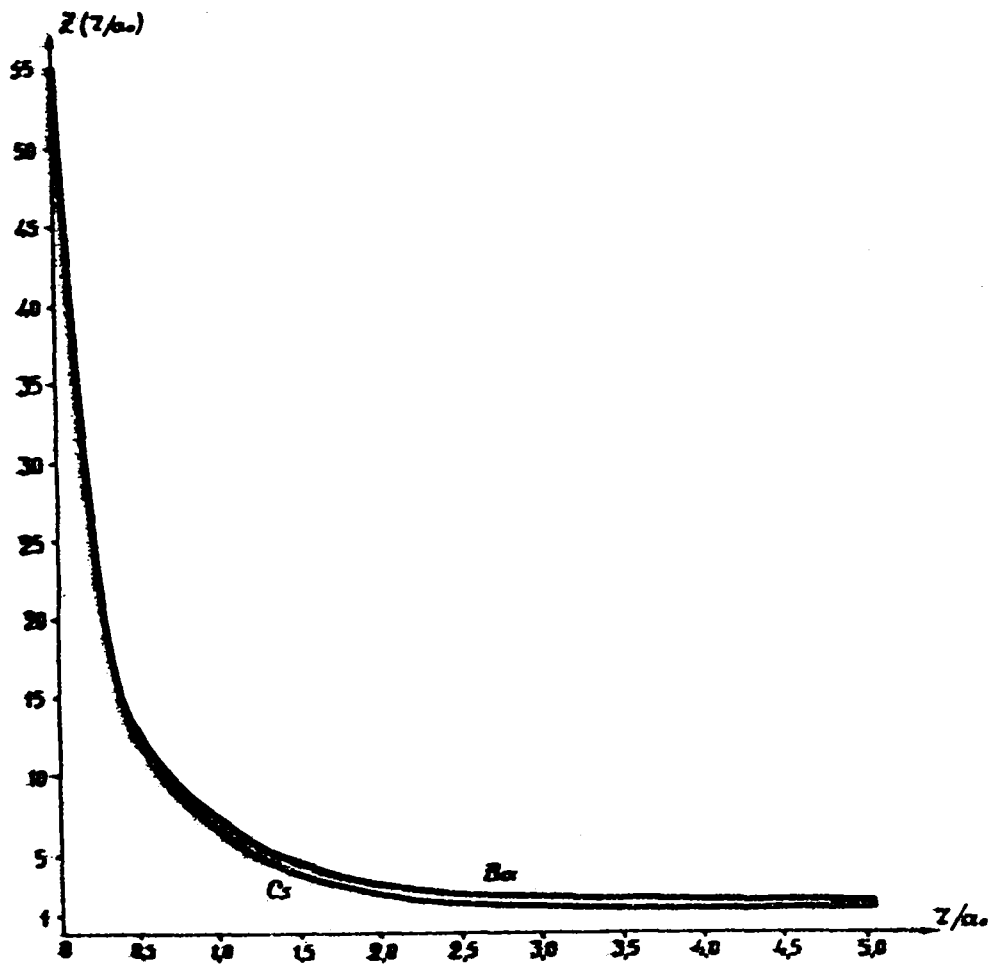
Fig. 1

Table 1

Key:

Элемент   = Element

Переход   = Transition

эксп.   = exp.

Элемент	Переход	f	f_2	f_1	f эксп.
He	1^1 -2^1P	0,350	0,3054	0,5268	0,349 [6] / 0,276 [7]
	1^1 -3^1P	0,0962	0,0839	0,0553	0,093 [6] / 0,0734 [7]
	1^1 -4^1P	0,03934	0,03434	$3,340 \times 10^{-4}$	0,0302 [8]
	1^1 -5^1P	0,01963	0,01724	$1,6043 \times 10^{-6}$	0,0153 [9]
Li	2^2 -2^2P	0,5857	0,6129	0,3244	0,60 [10] / 0,753 [11] / 0,744 [9]
	2^2 -5^2P	$3,056 \times 10^{-3}$	$2,987 \times 10^{-3}$	$5,653 \times 10^{-4}$	$3,16 \times 10^{-3}$ [12]
K	4^2 -5^2P	0,1890	0,2566	0,1808	0,18 [10] / 0,0091 [8]
Cs	6^2 -7^2P$_{3/2}$	0,2402	0,3928	0,1245	0,21 [10] / 0,0174 [13]
	6^2 -7^2P$_{1/2}$	0,0993	0,1631	0,0634	0,105 [10] / $2,84 \times 10^{-3}$ [13]
Rb	5^2 -6^2P$_{1/2}$	0,08263	0,1235	0,0611	0,065 [10]
	5^2 -6^2P$_{3/2}$	0,1817	0,2709	0,1213	0,125 [10]
Ba	6^1 -6^1P$_1$	0,9026	1,5496	-	1,40 / 0,90 [10]

REFERENCES

[1]   BETHE, H., Annls Phys. (LpZ.) 5 (1930) 325.

[2]   HARTREE, D., Rasčety atomnyh struktur (Calculation of atomic structures) Moscow IYA (1960).

[3]   BATES, D.R., DAMGAARD, A., Phil. Trans. Soc. London, A-242, (1949) 101.

[4]   WEINSTEIN, L.A., Trudy FIAN (Proc. Lebedev Physics Institute, Acad. Nauk SSSR) 15 (1961) 3.

[5]   VAZOV, FORSYTHE, Asimptotičeskie metody v teorii linejnyh differencial'nyh uravnenij (Asymptotic methods in the theory of linear differential equations).

[6]   LAUDOLT-BÖRNSTEIN, Zahlenwerte und Funktionen aus Physik, Chemie und Astronomie (Coefficients and functions from physics, chemistry and astronomy) Vol. 1, Part I, 6th ed. (1950).

[7]   SCHIFF, B., PEKERIS, L., "Phys. Rev.", 134, A-638 (1964).

[8]   "Atomic Transition Probabilities", Vol. 1-2, Washington, NBS, 1966-1969.

[9]   DALGARNO, A., STEWART, A.L., Proc. Phys. Soc., London, A-76 (1960) 49.

[10]   CORLISS, C., BOZMAN, U., Verojatnosti perehodov i sily oscilljatorov 70 elementov (Transition probabilities and oscillator forces of 70 elements) Moscow, Mir Press (1968).

[11]   WEISS, A.W., ASTROPHYS, J., 138 (1963) 1262.

[12]   FILIPPOV, A.N., Zh. eksp. teor. Fiz. 2 (1932) 24.

[13]   STONE, P.M., Phys. Rev., 127 (1962) 1151.

[14]   FRISCH, E., Optičeskie spektry atomov (Optical atomic spectra) Moscow, Fizmatgiz (1963).

METHOD OF ESTIMATING COOLANT FISSION FRAGMENT ACTIVITY AND THE RELEASES OF NUCLEAR POWER PLANTS WITH ROD-TYPE FUEL ELEMENTS COOLED BY BOILING WATER

A.G. Guseinov, M.G. Kobozev, Yu.V. Kharizomenov

1. Introduction

The activity of the primary circuit (surfaces of steam pipes, separators, turbine, condenser, ejector, etc.) during reactor operation is largely determined by the activity of the isotope formed in the $^{16}O(n,p)^{16}N$ reaction with a half-life of 7.4 sec and gamma emission with $E_\gamma = 6.1-7.1$ MeV.

When a reactor with zirconium-clad rod elements is shut down, the primary circuit activity will be governed mainly by fission fragment activity. In our calculations it was assumed that there were no fuel cladding failures likely to lead to emergency situations.

The basic assumptions for our investigation were:

1. Fission fragments get into the coolant from fuel elements with microscopic cracks in the cladding;

2. The proportion of failed elements is 0.1% of the total in the core;

3. The processes of precipitation, entrainment and distribution of the fragments between steam and water take place in accordance with a model used for calculating corrosion products.

To allow for differences in the behaviour of gaseous and solid fission fragments, we introduce two sets of coefficients, $(w,\gamma,k)^g$ and $(w,\gamma,k)^s$, for gaseous and solid fragments respectively:

$w^i(\sec^{-1})$ = coefficient of fragment precipitation from coolant;

$\gamma^i(\sec^{-2})$ = coefficient of entrainment of fragments from the surface of any part of the circuit;

k = coefficient of distribution of fragments between steam and water;

i = serial number of a fragment;

q = serial number of a section of the circuit.

A precise assessment of the fission fragment build-up in the coolant circuit would necessitate considering all possible decay chains of fragments escaping from defective elements. However, the process of considering and solving all the transport and build-up equations, with allowance for the time-dependent yields of different fragments, would be very complex and would require too much computer time. Moreover, after two years' reactor operation the system will be saturated with concentrations of the principal fission fragments and these will account for practically all the circuit activity. Therefore, if we want to know the activity of the primary circuit in a reactor which has been in operation more than two years, we can use the absolute cumulative fission fragment yields supplied in Ref. $\boxed{1}$, which remain steady for a long time after the fission of one ^{235}U nucleus.

By absolute fragment yield we mean the probability of formation of a specific type of fragment (x) in a given fission event, expressed as a percentage:

$$y\% = \frac{N(x)}{p} \cdot 100\% . \tag{1}$$

where $N(x)$ is the number of atoms of the fragment x, p is the number of fissions in the ^{235}U sample and $y(\%)$ is the absolute percentage yield of the fragment x.

In this approximation we obtain results which are slightly too high for fission fragments with half-lives of more than one year and also for their decay products. There are approximately 21 such fragments. Note that for practical purposes the only long-lived fragment of interest here is ^{137}Cs ($T_{\frac{1}{2}} = 30$ yr, $E_\gamma = 0.661$ MeV).

Thus in this approximation there is no need to consider all the decay chains and accumulations of each fission fragment in correlation with the other fragments. With only slight loss of accuracy it is possible to consider the processes of build-up, precipitation and entrainment of fragments independently of other fragments and their accumulated yields. Such an approach is justified by the acceptable accuracy of the results and by the simplicity and completenesss of the treatment.

In the present study the model is applied on a differential basis to the various sections of the circuit, although the values of the coefficients (w,γ,k) employed are known accurately in orders of magnitude and, in view

of this, it can scarcely be expected that dividing the circuit into separate sections will give more accurate results than considering the circuit as a whole. However, the differential approach to calculating the activity seems desirable if the procedures we intend to follow subsequently involve variation of parameters, comparison of theoretical and experimental results, and refinement of the coefficients for different reactors.

The rate of fragment emission (gaseous and solid) from the fuel elements was determined with the formula $[2]$

$$6_i = \left(\frac{v_i}{\sqrt{\lambda_i}}\right) \cdot \frac{3.29 \cdot 10^{13} \cdot \overline{N_k} \cdot y_i \cdot n_k \cdot m \cdot \eta \cdot 10^{-5}}{m \sqrt{\lambda_i}} \quad [\frac{nuclei}{sec}] \qquad (2)$$

Here: i is the number of the fragment;

v_i is the probability of fission fragment escape from a fuel element can;

3.29×10^{13} (fission/sec) is the number of fissions corresponding to a power of 1 kW;

$\overline{N_k}$(kW) is the mean power of a fuel channel;

n_k is the number of channels in the reactor;

y_i (%) are the fission yields;

η (%) is the relative number of defective fuel elements;

λ_i is the decay constant of the ith fragment; and

m is the number of elements in a fuel channel.

The parameter $\frac{v_i}{\sqrt{\lambda_i}}$ for fragments with half-lives $T_{\frac{1}{2}} \geqslant 1000$ sec is 10^{-5}–10^{-6} $[2]$ In our calculations we took it to be 10^{-5} for all fragments.

2. Balance equations for volume and surface activities

For a better understanding of the problem, let us consider the flow diagram of a nuclear heat and power plant with a boiling water reactor, as shown in Fig. 1. The following notation is used:

P_q^b (kg) is the quantity of water in the qth section of the circuit;

P_q^n (kg) is the quantity of steam in the qth section;

S_q (m^2) is the internal area of the qth section wet by the coolant;

G_1 (kg/sec) is the coolant flow rate through the reactor;

G_2 (kg/sec) is the steam flow rate at the outlet from the drum-
separator;

G_T (kg/sec) is the steam flow to the turbine;

G_3 (kg/sec) is the steam flow to the boilers at rated load;

G_3' (kg/sec) is the additional steam flow to the boilers at peak load;

G_{np} (kg/sec) is the water consumption on blow-down;

A_{qi} (Ci/kg) is the mean volumetric activity of the coolant in the qth
section of the circuit due to the ith fragment;

C_{qi} (Ci/m^2) is the mean surface activity of the qth section of the
circuit due to the ith fragment;

t (sec) is the operating time of the reactor;

S_q (m^2) is the internal surface of the qth section of the circuit
wet by the coolant; and

P_q^b (kg) and P_q^n (kg) are the quantity of steam and water in the qth
section of the circuit.

The values used for calculating the fragment migration parameters are
listed in Table 1. As can be seen from the table, the gaseous fragments
do not settle on the surfaces but are to be found either in the steam or
the water. Only the solid fragments are precipitated. The distribution
coefficient of solid fragments between steam and water is taken as
6.5×10^{-4} although, as follows from Ref. $\boxed{3}$, the quantity "k" can
vary within the range 6×10^{-5}–0.1 for different isotopes.

Let us write the balance equations for the volumetric and surface
activity of different sections of the circuit at peak load operation of
the plant, when there is an additional flow of steam to the boilers, so
that $G_3' \neq 0$ (see Fig. 1).

We shall number the various sections of the circuit in the following
sequence:

1 = core

2 = separator tubes leading up from the reactor to the drum-separator

3 = drum-separator

4 = turbine

5 = condenser

6 = boilers

7 = condensate pump

8 = deaerator

9 = feed pump

10 = circulation pump

Then the balance equations for the volumetric activity due to the ith fragment may be written as follows:

$$\frac{dA_{1i}}{dt} = \frac{6 \cdot \lambda_i}{3 + n^c \cdot p_1} + \frac{G_1}{p_1} A_{10i} + \frac{\gamma S_1 C_{1i}}{p_1} - A_{1i}\left(\lambda_i + \omega + \frac{G_1}{p_1}\right) \qquad (1)$$

$$\frac{dA_{2i}}{dt} = \frac{G_1}{p_1} A_{1i} + \frac{\gamma S_2 C_{2i}}{p_2} - A_{2i}\left(\lambda_i + \omega + \frac{G_1}{p_2}\right) \qquad (2)$$

$$\frac{dA_{3i}}{dt} = \frac{G_1}{p_3} A_{2i} + \frac{\gamma S_3 C_{3i}}{p_2} - A_{3i}\left(\lambda_i + \omega + \frac{p_3 \cdot \kappa \cdot G_2}{p_3^n \cdot p_3} + \frac{p_3(1-\kappa)(G_1 - G_2)}{p_3^6 \cdot p_3}\right) \qquad (3)$$

$$\frac{dA_{4i}}{dt} = \frac{p_3 \kappa G_7}{p_3^n p_4} A_{3i} + \frac{\gamma_7 S_4 G_{4i}}{p_4} - A_{4i}\left(\lambda_i + \omega + \frac{G_\kappa + G_3}{p_4}\right) \qquad (4)$$

$$\frac{dA_{5i}}{dt} = \frac{G_\kappa}{p_5} A_{4i} + \frac{\gamma S_5 C_{5i}}{p_5} - A_{5i}\left(\lambda_i + \omega + \frac{(1-\kappa)p_5 G_\kappa}{p_3^6 p_5} + \frac{p_3 \kappa G_\kappa}{p_5^n p_5}\right) \qquad (5)$$

$$\frac{dA_{6i}}{dt} = \frac{G_1 - G_\kappa}{p_6} A_{4i} + \frac{\gamma S_6 C_{6i}}{p_6} + \frac{p_3 \kappa(G_2 - G_7)}{p_3^n \cdot p_6} A_{3i} - A_{6i}\left(\lambda_i + S + \frac{p_6(1-\kappa)(G_2 - G_\kappa)}{p_6^6 \cdot p_6}\right. \qquad (6)$$

$$\left. + \frac{p_6 \cdot \kappa \cdot G_3}{p_6^n p_6}\right)$$

$$\frac{dA_{7i}}{dt} = \frac{(1-\kappa)p_5 \cdot G_\kappa}{p_5^6 \cdot p_7} A_{5i} + \frac{\gamma S_7 C_{7i}}{p_7} - A_{7i}\left(\lambda_i + \omega + \frac{G_\kappa}{p_7}\right) \qquad (7)$$

$$\frac{dA_{8i}}{dt} = \frac{(1-\kappa)p_6(G_2 - G_\kappa)}{p_6^6 \cdot p_8} A_{6i} + \frac{\gamma S_8 C_{8i}}{p_8} + \frac{G_\kappa}{p_8} A_{7i} - A_{8i}\left(\lambda_i + \omega + \right. \qquad (8)$$

$$\left. + \frac{(1-\kappa)(G_2 + G_{np})}{p_8^6} + \frac{(G_\kappa + G_3)\cdot\kappa}{p_8^n}\right)$$

$$\frac{dA_{9i}}{dt} = \frac{p_8(1-\kappa)(G_2 + G_{np})}{p_8^6 \cdot p_9} A_{8i} + \frac{\gamma S_9 C_{9i}}{p_9} - A_{9i}\left(\lambda_i + \omega + \frac{G_2 + G_{np}}{p_9}\right) \qquad (9)$$

$$\frac{dA_{10i}}{dt} = \frac{p_3(1-\kappa)(G_1 - G_2 - G_{np})}{p_3^6 \cdot p_{10}} A_{3i} + \frac{G_2 + G_{np}}{p_{10}} A_{9i} + \frac{\gamma S_{10} C_{10i}}{p_{10}} -$$

$$- A_{10i}\left(\lambda_i + \omega + \frac{G_1}{p_{10}}\right) \qquad (10)$$

The balance equations for the surface activity of the solid fragments
for the various sections are similar:

$$\frac{dC_{qi}}{dt} = A_{qi} \cdot \frac{P_q \cdot w^T}{S_q} - C_{qi} \cdot (\lambda_i + \gamma_q^T)$$ (11)

where q = 1, 2, 3, ... 10, $\gamma_q^T = \delta_T^T$ for q = 4, and $\gamma_q^T = \gamma^T$ for q ≠ 4.
Here i is the serial number of the fragment and q is the number of the
circuit section.

As can be seen from the system of equations set out in expressions
(1, 11), the quantity $A_{qi}(t)$ represents the activity of 1 kg of coolant
in any q^{th} section. This quantity characterizes the activity of steam
or water as the case may be. For example, in the fourth section (the
turbine) $A_{4i}(t)$ characterizes the mean activity of 1 kg of steam, whilst
in the eighth, ninth and tenth sections $A_{qi}(t)$ characterizes the activity
of water.

In our system of equations it is also assumed that the decontamination
factor of the blow-down water in the filter is 100% and that fully de-
contaminated water flows from the filter to the deaerator. In addition,
the coefficients of precipitation of fragments from water and steam are
considered to be identical.

The balance equations take no account of the part of the circuit
linking the turbine with the regenerative feed heater and the condenser (see
Fig. 1), because this has little effect on the results.

The system of equations is solved for the uniform initial conditions

$$\left.\begin{array}{l} A_{qi}(t)\big|_{t=0} = 0 \\[2em] C_{qi}(t)\big|_{t=0} = 0 \end{array}\right\}$$ for any values of q, i

3. Asymptotic solution of the system of equations 5-6

Let us write this system as follows:

$$\frac{dA_q}{dt} = \sum_{q'} a_{qq'} A_{q'} + f_q + \frac{k_q S_q}{P_q} C_q$$

$$A_q|_{t=0} = 0$$

$$\frac{dC_q}{dt} = \frac{\omega P_q}{S_q} A_q - (\lambda + k_q) C_q$$

$$C_q|_{t=0} = 0$$

$$q, q' = 1, 2, \dots, 10$$

$$\tag{8}$$

In the system of equations in expression (8) the coefficients $a_{qq'}$ and the source term f_q have the following values:

$$f_1 = \frac{6\lambda}{3\pi b^* \cdot p_1} \quad ; \quad f_{q \neq 1} = 0 \quad ;$$

$$a_{11} = \left(\lambda + \omega + \frac{G_1}{p_1}\right); \quad a_{22} = \left(\lambda + \omega + \frac{G_1}{p_2}\right),$$

$$a_{33} = \left(\lambda + \omega + \frac{\kappa G_2}{p_3^a} + \frac{(1-\kappa)(G_1 - G_2)}{p_3^b}\right) \quad ; \quad a_{44} = \left(\lambda + \omega + \frac{G_\kappa + G_3}{p_4}\right);$$

$$a_{55} = \left(\lambda + \omega + \frac{(1-\kappa)G_\kappa}{p_5^b} + \frac{\kappa G_\kappa}{p_5^a}\right); \quad a_{66} = \left(\lambda + \omega + \frac{(1-\kappa)(G_3 - G_\kappa)}{p_6^c} + \frac{\kappa G_3}{p_6^d}\right);$$

$$a_{77} = \left(\lambda + \omega + \frac{G_\kappa}{p_7}\right); \quad a_{88} = \left(\lambda + \omega + \frac{(1-\kappa)(G_2 + G_\gamma p)}{p_8^c} + \frac{\kappa(G_\kappa + G_3)}{p_8^a}\right);$$

$$a_{99} = \left(\lambda + \omega + \frac{G_2 + G_{\gamma p}}{p_9}\right); \quad a_{10,10} = \left(\lambda + \omega + \frac{G_1}{p_{10}}\right);$$

$$\tag{9}$$

$$a_{1,10} = \frac{G_1}{p_1} \quad ; \quad a_{2,1} = \frac{G_1}{p_2}; \quad a_{3,2} = \frac{G_1}{p_3}; \quad a_{4,3} = \frac{p_3 \cdot \kappa \cdot G_\gamma}{p_3^a \cdot p_4};$$

$$a_{5,4} = \frac{G_\kappa}{p_5}; \quad a_{6,3} = \frac{p_3 \cdot \kappa (G_2 - G_\gamma)}{p_3^a \cdot p_6}; \quad a_{6,4} = \frac{G_\gamma - G_\kappa}{p_6};$$

$$a_{7,5} = \frac{(1-\kappa) p_5 \cdot G_\kappa}{p_5^c \cdot p_7}; \quad a_{8,6} = \frac{p_6(1-\kappa)(G_2 - G_\kappa)}{p_6^c \cdot p_8}; \quad a_{8,4} = \frac{G_\kappa}{p_8};$$

$$a_{9,8} = \frac{p_8(1-\kappa)(G_2 + G_{\gamma p})}{p_8^c \cdot p_9}; \quad a_{10,3} = \frac{p_3(1-\kappa)(G_1 - G_2 - G_{\gamma p})}{p_3^c \cdot p_{10}}; \quad a_{10,9} = \frac{G_2 + G_{\gamma p}}{p_{10}}$$

while for the remainder $a_{qq'} = 0$.

Since we were estimating fragment activity for a long period of reactor operation, we looked for asymptotic values of the quantities A_q and C_q for $t \to 0$, which should be supplied by the system of equations in expression (8) on the basis of the physical picture of the activity build-up.

In fact, it can be shown that the solution of the system for the case where the effect of the surface activity term is small (as in our case: $\gamma_q = 5 \times 10^{-8} - 2 \times 10^{-6}$ (sec^{-1}), w = 3.5 $\times 10^{-5}$ (sec^{-1}) takes the form

$$A_q(t) = \sum_{k=1}^{q} \frac{\alpha_q^{(k)}}{a_{kk}}\left(1 - e^{-a_{kk}t}\right) + \int_0^{t} \sum_{k=1}^{q} \beta_q^{(k)} e^{-(t-\tau)a_{kk}} \sum_{e=0}^{\infty} \lambda^e F_e(\tau)\,d\tau \tag{10}$$

$$q = 1, 2, \ldots, 10; \qquad \lambda = a_{1,10} < 1$$

and the coefficients $\alpha_q^{(k)}$ and $\beta_q^{(k)}$ are found from the following expressions:

$$\left. \begin{array}{l} \alpha_1^{(1)} = f_1 + \dfrac{\delta q\, S_1\, C_1^{\infty}}{P_1} \\[4mm] \beta_1^{(1)} = 1 \end{array} \right\} \tag{11}$$

All succeeding $\alpha_q^{(k)}$ and $\beta_q^{(k)}$ are found with recurrent relations of the form

$$\alpha_q^{(k)} = \frac{a_{q,q-1} \cdot \alpha_{q-1}^{(k)}}{a_{q,q} - a_{k,k}} \quad ; \quad \alpha_q^{q} = \frac{\delta q\, S_q}{P_q} C_q^{\infty} - \sum_{k=1}^{q-1} \alpha_q^{(k)} \tag{12}$$

$$k < q$$

$$\beta_q^{(k)} = \frac{a_{q,q-1} \cdot \beta_{q-1}^{(k)}}{a_{q,q} - a_{k,k}} \quad ; \quad \beta_q^{q} = - \sum_{k=1}^{q-1} \beta_q^{(k)} \tag{13}$$

$$k < q$$

The functions $F_e(t)$ then take the form

$$F_e(t) = a_{1,10}\left\{ \gamma_1^{(e)} + \sum_{k=1}^{10} \gamma_2^{(e)k} e^{-a_{k,k}t} + \ldots + \frac{t^e}{e!} \sum_{k=1}^{10} \gamma_{e+2}^{(e)k} e^{-a_{k,k}t} \right\} \tag{14}$$

where the coefficients $\gamma_1^{(e)}, \ldots \gamma_{e+2}^{(e)k}$ depend on $a_e^{(k)}$ and $\beta_e^{(k)}$.

Substituting Eq. (14) in Eq. (10), we obtain for the volumetric activities

$$A_q(t) = \sum_{k=1}^{q} \frac{\alpha_q^{(k)}}{a_{k,k}}\left(1 - e^{-a_{kk}t}\right) + a_{1,10} \sum_{e=0}^{\infty} \lambda^e \gamma_1^{(e)} \sum_{k=1}^{q} \frac{\beta_q^{(k)}}{a_{kk}} + \tag{15}$$

plus the terms containing the products $\frac{t^m}{m!} \ell^{-a_{kk}t}$ (m = 1, 2, ...). When $t \to \infty$, Eq. (15) gives

$$A_q^{\infty} = \sum_{k=1}^{q} \frac{\alpha_q^{(k)}}{a_{k,k}} + a_{1,10} \sum_{e=0}^{\infty} (a_{1,10})^e \gamma_1^{(e)} \sum_{k=1}^{q} \frac{\beta_q^{(k)}}{a_{k,k}} = const \tag{16}$$

Rewriting the system in expression (8) in matrix form we have

$$\left\{ \begin{array}{l} \dfrac{d\,\bar{B}}{dt} = \hat{C}\,\bar{B} + \bar{F} \\[2mm] \bar{B}\big|_{t=0} = 0 \end{array} \right. \tag{17}$$

where

$$\bar{B} = \left\{ \begin{array}{c} A_1 \\ A_2 \\ \vdots \\ A_{10} \\ C_1 \\ C_2 \\ \vdots \\ C_{10} \end{array} \right\} , \qquad \bar{F} = \left\{ \begin{array}{c} f_1 \\ 0 \\ \vdots \\ \\ \vdots \\ 0 \end{array} \right\} \tag{18}$$

The elements $C_{e,m}$ of the matrix $\hat{C}$ are the coefficients

$$\left. \begin{array}{l} a_{e,m} \; \big(\text{see (9)}\big) \; , \quad \text{when} \quad e,m \, < \, 10 \\[2mm] b_{e,\,e+10} = \dfrac{\gamma_e\, S_e}{p_e} \; ; \quad e \leq 10 \\[2mm] \lambda_{e,\,e-10} = \dfrac{\omega^r p_{e-10}}{S_{e-10}} \; ; \quad e > 10 \\[2mm] g_{e,e} = \big(\lambda + \gamma_{e-10}\big) ; \quad e > 10 \end{array} \right\} \tag{19}$$

From Eq. (16) it follows that, in order to find the asymptotic solution of Eq. (17), we can put $\dfrac{d\bar{B}}{dt} = 0$. Then for infinite reactor operating time we have $\bar{B}_\infty = -\hat{C}\bar{F}$, where $\hat{C}^{-1}$ is a matrix which is the reciprocal of $\hat{C}$.

Solution of the system in expression (8) is considerably simplified for the case of gaseous fission fragments $(k = 1; \; w = 0; \; \gamma q = 1)$. In this case all $C_q \equiv 0$ and the system in expression (8) $(q = 1, 2, \ldots, 10)$ takes the following form:

$$\frac{dA_1}{dt} = f_1 - \left(\lambda + \frac{G_1}{P_1}\right)A_1$$

$$\frac{dA_2}{dt} = \frac{G_1}{P_2}A_1 - \left(\lambda + \frac{G_1}{P_2}\right)A_2$$

$$\frac{dA_3}{dt} = \frac{G_1}{P_3}A_2 - \left(\lambda + \frac{G_2}{P_3^n}\right)A_3 \quad .$$

$$\frac{dA_4}{dt} = \frac{G_T P_3}{P_4 \cdot P_3^n}A_3 - \left(\lambda + \frac{G_K + G_3}{P_4}\right)A_4 \tag{20}$$

$$\frac{dA_5}{dt} = \frac{G_K}{P_5}A_4 - \left(\lambda + \frac{G_K}{P_5^n}\right)A_5$$

$$\frac{dA_6}{dt} = \frac{P_3(G_2 - G_T)}{P_3^n \cdot P_6}A_3 + \frac{G_1 - G_K}{P_6}A_4 - \left(\lambda + \frac{G_3}{P_6^n}\right)A_6$$

$$A_q\big|_{t=0} = 0 \qquad q = 1, 2, \ldots 6$$

Analysing the solution of the system in expression (20), we see that the solution for $t \geqslant 0.5$ years is practically the same as for $t = \infty$ and can be sequentially determined from the system

$$A_1 = \frac{f_1}{\lambda + \frac{G_1}{P_1}} \quad ; \quad A_2 = \frac{G_1}{P_2}A_1 \bigg/ \left(\lambda + \frac{G_1}{P_2}\right) \; ,$$

$$A_3 = \frac{G_1}{P_3}A_2 \bigg/ \left(\lambda + \frac{G_2}{P_3^n}\right) \quad ; \quad A_4 = \frac{G_T P_3}{P_4 \cdot P_3^n}A_3 \bigg/ \left(\lambda + \frac{G_K + G_3}{P_4}\right) \; , \tag{21}$$

$$A_5 = \frac{G_K}{P_5}A_4 \bigg/ \left(\lambda + \frac{G_K}{P_5^n}\right) \; ,$$

$$A_6 = \left[\frac{P_3(G_2 - G_T)}{P_3^n \cdot P_6}A_3 + \frac{G_1 - G_K}{P_6}A_4\right] \bigg/ \left(\lambda + \frac{G_3}{P_6^n}\right)$$

The asymptotic solution of the system of equations in expression (1, 11) gives the following values for the volumetric activity of the different sections:*/

$$\sum_i A_{qi} \approx \left(10^{-5} \div 10^{-3}\right) \text{ Ci/kg} \tag{21a}$$

---

*/ These values were obtained on the assumption of a reactor power of 125 MW.

4. Estimating discharges of radioactive fission fragments

As can be seen from the flow diagram of the nuclear heat and power plant, the radioactive fragments accumulating in the circuit are removed from the 5th, 6th and 8th sections as the coolant is circulated. In our calculations it was assumed that the radioactive fragments present in the steam part of the above sections are entirely removed from the circuit (see the balance equations for the 5th, 6th and 8th sections).

The gaseous and solid fragments are distributed between the steam and water in accordance with the distribution coefficient

$$K = \begin{cases} 1 \text{ for gaseous fragments} \\ 6.5 \times 10^{-4} \text{ for solid fragments} \end{cases}$$

From the balance equations for the volumetric activity it is easy to find relations for estimating the amount of radioactive discharges from sections 5, 6 and 8:

$$B_{5i} \ (\text{Ci/d}) = A_{5i} \ \frac{P_5 \cdot K \cdot G_K}{P_5^n} \ 0.865 \cdot 10^5 \ ; \quad B_5 = \sum_i B_{5i} = \frac{P_5 K G_K}{P_5^n} 0.865 \cdot 10^5 \sum_i A_{5i}$$

$$B_{6i} \ (\text{Ci/d}) = A_{6i} \ \frac{P_6 \cdot K \cdot G_6}{P_6^n} \ 0.865 \cdot 10^5 \ ; \quad B_6 = \sum_i B_{6i} = \frac{P_6 K G_6}{P_6^n} 0.865 \cdot 10^5 \sum_i A_{6i} \quad (22)$$

$$B_{8i} \ (\text{Ci/d}) = A_{8i} \ \frac{P_8 (G_K + G_3) K}{P_8^n} \ 0.865 \cdot 10^5 \ ; \quad B_8 = \sum_i B_{8i} = \frac{P_8 (G_K + G_3) K}{P_8^n} 0.865 \cdot 10^5 \sum_i A_{8i}$$

Here B_{5i}, B_{6i} and B_{8i} are the discharges of radioactive fission products due to the ith fragment from the 5th, 6th and 8th sections respectively. B_5, B_6 and B_8 are the total discharges (Ci/d) from these sections. The total discharge of radioactive fragments into the vent pipe will be

$$B = \sum_i \left(B_{5i} + B_{6i} + B_{8i} \right) = B_5 + B_6 + B_8 \quad \text{Ci/d} \quad (22a)$$

According to our estimates the total discharge of radioactive fragments into the vent pipe (for this particular heat and power plant) is ~ 27 Ci/d.MW.

Our discharge estimates, referred to unit capacity, are shown in Table 2. The results agree satisfactorily with data for nuclear power stations with boiling water reactors /4-6/ (see Tables 3 and 4)/

Our estimates also show that a hundredfold increase in the distribution coefficient of solid fragments (K) leads to a hundredfold increase in the radioactive discharges due to solid fragments. In this case the volumetric activities for the different sections $\sum_i B_{qi}$ (Ci/kg), vary on average by a factor of 3-5.

A large variation in the parameter K is most significant for sections where discharges of radioactive fragments occur or where $\frac{Q_{steam}}{Q_{water}} \gg 1$ which means that the volumetric activity increases considerably in those sections with increasing K.

Conclusions

1. The assumptions made in order to obtain upper estimates of the dose situation at various parts of the circuit are well justified and values obtained with the model employed are in satisfactory agreement with experimental data $\lfloor 4 \rfloor$, both for the activity of the different sections of the circuit and for the radioactive discharges.

Our analysis also included a detailed analysis of the fission fragment spectrum, but the results are omitted here for the sake of brevity.

2. The fission fragment activity of the primary circuit - for a nuclear power plant of the type considered - is most significant in relation to releases of radioactivity.

3. To obtain a more universal set of parameters (w, γ, k) it will be necessary to analyse the sensitivity of the results to variations of all the parameters, and to compare the theoretical data with experimental values for similar nuclear power plants.

REFERENCES

$\lfloor 1 \rfloor$ GUSEV, N. et al., Gamma-izlučenie r/a izotopov i produktov delenija (Gamma radiation of radioactive isotopes and fission products) Gos. izdat. fiz. mat. literatury, Moscow (1958).

$\lfloor 2 \rfloor$ Nucleonics, vol. 22, 6 (1964) 39.

$\lfloor 3 \rfloor$ MARTYNOVA, O.I. et al., Atomn. Energ. 23 4 (1967) 305.

$\lfloor 4 \rfloor$ BLOMKE, I.D., HARRINGTON, F.E., "Waste management at nuclear power stations", Nuc. Saf. 9, 3 (1968) 238.

$\lfloor 5 \rfloor$ Nucleonics, No. 2 (1966) 39.

$\lfloor 6 \rfloor$ Atomnaja tehnika za rybežom, No. 3 (1967).

Table 1

Parameters for describing fragment migration

Key:

газ   = gas

тв   = sol.

сек   = sec

Table 2

Radioactive discharges from sections 5, 6 and 8,
referred to unit capacity

Key:

№ участков   = No. of sections

кюри/сутки мвт = Ci/d.MW

$$B\left[\dfrac{\text{тв.осколков кюри}}{\text{сут.мвт}}\right] = B^{\text{solid fragments}}\left[Ci/d.MW\right]$$

$$B\left[\dfrac{\text{газ осколков кюри}}{\text{сут.мвт}}\right] = B^{\text{gaseous fragments}}\left[Ci/d.MW\right]$$

$$B\left[\dfrac{\text{тв+газ осколк. кюри}}{\text{сут.мвт}}\right] = B^{\text{solid + gaseous fragments}}\left[Ci/d.MW\right]$$

Table 3

Radioactive discharges from foreign nuclear power stations[*]

Key:

АЭC/мощность	= Name and capacity	Выбросы /кюри/сутки мвт/	= Discharges (Ci/d.MW)
Р/а газы	= radioactive gases	аэрозоли	= aerosols
Дрезден 1	= Dresden-1 (700 MW)	Биг-Рок-Пойнт	= Big Rock Point (157 MW)
Гумбольт-Бей	= Humboldt Bay (165 MW)	Елк-Ривер	= Elk River (58 MW)

---

[*] The release data for these stations were obtained after the gases
had been cooled for 18–30 min and passed through aerosol filters.

Table 4

Activity of radioactive inert gases discharged (Ci/d.MW)

Кеу:

АЭС	= Nuclear power station
КRB	= KRB
Гарильяно	= Garigliano
Bonus	= Bonus
Рассматриваемая АТЭЦ	Nuclear heat and power plant (Fig. 1)

Table 1

Параметры для описания миграции осколков

$\omega^{м5}$	$r^{м5}$	$\kappa^{м5}$	$\omega^{тв}$	$r^{тв}$	$\kappa^{тв}$	$\sigma_т$	$\sqrt{\frac{\eta}{\lambda_i}}$	ℓ
сек⁻¹	сек⁻¹	-	сек⁻¹	сек⁻¹	-	сек⁻¹	сек⁻¹/2	%
0	I	I	$3,5.10^{-5}$	5.10^{-8}	$6,5.10^{-4}$	2.10^{-6}	10^{-5}	0,I

Table 2

Радиоактивные выбросы с участков 5,6,8, приведенные к единице мощности

№ участков	5	6	8	$\Sigma\,\beta\gamma$ (кюри/сутки мвт)
$B\left[\frac{тв.\,осколков}{н-pм}{сут.\,Nвт}\right]$	0,08	0,004	0,15	0,23
$B\left[\frac{газ.\,осколков}{н-pм}{сут.\,Nвт}\right]$	20,70	5,75	-	26,45
$B\left[\frac{тв.+газ.\,осколк.}{н-pм}{сут.\,Nвт}\right]$	20,78	5,754	0,I5	26,68

Результаты по оценке величины радиоактивных выбросов удовлетворительно согласуются с данными для АЭС с кипящими реакторами 4-6 (см. таблицы 3 и 4).

Table 3

Радиоактивные выбросы зарубежных АЭС (ж)

| АЭС (мощность) | Выбросы (кюри/сутки мвт) | |
	Р/а газы	аэрозоли
Дрезден I (700 мвт)	3,I	$0,430.10^{-6}$
Биг-Рок-Пойнт (157 мвт)	19	$0,64.10^{-3}$
Гумбольт-Бэй (165 мвт)	7,4	$0,36.10^{-4}$
Елк-Ривер (58 мвт)	0,16	$0,52.10^{-7}$

ж На рассмотренных АЭС данные по выбросам получены после 18-30 минут выдержки выбрасываемых газов и очистки их с помощью аэрозольных фильтров.

Table 4

Активность выброса радиоактивных благородных газов (к/сут. мвт)

| АЭС | Изотопы | | | | | | |
	85	87	88	133	135	135	138
KRB	0,125-0,193	0,174-0,25	0,36-0,5	0,275-0,34	0,39-0,72	0,325-0,83	0,94-1,2
Гарильяно	$0,0^228$	$0,0^252$	-	$0,0^226$	$0,0^298$	-	0,05
Bonus	$0,0^336$	$0,0^32$	$0,0^322$	$0,0^46$	$0,0^332$	-	0,00II
Рассматриваемая АТЭЦ	0,077	0,252	0,237	0,062	0,220	0,375	I,I
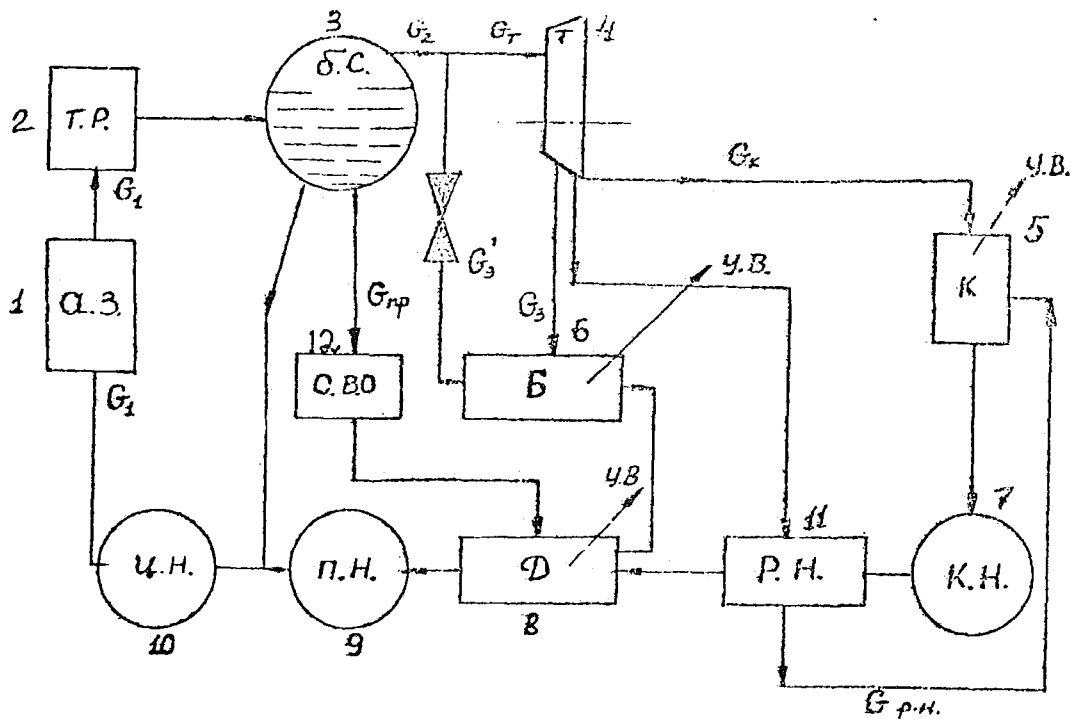
Fig. 1

Flow diagram of nuclear heat and power plant

Key:

1 = Core		2 = Separator tubes	
3 = Drum-separator		4 = Turbine	
5 = Condenser		6 = Boilers	
7 = Condensate pump		8 = Deaerator	
9 = Feed pump		10 = Circulating pump	
11 = Regenerative feed heaters		12 = Water purification plant	

Y.B. = Air vent; G_1, G_2, G_T, G_3, G_3', G_K, G_{np}, $G_{p.H}$ (kg/sec) are the coolant flow rates in different parts of the circuit.

CHAPTER IV

PROGRAMMING, INFORMATION AND
STANDARDIZATION QUESTIONS

ALGOL PROGRAMMES FOR DETERMINING NUCLEAR PARAMETERS FROM
AN ANALYSIS OF THE EXCITATION FUNCTION
(ERICSON'S STATISTICAL THEORY)

A.I. Baryshnikov

Practical and theoretical investigations carried out since 1960 have
shown convincingly that excitation functions measured with high energy
resolution of the primary particles for compound-nucleus reactions at high
excitation energy (12-30 MeV) have a fluctuation structure (Fig. 1).
According to Ericson's statistical theory these fluctuations do not have
a resonance character and cannot be explained by the individual nuclear
levels. The fluctuation is the result of interference between the many
partial levels existing within a certain energy interval, called the
coherent energy Γ, which is the reciprocal of the lifetime of the compound
state.

Even in his very early publications $\left[1, 2\right]$ Ericson pointed to the
amount of information derivable from the excitation functions and proposed
methods of analysing them to determine a number of nuclear parameters.

Subsequent investigations have explored and expanded these possibilities,
and the various methods of determining nuclear parameters from the excitation
functions and angular distributions have been analysed in detail by the
author in a review paper.

The present paper supplies ALGOL programmes which can be used for
determining nuclear parameters from correlation analysis of the excitation
function and for comparing the theoretical probability distribution with
the experimental histogram of the distribution, $Z(\frac{\sigma}{<\sigma>})$.

I.   ALGOL programme for correlation analysis (APKA)

With this programme it is possible to determine:

(1)   The auto- and cross-correlation functions for all exit channels of
the reaction

$$R^{ij}(\varepsilon) = \frac{\langle[\sigma^i(E+\varepsilon)-\langle\sigma^i\rangle][\sigma^j(E)-\langle\sigma^j\rangle]\rangle}{2\langle\sigma^i\rangle\langle\sigma^j\rangle} +$$

$$+ \frac{\langle[\sigma^i(E)-\langle\sigma^i\rangle][\sigma^j(E+\varepsilon)-\langle\sigma^j\rangle]\rangle}{2\langle\sigma^i\rangle\langle\sigma^j\rangle} ;$$

(1)

If i $\neq$ j, the cross-correlation function is determined.

If i = j, the auto-correlation function is determined.

(2) When i = j and ε = 0 the coefficient of the auto-correlation function is determined:

$$C(0) = R^{ij} \left(\varepsilon = 0 \right) \qquad \cdot \qquad (2)$$

(3) The coefficient of the cross-correlation function

$$C^{ij}(0) = \frac{R^{ij}\left(\varepsilon = 0\right)}{\sqrt{C^i(0)C^j(0)}} , \qquad (3)$$

the numerical value of which determines the degree of correlation between the channels "i" and "j".

(4) The normalized mean square deviation, which is numerically equal to the coefficient of the auto-correlation function (ε = 0):

$$C(0) = \frac{\langle \sigma^2 \rangle - \langle \sigma \rangle^2}{\langle \sigma \rangle^2} \qquad (4)$$

(5) The coherent energy (by several methods):

(a) From the condition that the auto-correlation function decreases by a factor of two in relation to R(ε = 0) = C(0), since with ε = Γ we have

$$R\left(\varepsilon = \Gamma\right) = \frac{1}{2} C(0) \qquad (5)$$

(b) By comparing the Lorentz function R(Γ,ε) with the auto-correlation function R(ε) when $\varepsilon \gg \Gamma$, since

$$R(\Gamma,E) = C(0) \frac{\Gamma^2}{\Gamma^2 + \varepsilon^2} \approx R\left(\varepsilon \leqslant \Gamma\right); \qquad (6)$$

(c) By analysing the fluctuations of the auto-correlation function when $\varepsilon > 2\Gamma$:

$$\left\langle R^2(\varepsilon)\left[\frac{I - \varepsilon}{I}\right]\right\rangle \cong R^2(\varepsilon = 0) \frac{\pi}{2} \left(\frac{\Gamma}{I}\right), \qquad (7)$$

where I is the range of energy variation of the excitation function.

If the excitation function has a constant mean value over the whole range I, the auto-correlation function oscillates about the ε-axis. These oscillations are due to the use of a finite range of averaging of I for the excitation function.

If the mean cross-section of the excitation function is not constant over the range I, the auto-correlation function will not oscillate about the ε-axis and the results of the auto-correlation analysis ($C(0)$ and Γ) will not be true.

Methods of eliminating the effect of the mean cross-section not being constant are described in the review paper. ALGOL programmes for these calculations have been compiled but will not be published until they have been checked numerically.

II. ALGOL programme for calculating the probability distribution (RVEG)

The RVEG programme can be used to determine:

(1) The experimental histogram of the probability distribution $Z(\frac{\sigma}{<\sigma>})$ for the excitation function of interest, for different variation steps of the argument $\frac{\sigma}{<\sigma>}$ (from 0.4 to 0.2), where σ and $<\sigma>$ are the cross-section and the mean cross-section respectively.

(2) The effective number of reaction channels N_{eff} (number of partial levels of the compound nucleus which participate in a given reaction channel) and the proportion of the direct interaction process, $-y_D$ $\quad y_D = \frac{G_D}{<G>}$; this is done by comparing the theoretical probability distribution $P(\frac{\sigma}{<\sigma>})$ with the experimental histogram $Z(\frac{\sigma}{<\sigma>})$ with simultaneous consideration of the dual experimental relationship between N and y_D:

$$\text{a)} \qquad C(0) = \frac{1}{N}(1 - y_D^2) \qquad\qquad (8)$$

$$P(y) = \left(\frac{N}{1-y_D}\right)^N \cdot y^{N-1} e^{-\frac{N(y+y_D)}{1-y_D}} \left\{ \frac{J_{N-1}\left(2iN\frac{\sqrt{y\,y_D}}{1-y_D}\right)}{\left(iN\frac{\sqrt{y\,y_D}}{1-y_D}\right)^{N-1}} \right\}, \qquad (9)$$

where $- \ y = \frac{G}{<G>}$,

J_{N-1} is the N-1 order Bessel function from the imaginary argument. After putting the Bessesl function in the form of a series (N being an integer) we have

$$J_{N-1}(2i\sqrt{x}) = i^{N-1}\sqrt{x^{N-1}} \sum_{j=0}^{\infty} \frac{x^j}{(N-1+j)!\,j!} , \qquad (9x)$$

and the probability distribution becomes

$$P(y) = \left(\frac{N}{1-y_D}\right)^N y^{N-1} \cdot e^{-\frac{N(y+y_D)}{1-y_D}} \sum_{j=0}^{\infty} \frac{\left[N^2 \frac{y\,y_D}{(1-y_D)^2}\right]^j}{(N-1+j)!\,j!} \qquad (9\,a)$$

The normalized mean square deviation is also determined here from the equation

$$C(O) = \frac{\langle \sigma^2 \rangle - \langle \sigma \rangle^2}{\langle \sigma \rangle^2} \; .$$

(4)

(3) The maximum possible number of effective channels in the reaction is determined from equation (8) for $y_D = 0$:

$$N^{max}(\theta) = \frac{1}{C(0,\theta)} \; ;$$

(10)

The results of processing the excitation functions (Fig. 1) of the reaction $^{52}Cr(pp_1)^{52}Cr$ with these programmes are illustrated in Figs (2) and (3).

In the case of N not being an integer [3, 4] we have

$$P(y) = \left(\frac{N}{1-y_D}\right)^N y^{N-1} e^{-\frac{N(y+y_D)}{1-y_D}} \sum_{j=0}^{\infty} \frac{[N^2 \frac{y y_D}{1-y_D}]^j}{\Gamma(N-1+j) j!}$$

(10a)

$$\Gamma(m) = (m-1) \Gamma(m-1)$$

REFERENCES

[1] ERCISON, T., Adv. Phys., 9 (1960) 425.

[2] ERICSON, T., Annls Phys., 23 (1963) 390.

[3] BATEMAN, H. et al., Tablicy integral'nyh preobrazovanij (Tables of integral transformations) Vol. 2 Izd. "Nauka" (1970).

[4] DWIGHT, H.B., Tablicy integralov (Tables of integrals) Izd. inostran. literatury (1948).
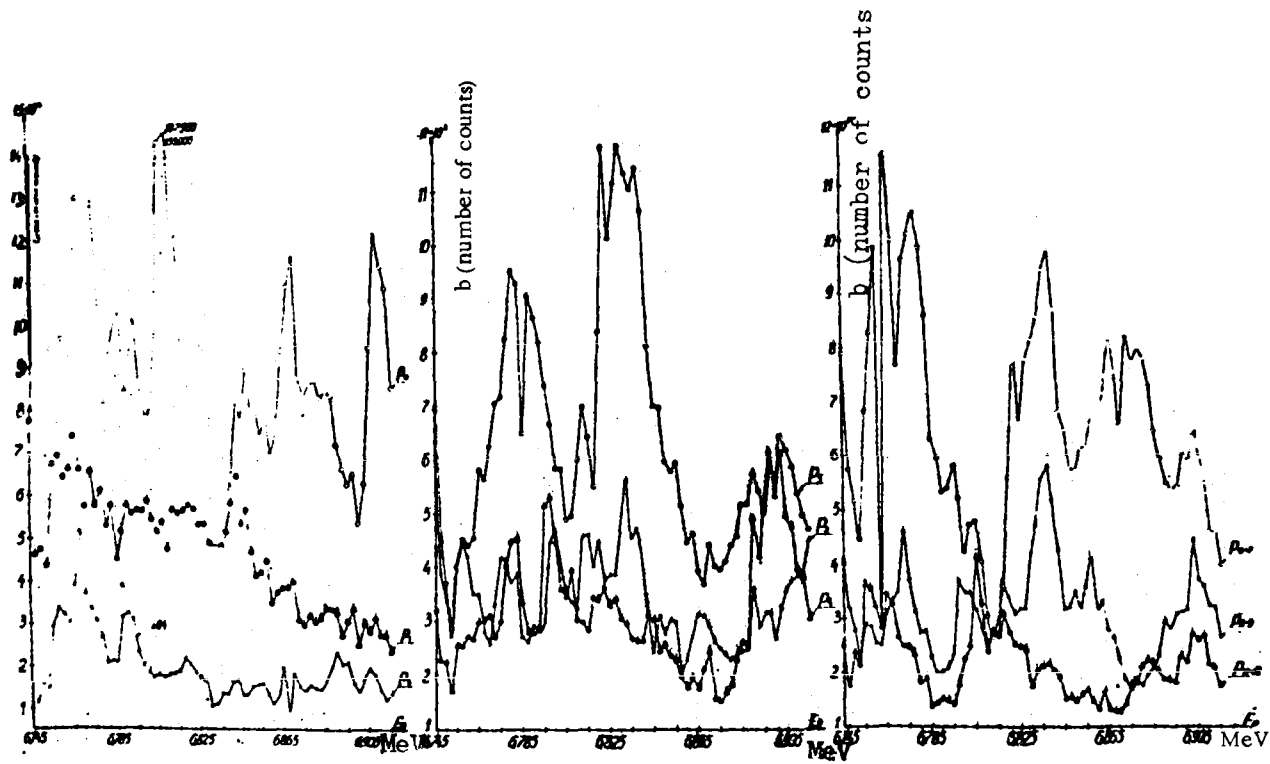
Fig. 1. Excitation functions of the reaction $^{52}Cr(p,p)^{52}Cr$. The exit channel of the reaction is shown on the graphs.
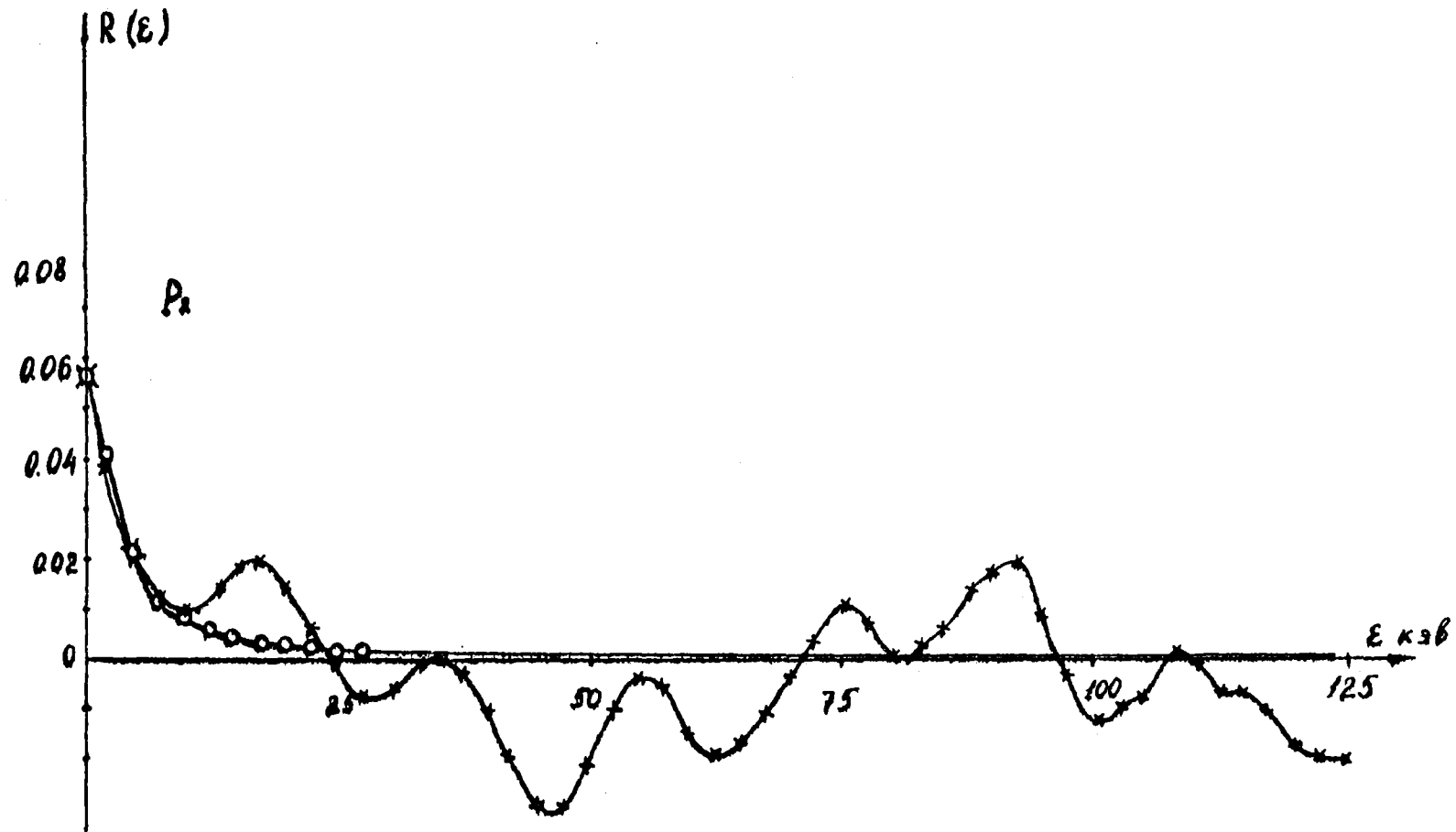
Fig. 2. x = auto-correlation function of the reaction
         o = Lorentz function
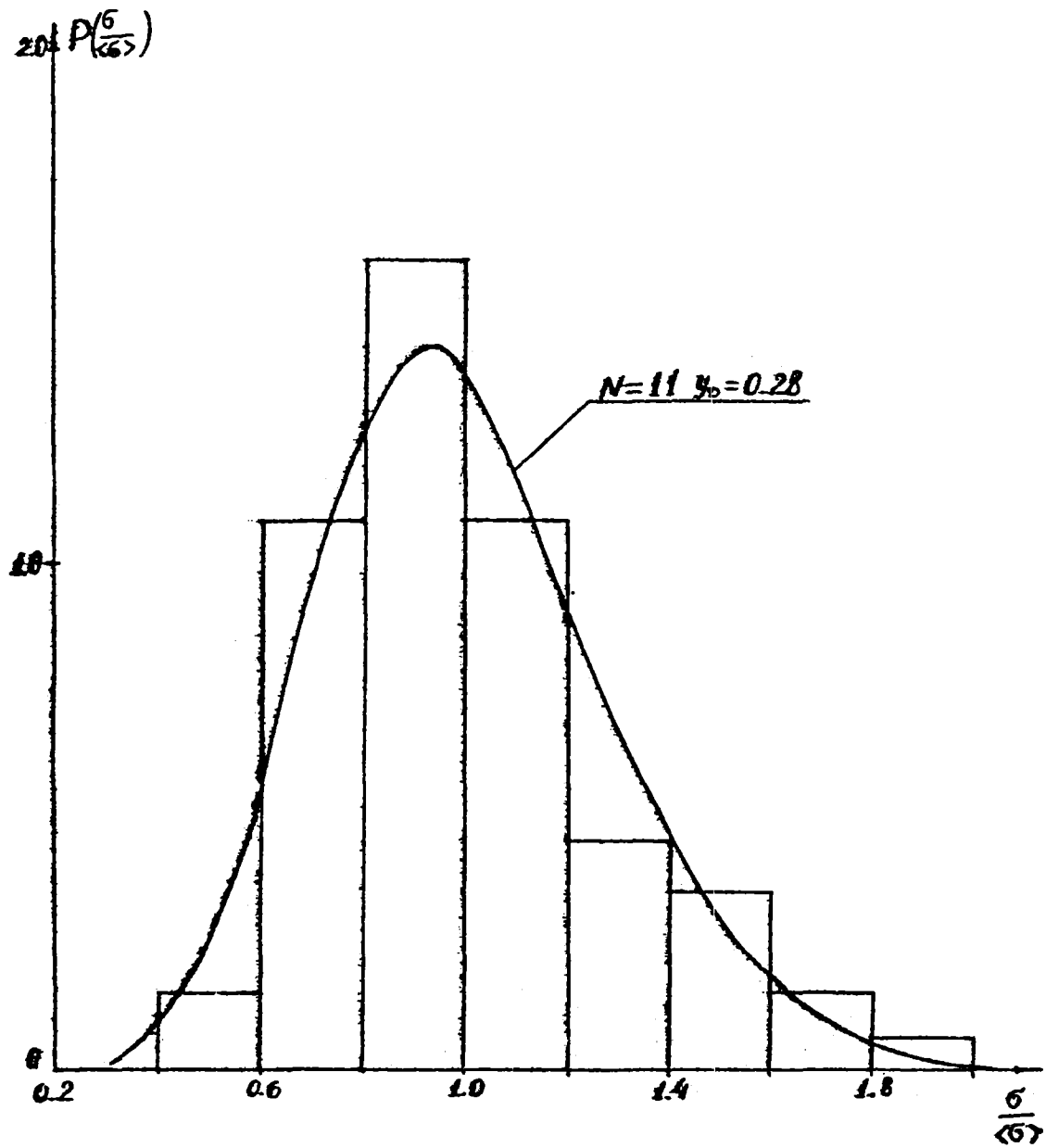
Fig. 3. Experimental histogram of $Z(\frac{\sigma}{<\sigma>})$ and the
theoretical probability distribution $P(\frac{\sigma}{<\sigma>})$
for the reaction $^{52}Cr(pp_{11})^{52}Cr$.

APKA Programme

Initial data

INTEGER

     M - maximum number of excitation functions investigated

     N - maximum number of points in the excitation function

     D - number of points in the auto- and cross-correlation functions

  I,J - number of excitation function (number of reaction channel)

REAL

     Q - energy variation step in excitation function in keV

ARRAY

     F $\big[$1 : M,1 : N$\big]$ - array of excitation functions

     Operating variables used for controlling the output of:

INTEGER

     K - the number of the point in the auto- and cross-correlation function
        (ε is the deviation from energy E)

     L - the number of the point in the excitation function (value of
        energy E)

     W - the number of the point of the auto-correlation function

REAL

     A - the sum of the values of the excitation function;   the ratio
        R[K]/R[0];   the difference in the values of the auto-correlation
        and Lorentz functions

     B - the sum of the squares of the excitation functions

    S1 - the mean value of the cross-section of the J excitation function
        being analysed;   the value of the coherent energy in keV obtained
        by analysing the fluctuations of the auto-correlation function
        (see equation (7)).

     V - the cross-correlation coefficient

    C1 - the normalized mean square deviation

     E - the sum of the products of the terms in the auto- and cross-
        correlation functions;   the variable value of the coherent
        energy in the Lorentz function

V - the sum of the products of the terms in the auto- and cross-
correlation functions; the maximum number of points in the
excitation function

SUM - the intermediate value

B1 - the mean value of the square of the excitation functions

$G = \frac{S1 + G2}{2}$ - the mean coherent energy

ARRAY

T[1 : M, 1 : N]   - the deviations of the excitation function from
                                 the mean values

S [1 : M]   - the mean values of all M excitation functions

LO [0 : D]   - the Lorentz function

R [0 : D]   - the values of the auto- and cross-correlation functions

P [1 : N]   - the excitation function being analysed

CO [1 : M]   - the values of the auto-correlation functions when K = 0
                                 ($\varepsilon = 0$)

```
BEGIN

INTEGER M, N, D, K, L, I, J;

REAL A, B, S1, B1, C1, E, V, SUM, Q;

COMMENT ( input of initial data)

COD ('R10-2', M, N, D, Q);

BEGIN

ARRAY F, T[1:M, 1:N], S, CO, CIJO[1:M], LO, R[0:D], P[1:N];

COMMENT DO 'F' 700 'S' 10 'LO' 51 'P' 70 'T' 700 'R' 51
'LO' 51 'R' 51 'P' 70;

COMMENT ( input of excitation function array)

COD ('R10-2', F);
```

COMMENT (calculation of mean cross-section and

normalized mean square deviation of the J excitation function

with print-out and filling of T array)

```
FOR J:=1 STEP 1 UNTIL M DO

BEGIN  A:=0; B:=0; C1:=0;

FOR L:=1 STEP 1 UNTIL N DO

BEGIN P[L] := F[J,L];

A:=A+P[L]; B:=B+P[L]↑2

END;

B1:=A/N;

S[J]:=A/N;

C1:=B1/(S[J]↑2)-1;

CIJO[J]:=C1;

FOR L:=1 STEP 1 UNTIL N DO

T[J,L]:=F[J,L]-S[J]; S1:=S[J];

cod('P2-10', J, P, S1, C1)

END; J:=0;
```

COMMENT (computation of the auto- and cross-correlation functions

and the cross-correlation coefficient with print-out of their values

and filling of the CO array)

```
H:J:=J+1; I:=J-1;

HH:I:=I+1;

FOR K:=0 STEP 1 UNTIL D DO

BEGIN E:=0; V:=0; FOR L:=1 STEP 1 UNTIL N-K DO
```

```
BEGIN  E:=E+T[J,L]*T[I,L+K];
       V:=V+T[J,L+K]*T[I,L];
END;
   SUM:=0.5*(E+V)/(S[J]*S[I]);
   R[K]:=SUM/(N-K)
END;
V:=0; K:=0;
IF  I≠J  THEN
V:=R[K]/(SQRT(CIJO[I]*CIJO[J]))
ELSE  CO[I]:=R[K];
code('P2-10' J, I, R, V);
```

COMMENT   (proceed to calculation of coherent energy from auto-correlation function),_

```
IF  I=J  THEN  GOTO  H1  ELSE
```

COMMENT   (proceed to calculation of the cross-correlation functions between J channel and the following I (I>J) reaction channels)

```
IF  I<M  THEN  GOTO  HH  ELSE
```

COMMENT (proceed to next excitation function)

```
IF  J<M  THEN  GOTO  H;
```

COMMENT (calculate coherent energy, Γ and Lorentz function)

```
H1:
BEGIN  INTEGER  W;
```

COMMENT   (determine coherent energy Γ in keV from fluctuation of auto-correlation function [see equation (7)] and print out)

```
BEGIN  REAL  G, G1, G2; A:=SUM:=B:=K:=E:=0;
H2:K:=K+1; A:=R[K]/R[0];
IF  I=J  THEN
BEGIN
   W:=2*K; G1:=W;
END;
IF  A>0.5  THEN  GOTO  H2;
W:=G1;
```

```
V:=N; SUM:=0; S1:=0;
FOR K:=W STEP 1 UNTIL D DO
SUM:=SUM+R[K]↑2*(1-K/V);
S1:=2*V*SUM*Q/(3,14157*(D-W)*R[0]↑2);
COD('R2-10', S1);
```

COMMENT (determine Γ in keV by comparing the auto-correlation and the Lorentz functions and calculate the Lorentz function with print out)

```
BEGIN A:=0; B:=0; E:=0; V:=0; SUM:=0; K:=0.5*W;
cod('P2-10', K, G1);
IF K=1 THEN E:=0;
IF K=2 THEN E:=0.5;
IF K=3 THEN E:=1.5;
IF K<10 THEN
 BEGIN IF K>4 THEN E:=K-3
 END
 ELSE
 E:=K-4;
 cod('P2-10', E);
 H3: E:=E+0.1; SUM:=0;
 FOR K:=0 STEP 1 UNTIL 0.5*W DO
 BEGIN
 A:=R[K]-R[0]*E↑2/(E↑2+K↑2);
 SUM:=SUM+A
 END
 G2:=E*Q; G1:=E;
 IF SUM>0 THEN GOTO H3;
 cod('P2-10', E, SUM);
 E:=G1;
 FOR K:=0 STEP 1 UNTIL D DO
 LO[K]:=R[0]*E↑2/(E↑2+K↑2);
 cod('P2-10', G2, LO)
 END;
```

COMMENT (determine mean coherent energy with print out)

```
6: = 0.5*(s1+62); s1:=0;
cod('P2-10', 6)
END
```
END;

COMMENT (proceed to calculation of the cross-correlation functions between the J channels and the following I (I> J) reaction channels)

IF I<M THEN GOTO HH;

COMMENT (print out the values of the auto-correlation function for K = 0 (ε = 0)
```
cod('P2-10', CO);
cod('PR2 -10', CO);
END
```
END;

RVEG Programme

Initial data

INTEGER

P — maximum number of excitation functions investigated

W — maximum number of points in the excitation function

Q — maximum number of points in the probability distribution curve

ARRAY

$F[1 : P, 1 : W]$ — array of excitation functions

$C[1 : P]$ — array of normalized mean square deviations for the excitation functions investigated / calculated /

Operating variables used for controlling the output of:

INTEGER DD — the volume of print out

N — number of effective channels

I — number of excitation function (reaction channel)

L — number of cell in array M1; number of terms in expansion of the Bessel function

K — number of interval along the axis $\sigma/\langle\sigma\rangle$

Q1 — range of renormalization of histogram

REAL

A1 — sum of all points and mean value of excitation function; intermediate values

A2 — intermediate values

J — variation step of $\sigma/\langle\sigma\rangle$; value of ψ in the probability distribution $P(\psi)$

I1 — intermediate value

M — maximum number of effective channels; intermediate values

D — proportion of the process of direct interaction

Z1, B, B1, B2, B3, B4, B5, B6, SUM, R — intermediate values

V — normalized mean square deviation of the I excitation function

ARRAY

$N1[1 : W]$ — excitation function being analysed

$N1[1 : W]$ — array $\sigma/\langle\sigma\rangle$ of function being analysed

$Z[1 : Q]$ — experimental and normalized histogram

$PR[1 : Q]$ — array of distribution probability $P(\psi)$

PRP[1 : Q]— array of distribution probability P(ψ)

PRR [1 : Q] — arrays of distribution probability after the cyclic
permutation necessary for comparing them

PE [1 : DD] — array of numerical output

Γ[1 : 10] — gamma function array (1.0, .95135, .91817, .89747,
.88726, .88623, .89352, .90864, .93138, .96177)

```
BEGIN
INTEGER  P, Q, I, L, K, W, Q1, L1, DD, Z1;
REAL  A1, A2, J, I1, N;
COMMENT  (input of initial data)
COD ('P10-2', P, W, Q);
DD: = 3*Q + W + 25;
BEGIN  ARRAY  F[1:P, 1:W], c[1:P], M1, N1[1:W], Z, PR, PRP,
  PRR [1:Q], PE[1:DD], Γ[1:10];
COMMENT  DO 'F' 700 'C' 10 'M1' 'N1' 20 'Z1' 'PR' 'PRP' 'PRR' 15 'PE' 140 'Γ' 10;
COMMENT  (input of initial data)
COD ('R10-2', F, J); I: = 0;
H: I: = I + 1;  A1: = A2: = 0;
FOR  L1: = 1  STEP  1  UNTIL  DD  DO  PE[L1]: = 0;
L1: = 1;
PE[L1]: = I;
COMMENT  ( calculation of mean square normalized deviation)
 ....;
BEGIN  FOR  L: = 1  STEP  1  UNTIL  W  DO
  BEGIN
    N1[L]: = F[I, L];
    PE[L+1]: = N1[L];
    A1: = A1 + N1[L];
    A2: = A2 + N1[L]↑2
  END;
  A1: = A1/W;
  A2: = A2/W;
  c[I]: = A2/(A1↑2) - 1;
  A2: = c[I];
  L1: = W + 2; PE[L1]: = A1; PE[L1+1]: = A2;
  L1: = L1 + 2;
```

COMMENT (construction of experimental histogram of the probability distribution Z($^{\sigma}/\!<\sigma>$) of the I excitation function for variation step of $^{\sigma}/\!<\sigma>$ = (0.4; 0.3; 0.2))

```
  FOR  L: = 1  STEP  1  UNTIL  W  DO  M1[L]: = N1[L]/A1;  I1: = 2.5;
```

```
H4: I1:= I1-0.5; FOR K:=1 STEP 1 UNTIL Q DO Z[K]:=0;
L:=0; J:=0.2*I1;
PE[L1]:=J;
H5: K:=0; L:=L+1; IF L<W THEN
BEGIN
H6: K:=K+1;
COMMENT (transfer to new range of σ/<σ>  )
IF M1[L] > 0.2 * K * I1 THEN GOTO H6
ELSE
IF M1[L] > 0.2 * (K-1) * I1 THEN
COMMENT (transfer to new value of excitation function)
BEGIN Z[K]:= Z[K]+1; GOTO H5.
END
END;
```

COMMENT (normalize area under histogram to unity and record corrected histogram)

```
Q1:= Q*0.2/J;
FOR K:=1 STEP 1 UNTIL Q1 DO
Z[K]:= Z[K]/(0.2*I1*W); ·
FOR K:=1 STEP 1 UNTIL Q DO
PE[L1+K]:= Z[K]; L1:=L1+Q+1;
PE[L1]:= 98989898989; L1:=L1+1;
```

COMMENT (transfer to new variation step of σ/<σ>)

```
IF I1 >1 THEN GOTO H4
END
```

COMMENT (calculate theoretical probability distribution P(σ/<σ>) of excitation function being analysed for variation step of σ/<σ> = 0.2, print out proportion of direct interaction process, number of effective channels N and probability distribution at specific value of C [J])

```
FOR K:=1 STEP 1 UNTIL Q DO PR[K]:=0;
BEGIN REAL M,D,B,B1,B2,B3,B4,B5,B6,SUM,R,V;
N:=0; V:= C[I]; M:=1/V;
```

```
PE[L1]:= V; PE[L1+1]:= -M;
PE[L1+2]:= I; PE[L1+3]:= 999999999;
COD ('P2-10', PE);
FOR L1:=1 STEP 1 UNTIL DD DO PE[L1]:= 0;
L1:=1;
H3: N:= N+1; Z1:= 1;
IF L1 > 125 THEN
BEGIN COD ('P2-10', PE);
FOR L1:=1 STEP 1 UNTIL DD DO
PE[L1]:= 0;
L1:=1
END;
ELSE L1:= L1+1;
HHH: B1:= 1 - V * N;
IF B1 < 0 THEN
BEGIN N:= N-1+0.1; M:= 1/C[I]; Z1:= Z1+1;
IF N ≤ M THEN GOTO HHH
END;
PE[L1]:= I; PE[L1+1]:= N;
COMMENT (transfer to control point at end of programme)
IF B1 < 0 THEN GOTO H2;
D:= SQRT(B1);
PE[L1+2]:= D;
B1:= f[Z];
A2:= 1;
COMMENT (transfer to eliminate part of programme)
IF N=1 THEN GOTO H1;
COMMENT (transfer to end of programme, recording limiting number
of channels N = 29, and re-recording the distribution and the
control point)
IF N > 29 THEN GOTO H2;
COMMENT ( transfer to eliminate part of programme)
IF N < 18 THEN GOTO H2H;
M:= 1;
IF Z1=1 THEN B:= N-18 ELSE B:= ENTIER(N)-18;
```

```
FOR K:= 1  STEP 1 UNTIL B DO
M: = M*(N-K);
A2:= 1/M; IF I=1 THEN B:=N ELSE B:= ENTIER(K);
FOR K:=1 STEP1 UNTIL 17 DO B1:=B1*(N-B+K);
COMMENT ( transfer to eliminate part of programme)
IF N>18 THEN GOTO H1;
H2H: IF I=1 THEN B:=N-2 ELSE B:= ENTIER(K)-2;
FOR K:=1 STEP 1 UNTIL B DO
B1:= B1*(N-K);
H1:A1: = 1/B1; B:= N/1-D); B2:= B4 (0.2*N);
B3:= EXP(- 0.2*B*D);
FOR K:=1 STEP 1 UNTIL Q DO
BEGIN J=0.2*K -0.1;
B4:= J*(0.5*(N-1));
B5:= B*J*D*B; B6:= EXP(-0.2*B*J);
COMMENT (in the absence of direct interaction D = 0)
IF B5=0 THEN
BEGIN
L:=0;
PR[K]:= A1*10*5*B3*B2*B6*B4* B3*B2*B6*B4*B3*B2*
*(A2*10*5)*B6*B3*B2*10*(-3)*B6*B3*B2*B6* 10*(-7);
IF PR[K]< 10*(-8) THEN PR[K]:=0
END;
COMMENT (in the presence of direct interaction D ≠ 0)
IF B=5 THEN
BEGIN
PE[L1+3]:=L; PE[L1+4]: = 979797979
END;
IF B5>0 THEN
BEGIN L:=0; SUM:= 10*(-15);
R:= 10*(-15);
H2:L:=L+1;
R:= R*B5/((N+L-1)*L); SUM:= SUM+R;
B1:=R;
```

```
IF  R < 5 * 10↑15  THEN
BEGIN
  I1: = R ; M: = SUM;

  COMMENT (transfer to increase the number of terms in the
  expansion of the Bessel function)
  IF  R/SUM > 0.01   THEN   GOTO  H2;
  COMMENT (print out number of effective channels)


  PE[L1+3]: = L;  PE[L1+4]: = 969696969
END;
IF  R > 5 * 10↑15  THEN
BEGIN
  L: = L-1;  SUM: = M * 10↑(-15);  R: = I1 * 10↑(-15);
  SUM: = SUM * 10↑(-8);
  R: = R * 10↑(-8);
ZM: L: = L+1;
  R: = R * B5/((N+L-1) * L);  SUM: = SUM+R;
  COMMENT (transfer to record distribution, input of
  overflow)

  IF  SUM > 10↑13  THEN GOTO  MZM;
  COMMENT (transfer to increase number of terms in the
  expansion of the Bessel function)
  IF  R/SUM > 0.01  THEN  GOTO  ZM;
  COMMENT ( print out number of effective channels)
  PE[L1+3]: = L;  PE[L1+4]: = 959595959
END;
IF  B1 > 5 * 10↑15  THEN
BEGIN
  SUM: = SUM + 10↑(-15) * M * 10↑(-8);
  PR[K]: = A1 * 10↑5 * B3 * B2 * B6 * B4 * B3 * 10↑5 * B6 * B4 * B3 * 10↑8
  * B2 * B6 * (A2 * 10↑8) * B3 * B2 * B6 * B3 * B2 * B6 * B2 * SUM * 10↑12 ,
END
ELSE
PR[K]: = A1 * 10↑5 * B3 * B2 * B5 * B4 * B3 * 10↑5 * B6 * B4 * B3 * B2 * B5*
```

```
A2 * 10↑8 * B3*B2*B6 * B3*B2*B6 * B2 * SUM* 10↑(-3));
IF PR[K]< 10↑(-18) THEN PR[K]:= 0'
END
END;
MZM;
COMMENT (print out proportion of direct interaction process and
distribution of probabilities for N ≠ 2)
L1:= L1+4;
FOR K:= 1 STEP 1 UNTIL Q DO
PE[L1+K]:= PR[K]; L1:= L1+Q +1; PE[L1]:= 919191919;
COMMENT (transfer for cyclic overflow of arrays PRR, PR, PRP and
eliminate part of programme operating only when N = 2)


IF N>2 THEN GOTO H8;
COMMENT (calculation for N = 2)
IF N=1 THEN FOR K:=1 STEP 1 UNTIL Q DO PRP[K]:= 0;
N:= N+1; COD (↑2-10', N);
L1:= L1+1;
PE[L1]:= I; PE[L1+1]:= N;
B1:= 1-V*N;
COMMENT (transfer to end of programme, recording zero array
of PRR for N = 2)
IF B1<0 THEN GOTO H21;
D:= SQRT(B1);
PE[L1+2]:= D;
A1:= 1;
B:= N/(1-D); B2:= B↑(0.2*N); B3:= EXP(-0.2*B*D);
FOR K:=1 STEP 1 UNTIL Q DO
BEGIN J:= 0.2*K-0.1;
B4:= J↑(0.5*(N-1));
B5:= B*J*D*B; B6:= EXP(-0.2*B*J);
IF B5=0 THEN
BEGIN SUM:=1; PRP[K]:= A1*10↑5*B3*B2*B6*B4*B3*B2*
B6*B4*B3*B2*B6*B3*B2*B6*B3*B2*B6*10↑(-5);
```

```
L:=0;
IF PRP[K] < 10↑(-18) THEN PRP[K]:= 0
END;
IF B5=0 THEN
BEGIN
PE[L1+3]:=L; PE[L1+4]:=979797979
END;
IF B5>0 THEN
BEGIN L:=0; SUM:=10↑(-15); R:=10↑(-15);
H7:L:=L+1;
R:= R*B5/((N+L-1)*L); SUM:=SUM+R; B1:=R;
IF R < 5*10↑15 THEN
BEGIN
I1:=R; M:=SUM;
```

COMMENT (transfer to increase number of terms in the expansion of the Bessel function)

```
IF R/SUM > 0.01 THEN GOTO H2;
```

COMMENT (record number of effective channels)

```
PE[L1+3]:=L; PE[L1+4]:=969696969
END;
IF R > 5*10↑15 THEN
BEGIN
L:=L-1; SUM:= M*10↑(-15); R:=I1*10↑(-15);
R:= R*10↑(-8);
SUM:= SUM*10↑(-8);
ZM1:L:=L+1;
R:= R*B5/((N+L-1)*L); SUM:= SUM+R;
```

COMMENT (transfer to record probability distribution in view of overflow)

```
IF SUM > 10↑15 THEN GOTO M2M1;
```

COMMENT (transfer to increase number of terms in the expansion of the Bessel function)

```
IF R/SUM > 0.01 THEN GOTO ZM1;
```

COMMENT (record number of effective channels)

```
        PE[L1+3]:= L; PE[L1+4]:= 959595959
      END ;
      IF B1 > 5*10↑15 THEN
      BEGIN
        A2:=1;
        SUM:= SUM + 10↑(-15)*M*10↑(-8);
        PRP[K]:= A1*10↑5*B3*B2*B6*B3*B2*B6*B2*SUM*10↑12 ;
        B3*10↑8*
        B2*B6*(A2*10↑8)*B3*B2*B6*B3*B2*B6*B2*SUM*10↑12;
      END ;
      ELSE
      PRP[K]:= A1*10↑5*B3*B2*B6*B4*B3*10↑5*B6*B4*B3*
      *B2*B6*10↑5*B3*B2*B6*B3*B2*B6*B2*SUM;
      IF PRP[K]< 10↑(-18) THEN PRP[K]:=0
      END
    END;
  M2M1:
  COMMENT (print out proportion of direct interaction process and
  probability distribution for N = 2)
  L1:= L1+4;
  FOR K:=1 STEP 1 UNTIL Q DO
  PE[L1+K]:= PRP[K]; L1:=L1+Q+1; PE[L1]:= 929292929;
  COMMENT (transfer to compare histogram with theoretical probability
  distribution for two neighbouring N)
  IF N=2 THEN GOTO H9;
  H8: FOR K:=1 STEP 1 UNTIL Q DO
  BEGIN PRR[K]:= PR[K]; PR[K]:= PRP[K]; PRP[K]:= PRR[K]
  END;
  H9: B1:=0; B2:=0;
  FOR K:=1 STEP 1 UNTIL Q DO
  BEGIN B:= PR[K]-Z[K]; A1:= B1+B↑2;
    R:= PRP[K]-Z[K]; B2:= B2+R↑2
  END;
  L1:=L1+1; PE[L1]:= 987654321;
```

```
COMMENT  (transfer to increase N in theoretical probability
distribution).
IF B2 < B1  THEN GOTO  H3; .
PE[L1] := 123456789; K := 0;
MM: K := 1; L := K+1;
B1 := PRP[K] - PRP[L];
COMMENT  (transfer to determine point with maximum value in
probability distribution)
IF  B1 < 0  THEN  GOTO  MM;
K := L-1;
B1 := Z[K] - PRP[K];
COMMENT  (transfer to increase N in theoretical probability
distribution
IF  B1 > 0  THEN GOTO  H3;
K := 0;
MM1: K := K+1; L := K+1;
B1 := Z[K] - Z[L];
IF  B1 < 0  THEN GOTO  MM1;
K := L-1;
B1 := Z[K] - PRP[K];
PE[L1] := 818181818;
IF B1 > 0 THEN  GOTO  H3;
H2:
H21:
PE[L1] := 191919191
END;
COD ('P2 - 10', PE);
IF  L < P THEN GOTO H
END
END;
```

COMPARISON OF TECHNIQUES AND METHODS FOR MEASURING THE
PARAMETERS OF INTENSE NEUTRON FIELDS (FIRST STAGE)

G.A. Borisov, R.D. Vasilev, N.B. Galiev,
E.I. Grigorev, V.P. Yaryna

1. Introduction

At the present time the All-Union Research Institute of Physico-
Technical and Radiotechnical Measurements (VNIIFTRI) is carrying out work
aimed at standardizing all the techniques of measuring the basic parameters
of neutron fields (integral neutron flux density, differential flux density,
etc.) based on the activation method.

One task will be to establish the possible causes of disagreement in the
results of neutron field parameter measurements performed in different
organizations. The causes of such disagreement may be:

1. Differences in the nuclear physics constants and activation
   cross-sections used;

2. Errors in measuring the activity of activation detectors;

3. Inaccuracy in determining the number of nuclei of an isotope
   in a detector;

4. Errors in the method of interpreting the activity values of the
   detectors used.

VNIIFTRI is proposing that in 1971-72 all interested organizations
should collaborate in a comparison of the methods and techniques needed
to measure differential neutron spectra.

The aim of the programme is, firstly, to compare the characteristics
of the activation detectors used in different organizations in order to
discover the differences responsible for disagreement and find ways of
eliminating them and, secondly, to establish the most simple and accurate
methods of unfolding differential neutron spectra.

The information contained in the answers to the questionnaire will
enable the Institute to undertake a broad programme of work on the standardiza-
tion of neutron field parameter measurements. The information will also be
used for comparing methods of unfolding neutron spectra and for comparisons
of activations obtained with the most widely used detectors.

2. Comparison programme

The proposed comparisons of detector characteristics and methods of unfolding spectra will be performed in two stages.

In the first stage the participants in the comparison will send the Institute information on the reactions and detectors they employ, including the nuclear physics characteristics of the detectors, and will indicate the detectors which are most widely used and which they feel should be compared first of all. This information should be included in the questionnaire supplied.

In the second stage the Institute will send out to the organizations which have answered the questionnaire the values of the activation integrals calculated for one or several test spectra and cross-sections used by a given participant, and they will be invited to unfold a test spectrum or spectra. The Institute will compare the results of the unfolding. All participants in the comparison will be informed of the results.

3. Conclusion

All the organizations taking part in the comparison will be informed of the results of the analysis of the questionnaires. Similar inter-comparisons operated by CMEA or the International Bureau of Weights and Measures might become an important source of information on nuclear physics constants and cross-sections of interest to those participating in the survey. The questionnaire should also show whether it would be desirable later on to hold a conference on the standardization of methods and techniques of measuring neutron field parameters.

QUESTIONNAIRE

A. Activation detectors

The answers to the first 15 points in the questionnaire should be incorporated in a special table, the number of the question corresponding to the number of the table column. A specimen table is attached.

1. What reactions do you use for spectrum measurement?

2. Indicate the values of E_{eff} used and the reference.

3. Indicate the values of σ_{eff} used and the reference.

4. Indicate the half-life of the product nucleus and the reference.

5. What chemical compound is used for your detector?

6. What type of material is used and what is its enrichment?

7. What are the shape, size and weight of the detector?

8. How do you determine the number of nuclei of the isotope in the detector?

9. Minimum neutron flux density with energy above E_{eff}.

10. Irradiation time.

11. Cooling time after irradiation.

12. Method of measuring the activity.

13. Type of radiation measured and its energy.

14. Correction coefficients and constants used in measuring activity (gamma radiation yield, self-absorption coefficient, internal conversion coefficient etc.).

15. Method of calibrating the measuring equipment.

16. Supply tables of the activation cross-sections for the reactions you use, showing the cross-section values together with the permissible error and the amount of detail you find necessary for unfolding a differential neutron spectrum.

17. Indicate those detectors which in your opinion should be included in the first comparison.

18. Would you welcome the centralized issue of tested activation detector kits?

B. Methods of unfolding differential neutron spectra

1. Describe briefly your method or methods of unfolding a spectrum. What in your opinion is the confidence level of the unfolded spectrum? Where was this method first described?

2. Would you welcome the centralized issue of standard computer programmes for unfolding differential neutron spectra?

3. What in your opinion would be of most help in standardizing the process of unfolding neutron spectra by the activation method?

Table

Key:

Реакция	=	Reaction
$E_{эфф}$, Мэв	=	E_{eff}, MeV
$\sigma_{эфф}$, мбарн	=	σ_{eff}, mbarn
$T_{1/2}$	=	$T_{\frac{1}{2}}$
Химическое соединение	=	Chemical compound
Марка и обогащение	=	Type and enrichment
форма и размеры	=	Shape and size
Число ядер	=	Number of nuclei
Мин.поток, нейтр./смсек	=	Minimum flux, n/cm.sec
Время облучения	=	Irradiation time
Время выдержки	=	Cooling time
Метод измерения активности	=	Method of measuring activity
Излучение и его энергия, мэв	=	Radiation and its energy, MeV
Поправочные коэффициенты и константы	=	Correction coefficients and constants
Метод градуировки	=	Method of calibration
дня	=	Days
О.С.Ч. естественная смесь изотопов	=	O.S.Ch. natural isotopic mixture
Таблетка	=	Tablet, ϕ 10 mm, 800 mg

Взвешивание на   =   Weighing on analytical balance
аналитических
весах
2 часа   =   2 hours

2-3 дня   =   2-3 days

Гамма спектрометр   =   Gamma spectrometer

Выход γ-лучей на   =   Gamma-ray yield per disintegration 33%
распад 33%

Градуировка   =   Calibration of photoefficiency O.S.G.I.
фотоэффективности
О.С.Г.И.

Table

№	Реакция	Еэфф Мэв	σ эфф мбарн	$T_{1/2}$	Химическое соединение	Марка и обогащение	Форма и размеры	Число ядер	Мин. поток нейтр. н/см²сек	Время облучения	Время выдержки	Метод измерения активности	Излучение и его энергия Мэв	Поправочные коэффициенты и константы	Метод градуировки
0	1	2	3	4	5	6	7	8	9	10	11	12	13	14	15
I	$J^{127}(n,2n)J^{126}$	II	1000	13.1 ± 0,5 дня	$C_7H_5O_2J$	О.С.Ч. естественная смесь изотопов	Таблетка ⌀10 мм 800 мг	Взвешивание на аналитических весах	10^9	2 часа	2-3 дня	Гамма-спектрометр	γ-0.65	Выход γ-лучей на распад 33%	Градуировка по фотоэффективности О.С.Г.И.

RECOMMENDED EFFECTIVE THRESHOLD AND CROSS-SECTION VALUES

E.A. Kramer-Ageev, V.S. Troshin, G.A. Borisov,
R.D. Vasilev, N.B. Galiev, E.I. Grigorev,
V.P. Yaryna

The effective threshold method for describing threshold cross-sections is described in Refs $\boxed{1}$, $2\boxed{}$. The table below contains the recommended effective thresholds E_{eff}, the effective cross-sections σ and the errors in the effective cross-sections for the chosen class of spectra $\boxed{3}$. The methods by which the recommended data were determined as well as a complete list of the references used are contained in Ref. $\boxed{3}$.

Table

Key:

№	= No.	Реакция	= Reaction
$E_{эфф}$, Мэв	= E_{eff}, MeV	$\sigma_{эфф}$, мбарн	= σ_{eff}, mbarn

Погрешность% = Error, %

№ п/п	Реакция	$E_{эфф}$, Мэв	$\sigma_{эфф}$, мбарн	Погрешность, %
I	2	3	4	5
I.	$^{237}Np\,(n,f)$	0,65	1420	2
2.	$^{103}Rh\,(n,n')\,^{103m}Rh$	0,80	950	6
3.	$^{115}Jn\,(n,n')\,^{115m}Jn$	I,I5	302	4
4.	$^{238}U\,(n,f)$	I,60	608	2
5.	$^{232}Th\,(n,f)$	I,60	145	4
6.	$^{31}P\,(n,p)\,^{31}Si$	2,55	122	5
7.	$^{64}Zn\,(n,p)\,^{64}Cu$	2,60	129	9
8.	$^{32}S\,(n,p)\,^{32}P$	2,65	252	4
9.	$^{58}Ni\,(n,p)\,^{58}Co$	2,70	450	8
I0.	$^{54}Fe\,(n,p)\,^{54}Mn$	3,00	372	8
II.	$^{35}Cl\,(n,\alpha)\,^{32}P$	3,70	190	8
I2.	$^{27}Al\,(n,p)\,^{27}Mg$	4,50	48,0	I0
I3.	$^{28}Si\,(n,p)\,^{28}Al$	5,50	125	6
I4.	$^{90}Zr\,(n,p)\,^{90}Y$	6,20	I5,5	7
I5.	$^{56}Fe\,(n,p)\,^{56}Mn$	6,60	60	3
I6.	$^{59}Co\,(n,\alpha)\,^{56}Mn$	7,I0	I3,8	3
I7.	$^{24}Mg\,(n,p)\,^{24}Na$	7,I5	128	2
I8.	$^{27}Al\,(n,\alpha)\,^{24}Na$	7,45	82,5	3
I9.	$^{203}Tl\,(n,2n)\,^{202}Tl$	9,90	I224	2
20.	$^{127}J\,(n,2n)\,^{126}J$	I0,95	I000	2
2I.	$^{65}Cu\,(n,2n)\,^{64}Cu$	II,2	608	6
22.	$^{55}Mn\,(n,2n)\,^{54}Mn$	II,70	740	2
23.	$^{19}F\,(n,2n)\,^{18}F$	I2,8	50	2
24.	$^{63}Cu\,(n,2n)\,^{62}Cu$	I2,90	526	3

REFERENCES

[1]   KRAMER-AGEEV, E.A., TROSHIN, V.S., Atomn. Energ. <u>29</u> 1 (1970).

[2]   KHARIZOMENOV, Yu.V., SUVOROV, A.P., Bjul. inf. Centr. jad Dannym,
       Issue No. 3 (1966) 462.

[3]   KRAMER-AGEEV, E.A., et al., Izmer. Tekh. (in press).

CORRIGENDA

to article by S.M. Zakharova entitled "80- and 21-group
cross-sections for absorption of neutrons by ^{237}Np and
isotopes of gadolinium" (Bjul. inf. Centr. jad. Dannym
Issue No. 5 (1968) 189).

1. On page 193 the expression $D(u,J) = \dfrac{\bar{D}}{2g}$, where $\bar{D} = \begin{cases} 2D \text{ observed when } I = 0 \\ D \text{ observed when } I \neq 0 \end{cases}$

    should be replaced by $D(u,J) = \bar{D}$, where $\bar{D} = \begin{cases} 2D \text{ observed when } I = 0 \\ D \text{ observed when } I \neq 0 \end{cases}$

2. On page 193 the expression $r_o = 1.25f$ should be replaced by
    $r_o = 1.31f$.

3. In the article it is stated that the factor S, correcting for the
    fluctuation of the mean neutron widths, had been taken into account.
    In fact, in the programme used for the computer calculation (Ref. $\lfloor 3 \rfloor$
    in the article) S is assumed to be 1.